VTT RESEARCH NOTES 2466

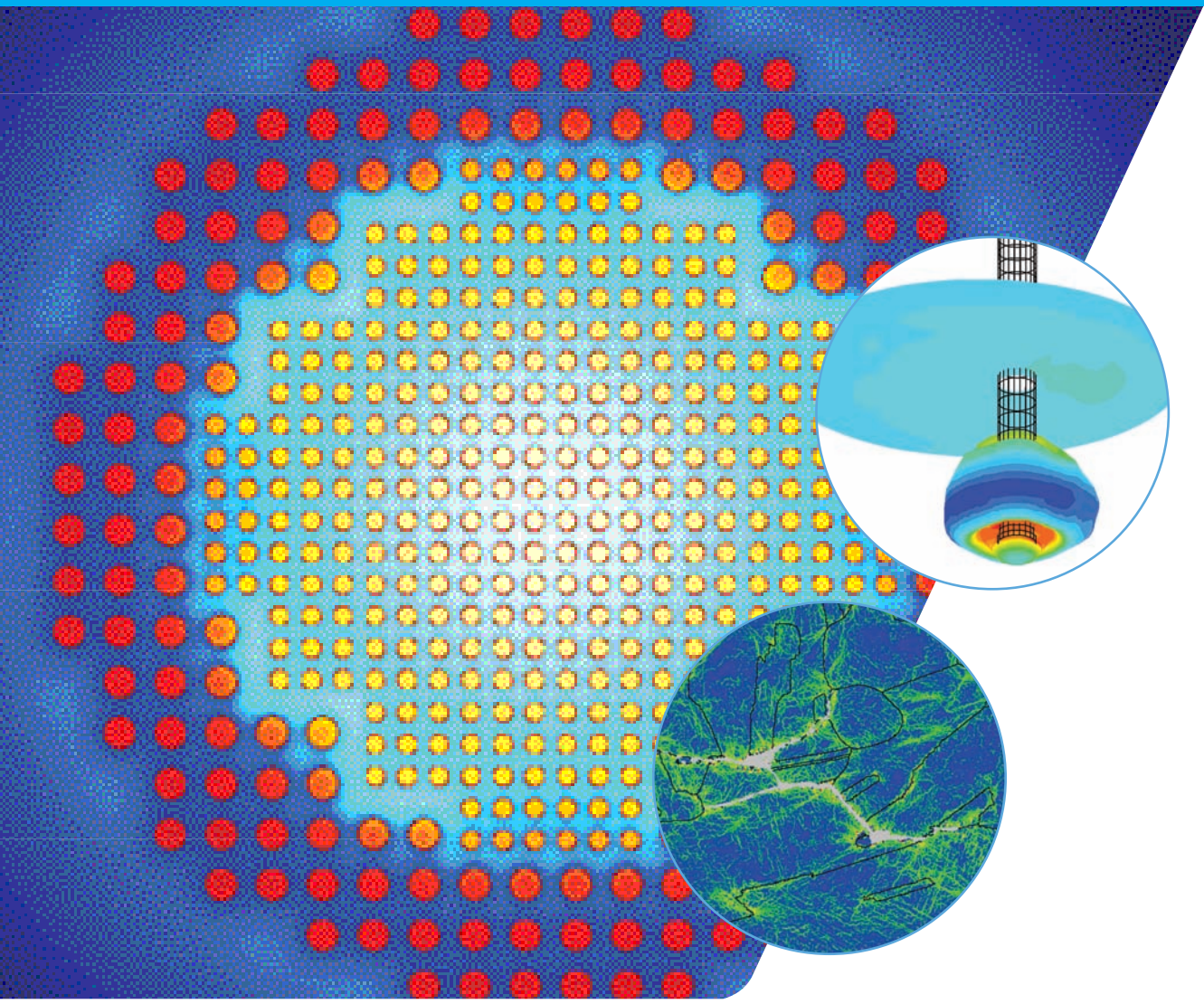

Eija Karita Puska (Ed.)

SAFIR2010

The Finnish Research Programme on Nuclear Power Plant Safety 2007–2010 Interim Report

VTT TIEDOTTEITA – RESEARCH NOTES 2466

SAFIR2010

The Finnish Research Programme on Nuclear Power Plant Safety 2007–2010

Interim Report

Eija Karita Puska (Ed.)

ISBN 978-951-38-7266-3 (soft back ed.)
ISSN 1235-0605 (soft back ed.)

ISBN 978-951-38-7267-0 (URL: http://www.vtt.fi/publications/index.jsp)
ISSN 1455-0865 (URL: http://www.vtt.fi/publications/index.jsp)

JULKAISIJA – UTGIVARE – PUBLISHER

VTT, Vuorimiehentie 5, PL 1000, 02044 VTT
puh. vaihde 020 722 111, faksi 020 722 7001

VTT, Bergsmansvägen 5, PB 1000, 02044 VTT
tel. växel 020 722 111, fax 020 722 7001

VTT Technical Research Centre of Finland, Vuorimiehentie 5, P.O. Box 1000, FI-02044 VTT, Finland
phone internat. +358 20 722 111, fax +358 20 722 7001

Edita Prima Oy, Helsinki 2009

SAFIR2010. The Finnish Research Programme on Nuclear Power Plant Safety 2007–2010. Interim Report. Eija Karita Puska (Ed.). Espoo 2009. VTT Tiedotteita – Research Notes 2466. 535 p.

Keywords nuclear safety, safety management, nuclear power plants, human factors, automation systems, operating practices, control room technology, nuclear fuels, reactor physics, thermal hydraulics, core transient analysis, steam generators, modelling, accidents, structural safety

Abstract

Major part of Finnish public research on nuclear power plant safety during the years 2007–2008 has been carried out in the SAFIR2010 programme. The steering group of SAFIR2010 consists of representatives from Radiation and Nuclear Safety Authority (STUK), Ministry of Employment and the Economy (MEE), VTT Technical Research Centre of Finland (VTT), Teollisuuden Voima Oyj (TVO), Fortum Power and Heat Oyj, Fortum Nuclear Services Oy (Fortum), Tekes – the Finnish Funding Agency for Technology and Innovation (Tekes), Helsinki University of Technology (TKK) and Lappeenranta University of Technology (LUT). In addition to representatives of these organisations, the Steering Group has permanent experts from the Swedish Radiation Safety Authority (SSM) and Fennovoima Oy (Fennovoima).

SAFIR2010 research programme is divided in eight research areas that are Organisation and human, Automation and control room, Fuel and reactor physics, Thermal hydraulics, Severe accidents, Structural safety of reactor circuit, Construction safety, and Probabilistic Safety Analysis (PSA).

Research projects of the programme are chosen on the basis of annual call for proposals. The annual volume of the SAFIR2010-programme in 2007–2008 has been 6,3–6,7 M€ and approximately 50 person years. Main funding organisations in 2007–2008 were State Waste Management Fund VYR with 2,7–3,0 M€ and VTT with 2,4–2,5 M€ annually. In 2008 research was carried out in 30 projects.

The research in the programme has been carried out primarily by VTT Technical Research Centre of Finland. Other research units responsible for the projects solely or in co-operation with other institutions include Lappeenranta University of Technology, Helsinki University of Technology, Tampere University of Technology, Fortum Nuclear Services Oy, Finnish Institute of Occupational

Health and Finnish Meteorological Institute. In addition, there have been a few minor subcontractors in some projects.

The programme management structure consists of the steering group, a reference group in each of the eight research areas and a number of ad hoc groups in the various research areas.

This report gives a summary of the technical results of the SAFIR2010 programme from the years 2007–2008.

Preface

SAFIR2010, The Finnish Research Programme on Nuclear Power Plant Safety 2007–2010 continues the tradition of Finnish national research programmes in nuclear energy. Organisation of public nuclear energy research in Finland as national research programmes was started in 1989 by the Ministry of Trade and Industry. Since then national programmes have been carried out first separately in the fields of operational aspects of safety and structural safety (YKÄ 1990–1994, RETU 1995–1998, RATU 1990–1994, RATU2 1995–1998), and then in combined programmes (FINNUS 1999–2002, SAFIR 2003–2006). Simultaneously research has been carried out in the national nuclear waste management programmes (JYT 1989–1993, JYT2 1994–1996, JYT2001 1997–2001, KYT 2002–2005, KYT2010 2006–2010).

SAFIR2010 research programme is divided in eight research areas that are Organisation and human, Automation and control room, Fuel and reactor physics, Thermal hydraulics, Severe accidents, Structural safety of reactor circuit, Construction safety, and Probabilistic Safety Analysis (PSA).

In the years 2007–2008 the research has been carried out primarily by VTT Technical Research Centre of Finland. Other research units responsible for the projects solely or in co-operation with other institutions include Lappeenranta University of Technology, Helsinki University of Technology, Tampere University of Technology, Fortum Nuclear Services Oy, Finnish Institute of Occupational Health and Finnish Meteorological Institute. In addition, there have been a few minor subcontractors in some projects.

The programme management structure consists of the steering group, a reference group in each of the eight research areas and a number of ad hoc groups in the various research areas. The steering group of SAFIR2010 consists currently of representatives from Radiation and Nuclear Safety Authority (STUK), Ministry of Employment and the Economy (MEE), VTT Technical

Research Centre of Finland (VTT), Teollisuuden Voima Oyj (TVO), Fortum Power and Heat Oyj, Fortum Nuclear Services Oy (Fortum), Finnish Funding Agency for Technology and Innovation (Tekes), Helsinki University of Technology (TKK) and Lappeenranta University of Technology (LUT). In addition to representatives of these organisations, the Steering Group has permanent experts from the Swedish Radiation Safety Authority (SSM) and Fennovoima Oy (Fennovoima).

Besides the research done within SAFIR2010 and education of experts via this research, SAFIR2010 is an important national network and forum of information exchange for all parties involved.

This report has been prepared by the programme management in cooperation with the project managers and project staff.

More information on SAFIR2010 is found in http://www.vtt.fi/safir2010.

Contents

Abstract 3

Preface 5

1. Introduction 10
   - 1.1 Role of SAFIR2010 in Finnish Nuclear Safety Research 10
   - 1.2 Research areas and projects 12
   - 1.3 Statistical information 17
   - 1.4 Administration 20
   - 1.5 Structure of the report 21
   - 1.6 Acknowledgements 21

2. Safety management and organisatorial learning (MANOR) 23
   - 2.1 MANOR summary report 23
   - 2.2 Safety culture and organizational learning 32

3. Expert work in safety critical environment (SAFEX) 42
   - 3.1 SAFEX summary report 42
   - 3.2 Knowledge sharing in interorganizational context 50

4. Model-based safety evaluation of automation systems (MODSAFE) 61
   - 4.1 MODSAFE summary report 61

5. Certification facilities for software (CERFAS) 71
   - 5.1 CERFAS summary report 71

6. Operator practices and human-system interfaces in computer-based control stations (OPRACTICE) 84
   - 6.1 OPRACTICE summary report: Designing large-screen overview displays for nuclear power plant control rooms 84

7. Development and validation of fuel performance codes (POKEVA) 99
   - 7.1 POKEVA summary report 99
   - 7.2 LOCA Test Simulation with FRAPTRAN-GENFLO (POKEVA) 112

8. Tridimensional core transient analysis methods (TRICOT) 120

8.1 TRICOT summary report 120
8.2 The porous medium model PORFLO for 3D two-phase flow and its application to BWR fuel bundle simulations 131

9. Total reactor physics analysis system (TOPAS) 142
9.1 TOPAS summary report 142
9.2 Development of the PSG2 / Serpent Monte Carlo Reactor Physics Burnup Calculation Code 151

10. Numerical modelling of condensation pool (NUMPOOL) 160
10.1 NUMPOOL summary report 160

11. Improved thermal hydraulic analyses of nuclear reactor and containment (THARE) 173
11.1 THARE summary report 173
11.2 APROS CCFL model validation 182

12. CFD modelling of NPP horizontal and vertical steam generators (SGEN) 191
12.1 SGEN summary report: CFD modeling of horizontal steam generators 191

13. Improvement of PACTEL facility simulation environment (PACSIM) 205
13.1 PACSIM summary report 205

14. Condensation experiments with PPOOLEX facility (CONDEX) 216
14.1 CONDEX summary report 216
14.2 PPOOLEX Wall Condensation Experiments 228

15. Large break loss of coolant accident test facility study (LABRE) and Large break loss of coolant accident test rig (LABRIG) 237
15.1 LABRE/LABRIG summary report 237

16. Participation in development of European calculation environment (ECE) 242
16.1 ECE summary report 242

17. The integration of thermal-hydraulics (CFD) and finite element (FEM) computer codes in liquid and solid mechanics (MULTIPHYSICS) 249
17.1 MULTIPHYSICS summary report 249

18. Release of radioactive materials from a degrading core (RADECO) 261
18.1 RADECO summary report 261

19. Primary circuit chemistry of fission products (CHEMPC) 276
19.1 CHEMPC summary report 276

20. Core melt stabilization (COMESTA) 287
20.1 COMESTA summary report 287
20.2 HECLA Experiments on Melt–Concrete Interactions 295

21. Hydrogen risk in containments and particle bed issues (HYRICI) 304
21.1 HYRICI summary report 304

21.2 STYX dry-out heat flux testing with lateral coolant inflow 315

22. Risk-informed inspections of piping (PURISTA) 326
22.1 PURISTA summary report 326

23. Fatigue endurance of critical equipment (FATE) 339
23.1 FATE summary report 339

24. Water chemistry and oxidation in the primary circuit (WATCHEM) 354
24.1 WATCHEM summary report: Development and verification of in situ techniques to study oxidation and water chemistry effects in the primary circuit 354

25. Monitoring of the structural integrity of reactor circuit (RAKEMON) 363
25.1 RAKEMON summary report 363
25.2 Ultrasonic inspection simulations with Civa version 8 371

26. Fracture assessment of reactor circuit (FRAS) 382
26.1 FRAS summary report 382
26.2 Simulation of thermal striping in a HDR experiment 395

27. Influence of material, environment and strain rate on environmentally assisted cracking of austenitic nuclear materials (DEFSPEED) 403
27.1 DEFSPEED summary report 403
27.2 Strain localisation in sensitised Type 304 stainless steel in simulated BWR-environment 418

28. Service life management system of concrete structures in nuclear power plants (SERVICEMAN) 430
28.1 SERVICEMAN summary report 430
28.2 Service Life Management System of Concrete Structures in Nuclear Power Plants 438

29. IMPACT2010 (IMPACT) and Structures under soft impact (SUSI) 446
29.1 IMPACT and SUSI summary report 446

30. Challenges in risk-informed safety management (CHARISMA) 474
30.1 CHARISMA summary report 474
30.2 Reliability analysis of digital I&C systems in nuclear power plants 485

31. Implementation of quantitative fire risk assessment in PSA (FIRAS) 495
31.1 FIRAS summary report 495
31.2 Estimation of pyrolysis model parameters for condenced phase materials 506

32. Extreme weather and nuclear power plants (EXWE) 518
32.1 EXWE summary report 518
32.2 Abrupt climate change and nuclear power plant safety 525

1. Introduction

1.1 Role of SAFIR2010 in Finnish Nuclear Safety Research

Eija Karita Puska
VTT

SAFIR2010 is the current Finnish National Research Programme on Reactor Safety for the period 2007–2010. It is strongly based on the chapter 7a, "Ensuring expertise", of the Finnish Nuclear Energy Act. The objective is "to ensure that, should such new factors concerning safe operation of nuclear facilities emerge that could not be foreseen, the authorities have such sufficient and comprehensive nuclear engineering expertise and other facilities at their disposal that can be used, when necessary, to analyse without delay the significance of such factors".

The objective of SAFIR2010 is realised in the research work carried out and in the training of experts in these research projects. High scientific quality is required from the research projects. Besides producing top level scientific results SAFIR2010 is also an increasingly important platform in education of experts. SAFIR2010 is also an important network in Finland both in domestic and in international matters.

The planning period for the national research on nuclear power plant safety up to 2010 contains granting licences and permits for the power plants in use and that under construction or the overall evaluation related to licence conditions: The operation permit of plant units Loviisa 1 and 2 were renewed in 2007 and the periodic safety review included in the operation permit conditions of the plant units Olkiluoto 1 and 2 will be implemented. Olkiluoto 3 unit currently under construction will also proceed to the operation permit phase. During the period from April 25, 2008 to February 5, 2009 Teollisuuden Voima Oyj, Fennovoima Oy and Fortum Oyj and Fortum Power and Heat Oy presented the Ministry of Employment and the Economy with applications for a decision-in-

principle, addressed to the Government, on constructing new nuclear power plant units. These processes are reflected in many ways in the national safety research.

Research on nuclear safety requires profound training and commitment. The research programme serves as an important environment providing long-term activity. During the period of SAFIR2010 and years thereafter the experts who have taken part in construction and use of the currently operating plants are retiring. The licensing processes and the possibility to recruit new persons in research projects give an opportunity to experts from different generations to work together and thus transfer the knowledge to the younger generation.

Globalisation and networking highlight the importance of national safety research. The national research programme is an important channel for information exchange, and provides a chance to direct limited national resources to the most useful international research programmes in a more focused manner.

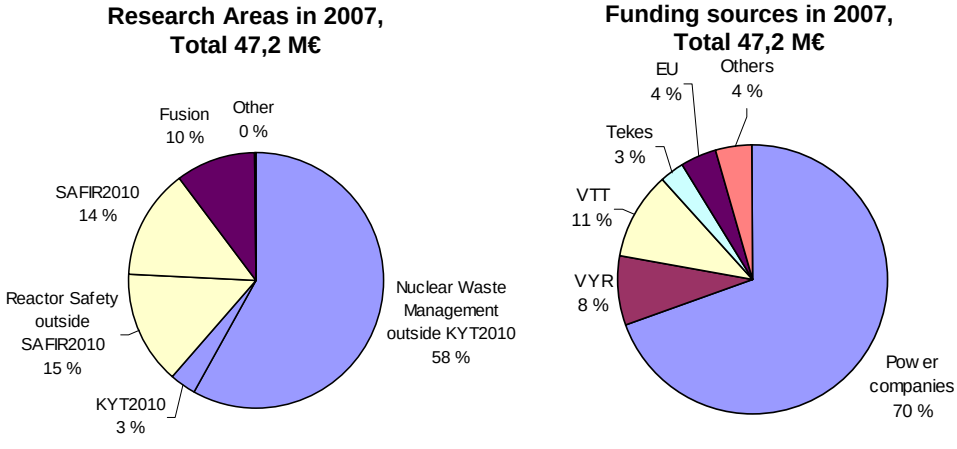

Figure 1.1.1. Nuclear energy research and funding sources in Finland in 2007.

Nuclear safety research in Finland consists of three components: regulatory research, utility research and public research. SAFIR2010 programme covers approximately half of the total reactor safety research volume in Finland currently. In 2007 the programme volume was € 6.5 million and 50 person years. The planned volume of the programme in 2008 is € 6.7 million. The major funding partners are VYR with € 2.95 million, VTT with € 2.48 million, Fortum with € 0.11 million, TVO with € 0.06 million, NKS with € 0.15 million, EU with only € 0.03 million and other partners with € 0.93 million. The final realised

figures for 2008 will be available in spring 2009. In 2009 and 2010 the annual volume is expected to remain at the same level.

Figure 1.1.2. Finnish organisations in the SAFIR2010 Steering Group in 2007–2008.

The steering group of SAFIR2010 consists of representatives from Radiation and Nuclear Safety Authority (STUK), Ministry of Employment and the Economy (MEE), VTT Technical Research Centre of Finland (VTT), Teollisuuden Voima Oyj (TVO), Fortum Power and Heat Oy, Fortum Nuclear Services Oy (Fortum), Tekes – the Finnish Funding Agency for Technology and Innovation (Tekes), Helsinki University of Technology (TKK) and Lappeenranta University of Technology (LUT). In addition to representatives of these organisations, the Steering Group has permanent experts from the Swedish Radiation Safety Authority (SSM) and Fennovoima Oy (Fennovoima).

1.2 Research areas and projects

Research in SAFIR2010 is conducted according to the Framework Plan [1], and decisions of the Steering and Reference Groups and additional quidance [2]. The research is to a large extent continuation of the research themes in the preceeding programme SAFIR [3, 4]. The research areas and research needs have been defined in the Framework plan. SAFIR2010 research programme is divided in eight research areas, which are:

1. Organisation and human factors
2. Automation and control room
3. Fuel and reactor physics
4. Thermal hydraulics
5. Severe accidents
6. Structural safety of reactor circuit
7. Construction safety
8. Probabilistic safety analysis (PSA).

These research areas include both research projects of the named topic and interdisciplinary co-operation projects. Each research area has a Reference Group that consists of experts from all organisations involved in the Steering Group. The Reference Groups have responsibility on scientific guidance and supervisory in their area.

In 2008 research was carried out in 30 projects. VTT was the responsible research organisation in 25 of these projects and VTT is also the coordination unit of the programme. In 2007 SAFIR2010 produced 149 Specified research results (Deliverables), 195 Publications, and 13 Academic degrees. Corresponding numbers for 2008 will be found in the Annual Report 2008 that will be published in April 2009. In Table 1.1.1 the summary of the volumes of the projects in 2007–2008 is given.

Table 1.1.1. SAFIR2010 projects in 2007 and 2008.

Research area	Project	Acronym	Organisation(s)	Funding k€ 2007	Funding k€ 2008**	Volume person months 2007	Volume person months 2008**
1.							
	Safety management and organisatorial learning	MANOR	VTT	183,625	215	12	14
	Expert work in safety critical environment	SAFEX	HUT, TLL	90,179	100,2996	11,6	10,6
2.							
	Model-based safety evaluation of automation systems	MODSAFE	VTT, HUT	185,57	190,6	15,5	15,3
	Certification facilities for software	CERFAS	VTT, TUT	110	110	12,6	11,9
	Operator practices and human-system interfaces in computer-based control stations	OPRACTICE	VTT	226,627	226	17	16,5
3.							
	Development and validation of fuel performance codes	POKEVA	VTT	341,449	322	34,1	27
	Tridimensional core transient analysis methods	TRICOT	VTT	305,198	330	23,1	25,5
	Total reactor physics analysis system	TOPAS	VTT	285,381	294	25,5	25
4.							
	Numerical modelling of condensation pool	NUMPOOL	VTT	98,823	100	7	7
	Improved thermal hydraulic analyses of nuclear reactor and containment	THARE	VTT	296,123	318	24,5	19

	CFD modelling of NPP horizontal and vertical steam generators	SGEN	VTT	-	127	-	9,5
	Improvement of PACTEL facility simulation environment	PACSIM	LUT	-	81	-	11
	The integration of thermal-hydraulics (CFD) and structural analyses (FEA) computer codes in liquid and solid mechanics	MULTIPHYSICS	Fortum, VTT	76	-	5,4	-
	Participation in development of European calculation environment	ECE	LUT	31	-	8	-
	Condensation experiments with PPOOLEX facility	CONDEX	LUT	254	290	26,3	22,5
	Large break loss of coolant accident test study	LABRE	LUT	36	-	5	-
	Large break loss of coolant accident test rig	LABRIG			30		3
5.							
	Release of radioactive materials from a degrading core	RADECO	VTT	85,24	85	5,7	5
	Primary circuit chemistry of fission products	CHEMPC	VTT	316,023	209	35,7	14,4
	Core melt stabilization	COMESTA	VTT	232,909	280	16,1	14,7
	Hydrogen risk in containments and particle bed issues	HYRICI	VTT	153,165	152,25	10,34	10,3
6.							
	Risk-Informed Inspections of Piping	PURISTA	VTT	218,152	218	16,4	13,7
	Fatigue endurance of critical equipment	FATE	VTT	117,29	114	7	6

	Water chemistry and oxidation in the primary circuit	WATCHEM	VTT, UTCM (Bulgaria), TUT	170,25	148	12	9,5
	Monitoring of the structural integrity of reactor circuit	RAKEMON	VTT	214,737	206	16	14
	Fracture assessment of reactor circuit	FRAS	VTT, TVO	365,029	422	30,5	26
	Influence of material, environment and strain rate on environmentally assisted cracking of austenitic nuclear materials	DEFSPEED	VTT	346,559	445	28,4	20,5
7.							
	Service life management system of concrete structures in nuclear power plants	SERVICEMAN	VTT, ÅF-Enprima	123,418	210	9	14,9
	IMPACT2010	IMPACT	VTT, IRSN & others	632,161	490	47,3	40
	Structures under soft impact	SUSI	VTT, TUT	163,657	190	12	13
8.							
	Challenges in risk-informed safety management	CHARISMA	VTT	254,161	331,8	20,3	23,1
	Implementation of quantitative fire risk assessment in PSA	FIRAS	VTT	164,585	165	12,6	9,8
	Extreme weather and nuclear power plants	EXWE	FMI	57	135,216	7,18	15,8
0.							
	Programme administration and information	SAHA2007 SAHA2008*	VTT	198,5	172,264	9,5	8,5
	Total			**6332,8111**	**6707,43**	**523,3**	**478,5**

* For periods 1.1.2007–31.3.2008 and 1.4.2008–31.3.2009 with VAT 22% included.
** From updated annual plan 2008. Confirmed realised figures in annual report 2008.

1.3 Statistical information

The annual volume of the SAFIR2010-programme in 2007–2008 has been 6,3–6,7 M€ and approximately 50 person years. Main funding organisations in 2007–2008 were State Waste Management Fund VYR with 2,7–3,0 M€ and VTT with 2,4–2,5 M€ annually. In 2008 research was carried out in 30 projects. The research in the programme has been carried out primarily by VTT Technical Research Centre of Finland. Other research units responsible for the projects solely or in co-operation with other institutions include Lappeenranta University of Technology, Helsinki University of Technology, Tampere University of Technology, Fortum Nuclear Services Oy, Finnish Institute of Occupational Health and Finnish Meteorological Institute. In addition, there have been a few minor subcontractors in some projects.

Distribution of total funding in the SAFIR2010 research areas in 2007–2008 is shown in Figure 1.1.3. The corresponding distribution of the VYR-funding to the various research areas is shown in Figure 1.1.4. Distribution of funding and person years in the eight research areas of SAFIR2010 in 2008 have been illustrated in Figures 1.1.5 and 1.1.6, respectively.

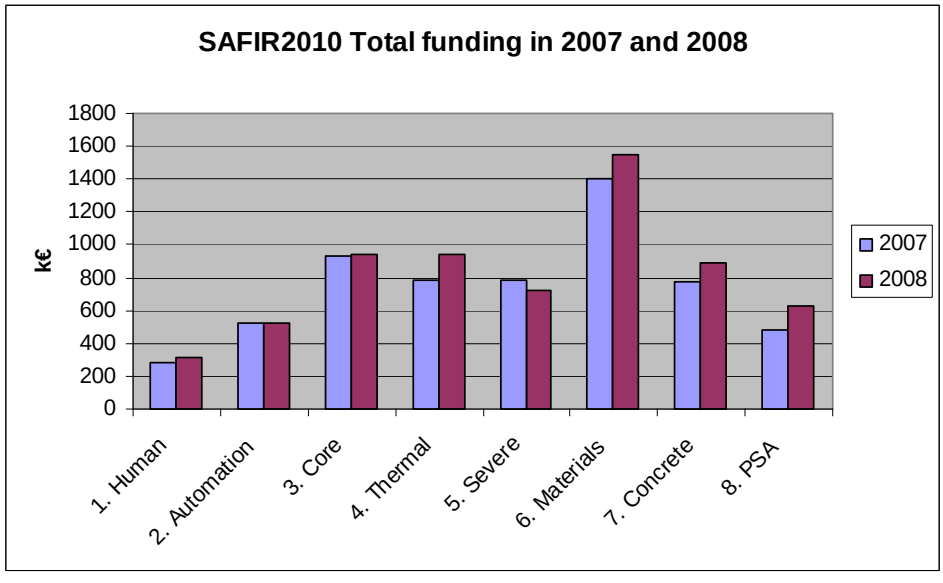

Figure 1.1.3. Distribution of total funding in the SAFIR2010 research areas in 2007–2008.

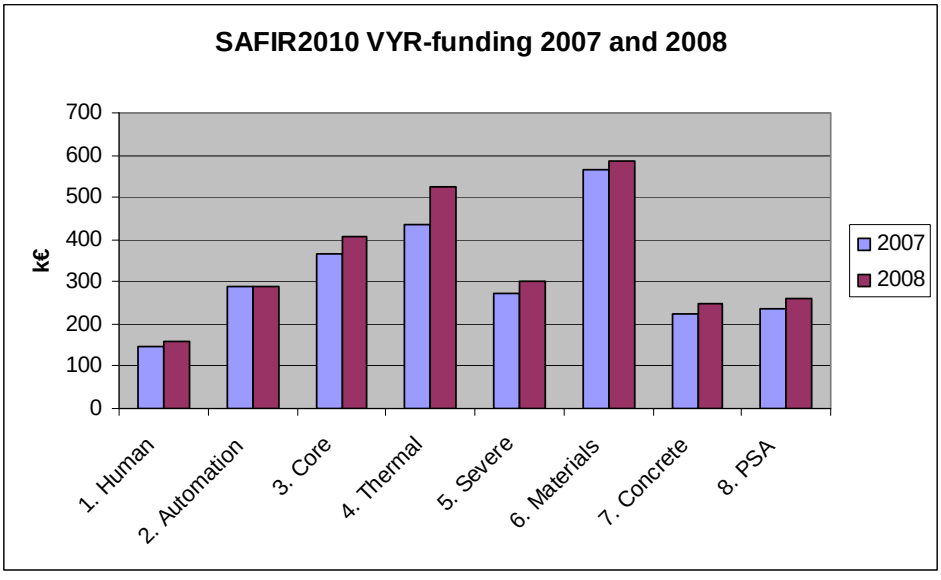

Figure 1.1.4. Distribution of VYR funding in the SAFIR2010 research areas in 2007–2008.

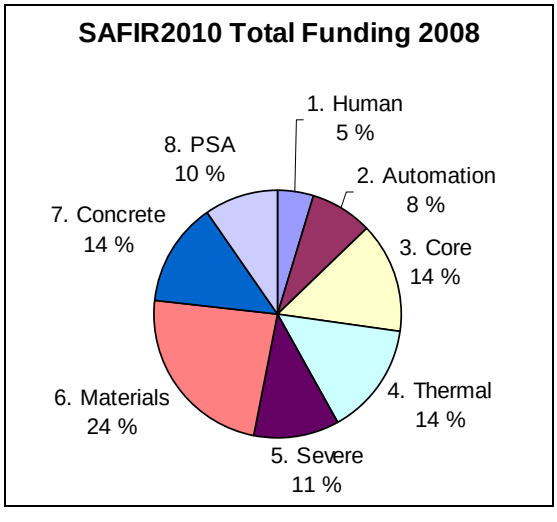

Figure 1.1.5. Distribution of funding in the SAFIR2010 research areas in 2008.

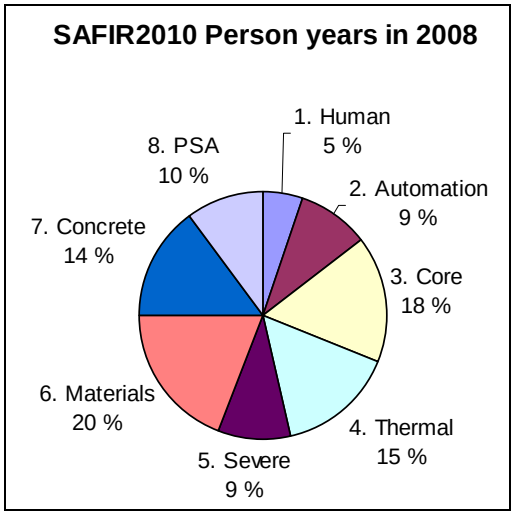

Figure 1.1.6. Distribution of person years in the SAFIR2010 research areas in 2008.

Figues 1.1.7 and 1.1.8 illustrate the funding sources and cost structure of SAFIR2010 in the year 2008.

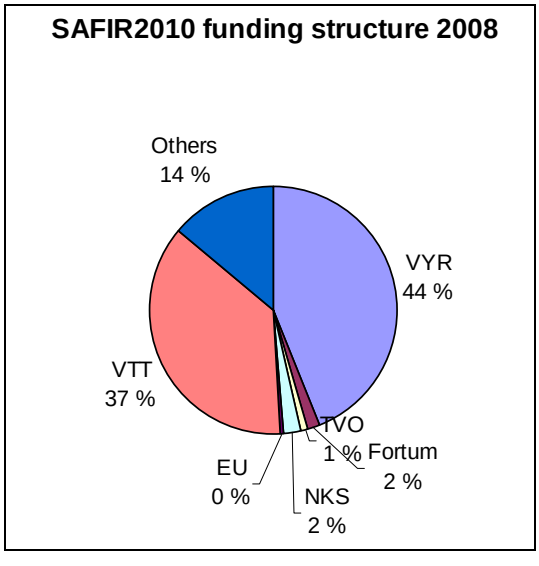

Figure 1.1.7. Funding sources in SAFIR2010 in 2008.

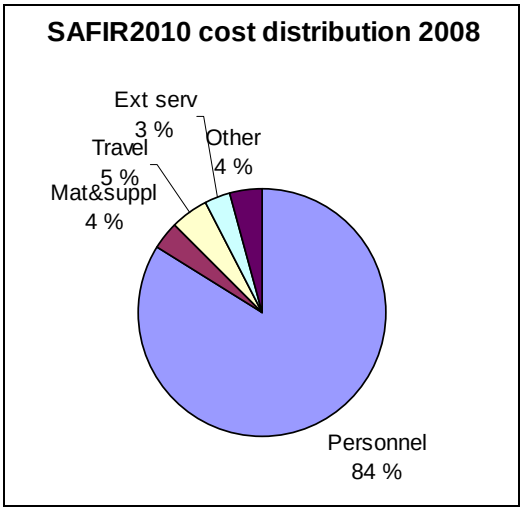

Figure 1.1.8. Cost structure in SAFIR2010 in 2008.

1.4 Administration

The programme management bodies, the Steering Group and the eight Reference Groups, have met on regular basis 4–5 times annually. The Ad Hoc groups that have a vital role for several projects have carried out successfully their tasks. The ad hoc groups have met upon the needs of the specific project. The programme is managed by the coordination unit VTT, the programme director, the project co-ordinator and the project managers of the individual research projects.

The information on the research performed in SAFIR2010 has been communicated formally via the quarterly progress reports, the annual plans and annual reports [5–7] of the programme and the www-pages of the programme. Additional information has been given in seminars organised by various research projects. The detailed scientific results have been published as articles in scientific journals, conference papers, and separate reports.

In addition to conducting the actual research according to the yearly plans, SAFIR2010 has been an efficient way of information exhange with all organisations operating in the nuclear energy sector and as an open discussion forum for participation in international projects, allocation of resources and in planning of new projects.

1.5 Structure of the report

The report contains presentation of the main scientific achievements of the projects in Chapters 2–32 both in the format of project overviews and special technical reports. For the statistical information on publications, academic degrees and project personnel as well as the list of the Steering Group, Reference Group and Ad Hoc Group members reference is made to the Annual Plans and Annual Reports (Annual Report 2008 to appear in April 2009) at the SAFIR2010 www-pages.

1.6 Acknowledgements

The results of the SAFIR2010 programme have been produced by all those involved in the actual research projects. Their work is highly esteemed.

The contributions of project managers and project staff that form the essential contents of this report are acknowledged with gratitude.

The work of the persons in the Steering Group, Reference Groups and Ad Hoc Groups that has been carried out with the expense of their home organisations is highly appreciated.

References

1. Järvinen, M.-L. et al. National Nuclear Power Plant Safety Research 2007–2010, Proposal for SAFIR2010 Framework Plan. Ministry of Trade and Industry, MTI Publications 32/2006. ISBN 952-489-037-2, ISSN 1459-9376. 87 p.

2. SAFIR2010 Toimintakäsikirja (*SAFIR2010 Operations manual, living document at the project www-pages, In Finnish*).

3. Räty, H., Puska, E.K. (Eds.). 2006. SAFIR.The Finnish Research Programme on Nuclear Power Plant Safety 2003–2006. Final Report. Espoo, VTT. 379 p. + app. 98 p. VTT Tiedotteita – Research Notes 2363. ISBN 951-38-6886-9; 951-38-6887-7. http://www.vtt.fi/inf/pdf/tiedotteet/2006/T2363.pdf.

4. Puska, E.K. (Ed.). 2006. SAFIR. The Finnish Research Programme on Nuclear Power Plant Safety 2003–2006. Executive Summary. Espoo, VTT. 36 p. + app. 33 p. VTT Tiedotteita – Research Notes 2364. ISBN 951-38-6888-5; 951-38-6889-3. http://www.vtt.fi/inf/pdf/tiedotteet/2006/T2364.pdf.

5. Puska, E.K. & Suolanen, V. SAFIR2010 Annual Plan 2007. VTT Research Report VTT-R-06442-07. 36 p + app. 177 p.

6. Puska, E.K. & Suolanen, V. SAFIR2010 Annual report 2007. VTT Research Report VTT-R-02381-08. 105 p + app. 188 p.

7. Puska, E.K. & Suolanen, V. SAFIR2010 Annual Plan 2008. VTT Research Report VTT-R-02382-08. 34 p + app. 166 p.

2. Safety management and organisatorial learning (MANOR)

2.1 MANOR summary report

Teemu Reiman
VTT

Introduction

Nuclear power plants are complex socio-technical systems. In addition to complexity of technology, overall system complexity arises from the organizing of work, standard operating procedures, decision-making routines and daily work practices. Work is specialised, meaning that tasks require special know-how which takes long to acquire. The chain of operations involves many different parties and technical fields. The daily work in is increasingly carried out through various technologies, information systems and electronic tools. This has led to decrease in craftwork where people were able to immediately see the results of their work.

In addition to inherent complexity, different kinds of internal and external changes bring new challenges for safety management. For example, organizations keep introducing new technology and upgrading or replacing old technology. Technological changes influence the social aspects of work, such as information flow, collaboration and power structures. Different kinds of business arrangements, such as mergers, outsourcing or privatisation, also have a heavy impact on social matters and culture. The exact nature of the impact is often difficult to anticipate and the safety consequences of organizational changes are challenging to manage [8]. Due to the complexities of the system the boundaries of safe activity

are becoming harder and harder to perceive. At the same time economic pressures and strive for efficiency push organizations to operate closer to the boundaries and shrink unnecessary slack. Over time, organizations can drift into failure [2].

In the recent years safety researchers have started to develop new approaches for analysing and supporting human and organizational reliability and the overall safety of the system. The current state-of-the-art safety science strives towards more realistic and comprehensive view on organizational activity. Humans are not only sources of failures, but also the creators of safety and reliability, as well as the guardians and last line of defence against the unruly technology. Sociotechnical systems have their own internal logics of functioning, which must be understood if safety is sought to be managed and a sound safety culture created. The understanding of the dynamics of the sociotechnical system is the key to understanding system safety.

Main objectives

The main objective of the research project is to study the facilitators and hindrances to organizational learning and development of safety culture in the nuclear power industry. The aim is to help the power companies and the regulator to create safety management practices that support the evaluation and management of the working practices and organizational performance based on a sound safety culture.

The specific goals of the MANOR 2007–2010 project are

- To further develop organizational psychological theory on safety critical organizations and promote Finnish competence in the area of human and organizational factors
- Support the development of safety management practices at the nuclear power plants in order to enhance their cability to
  - evaluate and direct their activities and processes
  - recognise weak signals and vulnerabilities
  - learn from incidents and near-misses
- Clarify the central characteristics and requirements of safety culture in the Nordic nuclear industry and inspect the possibilities of safety management practices in influencing safety culture
- Create a tool for evaluating safety culture and for selecting development methods that focus on human and organizational factors

Research strategy and specific activities

The MANOR project is carried out by conducting case studies and benchmarking in combination with theoretical work on safety management, organizational learning and safety culture.

- A longitudinal case study with OKG power plant is in progress concerning the effectiveness and justification of human factors initiatives.
- Case study on utilization of operating experience is being conducted with the Finnish power plants and STUK.
- A preliminary review of safety culture challenges in subcontracting at the nuclear industry has been made.
- In collaboration with the Nordic nuclear safety research (NKS) platform and Swedish researchers from KTH and RiskPilot, a study on the requirements and methods of organizational safety reviews at the Nordic NPPs has been conducted.
- In collaboration with the Nordic nuclear safety research (NKS) platform and Swedish researchers from KTH and RiskPilot, a study on safety culture evaluation and development has been started.
- Theoretical work on the clarification of the requirements of strong safety culture has been made, and a Finnish language publication on safety culture has been written [9].
- MANOR project has been active in the Nordic HUSC (Human Performance and Safety Culture) network, including a steering board membership and the planning of HUSC safety culture symposium held December 4th at Arlanda.
- One dissertation has been published in the field of psychology: Reiman, T. 2007. Assessing organizational culture in complex sociotechnical systems – Methodological evidence from studies in nuclear power plant maintenance organizations [6].

Effect of organization on human performance and safety

The organizational structures and processes, as well as the tools and technology, affect the way people work. The social context of work creates norms and

shapes perceptions of what is important and appropriate, and what is meaningless. Together these organizational structures, processes and norms (organizational culture) define what is considered normal work, how it should be carried out, what the potential warning signals are, and how to act in abnormal situations. Cultural norms define the correct ways to behave in risk situations and correct ways to talk about safety, risks or uncertainty. This influences the perception of risks and hazards, as well as the feeling of individual responsibility.

Weick has emphasized that "strong cultures can compromise safety if they provide strong social order that encourages the compounding of small failures" [13, p. 75; cf. 10]. He has further argued that "organizations are defined by what they ignore – ignorance that is embodied in assumptions – and by the extent to which people in them neglect the same kinds of considerations" [13, p. 74]. Thus, it is important to consider how the organizational culture affects human performance and perception of hazards and risk.

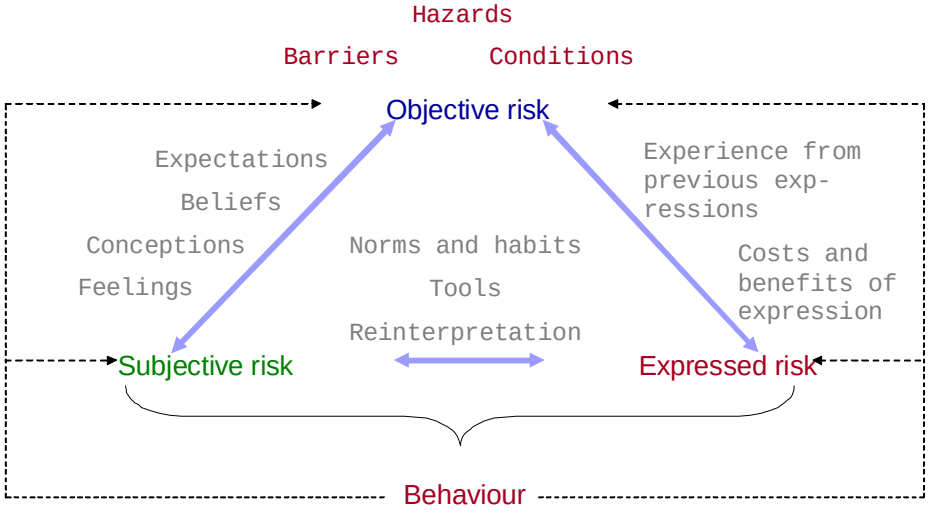

Figure 2.1.1. In order to understand human performance and safety it is important to separate the highly interactive concepts of objective, subjective and expressed risk.

Figure 2.1.1 illustrates the socially constructed nature of risk. The figure separates objective, subjective and expressed risk. Objective risk denotes the product of the probability and consequences of the hazard, taking into account the conditions and safety barriers which both reduce the probability and mitigate

the consequences. Subjective risk means the employee's perception of and understanding of the hazards and their significance in the given context. Risk perception is influenced by the employee's duties, as well as his or her department and work role [1, 3, 7]. Thus, people may observe risks in their organization in systematically different ways. Although employees may, generally speaking, understand that operations include risks, it may be difficult to see how one's own work or work group affects risks. Commitment to safety may be emotional, without fully understanding the practical requirements of ensuring safety in one's own tasks [7].

The expression of risk is influenced by the feedback from previous expressions of risks; whether or not colleagues and management has been receptive to them. The norms that create expectations on what people think others want to hear influence the risk expression in a form of self-censorship. For example, a worker who always points out risks and uncertainties may be labelled as a troublemaker or as "bird of ill omens". Another norm affecting risk expression in the other direction is the perceived need to upgrade expressed risk in order to get management attention. This in turn can lead to a cultural norm where the basic assumption is that people are always exaggerating the risks, and the feeling of subjective risk by whoever is listening is subsequently diminished. When the subjective risk and expressed risk are not in line, the phenomenon is called cognitive dissonance. Whichever is more plausible and fits better with one's self-image and the organizational culture – subjective risk or expressed risk – is taken as a foundation for reinterpreting the other [12].

Figure 2.1.1 implies that human factors efforts to improve system safety can target:

- the reduction of objective risk by contributing to the design of robust systems, applicaple safety barriers and reasonable work conditions
- the accurate subjective perception of risk
- the willingness of the employees to express their subjective feelings freely by creating an open and supportive climate
- the human performance in situations involving acceptable risk in order to guarantee that the risks do not actualise.

Organizations should determine the kinds of risks in which human activities must be restricted using technology or procedures and those that call for 'education', that is, ensuring that employees have a concrete understanding of the risk and

the uncertainties, as well as a clear picture of the connection between the hazards and their own work. Various human performance tools can also be applied to help in identification and handling of risks [cf. 7].

Challenges of applying human and organizational factors knowledge

Implementing the results of constantly evolving safety research into practice is a challenge for any safety critical organization. This is especially true with regard to knowledge concerning human and organizational behaviour. Current safety science does not separate human and technical aspects from each other as strictly as has been done in the traditional approaches. Organizations are sociotechnical systems which include technology, people, and the interaction of individuals with each other as well as with technology. Thus, understanding and managing organizational processes and practices has become one of the primary concerns of safety science.

The fundamental purpose of human and organizational factors work is to be able to anticipate and prevent small and large scale safety problems – technical or human – before there are any clear signs of problems. Demonstrating the benefits of “non-events”, showing what has been avoided or how the safety has improved as a result of human factors work is demanding.

Human performance enhancement tools, such as three way communication, pre and post job briefs and peer checking, can provide a good way of facilitating the human factors in nuclear power plant domain. However, the tools are only as good as their users, designers and implementers. The tools cannot compensate for a lack of understanding on technical issues or hazards, nor can they compensate for inadequate organizational processes or human resource management in terms of training and competence development. The tools that are taken into use should also be based on a sound theory of human behaviour. Many of human performance tools in the safety management field are often fashion-driven rather than theory driven [5].

Recent popularity of behaviour based safety (BBS) approaches including task observation and behaviour training stems from their simplicity, applicability and the scientific coating given to the “stick-and-carrot” principles. The aim of most behaviour modification programs is to identify behaviour which is not in accord with work procedures, and to bring it into compliance. Yet a culture of safety is more than a culture of compliance [4]. The safe behaviour programs run the risk of assuming that the unsafe acts of the shop-floor personnel are the causes of

accidents – both occupational as well as nuclear. BBS tools focus on readily observable behaviour that occurs frequently enough for counting. Thus, the tools neglect behaviour in abnormal situations [4] such as a failure repair conducted on critical machinery under pressure from management to get the plant operational. BBS tools ignore the important role of understanding in promoting safe behaviour.

The most important thing is that the tools should promote and increase understanding of the hazards and of the ways they are managed, and how one's own work influences them. Hopkins [4, p. 591] provides an example of the Longford gas plant explosion and answers the question of whether behavioural observation would have prevented the accident: "The explosion was triggered by actions of front line workers trying to re-start a pump. Neither they, nor their supervisors, nor even the plant manager realized that this behaviour was unsafe, and no behavioural observer would ever have picked it up." A wide understanding of the organizational culture, the nature of the hazards and theories of human performance and safety is needed in order to be able to utilise human performance tools in an effective manner.

Applications

People act according to their understanding of the world [11], including that of their work and its hazards as well as the control measures [5]. This understanding is influenced by organizational structures, processes and norms as well as the tools and technology used. In time the understanding that people have influences how the structures and processes are shaped, and how the norms develop. In terms of safety management, it is important to be aware of the organizational phenomena and their effect on human performance and safety. It is also important to try to influence understanding and safety culture at the organization. The first step in improving human performance is providing the personnel basic knowledge about human performance [5] and about the hazards and potential accident mechanisms of the nuclear power plant.

Use of task analysis tools to identify the typical bottlenecks, errors, conflicting goals, physical and cognitive loads, and decision making requirements is a good way to improve performance on certain safety critical tasks. It is important to involve the workers in the analysis and discuss the findings and possible countermeasures with them. Team discussions of key tasks are a good way to communicate results and get feedback.

Studies have shown that the most effective level of targeting development initiatives is the group or team level [5, 7]. The norms and social identity of the group are of crucial importance in facilitating safe and effective behaviour. This can be accomplished by e.g. group discussions on hazards and needed countermeasures, seminars and workshops, use of semi-autonomous work teams and involvement of the group in design and implementation of procedures and safety related activities.

The hazards that the nuclear power plant organization has to manage have to be made clear to the workers. Furthermore, the subjective and cultural tendencies to perceive risks need to be taken into account in safety management. It is important to acknowledge that it is the subjective perception of risk that guides behaviour, not the objective risk per se. The various uncertainties related to the nuclear power plant and the technology used should be discussed in the organization. It is important that the organizational culture does not develop a too strong belief in the possibility of being certain and able to anticipate everything. Further, the organizational and technical means of controlling risks should be considered in terms of their influence on employees' understanding of their work as well as their overall job motivation.

References

1. ACSNI. Organising for safety. Third report of the Human Factors Study Group of the Advisory Committee on Safety in the Nuclear Industry. Health & Safety Commission. London: HMSO, 1993.

2. Dekker, S.W.A. Ten questions about human error. A new view of human factors and system safety. New Jersey: Lawrence Erlbaum, 2005.

3. Flink, A.-L., Reiman, T. & Hiltunen, M. Heikoin lenkki? Riskienhallinnan inhimilliset tekijät. Helsinki: Edita, 2007.

4. Hopkins, A. What are we to make of safe behaviour programs? Safety Science, 2006. Vol. 44, pp. 583–597.

5. Reason, J. & Hobbs, A. Managing maintenance error. A practical guide. Hampshire: Ashgate, 2003.

6. Reiman, T. Assessing organizational culture in complex sociotechnical systems – Methodological evidence from studies in nuclear power plant maintenance organizations. VTT Publications 627. Espoo: VTT, 2007. http://www.vtt.fi/inf/pdf/publications/2007/P627.pdf.

7. Reiman, T. & Oedewald, P. Turvallisuuskriittiset organisaatiot – Onnettomuudet, kulttuuri ja johtaminen. Helsinki: Edita, 2008.

8. Reiman, T., Oedewald, P., Rollenhagen, C. & Kahlbom, U. Management of change in the nuclear industry. Evidence from maintenance reorganizations. MainCulture Final Report. NKS-119. Roskilde: Nordic nuclear safety research, 2006.

9. Reiman, T., Pietikäinen, E. & Oedewald, P. Turvallisuuskulttuuri. Teoria ja arviointi. VTT Publications 700. Espoo: VTT, 2008. http://www.vtt.fi/inf/pdf/publications/2008/P700.pdf.

10. Sagan, S.D. The limits of safety. Organizations, accidents, and nuclear weapons. New Jersey: Princeton University Press, 1993.

11. Sandberg, J. & Targama, A. Managing understanding in organizations. London: Sage, 2007.

12. Weick, K.E. Sensemaking in organizations. Thousand Oaks: Sage, 1995.

13. Weick, K.E. Foresights of failure: an appreciation of Barry Turner. Journal of Contingencies and Crisis Management, 1998. Vol. 6, pp. 72–75.

2.2 Safety culture and organizational learning

Teemu Reiman and Pia Oedewald
VTT

Abstract

System safety is an emergent property of the entire sociotechnical system. Safety management requires the management of the organization. For that an action-oriented model of organizational safety culture is needed. In this article safety culture is defined as the ability and willingness of the organization to understand safety, hazards and means of preventing them, as well as ability and willingness to act safely, prevent hazards from actualising and promote safety. A model of safety culture is presented. The main elements of an organizational safety culture are defined as organizational dimensions, psychological states and social processes. The influence of safety culture on organizational learning is illustrated. It is concluded that effective safety management requires utilizing and steering the organizational dimensions, controlling the social processes, and monitoring and influencing the psychological states of the personnel. The safety culture model can be used in evaluating the safety culture at various organizational levels from units and departments to network of organizations.

Introduction

Safety critical organization can be defined as “any organization that has to deal with or control such hazards that can cause significant harm to the environment, public or personnel” [13]. Control of risk and management of safety is one of their primary goals. Risk control in safety critical organizations and nuclear power plants in particular is largely based on quantitative safety analyses, standard operating procedures and defences-in-depth. The primary aim has been to constrain technical, human and organizational variability in performance. Organizational reliability and safety has been sought by the consistency and invariability of routines and activities.

Current safety science has moved beyond mechanistic and error-oriented approaches to system safety. At the same time the view and theories of the organization have become more nuanced and complex. This development has

led into questioning the deterministic models of system safety as well as models based on a mechanistic conception of organizational functioning [2, 6, 13]. Safety has become more qualitative and less quantitative. Safety is a dynamic non-event [18] and not a consistent and invariable outcome of formal organizational systems and technical barriers [2, 6, 13, 18].

The reality of organizational life is usually very different from that defined in the formal documents, systems and organizational structure. Workers need to adapt to local circumstances and sometimes contradictory goals, and work with the skills, resources, tools and time that they have. The bending of rules or "innovative" utilization of tools may indicate that there is a genuine need for change in the practices. In many cases the small, local adjustments of procedures are not negligence but usually done with good intentions (to get the job done, to save money). The work and the organizational processes can be such that employees have to bend the rules in order to get the work done.

The nature of accidents is also changing [2]. They are not anymore caused by single human errors but rather by normal people doing what they consider to be their normal work [cf. 5, 6]. Furthermore, reliance on technology creates new types of hazards. Dekker [2] argues that one of the problems faced by human factors research of today is that apparently safe systems can drift into failure [see also 9]. He further states that the tendency of psychology to attribute errors to irrationality or motivational factors of individuals (such as deliberately breaking rules) has led to neglect of organizational level issues such as cultural norms, organization processes and structure [2]. Instead, the suggested remedies are usually more training or injunctions to follow rules.

We have argued that safety is an emergent property of the entire sociotechnical system [13]. It is important to realise that safety is not a system; the organization is [13]. Safety management requires the management of the organization. This approach sets also the old and established concepts such as safety culture, operating experience, organizational learning and human error into a new perspective.

In this article we will present a model of the main elements of safety culture. Safety culture can be viewed as the prerequisite of a long term system safety. Thus, any safety critical organization should consider the areas covered with modern safety culture thinking in their safety management. We will also discuss the association between organizational learning and safety culture.

Organizational safety culture

The essence of safety culture is the ability and willingness of the organization to understand safety, hazards and means of preventing them, as well as ability and willingness to act safely, prevent hazards from actualising and promote safety. Safety culture refers to a dynamic and adaptive state. It can be viewed as a multilevel phenomenon of organizational dimensions, social processes and psychological states of the personnel [14].

Cultural approaches share an interest on meanings and beliefs which members of an organization assign to organizational elements (structures, systems and tools) and how these assigned meanings influence the ways in which the members behave themselves [1, 12, 15, 19]. However, technology and technological solutions form an important part of culture. The visible and structural properties of an organization, such as management systems, organizational structures and information systems, are part of the overall organizational culture. Cognitive skills, personal work orientation, communication skills and mental readiness to perform in abnormal conditions can be important to safety as well [10]. A mark of a good safety culture is the ability to take into account differences in motivation and skills of individual workers and balance these with demands of various tasks without compromising high safety levels or overall work climate.

We have outlined the main elements of an organizational safety culture as being organizational dimensions, psychological states and social processes [see also 14]. The dimensions are based on the model of the core elements of organizational culture created by Reiman and Oedewald [11, 12]. The revised model is called “OPS framework” (from Organizational, Psychological, and Social elements). Main difference to the old organizational culture framework [11] is that current model serves as a checklist for assessing the organizational capability for high level safety performance. The structure of the model is slightly different if the aim is to understand the dynamics of the entire organization or to evaluate the potential for safe work. The OPS model depicts the organizational structures and processes that can be clearly identified as influencing the personnel’s capability and willingness for risk-informed and safety conscious behaviour. These are for example; risk management practices, training, resourcing, change management and supervisory activity (see Figure 2.2.1). The previous model did not describe in detail which properties of the organizational structure and management system should be covered in the assessment. Also, personnel’s conceptions and experiences are now described as

"psychological properties". The psychological properties that illustrate high level safety culture in the organization are now identified, based on the research in different fields.

The OPS framework strives toward dynamic and change-oriented model providing an opportunity for both evaluation and development. The aim of the OPS evaluation framework is to provide an answer to the questions "what is happening in the organization", and "how to make something happen in the organization". Thus, the framework offers a more action-oriented model for both the evaluation and the development of safety culture.

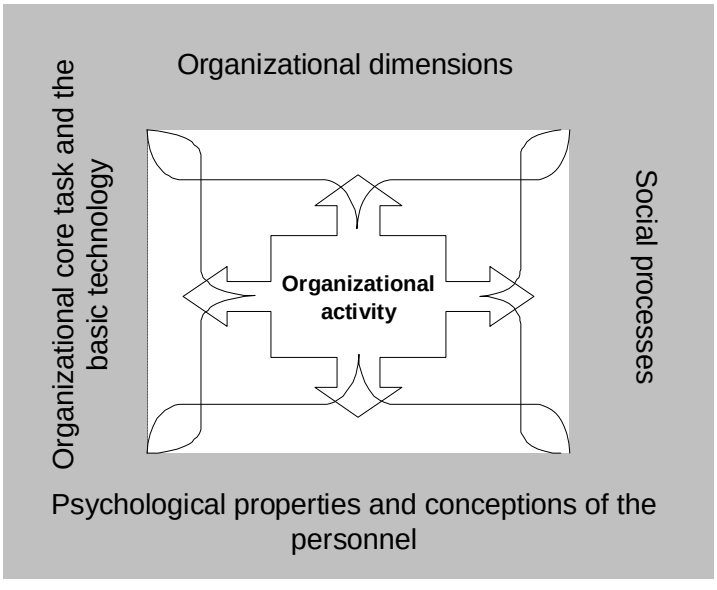

Figure 2.2.1. The "block model" of safety culture.

Figure 2.2.1 depicts the main elements of organizational safety culture. These elements together with the demands of the core task and the basic production technology define the frames of organizational activity by setting constraints and possibilities for action. Activity in turn influences the elements over time.

Organizational dimensions represent those key activities that the organization has to carry out in order to ensure safety. Psychological dimensions represent the "outcomes", which the organizational dimensions seek to create to the working community. Social processes represent the social phenomena affecting how organizational dimensions are interpreted, how events and incidents are perceived

and how practices and risk perceptions are socially negotiated in the organization. Social processes deal with intentional changes, unintentional variations, trade-offs, gradual local adjustments of work and reinterpretations of organizational activities and demands of work. Social processes can be seen as mechanisms that "quietly" lead the organization to some state of organizational and psychological dimensions.

Organizational dimensions as a way to manage safety

The organizational dimensions are analytical tools for considering those aspects of organizational activity that can be intentionally managed and influenced. Organizational safety management is carried out through these dimensions. It is important to note that organizational dimensions are tools, not ends as such. They are tools to monitor and control the technology and the social processes and influence the psychological states of the personnel.

The aim of safety management is to develop and sustain optimal motivational and knowledge structures in the organization i.e. the psychological states. Organizational dimensions are the layer on which development activities are carried out and which can be managed by interventions, technological innovations and change initiatives.

Figure 2.2.2. The specific contents of the organizational dimensions.

The psychological states of the personnel can be used as leading indicators of safety culture. In other words, they indicate the effectiveness of the organizational dimensions in managing safety and controlling the work in the social context. These psychological phenomena indicate how well the personnel are able and willing to take care of safety. Social processes mediate the effect of the organizational dimensions on the psychological states. In terms of safety management the influence of social processes is important to take into account and control as well as possible.

Understanding of social processes is needed in order to get an overview of the rationale for the current elements of safety culture. Social processes can explain why the organizational dimensions have formed the way they have, and why the dimensions are having a certain effect on the personnel. Thus, effective safety management requires *utilizing* and *steering* the organizational dimensions, *controlling* the social processes, and *monitoring* and *influencing* the psychological states of the personnel.

Examples of social processes

Social norms may affect workers' behaviour more than the formal rules and instructions. Norms of proper conduct are one key mechanism which integrates the group and creates a shared identity. Norms are informal rules about how to behave inside the group as well as toward outsiders. They affect what is considered acceptable communication, e.g. how much uncertainty one can express and whether or not it is acceptable to question your colleague or your boss.

Formation of social identity and norms means a process where a group defines who they are and what kind of behaviour is acceptable from their members. Social identity refers to a sense of belonging to a certain organization, profession or group in the organization and the differentiations made between the ingroup and other groups [4]. Humans have a basic need to belong to a group and to be social and accepted by the group of people to which one feels like belonging. Motive to conform and avoid embarrassment affects the behaviour of individuals in groups. Too strong a social identity can hinder learning from incidents that have happened elsewhere (at another plant or another work group in the same plant) in the form of "cannot happen here" -thinking.

Optimizing and local adaptation of practices refers to a process where the work practices are adapted to local goals and conditions. People constantly adjust their practices depending on perceived demands and resources, they

optimize by doing what they consider important, and by devising new ways of achieving same results. The demands placed by the goals of safety, efficiency and production are socially negotiated in work situations. Compromises have to be made, and goals have to be weighted and prioritised. If these compromises and situational adaptations work and have no visible side-effects, they become the new informal norm or practice. From the perspective of the sociotechnical system this can mean organizational drift. Snook [16, p. 194] writes: "Practical drift is the slow steady uncoupling of practice from written procedure ... After extended periods of time, locally practical actions within subgroups gradually drift away from originally established procedures ... Constant demands for local efficiency dictate the path of the drift."

Normalization of deviance means a process where small changes – new behaviours, technical anomalies, or variations that are slight deviations from the normal course of events – gradually become the norm, providing a basis for accepting additional deviance [17]. Normalization of deviance produces disregard and misinterpretation – neutralization – of potential danger signals. Normalization of deviance is reinforced by cultural beliefs and expectations, routines of daily work and by commitment to past decisions and past line of action. Normalization of deviance it thus closely connected to sensemaking as well as to social identity maintenance and formation of habits and routines.

Habit and routine formation means a social process where recurring tasks become routine, and certain habits and "ways of the house" start to develop. Habit and routine formation leads to diminished reflection of working practices and conceptions, but also to a higher sense of control and predictability of the environment.

Social processes affect organizational learning

One of the central social processes of safety culture is sensemaking. Sensemaking is a process of active agents together structuring the unknown so as to be able to act [19]. Reality is an ongoing accomplishment that emerges from efforts to create order and make retrospective sense of what occurs. Sensemaking refers to the process where the so called external reality is enacted by personnel, where people create the "reality" they later perceive and interpret. Decisions are often justified by emphasising some "facts" over others, by reconstructing the pre-decision making history. Sensemaking is driven by plausibility and coherence rather than accuracy. People do not make sense of

events only once, but rather engage in a continual revision of their understanding based on historical and social influence. [19]

Sensemaking influences learning from events. Studies show that the more serious the event is (to the individual or society), the more disagreeable is the idea of the accident being pure chance [13]. Chance implies that the same incident could target or could have targeted the person doing the evaluation of the incident. This is why people so readily stress the fact that an incident could have been prevented and the person involved must have caused it [3, 7]. Causal explanations of incidents and accidents have implications for organizational control [8, 17]. Locating the responsibility for incidents in individual decision makers allows quick (and "dirty") remedies such as firing, transferring or retraining the individuals [17, p. 392].

Such organizational learning that would increase the capability and willingness of the organization to manage safety is challenging. Too often organizations learn to repeat their mistakes and to better justify why they can not change practices. Organizations with a strong safety culture differ from other organizations in that they have adopted a philosophy of continuously reinterpreting the environment, possible problems and solutions. Even weak signals get a strong reaction. They strive for system reforms instead of local repairs when facing failures or errors [10]. They seek to identify the contributing factors to incidents and near-misses on an organizational level. Human errors are treated as consequences (of organizational failure) not causes of technical failure [cf. 5, 10].

We argue that OPS model can be useful in organizational learning initiatives. Organizations should ensure that they have adequate organizational conditions for safe work. The model of organizational dimensions provides an analytical tool to seek for areas for improvement in event investigations and organizational evaluations. The organization should learn about the aspects described in the OPS model; also about the adequacy of their current practices for organizational learning (Figure 2.2.2).

Conclusions

Manor-project has created a model of safety culture which corresponds to the latest development in the organization science and safety science fields. The OPS safety culture model can be used in evaluating the safety culture of a nuclear power plant, a single department or a networked activity in the field.

Furthermore, the model of the organizational dimensions can be used as a checklist in different development activities that aim to cover the human and organizational factors. For example, operating experience work should provide input for the organizational dimensions.

Further research is needed to develop valid methods for empirically measuring the various elements of the organizational safety culture. The dimensional structure of the social processes requires further research as well.

References

1. Czarniawska-Joerges, B. Exploring complex organizations. A cultural approach. Newbury Park, CA: Sage, 1992.

2. Dekker, S.W.A. Ten questions about human error. A new view of human factors and system safety. New Jersey: Lawrence Erlbaum, 2005.

3. Fiske, S.T. & Taylor, S.E. Social cognition. 2nd edition. McGraw-Hill, 1991.

4. Haslam, S.A. Psychology in organizations. The social identity approach. Second edition. London: Sage, 2004.

5. Hollnagel, E. Barriers and accident prevention. Aldershot: Ashgate, 2004.

6. Hollnagel, E., Woods, D.D. & Leveson, N. Resilience engineering. Concepts and precepts. Aldershot: Ashgate, 2006.

7. Oedewald, P. & Reiman, T. Special characteristics of safety critical organizations. Work psychological perspective. VTT Publications 633. Espoo: VTT, 2007. http://www.vtt.fi/inf/pdf/publications/2007/P633.pdf.

8. Perin, C. Shouldering risks. The culture of control in the nuclear power industry. New Jersey: Princeton University Press, 2005.

9. Rasmussen, J. Risk management in a dynamic society: A modelling problem. Safety Science, 1997. Vol. 27, pp. 183–213.

10. Reason, J. The human contribution. Unsafe acts, accidents and heroic recoveries. Farnham: Ashgate, 2008.

11. Reiman, T. Assessing organizational culture in complex sociotechnical systems – Methodological evidence from studies in nuclear power plant maintenance organizations. VTT Publications 627. Espoo: VTT, 2007. http://www.vtt.fi/inf/pdf/publications/2007/P627.pdf.

12. Reiman, T. & Oedewald, P. Assessment of Complex Sociotechnical Systems – Theoretical issues concerning the use of organizational culture and organizational core task concepts. Safety Science, 2007. Vol. 45, pp. 745–768.

13. Reiman, T. & Oedewald, P. Turvallisuuskriittiset organisaatiot – Onnettomuudet, kulttuuri ja johtaminen. Helsinki: Edita, 2008.

14. Reiman, T., Pietikäinen, E. & Oedewald, P. Turvallisuuskulttuuri. Teoria ja arviointi. VTT Publications 700. Espoo: VTT, 2008. http://www.vtt.fi/inf/pdf/publications/2007/P700.pdf.

15. Schultz, M. On studying organizational cultures. Diagnosis and understanding. Berlin: Walter de Gruyter, 1995.

16. Snook, S.A. Friendly fire. The accidental shootdown of U.S. Black Hawks over Northern Iraq. New Jersey: Princeton University Press, 2000.

17. Vaughan, D. The Challenger launch decision. Chicago: University of Chicago Press, 1996.

18. Weick, K.E. Organizational culture as a source of high reliability. California Management Review, 1987. Vol. 29, pp. 112–127.

19. Weick, K.E. Sensemaking in organizations. Thousand Oaks: Sage, 1995.

3. Expert work in safety critical environment (SAFEX)

3.1 SAFEX summary report

Krista Pahkin and Anneli Leppänen
Finnish Institute of Occupational Health

Eerikki Mäki, Tanja Kuronen-Mattila and Eila Järvenpää
Helsinki University of Technology

Abstract

Currently nuclear industry organizations worldwide are facing the challenge of preserving existing expertise, competence and knowledge in their organizations due to the expected large number of retiring employees. In order to be able to preserve this expertise in organisations as well as on a more general level in the national nuclear community, we need to increase and deepen our understanding of the work, work processes, competences and work environment of these experts.

The SafeExpertNet research project focuses on the work and work processes of nuclear experts and determines how organisations can support the maintenance and development of expertise. The study comprised two phases: 1) A qualitative cross-sectional case study was conducted in two nuclear industry organizations in 2007, 2) a questionnaire survey for experts from three nuclear industry organizations was conducted in 2008 (n = 170, response rate 59).

The results showed that the work practices of nuclear industry organizations face challenges in the creation and preservation of expertise. One of the challenges is competence development: how to carry out efficient induction for

new employees and ensure they receive enough meaningful and challenging projects, as this was regarded as the most effective way of learning. Collaboration between experts in the entire nuclear industry sector is also important for the creation and preservation of expertise. Many obstacles to interorganizational collaboration are already recognized, as are practices that support collaboration. Thus, managerial action can be taken to improve the utilization of the Finnish nuclear power network's knowledge resources.

Introduction

Efficient and effective management of knowledge is relevant to all industries where knowledge and expertise are the "raw material" of the business itself and its results, products or services. Managing knowledge involves tools and practices that are applied to accessing, preserving, generating, utilizing and transferring individual and collective knowledge [1]. Knowledge and expertise are not only the property and intellectual capital of individual persons, but also an important asset for the whole company. A company should thus actively preserve the knowledge and know-how of experts, otherwise it risks losing this resource when an expert leaves his/her job. Knowledge management is not an easy task; in order to be successful, one should not only know the content of different practices within the company, but also know what the content of the work is like at different organizational levels.

Currently nuclear industry organizations worldwide are facing the challenge of preserving expertise, competence, and knowledge as their workforce ages. The reduced number of recruits and students entering the industry may not be enough to provide the workforce needed. Many other industries share similar challenges, but the preservation of expertise in the nuclear industry is even more important due to the safety-critical nature of the work carried out in these organizations.

As a response to the risk of knowledge loss, nuclear organizations have engaged in knowledge-retaining efforts. New information and communication systems and organizational practices have been implemented to safeguard nuclear expertise. For example, the International Atomic Energy Agency (IAEA) has proposed nuclear organizations design and adopt people-centred programs that encompass themes such as workforce planning, recruitment, training, succession planning, leadership development and knowledge management [2]. In order to address the current risks to nuclear expertise, attention should be focused on

these different areas and the corresponding human resource (HR) functions within the organizations.

Although all kinds of organizations aim at preserving their knowledge resources and accumulated expertise from their operative history, knowledge renewal is also vital. Knowledge is not created or developed in a vacuum, but in interaction with other experts. Expertise is often based on the personal cognitive and technical skills and abilities of individuals. At the organizational level, the complementary expertise of individual experts needs to be identified and combined. Collaboration between different individuals and organizations integrates diversified and distributed expertise, which can lead to new technical knowledge and organizational competencies.

Organizations apply formal practices and processes in order to combine distributed knowledge and expertise. Individual experts may also apply informal practices to access the knowledge they need. For example, communities of practice [3] are used to develop member's capabilities and to exchange knowledge. Numerous studies show that (informal) social networks are crucial for locating and attaining knowledge [e.g. 4, 5]. Both formal and informal practices and processes can be used for accessing and sharing knowledge and expertise that cross functional, organizational, or even industrial boundaries. Formal and informal networks or collaboration opportunities are not separate from each other. Formal collaboration opportunities or other support provided by the management is a necessary precondition before one can establish informal communities of practice [3].

Main objectives

The SafeExpertNet project focuses on studying the work and work processes of nuclear experts and identifying how the organisation can support the maintenance and development of expertise.

The SafeExpertNet research project aims at providing new scientific knowledge and an improved understanding of expert work in nuclear power plants and the nuclear power sector. It also studies the work processes and identifies the knowledge and competences of these experts. The objective is to define and develop practices for preserving and developing expertise in nuclear power plants. These include practices such as recruiting and competence development.

Another goal is to gather new information about the nuclear expertise community, and the roles of its different parties (including nuclear power plants, regulators/authorities, research and educational organisations). The focus is on describing expertise in the nuclear power network and defining and developing knowledge-sharing and utilization of expertise in the entire nuclear power community.

Methods

The first task of the SafeExpertNet project was to examine the nature of expert work and the HRD functions that support the development and preservation of expertise in nuclear industry organizations. In this study we analysed the creation and preservation of expertise in nuclear industry organizations, and the role of HRD practices in improving it.

The study comprised two phases:

1) A qualitative cross-sectional case study was conducted in two different nuclear industry organizations in 2007. A total of 18 experts, 9 managers, and 2 HR professionals participated in thematic interviews about the nature of their expertise, its development, and the organizational support they receive for developing it. The experts work mainly in safety management tasks, such as reactor monitoring, risk calculation (PSA), structural design, material technology, and radiation safety.

2) In 2008, 170 experts from three nuclear industry organizations answered a questionnaire on the organizational practises at work in the improvement of expertise. The response rate was 59%. The questionnaire included 86 questions about such topics as the way work groups work, the actions of their closest superior and management, work goals, the safety-critical aspects of work, and the level of stress. The format for answering most of the individual items was a Likert-type scale.

Main results

Improvement of expertise in nuclear industry organizations

The interviews show that it takes approximately five years for a new recruit to become an expert. This poses the challenge of how to motivate recruits to work for several years in a complex technical field that takes time and is difficult to master.

According to the interviewees, there are numerous ways of gaining nuclear expertise. A newly recruited person can develop into an expert by e.g. reading and updating documents, engaging in discussions with experienced experts, taking part in meetings and work groups, networking with experts within and across organizations, educating oneself through training courses, and acting as a consultant. Working on a meaningful and challenging project, however, was regarded as the most effective way of learning.

The interviewees listed various HR practices they felt were relevant to developing expertise, but they also presented new ideas as to how HR practices can be developed in the future. They proposed that a detailed risk management plan for expertise and knowledge be carried out at the organizational unit level, and that more resources be acquired to safeguard expertise. Career planning should be more systematic and different career paths should be made more visible.

The results of the questionnaire survey showed that the development of individual expertise was related to the content of work (r = .627***), the actions of the closest superior (r = .619***), the functionality of the work group (r = .561***) and to the way a superior takes into account the safety-critical aspects of the work (r = .551***). Development of individual expertise was also related to the way the organization as a whole viewed safety culture (r = .515***).

The functionality of 12 different HR practices was also evaluated in the questionnaire. In general the respondents were most satisfied with the internal and external training, and the utilization of operation events as a learning opportunity. Job rotation (inside their area of expertise) and knowledge risk management were seen as the weakest areas.

Responses regarding the functionality of the organisation (the way work groups work, the actions of the closest superior and management, clear work goals etc.) and the well-being of employees (level of stress, work enjoyment etc.) were of the same level as in other expert organisations.

Knowledge sharing within the network of Finnish nuclear power experts

The second task of the SafeExpertNet project was to identify the national nuclear power expertise network and its participating parties. In this task, the sharing of knowledge and expertise and various forms of collaboration in the expert network, as well as the factors supporting or prohibiting it, were examined.

14 nuclear power experts from eight different organizations were interviewed in 2008. Interviews aimed to explore how knowledge sharing and collaboration takes place within the network of Finnish nuclear power experts. In addition to the interviews, the aforementioned questionnaire produced comments that indicated challenges and opportunities for interorganizational collaboration and knowledge sharing. Questionnaire respondents (n = 170, response rate 59%) produced 76 comments related to the factors that support interorganizational collaboration and 63 comments related to factors that inhibit interorganizational collaboration. Many of the comments were similar.

The results from the interviews show that the importance of knowledge sharing and networking within the Finnish nuclear power expert networks is predominantly recognized. The interviewees regularly emphasized the importance of building and nurturing connections between experts. Furthermore, many survey respondents expressed a need for increased interorganizational collaboration. The results also suggest that competition between organizations may constrict collaboration in some areas of expertise. Although Finnish nuclear power organizations may have some differing objectives, one shared goal was repeatedly mentioned: *"Our objective is to produce nuclear energy safely"*.

The interview results show that new recruits do not become members of the Finnish nuclear power network automatically, nor do they instantly become aware of how to find, share, and utilize knowledge and expertise in the network. Many interviewees reported that it takes time to grow and to become a member of an expert network. This is by no means an unexpected result. But still; are there methods to accelerate and support earlier integration into the expert networks?

In addition to the national nuclear expertise network, the importance of international contacts and collaboration was emphasized. The small size of the Finnish nuclear power network facilitates collaboration, while international contacts provide access to knowledge and expertise that does not exist in Finland.

Applications

The SafeExpertNet project is part of the *"Organisation and human factors"* research area of the SAFIR2010 programme.

The results of the project can be immediately used in the nuclear power community. The knowledge on nuclear experts' work, work processes and competences enables organisations and experts themselves to better understand

the work environment and respond to changes in it. The improved knowledge of HR practices further contributes to continuous improvement and a more holistic view of the work, knowledge and career of nuclear experts.

The modelling of the nuclear power community, its actors and their expertise builds a strong basis for collaboration, utilization of expertise and development of the knowledge that will be needed in the future.

Conclusions

The results revealed that nuclear industry organizations face great challenges in the creation and preservation of expertise. One of the challenges is how to carry out efficient induction for new employees and ensure that they are assigned with meaningful and challenging projects, as this was regarded as the most effective way to learn.

As a solution the experts suggested a detailed risk management plan for expertise and knowledge to be carried out at the organizational unit level, and that more resources be acquired to safeguard expertise. Career planning should be more systematic and different career paths should be made more visible.

The actions of the closest superior and the functionality of the work group were also strongly connected to the development of individual expertise, and for this reason, they should be considered important contributing factors. Supportive superior work, an open and incentive-building work group and meaningful work are very important for the well-being of not only individual employees, but also the whole work community, regardless of the area of expertise.

The results indicate that the development of the expert network requires managerial and organizational support. From the organizational perspective, expert networks and individual experts cannot reach their full potential without the active support of management. Organizations should provide opportunities to form networks and participate in network collaboration crossing organizational boundaries, remove both individual and organizational barriers limiting collaboration, and support the development of skills and capabilities in order to contribute and gain from network collaboration.

If nuclear power organizations acknowledge that the development of expertise can be supported by networking and interorganizational knowledge-sharing and learning, the results of the SafeExpertNet project can assist these efforts by offering some ideas for promoting collaboration. Many obstacles to interorganizational collaboration are already recognized, as are practices that

support collaboration. Thus, managerial action can be taken to improve the utilization of the Finnish nuclear power network's knowledge resources.

References

1. Mäki, E. Exploring and Exploiting Knowledge. Research on Knowledge Processes in Knowledge-Intensive Organizations. Doctoral Thesis. Espoo, Finland: Helsinki University of Technology, 2008.

2. IAEA. Risk Management of Knowledge Loss in Nuclear Industry Organizations. Vienna: IAEA, 2006.

3. Wenger, E. & Snyder, W. Communities of Practice: The Organizational Frontier. Harvard Business Review, January-February 2000.

4. Cross, R., Parker, A., Prusak, L. & Borgatti, S. Knowing What We Know: Supporting Knowledge Creation and Sharing in Social networks. Organizational Dynamics, 2001. Vol. 30, No. 2, pp. 100–120.

5. McKenzie, M.L. Managers Look to the Social Network to Seek Information. Information Research, 2005. Vol. 10, No. 2, paper 216. http://InformationR.net/ir/10-2/paper216.html.

3.2 Knowledge sharing in interorganizational context

Eerikki Mäki, Tanja Kuronen-Mattila and Eila Järvenpää
Helsinki University of Technology

Abstract

The study explored interorganizational collaboration and knowledge sharing between Finnish nuclear power experts. Data from 13 semi-structured interviews and 139 open ended comments from survey respondents were used to find out how motivation, culture, knowledge, and opportunities affect interorganizational collaboration and knowledge sharing. Both positively and negatively influencing factors on collaboration and knowledge sharing were found, positively influencing factors were dominant. The research offers a model that can be applied for assessing how collaboration and knowledge sharing among Finnish nuclear power experts can be supported and which factors should be considered when developing or evaluating collaboration and knowledge sharing practices.

Introduction

Three primary drivers motivate for interorganizational collaboration [1]. Interorganizational collaboration may reduce transaction costs, help at positioning in markets, and offer an opportunity to access new knowledge and capabilities. In the context of this study, the last driver is the most interesting. Through interorganizational collaboration organizations can evoke opportunities to combine diverse knowledge and expertise, and generate new knowledge [2]. However, diversity of people and knowledge of collaborating organizations can create divergent expectations towards collaboration, misunderstandings and uncertainty, and thus diversity must be seen as one critical factor causing interorganizational collaboration failures [3]. Therefore, operational, organizational, and cultural fit between collaborating organizations helps at achieving the objectives of the interorganizational collaboration [4].

Interorganizational learning may take place when knowledge is transferred from one organization to another, or when completely new knowledge is created in the collaborative interface. To make learning possible, collaborating organizations need to be receptive to knowledge and willing to share knowledge at the same

time [5]. In addition to the intended task-specific benefits, close collaboration may generate skills and know-how exploitable in future collaborative relationships [6, 7].

Knowledge exchange and combination of knowledge are the basic elements in creating new knowledge [8]. An organization's ability to exploit and utilize available knowledge resources is dependent on its individuals' capabilities [9] and organizational absorptive capability [10]. All kinds of collaborative relationships necessitate knowledge transfer across organizational boundaries. Knowledge can be transferred by personnel interaction (knowledge sharing), technology sharing, personnel transfer, and strategic integration [11]. Sometimes knowledge sharing is related to informal and knowledge transfer to formal procedures [12], but this paper does not make a difference between knowledge sharing and knowledge transfer.

Knowledge sharing

Knowledge sharing refers to "*the process by which knowledge held by an individual is converted into a form that can be understood, absorbed, and used by other individuals"* [13]. Communication and knowledge sharing between people has two aims [14]. First, *instrumental communication* aims at delivering messages that are needed to accomplish job-related tasks. The forms and media of instrumental communication are usually predefined. Second, *expressive communication* is employed by social reasons. Expressive communication is used for sharing different types of experiences, for nurturing friendship, for getting to know others, etc. Instrumental communication (or lack of it) has more or less obvious and salient (short-term) implications for work performance, while expressive communication and interaction helps organizations' members to become familiar with each other. Expressive communication helps to build trust [15] and social capital [8] between organizational members. Trust and social capital are supposed to have positive, long-term implications, e.g., an increased knowledge pool and improved knowledge availability.

Sharing of expert knowledge can be challenging because employees and groups might have dissimilar needs and motives for knowledge [9], and divergent skills and competences for processing knowledge [16, 9]. Four factors influence the success or failure of knowledge sharing between individuals within an organization [13]: the nature of knowledge, the motivation to share

knowledge, opportunities to do it, and the culture of the organization. This is depicted in Figure 3.2.1.

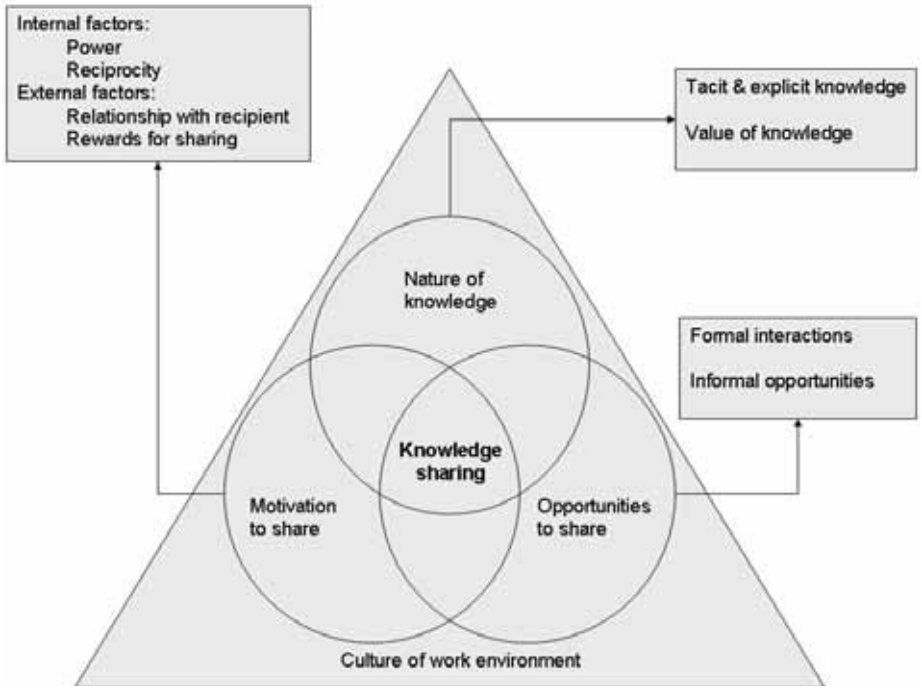

Figure 3.2.1. Factors influencing knowledge sharing (modified from [13]).

The model presented in Figure 3.2.1 suggests that all four factors must be simultaneously present or favorable to make knowledge sharing possible. First, there needs to be internal and external motivation to share knowledge. It is suggested that the quantity of knowledge sharing may perhaps be motivated and enhanced by external rewards but the quality cannot [17]. The motivation to share knowledge depends on a feeling of reciprocity: people are willing to share their knowledge if they get something back in return [18]. Internal motivation is particularly important when tacit knowledge needs to be shared [19].

Second, the nature of knowledge affects its transferability. Tacit and embedded knowledge can be challenging to share [20, 21, 22]. This is due to the difficulty of articulating such knowledge and the need for an interactive channel between the source and the receiver. In addition, this kind of knowledge is also difficult to receive because it requires a lot of prior understanding from the receiver [23, 24].

Third, knowledge sharing requires opportunities to do so. Interaction required for knowledge transfer between the members of an organization can vary from low to high [25]. Knowledge is shared in formal and in informal occasions. Knowledge sharing opportunities are lost if the source and the potential receiver do not have a connecting forum [26]. Opportunities to share knowledge can be supported by social capital [27, 8] or the opportunity for interaction can be provided by technological applications [25]. Social capital means [8] ‘‘*the sum of actual and potential resources embedded within, available through, and derived from the network of relationships possessed by an individual or a social unit.*” Additionally, the opportunity can be lost because the source is unaware of knowledge needs elsewhere in the organization [20].

Fourth, organizational culture(s) affects knowledge sharing through adopted norms, values, and practices [28]. Of the four factors depicted in Figure 3.2.1, the cultural dimension is the most ambiguous one. Cultural aspects affect an organization’s members’ motivation to share knowledge, opportunities to do so, and types of organizational knowledge.

The model presented in Figure 3.2.1 does not pay much attention to the receiver’s motivation or ability to receive knowledge. These are also important aspects because successful knowledge sharing is not dependent solely on the source but also on the receiver. Motivation to receive shared knowledge is affected by the perceived value of the knowledge [29] and the willingness to receive and adopt knowledge produced elsewhere [29, 26, 30]. Receiving and integrating knowledge from divergent professional groups is difficult because different groups do not necessarily have a shared understanding or ability to convey these messages [31]. Close and intensive interaction is likely to generate more homogenous than heterogeneous meanings because actors start to generate a similar knowledge basis. This, in turn, makes knowledge sharing and receiving easier [9, 32].

This paper explores the prospects of knowledge sharing and collaboration among Finnish nuclear power experts using the theoretical model presented in the Figure 3.2.1. Specifically, the research aims to find out how Finnish nuclear power experts from different organizations can collaborate and share knowledge.

Material and methods

Data

The results presented in this paper are based on two types of data. First, 13 interviews in seven different organizations in the nuclear power industry were conducted. These organizations were: FNS (Fortum Nuclear Services) (3 interviews), VTT (VTT Technical Research Centre of Finland) (4), LUT (Lappeenranta University of Technology) (1), Fennovoima (1), STUK (Radiation and Nuclear Safety Authority) (2), TVO (Teollisuuden Voima Oyj) (1) and TEM (Ministry of Employment and the Economy) (1). The interviewees can be considered as key informants on the matter in each organization. Thus, the interviewees were selected purposefully (purposive sample) in order to achieve as precise picture of the collaborative actions in the network as possible. Five of the interviews were conducted face to face and eight via telephone. Telephone interviews were possible, since the structure and questions of the interview were predefined. Interviews lasted from 30 to 60 minutes. Interviews aimed at finding out the collaboration partners of the interviewees, roles and responsibilities of collaborating organizations, methods and procedures of collaboration, possible obstacles of collaboration, and possible opportunities to improve collaboration.

Second, survey data from three different organizations (TVO, FNS and Fennovoima) was collected. For this paper, two open ended questions from the survey were analyzed. These questions were 1) What improves or advances the expert collaboration between organizations? and 2) What prevents or hinders the expert collaboration between organizations? Questionnaire respondents (N = 170, response rate 59%) produced 76 comments related to the factors that improves or advances the expert collaboration between organizations and 63 comments related to the factors prevents or hinders the expert collaboration between organizations. Many respondents produced similar comments.

Context of the research

The context of research is the national nuclear expertise network. The core of this network is embodied around the nuclear power companies (Fortum Loviisa power plant and TVO), regulatory bodies (STUK – Radiation and Nuclear Safety Authority and TEM – Finnish Ministry of Employment and the Economy) and VTT (VTT Technical Research Centre of Finland). VTT contributes to the expertise

of the network by producing research and developing expertise. Other members of this network include universities (Helsinki University of Technology and Lappeenranta University of Technology), Fortum Nuclear Services, Posiva (nuclear waste management company) and Fennovoima. Fennovoima is an energy company planning to start nuclear energy production in Finland in the future. In addition, there are several small companies in different areas of expertise that contribute to the expertise and knowledge of this network. The network and its members are also active internationally. International collaboration can be identified at least between power companies (especially with Swedish power companies) and regulatory bodies.

Qualitative content analysis was used for data analysis. Content analysis means that words, phrases, or concepts from the text data are extracted into meaningful categories [e.g., 33]. The data set was categorized using the model [13]. Data from the surveys and interviews were analyzed similarly.

Results

Based on the interviews the collaboration between network members was considered effective and fluent. The organizations have a common goal, safe energy production. This objective guides their operation and collaboration. Each member has its specific role and expertise area in the network. These roles are well known throughout the network. The formal collaboration is mostly defined by these official roles and tasks which are usually clearly defined. For example, supervision by the authorities determines much of the collaboration and communication between power companies and STUK. On the other hand, the communication between nuclear power producers was believed to be restricted due to their competitive position in the market. In addition to interorganizational collaboration, much collaboration takes place also between individual experts. From the individual experts' perspective the goal of collaboration and networking are more related to developing personal competences and expertise.

Opportunities to collaborate and share knowledge include formal and informal opportunities. Related to the formal opportunities the respondents emphasized that common seminars, common work projects, conferences, working in other work related professional organizations (e.g. Finnish nuclear society), formal training (e.g. nuclear safety courses), formal research and development programs (e.g. SAFIR2010, The Finnish Research Programme on Nuclear Power Plant Safety), and proactive and systematic planning and supporting of recruits

expertise development are good means to support collaboration and knowledge sharing among Finnish nuclear power experts. Informal opportunities and factors that support collaboration and knowledge sharing include small number of experts in Finland (which makes expertise easily recognizable and attainable), and low hierarchies. Factors that were found to influence negatively on collaboration and knowledge sharing opportunities include competition between different organizations, an insufficient planning of network collaboration, a need to reduce costs (e.g. collaboration and networking requires resources), and inability to find a partner (e.g. expert) with whom to collaborate.

Several factors increased *motivation to collaborate and share knowledge* in the interorganizational context. These include common objectives (e.g. safe nuclear power), good personal relationships between people in different organizations, a feeling of reciprocity in knowledge sharing, an ability to recognize how own knowledge and expertise can contribute the industry, openness and trust between people in Finnish nuclear power experts, and a sense of being a member of Finnish nuclear power expert community. On the other hand, there were also factors that decreased motivation to collaborate and share knowledge in the interorganizational context. These include shortage of time to collaborate and share knowledge, organizations' diverse objectives or expectations toward collaboration and knowledge sharing (e.g. different time horizons, or different expectations on how to benefit from collaboration), occasionally poor social relationships between the members of different organizations, and rewarding collaboration insufficiently.

Factors related to the *nature of knowledge* mainly supported collaboration. New knowledge and accumulation of expertise was highly appreciated among the respondents. Appreciation of knowledge did not make experts to bond emotional ownership on their knowledge. Consequently, possessing highly valued knowledge was not a reason to constrain or limit knowledge sharing.

Cultural factors that influenced collaboration and knowledge sharing were mainly positive. Collaboration and knowledge sharing were supported by common working history of nuclear power experts, importance of collaboration itself, tradition of collaboration, openness of information, and encouragement toward collaboration. The only negatively influencing cultural factor according to the respondents was dissimilar working practices in different organizations.

Conclusions

This study aimed to identify how collaboration and knowledge sharing opportunities occur in the community of Finnish nuclear power experts. The study discovered both positively and negatively influencing factors. At the time of the study, the positively influencing factors outnumbered the negative ones. This helps at further development of collaboration.

The four factors influencing on collaboration and knowledge sharing (opportunities, motivation, nature of knowledge and culture) are highly interdependent. For example, the nature of knowledge influences the opportunities to share knowledge, and the motivation to share knowledge influences the culture of collaboration and knowledge sharing in general. Opportunities for informal interaction support expressive communication, which leads to improved availability of expert knowledge in the network [15, 8, 20]. Therefore, organizations should provide opportunities of informal interaction. Formal and informal knowledge sharing opportunities also increase motivation to share knowledge [18].

The small number of interviews may limit the generalization of the results. The interviewed people had rather long working history, or central position in the network. It is possible that their views on network collaboration may be more positive than the views of younger experts. The research offers a model that can be applied for assessing how collaboration and knowledge sharing among Finnish nuclear power experts can be supported and which factors should be considered when collaboration and knowledge sharing practices are developed or evaluated.

References

1. Kogut, B. Joint Ventures: Theoretical and Empirical Perspectives. Strategic Management Journal, 1988. Vol. 9, No. 4, pp. 319–332.

2. Paija, L. Yritysverkostot: Miksi, miten – ja miksi ei? In: Ollus, M., Ranta, J. & Ylä-Anttila, P. (Eds.). Yritysverkostot – kilpailua tiedolla, nopeudella ja joustavuudella. Helsinki: Sitra, 1999.

3. Blomqvist, K. Partnering in the dynamic environment: The role of trust in asymmetric technology partnership formation. Doctoral Thesis. Lappeenranta: Lappeenranta University of Technology, 2002.

4. Kanter, R. Collaborative Advantage: The Art of Alliance. Harvard Business Review, 1994. Vol. 72, No. 4, pp. 96–108.

5. Larsson, R., Bengtsson, L., Henriksson, K. & Sparks, J. The Interorganizational Learning Dilemma: Collective Knowledge Development in Strategic Alliances. Organization Science, 1998. Vol. 9, No. 3, pp. 285–305.

6. Simonin, B. The importance of collaborative know-how: An empirical test of the learning organization. Academy of Management Journal, 1997. Vol. 40, No. 5, pp. 1150–1174.

7. Inkpen, A. Creating Knowledge Through Collaboration. California Management Review, 1998. Vol. 39, No. 1, pp. 123–140.

8. Nahapiet, J. & Ghoshal, S. Social Capital, Intellectual Capital, and the Organizational Advantage. Academy of Management Review, 1998. Vol. 23, No. 2, pp. 242–266.

9. Markus, M. Toward a Theory of Knowledge Reuse: Types of Knowledge Reuse Situations and Factors in Reuse Success. Journal of Management Information Systems, 2001. Vol. 18, No. 1, pp. 57–91.

10. Cohen, W. & Levinthal, D. Absorptive Capacity: A New Perspective on Learning And Innovation. Administrative Science Quarterly, 1990. Vol. 35, No. 1, pp. 128–152.

11. Inkpen, A. & Dinur, A. Knowledge Management Processes and International Joint Ventures. Organization Science, 1998. Vol. 9, No. 4, pp. 454–468.

12. Oshri, I., Pan, S. & Newell, S. Trade-Offs Between Knowledge Exploitation and Exploration Activities. Knowledge Management Research & Practice, 2005. Vol. 3, No. 1, pp. 10–23.

13. Ipe, M. Knowledge Sharing on Organizations: A Conceptual Framework. Human Resource Development Review, 2003. Vol. 2, No. 4, pp. 337–359.

14. Thomas, J., Kellogg, W. & Erickson, T. The Knowledge Management Puzzle: Human and Social Factors in Knowledge Management. IBM Systems Journal, 2001. Vol. 40, No. 4, pp. 863–884.

15. Jones, G. & George, J. The Experience and Evolution of Trust: Implications for Cooperation and Teamwork. Academy of Management, 1998. Vol. 23, No. 3, pp. 531–546.

16. Weiss, L. Collection and Connection: The Anatomy of Knowledge Sharing in Professional Service Firms. Organization Development Journal, 1999. Vol. 17, No. 4, pp. 61–77.

17. Hendriks, P. Why Share Knowledge? The Influence of ICT on the Motivation for Knowledge Sharing. Knowledge and Process Management, 1999. Vol. 6, No. 2, pp. 91–100.

18. Watson, S. & Hewett, K. A Multi-Theoretical Model of Knowledge Transfer in Organizations: Determinants of Knowledge Contribution and Knowledge Reuse. Journal of Management Studies, 2006. Vol. 43, No. 2, pp. 141–173.

19. Osterloh, M. & Frey, B. Motivation, Knowledge Transfer, and Organizational Forms. Organization Science, 2000. Vol. 11, No. 5, pp. 538–550.

20. Haldin-Herrgard, T. Difficulties in Diffusion of Tacit Knowledge in Organizations. Journal of Intellectual Capital, 2000. Vol. 4, No. 1, pp. 357–365.

21. Goh, S. Managing Effective Knowledge Transfer: An Integrative Framework and Some Practice Implications. Journal of Knowledge Management, 2002. Vol. 6, No. 1, pp. 23–30.

22. Cummings, J. & Teng, B.-S. Transferring R&D Knowledge: The Key Factors Affecting Knowledge Transfer Success. Journal of Engineering and Technology Management, 2003. Vol. 20, pp. 39–68.

23. Szulanski, G. Exploring Internal Stickiness: Impediments to the Transfer of Best Practice within the Firm. Strategic Management Journal, 1996. Vol. 17, pp. 27–244.

24. Hansen, M. The Search-Transfer Problem: The Role of Weak Ties in Sharing Knowledge Across Organizational Subunits. Administrative Science Quarterly, 1999. Vol. 44, No. 1, pp. 82–111.

25. Gammelgaard, J. & Ritter, T. The Knowledge Retrieval Matrix: Codification and Personification as Separate Strategies. Journal of Knowledge Management, 2005. Vol. 9, No. 4, pp. 133–143.

26. Hansen, M. & Nohria, N. How to build collaborative advantage. MIT Sloan Management Review, 2004. Fall, pp. 22–30.

27. Cross, R., Parker, A., Prusak, L. & Borgatti, S. Knowing what we know: Supporting knowledge creation and sharing in social networks. Organizational Dynamics, 2001. Vol. 30, No. 2, pp. 100–120.

28. De Long, D. & Fahey, L. Diagnosing Cultural Barriers to Knowledge Management. Academy of Management Executive, 2000. Vol. 14, No. 4, pp. 113–127.

29. Gupta, A. & Govindarajan, V. Knowledge Flows within Multinational Corporations. Strategic Management Journal, 2000. Vol. 21, No. 4, pp. 473–496.

30. Huysman, M. & de Wit, D. Practices of Managing Knowledge Sharing: Towards a Second Wave of Knowledge Management. Knowledge and process management, 2004. Vol. 11, No. 2, pp. 81–92.

31. Hoopes, D. & Postre, S. Shared Knowledge, “Glitches”, and Product Development Performance. Strategic Management Journal, 1999. Vol. 20, No. 9, pp. 837–865.

32. Postrel, S. Islands of Shared Knowledge: Specialization and Mutual Understanding in Problem Solving Teams. Organization Science, 2002. Vol. 13, No. 3, pp. 303–320.

33. Silverman, D. Interpreting qualitative data: methods for analysing talk, text and interaction. London: Sage, 1993.

4. Model-based safety evaluation of automation systems (MODSAFE)

4.1 MODSAFE summary report

Kim Björkman[1], Juho Frits[2], Keijo Heljanko[2],
Ilkka Niemelä[2] and Janne Valkonen[1]

[1] VTT
[2] Helsinki University of Technology (TKK)

Abstract

The objective of the MODSAFE project is to evaluate and develop methods based on formal model checking and apply them in the safety analysis of NPP safety automation. In the first project year a review of formal methods and models for safety evaluation of industrial and nuclear safety systems was made, basic methodology for applying model checking to safety evaluation was developed, and the feasibility of the approach was studied using two case examples. This work was based on using techniques developed for hardware model checking and the case studies employed the NuSMV model checking tool. In the second project year methodology for using timed automata as a basis for model checking safety systems was developed and a more elaborate case study involving also failure models was completed. The results show that by using current model checking techniques it is possible to verify whether a design model of a moderate size safety system satisfies its key safety requirements or not, even when system failures must be taken into account.

Introduction

Modern digitalized I&C systems are employed in critical applications creating new challenges for safety evaluation. However, such validation work still relies heavily on subjective evaluation which covers only a limited part of the possible behaviours and therefore more rigorous formal methods are needed. Model checking [7] is a promising formal method that can be used for verifying the correctness of system designs. It has not previously been applied in the safety evaluation of nuclear power plant (NPP) automation systems (at least in Finland) but internationally it has been used in verifying the correct behaviour of, e.g., hardware and microprocessor designs, data communications protocols and operating system device drivers.

A number of efficient model checking systems are available offering analysis tools that are able to determine automatically whether a given state machine model satisfies desired safety properties. Model checking can also handle delays and other time-related operations, which are crucial in safety I&C systems and are challenging to design and verify.

Main Objective

The objective of the MODSAFE project is to evaluate and develop methods based on formal model checking and apply them in the safety analysis of NPP safety automation (I&C). The purpose is to get a group of methods and tools that can support the practical safety evaluation work and benefit utilities, regulator, and vendors.

The goals of the project for the first two years include reviewing the state of the art in employing formal methods and models for safety evaluation of industrial and nuclear safety systems, developing basic methodology for applying model checking to safety evaluation, and studying the feasibility of the approach. The project focuses on a number of case studies which direct the development of the required methodology and serve as benchmarks for evaluating the feasibility and applicability of the approach.

The rest of the report is structured as follows. First, some background information on model checking is given. Then further details are given on the main results: the state of the art review and the analysis of three case studies.

Model Checking

Model checking [7] is a computer aided verification method developed to formally verify the correct functioning of a system design model by examining all of its possible behaviours. The models used in model checking are quite similar to those used in simulation as basically the model must describe the behaviour of the system design for all sequences of inputs. However, unlike simulation, model checkers examine the behaviour of the system design with all input sequences and compare it to the specification of the system. In model checking, at least in principle, the analysis can be made fully automatic with computer aided tools. The specification is expressed in a suitable specification language, temporal logics being a prime example, describing the allowed behaviours of a system. Given a model and a specification as input, a model checking algorithm decides whether the system violates its specification or not. If none of the behaviours of the system violate the given specification, the (model of the) system is correct. Otherwise the model checker will automatically give a counterexample execution of the system demonstrating why the property is violated. The MODSAFE project has used two model checkers, NuSMV originally designed for hardware model checking and Uppaal supporting model checking timed automata. These tools are introduced below.

Symbolic Model Checking

NuSMV [6, 11] is a state-of-the-art symbolic model checker that supports synchronous state machine models where the real-time behaviour has to be modelled with discrete time steps using explicit counter variables that are incremented at a common clock frequency. NuSMV supports model checking using both the Linear Temporal Logic (LTL) and Computation Tree Logic (CTL) [7] making it quite flexible in expressing design specifications. The model checking algorithms employed in this work are based on symbolically representing and exploring the state space of the system by using Binary Decision Diagrams (BDDs) [5]. In addition, SAT (propositional satisfiability) based bounded model checking is also supported by NuSMV [3] for finding bugs in larger designs. The sophisticated model checking techniques used by NuSMV can handle non-determinism induced by free input variables well but modelling the real-time aspects can be more challenging due to the inherently discrete time nature of the synchronous state machine model employed by NuSMV.

Timed Automata Model Checking

Uppaal [12] is a model checking tool for timed systems based on modelling the system as a network of timed automata that communicate through message channels and shared variables. The timed automata have a finite control structure and real-valued clocks [1] making the modelling of timers of a system design fairly straightforward. Networks of timed automata can express the real-time behaviour of the system in continuous time and still be automatically analyzed. This is feasible because all the possible behaviours of the system can be captured using a finite graph where different clock valuations with, intuitively, the same behaviour are grouped into a finite number of equivalence classes called regions [1]. The model checking algorithms use symbolic methods to compactly represent the clock valuations associated with each state of the system in quite a memory efficient manner. The model checking algorithms employed inside Uppaal [2, 10] are able to check a subset of the temporal logic TCTL (Timed Computation Tree Logic) [2] by explicit state model checking that explicitly traverses the finite graph induced by the behaviour of the system. The main strength of Uppaal is in analyzing complex timing behaviour of a system. However, it is not too well suited with systems with a very high amount of non-determinism as induced by, e.g., reading a large number of input variables (sensor readings) provided by the environment because each combination of inputs is explicitly explored by the employed model checking algorithms.

Main results

NPP Safety Automation Systems Analysis – State of the Art

A review of the formal methods and models applied in safety evaluation of industrial and nuclear safety systems was made in the beginning of the project (see [14]). The reviewed methods were evaluated with respect to their applicability in the analysis of NPP safety automation systems. An important topic was also the compatibility of the methods with the practices and models used in different phases of NPP safety automation design. Furthermore, the role of model checking in the NPP automation safety case was discussed.

Case Emergency Cooling System

The project has utilised several example systems (case studies) to try model checking in different environments and see how the method suits for solving various types of verification problems. One of the cases was the emergency cooling system of a nuclear power plant. The purpose of the system is to take care of the reactor core's cooling if normal cooling systems are unavailable (see Figure 4.1.1). A finite state model of the system was created for testing the suitability of model checking to verify safety properties. The objective was to verify the correctness of the system's logical functions and test different approaches to modelling.

Several properties of the system were verified with model checking and no erroneous behaviour between the system model and its specification was found (as was anticipated). However, the purpose of the case study was to try model checking method and see how it could be used in future cases. The potential and power of the method were clearly demonstrated and the case gave a good basis for further work.

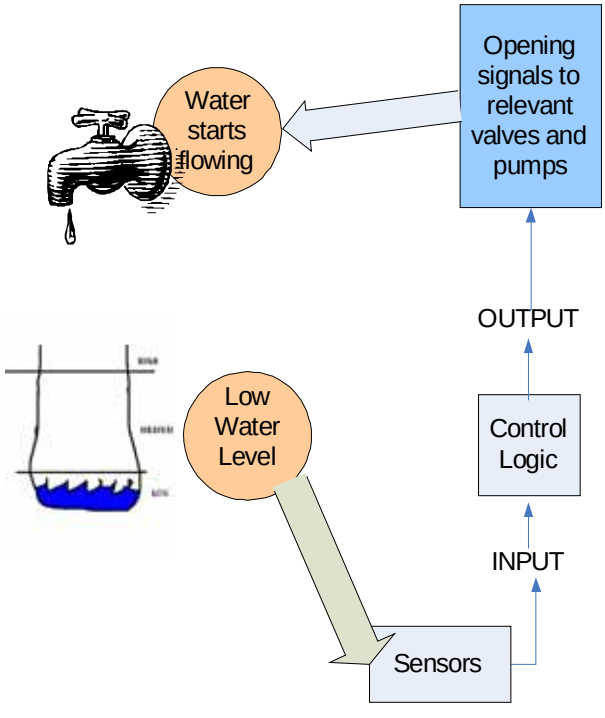

Figure 4.1.1. Emergency cooling system's functional principle [15].

Case Arc Protection System

Another case study concerned a real electric arc protection system that can be used to protect switchgear and electrical instrumentation. The system consists of a master unit, over current sensor units, and light sensor units. Sensors are installed into the protected system and connected to the master unit via optical cables. The master unit collects the alarm signals from sensors, and when necessary, launches circuit breakers that close the power feed from the protected device leading to termination of the electric arc. The master unit is based on a Programmable Logic Controller (PLC) so that the tripping logic can be freely designed for the protected system. This gives the possibility for selective tripping meaning that the protected system can be divided into several protection zones with different tripping conditions. The switching diagram of the system is in Figure 4.1.2.

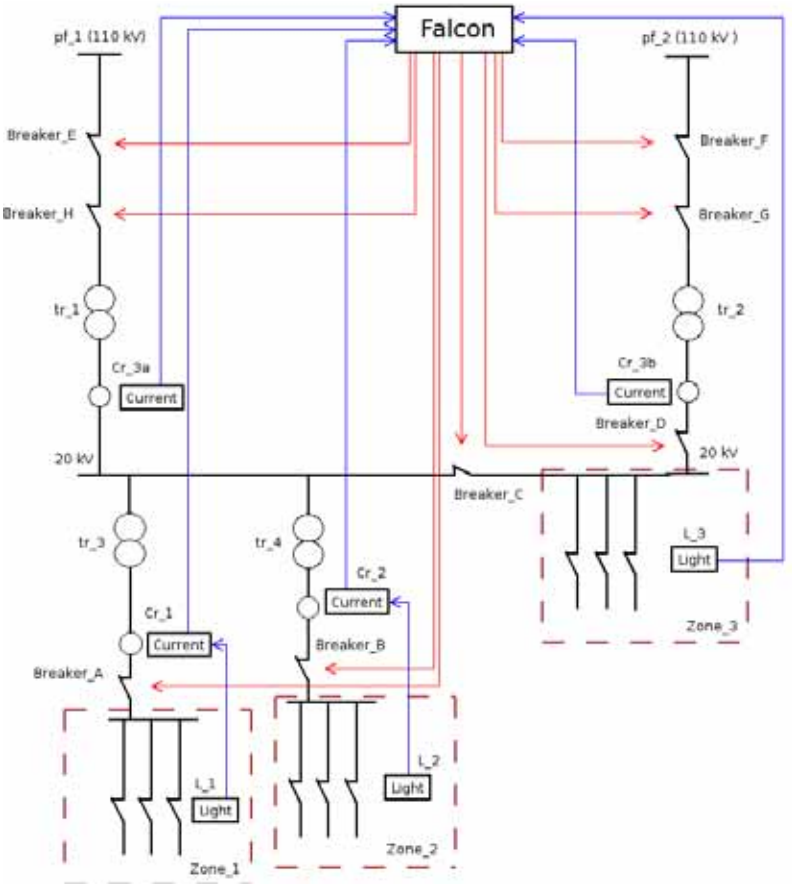

Figure 4.1.2. Switching diagram of the arc protection system [8].

For this case study basic methodology for modelling such safety instrumented systems was first developed based on hardware model checking techniques and the NuSMV tool [8]. As delays and timing related issues turned out to be essential in such systems, alternative model checking methodology based on timed automata and the Uppaal tool was also investigated [9]. The applicability of model checking was studied with respect to verifying the correspondence of implementation of control logic and its specification, and verifying the correctness of system design against safety properties. Also the environment of the arc protection system had to be modelled. The challenge was to find the right level of abstraction for the environment in order to guarantee the sufficient correspondence between the model and reality and to maintain the size of the model computationally feasible. The results show that the system design could be verified against its safety properties using hardware model checking techniques and the NuSMV tool as well as using timed automata and the Uppaal tool. For further information on the verification results, see [8, 9, 13, 15].

Case Stepwise Shutdown

A third case study was called the stepwise shutdown logic (see Figure 4.1.3). It is used for stepwise control of the process towards the normal operating state in case of disturbances. The system is triggered if some of the process variables, for example the measurement of the temperature, deviate from the values set for normal operation. The purpose of the system is to reduce the possibility that the process enters a state where the more complicated and heavier actual shutdown function of the process is needed.

The system was modelled using NuSMV and Uppaal tools and it was possible to verify basic safety properties of the system using both tools [4]. Besides model checking the design of the control logic, the fulfilment of the single failure criterion was analysed with several different failure models using the NuSMV tool. It was assumed that a failure could only affect one input signal of each process variable measurement at a time and that the logical components function correctly. In the most complicated failure model, failures may remain undetected, failed input signals get a non-deterministic value, and input signals may fail or recover at any time step. The evaluation of the case system showed that it is possible to determine the fulfilment of single failure criteria with model checking. For further information, see [4].

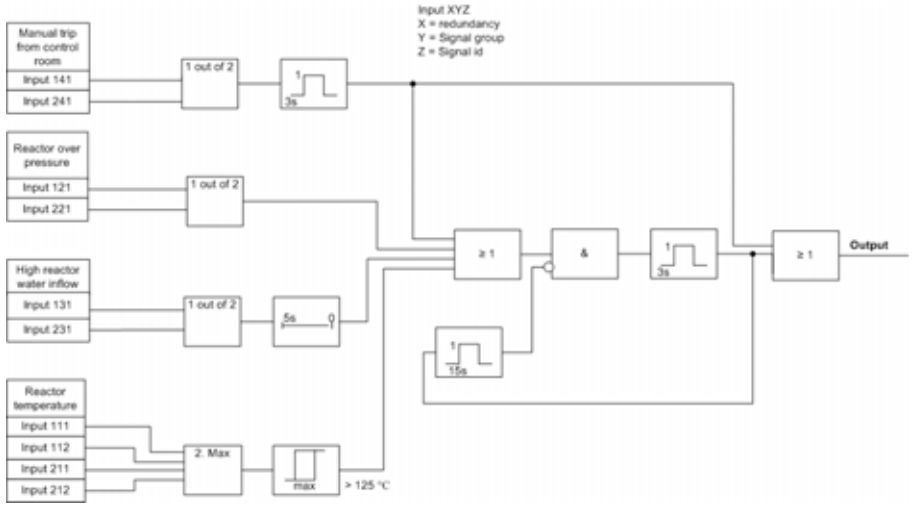

Figure 4.1.3. Stepwise shutdown logic.

Safety Cases

The applicability of model checking as part of safety case development was investigated along with the case study on stepwise shutdown. Safety case is a way of presenting a clear, defensible argument that a system is adequately safe to operate in its intended environment. Two safety case methodologies, Claims-Arguments-Evidence (CAE) and Goal Structuring Notation (GSN), were tested and their features compared. In addition, an exploratory safety case was outlined with both methodologies to see how they differ and what is required for making safety cases.

GSN has greater expressive power than CAE because it has more entity types. CAE is simpler to follow but it needs more narrative to explain and justify the structure of the safety case and meaning of the entities. Deciding the suitable level of details in safety case development is challenging. However, safety case type tree structure is one possible way of visualising and documenting the results of model checking.

Conclusions

Digitalized I&C systems are able to perform more and more complicated control tasks. They often combine real-time aspects such as timers with non-trivial control logic making their design and validation very challenging. The MODSAFE project aims at evaluating and developing methods based on formal model checking and applying them in the safety analysis of NPP safety automation (I&C).

During the first two years of the project, the state of the art of NPP safety automation systems analysis was reviewed and a basic methodology for applying model checking to safety evaluation developed. Model checking was utilised in analysing a number of case examples through which the methodology development got feedback and further ideas. It was also shown that model checking can be used to determine the fulfilment of single failure criteria.

In general, the results of the project show that model checking has potential to become a valuable tool that can be used both in the design and licensing of safety automation. It will benefit utilities, regulators, and system vendors.

The upcoming project years will concentrate on investigating how to enhance scalability of model checking based validation techniques to larger systems and how to combine validation results obtained from different levels of design. Developing model checking methods for embedded software systems and combining the strengths of symbolic model checking and timed explicit state model checking are other future challenges for the MODSAFE project.

Publications

During the first two project years, two conference articles [4, 13], two research reports [14, 15], and two Master's Theses [8, 9] have been published. In addition, at the time of writing this, there are one conference article and a project report under preparation.

References

1. Alur, R. & Dill, D.L. A theory of timed automata. Theoretical Computer Science, 1994. 126(2): pp.183–235.

2. Alur, R., Courcoubetis, C. & Dill, D.L. Model-checking for real-time systems. Fifth Annual IEEE Symposium on Logic in Computer Science, Philadelphia, Pennsylvania, June 4–7, 1990. IEEE Computer Society Press, pp. 414–425.

3. Biere, A., Heljanko, K., Junttila, T., Latvala, T. & Schuppan, V. Linear Encodings of Bounded LTL Model Checking. Logical Methods in Computer Science, 2006. 2(5:5): pp. 1–64.

4. Björkman, K., Frits, J., Valkonen, J., Lahtinen, J., Heljanko, K., Niemelä, I. & Hämäläinen, J.J. Verification of Safety Logic Designs by Model Checking. Sixth American Nuclear Society International Topical Meeting on Nuclear Plant Instrumentation, Control, and Human-Machine Interface Technologies, NPIC&HMIT 2009, Knoxville, Tennessee, April 5–9, 2009. On CD-ROM. American Nuclear Society, LaGrange Park, IL 2009.

5. Bryant, R.E. Graph-Based Algorithms for Boolean Function Manipulation. IEEE Trans. Computers, 1986. 35(8): pp. 677–691.

6. Cavada, R., Cimatti, A., Jochim, C.A., Keighren, G., Olivetti, E., Pistore, M., Roveri, M. & Tchaltsev, A. NuSMV 2.4 User Manual, ITC-IRST, http://nusmv.irst.itc.it/ (2009).

7. Clarke, E.M. Jr., Grumberg, O. & Peled, D.A. Model Checking. The MIT Press, 1999.

8. Koskimies, M. Applying model checking to analysing safety instrumented systems. Research Report TKK-ICS-R5. Espoo, Finland: Helsinki University of Technology, Department of Information and Computer Science, June 2008.

9. Lahtinen, J. Model checking timed safety instrumented systems. Research Report TKK-ICS-R3. Espoo, Finland: Helsinki University of Technology, Department of Information and Computer Science, June 2008.

10. Larsen, K.G., Pettersson, P. & Yi, W. Uppaal in a nutshell. International Journal on Software Tools for Technology Transfer, 1997. 1(1–2): pp.134–152.

11. NuSMV Model Checker v.2.4.3. http://nusmv.irst.itc.it/ (2009).

12. Uppaal integrated tool environment v. 4.0.6, http://www.uppaal.com/ (2009).

13. Valkonen, J., Koskimies, M., Pettersson, V., Heljanko, K., Holmberg, J.-E., Niemelä, I. & Hämäläinen, J.J. Formal verification of safety I&C system designs: Two nuclear power plant related applications. Enlarged Halden Programme Group Meeting – Proceedings of the Man-Technology-Organisation Sessions, C4.2. Halden, Norway: Institutt for Energiteknikk, 2008.

14. Valkonen, J., Karanta, I., Koskimies, M., Heljanko, K., Niemelä, I., Sheridan, D. & Bloomfield, R.E. NPP Safety Automation Systems Analysis – State of the Art. VTT Working Papers 94. Espoo, Finland: VTT Technical Research Centre of Finland, 2008. 62 p. http://www.vtt.fi/inf/pdf/workingpapers/2008/W94.pdf.

15. Valkonen, J., Pettersson, V., Björkman, K., Holmberg, J.-E., Koskimies, M., Heljanko, K. & Niemelä, I. Model-Based Analysis of an Arc Protection and an Emergency Cooling System – MODSAFE 2007 Working Report. VTT Working Papers 93. Espoo, Finland: VTT Technical Research Centre of Finland, 2008. 51 p. http://www.vtt.fi/inf/pdf/workingpapers/2008/W93.pdf.

5. Certification facilities for software (CERFAS)

5.1 CERFAS summary report

Hannu Harju, Jussi Lahtinen and Jukka Ranta
VTT

Mika Johansson and Risto Nevalainen
Tampere University of Technology, Pori

Abstract

As a part of Finnish nuclear research program SAFIR2010 a project called CERFAS started in 2007 to define necessary software certification services for nuclear industry needs. Main areas of the service development activities are process assessment and product evaluation. Several additional modules and methods may be needed and will be developed during the project. During 2007 the project produced three state-of-the-art reports and evaluated certification schemes also in other domains. In 2008 a first draft of the service was developed and piloted in an industrial case.

The main purpose of CERFAS is to develop facilities for a consortium called Software Certification Service. Conditions for services of consortium are the application of diverse expertise and effective evaluation tools. This leads into networking both in the project and in the certification services.

Introduction

Certification of software products by independent evaluation has been practiced in the software industry since early 1990s, especially in Europe and later in the United States. In Finland, a type acceptance certificate is required mainly in highest safety class of I&C equipments and systems in NPP, and recommended in lowest safety classes. In the research project “Certification facilities for software (CERFAS)”, the objective is to develop facilities for flexible, supported, commercially exploitable, high quality *Software Certification Service, SCS*, able to certificate safety critical software for the demands in Finnish nuclear area.

As a part of the development of the SCS, three state-of-the-art reports were published [1, 2, 3]. The first of these reports examines the state-of-the-art of research and practice of software safety concentrating on software product certification. The report discusses the certification practices of software products by independent evaluation in the software industry. The report gives an overview of aspects related to establishing a software certification service: legal liability viewpoints, distinctions between different viewpoints on certification, and standardisation efforts on software product safety certification.

The second CERFAS-report examines the state-of-the-art of process certification and evaluation, based mainly on generic and domain specific standards, reference models, and commercial process assessment approaches. The report was written mainly for certification bodies and licensers as a starting point to develop selected areas of certification service. The focus is mainly in process assessment and its current state-of-the-art in software and systems engineering.

The third report gives an overview of the first version of the Software Certification Service. The report provides basic principles of developing criteria for certification of software products. One of those principles emphasises that “Safety is a system problem, but deals with software developers.” In software safety certification the problem is not only in software, but also in its environment. Furthermore, some of the basic principles laid down in the report lead to development of criteria for the determination of whether a certified software product will be correct and suitable, verified and validated. In addition, the third report gives detailed guidelines in evaluating the software safety based on the important safety guides written in nuclear power plant field.

Certification can be defined as “the process of assessing whether an asset conforms to predetermined certification criteria appropriate for that class of asset”. This idea of conformance with criteria is the fundamental principle of

certification. Certification can be based both on generic sets of criteria and nuclear specific requirements. These two approaches have been combined in the project.

In CERFAS, certification is seen as a service to support software qualification and further licensing. The project needs an internationally recognised and accredited Certification Body (CB); promising CB's available in Finland are VTT and Inspecta.

Most important nuclear specific requirements are standards, which include requirements for safety critical systems and software. The most relevant for software safety is IEC 60880 [4], which can be used also as a reference for certification in safety class 2 I&C systems. The other main reference is the generic functional safety standard IEC 61508 Part 3 [5]. Comparison of IEC 60880 and IEC 61508 Part 3 was conducted. The purpose of the task was to extract the absolute requirements from both standards and to find out how these requirements compare to each other in terms of strictness and scope.

Safety cases provide a formal argument that a system is safe. The recorded safety cases support education of certifiers and evaluators, and the update and correction activities of software maintenance.

Evidence is gathered through software process assessment and product evaluation. In CERFAS process assessment is based on the SPICE standard. Product evaluation consists of analysing technical design solutions by methods such as reviews, static and dynamic analyses, fault injection, etc.

Certification of software and systems

Certification as a service

In general, certification is seen in CERFAS as a service to support system/software qualification and further licensing. Various areas of methods are needed to support certification, see Figure 5.1.1. Some examples are process assessment, product evaluation and use of different models and analyses. Figure 5.1.2 gives an overview of a process assessment procedure used in Software Certification Service.

For certification, an accredited Certification Body (CB) is needed. Some CB's have already a strong position in certification of safety-critical systems, for example TÜV in Germany. Type testing or other kind of Independent Verification and Validation (IV&V) is typically a fundamental part of the certification. Any CB needs a variety of services to run a certification service and to integrate different approaches as a coherent system.

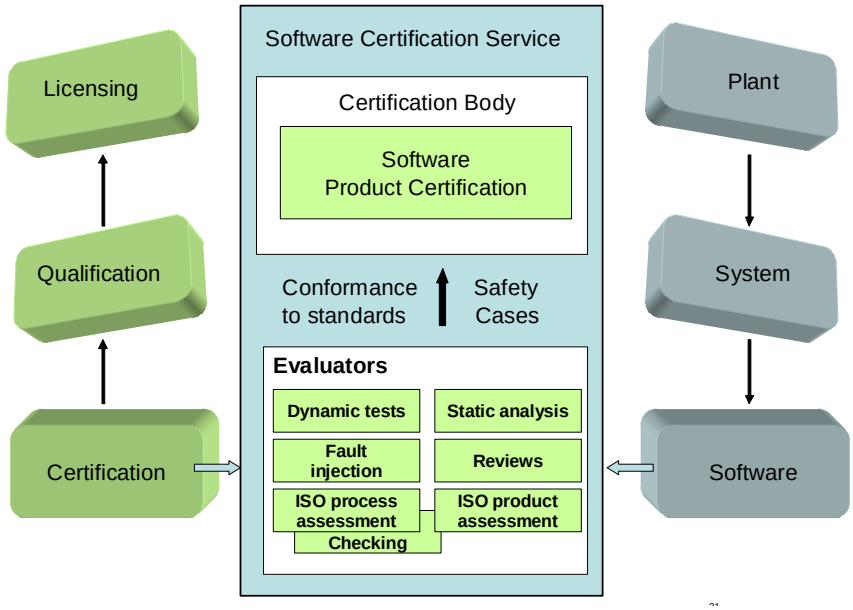

Figure 5.1.1. CERFAS project gives facilities for the Software Certification Service that includes Certification Bodies and evaluators.

The software under certification is in most cases basic software (for example platform or COTS module), but also application software in those cases where it is independent of application projects. The certification supports qualification of applications (software and system), which in turn supports the licensing issues.

The idea in CERFAS project is to integrate existing approaches together to facilitate effective and high quality certification. As a result, trust in software and system increases and further qualification and licensing phases are easier for supplier and utilizer.

Each certification type has its own assessment elements. The framework in CERFAS (see Figure 5.1.1) assumes that certification is based on some reference model, norm or set of criteria. Certificate itself is then a conformance statement against those requirements. Typically such statement is justified by some methods, which include external audits, IV&V's, reviews and inspections, code analysis and type tests. System wide certificates include some hardware related methods, like aging tests and electromagnetic tests.

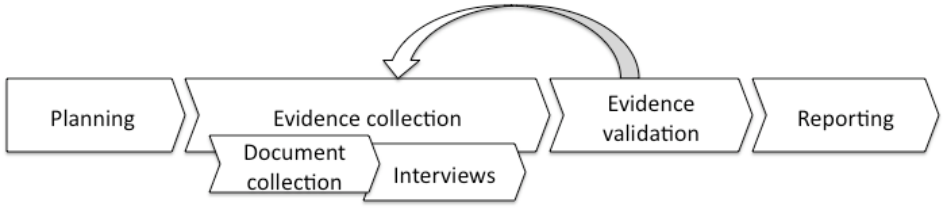

Figure 5.1.2. General process assessment scheme used in Software Certification Service.

Comparison of IEC 60880 and IEC 61508-3

IEC 61508 is an umbrella standard concerning basic functional safety issues in all kinds of industry. The part 3 of IEC 61508 covers the software requirements of such safety-related systems. Requirements for all software lifecycle activities are considered.

IEC 60880 provides requirements for the software of computer-based I&C systems of nuclear power plants performing category A functions as defined in IEC 61226. The standard provides requirements for the purpose of achieving highly reliable software. The standard is similar to the IEC 61508 standard in the sense that it covers requirements for all software lifecycle activities.

Even though the scopes of the standards are similar, the assumptions and approaches in the standards are different. Because of these differences, some topics and requirements can not be compared in terms of strictness.

IEC 60880 often has an emphasis on the required matters, or tasks, whereas IEC 61508-3 discusses the methods that can be used to meet these requirements. For instance, where IEC 60880 requires a specific property to be verified, IEC 61508-3 requires the use of a specific verification method. In addition, it is characteristic for IEC 61508-3 to use rather generic phrasing. It typically requires completeness, correctness and consistency. On the other hand, IEC 60880 requirements focus more on how these attributes are attained.

Granted that the IEC 60880 requirements are often more detailed than the requirements of IEC 61508-3, it cannot be argued that IEC 60880 is a stricter standard. The detailed requirements can possibly guide the evaluator to perform the evaluation more rigorously, but the details do not add to the strictness itself. It is more meaningful to argue that the details increase the unambiguity, or expressiveness of the standard rather than strictness.

Consequently, no significant differences in the strictness of the standards could be found. Most of the found differences were open to interpretations. Some evident differences do nonetheless exist.

The differences in the standards' scopes were mainly due to the nuclear specificity of IEC 60880. Other than that, IEC 60880 discusses pre-developed software more extensively than IEC 61508-3. Also, there is no equivalent in IEC 60880 for the functional safety assessment of IEC 61508.

Safety Case argues for the sufficiency of safety

Safety case is defined as "A document body of evidence that provides a convincing and valid argument that a system is adequately safe for a given application in given environment" [6]. Safety cases provide a formal argument that a system is safe and show that any risks associated with its operation have been reduced to an acceptable level. In the safety domain, explicit safety cases are increasingly required by law, regulations, and standards. At present, several kinds of safety cases have been constructed. The following list presents some of them:

1. Goal based approach for safety case. "Increasingly, regulatory agencies are making the case for a goal-based approach, in which claims (or goals) are made about the system, and arguments and evidence support those claims" [6].
2. Requirements based approach for safety case. This safety case technique provides a systematic and complete way to show compliance to one or more standards.
3. Vulnerable based approach for safety case. The safety case provides arguments that risk of occurring failures due to a software malfunction is sufficiently low.

What ever the approach is, it covers the other two approaches. According to [6], the safety case is defined in terms of three elements: 1) Claims about properties of the system, 2) Evidence used as the basis of the safety argument, and 3) Argument that links the evidence to the claims via a series of inference rules (Figure 5.1.3).

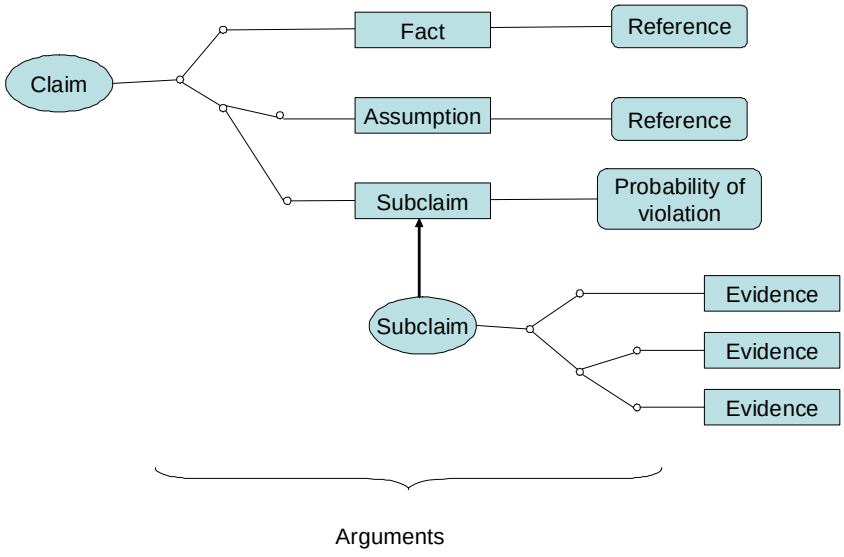

Figure 5.1.3. Example of constructing a Safety Case.

A claim is an objective which has to be achieved, for example, demonstrating that a system is safe, proving that a theorem is true, or showing that a hazard will not arise because of a given single point failure.

The following three types of arguments can be used: 1) Deterministic – relying upon axioms, logic and proof, 2) Probabilistic – relying upon probabilities and statistical analysis, and 3) Qualitative – relying upon adherence to standards, design codes etc.

Confidence in acceptance of safety cases is an important issue. It is affected by both information uncertainty and inadequate understanding. Quality of safety case is related to the concept of a good and acceptable argument and sufficient evidence. A good argument should be refutable by appropriate evidence. For example, bad product evidence of metrics, testing or analysis can refute claims. Whereas, argumentation based on compliance with process requirements as an argument for safety, is not refutable. The argument only supports the claim for safety; it will never be able to prove that the system is safe. A good argument

- is always refutable by the evidence
- is acceptable; it is one that is known to be true or is otherwise believable
- is based on an unambiguous interpretation
- provides sufficient supporting evidence
- is relevant to the appropriate claim.

Evaluators in Software Certification Service

Process assessment elements of certification

High-level and capable software development process is an essential part of achieving software quality. ISO 12207 is the basic standard to define software processes. ISO 15504 (known as SPICE-standard) considers all these defined processes, but only some are relevant for certification purposes. Many nuclear specific standards include quite similar concepts of processes as SPICE, and they are also used as normative sources, for example, IEC 60880 is originally based on processes of ISO 12207.

Process assessment is based on evidence, and it is quite close to safety case approach in that sense. In SPICE, evidence is called an “indicator”. Capability level 1 indicators are base practices and work products. Each work product includes a set of characteristics. Capability level 2–5 indicators are generic practices and work products, and process resources. Systematic mapping of process indicators to requirements of nuclear specific standards gives a quite good coverage of evidence for certification.

So far, CERFAS project has not yet defined any specific process set from ISO and/or IEC standards to be used in certification. We developed a method called TVO SWEP (Software Evaluation Procedure) during 2002–2005 to be used for qualification of safety class 3 software. All fifty SPICE processes are not relevant, and also the cost-effectiveness of process assessment indicates that only a few processes should be used. The criterion for process selection has been alignment and integration of ISO 12207 processes and related nuclear specific standards.

During the CERFAS project TVO-SWEP model was upgraded to cover safety class 2. Most of the new requirements, taken from IEC 60880, were added as new indicators to the base model. Some new processes were also required to fully cover the scope of IEC 60880, concerning the security of the development and qualification of the development tools. For the piloting purposes, the tool qualification was added. The number of processes and indicators is presented in Table 5.1.1.

Table 5.1.1. The size of TVO-SWEP model.

Process set	Processes	Base Practices	Subpractices (nuclear specific requirements)
ISO/IEC 15504-5 processes selected for TVO-SWEP	22	617	0
TVO-SWEP for safety class 3 (1. edition)	22	621	807
TVO-SWEP for safety class 2 (2. edition)	23	625	1277

The first assessment with the new edition of the model was performed in spring 2008, and experiences collected during assessment were analysed. The process set of the model fulfilled its purpose both from assessment and reporting point of view. Assessment was documented using an Excel based tool, which provided rapid prototyping features, but managing almost 2000 entities in Excel was not a user-friendly option.

The “third edition” of the TVO-SWEP model, to be released in 2009, will not include any more standards or requirements, but the existing model will be rearranged to better match the idea of the capability model of SPICE. Also some new processes are created, at least for security issues. Another candidate for a new process is safety management or “safety culture”. One important source of input for development is benchmarking of the model against similar models in other industry areas such as automotive and rail transportation.

Product based evidence

In reviews the artefacts produced by a software project and development process are inspected. Artefacts to be considered can be project plans, requirements specifications, architectural and structural plans and designs from various stages of the development process, and the actual code or some other lowest level description of the software. Reviews typically use tables and cross references to map statements between documents, e.g., traceability of requirements from specification to verification. For purposes of CERFAS VTT has experience in performing reviews and also the availability of software testing professionals to be used as consultants or service providers seems fairly good.

Static analysis of software is performed by analysing the source or object code without executing the program. The analysis considers the structure, architecture, use of the programming language, and potential programming errors. The object of interest can be, e.g., modularity, function call structure, or how and what aspects of the language have been used.

There are a number of metrics with which the complexity of the software can be analysed. Metric can also be applied to the specifications and design in addition to actual software code. A simple metric of software is the number of lines of code and correspondingly a metric of the requirements specification is the number of requirements.

Automated tools are an essential part of static analysis. The amount of manual work would be huge for many of the involved tasks. Manually performed static analysis is often referred to as program comprehension or understanding. There are a number of commercial tools devoted to different aspects of static analysis. These tools are however mostly suitable to be used during the development of the software and not of particular interest for verification. The availability of tools for static analysis is good and there are numerous vendors of commercial applications.

Model checking is a formal method of static analysis. The analysis is performed on a model of the software. Certain properties of the software, or more specifically the model, can be formally proved. The properties are described using temporal logic. Model checking is a relatively young and continually evolving method and the availability of tried and tested commercial tools is poor. Also the method is mostly suitable for small fragments of programs due to the rapidly increasing computational effort needed. However, checking critical fragments and structures or those used repeatedly in the software can be efficient in verifying the reliability of the software. A pool of knowledge and experience has been gathered in a joint project named MODSAFE in SAFIR2010.

In symbolic execution the program is executed from the source code instead of compiling the software. The tools of symbolic execution are therefore language specific. The approach uses symbolic variables which can have different values and value ranges instead of numbers. E.g., a symbolic integer variable, *I*, could have the value "$I > 3$ and $I \leq J$", where *J* is another variable. The execution expresses the values of output variables as functions if input variables. Due to the method of expressing variable values symbolic execution can handle infinite state machines, because each possible value of the variables need not be explored separately.

Dynamic analysis encompasses methods in which the software is executed using varying inputs. This is the typical testing performed practically on all software. The method facilitates the observation of properties such as run time errors, performance, errors due to timing and concurrency of parallel software threads. An important aspect of efficiency of the method is the coverage of the test cases. The inputs should cover all relevant real operating conditions as well as all of the code and error and exception situations. Typical errors to be found include programming errors such as unintentional use of an incorrect operator or variable and a call to a wrong function or with wrong variables or input parameters.

The availability of dynamic analysis is fairly good. There are numerous companies providing tools and services. A certification service provider could use testing professionals as consultants to analyse and evaluate the tests performed by the software manufacturer.

Fault injection into the source or object code or during execution can be used for analysis of, e.g., rarely executed sections of the software, recovery from errors, or the effectiveness and coverage of other debugging methods. It is closely related to dynamic analysis. Code mutations can be used to guide the execution path to exercise certain fragments of code to increase the coverage of the test cases. Runtime injection of errors can further simulate, e.g., hardware malfunctions or memory corruption. There are tools to automatically inject errors into the code but creating and choosing good errors usually requires manual work. The availability of tools and services for fault injection is far worse than for dynamic analysis, static analysis, or reviews.

Symbolic execution can be combined with both fault injection and model checking. Tools exist to inject the faults into symbolic execution and to incorporate model checking techniques into the analysis. These are, however, still research tools but seem to indicate a trend of different approaches being combined into unified analyses.

Conclusions

Nuclear power industry has a classification for their safety I&C systems. Safety-critical I&C systems belong to safety class 2 and safety-related systems belong to either safety class 3 or 4. All digital I&C systems in these safety classes must be qualified and further licensed before commissioning. Certification is required mainly for safety class 2 systems.

The toolset for certification will be developed in several increments in CERFAS. In each phase, tools are used in real pilots to get feedback and to collect further needs for certification. At the time of writing this article, the first pilot is completed and analyzed. Tools and methods are updated according to feedback and needs of the second industrial case.

Other industries may have quite similar needs for certification and qualification as nuclear power plants. For example, control of railway and subway networks and traffic, space and aviation applications, car and vehicles and electro-medical devices have similar needs and requirements for safety. Experience from other domains is collected and shared in upcoming workshops.

Comparison of the standards IEC 60880 and IEC 61508-3 was performed. The differences in the standards' scopes were mainly due to the nuclear specificity of IEC 60880 and Safety Integrity Levels of IEC 61508. No significant differences in the strictness of the standards could be found.

Conformance to standards is presented in Safety Case, which provides an efficient method of justifying and demonstrating safety of the software and its system in several domains. In addition, Safety Case templates can be utilised in education of certifiers and evaluators.

Many de-jure and de-facto standards like SPICE, are developed to assess software processes. The most rigid versions of these models are used to certify software processes. Several less disciplined approaches are also needed in process assessment, and they are defined and classified by their credibility and effort.

It is well known that dynamic testing is the main method to demonstrate quality of the system and software. Also, we know that by this method we can not show the absence of faults and failures. The absence of faults is shown by proving the code to be correct with respect to predetermined requirements.

References

1. Harju, H. & Pakonen, A. State of the Art of Software Certification. SAFIR2010, CERFAS, Research report VTT-R-09699-07, 2007.

2. Nevalainen, R. & Johansson, M. Software Process and Product Quality Evaluation in Safety Critical Domains. CERFAS State of the Art Report. Tampere University of Technology. Pori. Research Report 5, 2008.

3. Harju, H. Software Certification Service: Facilities for type approval of system software product. SAFIR2010, CERFAS. Research report VTT-R-09700-07, 2007.

4. IEC 60880. Nuclear Power Plants – I&C systems important to safety – Software aspects for computer based performing category A functions. IEC 2006.

5. IEC 61508. Functional safety of electrical/electronic/programmable electronic safety-related systems. IEC 1998.

6. Bishop, P.G. & Bloomfield, R.E. A methodology for safety case development, in Safety-Critical Systems Symposium, Birmingham, UK, February 1998.

6. Operator practices and human-system interfaces in computer-based control stations (OPRACTICE)

6.1 OPRACTICE summary report: Designing large-screen overview displays for nuclear power plant control rooms

Jari Laarni, Leena Norros, Leena Salo and Hanna Koskinen
VTT

Abstract

Finnish nuclear power plants (NPPs) are renewing their automation systems, control rooms (CRs) and human-system interfaces (HSIs). In control rooms there will be a change from analog technology to digital technologies and desktop-based workstations. The changes are challenging, and they have a great impact on operator practices. These issues have been studied in the O'PRACTICE (Operator practices and human-system interfaces in computer-based control stations) project by the VTT's Human activity and systems usability team. In this paper we present results of studies in which we have investigated the usage of large screen overview displays (LSDs) and participated in the design of large displays for the nuclear power plant control room.

Based on the results, a LSD concept has been outlined. The results suggest that the large screens should be some kind of a hybrid of CR panels, desks and the displays of the process computer system synthesizing their best features. They should support the development of an overview of the power process, development of situation awareness, rapid detection of failures and problem

states and collaboration and co-ordination of activities. Their role and usage practice are dependent on the state of the power process.

We have also participated in the evaluation of LSDs based on the Information Rich Design (IRD) concept developed by Institutt for energiteknikk (IFE) and Fortum. The final prototype is a hybrid of displays based on the IRD concept and traditional displays based on process and instrumentation (PI) diagrams. It was found that the Fortum IRD pilot displays can function both as overview displays providing useful information of the overall state of the power process and as supplementary displays that help operators to early detect failures and problems in the power process.

Introduction

Both Finnish NPPs have renewed or are just renewing their automation systems, CRs and HSIs. In CRs there will be a change from analog panel-based HSIs to digital desktop-based workstations. Since CR modernizations and changes in HSIs provoke risks, there is a clear need to pay closer attention to the accomplishment of CR and HSI renewals. Especially, there is a need to develop new tools and practices that help to manage problems caused by digital technologies.

One aim of our research in the O'PRACTICE-project is to help the design of new displays, HSIs and operating procedures by outlining the concept of operations for digitalized CRs and by developing new design methods and practices. A digital CR is a control centre which is based on desktop-based user interfaces, LSDs, touch screens, intelligent management of alarms and computerized procedures [1]. The concept of operations describes how the operating crew is organized, and by which way it monitors and controls the power process both in normal and exceptional operating conditions [1]. The second aim is to develop new methods and practices for the evaluation of the safety of HSIs. This part of the O'PRACTICE-project is a continuation of the work done in the IDEC (Interaction Approach to the Development of Control rooms) project included in the SAFIR 2003–2006 program in which the CASU (Contextual Assessment of Systems Usability) method was developed for the integrated validation of NPP CRs and HSIs. As results of these two tasks a realistic concept of operation for digitalized control rooms can be developed, new innovative concepts for presentation of process information can be designed, and more reliable and valid methods for the evaluation of CRs and HSIs can be presented.

In this paper, we will present some results of studies in which the role of large-screen overview displays in the CR context has been investigated. We will also present results of studies in which displays based on a novel information presentation concept (i.e. Information Rich Design -concept) have been evaluated. Results on studies concerning our other focus areas in the O'PRACTICE project (i.e. operating procedures as collaborative tools and further development of systems validation methodology) are found, e.g., in [2] and [3].

Opportunities and challenges of computer-based control rooms

Even though computer-based information systems provide new opportunities, they also involve challenges. Previous results suggest that changes in HSIs may have unexpected consequences, and it is also possible that totally new tasks emerge [4]. Our claim is that the concept of operations will be changed with the modernization of automation systems and HSIs, since these changes will not only change the interface management tasks, but it will also affect the primary tasks concerning the monitoring of plant performance and controlling the plant. We propose that possible problems can be solved by developing new kinds of computer-based displays and new ways to visualize process data.

There is a general hope that digital technology would have a profound positive impact on operator work, and it would improve operators' ability to monitor the power process and control the plant. For example, there are possibilities for a better integration of HSI resources so that all information that a user needs at a particular moment of time can be integrated [4]. There are also possibilities for increased flexibility in information presentation so that all information can be presented in a way that better supports the ongoing task [4]. In addition, due to the portability of digital technology, all HSIs can be accessed through a workstation located in a particular place [4]. All these improvements provide a better detection of failures, better overall situation awareness and better decision making.

However, even though the introduction of digital technology in the control room environment provides new opportunities, it has also raised several problems [5]. It is possible that monitoring and operating the system through desktop-based workstations increases the operator's separation from the process [4]. Due to the limiting viewing area of the display screen, only a small amount of information can be seen at any one time. If more information is needed, operators must have knowledge of where it is located in a virtual information

space, and in order to access this information the operator has to navigate through the information space and retrieve it. Because of small screen area the amount of interface management tasks may thus considerably increase [4]. Computer-based systems also provide less feedback about the success of the operators' responses and about the control operations the other operators are conducting [5]. For example, the manipulation of knobs, sliders and switches provides rich tactile feedback to the operator; mouse-based operations are clearly deficient in this respect. In a traditional CR based on analog technology, it is also easy to be aware of other operators' activities by observing their position at the panels and desks that contain spatially-fixed displays and controls [4]. With the introduction of desktop-based workstations it is more difficult to interpret what the other operators are doing.

Development of the large-screen display concept

Large screen overview displays may play an important role in digital CRs based on desktop-based workstations in the presentation of process information (see Figure 6.1.1). The hope is that they could solve some of the above-mentioned problems caused by digital technology. For example, LSDs may provide an overview of the state of the process and information of important process changes, disturbances and alarms in a way that is easy to detect and comprehend [6]. By providing an overview of the state of the system they can help users to develop a better mental model of the process, and thus also improve the awareness of the momentary state of the process (i.e. situation awareness) both at the individual and at the team level [6]. They can also support teamwork and crew coordination by providing information of what other operators are doing [6]. In addition, the LSDs may help operators to locate themselves in the information space and tell them by which way they can navigate from one display page to another [6]. Since more information can be presented at the same time on a large screen, there is less need to scroll the display, open new windows or change the display content. By this way the LSDs should help to reduce the load caused by the display management tasks.

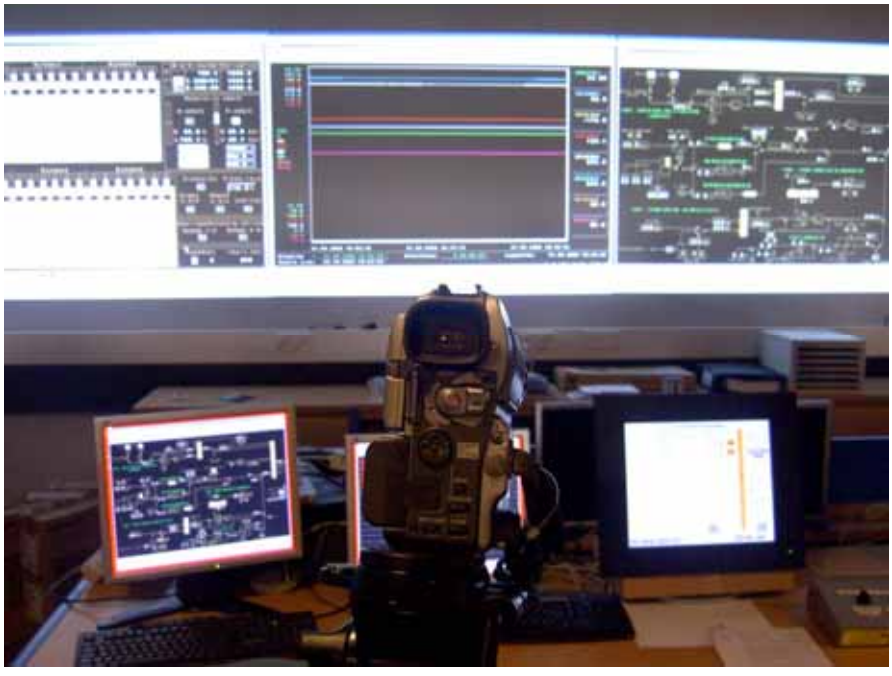

Figure 6.1.1. Large screen displays at the Fortum development simulator.

On the other hand, the design of LSDs for the CR environment is challenging. They are not only bigger in size, but they are also qualitatively different from desktop-based workstations, and therefore user-interface metaphors and design principles applied in the design of small displays are not necessarily adequate in the design of LSDs. Overall, quite little is known about the usage practices of LSDs in NPP CRs. Our earlier study showed that LSDs have several useful features making them suitable for the CR context [7]. It was found that the LSDs may be useful in continuous monitoring of specific information especially during revisions, in training, and during failure situations. They can also promote crews' shared understanding of the process state but their role in cooperation could be further developed by discussing their possibilities during training.

Three design workshops in which operators, trainers and designers from the two Finnish NPPs participated have been arranged. The aim in the design workshops was to collect their ideas and suggestions about the design of future CRs. Based on the results of the workshops, a preliminary LSD concept was outlined.

The method we have used is a mixture of different types of techniques within the context of participatory design [8]. Our method is based on dialogic communication between researchers and process experts, and an attempt to build up a dialogic relationship between different stakeholders takes place in a special kind of future workshops arranged. The workshops aim to bridge the gap between and to integrate expertise of different participants in a way that makes possible to illuminate the phenomenon from different perspectives. The workshop participants first develop in small groups a future plan in which the actual state of the operator work is imagined from the future perspective by considering which kind of problems they have at the moment and by which way the problems could be tackled within a longer time perspective. Secondly, reflective thinking is promoted by letting each group of experts at the time to present their ideas while others are listening.

We have found that since the nuclear power process is very complex, profound expertise in the nuclear field is a key prerequisite for success in the design of new tools for the CR environment [8]. We have also found that the development of mutual understanding between different stakeholders is a complex process that needs time. Even though the used dialogic method has shown to be promising, new ways to build communication and understanding between operators, researchers and designers are under development.

The results of the workshops suggest that the LSD concept should answer questions such as: By which way are LSDs used in different plant states? How is information presented on the large screen display? The role, usage practices and content of large screens depend on the state of the plant, that is, different kind of information should be presented on the LSDs during normal power operation state than, for example, during outages or during start-ups and shutdowns [9]. Questions of the usage practices of LSDs can be classified into four groups: those that are related to interactivity, integrability, co-operativity and division of responsibility (see Figure 6.1.2). Questions of the information content and presentation format can be, in turn, classified into six groups: those that indicate level of abstractness, structuralness, dynamicism and customization, and extent of description and target group.

Most of the participants of the workshops thought that the responsibility of the management and design of LSDs should be shared, and the representatives of operators should be able to participate in the design of LSDs [9]. The interactive use of LSDs was not considered an essential feature of the LSDs. The best alternative would be if the content of large screens would change automatically

without operator involvement. A general agreement was that LSDs should be integrated with other information systems of the plant, even though this may be difficult to achieve due to safety requirements. The co-operative use of LSDs was not considered important. On the other hand, the participants thought that it would be useful if it could be seen on LSDs information of operations other operators are executing.

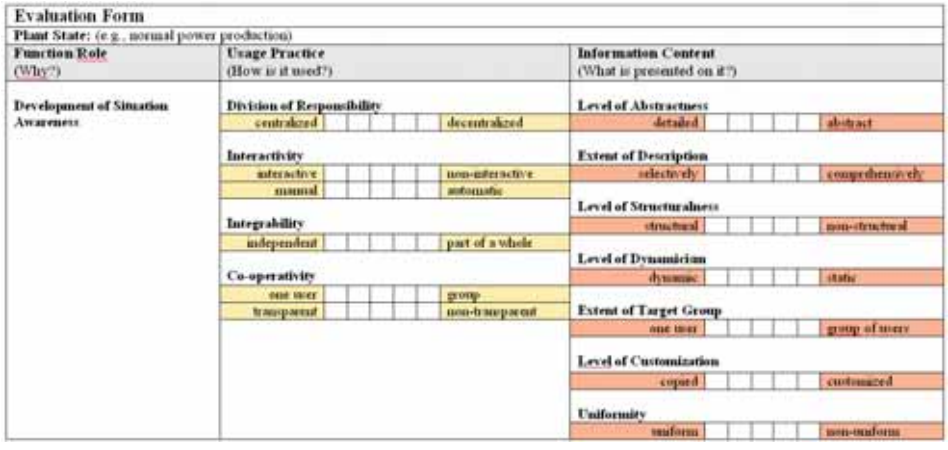

Figure 6.1.2. Evaluation form for the development of situation awareness showing the basic categories of the LSD concept. Similar forms are drawn for other functions of the LSDs.

There were different views of the preferable abstraction level of information on LSDs: On the one hand it was hoped that it could be presented as detailed information on LSDs as possible; on the other hand it was hoped that the LSDs should show only highly processed abstract information [9]. Neither was there a single view of how extensively and comprehensively information should be presented on LSDs. Some operators thought that the information should be presented as comprehensively as in the panels and desks of the conventional CR, some of them thought that only the most essential information should be presented on LSDs.

The participants hoped that LSDs could show a basic description of the plant based on PI-diagrams that include non-structural dynamic information (such as trend displays) of particular subsystems [9]. Even though dynamic information is preferred over static one, also static information is needed to help operators to segment the display. The content of a specific large screen can be designed for a single operator or for a group of operators. The reactor and turbine operator may

also have their ‘own’ LSDs that are specifically tailored for their information needs. An example of a suggestion for the placement of LSDs is illustrated in Figure 6.1.3.

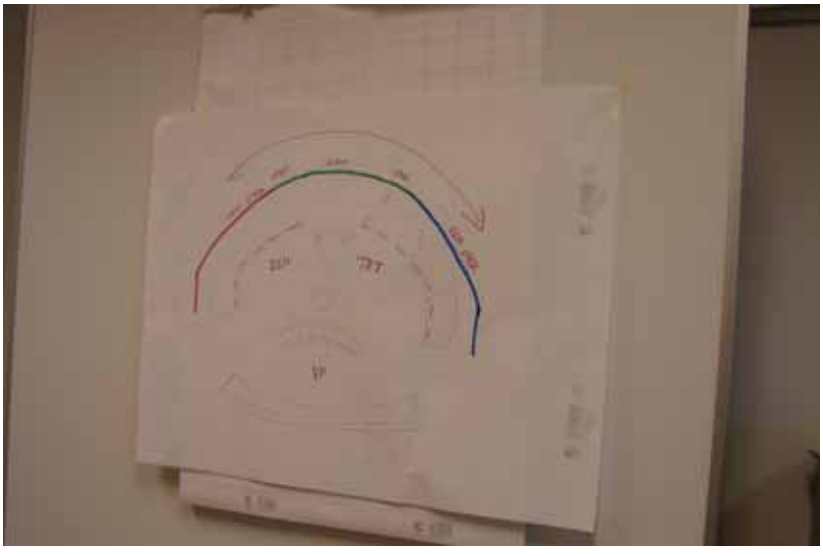

Figure 6.1.3. Example of a suggestion for the placement of LSDs in a NPP CR.

Evaluation of displays based on novel display concepts

Since LSDs are qualitatively different from other kind of displays, there is a good reason to develop new types of interface metaphors and design concepts providing suggestions of how to design and develop LSDs for process industry. We have participated in recent years in the evaluation of two kinds of displays based on Ecological Interface Design (EID) and IRD concept in close collaboration with the Halden Reactor Project (HRP) and IFE. The results of our EID studies have been presented in several conferences and published in several papers, see e.g. [10]. The detection of changes and process failures can also be improved by developing displays that emphasize important information by making it more salient and de-emphasize the less important information by reducing its visibility. Displays based on the IRD concept have been developed by IFE for those purposes for Norwegian oil companies [11].

The Fortum IRD pilot is the first application of the IRD concept for the monitoring of the nuclear power process. It has been developed collaboratively

by designers from IFE and Fortum. Some of the central aims in the development of IRD displays have been to provide overview information, support early detection of failures and disturbances and help operators to diagnose the problem and stabilize the process [11]. The IRD concept is based on such design principles as display normalization, Dull Screen principle and information richness [11]. The aim of display normalization is to help operators to immediately detect deviations from the baseline. Two types of graphical objects have been developed, normalized mini trends and normalized bar-like symbols without mini trends. The aim of the Dull Screen principle is to prevent visual noise by using colouring rules that make essential information more salient [11]. "Information richness", in turn, refers to the principle of attaching a large amount of critical information to each diagram. For example, some normalized trends include a lot of information concerning the position of a valve.

Figure 6.1.4. The four Fortum IRD pilot displays that were designed in the project.

During 2008 we have interviewed designers of the displays, and observed the design process of the Fortum pilot displays at design workshops. We have also conducted a usability test of the Fortum IRD pilot, and gathered information about users' experiences and conceptions. In addition, we have carried out a heuristic evaluation of the Fortum IRD pilot displays by ourselves. In this paper we will focus on designers' comments; the results of the all the IRD studies are briefly summarized at the end of the section. A more extensive presentation of the results can be seen in another paper entitled "Evaluation of the Fortum IRD pilot" [6].

IFE designers' views

The development of the Fortum IRD pilot displays is based on a couple of workshops with IFE designers, Fortum designers and domain experts (i.e. operator designers). The first preliminary version of the displays was developed at the early stage of the project. After that some new variables came in and they were included in the system (see Figure 6.1.4). The IFE designers called this approach rapid prototyping, which they have also used in the oil industry. In this method the first version is some kind of an idea generator that stimulates the designers' thinking. It was estimated that approximately at least four to six months is needed in this kind of design process to generate the final prototype.

The IFE designers admitted that one typical problem in this type of projects is that clear principles and intentions easily water down and accommodate to the new requirements. In the beginning of the development Fortum IRD pilot displays, the IFE designers started with a clear intention that the pilot IRD displays would be complementary to the operator displays of the process monitoring system (PMS). Since the aim was not to present all information on the LSD, they had to select the most appropriate variables. They thought that there is a danger that at some point more and more information is added in order to make the display absolutely complete. Even though more information was eventually included than was at first suggested, the IFE designers thought that they are quite satisfied to the final prototype.

Overall, the IFE designers thought that they had had no need to modify the original concept to a large extent, and they had not had to make any difficult compromises. However, according to them, it is always necessary to make some special kind of adjustments according to the specific domain. For example, new kinds of symbols have been developed during the design of the Fortum pilot.

In the oil industry the IFE designers have found that in the first meetings operators do not like the normalization and alignment of trends and bars. They think that due to normalization the presentation of information is not physically correct any longer, and therefore, they lose touch to the physical world. According to the IFE designers, it is very important that the operators know what it means that the information is normalized. Because of this, when implementing IRD displays it is important that sufficient training is arranged for operators in which it is explained the rationale behind the IRD approach.

One lesson the IFE designers have learned during the project is that the nuclear power process is quite different from the oil industry process. In the oil

industry the process is very volatile and dynamic, and the operators have to carry out operations within minutes or even seconds. The operators do not rely on procedures because they have no time to do that. In the nuclear industry operators use more procedures, since the process is much slower and the operators have, thus, more time to look at them. Therefore, the designers thought that they should better take into consideration how the LSDs could support the use of procedures.

Fortum and operator designers' views

The Fortum designers and operator designers were quite satisfied of the fact all the relevant information could be presented. Some information that is important for the monitoring and operation of the plant has been added at the later stages of the project. For example, more information of individual components is shown that was displayed in the first version of the pilot. Overall, the amount of information is order of the same magnitude than in the earlier designed PMS-based overview displays.

Considering the function of the Fortum IRD prototype, it was thought that the IRD displays should be some kind of a support system for operators. They should provide an overview of the state of the power process, and at the first hand they should support the management of the power process as a whole. That is, with a single glance into the LSD, the operator could immediately see what is going on in the process. The LSD displays should also be a stand-alone system that is independent of the automation system. This could be possible because the LSDs are only aimed for monitoring, and there is no need for a two-way transmission of information.

Even though the designers thought that the IRD displays should be a quite independent entity, consistency with other information systems was considered to be an important design feature. For example, colour philosophy should be consistent so that the same set of colours should be used in all displays in the CR. It was also considered important that the direction of the presentation of the process is consistent with other displays.

The Fortum and operator designers discussed whether the displays could also be used in other plant states. A general view was that it is important that it can be applied also in other plant states, for example, in hot shutdown and start-up, but different displays should be designed for these conditions. On the other hand, some of them were not very convinced whether the IRD displays are also

valuable in emergency situations, since in these conditions different instructions are used. Another problem is that normalized graphical information loses its value when the plant state changes. For example, since the line showing the measured value does not stay any longer at the middle of the trend graph after the change of the plant state, the normalization has to be done again after it.

There were some controversies whether exact numerical values should be presented or not in the vicinity of trends and bar graphs. Even though most of them were removed, some of them were considered more important and they were kept there. All numerical values are, however, shown when the measurement value exceeds the alarm limit. It was also considered useful that the reliability of the presented information could be clarified.

The Fortum designers and operator designers were convinced that the fluent use of IRD displays needs practice. Because of this, operators may at the beginning resist the new displays, but it is probable that by time the resistance would diminish. It would be important that the operator designers that had participated in the design process also could participate in the training session and explain the rationale behind the design choices made.

Summary findings

The results suggest that the Fortum IRD pilot displays have shown to be applicable to the detection, identification and diagnosing of failure states in the nuclear power process [6]. The displays have many useful features such as presentation of history information through trend graphs, use of Gestalt grouping principles in element clustering and information richness of graphs. These features make the displays nice looking and can also help operators in the identification and diagnosing of failures if they have enough time to practise the use of the displays [6]. On the other hand, the displays have also several features that make them poorly suited to their purpose. For example, the Fortum IRD pilot is designed mainly for one plant state, the 100% power level, but according to user comments, an overview display should be usable also in other plant states. Secondly, although trend information was considered very useful, the usefulness of trend normalisation was somewhat doubted. Also, according to the operators, the overuse of the colour grey, the lack of exact numeric parameter values and component labels, and the misplacement of some components hampered the detection of failures. Our claim is that these problems are caused by the fact that the final prototype is some kind of hybrid of IRD displays and

traditional displays based on PI-diagrams [6]. One possibility in the future is to continue to develop this kind of a hybrid version which is a combination of traditional overview displays and IRD displays. Another possible way to continue is to develop a small-scaled IRD display for early detection of failures and develop a separate set of overview displays that are based on existing overview displays and whose structure is based on plant mimics.

Conclusions

One of our central aims in the O'PRACTICE project has been to find the questions we need to answer in the design and development of new digital HSIs for NPP CRs. These questions are included in the LSD concept that provides a general framework for the design of LSDs. We claim that new design solutions should be evaluated against this framework by checking which kind of answers they give to these questions. It is, for example, probable that 'traditional' CRs based on analog panels and desks provides different kind of answers to these questions than CRs based on digital technology and desktop-based workstations.

There is quite much evidence of advantages of information visualisations' ability to bring the user distant from the system physically closer to it in information space. Complex visualisations make essential information immediately available and provide an ability to comprehend a huge amount of data with a single glance [12]. They also provide access to emergent or hidden properties of the data that are difficult to anticipate [12]. Overall, on the one hand, visualisations help users to see the forest from the trees, on the other hand, they also help users to quickly see small deviations from the normal state.

Even though visualisations provide advantages, our results also suggest that they have some drawbacks. A simple fact is that every diagram visualising process data takes room from some other information that may be equally or even more important. Designers have thus to manage the trade-off between highlighting some information supporting some operator task (e.g. early detection of process failures) and suppressing information supporting some other task (e.g. comprehension of the overall state of the process). Every diagram highlighting essential information that is inserted in the PI-diagram easily breaks the integrity of the diagram and makes difficult to perceive the spatial relationships of the plant systems. From the standpoint of display design, the key question is whether the visualisations are integrated into the PI-diagrams or whether they are shown on a separate display. The paradox is that visualisations

that should help operators to get an overview of the plant state may even deteriorate the operator's ability to comprehend it.

Our studies in the O'PRACTICE project have so far concentrated on the design and development of visual displays. Issues related to the presentation of process information through other sensory (i.e. auditory and tactual) channels have not yet been tackled; nor have we studied the role of different types of input devices in the CR environment. Our next aim is to develop a concept of operations for digital NPP CRs in which the role of multimodal interfaces and input devices will also be discussed. Our hypothesis is that this task much more demanding than what we have done so far. This work is supported by the work done in a VTT-funded project called NASE (Novel Affordances of Smart Environments) in which the aim is to develop novel interaction concepts and a prototype for a more efficient and effective operation of the power process.

Overall, we are only at the beginning in the understanding of the effects of digitalisation and in the application of novel visualisations to the design of CR HSIs, but what is already clear is that the digitalization of CR HSIs has both positive and negative consequences concerning safety operation of NPPs, and new types of displays will not solve all the problems associated with the maintenance of accurate situation awareness, detection of process failures and collaboration and co-operation between operators.

References

1. EPRI 1008122. Human factors guidance for control room and digital human-system interface design and modification: Guidelines for planning, specification, design, licensing, implementation, training, operation, and maintenance. Palo Alto, CA: EPRI, 2004.

2. Norros, L. & Salo, L. Acting with procedures in complex work – A challenge for work design. Activity Analyses for Developing Work – Book of Abstracts. International Ergonomic Association Symposium (ACTIVITY2008). Helsinki, Finland, May 12–14, 2008. Helsinki: FIOH, 2008.

3. Liinasuo, M. & Norros, L. Usability Case – integrating usability evaluations in design. COST294-MAUSE Workshop on Downstream Utility, November 6, 2007, Toulouse, France. Pp. 11–13.

4. EPRI 1002830. Information display: Considerations for designing modern computer-based display systems. Palo Alto, CA: EPRI, 2003.

5. Laarni, J., Salo, L. & Norros, L. A step towards more agile and adaptive management of nuclear power plant control room renewals – lessons learned from a project in Finland. In: Proceedings of the Enlarged Halden Programme Group meeting, Gol, Norway, March 11–16, 2007.

6. Laarni, J., Koskinen, H., Salo, L., Norros, L., Braseth, A.-O. & Nurmilaukas, V. Evaluation of the Fortum IRD pilot. In: Proceedings of the 6th American Nuclear Society International Topical Meeting on Nuclear Plant Instrumentation, Control, and Human-Machine Interface Technologies, NPIC&HMIT 2009. (In press.)

7. Salo, L., Laarni, J. & Savioja, P. Operator experiences on working in screen-based control rooms. In: Proceedings of the 5th ANS International Topical Meeting on Nuclear Plant Instrumentation, Controls, and Human Machine Interface Technology, Albuquerque November 12–16, 2006.

8. Laarni, J., Koskinen, H. & Norros, L. Activity-driven design of collaborative tools for nuclear power plant control rooms. Activity Analyses for Developing Work – Book of Abstracts. International Ergonomic Association Symposium (ACTIVITY2008), Helsinki, Finland, May 12–14, 2008. Helsinki: FIOH, 2008.

9. Laarni, J., Norros, L., Koskinen, H. & Salo, L. Designing large screen displays for process monitoring and control. In: Proceedings of the Enlarged Halden Project Group Meeting, Loen, Norway, May 18–23, 2008.

10. Norros, L., Salo, L., Savioja, P. & Laarni, J. Communicating the meaning of process state information – Comparing operator practices when using three forms of information presentation. In: Proceedings of the Enlarged Halden Programme Group meeting, Gol, Norway, March 11–16, 2007.

11. Veland, Ø. & Eikås, M. A novel design for an ultra-large screen display for industrial process control. In: Dainoff, M.J. (Ed.) Ergonomics and Health Aspects, HCI International 2007, LCNS 4566. Berlin: Springer, 2007. Pp. 349–358.

12. Ware, C. Information visualization. Perception for design. San Francisco: Morgan Kaufmann.

7. Development and validation of fuel performance codes (POKEVA)

7.1 POKEVA summary report

Seppo Kelppe
VTT

Abstract

Advancements in updating, improving, and extending of fuel performance codes in use at VTT have been accomplished. Continuing effort to introduce a probabilistic transient analysis tool has resulted in a concept of core-wide assessment that will be used to estimate the number failing rods in an accident. Steady-state codes have been further validated. Selected models have been critically reviewed. In addition to uranium dioxide, doped pellets, inert matrix fuel and thorium dioxide fuel have been studied. Development efforts at VTT are being combined with similar programmes through international collaboration. Vital training of young experts urgently required to compensate personnel turnover has continued.

Introduction

In the project, development is being carried out to meet the demands on availability of methods for nuclear fuel performance assessments. A permanent goal is to create and maintain calculation tools, i.e., systems of computer codes for steady-state and accident conditions which can be utilized independently of those in the possession of the plant designers and fuel vendors. Systematic validation and maintenance as well as continuous feed of experimental data are

inseparable elements of code development. Some of the existing codes base on obsolete modelling and architecture, and renewal of the system consisting of new parts or entirely new codes is one of the long term objectives.

Reactor fuel, as regards both its construction and materials, is a product under continuous development. The progress largely stems from expectations on improved efficiency, particularly through striving for higher fuel discharge burnups, and it will bring about a need to revise both acceptance criteria and the models and codes that are used for assessments.

Series of codes are in use at VTT that basically can cover the phenomena and conditions in which analyses are called for. Two parallel lines of steady-state and accident behaviour codes can be applied for independent studies. At VTT, methods of applying probabilistic studies with fuel performance codes have been created; those for steady states are in routine use, a probabilistic accident analysis system is in a demonstration state. Coupled codes in which a fuel performance code is combined with an advanced description of thermal hydraulics have been introduced and intensively utilised in limited types of applications. Finite Element Method (FEM) has been extensively introduced to improve the accuracy of the description of mechanical behaviour.

Certain areas of fuel behaviour are not fully comprehended and need more experimental work and subsequent modelling. Close relation of research activities with emerging fuel types and materials needs to be kept.

Fuel behaviour research – reactor tests and examinations of irradiated material, in particular – are in practice possible to carry out in collaborative projects only. Finnish participation in the OECD/IRSN CABRI Water Loop Project (CIP) and the OECD Studsvik Cladding Integrity Project (SCIP) are continuing and are coordinated and channelled in Finland through VTT. OECD Halden Reactor Project continues to be a valuable one-of-a-kind general fuel research programme. Well-established connections to the US Nuclear Regulatory Commission and its national laboratories PNNL and ANL are maintained. Some of the fuel cladding material aspects are addressed at the VTT Materials Performance Technology Centre.

Main objectives and items of work

- Method for a probabilistic whole-core accident simulation to produce estimate of the number of failing rods

- Elaboration of the coupled thermal hydraulic and fuel performance mode FRAPTRAN-GENFLO
- FUMEX II cases calculated with the re-calibrated ENGIMA fission gas release model
- Analyses on inert-matrix and thoria fuels (HP)
- Analyses on doped VVER fuel (HP)
- High temperature oxidation model to APROS simulator
- Comprehensive review of the VTT version of the ENIGMA code: review of development history, fission gas release and UO_2 thermal conductivity state-of-the-art reviews (partly met; continuing)
- Code version management (partly met; continuing)
- Comparative validation of three FRAPTRAN versions (SSM/VTT; PNNL/VTT) (not met; under preparation).

Core-Wide Accident Analyses

The goal is to routinely handle core-wide performance phenomena in accident conditions to the extent required in the YVL 6.2 guideline. This includes estimation of the number of failing rods in a given transient.

Determination of the failed rod through a probabilistic procedure makes an advancement towards a best-estimate procedure. This work that was initially started in 2006 has now proceeded to a demonstration [1]. See Figure 7.1.1 for the procedure.

In the application here three successive methods are used to reduce the enormous number of single calculations required by a probabilistic method. First, the rods are divided into groups by their respective similarities. Criteria for the grouping include irradiation time, relative power, and the position of the rod in the thermal hydraulic channel. Secondly, the calculation is made in such a way that the cases are distributed among 59 global groups with the same global parameters (Table 7.1.1). By this, the results from calculation of the tolerance intervals can be utilised. And finally, neural networks – a totally new approach – has been introduced to explain the connections between input and output parameters. The results of fuel performance code simulations have been used to teach the neural network and, with the networks, all the rods in the reactor have been calculated 59 times with different local parameter values.

Table 7.1.1. Local and global parameters in probabilistic accident analysis (shaded not used yet).

Parameter	**Locality**	**Distribution**
Swelling parameter	global	normal(1.0; 0.012)
Creep parameter	global	normal(1.0; 0.5)
Fission gas release parameter	global	normal(1.0; 0.5)
Thermal conductivity parameter	global	normal(1.0; 0.1)
Clad corrosion parameter	global	normal(1.0; 0.02)
Clad outer diameter	local	triang(9.05; 9.1; 9.18)
Clad inner diameter	local	triang(7.7199;7.72; 7.79)
Pellet outer diameter	local	triang(7.53; 7.57; 7.5701)
Pellet centre hole diameter	local	triang(1.4; 1.5; 1.6)
Pellet density	local	triang(10.4; 10.55; 10.7)
Fuel grain size	local	normal(12.5; 1.0)
Power	local	normal(1.0; 0.005)
Power	global	
Reactivity coefficients	global	
Control rod worths	global	
Coolant pressure	global/local	
Coolant temperature	global/local	
Clad yield strength	local	

So far highly conservative assumptions have been made. Some of these are to deliberately increase the probability of failures for demonstration purposes, partly due to remaining difficulty to couple the thermal hydraulics appropriately. It is expected that the applied rough assumption based on coolant temperature acquired from an APROS simulation can be replaced by GENFLO boundary conditions shortly.

Although not too realistic, the results are encouraging in that the usefulness of neural network has been demonstrated. Before proceeding, a careful assessment on the proper selection of the varied parameters is suggested. Being a novel solution, the method with neural networks still requires a critical verification.

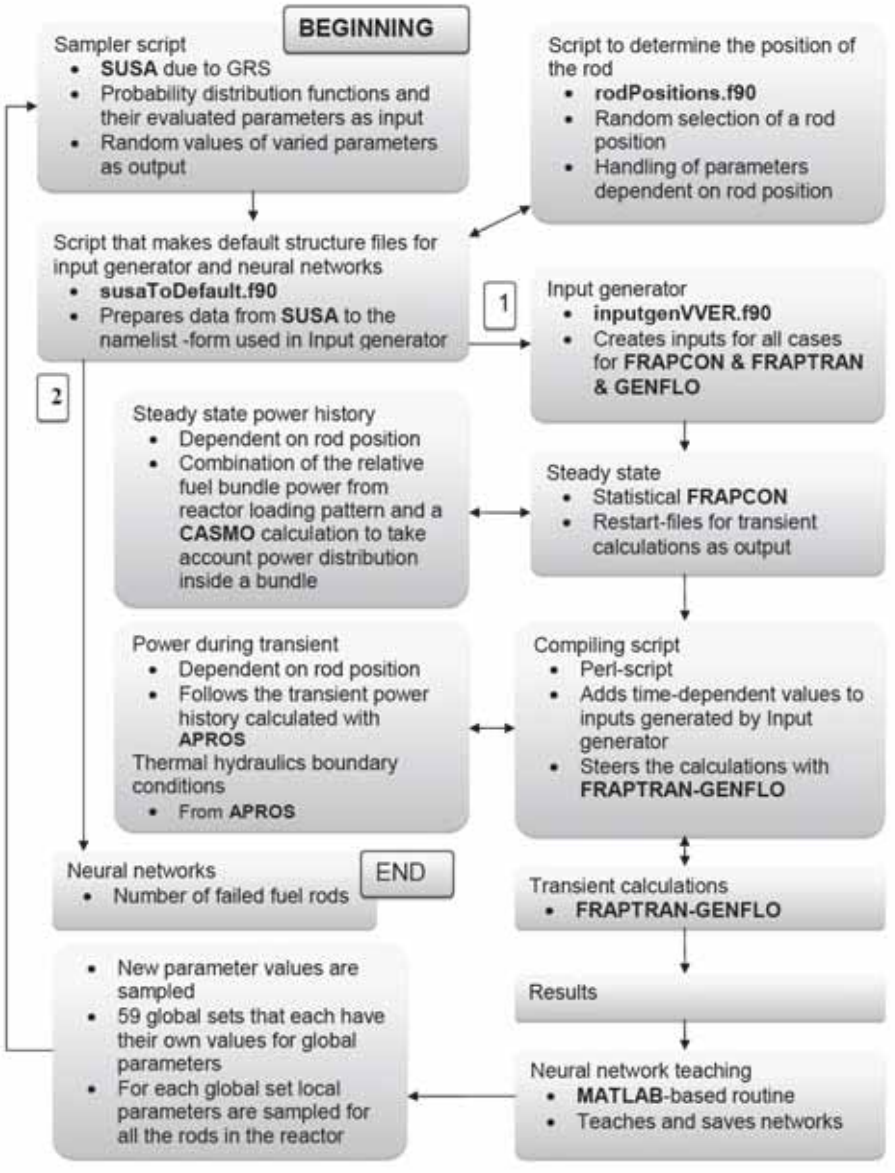

Figure 7.1.1. Procedure of probabilistic core-wide fuel accident behaviour assessment.

FRAPTRAN-GENFLO Development

Much of the FRAPTRAN-GENFLO development happens momentarily to establish an active link in order to produce boundary for the probabilistic accident analysis in desired detail and format. [2] The thermal hydraulic interface in FRAPTRAN-GENFLO that has suffered from apparent faulty coding is being rectified. Alternatives to give FRAPTAN-GENFLO boundary conditions from a system code have been elaborated. A new mode has been introduced to independently define steam and water flows with mixed or separate enthalpies for each of the phases. Preliminary test runs with PWR LOCA simulations have been successful.

Another major target of development and application has been the simulations of the OECD Halden integral LOCA test described at certain length in the POKEVA special report.

Steady-State Modelling Review and ENIGMA Validation

In the current fission gas release model in the modified ENIGMA 5.9b study-state code, the original formulation is broadly retained, while the parameters have been recalibrated. This is repeated from time to time as new release data comes available. As part of the validation the nine “mandatory” cases of the former IAEA CRP FUMEX II Benchmark were recalculated with the current version [3]. The cases include eight steady-state and transient fuel performance tests made in test reactors and the ninth test case is a set of hypothetical calculations with simple boundary conditions. The FUMEX-II cases broadly illustrate the current performance of the VTT modified ENIGMA version. The ENIGMA code shows good numerical robustness. Generally the code seems to predict the measured fission gas release values reasonably (Table 7.1.2). There is some scatter between the calculated and measured results but no general trend to under or overprediction. Also the fuel rod centre temperatures are quite accurately reproduced. An example of results is in Figure 7.1.2.

A review of the VTT development history of ENIGMA was prepared [4]. This will serve the aim of improving the housekeeping of the number of versions that have introduced over the years. Systematic version management tools have been examined. Of the development, a simple high burnup structure model, addition of VVER specific property data, recalibrated fission gas release model with burnup enhancements, and the RADAR 99 power profile model deserve to be mentioned.

Table 7.1.2. Fission gas release calculated with re-calibrated ENIGMA model (FUNEX II).

		MWd/kgU	FGR %	FGR %	%
IFA-534.14 rod 18	PWR-15x15	62.3	6.25	4.68	33.52
IFA-534.14 rod 19	PWR-15x15	62.2	9.37	8.89	5.35
IFA-597.3 rod 7	BWR-8x8	69.9	14.06	12.60	11.57
IFA-597.3 rod 8	BWR-8x8	70.0	9.32	15.80	-41.00
Regate rod H09	PWR-17x17-rodlet	47.4	3.96	9.3	-57.42
Riso-3 rod NA3	PWR-rodlet	40.4	25.75	35.5	-27.47
Riso-3 rod NA4	PWR-rodlet	35.74	29.25	40.9	-28.48
HBEP rod BK365	PWR-rodlet	61.2	5.09	2.40	112.08

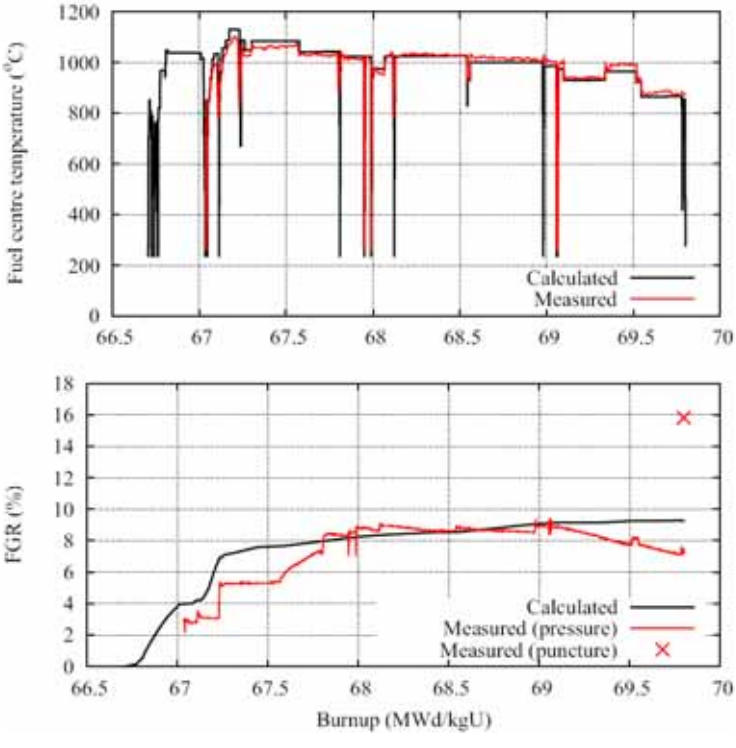

Figure 7.1.2. Performance of the ENIGMA code in an example case of FUMEX II CRP.

ENIGMA is run at VTT both in Windows and unix platforms with equal availability.

A detailed comparative assessment of the fission gas release and uranium dioxide pellet thermal conductivity was made [5]. The critical review contains detailed descriptions of the models and points out shortcomings and suggests areas of improvements. The summary identifies a number of differences between ENIGMA and other models which should be further studied in the ongoing work at VTT to improve ENIGMA performance. A degree of ENGMA's underpredicting fuel temperatures is suggested.

Options identified for model improvement include 1) introducing precipitate and gas concentration factors, as well as radiation influence factors in the diffusion coefficient, 2) improving the conductivity correlation to account for post-ramp annealing and lessening the underestimation of rod temperature in select cases, 3) replacing the thermal re-solution mechanism with a more physical irradiation-induced chip re-solution model, 4) replacing the current grain boundary bubble growth rate release threshold with an equivalent threshold for gas concentration, and 5) implementing mechanistic models to enhance fission gas release predictions at high burnup.

Halden Test Assessments

Inert Matrix and Thoria Fuel. [6] Material properties of calcia stabilized zirconia inert matrix (CSZ-IM) and thoria fuel were introduced to the ENIGMA code Due to lack of data a simplified approach was adopted. It is comprised of mass proportions as weight factors with respective correlations for urania, thoria, zirconia and calcia. After implementing these to the code, calculations were performed using the irradiation history of the rods irradiated in the Halden research reactor as input.

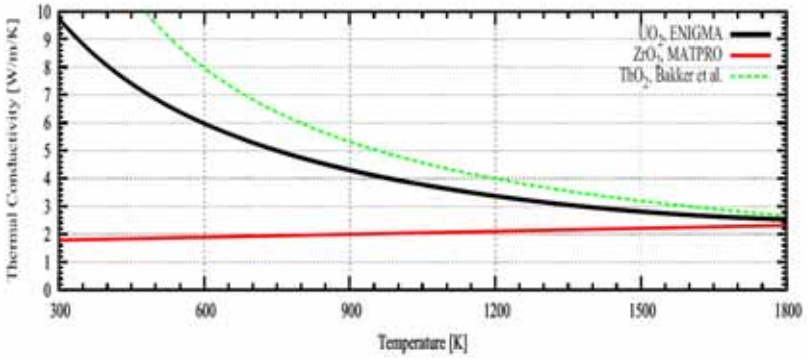

Figure 7.1.3. Comparison of thermal conductivities of fuel materials.

The test performed in Halden comprised six rods with highly enriched uranium as fissile material. Four of these were taken under closer examination – the two inert matrix rods (one of them hollow), inert matrix doped with thoria, and a thoria rod. Calculated temperatures and rod internal pressures were then compared with the data obtained from the experiment. Calculations showed that the temperatures were underestimated with all of the rods, the biggest difference being with the thoria rod.

It became apparent from the results that urania reduces the thermal conductivity of mixed oxide fuel more than its mass proportion implies. This conclusion was also made in a study conducted at Idaho National Engineering and Environmental Laboratory where thoria properties were implemented to the FRAPCON-3 code.

The next step in developing ENIGMA code would be to include the nonlinear correlation for fuel compound weight factors in heat conductivity model as used in modified FRAPCON-3. Similarly, micro structural effects could be one of the things explaining the difference between measured and calculated temperatures in inert matrix fuels. Another attribution possibly results from the conductivity correlation for zirconia adapted from MATPRO that seems to overrate conductivity. Rod internal pressures were also under scope, and with the inert matrix rods the calculation managed to reproduce pressure jumps indicating fission gas release, but the pressure levels were overestimated. A possible explanation could be that zirconia thermal expansion is overestimated. With thoria doped inert matrix, calculation failed to show any pressure jump, and with thoria rod pressure is underestimated with increasing linear heat rate. This in turn is a result of badly reproduced temperatures. In conclusion, more suitable

and more sophisticated correlations are needed to take account of material properties of these mixed oxide fuels.

Doped pellet VVER test analyses. [7] The Halden IFA-676 test has been qualified making use of the ENIGMA fuel performance code. In the test, three pairs of instrumented fuel rodlets with different fuel types: large grained VVER-1000 fuel, reference VVER fuel of standard grain size, and Gd_2O_3-doped VVER fuel are being irradiated in the Halden test reactor. At the time of calculation the cluster had been irradiated for one year only. The four undoped rods with high enrichment had reached burnups around 14 MWd/kgUO_2, the Gd-doped rods merely 4 MWd/kgUO_2. The main objective is to study the behaviour of the large grain VVER-1000 fuel at high burnups. The irradiation of IFA-676 and qualification of the results are being continued.

The calculated fuel centreline temperatures are in good agreement with the measurements. However, the calculated temperatures somewhat systematically remain below the measured. An example comparison is in Figure 7.1.4. The assumed change in thermal conductivity due to added gadolinia works fairly well with low burnups here.

It has been acknowledged that the dimensional changes of a rod, as described in the current ENIGMA code require more attention. The results here suggest the same even in the case there is no pellet-to-clad contact yet.

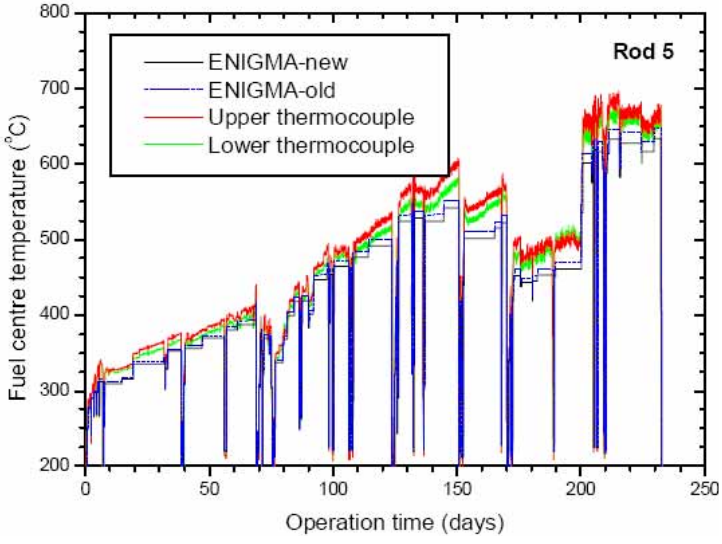

Figure 7.1.4. Measured and calculated fuel temperatures in a gadolinia-bearing test rod.

High-temperature Oxidation Model to APROS

The purpose of the development project was to renew the high-temperature zirconium oxidation model used in the APROS code. Material availability and temperature limiters, two most commonly used best-estimate type correlations, and hydrogen production and steam consumption calculation were added in the model. The correlation for the high-temperature zirconium oxidation calculation is selected by the user. [8]

The functionality of the implemented limiters was tested with two example cases. The numerically calculated values agreed well with the analytical values. Also the interface of the model was changed because the renewed model needs more data than the old model. However, the implementation should require minor modifications of the APROS main code.

To verify the numerical correctness of the implementation, two cases were analysed. A tube with a length of 1000 mm, inner radius of 4.0 mm and outer radius of 5.0 mm was selected for an example geometry. The purpose of the first test case is to test the zirconium availability limiter with prolonged oxidation time, i.e. slowly increasing temperature (1 °C/s). The aim of the second case is to test the temperature limiters by utilising a high linear heat rate of 100 °C/s.

Calculated hydrogen production for the second case is given in Figure 7.1.5.

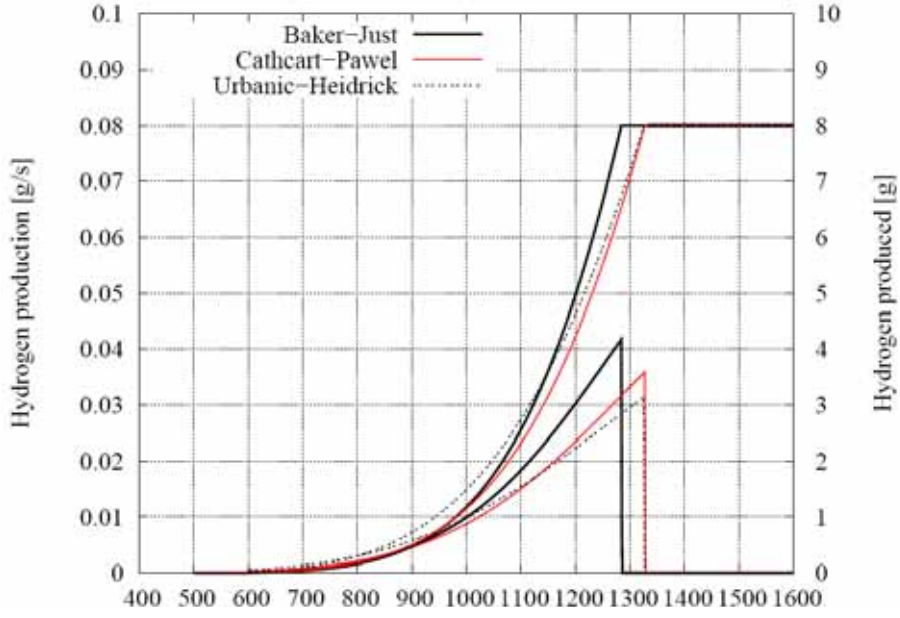

Figure 7.1.5. Results of the high-temperature oxidation model implemented in APROS.

Expected Collaboration

Discussion with several institutions having similar goals have been carried out. The closest contacts are continued and expected with the OECD Halden Reactor Project, the Swiss Paul Scherrer Institute, the Swedish authority SSM with the consult Quantum Technologies AB, the French Institut de Radioprotection et de Sûreté Nucléaire, and the US Pacific Northwest National Laboratory.

Applications

The steady-state codes have been utilised in thermal mechanical assessments of power reactor fuels under contracts with the nuclear utilities. The coupled thermal hydraulic code FRAPTRAN-GENFLO has been applied, above all, in planning and qualification of OECD Halden Project's loss-of-coolant accident tests [9, 10, 11].

Conclusions

Remarkable progress has been made with improvements and further validation of the fuel performance computer codes in use at VTT. Here, the emphasis has been on high burnups and transient and accident conditions. Further development, close connections to experimental research, and international collaboration continue.

References

1. Rintala, J. Probabilistic Analyses for Rod Behaviour in Accident Conditions: Demonstration, VTT-R-10519-07, VTT Technical Research Centre of Finland, 5.5.2008. 21 p.

2. Stengård, J.-O. & Hämäläinen, A. Updated FRAPTRAN-GENFLO User's Instructions. VTT-R-00682-09, VTT Technical Research Centre of Finland, 2.2.2009.

3. Knuutila, A. & Pietarinen, K. Re-calculation of the FUMEX II cases with VTT modified ENIGMA fuel performance code. VTT-R-01113-07, VTT Technical Research Centre of Finland, 30.1.2007. 22 p.

4 Kekkonen, L. Outline of the Past Development of the ENIGMA Code at VTT. VTT-R-01905-08, VTT Technical Research Centre of Finland, 22.2.2008.

5. Ghan, S. A Comparative Review of the VTT ENIGMA Fission Gas Release and UO_2 Thermal Conductivity Models. VTT-R-10996-08, VTT Technical Research Centre of Finland, 19.12.2008. 25 p.

6. Arffman, A. Preliminary Qualification and Calculation of Thorium and Inert Matrix Fuel (IFA-652.1-3) with the VTT ENIGMA Code. VTT-R-01874-08, VTT Technical Research Centre of Finland, 22.2.2008. 27 p. + app. 40 p.

7. Kekkonen, L. ENIGMA Calculation on Halden VVER Test IFA-676.1. VTT-R-010530-07, VTT Technical Research Centre of Finland, 22.2.2008. 20 p.

8. Pietarinen, K. High Temperature Zirconium Oxidation Model for the APROS Code. VTT-R-1857-08, VTT Technical Research Centre of Finland, 25.2.2008. 9 p. + app. 15 p.

9. Knuutila, A., Miettinen, J., Stengård, J.-O. & Kelppe, S. Development of FRAPTRAN-GENFLO and its application to IFA-650 LOCA test series. Enlarged Halden Programme Group Meeting, Storefjell, Norway, 11.–16.3.2007. 12 p.

10. Stengård, J.-O. Pre-test analyses on the Halden VVER LOCA test IFA-650.6 with FRAPTRAN-GENFLO. VTT-R-04069-07, VTT Technical Research Centre of Finland, 3.5.2007. 10 p.

11. Miettinen, J., Stengård, J.-O. & Kelppe, S. Qualification Efforts of Halden IFA-650 LOCA Test Results. Enlarged Halden Programme Group Meeting, Loen, Norway, 18.–23.5.2008. 12 p.

7.2 LOCA Test Simulation with FRAPTRAN-GENFLO (POKEVA)

Jan-Olof Stengård, Jaakko Miettinen and Seppo Kelppe
VTT

Dedicated to the memory of LicTech Jaakko Miettinen, 31.3.1947–7.8.2008.

Abstract

In assuring reactor safety with increasing target burnups, fuel behaviour in postulated accident conditions is receiving high attention. Within the OECD Halden Project in Norway, a programme of integral reactor tests in closely simulated light-water reactor loss-of-coolant accident (LOCA) conditions and with high-burnup power reactor fuel has been implemented [1]. The tests, designated as the IFA-650 series, now encompass seven abundantly instrumented in-pile tests and versatile post irradiation examinations.

From the very beginning, VTT has been active in planning and qualifying the tests whereby the VTT GENFLO [2, 3] and amended USNRC FRAPTRAN codes, and their combination have been instrumental. In the following, success of some of the simulations with due consideration of the special features of the test arrangement are reviewed.

In the Halden IFA-650 series, testing, post-test examinations, and related supporting and qualifying analyses continue.

Introduction

The Halden IFA-650 LOCA test series is an unequalled topical enterprise. The tests are emphasised to produce fuel and cladding performance data from high-burnup rods. The tests so far have been quite successful and the continuing programme is subject to high expectations.

A particular concern with LOCA is that the fuel fragments may “relocate” or fill up the ballooned volume of the cladding and locally increase the linear power. With higher-burnup fuel, the pellet would turn into finer fragments, and the relocation as well as the dispersal of fuel out of the cladding are postulated to be stronger.

The start of the IFA-650 tests in 2003 coincided with the VTT idea to create a coupled thermal hydraulic and fuel performance model in which the VTT in-house GENFLO code and the USNRC-originated FRAPTRAN fuel code would be run in an interactive combination. This has been largely successful; however, realisation of applying the compound model to an IFA-650 type arrangement is not all that straightforward, and a lot of feed-back has been acquired from the experimenting.

Experimental LOCA Test Setup

The experimental IFA-650 arrangement is schematically shown in Figure 7.2.1.

Despite its basic simplicity, the test set-up has several challenging features: the long small-diameter pipelines, small flow orifices, a small-capacity water spray system, and the electrically heated sheath around the test rod, to list a few. Phenomenologically, the importance of radiation as the main heat transfer mode radially and the more or less efficient natural circulation of steam axially, together with the idea of simulating the residual heat by a small fission power all require considerable flexibility and adaptation of the models basically describing power reactor geometries.

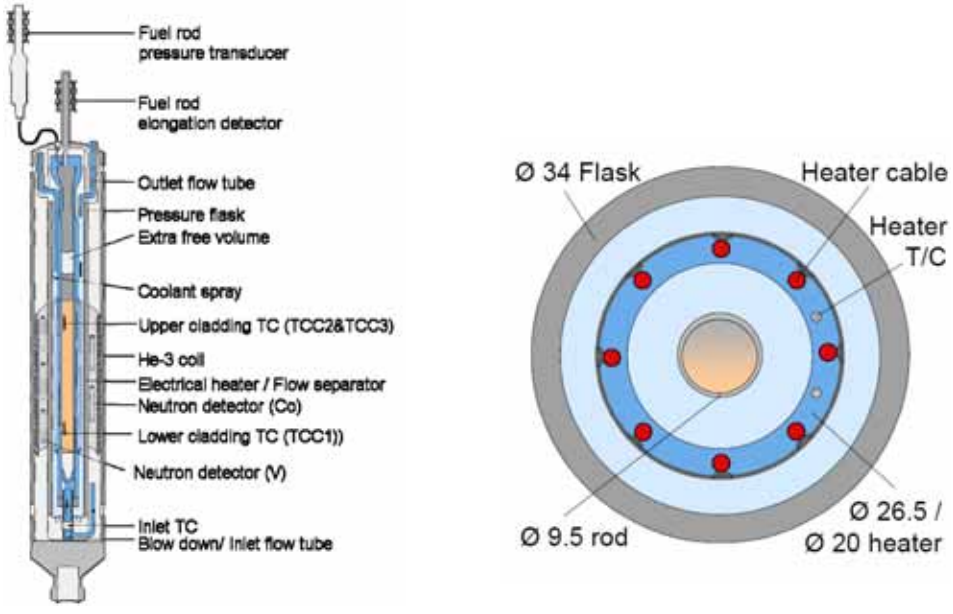

Figure 7.2.1. Features of the experimental setup in the Halden integral LOCA tests.

Thermal Hydraulic Modelling of the IFA-650 Test Section in GENFLO

The original thermal hydraulic model of the IFA-650 loop calculation was made on the best understanding of the loop characteristics during forced flow, natural circulation and LOCA blow-down conditions. The main emphasis in the test sequence is the heat-up part when the rod is cooled by radiation heat transfer and by natural circulation by superheated steam.

The basic GENFLO nodalisation for IFA-650 is shown in Figure 7.2.2.

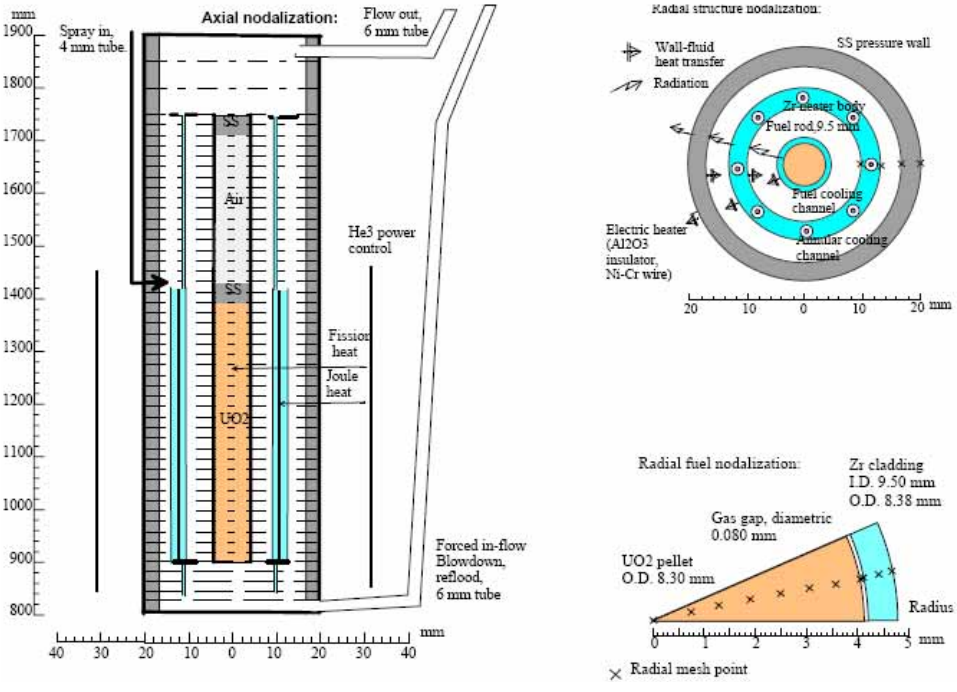

Figure 7.2.2. GENFLO nodalisation for IFA-650 experiments.

During the forced flow conditions the main flow path is through the annular flow channel surrounding the fuel rod and partially through the outer flow channel between the electrically heated shroud and the pressure vessel immersed into the reactor pool. After departing from the forced flow mode, the single-phase water is cooling the heated rod by natural circulation with upwards flow around the fuel rod, with a negative flow occurring in the outer annulus.

After the blow-down and fuel rod heat-up, the radiation heat transfer is adjusted in such a way that the stabilised temperatures of the fuel rod and the electrically

heated shroud agree with the measure data, if no spray cooling is applied. The holes between the inner and outer annular spaces are assumed to allow natural circulation by single-phase steam, whereby superheated vapour would flow upwards in the inner annulus and the cooled vapour down in the outer annulus.

For sufficient steam supply to keep up the oxidation at high temperatures, a small spray device is provided. Here the spray is operated in pulses. From the nozzle diameter, droplet diameter of about 0.3 mm is deduced. The flow is laterally directed towards the fuel rods. In the way it is used, this spray may only have a weak cooling effect.

The radiation balance is controlled by the emissivities of the rod and shroud surfaces. With the GENFLO model's simplified concept, emissivities for each experiment were found empirically. The best-fit emissivities range from 0.80 to 0.93 for the rod, and from 0.65 to 0.78 for the shroud. To reproduce the results, the rod emissivity needs to be increased when going higher in burnup. The varying deduced emissivities reflect differences in surface conditions from test to test.

Mechanical Model in VTT FRAPTRAN

A finite-element-method based mechanical model for cladding and pellet elastic-plastic behaviour has been created at VTT [4] and has been applied here. In addition to being robust in performance, the model allows handling cladding and pellet creep, pellet-to-clad frictional contact, and large deformations like ballooning when desired. The model is optional to the original FRACAS models in FRAPTRAN.

Examples of Halden LOCA Test Simulations

With this effort, support has been given to test planning by offering suggestions of the main test parameters – the fission power and the power of the electric heater. The simulation of the IFA-650 tests have been made with the GENFLO thermal hydraulic model, with the VTT modified FRAPTRAN fuel behaviour model, or with their interactive combination. In all cases covered here, the VTT mechanical model option for mechanics has been applied due to its superior performance over the built-in FRAPTRAN modules in ballooning situations.

From test to test some tuning has been required to be able to reproduce the measured behaviour. The parameters involved are emissivities, factors affecting the plenum temperature, amount of water in a spray pulse, and flow friction in

the pipes. Persistent attempt to define general boundary conditions to substitute for any tuning is made.

In the fourth run – **IFA-650.4** – the cladding peak temperature target of 800°C was reached. Ballooning and burst occur at 336 s. Considerable fuel relocation was observed: the fuel stack above the burst location collapsed into the balloon and about 200 mm of the clad is emptied of pellets. Consequently, the linear power is increased at the balloon. Some fuel was dispersed out of the rod through the burst opening.

There are two cladding thermocouples at the upper end of the rod (about 100 mm from top). There is a heater thermocouple at the elevation of 205 mm from the bottom, near the burst location, and another in the upper end, near the cladding thermocouple.

In calculation, the configuration of the relocated fuel is roughly simulated as follows: First a parametric study was made to make the calculated heater temperature meet the measured at the lower location by varying the rod power. The best match resulted with an applied linear power of 1.8 kW/m. Heater temperatures are given in Figure 7.2.3. If one assumed that the balloon is filled with solid fuel, the power would have risen to 3 kW/m. After the burst at 336 s, the linear powers are deliberately adjusted to be zero at the nodes at the top where there are no pellets left inside the cladding, and the case was repeated with several power levels from 1.25 to 2.2 kW/m at the balloon site. Power in other axial locations was not affected in the calculation.

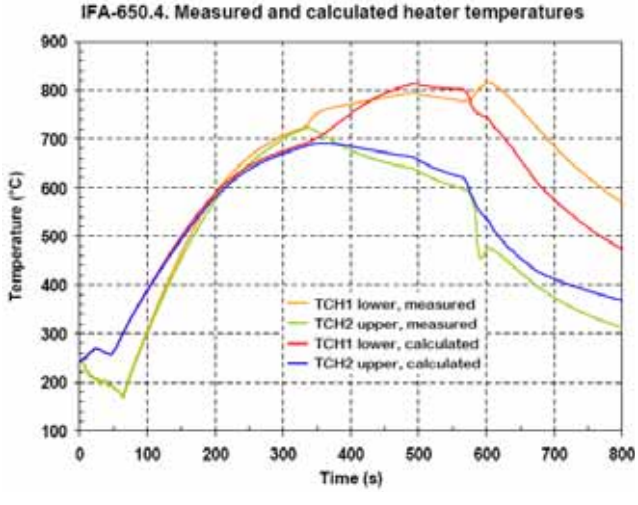

Figure 7.2.3. Observed and calculated heater temperatures in Halden IFA-650-4.

The outcome is in Figure 7.2.4. The cladding temperature is rapidly decreasing in the upper end of the rod, while a fair temperature increase for the ballooning region is expected eventually stabilising in each case at about 150 s after the relocation. With the best-estimate power of 1,8 kW/m the peak temperature is 970 °C.

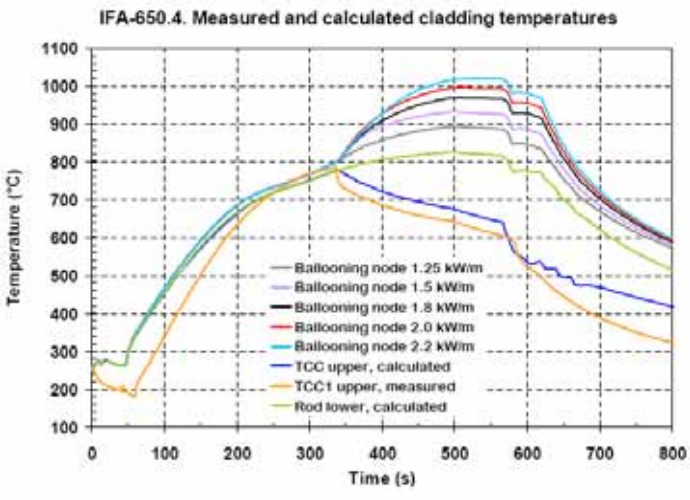

Figure 7.2.4. Halden IFA-650.4 clad temperatures, with parameter variation.

The result of the FRAPTRAN calculation is that the balloon will be nearly filling the space inside the heater (Figure 7.2.5), which is in concert with the test result. The calculated burst time is somewhat earlier that the observed.

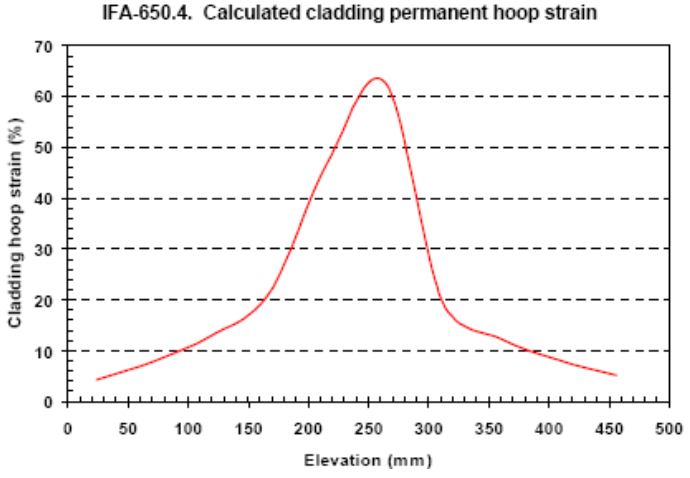

Figure 7.2.5. Calculated cladding plastic deformation in Halden IFA-650.4.

In the **IFA-650.6** test (Loviisa VVER fuel) [5], the location of the hot-spot in the transient comes close to the lower thermocouple elevation by a fortunate chance. Further, the burst opens in the opposite direction circumferentially yielding a clean temperature measurement on the ballooning cladding. In the thermocouple reading we do see an increase in the surface temperature heat-up rate, momentary though as the test is shortly terminated (Figure 7.2.6). The fluctuations in the calculated upper end temperature relate to the operation of the spray. In reality they seem to be suppressed.

As in some previous occasions one runs into difficulty with the unexplained offset of axial cladding temperatures that probably stems from the rig setup. This is not seriously affecting the conclusions from the test but makes it tricky to model. There is a distinct overestimation of the temperatures in the upper end. Heater temperatures (not shown) are reproduced with better success.

The rod did balloon and burst. The post-test gamma scan showed some fuel relocation but no marked dispersal. At the instant of calculation there was no quantitative information on the clad strain. FRAPTRAN-GENFLO result for maximum circumferential strain was 60%. The burst time was calculated correctly at 526 s after the blow-down. Due to the delayed heat-up, the duration of the experiment became so long that the test was terminated only 40 s after the clad burst.

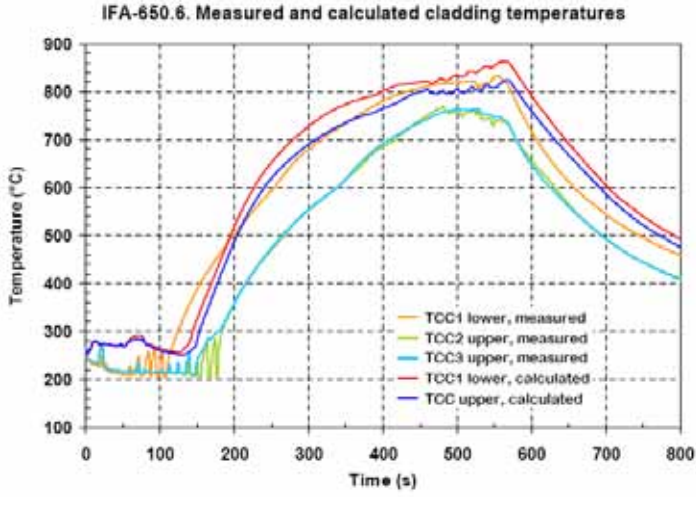

Figure 7.2.6. Cladding and heater temperatures in Halden IFA-650.6.

Conclusions

The integrated LOCA tests in the OECD Halden IFA-650 series have been successfully simulated. Use has been made of the VTT GENFLO and amended USNRC FRAPTRAN codes or their interactive combination. Dedicated nodalisation and code inputs have been generated to describe the many features of the test devise and conditions.

Results have been provided and used to make decisions on vital test parameter values before the conduct of each test, and to qualify and interpret the result in post-test calculation. In parallel, the exercise has supported development and validation of the more general FRAPTRAN-GENFLO version intended for power reactor applications.

An early by-result was attracting the attention of the community to the high importance on one hand, and the great difficulty on the other, to properly handle the bounding thermal hydraulic conditions in this seemingly simple test facility.

The FRAPTRAN-GENFLO development at VTT, the LOCA testing in Halden, and the interpretation and extrapolation of the test results over the world continue.

References

1. Wiesenack, W., Kekkonen, L. & Oberländer, B. Axial gas transport and loss of pressure after ballooning rupture of high burn-up fuel rods subjected to LOCA conditions. PHYSOR 2008; International Conference on the Physics of Reactors Interlaken Switzerland, September 14–19, 2008.

2. Miettinen, J. & Hämäläinen, A. GENFLO: A Thermal Hydraulic Solution for Accident Simulation. VTT Research Notes 2163, Espoo 2002. ISBN 951-38-6083-3. 75 p. + app. 4 p. http://www.vtt.fi/inf/pdf/tiedotteet/2002/T2163.pdf.

3. Miettinen, J. et al. Improvements in Transient Fuel Performance Modelling. In: SAFIR: The Finnish Research Programme on Nuclear Power Safety 2003–2006. Final Report. Pp. 69–78.

4. Knuutila, A. Improvements on FRAPCON3/FRAPTRAN mechanical modelling. Research Report VTT-11337-06, 29.11.2006. VTT Technical Research Centre of Finland, 96 p.

5. In: 7th International Conference on VVER Fuel Performance, Modelling and Experiment Support, Albena, Bulgaria, September 2007.

8. Tridimensional core transient analysis methods (TRICOT)

8.1 TRICOT summary report

Hanna Räty, Antti Daavittila and Anitta Hämäläinen
VTT

Dedicated to the memory of LicTech Jaakko Miettinen, 31.3.1947–7.8.2008.

Abstract

The fundamental objective of the project is to continue the development of the truly independent transient calculation system concentrating on three-dimensional reactor dynamics computer codes and thermal hydraulics models, which can be utilized by the safety authority and other end-users for safety analyses. During the first half of the SAFIR2010 programme, the main emphasis has been on the subtasks related to internal coupling of TRAB-3D neutronics and SMABRE hydraulics, and the development of the 3D thermal hydraulics model based on the porous medium approach. Participation in international work groups and benchmark activities has provided crucial support for the development work. Education of new experts has, as always, been a priority.

Introduction

VTT has developed its own dynamics calculation codes for independent safety analyses since 1970's during the predecessors of the SAFIR2010 research programme. The TRAB, TRAB-3D and HEXTRAN codes have been successfully used for transient analyses of BWRs, PWRs and VVERs in Finland and elsewhere, most

recently in the licensing process of the Olkiluoto-3 plant. To be state-of-the-art internationally the models of the codes must be constantly improved as the knowledge of physical phenomena and computer capabilities increase. Furthermore, new fuel and reactor designs, new loading strategies and the continuing trend towards higher fuel burnups make it necessary to further improve as well as validate the code system to be able to cope with the new challenges.

Main objectives

The fundamental objective of the project is to continue the development of the three-dimensional reactor dynamics computer codes (TRAB-3D and HEXTRAN) developed at VTT, especially in the area of thermal hydraulics. The goal is to have a truly independent transient calculation system, which can be utilized by the safety authority and other end-users for safety analyses that are independent from those of power plant designers and fuel vendors. To achieve this, the codes must be constantly developed in order to be on the same level as other codes used for similar purposes internationally.

In addition to the development work itself, it is essential that the new models are validated against measurements and the results of other codes. Much of this work can be done as international co-operation in the form of calculating benchmark problems. Another objective is to educate new experts to this field.

Internal coupling of TRAB-3D/SMABRE for PWR

The objective of subtask TRAB-3D/SMABRE of SAFIR2010/TRICOT project is to improve thermal hydraulics in the reactor dynamics computer code, TRAB-3D, by coupling it internally to the SMABRE code. TRAB-3D [1] is a reactor dynamics code with three-dimensional neutronics and one-dimensional thermal hydraulics in a core and in a BWR circuit. The code can be used for transient and accident analyses of boiling (BWR) and pressurized water (PWR) reactors. The system code SMABRE [2] models the thermal hydraulics of light water reactors. Both codes have been entirely developed at VTT.

Main advantages of the internal type of coupling are possibilities to handle coolant flow reversals in core flow channels as well modeling cross flows in an open reactor core like EPR. Also the porous media model could be coupled for the thermal hydraulics to simulate 3-dimensional hydraulics. On the other hand, the possibility of describing flow 3-dimensionally in the core demands renewal of hot channel concept.

The basics for internal coupling were created for BWRs in the EMERALD project as a part of the SAFIR-Programme [3, 4, 5]. In TRICOT, the work has continued for the PWR [6]. The internal coupling of TRAB-3D and SMABRE needed large modifications and new modules especially in SMABRE, which should still have all the old calculation capabilities with parallel coupling intact.

Up to now, the main features of coupling have been performed mainly by the SMABRE developer who passed away recently. This unexpected and unfortunate accident has forced the studies to new paths. The status of the different code versions has been studied and identification of modifications leading to deviating results in traditional parallel coupling has been performed and comparison of the coupling types has been started.

Internal coupling of TRAB-3D/SMABRE

In internal coupling TRAB-3D performs the neutronics calculation, SMABRE will take care of the hydraulics calculation of the whole cooling circuit including the reactor core, and the heat transfer calculation may be carried out by either code by the user's choice. Whereas in parallel coupling TRAB-3D performs the core hydraulics and heat transfer, and the coarse SMABRE core hydraulics with fewer channels are solved in parallel.

At the beginning, SMABRE was adapted to modeling of large number of flow channels resulting in shorter calculation time than in the original solution. Secondly, several TRAB-3D models were made available through SMABRE in internal coupling.

In SMABRE the thermal hydraulics is solved by a matrix inversion, and for each neutronic time step only one thermohydraulic time step is needed. The phase separation is solved by using the drift flux model. The wall friction between the two-phase mixture and wall is calculated by using the mixture loss formulation. In TRAB the phase separation is calculated by using the slip model using separate slip correlations. The wall friction for the two-phase mixture is calculated from the combination of the single phase friction for the total mass flow and the two-phase multiplier. SMABRE and TRAB-3D models are available by defining user options.

SMABRE's heat transfer model was supplemented to take into account different characteristics for different fuel types, and by including models from TRAB-3D for heat conductivities, capacities and gas gap heat transfer. Also the number of radial mesh points in fuel pellet was increased to what is typically used in TRAB-3D.

Next steps in development are modeling of the heavy reflector around the core, the option to connect several fluid channels with one fuel assembly, and vice versa, the option to couple several fuel assemblies with one fluid channel. The simultaneous development with the high pressure light water reactors, HPLWR, generates useful cross-checking possibilities and an application for internal coupling.

Comparison of TRAB-3D/SMABRE coupling types

For comparing the couplings in PWR, the plant model, consisting of whole primary loop of EPR and secondary loop from the feedwater tank to the turbine valves have been used. The EPR reactor core with 241 hydraulic channels and 20 axial core nodes has been modeled and a typical PWR fuel is used in comparisons.

For these comparisons nominal primary pressure of the steady state has been increased slightly. As a dynamic test case a pump seizure transient has been performed with different coupling types, code versions and with SMABRE or TRAB-3D heat transfer options. Some results of comparisons are depicted in the figures. Figure 8.1.1 shows the ratio of core inlet mass flow distribution in the core channels and the radial power distribution between the internal and parallel coupling. The flow distribution is calculated by two different models, by TRAB-3D hydraulics in parallel coupling and SMABRE hydraulics in internal coupling. The power distribution is always calculated by TRAB-3D neutronics, and the differences results from different thermal hydraulic models and the coupling itself. The differences are very small.

For the parallel coupling with the old and new code versions, the distributions of the core parameters are even better, as it should be. During the transient, also the main parameters in the primary and secondary circuit are equal in comparing parallel coupling between old and new code versions. This is shown in Figure 8.1.2, where total core mass flow and maximum of channel outlet equilibrium quality is presented. (Note that in internal coupling the outlet equilibrium quality is calculated in the midpoint of the last node and in parallel coupling half a node later, at node boundary). The results from internal and parallel coupling deviate during the transient. The differences are not large and may be result from used options, for example the effect of SMABRE and TRAB heat transfer options on results, or from the internal coupling itself. Research continues with testing the new options and validation, which is nessessary after large code modifications.

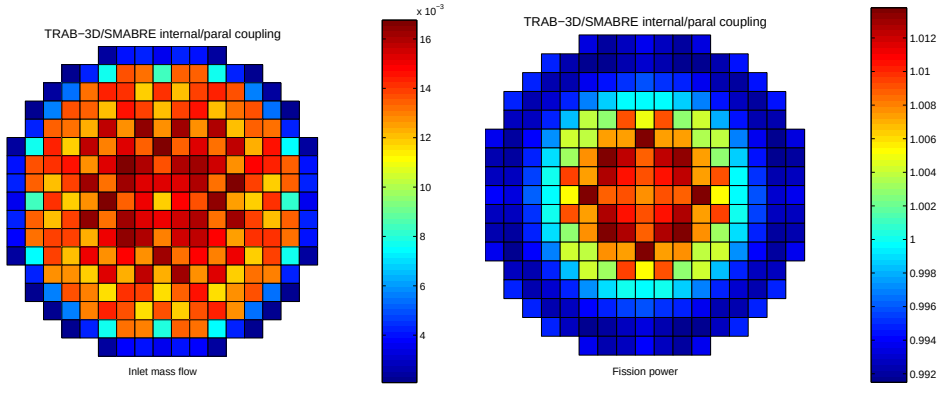

Figure 8.1.1. Steady state bundle flow at core inlet and fission power distribution calculated by TRAB-3D-SMABRE with internal coupling relative to distribution with parallel coupling.

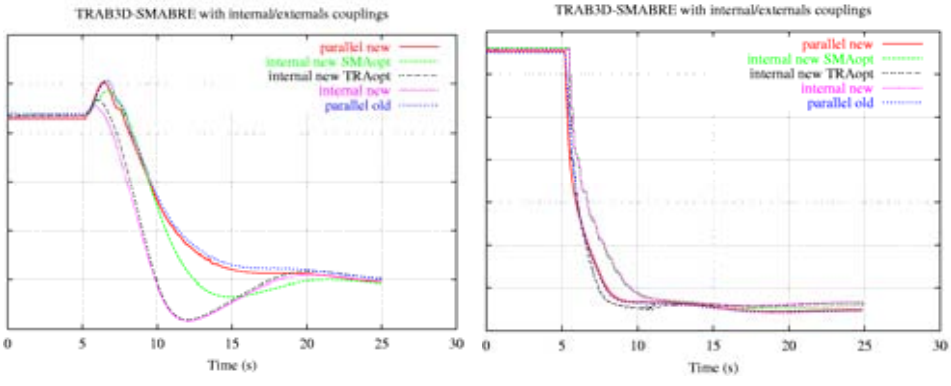

Figure 8.1.2. Total core mass flow and maximum of channel outlet equilibrium quality in pump seizure transient with two coupling types, old and new code versions and with SMABRE and TRAB sets of heat transfer options.

TRAB-3D Validation through comparisons with TRACE/PARCS

In addition to VTT's own TRAB-3D reactor dynamics code that has been developed in the previous research programmes, VTT has the possibility to use the thermal hydraulics and system simulating computer code TRACE [7], which is presently the main tool endorsed by the NRC for nuclear reactor analysis. Concerning 3D neutronics calculations, TRACE now includes the Purdue Advanced

Reactor Core Simulator (PARCS [8]) as an integral part (a static library) of the TRACE package.

The availability of TRACE/PARCS opens new possibilities for TRAB-3D validation. Exactly the same problems can now be calculated with two computer codes by a single user, and input files directly compared by the same user, in order to minimize the modeling differences. Fortunately, the developers of both codes have participated in the same OECD NEA benchmark activities, and ready input data exists for some cases. Besides TRAB-3D validation, this work is motivated by getting familiar with and gaining some experience on TRACE/PARCS 3D transient calculations. TRACE has probably a significant role as an independent analysis tool for the regulator STUK in future.

Three cases were calculated with both TRAB-3D and TRACE/PARCS in 2007 [9]. Two were OECD NEA core transient cases (NEACRP A1 and C1), the third being the OECD NEA PWR MSLB exercise 2 separate core calculation. At this point the work was concentrated on separate core transients, because analysing the differences in plant models is a much more difficult task than comparing core models.

As an example of the comparison calculations, Figure 8.1.3 shows the time behaviour of fission power during the PWR MSLB transient. The case concerns a main steam line break (MSLB) at the TMI-1 nuclear power plant with one stuck control rod during the reactor scram. The cross section data was modified for the exercise in such a way that the return to fission power after the scram was ensured. The TRAB-3D calculation was performed with both 18 and 177 core thermal hydraulic channels, for TRACE 18 channels was used. The difference in reactor power at the point of the power maximum after the reactor scram is shown in Figure 8.1.4.

As an overall conclusion, it could be said that the 3D nodal neutronic model is not a significant source of uncertainty in transient analysis. The uncertainties and modeling options of thermal hydraulic details cause much larger deviations. For boiling water reactors thermal hydraulics play an essential role already in the reactor core, but the real differences come largely from plant modeling.

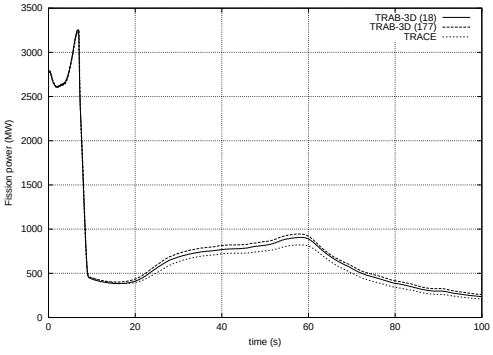

Figure 8.1.3. Power vs time during the PWR MSLB transient.

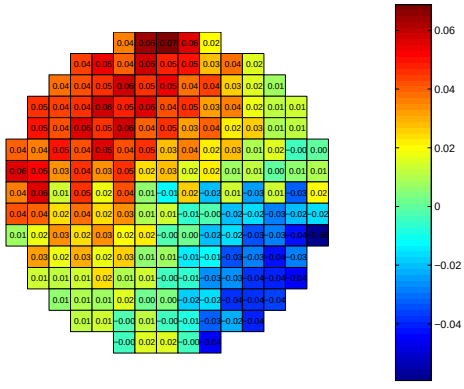

Figure 8.1.4. Power at the maximum after scram, TRAB-3D 18 channels vs. TRACE.

Uncertainty analysis

In the previous research programme the first version of a new sensitivity and uncertainty analysis tool for reactor dynamics codes was developed and tested with HEXTRAB-SMABRE [10]. The tool has now been updated for use with TRAB-3D/SMABRE calculations, as well as for series of hot channel and DNB calculations with the one-dimensional TRAB-CORE code. The usability of the tool has been improved and it is now more versatile for the management of large amount of reactor dynamics calculations. [11, 12]

The tool generates input data, performs calculations and calculates some statistical sensitivity measures, e.g. rank correlation coefficients and tolerance intervals for the output variables of reactor dynamic codes. The sensitivity analysis of output variables has also been added to the TRAB-CORE calculations.

As an example the tool was in 2008 applied to analyses of a worst leak size for a MSLB accident in a VVER. [12]

The sensitivity and uncertainty analysis tool will be developed and tested further towards practical application in safety analyses and capability to answer the requirements posed by the safety authority. Especially the interface to the fuel performance calculations will be developed.

Three-dimensional core hydraulics

The objective of this subproject is to develop methodology for 3D two-phase thermal-hydraulic modeling of the nuclear reactor core. The used porous medium approach is CFD-like, but does not use calculation mesh fitted to the structures. Instead, the fluid volumes of the mesh cells are described as porosity (volume not filled by structure). It is hoped that with this approach, it will be easier to create models, and calculation will be faster than with actual CFD [13, 14].

In PORFLO, the basic features of the computer code include assumption of porous medium, description of the problem in three-dimensional Cartesian coordinates and the use of either the five-equation model (with a mixture momentum conservation equation) or the six-equation model for the solution of the two-phase flow problem. The most important development steps made during 2008 were: the implementation of the six-equation model to PORFLO and the development of new iterative linear solvers and preconditioning methods for the solution of the pressure correction equations of both the five-equation SIMPLE algorithm and the newly developed (six-equation) Phase-Coupled SIMPLE algorithm.

Preliminary simulations of one of the NUPEC (**Nu**clear **P**ower **E**ngineering **C**orporation) BFBT (**B**WR **F**ull-size Fine-mesh **B**undle **T**ests) benchmark steady-state exercises were performed on a BWR (8×8) fuel bundle with a central water rod using the five-equation SIMPLE algorithm of PORFLO, as a transient simulation. A more detailed description on this subtask is presented as the special report of TRICOT in this interim report.

International research co-operation

Participation in the OECD Nuclear Energy Agency (NEA) working groups and benchmarks [15] is one of the most important ways of validating the methods and codes used in reactor analysis. This project will include the participation in the meetings of the NEA Working Party on the Scientific Issues of Reactor Systems (WPRS), which is responsible for the organization of the reactor dynamics benchmarks among other activities. VTT participates to the OECD/NEA Uncertainty analysis benchmark series (UAM) and to the fuel bundle benchmark (BFBT). The cooperation and information exchange on VVER safety within the AER framework together with other countries that use

VVER reactors will also be continued. In addition, young scientists have participated in international training courses.

Applications

The three-dimensional reactor dynamics codes TRAB-3D and HEXTRAN have been used for independent safety analyses of Finnish and foreign nuclear power plants. This project ensures the constant development of the codes, so that they will remain on the high, internationally recognized level. The whole calculation system, which also includes the reactor physics and fuel performance analysis tools, can be used for research as well as the needs of the safety authorities and power utilities in order to ensure safe and economic use of the nuclear power plants. The three-dimensional flow model for open core geometry will be especially well suited to analyses of western pressurized water reactors, such as the EPR.

Conclusions

During the years 2007 and 2008, significant progress has been made on all subtasks of the TRICOT project. The unexpected death of the main developer of the SMABRE and PORFLO codes resulted in serious challenges to the goals of the project, but the project staff has recovered well from the loss. Comparison analyses of different TRAB-3D/SMABRE coupling types show good results for pressurized water reactors. In the TRAB-3D validation subtask the United States Nuclear Regulatory Commission’s TRACE/PARCS computer code has been taken into use at VTT and first analyses performed, with results showing that the core modeling does not cause significant deviation between codes. Uncertainty analyses tools have been further updated, but the main progress of this subtask will take place later, due to personnel issues. The development of the 3D porous medium solver PORFLO has succeeded in creating a new computer code capable of e.g. calculating boiling water reactor fuel bundle internal void fraction distribution. This opens up totally new possibilities in 3D thermal hydraulics analyses of nuclear reactors.

References

1. Kaloinen, E. & Kyrki-Rajamäki, R. TRAB-3D, a New Code for Three-Dimensional Reactor Dynamics. In: 5th International Conference on Nuclear Engineering (ICONE-5). Nice, France, 26–30 May, 1997 [CD-ROM]. New York: the American Society of Mechanical Engineers. Paper ICONE5-2197. ISBN 0-79181-238-3.

2. Miettinen, J. Thermohydraulic model SMABRE for light water reactor simulations. Licentiate's thesis. Helsinki University of Technology, Department of Engineering, Physics and Mathematics, 2000. 151 p.

3. Miettinen, J. & Räty, H. Status of the EMERALD subtask for coupling of TRAB-3D and SMABRE. Project Report PRO1/P7037/03, VTT Processes, 31.12.2003. 6 p.

4. Miettinen, J. & Räty, H. The coupled code TRAB-3D-SMABRE for 3D transient and accident analyses. In: Räty, H. & Puska, E.K. (Eds.). SAFIR, The Finnish Research Programme on Nuclear Power Plant Safety 2003–2006, Final Report. Espoo: VTT Technical Research Centre of Finland, 2006. (VTT Research Notes 2363.) Pp. 48–59. ISBN 951-38-6886-9; 951-38-6887-7. ISSN 1235-0605. http://virtual.vtt.fi/inf/pdf/tiedotteet/2006/T2363.pdf.

5. Miettinen, J. & Räty, H. Status of the EMERALD subtask for coupling of TRAB-3D AND SMABRE. Project Report VTT-R-00982-06, VTT, 1.2.2006. 9 p.

6. Miettinen, J., Hämäläinen, A. & Räty, H. Status of internal coupling of TRAB-3D and SMABRE for PWR core. VTT Research report VTT-R-00718-08. Espoo, 2008.

7. TRACE V5.0 User's Manual, United States Nuclear Regulatory Commission, 2007.

8. PARCS v.2.6 User Manual, DRAFT (11/10/04), Purdue University, 2004.

9. Daavittila, A. TRAB-3D Validation through comparison calculations with TRACE/PARCS. Espoo: VTT Technical Research Centre of Finland, 2008. Research Report VTT-R-00124-08. 24 p.

10. Syrjälahti, E. New sensitivity analysis tool for the reactor dynamic codes. Espoo: VTT Technical Research Centre of Finland, 2005. Project Report PRO1/1016/05. 15 p.

11. Syrjälahti, E. Development of sensitivity and uncertainty analysis tool for reactor dynamics codes. Espoo: VTT Technical Research Centre of Finland, 2008. VTT Research Report VTT-R-00843-08. 15 p.

12. Syrjälahti, E. Preliminary main steam line break calculations with HEXTRAN/ SMABRE utilising the sensitivity analysis tool. Espoo: VTT Technical Research Centre of Finland, 2008. Research Report VTT-R-05475-08. 9 p.

13. Hovi, V. Calculations of Boiling Two-Phase Flow Using a Porous Media Model. Espoo: VTT Technical Research Centre of Finland, 2008. Research Report VTT-R-04858-08. MScTech thesis, Lappeenranta University of Technology. 112 p.

14. Miettinen, J. & Ilvonen, M. Solving porous media flow for LWR components. In: 15th International conference on Nuclear Engineering (ICONE-15). April 22–28, 2007. Nagoya, Japan. [CD-ROM]. Japan: Japanese Society of Mechanical Engineers (JSME), 2007. Paper ICONE-15-10291. 9 p. ISBN 978-4-88898-159-0.

15. Seppälä, M. HEXTRAN-SMABRE calculation of the VVER-1000 Transient benchmark, Main steam line break. Espoo: VTT Technical Research Centre of Finland, 2007. VTT Research report VTT-R-08573-07. 17 p. + app. 7 p.

8.2 The porous medium model PORFLO for 3D two-phase flow and its application to BWR fuel bundle simulations

Mikko Ilvonen and Ville Hovi
VTT

Abstract

This presentation describes the current status of the PORFLO code and the latest developments made in the second subtask of the SAFIR2010/TRICOT project. The present work is a continuation of the corresponding previous SAFIR project.

In PORFLO, the basic features of the computer code include assumption of porous medium, description of the problem in Cartesian coordinates and the use of either the five-equation model (with a mixture momentum conservation equation) or the six-equation model for the solution of the two-phase flow problem. The most important development steps made during 2008 were: the implementation of the six-equation model to PORFLO and the development of new iterative solvers and preconditioning methods for the solution of the pressure correction equations of both the five-equation SIMPLE algorithm and the newly developed (six-equation) Phase-Coupled SIMPLE algorithm. As a result of the new iterative solvers and preconditioning methods the computation time has been reduced almost by an order of magnitude.

Introduction

Three-dimensional calculation of a boiling two-phase flow in complex geometry is a very challenging task, to which no completely satisfactory solution has been found so far. As a result, several methods with varying numbers of conservation equations and various solution strategies have been proposed.

The development of a three-dimensional porosity model for the modeling of two-phase phenomena was started at VTT with the objective to be able to model the components of nuclear power plants, such as isolation condensers, while avoiding the need for a large and fine mesh or having to accurately describe the often quite complex geometry of the components. In other words: a compromise between the approaches taken in commercial CFD codes, which are often CPU time intensive when applied to complex geometries, and one-dimensional system codes, which are fast but cannot be accurately applied to three-dimensional simulations, was made. The model that was developed, originally by Jaakko Miettinen, is known as PORFLO.

PORFLO

As opposed to the common practice in CFD, in which the domain is split into nodes whose boundaries conform to the interfaces between solid structures and fluid, in PORFLO, the computational grid is orthogonally divided into rectangular hexahedra, regardless of the interfaces between solid and fluid; this is known as the concept of porous medium, in which the fraction of the total volume occupied by the two-phase fluid is defined as porosity, $\varepsilon = V_{\text{fluid}} / V_{\text{total}}$. The orientation of the grid is chosen so that the axes of the 3D Cartesian coordinate system are perpendicular to the faces of the hexahedra. The solution of the governing equations is then performed in the directions of the Cartesian coordinate system. The velocities on node faces are solved on a staggered grid arrangement.

There are currently two alternative strategies available for the solution of the flow problem in PORFLO: methods based on the five-equation model and a method based on the six-equation model, the Phase-Coupled SIMPLE algorithm [1]. These alternatives are presented briefly in the following sections.

The methods based on five-equation model in PORFLO

In the five-equation model, the two-phase flow problem is described with five equations: continuity equations written for both phases, momentum equation written for the mixture of the two phases and enthalpy equations written for both phases. The interaction between the phases, phase separation, is governed by an empirical correlation, the Zuber-Findlay drift-flux model.

The continuity equations are given through

$$\begin{aligned} &\text{liquid}: && \frac{\partial\left[(1-\alpha)\rho_{\text{l}}\right]}{\partial t} + \nabla\cdot\left[(1-\alpha)\rho_{\text{l}}\mathbf{u}_{\text{l}}\right] = -\gamma \\ &\text{vapor}: && \frac{\partial\left(\alpha\rho_{\text{g}}\right)}{\partial t} + \nabla\cdot\left(\alpha\rho_{\text{g}}\mathbf{u}_{\text{g}}\right) = +\gamma \end{aligned} \tag{8.2.1}$$

where t is time [s], $\mathbf{u}_{\text{g}}$ is vapor velocity [m/s], $\mathbf{u}_{\text{l}}$ is liquid velocity [m/s], α is void fraction [-], ρ_{g} is vapor density [kg/m^3], ρ_{l} is liquid density [kg/m^3] and γ is evaporation / condensation rate per unit volume [kg/m^{3}s].

The momentum equation is written for the mixture of phases:

$$\frac{\partial\left(\rho_{\text{m}}\mathbf{u}_{\text{m}}\right)}{\partial t} + \nabla\cdot\left[\left(\rho_{\text{m}}\mathbf{u}_{\text{m}}\right)\otimes\mathbf{u}_{\text{m}}\right] = -\nabla p + \nabla\cdot\mathbf{T} + \rho_{\text{m}}\mathbf{g} + \mathbf{F} \tag{8.2.2}$$

where **F** is the sum of body forces per unit volume [N/m^3], **g** is acceleration of gravity [m/s^2], p is pressure [Pa], **T** is the surface stress tensor [N/m^2], $\mathbf{u}_m$ is mixture velocity [m/s] and ρ_m is mixture density [kg/m^3].

The enthalpy equations for liquid and vapor, respectively, can be expressed as

$$\begin{aligned} &\text{liquid}: && \frac{\partial\left[(1-\alpha)\rho_l h_l\right]}{\partial t} + \nabla\cdot\left[(1-\alpha)\rho_l h_l \mathbf{u}_l\right] = q'''_{wl} + q'''_{lg} \\ &\text{vapor}: && \frac{\partial\left(\alpha\rho_g h_g\right)}{\partial t} + \nabla\cdot\left(\alpha\rho_g h_g \mathbf{u}_g\right) = q'''_{wg} - q'''_{lg} \end{aligned} \tag{8.2.3}$$

where h_g vapor enthalpy [J/kg], h_l liquid enthalpy [J/kg], q'''_{lg} heat transfer rate from liquid to vapor per unit volume [W/m^3], q'''_{wg} heat transfer rate from wall to vapor per unit volume [W/m^3] and q'''_{wl} heat transfer rate from wall to liquid per unit volume [W/m^3].

Pressure-velocity coupling

The two alternative solution strategies, the five and the six-equation models, have no bearing on the technique, with which the set of governing equations solved; instead they can be viewed as a common denominator for the approach taken to tackle the flow problem. The solution methods, or techniques, can be divided into two categories, direct methods and iterative methods, depending on the coupling of pressure and velocities.

Direct method

In the direct method implemented in PORFLO the mixture momentum equations are combined with the mixture continuity equations to provide a system of equations for pressure. Once the pressure field is solved the velocity field is obtained explicitly from the pressure field. The pressure field is solved only once during each time step. One of the benefits of direct methods is the amount of computations compared to iterative methods. One of the shortcomings, however, is that some of the terms of the momentum equations have to be treated explicitly to accommodate the solution of the resulting system of equations, which increases the explicitness of the overall solution procedure, even if fully implicit discretization was used to discretize the governing equations.

Iterative methods based on the SIMPLE family of algorithms

In iterative methods, the pressure and velocity fields are coupled indirectly, usually by devising a correction that is applied for the pressure or velocity fields, or both. The SIMPLE algorithm, Semi-Implicit Method for Pressure Linked Equations [2, Section 6.7, pp. 126–131], which is an iterative method, uses the mixture momentum and mixture continuity equations to derive a set of equations for the pressure corrections, which are then used to correct the pressure and velocity fields. The use of a correction leads to an iterative procedure where the conservation equations and pressure correction equations are solved, and the corrections are applied, consecutively during each iteration until the solution of the current time step has converged.

Iterative methods usually require more computations than direct methods, but on the other hand, fully implicit discretization can be applied to the momentum equations and even the convective terms can be included. There are three different variants from the SIMPLE-family of algorithms available in PORFLO: SIMPLE, SIMPLEC or SIMPLE-Consistent [3, Section 6.7, p. 193] and SIMPLER or SIMPLE-Revised [2, Section 6.8, pp. 131–134].

The sequence of the solution procedure with the five-equation model

The sequence of the solution procedure using the five-equation models implemented in PORFLO is presented in Figure 8.2.1. The solution procedure is similar in both the direct method and iterative methods implemented in PORFLO, with the exception that all the steps of the solution can be performed inside the iteration loop of the iterative methods.

The method based on six-equation model in PORFLO

In the six-equation model the two-phase flow problem is fully described; the continuity, momentum and enthalpy equations are written for both phases. The interaction between the phases is modeled with interphase force terms, such as interphase friction force and momentum transfer due to mass transfer. In general, the six-equation model facilitates mechanistic modeling to a greater extent than the five-equation model, but at the same time the interaction terms need to be modeled accurately to achieve realistic phase separation. The continuity equations, in Equation (8.2.1), and enthalpy equations, in Equation (8.2.3), remain the same as in the five-equation model presented in the subsection above, but the momentum equations are written for both phases instead.

Liquid momentum equation is expressed through

$$\frac{\partial\left[(1-\alpha)\rho_l \mathbf{u}_l\right]}{\partial t} + \nabla\cdot\left\{\left[(1-\alpha)\rho_l \mathbf{u}_l\right]\otimes \mathbf{u}_l\right\} = -(1-\alpha)\nabla p + \nabla\cdot\mathbf{T} + (1-\alpha)\rho_l \mathbf{g} + \mathbf{F}_{PC} + \mathbf{F}_{IF} + \mathbf{F} \qquad (8.2.4)$$

and vapor through

$$\frac{\partial\left(\alpha\rho_g \mathbf{u}_g\right)}{\partial t} + \nabla\cdot\left[\left(\alpha\rho_g \mathbf{u}_g\right)\otimes \mathbf{u}_g\right] = -\alpha\nabla p + \nabla\cdot\mathbf{T} + \alpha\rho_l \mathbf{g} - \mathbf{F}_{PC} - \mathbf{F}_{IF} + \mathbf{F} \qquad (8.2.5)$$

where $\mathbf{F}_{IF}$ is the interphase friction force [N/m^3], $\mathbf{F}_{PC}$ is the momentum transfer due to phase change [N/m^3] and $\mathbf{F}$ is the rest of the force terms (such as friction) [N/m^3].

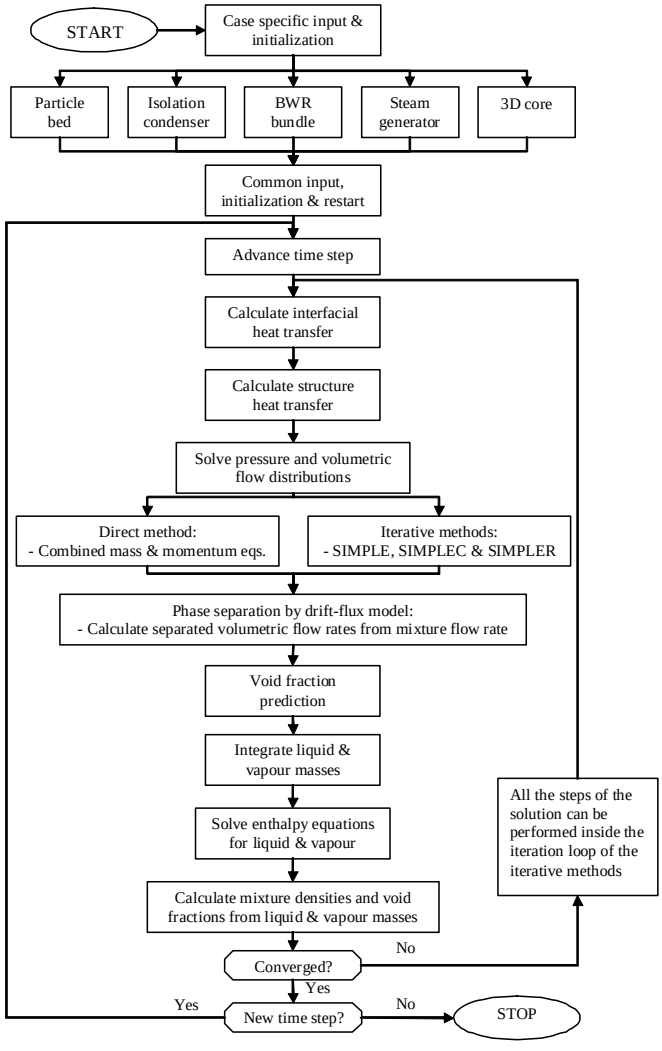

Figure 8.2.1. Solution procedure using the five-equation models.

The Phase-Coupled SIMPLE algorithm

The Phase-Coupled SIMPLE algorithm [1] is an extension of the SIMPLE algorithm to two-phase flows. The solution procedure is similar to the original SIMPLE algorithm, with the exception that the momentum equations are solved for both the vapor and liquid phases in the beginning of the iteration loop, and that the pressure correction equations contain correction terms caused by both of the two phases.

The solution procedure using the Phase-Coupled SIMPLE algorithm is presented in Figure 8.2.2. Heat transfer and enthalpy equations are solved, and material properties are updated, within the SIMPLE iteration loop, which increases the risk of divergent behavior, but decreases the computation time, since the solution of the other transport equations is cheap compared to the pressure correction equations.

Iterative linear solvers and preconditioning methods

Progress was made in the development and implementation of iterative linear solvers, intended for the solution of linear systems of equations arising from the solution procedures, in the fall of 2008. Two iterative solvers, Conjugate Gradient method (CG) and Bi-Conjugate Gradient method (BiCG), belonging to the Krylov subspace methods, were implemented in PORFLO as an extension to the existing Conjugate Gradient Squared method (CGS). Special attention was paid to suitable preconditioning methods for each solver, since the choice of the preconditioning method is often more significant than the choice of the iterative solver itself.

The conjugate gradient method was chosen for its capability to solve symmetric systems of equations, with fewer computations per iteration compared to other Krylov subspace methods (roughly half compared to BiCG and CGS). In addition, CG has been proven to be quite efficient and comparatively robust when suitable preconditioning has been applied. The only shortcoming of the conjugate gradient method is its inability to solve asymmetric systems of equations, momentum equations for instance; therefore its application is limited to the pressure equation of the SIMPLER algorithm and the pressure correction equations of the SIMPLE-family of algorithms at the moment.

Successive Symmetric Over-Relaxation (SSOR) was chosen as the preconditioning method to be used together with the conjugate gradient method. Quite promising results were obtained using this combination; the computation time required for a single iteration of the Phase-Coupled SIMPLE algorithm was reduced 76% compared to the un-preconditioned version of the conjugate

gradient method. A reduction of 86% was achieved compared to the solver based on Gaussian elimination, which was until recently the only solver capable of solving the pressure correction equations.

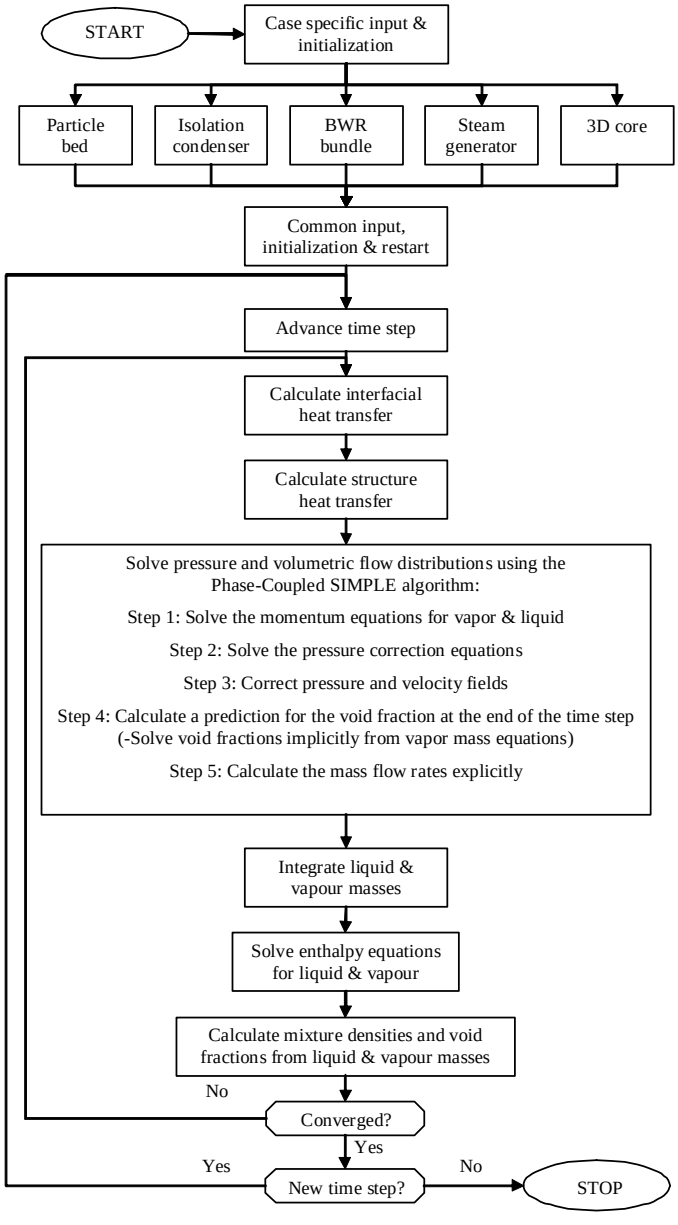

Figure 8.2.2. Solution procedure using the Phase-Coupled SIMPLE algorithm.

BiCG was the second new solver that was implemented in PORFLO, mainly for its capability to solve both asymmetric and symmetric systems. The un-preconditioned version of BiCG was completed, but in order to achieve significant reductions in the computation time, a suitable preconditioning method needs to be introduced into the algorithm. Successive Over-Relaxation (SOR) can be applied to BiCG without a significant increase in the amount of computations needed to perform a single iteration, which makes it a prime candidate for future development.

Simulations

Preliminary simulations of one of the NUPEC (**Nu**clear **P**ower **E**ngineering **C**orporation) BFBT (**B**WR **F**ull-size Fine-mesh **B**undle **T**ests) benchmark steady-state exercises were performed on a BWR (8×8) fuel bundle with a central water rod using the five-equation SIMPLE algorithm of PORFLO, as a transient simulation. System pressure was set at 6 MPa, total heating power at 3.52 MW, inlet mass flux at 1500 kg/m^{2}s and inlet enthalpy at 1100 kJ/kg. The domain was split using a nodalization of (83×83×36), which amounts to approximately 250 000 nodes. The steady state results, in Figures 8.2.3 and 8.2.4, where obtained at the end of a 9.5 s transient. The computation time spent on a single core of a 2.992 GHz quad-core processor was 25 days. The friction was set uniform over the whole domain during the preliminary simulations.

Discussion of simulation results

The velocity profiles, in Figure 8.2.3, are qualitatively correct: maximum velocities of mixture, liquid and vapor are located in the middle of the hottest channels, and there is a distinct difference between the velocities of hotter and colder channels. The vertical slip velocity, the velocity difference between vapor and liquid, corresponds nicely with the void fraction distribution, in Figure 8.2.4.

In a situation where the friction caused by the fuel rods is uniform over the cross section of the bundle, the fact that there is a local minimum of void fraction in the middle of the channels where the maximum velocities are located raises doubt. This might partly be due to the fact that vapor is generated on the heated surfaces; when a horizontal cross section of the fuel bundle is considered, roughly the following forces in the vertical direction, in Equation (8.2.2), need to be balanced: the pressure gradient, the weight of the fluid column, friction caused by the fuel rods and the force needed to accelerate the fluid when fluid

volume is increased by evaporation. The weight of the fluid column is smallest near the heated surfaces and increases towards the centers of the channels, since void fraction decreases towards the centers of the channels. The friction caused by the fuel rods is relative to dynamic pressure, $\frac{1}{2}\rho_{\mathrm{m}}v_{\mathrm{m}}^{2}$, and hence increases towards the centers of the channels, the same as velocities.

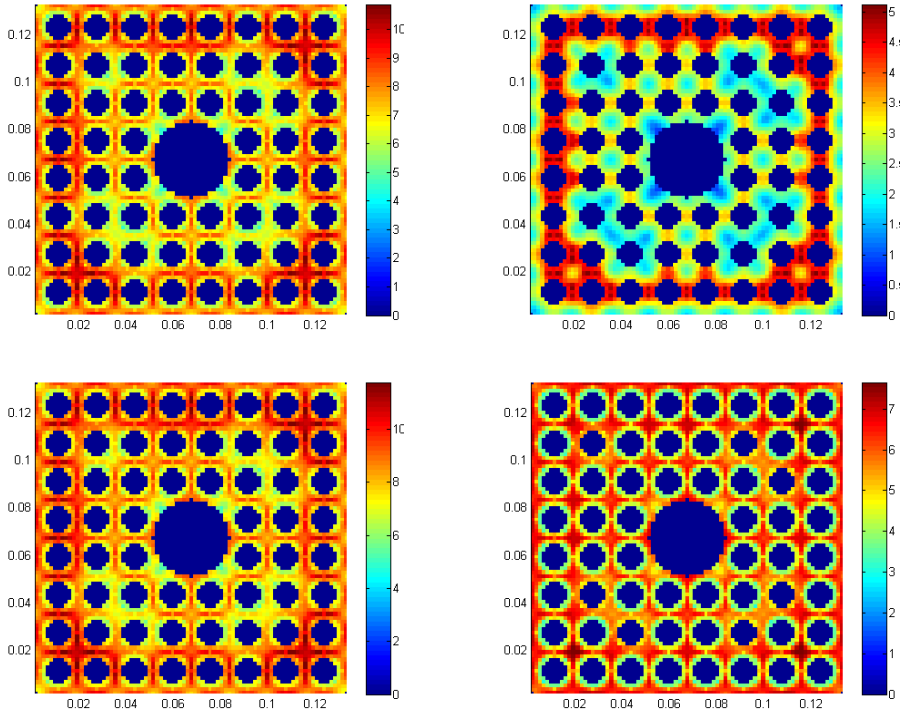

Figure 8.2.3. Vertical velocities at outlet [m/s]: mixture velocity (upper left), slip velocity (upper right), vapor velocity (lower left) and liquid velocity (lower right).

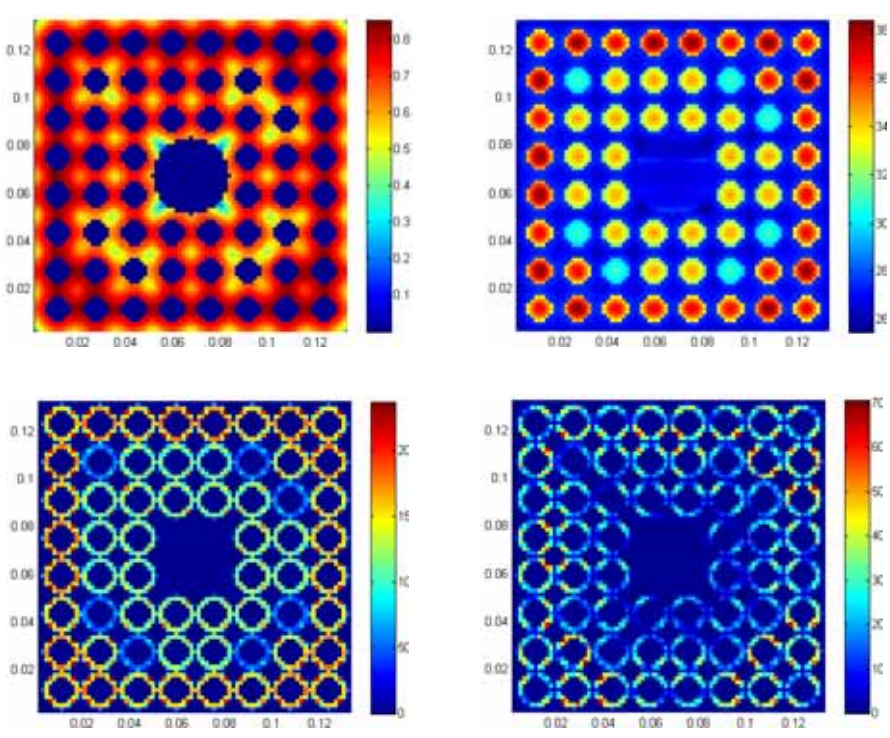

Figure 8.2.4. Contours of various parameters at outlet: void fraction [-] (upper left), temperature [°C] (upper right), volumetric heat flux for vapor generation [W/m^3] (lower left) and volumetric heat flux for liquid heating [W/m^3] (lower right).

While volume is constantly being created on the surfaces of the fuel rods, the fluid is either being accelerated near the heated surfaces or directed towards the center of the channel to preserve continuity, but since the driving force of the flow, the pressure gradient, is almost uniform over the cross section of the bundle, the pressure gradient cannot provide the force needed to accelerate the fluid; instead the fluid flows slower near the heated surfaces and thus the force needed to accelerate the fluid is compensated by a decrease in the friction caused by the fuel rods.

Conclusions

The results of the five-equation SIMPLE algorithm are quite realistic apart from the horizontal distribution of void fraction: since the drift-flux model acts as diffusion in the horizontal direction and only disperses and smoothes the

distribution, the location of the maximum void fraction will always be where it is formed – on the heated surfaces.

The development of the Phase-Coupled SIMPLE algorithm will be continued by improving the features that have been implemented, the interphase forces in particular, and by adding more features, such as the handling of lift forces and virtual mass forces. With careful consideration of the interphase force terms a more realistic void fraction distribution can be achieved.

In addition to the above, development of a basic turbulence model (k-ε) and parallelization of the code have been proposed. The work done on the iterative linear solvers and preconditioning methods will be continued, as well, to further decrease the computation time and facilitate the use of finer grids.

References

1. Vasquez, S.A. & Ivanov, V.A. A phase coupled method for solving multiphase problems in unstructured meshes. In: Proceedings of ASME FEDSM'00: ASME 2000 Fluids Engineering Division Summer Meeting. Boston, Massachusetts, June 11–15, 2000. Pp. 743–748.

2. Patankar, S.V. Numerical Heat Transfer and Fluid Flow. Hemisphere Publishing Corporation, 1980. 197 p. ISBN 0-89116-522-3

3. Versteeg, H.K. & Malalasekera, W. An Introduction to Computational Fluid Dynamics: The Finite Volume Method, Second Edition. Harlow: Pearson Education Limited, 2007. 503 p. ISBN 978-0-13-127498-3.

9. Total reactor physics analysis system (TOPAS)

9.1 TOPAS summary report

Petri Kotiluoto
VTT

Abstract

The purpose of the TOPAS project has been to maintain and develop stationary reactor physics code system, covering a wide range of calculation needs. Main results have been the development of a new Monte Carlo code Serpent, advanced methods for burnup calculations, and the development of sensitivity and uncertainty analysis methods. There has also been a strong interest in educating new competent people to work in field of reactor physics and nuclear safety. Several university degrees have been taken during the first two years of the project, and the educational objectives have been well fulfilled. International co-operation has also been active. The results of the project will serve the needs of both the safety authorities and the power utilities.

Introduction

Together with the reactor dynamics codes, the stationary reactor physics code system has to cover the whole range of calculations, from handling of basic nuclear data, i.e. cross section libraries, over fuel and core analyses in normal operating conditions to transient and accident studies using coherent models and methods. It should be possible to follow the whole life cycle of the nuclear fuel from a reactor physics point of view until its final disposal. The same or similar models can often

be used in both the static and the dynamic calculations. Additionally, it is of utmost importance to maintain competence and train new personnel in today's situation, when the use of nuclear power is increased at the same time as the present generation of nuclear experts is gradually retiring from work. Co-operation with the technical and other universities is necessary to make new students interested in this branch of science and thus ensure that the nuclear plants in Finland will be in the hands of competent people in the future, too. The tasks of the project have provided excellent possibilities for university students to perform work for their academic degrees.

Main objectives

The objective of the project has been to further develop VTT's computer code system for reactor analysis into a unified, up-to-date and sufficiently complete entirety in order to make it possible to perform all analyses that are needed in Finland in the field of nuclear reactor physics. It should be possible to follow the whole life cycle of the nuclear fuel from a reactor physics point of view. Especially the demands of new nuclear fuel designs and the new Finnish nuclear power plant have to be taken into account. The project also includes international co-operation and the education of new experts in nuclear reactor technology.

Main results

The work has been devided into five subprojects, which deal with nuclear cross sections, development and validation of nodal methods, Monte Carlo and other radiation transport methods, criticality safety and isotopic concentrations, and development of sensitivity and uncertainty analysis methodology.

VTT has participated in OECD NEA organised JEFF project. Through this participation, knowledge about latest evaluated nuclear data files (ENDF) is maintained. The NJOY code has been used to extract cross section data for various purposes. For instance, a cross section library has been created for the new Serpent Monte Carlo code (with the earlier working title PSG) [1].

Related to the development and validation of nodal methods, Studsvik Scandpower's (SSP) SIMULATE-3 and CASMO-4 codes have been further tested. In addition, "Basic CMS Training Course" organised by SSP has been attended both in 2007 and 2008. A research trainee has also made a survey on the status and usability of 1D data condensation methods and codes at VTT [2], and some new modules have been preliminary programmed to CROCO code, in order to enable input of SIMULATE data for the 1D condensation.

The Serpent code has been developed as a part of both the cross section and the Monte Carlo subprojects. Sepent is especially intended for reactor physics calculations at the fuel assembly level, e.g., to calculate homogenised few-group reaction cross sections, scattering matrices, diffusion coefficients, assembly discontinuity factors, and delayd neutron parameters in an infinite-lattice geometry. Recently also burnup calculation routines have been implemented. The first burnup calculation method was based on an external coupling to the ORIGEN2 depletion code using ABURN, a coupling code developed at VTT [3]. Thereafter, internal depletion routines based on the Transmutation Trajectory Analysis (TTA) method have been implemented, and the Serpent code has the capability to run stand-alone burnup calculation. In addition, an advanced matrix exponential method for the solution of Bateman equations in burnup calculation has also been developed.

More information about Serpent can be found, for instance, from the separate summary (in this publication), from the doctoral dissertation of J. Leppänen [4], and from the recently published web site http://montecarlo.vtt.fi.

Also a simplified full-core reactor physics code MORA (Monte Carlo Reactor Analysis) based on the homogenized multi-group Monte Carlo method has been developed [5, 6]. Figure 9.1.1 shows the CROCUS reactor kinetics benchmark geometry and the corresponding flux and pin-power distributions [6]. The MORA code has also been used for comparison calculations in JOYO fast reactor benchmark [7] and studies of the EPR conceptual initial core.

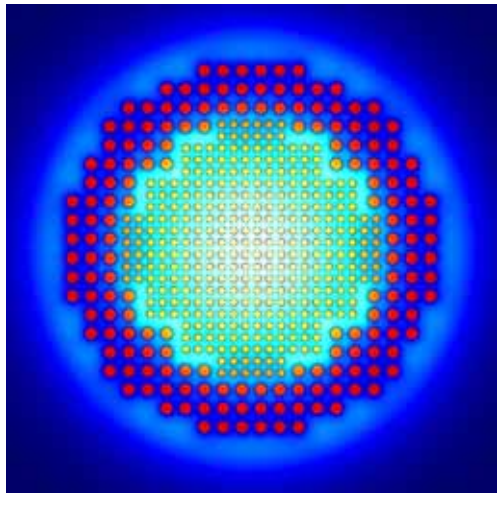

Figure 9.1.1. The CROCUS reactor core. Two nested lattices with different pin pitch. The PSG and MORA codes were used for calculating reactor point kinetics parameters in the CROCUS benchmark [6].

The well-known Monte Carlo code MCNP developed in Los Alamos National Laboratory (LANL) is widely used in neutron and photon transport calculations. Latest versions of MCNP5 and MCNPX have been taken into use at VTT. F. Wasastjerna [8] wrote a doctor's thesis in 2008 on the efficient use of MCNP in shielding calculations: the performed research was related to fusion neutronics, but the studied variance reduction methods are also highly relevant in reactor physics applications. The work was performed with separate funding.

In addition to the use of the Monte Carlo method also deterministic radiation transport calculation system has been maintained. This has included installation of the latest DOORS package and the BOT3P pre- and post-processing tool into VTT's linux cluster. DOORS package includes three-dimensional discrete-ordinates radiation transport code TORT developed in Oak Ridge National Laboratory (ORNL). In addition, P. Kotiluoto wrote a doctoral dissertation in 2007 on the development, validation and verification of the VTT's MultiTrans code, which uses adaptive tree multigrids and simplified spherical harmonics approximation [9]. A Linux version of the MultiTrans has also been created with some improvements to the code performance.

VTT is participating in an international consortium that will contract out radiochemical analysis of irradiated VVER-440 fuel in Dimitrovgrad. This data, when available, will be useful in verification of burnup calculation methods of isotopic concentrations [10]. For criticality safety analysis of, e.g., spent fuel storage and transportation, burnup credit (BUC) methodology has been investigated. Especially methods for coupled Monte Carlo and burnup calculations have been developed. The ABURN code [4] couples MCNP or PSG2 / Serpent code with isotope generation and depletion code ORIGEN2. Comparison calculations between the burnup script ABURN (coupling MCNP4C with ORIGEN2) and the two-dimensional transport theory code CASMO-4E have been made, for instance, for an EPR-type assembly [3]. In Figure 9.1.2, an example of the radial power difference between ABURN and CASMO-4E results is shown for 10 GWd/tU burnup [3]. Unfortunately, the developer of ABURN, Anssu Ranta-aho, resigned from VTT in 2008 and no longer works in the project. A new research trainee is familiarising himself with the Monte Carlo burnup calculation methods.

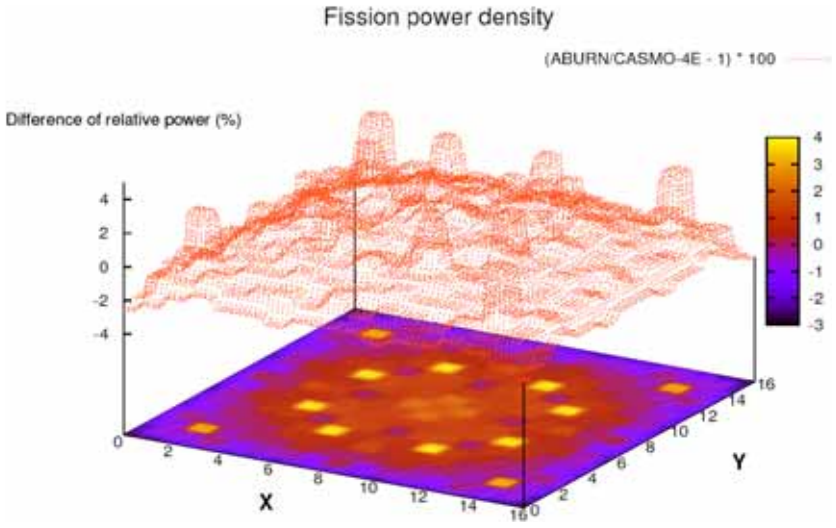

Figure 9.1.2. Difference of the radial power density at 10 GWd/tU for an EPR-type assembly [3].

There has been a growing interest towards uncertainty and sensitivity analysis in many fields. In reactor physics, uncertainty and sensitivity analysis is used to determine how different parameters and their associated uncertainty will affect the final computational value and its uncertainty. Traditionally, conservative models have been used, in order to ensure the nuclear safety. More realistic best estimate models could be used in the future, but this would require a reliable estimation of the associated uncertainty of the results.

In the TOPAS project, uncertainty and sensitivity analysis methods have been studied in-depth. M. Pusa has written a Master's thesis on the subject [11], and also a separate report has been written on the use of TSUNAMI code system for uncertainty and sensitivity analysis [12]. An example of evaluated uncertainty of ^{235}U, ^{238}U, and ^{239}Pu multigroup cross sections is shown in Figure 9.1.3.

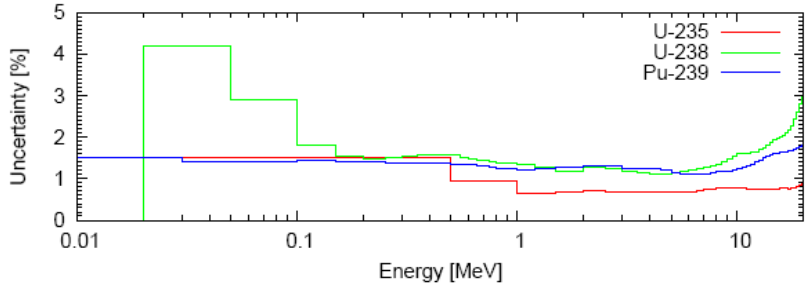

Figure 9.1.3. Evaluated uncertainty of ^{235}U, ^{238}U, and ^{239}Pu multigroup cross sections [11].

NEA has also launched an international LWR uncertainty analysis of modelling (UAM) benchmark: the benchmark has been divided into several stages, first three of them concerning steady-state reactor physics. These three benchmark studies have been attended. The work has included practical realisation of the methods by making several code modifications, for instance, to the KRAM solver in CASMO, in order to allow sensitivity and uncertainty analysis based on perturbation theory. Modifications and the use of CASMO code in sensitivity and uncertainty analysis are illustrated in a block diagram in Figure 9.1.4.

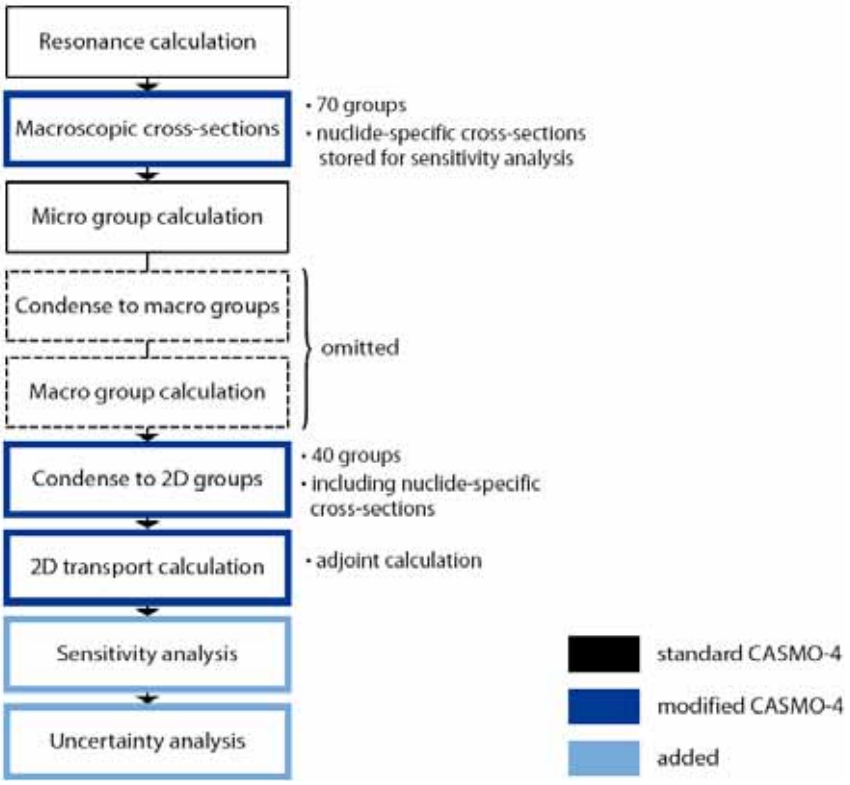

Figure 9.1.4. Block diagram of the modified CASMO code for uncertainty and sensitivity analysis.

Additional utility programmes have also been written, for instance, to transform covariance matrices of SCALE 5.1 to compatible CASMO cross section library format. Based on experience and feedback from the UAM benchmark, the developed methods represent the current state-of-the-art in reactor physics uncertainty and sensitivity analysis.

Education and international co-operation

From the educational point of view, TOPAS project has been remarkably succesfull during the first two years. Several project members have graduated, including three doctorates [4, 8, 9] and a M.Sc.Tech degree [9]. Currently, four young persons (YG, ≤ 35 y) are working for the project, including research trainees. At least one M.Sc. degree and one Lic.Tech. degree are expected to be finished in 2009. Several training courses have been attended by project staff, such as CMS training courses (both in 2007 and in 2008), MCNP/MCNPX workshop, Joliot&Hahn summer school, International School in Nuclear Engineering, and EXTEND course.

VTT has widely participated to the OECD NEA activities, such as Nuclear Science Committee (NSC), Nuclear Development Committee (NDC), JEFF cross section project, Working Party on Nuclear Criticality Safety (WPNCS), Working Party on the Scientific Issues of Reactor Systems (WPRS), Expert Group on Uncertainty Analysis for Criticality Safety Assessment (UACSA), and LWR uncertainty analysis of modelling (UAM) benchmark and expert group. Several international conferences have been attended.

Applications

The name of the project, total reactor physics analysis system (TOPAS), is not only formulated to cohere with the research programme name, but also to reflect the need for a code system that will cover the whole range of steady-state calculations, starting from basic nuclear data, and eventually being capable to perform core analysis, criticality safety studies, activity inventory, decay heat or radiation shielding calculations, or providing starting points for transient and accident analysis. The results of the project are aimed to fulfil the present and future needs of the safety authorities and power utilities in the reactor physics in order to ensure safe and economic use of the nuclear power plants.

Conclusions

Profound knowledge related to the use of Monte Carlo method has been gained by both developing an outstanding new radiation transport code Serpent and by studying the MCNP variance reduction methods. Different Monte Carlo burnup calculation methods have also been developed. In addition, new state-of-the-art methods and tools have been developed for sensitivity and uncertainty analysis

in reactor physics. Participation to an international LWR uncertainty analysis of modelling (UAM) benchmark has evidenced the high-level of the performed work.

During the first two years of the TOPAS project, three doctor's degrees and a M.Sc.Tech degree have been taken, and the educational objectives of the project have been well fulfilled. International co-operation has included NEA activities, such as NEA working groups and benchmark studies related to uncertainty analysis. The project personnel have had good opportunities for international networking and education by attending several international conferences, training courses, workshops, and summer schools.

References

1. Leppänen, J. PSG2 / Serpent – a Continuous-energy Monte Carlo Reactor Physics Burnup Calculation Code. User's Manual, VTT Technical Research Centre of Finland, 24 November, 2008. Available at: http://montecarlo.vtt.fi.

2. Räty, A. On the One-Dimensional Condensation of Cross-Sections for Transient Analysis. VTT Technical Research Centre of Finland, 2008. VTT Research Report, VTT-R-066007-08.

3. Ranta-Aho, A. Burnup calculations for an EPR-type assembly – Comparison of CASMO-4E and ABURN. In: Proceedings of the XIII Meeting on Reactor Physics Calculations in the Nordic Countries. Västerås, Sweden, 29–30 March, 2007.

4. Leppänen, J. Development of a New Monte Carlo Reactor Physics Code. D.Tech. Thesis, Helsinki University of Technology. Espoo: VTT Technical Research Centre of Finland, 2007. VTT Publications 640. 228 p. + app. 8 p. ISBN 978-951-38-7018-8. http://www.vtt.fi/inf/pdf/publications/2007/P640.pdf.

5. Leppänen, J. On the feasibility of a homogenised multi-group Monte Carlo method in reactor analysis. In: Proceedings of the International Conference on the Physics of Reactors. Interlaken, Switzerland, 14–19 September, 2008.

6. Leppänen, J. On the Calculation of Reactor Time Constants Using the Monte Carlo Method. In: Proceedings of the International Youth Nuclear Congress. Interlaken, Switzerland, 20–26 September, 2008.

7. Juutilainen, P. Simulating the Behaviour of the Fast Reactor JOYO. In: Proceedings of the International Youth Nuclear Congress. Interlaken, Switzerland, 20–26 September, 2008.

8. Wasastjerna, F. Using MCNP for fusion neutronics. D.Tech. Thesis, Helsinki University of Technology. Espoo: VTT Technical Research Centre of Finland, 2008. VTT Publications 699. 68 p. + app. 136 p. ISBN 978-951-38-7129-1. http://www.vtt.fi/inf/pdf/publications/2008/P699.pdf.

9. Kotiluoto, P. Adaptive tree multigrids and simplified spherical harmonics approximation in deterministic neutral and charged particle transport. Ph.D. Thesis, University of Helsinki. Espoo: VTT Technical Research Centre of Finland, 2008. 106 p. + app. 46 p. VTT Publications 639. ISBN 978-951-38-7016-4. http://www.vtt.fi/inf/pdf/publications/2008/P639.pdf.

10. Ranta-aho, A. On the need of high quality radiochemical data. A Finnish perspective. In: ICNC 2007 – 8th International Conference on Nuclear Criticality Safety. St. Petersburg, Russia, 28 May – 5 June, 2007.

11. Pusa, M. Vaikutusalojen tarkentamiseen ja niiden epävarmuuden vaikutusten arviointiin käytetyt matemaattiset menetelmät reaktorifysiikassa. (“Mathematical methods for evaluating cross-sections and the impact of their uncertainty in reactor physics”). M.Sc.Tech. Thesis, Helsinki University of Technology. Espoo: Helsinki University of Technology, 2007. 121 p. (In Finnish.)

12. Pusa, M. Herkkyys- ja epävarmuuslaskenta TSUNAMI-ohjelmissa. Espoo: VTT Technical Research Centre of Finland, 2008. VTT Research Report, VTT-R-02260-08. (In Finnish.)

9.2 Development of the PSG2 / Serpent Monte Carlo Reactor Physics Burnup Calculation Code

Jaakko Leppänen
VTT

Abstract

The PSG2 / Serpent Monte Carlo reactor physics burnup calculation code has been developed at VTT since 2004. This paper summarizes the four years of code development and introduces the methodology and the potential applications.

Introduction

The Monte Carlo method is a computing-intensive calculation technique, capable of detailed simulation of complicated processes consisting of separate well-defined sub-tasks. A good example of such process is the transport of radiation and sub-atomic particles through the surrounding medium. Typical transport applications of the Monte Carlo method include radiation shielding and dosimetry calculations, criticality safety analyses and the validation of deterministic transport codes.

In recent years, there has been an increasing interest in using the Monte Carlo method for various reactor physics applications, traditionally handled using deterministic transport methods. One of such applications is the production of input data for reactor simulator codes. This process is called homogenization, and it basically implies that the geometry and physics in the reactor core are reduced to such level that simple and efficient deterministic calculation methods, such as the nodal diffusion method, can be used for coupled full-core analyses.

The main advantage of using Monte Carlo codes for homogenization is the accuracy and the versatility of the calculation method. The same code and cross section libraries can be used for modelling any fuel or reactor configuration, without application-specific limitations. This is particularly valuable for the development of high-burnup fuels, advanced MOX technology and next-generation reactor concepts, which may lie beyond the capabilities of presently-used deterministic lattice transport codes.

The use of the Monte Carlo method for homogenization and group constant generation was also the inspiration for developing the PSG2 / Serpent Monte Carlo reactor physics code at VTT Technical Research Centre of Finland. This paper summarizes the work carried out during the past 4 years.

History

The main reason to start developing a completely new Monte Carlo neutron transport code from scratch was the fact that general-purpose codes, such as MCNP [1], are not particularly well suited for homogenization and group constant generation. The task usually requires considerable user effort and the calculation of certain input parameters lies completely beyond the standard tally capabilities of most codes. Another reason is that general-purpose Monte Carlo codes are usually not capable of burnup calculation, required for simulating the isotopic changes in the material compositions during irradiation. Coupled codes have been developed for the purpose, but they are often difficult to use and extremely slow since the calculation routines have not been optimized for the calculation of a large number of reaction rates.

The development of Serpent began in 2004, under the working title “Probabilistic Scattering Game”, or PSG. Code development, originally started as a free-time activity, became a full-time work at VTT in early 2005. The project was soon included in the SAFIR research programme [2] and a related doctoral thesis was completed in 2007 [3]. The name was changed from PSG to Serpent in 2008, mainly due to the ambiguous use of the acronym. Recent development has been focused on the implementation of built-in burnup calculation routines. The possibility to release the code to the OECD/NEA Data Bank for international distribution is currently under discussion.

Overview of the methodology

In technical terms, Serpent can be characterized as a three-dimensional continuous-energy Monte Carlo neutron transport code, capable of performing burnup calculation. The source routine limits the applications to the simulation of a self-sustaining chain reaction and certain features in the neutron tracking methods make the code particularly well suited for two- and three-dimensional lattice physics calculations. For this reason the Serpent code is often referred to as a “reactor physics code”, rather than a neutron transport code, even though the

universe-based geometry model allows the description of practically any three-dimensional reactor configuration.

Neutron tracking and geometry

Neutron transport in Serpent is based on the so-called Woodcock delta-tracking method [4]. This method enables a simple geometry routine that performs well in the modelling of complicated systems. The problem with the basic delta-tracking method is that the calculation tends to slow down in the presence of localized heavy absorbers, such as control rods or burnable absorber pins. Since LWR fuel assemblies often contain these absorbers, special techniques were developed for the PSG code to speed up the calculation. The old geometry routine worked well with cylindrical absorbers, but in order to overcome the efficiency problem altogether, a new method, based on the combination of delta-tracking and conventional surface-to-surface ray-tracing, was developed for the Serpent code.

Interaction physics and nuclear data

The interaction physics in Serpent is based on classical collision kinematics and ENDF reaction laws. The neutron interaction data is read from continuous-energy ACE format cross section libraries. The ACE data format was originally developed for the MCNP code [1], and the use of a shared library format has the advantage that Serpent can be validated by comparing to MCNP results without additional discrepancies originating from the fundamental interaction data. Another advantage is that cross section libraries based on different data evaluations are widely available from various public sources, such as the OECD/NEA Data Bank.

All reaction cross sections used by Serpent are reconstructed using the same energy grid for all nuclides. The use of a single unionized grid reduces the number of time-consuming iterations, which results in a major speed-up in the calculation. This is best seen in burnup calculation, in which the irradiated materials consist of several hundred actinide and fission product nuclides. The drawback of the methodology is that computer memory is wasted for storing redundant data. Although the memory demand is not impossible for today's computers, special methods have been developed for reducing the memory usage [5].

Homogenization and group constant generation

Serpent can be used for producing homogenized few-group constants for deterministic reactor simulator codes. The calculation is based on both standard Monte Carlo methods and some less conventional techniques developed for the purpose. All parameters are calculated without additional user effort. The standard output includes:

- Effective and infinite multiplication factors calculated using different methods
- Homogenized few-group reaction cross sections
- Group-transfer probabilities and scattering matrices
- Diffusion coefficients calculated using two fundamentally different methods
- P_n scattering cross sections up to order 5
- Assembly discontinuity factors for boundary surfaces and corners
- Assembly pin-power distributions
- Point reactor kinetics parameters
- Physical and effective delayed neutron fractions and decay constants in 6 or 8 precursor groups (depending on data)
- Normalized flux, power and reaction rates integrated over the geometry
- Parameters for the six-factor formula
- Various parameters related to the Monte Carlo transport simulation.

The effective delayed neutron parameters are calculated using a forward Monte Carlo technique developed at the NRG [6]. The few-energy group structure for group constant generation is arbitrary and defined by the user. The code also calculates fission source entropies for convergence studies. The total entropy is divided into x-, y- and z-components to monitor source convergence separately in each direction.

User-defined detectors (tallies) can be set up for calculating various integral reaction rates. The spatial integration domain can be defined by a combination of cells, universes, lattices and materials, or using a three-dimensional super-imposed mesh. The number and structure of detector energy bins is unrestricted. Various

response functions are available for the calculation, including material total and isotopic reaction cross sections and ACE format dosimetry data.

Burnup calculation

Serpent can be run both as a stand-alone burnup calculation code and as a part of an externally coupled system. The development of the calculation routines started in early 2008. At first, the code was coupled to the widely-used ORIGEN [7] depletion code using ABURN [8], a coupling code originally developed at VTT. The main focus, however, has been in the development of built-in burnup calculation routines.

Burnup calculation is a cyclic process, consisting of two main parts. At first, nuclear transmutation rates caused by neutron-induced reactions are calculated for each nuclide using standard Monte Carlo techniques. The reaction rates are then combined with radioactive decay constants and fission product yields to calculate the isotopic changes in each material. After the new material compositions have been resolved, the procedure is repeated for the next burnup step.

Serpent has two fundamentally different methods for solving the Bateman equations, describing the changes in the nuclide concentrations. The first option is the Transmutation Trajectory Analysis method (TTA), taking advantage of the analytical solution of linearized depletion chains [9]. The second method is an advanced matrix exponential solution, based on the Chebyshev Rational Approximation Method (CRAM), recently developed at VTT specifically for the Serpent code [10].

To speed up the calculation of one-group transmutation cross sections, the code uses a method originally developed for coupled burnup calculation codes [11, 12]. The flux spectrum for each irradiated material is tallied using the unionized energy grid structure. This spectrum is then used after the transport cycle for calculating the spectrum-averaged cross sections for the depletion calculation. The result is a significant speed-up in the calculation, since the reaction rates are not tallied during the transport simulation. The spectrum is calculated using a super-fine energy bin structure and the loss of accuracy is practically negligible. The only drawback of the method is that the information on statistical errors is lost.

Typical results

PSG, the predecessor of Serpent, has been thoroughly validated in LWR lattice calculations [3]. After the correction of a persistent flaw in the neutron free-gas model [13], all differences to MCNP results have been reduced to the level of statistical noise. Discrepancies compared to deterministic transport codes are generally larger, mainly due to the fundamental differences in the calculation methods and neutron interaction data.

The burnup calculation capability is still under development and the routines have not been thoroughly tested. Comparison to CASMO-4E results shows consistent depletion of U-235 and gadolinium isotopes in PWR assembly burnup calculations. The infinite multiplication factor is in a reasonably good agreement as well, but small discrepancies are observed in the build-up of plutonium isotopes and higher actinides. The differences seem to originate from the neutron capture rate of U-238, but more studies need to be carried out before reaching any conclusions.

The two methods used for solving the Bateman depletion equations are in a good agreement. The CRAM matrix exponential method can be considered superior to the TTA method, both in terms of accuracy and calculation time. Work is currently under way for implementing a better solution for the TTA depletion chains.

Code performance

Group constant generation for simulator codes is a repetitive process, often requiring hundreds of runs in order to cover all fuel assembly types and operating conditions within the reactor core. The calculation takes considerable time using the Monte Carlo method, especially when burnup calculation is involved. For this reason the Serpent code has been optimized for performance. Conveniently, some of the calculation techniques, originally implemented for the sake of simplicity, have later turned out be particularly efficient in lattice physics and burnup calculations. This is especially the case for the Woodcock delta-tracking method and the unionized energy grid used for all cross sections. The Serpent code also has the capability to run parallel calculation using the Message Passing Interface (MPI).

The typical running time for an LWR lattice transport calculation on a 2.6 GHz AMD Opteron PC varies from 10 to 20 minutes, when 3 million neutron histories are simulated. This results in a relative statistical error of less than

0.08% for homogenized few-group reaction cross sections and about 0.03% for k_{eff}. Direct comparisons suggest that Serpent runs 5 to 20 times faster than MCNP5 in group constant calculation. This type of direct comparison is a bit problematic, however, since MCNP is not specifically designed for the task and the calculation slows down significantly when a large number of reaction rates are tallied. This is not the case with Serpent, mainly due the unionized energy grid approach. The advantages of the technique are also seen in calculations involving materials that consist of a large number of nuclides. The transport cycle in Serpent usually slows down by a factor of 1.5 or less when modelling irradiated fuels. Similar comparison using MCNP5 gives a factor of 5 for the overall calculation time.

The situation becomes more complicated in burnup calculation. If the number of depletion zones is large, a significant fraction of CPU time is contributed to data processing between the burnup steps. The overall calculation time scales linearly with respect to the number of depletion zones. An LWR assembly burnup calculation involving 65 depleted materials, 37 burnup steps with predictor-corrector calculation and a total of 3 million active neutron histories can be completed in less than 24 hours.

Comparison to a similar calculation using Monteburns [14] suggests that Serpent may run over 80 times faster than coupled Monte Carlo burnup calculation codes based on MCNP. It should be noted, however, that the difference does not result so much from the efficiency of the code, but rather from the fact that MCNP slows down as the number of nuclides and reaction rate tallies becomes large, as discussed above. What is more important is that the Serpent code can run realistic full-scale assembly burnup calculations similar to deterministic transport codes, and the overall calculation time is counted in hours or days, rather than weeks or months.

Summary and conclusions

The development of the PSG2 / Serpent Monte Carlo reactor physics burnup calculation code has been carried out at VTT since 2004. The code is mainly intended for lattice physics calculations, such as homogenization and group constant generation for deterministic reactor simulator codes. The recently-implemented built-in burnup calculation capability also enables Serpent to be used for fuel cycle studies and other applications requiring the simulation of isotopic changes in the material compositions during irradiation.

Serpent has been validated by comparing to the widely-used MCNP code in LWR infinite-lattice calculations with good results. The development and testing of the burnup calculation routines is still under way. The code is optimized for performance and test calculations show that the overall calculation time is reduced significantly, compared to general-purpose Monte Carlo neutron transport codes. What is more important, however, is that Serpent can be considered a realistic near-future option to presently-used deterministic transport codes in assembly burnup calculations.

In addition to a doctoral thesis written on the PSG development [3], the code has been or is currently the subject or a part of three master's theses and several smaller student projects. The results and calculation methods used by the code have been reported in six international conferences during the past four years. One conference paper and two scientific review articles are currently under preparation. In addition to VTT, the code has been licensed to four other organizations for research and educational purposes. International release via the OECD/NEA Data Bank is currently under discussion. An official website for the Serpent code has been opened at http://montecarlo.vtt.fi.

References

1. X-5 Monte Carlo Team. MCNP – A General Monte Carlo N-Particle Transport Code, Version 5. LA-CP-03-0245, Los Alamos National Laboratory, 2003.

2. Leppänen, J. Development of Monte Carlo neutron transport methods for reactor physics applications. In: SAFIR The Finnish Research Programme on Nuclear Power Plant Safety 2003–2006 Final Report. VTT Research Notes 2363. Espoo: VTT Technical Research Centre of Finland, 2006. http://www.vtt.fi/inf/pdf/tiedotteet/2006/T2363.pdf.

3. Leppänen, J. Development of a New Monte Carlo Reactor Physics Code. D.Sc. Thesis, Helsinki University of Technology. VTT Publications 640. Espoo: Technical Research Centre of Finland, 2007. http://www.vtt.fi/inf/pdf/publications/2007/P640.pdf.

4. Woodcock, E.R. et al. Techniques Used in the GEM Code for Monte Carlo Neutronics Calculations in Reactors and Other Systems of Complex Geometry. In: Proc. of the Conference on Applications of Computing Methods to Reactor Problems. ANL-7050, Argonne National Laboratory, 1965.

5. Leppänen, J. Two Practical Methods for Unionized Energy Grid Construction in Continuous-Energy Monte Carlo Neutron Transport Calculation. (Article submitted to Ann. Nucl. Energy.)

6. Meulekamp, R.K. et al. Calculating the Effective Delayed Neutron Fraction with Monte Carlo. Nucl. Sci. Eng., 152 (2006), pp. 142–148.

7. Croff, A.G. A User's Manual for the ORIGEN2 Computer Code. ORNL/TM-7175, Oak Ridge National Laboratory, 1980.

8. Ranta-Aho, A. Burnup calculations for an EPR-type assembly. Comparison of CASMO-4E and ABURN. In: Proc. XIII Meeting on Reactor Physics Calculations in the Nordic Countries. Västerås, Sweden, March 29–30, 2007.

9. Cetnar, J. General solution of Bateman equations for nuclear transmutations. Ann. Nucl. Energy, 33 (2006), pp. 640–645.

10. Pusa, M. & Leppänen, J. Computing the Matrix Exponential in Burnup Calculations. Article submitted to Nucl. Sci. Eng.

11. Fridman, E. et al. Efficient Generation of One-Group Cross Sections for Coupled Monte Carlo Depletion Calculations. Nucl. Sci. Eng. 159 (2008), pp. 37–47.

12. Haeck, W. et al. An Optimum Approach to Monte Carlo Burnup. Nucl. Sci. Eng. 156 (2007), pp. 180–196.

13. Leppänen, J. PSG Status Report (March 2008). VTT-R-02580-08. Espoo: VTT Technical Research Centre of Finland, 2008.

14. Poston, D.I. & Trellue, H.R. User's Manual, Version 2.0 for Monteburns, Version 1.0. LA-UR-99-4999. Los Alamos National Laboratory, 1999.

10. Numerical modelling of condensation pool (NUMPOOL)

10.1 NUMPOOL summary report

Timo Pättikangas, Jarto Niemi and Antti Timperi
VTT

Abstract

Numerical methods for analyzing pressure suppression pools in boiling water reactors are developed. Some of the first experiments performed with the PPOOLEX facility are analysed with computational fluid dynamics (CFD) and Fluid-Structure Interaction (FSI) simulations. PPOOLEX vessel is a scaled-down model of a boiling water reactor containment with pressurized drywell and wetwell compartments. The compartments are connected with a vent pipe, whose outlet was submerged in a water pool of the wetwell. In the first experiments, air was blown into the drywell of the pressurized PPOOLEX vessel. The experiments and modelling are continued with steam discharges.

Simulation of an air discharge was performed by using the Fluent CFD code. The pressurization of the drywell, clearance of the vent pipe and pressurization of the wet well during the first tens of seconds of the experiment are resolved. The bubble dynamics at the outlet of the vent pipe is studied in some detail. The results are compared to measurements in the PPOOLEX experiment.

FSI analyses of the POOLEX and PPOOLEX experiments are performed, where the Star-CD CFD code and ABAQUS structural analysis code are coupled with MpCCI software. A linear perturbation method is used for preventing numerical instability which occurs in the pool simulations with explicit FSI

coupling. The calculations shows that FSI may have to be accounted for in simulating blowdown in pressure suppression pools.

Introduction

In boiling water reactors (BWR), the major function of the containment system is to protect the environment if a loss-of-coolant accident (LOCA) should occur. The containment is designed to accommodate the loads generated in hypothetical accidents, such as sudden rupture of a main steam line. In such an accident, a large amount of steam is suddenly released in the containment. An essential part of the pressure suppression containment is a water pool, where condensation of released steam occurs.

In a BWR, the pressure suppression containment typically consists of a drywell and a wetwell with a water pool. In a hypothetical LOCA, steam and air flow from the drywell through a vent pipe to the wetwell, where the outlet of the vent pipe is submerged in the water pool. In early part of the accident, mainly non-condensable air or nitrogen flows through the vent pipe into the wetwell. Then, the volume fraction of vapour increases in the gas mixture. When all the non-condensable gas from the drywell is blown into the wetwell, the blowdown consists of pure vapour. The pressure suppression pool changes this large volume of vapour to a small volume of water [1].

PPOOLEX test facility is a scaled-down model of a pressure suppression containment of a BWR. The PPOOLEX vessel shown in Figure 10.1.1 consists of a drywell compartment and a wetwell compartment with a water pool. The compartments are connected with a vent pipe, whose outlet is submerged in water pool in the wetwell. In experiments, air or vapour is blown into the drywell from air tanks or steam generator. The experimental facility is described in detail in the article on the CONDEX project [2].

In the first experiments performed with the PPOOLEX facility, the pressurized vessel was charged with air. These experiments are already interesting even though non-condensable gas was used. The charging of the drywell, expulsion of the water plug from the vent pipe, the bubble dynamics at the vent outlet and the charging of the wetwell can be studied. In addition, the displacements of the pool bottom during the experiments are measured. Further experiments have been performed with vapour [2].

In the following, CFD and structural analysis calculations performed for the first experiments with the PPOOLEX facility are described. The experiments are

modelled with the volume of fluid model of the Fluent CFD code. The CFD results are compared to pressure and temperature measurements. The bubble dynamics in the vent pipe is analysed in some detail.

In addition, the Fluid-Structure Interaction (FSI) analysis results on the experiments are also presented. In FSI analysis, the motion of the structures is taken into account when the pressure loads on the structures are calculated. FSI has significance in certain situations of the blowdown event [3, 4]. In this work, FSI calculations are performed using Star-CD 4.08 for CFD and ABAQUS 6.7 for structural analysis. The external MpCCI 3.0.6 software is used for coupling the CFD and structural analysis codes. Two-way coupled FSI calculations of the experiments have been numerically unstable with the explicit coupling scheme of MpCCI. A more stable implicit scheme is so far unavailable with the used codes. A linear perturbation method (LPM) [5, 6] is used for circumventing the numerical instability. The method is validated against numerical and experimental data in blowdown situations.

CFD modeling of discharges of non-condensable gas

In the experiment discussed below, air was blown into the drywell compartment of the PPOOLEX facility through a horizontal pipe. The increase of pressure in the drywell expelled the water plug from the vent pipe and large air bubbles were periodically formed at the pipe exit. The pressure in the wetwell compartment increased when air was flowing through the vent pipe into the wetwell compartment. The temperature both in the drywell and wetwell increased when the pressure increased. The instrumentation for measuring the pressure and temperature increase is illustrated in Figure 10.1.1.

In the PPOOLEX experiment CHAR-09 test 04, the maximum mass flow rate into the drywell was 0.755 kg/s, which corresponded to maximum flow velocity of about 16 m/s. The temperature of air flowing into the drywell decreased from about 21 °C to 14 °C during the first 30 s of the experiment. The mass flow rate is shown in Figure 10.1.2.

The simulations were performed with the commercial Fluent 6.3 CFD code. The flow of air and water was solved by using the Volume Of Fluid (VOF) model, which is based on tracking the interface between the two phases. The fully hexahedral mesh is shown in Figure 10.1.9, and it contains about 135 000 grid cells. In the present simulation, the time step was 0.5 ms.

In Figure 10.1.2, the calculated mass flow rate of air through the vent pipe to the wetwell compartment is illustrated. When air is blown into the drywell, the pressure increases and the water plug in the vent pipe starts to move. The vent pipe is cleared at time $t = 4.5$ s, and the mass flow rate reaches its first maximum value of 0.73 kg/s at time $t = 4.91$ s. This first maximum occurs during formation of the first air bubble at the outlet of the vent pipe. Then, the first bubble is detached from the pipe outlet and starts rising towards the water surface. The vent pipe is closed by the water flowing into the pipe and the mass flow rate of air in the vent pipe decreases rapidly towards zero. After this, new bubbles are formed in a cyclic manner.

In Figure 10.1.3, detachment of the first bubble is shown at the outlet of the vent pipe. The bubble surface is coloured with the vertical velocity. The water surface at $z = 2.14$ m is seen above the bubble. The bubble is detached at the pipe outlet at time $t = 5.02$ s. The velocity of the bubble surface is upwards near the pipe and downwards further away from the pipe. This phenomena determines the characteristic shape of the bubble. The vertical velocity of the bottom surface of the bubble is larger than the vertical velocity of its top surface. This can lead to fragmentation of the bubble if the bottom surface reaches the top surface of the bubble. In this case, however, the bubble reaches the water surface before fragmentation.

Figure 10.1.2 shows that the average interval between the bubbles was $\Delta t = 0.93$ s. Closer inspection of the data shows that the period of bubble formation changes somewhat when the mass flow rate into the drywell decreases during the experiment.

In Figure 10.1.4, analysis of the mass flow rate through the vent pipe is shown for the simulation data of Figure 10.1.2. The time interval between the bubbles is plotted as a function of the mass flow rate of air into the drywell. It is evident that the time period between the bubbles increases approximately linearly with the mass flow rate into the drywell.

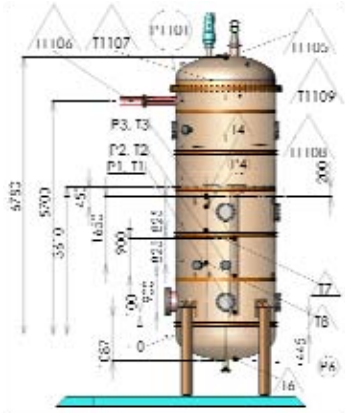

Figure 10.1.1. Pressure (Pn) and temperature (Tn) measurements in the PPOOLEX pressurized test facility (see ref. [2]).

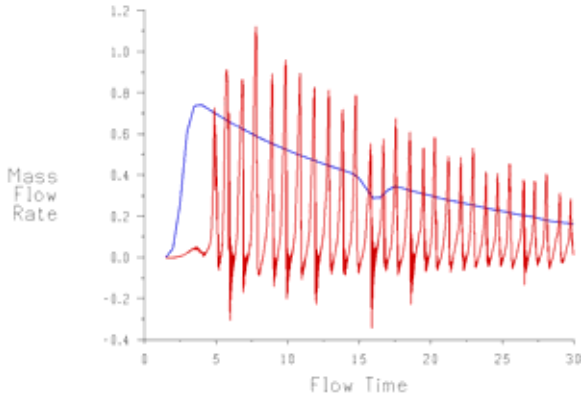

Figure 10.1.2. Measured mass flow rate (kg/s) into the drywell (blue line) and calculated mass flow rate through the vent pipe (red line) versus time (s). Experiment CHAR-09-04.

Figure 10.1.3. Surface of the first bubble at time t = 5.02 s coloured with vertical velocity (m/s). Simulation of experiment CHAR-09-04.

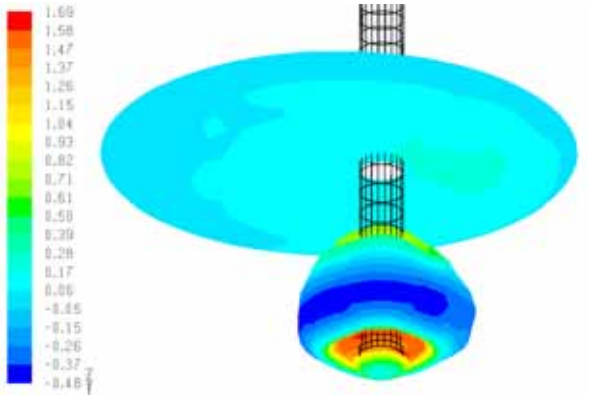

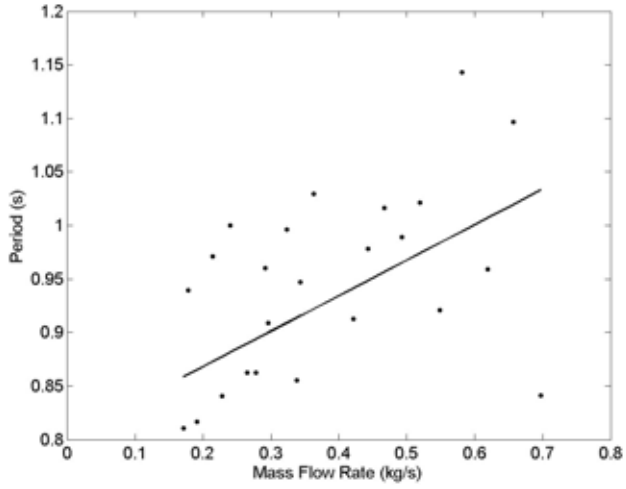

Figure 10.1.4. Time period between bubble formation at the outlet of the vent pipe as a function of mass flow rate into the drywell. CFD simulation results (dots) and linear fit (line) are presented for the experiment CHAR-09 test 04.

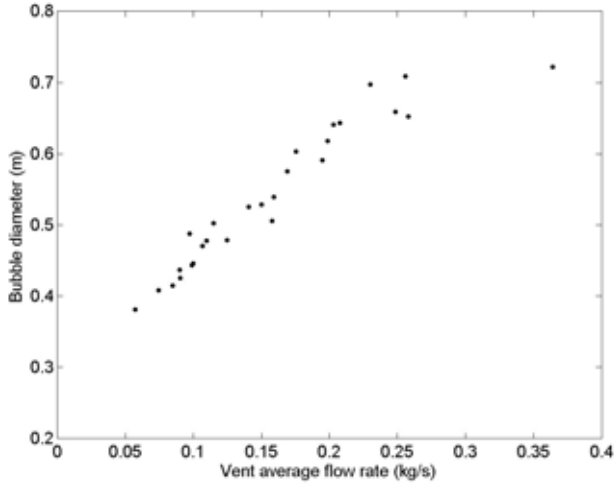

Figure 10.1.5. The diameters of the bubbles versus mass flow rate through the vent pipe. CFD simulation results for the experiment CHAR-09 test 04.

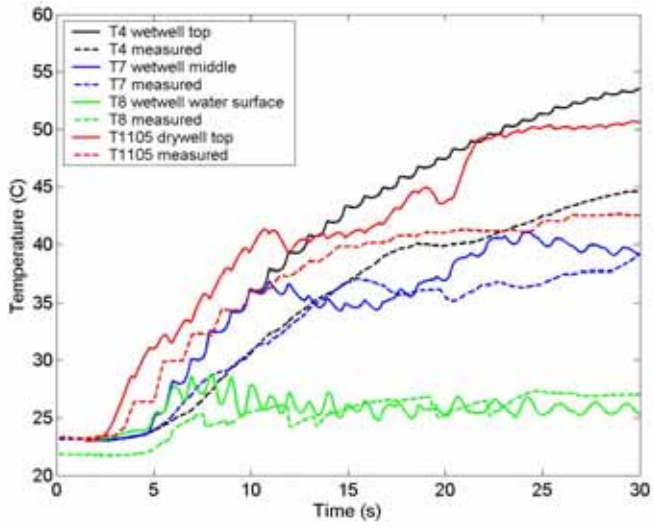

Figure 10.1.6. Comparison of calculated temperatures to the measured values in CHAR-09 test 04. The experimental results are from ref. [7].

In Figure 10.1.5, the bubble diameters are presented as a function of the average mass flow rate through the vent pipe. In the parameter range of the present simulation, the bubble diameter increases roughly linearly with the mass flow rate through the vent pipe. Note that such a linear scaling is not expected to be valid for smaller mass flow rates because the bubble diameter is expected to approach zero when the mass flow rate goes to zero.

In Figure 10.1.6, the calculated temperatures are compared to measured values. The calculated temperatures differ from the measured values especially in the wetwell top and in the drywell top. In the end of the simulation, the calculated temperatures are about eight degrees higher than the measured temperatures. Near the wetwell water surface and in the wetwell middle, the calculated values are closer to the measured ones. Stepwise rise pattern caused by bubble dynamics is clearly visible in the calculated temperature in the wetwell top and wetwell middle. In the measured values, it is much less apparent.

Fluid-structure interaction calculations

In the linear perturbation method (LPM), pressure load is transferred from the CFD model to the structural model, but no displacement feedback is sent back. The mass of the fluid is accounted for in the structural motion through a separate acoustic fluid which has two-way coupling with the structure. The method eliminates the numerical instability as the coupling between CFD and structural models is only one-way. A stable monolithic approach is used for the acoustic-

structural system [8]. In addition to validation calculations, basis of the method was examined mathematically with an order of magnitude analysis similar to that in [6].

Calculations with axisymmetric model

A simple axisymmetric model of the PPOOLEX facility was first used. The pool has rigid side wall and a bottom plate that experiences only vertical rigid-body motion. A harmonic pre-determined wall motion was assumed for the bottom plate so that the numerical instability was prevented in the moving-mesh CFD calculation. Frequency and amplitude of the wall motion were set to 10 Hz and 1 mm which are close to the values observed in the experiments [9]. The VOF model was used for tracking the free surface and both air and water were assumed incompressible. Turbulence was modelled with the k-ε model. Constant flow velocity of 10 m/s was used at the blowdown pipe inlet which is of the same order as in the experiments.

Figure 10.1.7 shows volume fraction of water in the pool at different instants of time. Pressures at the pool bottom are compared in Figure 10.1.8. Pressures obtained from the moving-mesh calculation and with LPM are in good agreement. The calculation with rigid walls shows only the blowdown load, i.e. the effect of wall motion on the pressure is not included. Also a conservative wall amplitude of 10 mm and a blowdown velocity of 100 m/s were tested showing similar results. LPM becomes invalid for sufficiently high flow velocity near moving walls. During blowdown, flow velocity in the pool can be relatively large near the pipe outlet but in the calculations validity of the method is unaffected by this. The method works well in this kind of case although the free surfaces of the acoustic fluid remain static during the calculation.

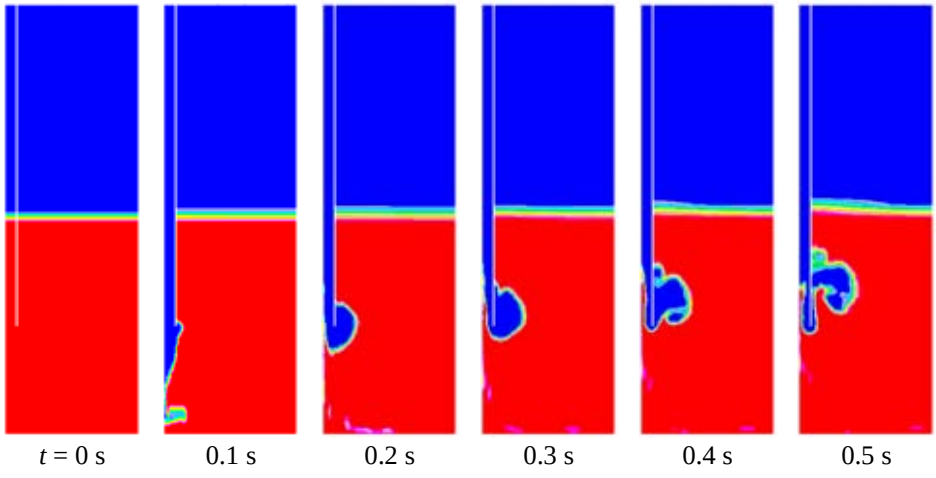

Figure 10.1.7. Volume fraction of water in calculation with axisymmetric model.

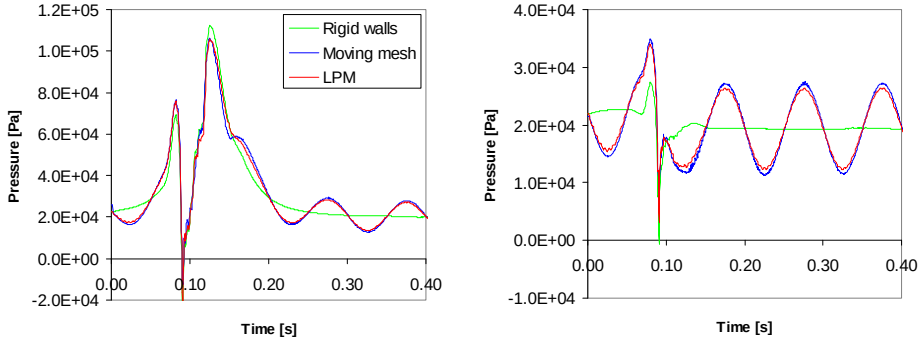

Figure 10.1.8. Wall pressure below pipe (left) and average wall pressure (right) in calculations with axisymmetric model.

Calculations with three-dimensional models

FSI calculations of PPOOLEX experiment SLR-05-02 were performed which is similar to the CHAR-09-04 experiment. For the structure, a fairly detailed FEM model consisting mainly of 4-noded shell elements was used. The structural model and acoustic fluid used for LPM for preventing numerical instability are presented in Figure 10.1.9, where the mesh used in the CFD model is also

shown. The VOF and k-ε models were used in the CFD calculations. Air was treated as ideal gas and a logarithmic equation of state suitable for compressible liquids was used for water.

Pressure and displacement at the pool bottom are presented in Figure 10.1.10. Calculation with FSI shows qualitatively correct results. The pressure load is expected to be smaller in the calculations because of delay in the mass flow sensor. Frequency of the pool motion is similar with or without FSI because structures of the PPOOLEX facility have almost the same mass as the pool water. Figure 10.1.11 shows results from calculations of the previous POOLEX facility. These calculations show much larger added mass effects due to relatively light structures. Condensation of steam in the considered experiment was not modelled which could explain the significantly higher stresses in the experiment. The calculations show, however, that FSI has to be accounted for in order to have qualitatively correct results.

Conclusions

The CFD simulations were found to predict well the main features of the experiments. The pressure rise in the drywell, the clearance of the vent pipe and the pressure rise in the wetwell are described quite accurately. The expulsion of the water plug and the bubble dynamics at the outlet of the vent pipe also corresponded well visual observations of the experiment. The temperature rise was, however, overestimated in the simulations, in particular, near the top of the drywell and wetwell compartments.

The different parts of the experiment CHAR-09 test 04 were analysed in detail. First, adiabatic compression of air in the drywell occurred. The pressure increase led to acceleration and expulsion of the water plug from the vent pipe. The expulsion occurred approximately when the drywell pressure exceeded the hydrostatic pressure at the submergence depth of the vent pipe.

The dynamics of the gas bubbles at the vent outlet have been analysed in detail because the change in the bubble volume is the source of the pressure loads on the pool structures. The average time interval between the bubbles was about Δt = 0.93 s, which agreed well with the experiments. A careful analysis of the simulation of CHAR-09 test 04 showed that the interval between the bubbles had weak dependence on the mass flow rate into the drywell of the vessel. At the largest flow rate (0.7 kg/s), the period was about Δt = 1.05 s and at the smallest flow rate (0.2 kg/s) it was about Δt = 0.85 s.

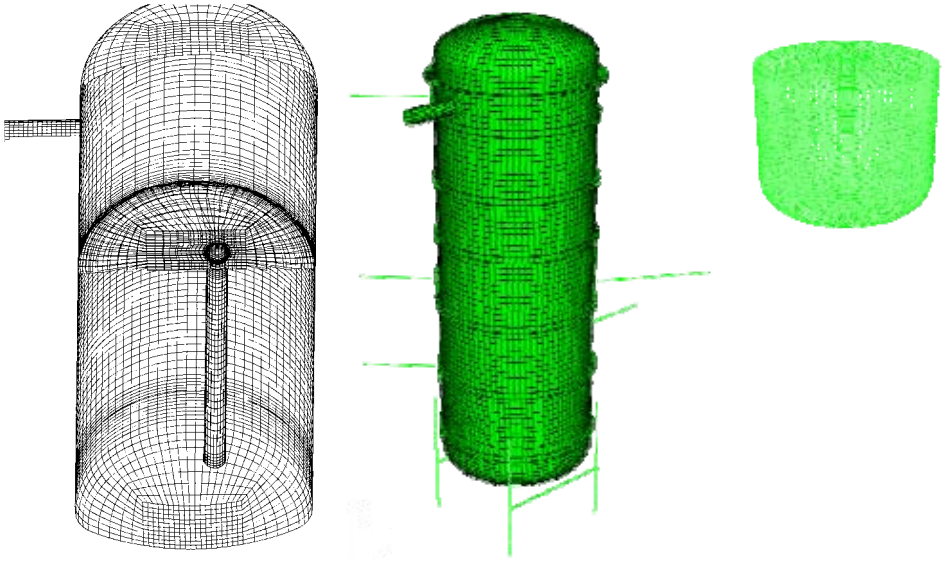

Figure 10.1.9. CFD (left) and FEM meshes (center and right) of the PPOOLEX structure and water.

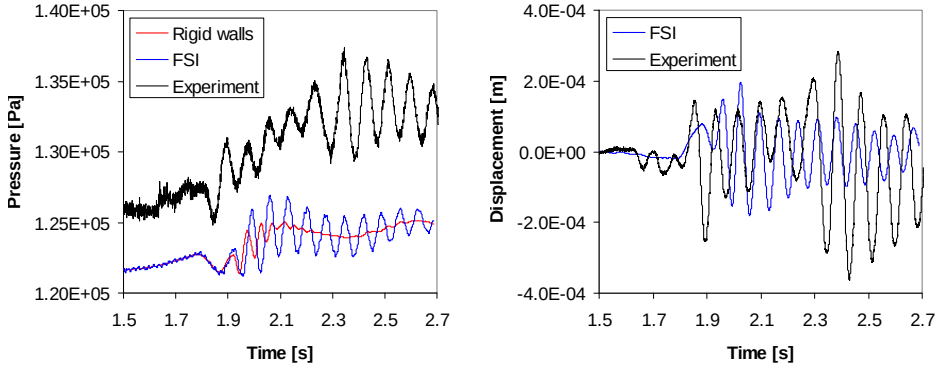

Figure 10.1.10. Pressure and displacement at the pool bottom in PPOOLEX experiment SLR-05-02. The times have been syncronized to the moment when the first bubble appears.

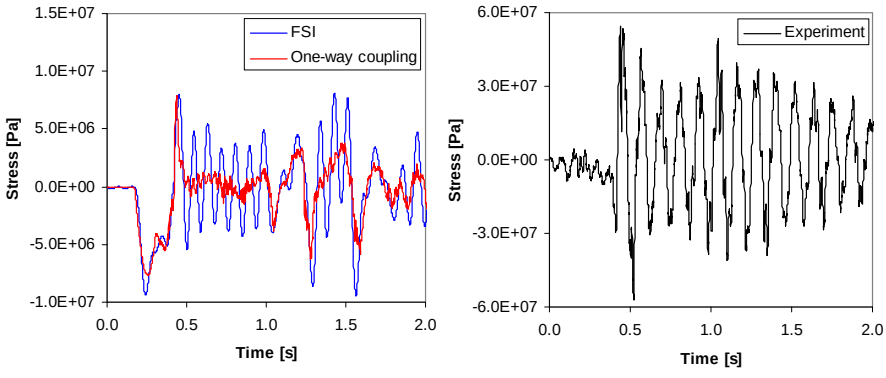

Figure 10.1.11. Stress at the pool bottom in POOLEX experiment STB-17-6. The times have been syncronized to the moment when the first bubble appears.

The bubble diameter at the vent outlet also depended on the flow rate. At, the smallest flow rate, the bubble diameter was about 0.4 m and at the largest flow rate it was about 0.7 m. These calculated results correspond well to the visual observations on the performed experiment.

FSI calculations of the experiments were performed by using the Star-CD, ABAQUS and MpCCI codes. An approximate method that makes possible numerically stable FSI calculations for the PPOOLEX facility was used. The method is based on linear perturbation method which necessitates small deformations of the vessel. Wall pressure obtained in the experiments and FSI calculations show clearly the oscillating component caused by wall motion. FSI may have to be accounted for in condensation pool simulations because the pool water modifies eigenfrequencies of the structure. Using only one-way coupling does not necessarily yield conservative results in this kind of situation. The linear perturbation method was validated also against moving-mesh calculations by using different blowdown velocities and amplitudes of the wall motion.

References

1. Lahey, R.T. & Moody, F.J. The thermal hydraulics of a boiling water nuclear reactor. 2nd Edition, American Nuclear Society, 1993.

2. Puustinen, M. et al. Condensation experiments with PPOOLEX facility. Special report on the CONDEX project in this volume.

3. Giencke, E. Pressure distribution due to a steam bubble collapse in a BWR pressure suppression pool. Nuclear Engineering and Design, 1981. Vol. 65, pp. 175–196.

4. Björndahl, O. & Andersson, M. Globala vibrationer vid kondensationsförlopp i wetwell orsakade av LOCA i BWR-anläggningar. SKI Rapport 99:3, 1998.

5. Huber, P.W., Kalumuck, K.M. & Sonin, A.A. Fluid-structure interactions in containment systems: small-scale experiments and their analysis via a perturbation method. 5th International Conference on Structural Mechanics in Reactor Technology, 1979.

6. Sonin, A.A. Rationale for a linear perturbation method for the flow field induced by fluid-structure interactions. Journal of Applied Mechanics, 1980. Vol. 47, pp. 725–728.

7. Puustinen, M. & Laine, J. Characterizing Experiments of the PPOOLEX Test Facility. Lappeenranta: Lappeenranta University of Technology, Nuclear Safety Research Unit, Research Report CONDEX 1/2007, 2008. 23 p. + app. 6 p.

8. Cook, R., Malkus, D., Plesha, M. & Witt, R. Concepts and applications of finite element analysis. Wiley & Sons Inc, 2002.

9. Laine, J. & Puustinen, M. Steam line rupture experiments with the PPOOLEX test facility. Lappeenranta: Lappeenranta University of Technology, Nuclear Safety Research Unit, Research Report CONDEX 2/2007, 2008.

11. Improved thermal hydraulic analyses of nuclear reactor and containment (THARE)

11.1 THARE summary report

Ismo Karppinen, Seppo Hillberg, Pasi Inkinen, Sampsa Lauerma, Joona Kurki, Markku Hänninen, Risto Huhtanen and Jarto Niemi
VTT

Abstract

The main objectives of the THARE project are to develop and validate calculation methods for safety evaluation of nuclear power plants. The CCFL model of the APROS code has been validated with the IVO upper tie plate experiments. The analysis capabilities of APROS have been verified with the integral OECD/ROSA and OECD/PSB-VVER experiments. TRACE code validation has been started with creating a model of ROSA/LSTF test facility. Containment analysis methods have been enhanced by developing and validating a wall condensation model in Fluent CFD code and by validating the spray model of the APROS code.

Introduction

The project is divided in three tasks, 1) validation of thermal hydraulic system analysis codes APROS and TRACE, 2) enhancements of containment thermal hydraulic analysis methods and 3) participation in the international research programs.

Validation of APROS and TRACE

Thermal hydraulic system analysis codes, like APROS and TRACE, rely largely on experimental correlations. When the codes are used in conditions beyond experimental data or applied in new problems the usability of the correlations and models has to be studied. Increase in computer performance allows more detailed modelling and makes it feasible to study new phenomena. Sometimes better resolution in modelling brings out new problems, like interaction of parallel flow channels or u-tubes. In addition, the way the problem is modelled and the simplifications and choices made by the user will affect results (user effect). Therefore continuous validation of models and experience gained from international co-operation are important. Moreover code validation gives excellent opportunities for trainees and young scientists to acquaint themselves with the capabilities of the safety analysis codes.

Validation of APROS with OECD research programs

The ongoing OECD research programs produce high quality experimental data and which is even more important facilitate interpretation of the results and discussions between experts participating in analysis with various computer codes.

OECD/ROSA

The OECD/ROSA studies design basis events (DBEs) and beyond-DBE transients to provide an integral and separate-effect experimental database, which will be used to validate code predictive capability and accuracy of models. The test 6-2 (SBLOCA in pressure vessel bottom), test 5-1 (Primary cooling through SG secondary depressurization) and test 3-1 (Natural circulation under high core power conditions) were chosen for APROS verification.

The ROSA/LSTF (Rig of Safety Assessment / Large Scale Testing Facility) is a full-height and 1/48 volumetrically-scaled system simulating a Westinghouse-type 3423 MWth PWR located in Japan. The APROS model consists of 392 nodes, 434 junctions and 2119 heat slabs, as well as automation components simulating processes such as scram, emergency core cooling systems (ECCS) and safety valves. A schematic picture of the test facility and the model nodalization are presented in Figure 11.1.1. More detailed description of the model is given in [1].

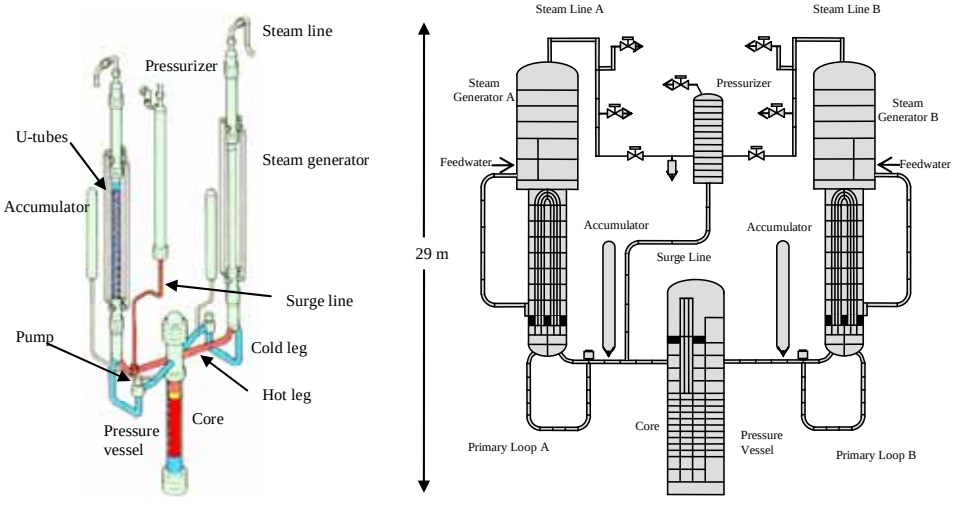

Figure 11.1.1. ROSA/LSTF test facility (left) and APROS model (right).

As an example of the code verification calculations the test 5-1 is presented here. The experiment simulated a cold leg small break loss-of-coolant accident (SBLOCA) with a break size of 0.5%, which corresponds to 50 mm break in the reference PWR. The break was located in the loop without pressurizer. The test studied primary circuit cooling with secondary side de-pressurization. In the scenario total failure of high and low pressure safety injection was assumed. As an accident management action the steam generator secondary-side de-pressurization was started 10 minutes after safety injection signal tripping by fully opening the relief valves in both steam generators [2]. Calculated pressures, presented in Figure 11.1.2, show very similar behaviour than measured in the experiment.

Participation in the ROSA project and especially analytical work with code calculations have deepened understanding of plant behaviour in accident conditions. For example internal circulation and mixing of cold bypass water in the upper head of the reactor pressure vessel is one found phenomena which have peen applied in modelling of power plants. Another model of the ROSA test facility was created using the TRACE code [3].

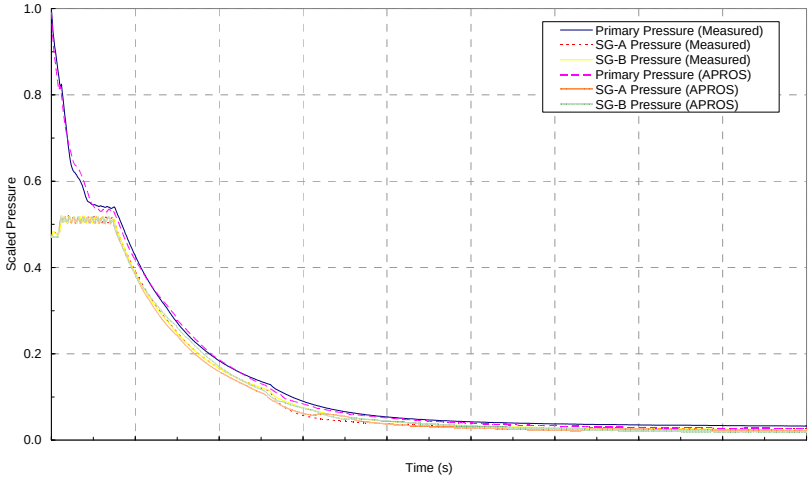

Figure 11.1.2. ROSA test 5-1 measured and calculated primary and secondary circuit pressures (data restricted).

OECD/PSB-VVER

PSB-VVER is a model of VVER-1000 reactor in Electrogorsk, Russia, in which a 200% cold leg break (LBLOCA) was one of the test included in the OECD research program. Among other participants VTT performed pre-test calculations of the test.

In the test three out of four hydro accumulators were used and two of them injected water to the upper plenum and one accumulator injected water to the downcomer. Two HPIS pump delivered cooling water to cold legs. One LPIS pump injected to cold and hot legs and the other LPIS pump to downcomer and upper plenum.

During the re-flood phase the analysis predicted that the core overheating began at 120 seconds. Due to high upward steam velocity in the downcomer pipe all emergency core cooling water, injected to the downcomer inlet chamber and cold legs, was drained to the break and none of that water penetrated to the downcomer pipe and further to the lower plenum and core. Emergency core cooling water, injected to the upper plenum, formed a pool and only part of that water penetrated into the core [4]. Due to several broken devices the final experiment was delayed. When the experiment 5a finally was performed core over heating was detected, but the ECCS water penetrated slowly to the core and quenched it around 450 s.

PWR-PACTEL

Lappeenranta University is modifying the PACTEL test facility so that it can be used to simulate a power plant with vertical steam generator. To support the PWR-PACTEL experimental program the planned characterizing experiments were calculated with the reference plant model. The aim of the calculations was to evaluate the behaviour of the real power plant in the test conditions and help planning the tests. The calculations are a supplementary work to the actual pre-test calculations with the model of the test facility. The calculated cases were a stepped primary side water inventory reduction and steam generator boil of test. Figure 11.1.3 shows schematic picture of the PWR-PACTEL test facility and APROS model of the steam generator. Please note that the hot and cold risers are separated with the so-called economiser plate.

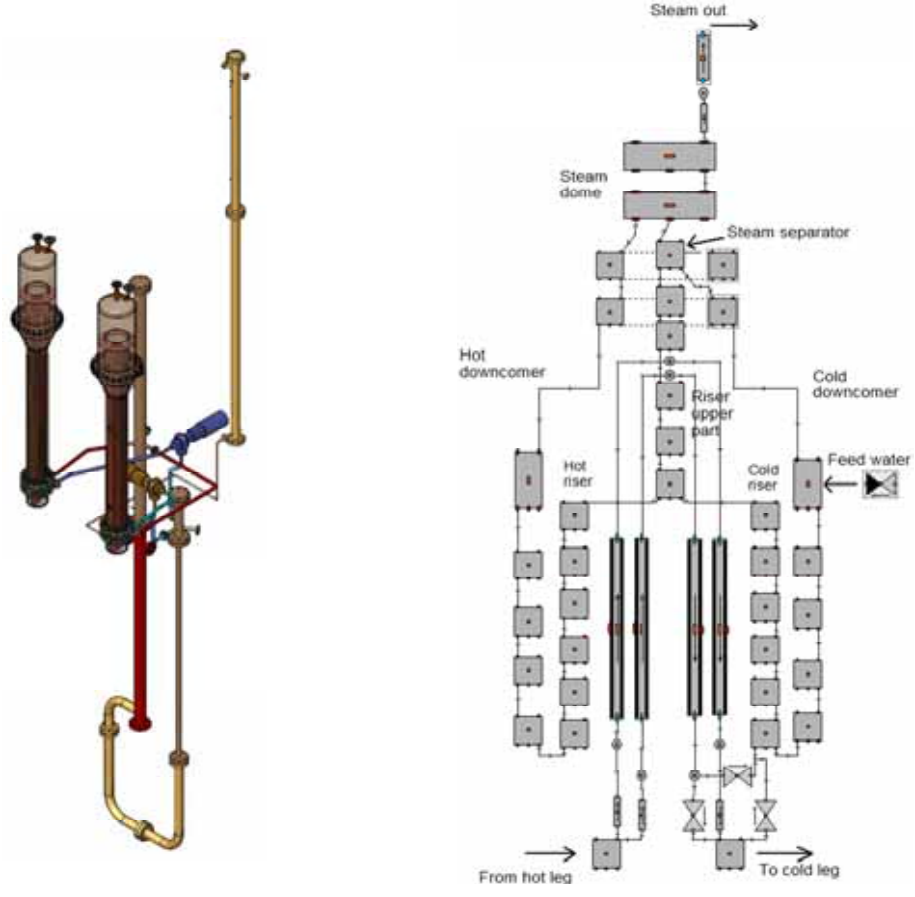

Figure 11.1.3. PWR-PACTEL test facility and APROS model of the steam generator.

In the steam generator boil of experiment (LOF = loss of feedwater) the feed water is closed and the steam generator will dry out gradually. The purpose of the test will be to study degradation of heat transfer in the steam generator. In the presented case a very low core power was used in order to produce slow boil of with quite stationary conditions with slowly decreasing water level. In the beginning of the transient the feed water was closed and the main circulation pumps were stopped. Figure 11.1.4 shows calculated temperature profiles in the U-tubes. In the initial state (time 0) the temperature difference from the inlet (node 1) to the outlet (node 14) is very small due to the low power level. When the primary pumps were stopped the inlet temperature increased and temperature difference became large (temperature profile at 1000 s). Most of the heat transfer takes place on the hot side of the steam generator (nodes 1–7). Heat transfer is maintained until the steam generator is almost empty. The hot side of the steam generator will dry out first, which can bee seen in the temperature profile at 9000 s. All the heat transfer takes place in the cold side (nodes 9–14). The steam generator was completely drained out at 10000 s [5].

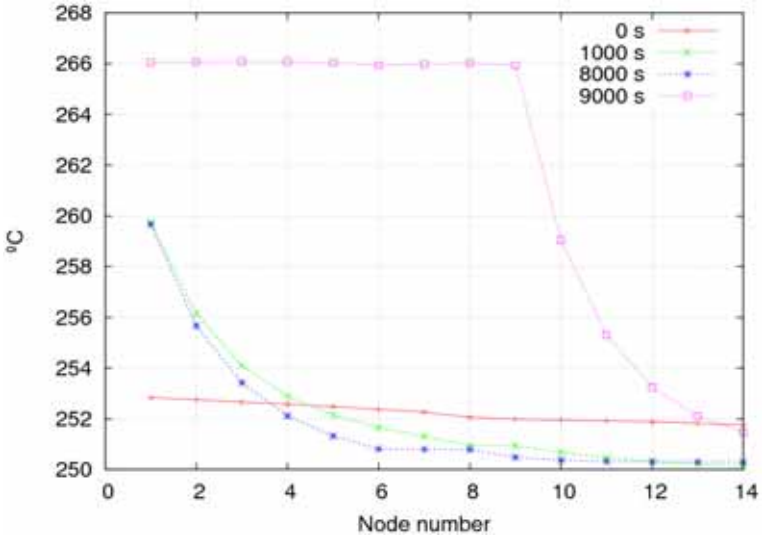

Figure 11.1.4. Calculated SG U-tube temperatures in LOF transient.

CCFL model validation

The upper tie plate counter current flow limitation model of APROS was validated against experimental data obtained at a full-scale test facility representing the

upper tie plate of the VVER-440 fuel channel [6]. The work is described in a separate article.

Containment thermal hydraulics

SARNET condensation benchmark

A condensation benchmark in SARnet co-operation in WP 12-2 (Containment Atmosphere Mixing) was calculated with Fluent CFD code. The first test case (benchmark-0) was a condensation test on a cold wall of a rectangular flow channel. Altogether 10 organisations took part in the numerical comparison (CEA, FZJ, FZK, JRCP, JSI, NRG, UJV, UNIPI, VEIKI, VTT). The results were discussed in the WP meetings and a common report was compiled [7].

APROS spray model validation with MISTRA experiments

In SARNET tests MASP1 and MASP2 the effectiveness of spray cooling was tested in the large 100 m^3 MISTRA tests facility. In the model the vessel was divided in four vertical layers and five radial sections (Figure 11.1.5). The initial stratified condition in the test vessel was formed with steam injection and with three cylindrical heat exchangers inserted inside the vessel close to the walls. Two top heat exchangers were kept at constant 140 ºC and the lowest one at 80 ºC temperature.

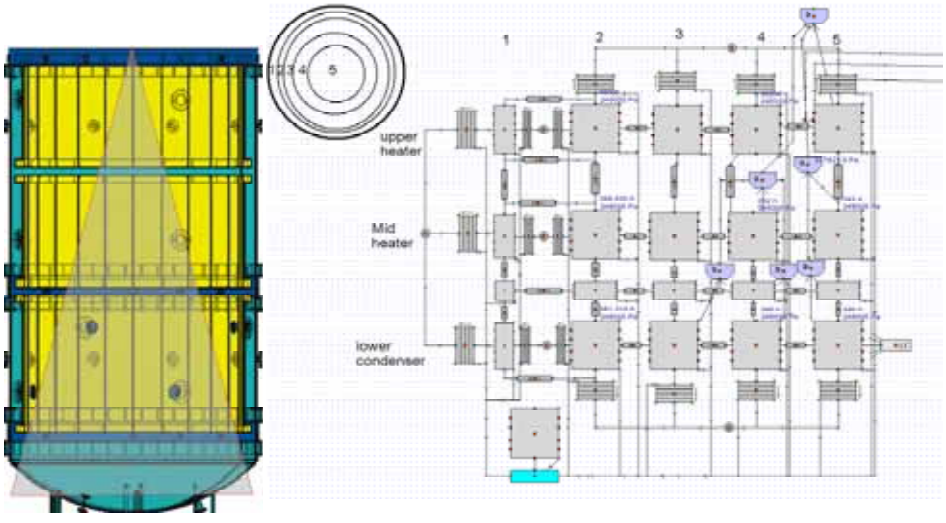

Figure 11.1.5. MISTRA test facility (on the left) and APROS model (on the right).

Simulated transient Masp1 started when the steam flow into the tank lower part was stopped. The tank pressure started to decrease as a consequence of the cooling mainly due to the lower cooler condenser. At 2100 s the spray injection was started. At 3900 s the spray injection was stopped and the system was again heated up by hot walls and heat exchangers. In Figure 11.1.6 the calculated pressure is compared with the measured pressure. During the cooling phase the calculated pressure decreases faster than the measured pressure. The reason is expected to be in the too efficient circulation in the calculation with the coarse lumped parameter model. After the spray cooling started at 2100 s, the calculated curve follows closely to the measured curve. After 3900 s, when the spray injection was switched off, the pressure increases due to heating of hot condensers and walls. The calculated pressure follows closely the measured value [8].

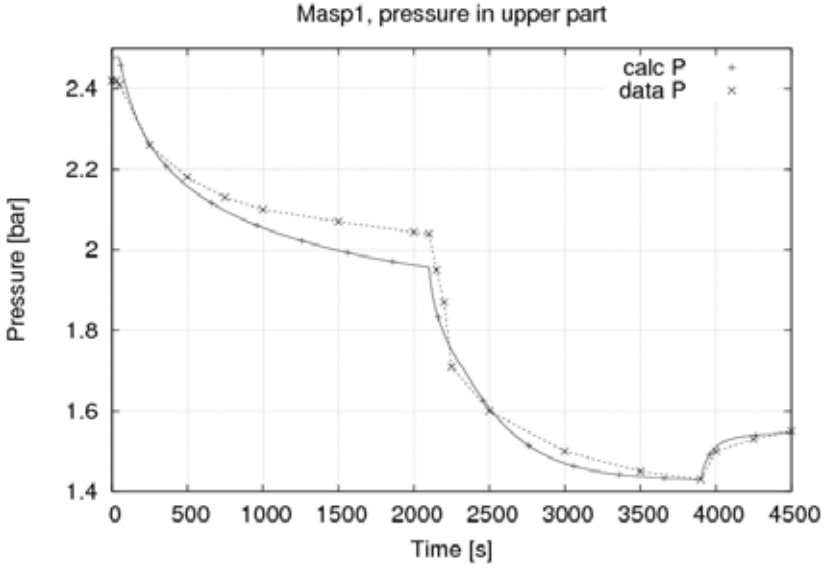

Figure 11.1.6. Calculated and measured pressure in the MISTRA MASP1 experiment.

Participation in the international research programs

Participation in the OECD working group of Analysis and Management of Accidents (WGAMA) and participation in the OECD research programs: PSB-VVER, ROSA, SETH2 and PKL2 is arranged through the THARE project.

Conclusions

Calculation methods for safety evaluation of nuclear power plants have been developed and validated. Both thermal hydraulic system analysis codes and CFD calculations have been used in the analysis and their usability have been studied and enhanced. An important objective has also been to train new thermal hydraulic code users and educate young experts.

References

1. Inkinen, P. OECD/ROSA-V Project Test 6-2 Simulation with APROS. Espoo 2008. VTT-R-01629-08.

2. Inkinen, P. OECD/ROSA Test 5-1 Simulation with APROS. Espoo 2009. VTT-R-00666-09.

3. Hillberg, S. TRACE model of the ROSA/LSTF. Espoo 2009. VTT-R-00319-09.

4. Junninen, P. PSB-VVER Large Break LOCA pre-test Analysis. Espoo 2008. VTT-R-00194-08.

5. Hillberg, S. Loss of Feed Water simulation with a PWR-PACTEL reference plant model. Espoo 2009. VTT-R-00805-09.

6. Kurki, J. Validation of APROS Upper Tie Plate CCFL Correlation in VVER-440 Geometry. Espoo 2009. VTT-R-00730-09.

7. Ambrosini, W., Bucci, M., Forgione, N., Oriolo, F., Paci, S., Magnaud, J.-P., Studer, E., Reinecke, E., Kelm, St., Jahn, W., Travis, J., Wilkening, H., Heitsch, M., Kljenak, I., Babić, M., Houkema, M., Visser, D.C., Vyskocil, L., Kostka, P. & Huhtanen, R. Comparison and Analysis of the Condensation Benchmark Results. The 3rd European Review Meeting on Severe Accident Research (ERMSAR-2008) Nesseber, Bulgaria, 23–25 September 2008. http://www.sar-net.org/upload/3-2_condensation-paper_final.pdf.

8. Hänninen, M. Simulation of MISTRA containment spray experiments with APROS. Espoo 2009. VTT-R-00654-09.

11.2 APROS CCFL model validation

Joona Kurki
VTT

Abstract

The upper tie plate countercurrent flow limitation correlation of APROS was validated against experimental data obtained at a full-scale test facility representing the upper tie plate of the VVER-440 fuel channel. Water and air treated as non-condensable gas were used as the fluids in the simulation. Values for the free parameters of the CCFL correlation were first defined, and then two experiments with different pressures were simulated. The simulation results show good agreement with the experimental results for the mass flow rates for which a quasi-stationary state could be established in the simulation software.

Introduction

Counter current flows (CCF) of water and steam occur in various transient situations in nuclear reactors, most notably during the reflooding phase of a loss-of-coolant accident (LOCA), where cold injection water flows against steam rising from the reactor core. As the upwards-flowing steam limits the downward flow of the cold injection water, and thus increases the time it takes to refill the reactor with water, it is evident that the flow limitation imposed by the counter current flow has a very strong effect on the safety of the reactor, and thus an analysis code's ability to predict this counter current flow limitation phenomenon (CCFL) is of great importance for safety analyses.

Validation of CCFL model

Previously, CCFL correlations developed only for single pipes and fuel bundles had been included in APROS. However, because the downcomer and the upper tie plate of the reactor have an important effect on the overall flow limitation in the above-mentioned transient situations, special CCFL correlations for these components were implemented in APROS [1, 2].

In the present work the upper tie plate CCFL correlation of APROS is validated against experimental data acquired from tests in a full-scale fuel-bundle test facility [3].

CCFL correlations

Counter current flow limitation correlations are usually based on the dimensionless Kutateladze numbers for liquid (k = l) and gas (k = g):

$$K_k = \frac{j_k \rho_k^{1/2}}{\left[g\sigma\left(\rho_\mathrm{l} - \rho_\mathrm{g}\right)\right]^{1/4}} \tag{11.2.1}$$

where ρ is density, j superficial velocity, g the gravitation constant and σ surface tension of water. These numbers are then correlated through equations of the form

$$K_\mathrm{g}^{1/2} + M_\mathrm{n} K_\mathrm{l}^{1/2} = C_\mathrm{n} \tag{11.2.2}$$

where the constants M_n and C_n are specific for each correlation [5].

The Glaeser correlation for the upper tie plate is [7]

$$K_\mathrm{g}^{1/2}\left(\frac{\nu_\mathrm{g}^{2/3}}{\mathrm{g}^{1/3} l}\right)^{1/2} + 0.014 K_\mathrm{l}^{1/2} = 0.027 \tag{11.2.3}$$

where v is the flow velocity and $l = d_\mathrm{c} \sin(0.5\theta_{\mathrm{ECC\text{-}BCL}})$, with d_c the characteristic diameter of the tie plate and $\theta_{\mathrm{ECC\text{-}BCL}}$ the angle between the hot leg with emergency injection and the broken hot leg. This correlation can be represented in the common form of a Kutateladze-type correlation (Equation 11.2.2) with

$$M_\mathrm{tp} = M_0\left(\frac{\mu_\mathrm{g}^{2/3}}{\rho_\mathrm{g}^{2/3} g^{1/3} l}\right)^{-1/2} \qquad C_\mathrm{tp} = C_0\left(\frac{\mu_\mathrm{g}^{2/3}}{\rho_\mathrm{g}^{2/3} g^{1/3} l}\right)^{-1/2} \tag{11.2.4}$$

where M_0 = 0.014 and C_0 = 0.027.

In APROS' two-fluid model, the CCFL correlations are implemented through defining the interfacial friction coefficients that correspond to the original correlations. For Kutateladze-type correlations, the following equation for the interfacial friction is used:

$$\tau_\mathrm{i} = \alpha(1-\alpha)\frac{\sqrt{g\left(\rho_\mathrm{l} - \rho_\mathrm{g}\right)}}{C_\mathrm{n}^4 d}\left[\sqrt{\rho_\mathrm{g}} + M_\mathrm{n}^2(1-\alpha)\sqrt{\rho_\mathrm{l}}\right]^2 \tag{11.2.5}$$

Equation (11.2.5) has been derived using the drift-flux model and the envelope theory flooding model [6]. It should be noted that Equation (11.2.5) corresponds to the Kutateladze-type correlation very well in steady-state calculation, but in transient situations the condition imposed by the correlation is naturally not strictly fulfilled.

The constants C_0 and M_0 in Equation (11.2.4) depended strongly on the geometry and of the flow channel and the flow regime, and thus, instead of using the original values of Glaeser, they were turned into user-definable variables in APROS. These values can be set through the APROS database variables `TH6_CCFL6_PARAM_1` (C_0) and `TH6_CCFL_PARAM_2` (M_0).

Defining the free parameters

The free parameters of the correlation, C_0 and M_0, must have reasonable values in order for the results to be realistic. Preliminary values for these constants were first determined by fitting a line ($y + ax - b = 0$) to the experimental results (see Figure 11.2.1), and then equating this line expression with Equation (11.2.2) in order to calculate the values of C_0 and M_0 from the fitting constants a and b. This procedure with the assumption of a liquid head of 80 cm above the perforated upper tie plate (p = 1.093 bar) led to constants C_0 = 0.127 and M_0 = 0.071.

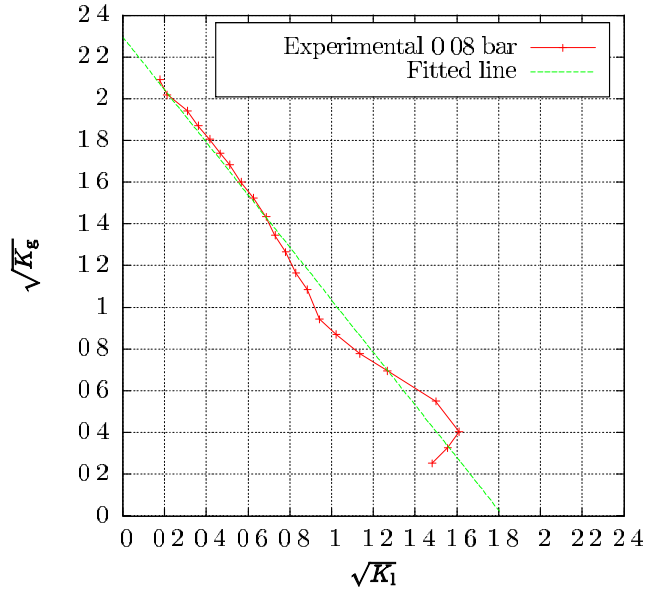

Figure 11.2.1. Fitting a line to the experimental data.

Because also other factors, such as hydraulic losses[1], play an important role in the flow limitation phenomenon, the correlation constants defined in the above-described fashion had to be further tuned in order to get good results. The final constants were defined through a process of trial and error in the simulation software. In the end, values $C_0 = 0.5$ and $M_0 = 0.071$ were used for the calculations.

Description of the experimental apparatus and operation

The correlation implemented in APROS was validated against experimental data obtained at a test facility representing the top area structures of the VVER-440, at the Hydraulic laboratory of Imatran Voima Oy. The purpose of the experiments was to study the influence of the flow restriction in vertical flow channels, such as the perforated upper tie plate and the fuel bundle structures below the plate, on the counter current flow behaviour of air and water at atmospheric pressures [3,4].

The test facility (see Figure 11.2.2) consisted of a vertical flow channel with different internal components. These components could be changed in order to make it possible to study the effect the geometries of these components have on the counter current flow behaviour.

At the test facility air was injected to the bottom part of the apparatus, and it flowed upwards through the internal components. At the same time water was injected to the top part of the test channel, from where it flowed downwards through the test section, towards the water collection chamber. Because of the flow limitation imposed by the upwards flowing air, the water may accumulate above the upper tie plate. As the accumulation of the water continues, a point is reached where the hydraulic pressure formed by the water column is large enough to overcome the flow limitation, and a part of the water blasts down. Thus the height of the water column above the upper tie plate is restricted.

The test procedure consisted of first establishing the air flow and then increasing the water flow until a stationary state with a predefined hydraulic head of either 0.2 m or 0.8 m (H_2O) was reached. In the stationary state, the

[1] According to paper [6] “The buoyancy, the interfacial friction, the liquid acceleration and the singular pressure losses are the most important forces playing a role in the countercurrent flow limitation phenomenon“.

height of the liquid column above the tie plate oscillates, but its time-average remains constant.

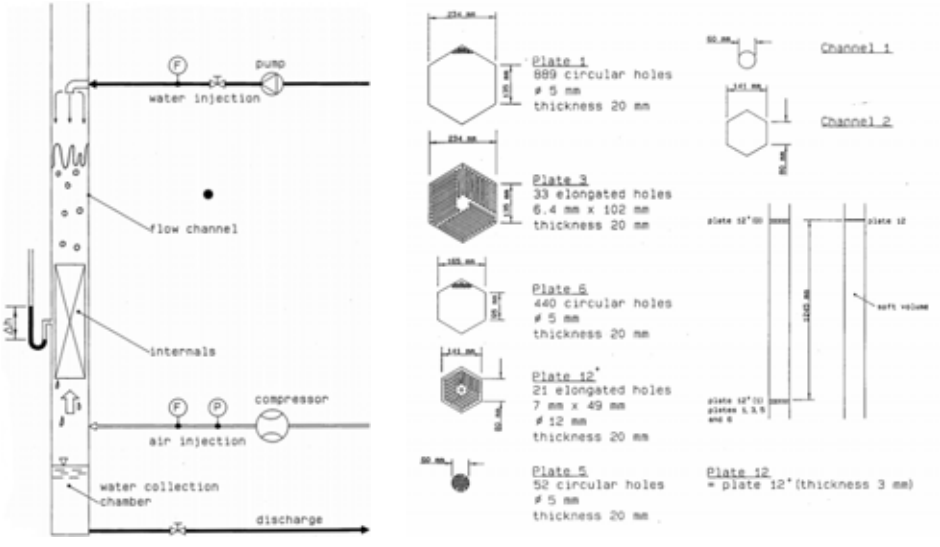

Figure 11.2.2. Left: a schematic diagram of the test setup for CCFL experiments, Right: perforated plates and flow channels used in the experiments [3].

APROS model of the test facility

APROS model of the test facility is illustrated in Figure 11.2.3. In the current work, only the plate 12 (VVER-440 tie plate in an empty hexagonal flow channel) experiments were calculated.

The upper and lower chambers, as well as the test channel above the tie plate, were modelled as single nodes. The lower part of the test channel is modelled with a pipe component with a single internal node – increasing the number of internal nodes had practically no effect on the results, but it made the simulation less stable. The upper tie plate is represented by a single branch with the length of 2.0 cm.

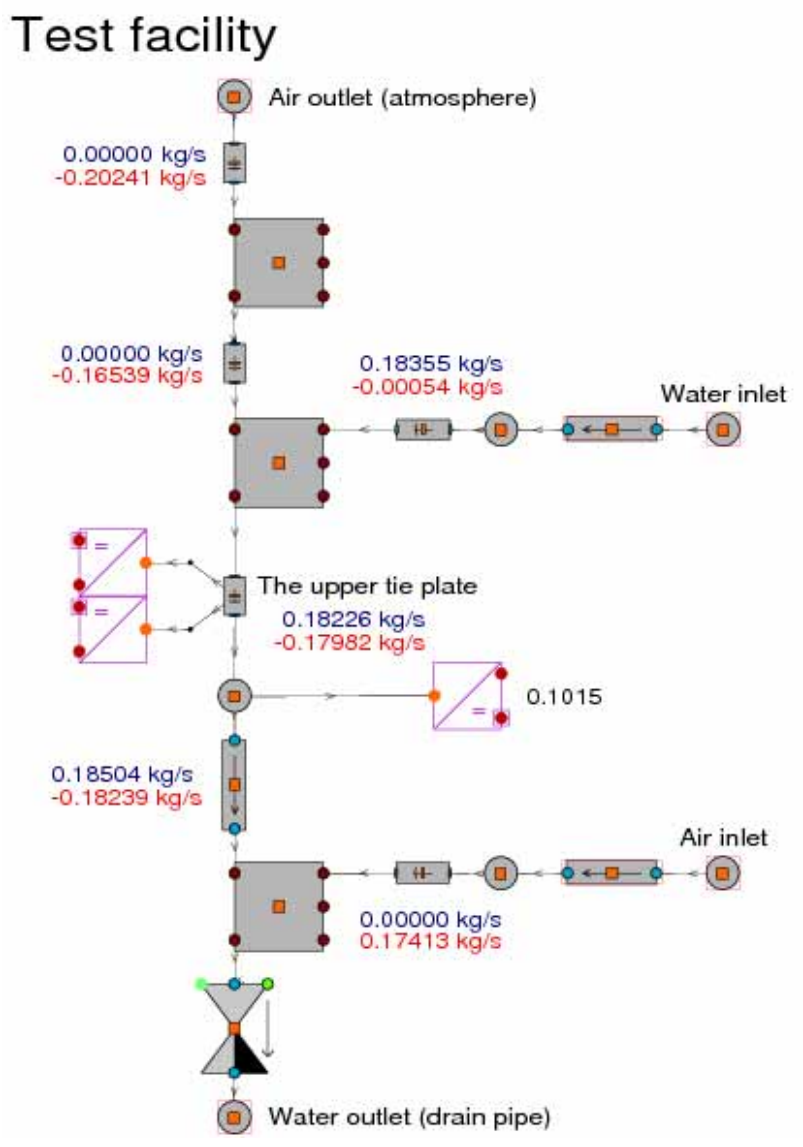

Figure 11.2.3. APROS model of the test facility.

The node above the upper tie plate was defined as completely separated (`NO_SEPAR_OPT = 1`) (i.e. it was assumed that in that node water was at the bottom and air at the top), and the momentum flux term was neglected in the tie plate branch (`BR_MOM_FLUX_USED = F`). Both these settings seem to be crucial in order for APROS to be able to arrive to a quasi-stationary state.

The CCFL-phenomenon was correlated only at the upper tie plate branch, since that is the narrowest part of the flow channel, and as such is the most important part contributing to limitation of the counter-current flow.

Pressure boundary conditions were imposed at the both outlets (p = 0.1013 MPa), and mass flow boundary conditions at the inlets. The system temperature, which was not specifically mentioned in the report [3], was taken to be 50°C. Air was used as the gas in the simulation[2]. Relative moisture of the air at the inlet was 8%.

Water level at the lower chamber was kept constant by controlling the bottom valve with a simple PI-control circuit.

The simulation procedure was essentially identical to the procedure taken at the real test facility; first the air flow was established, and then a water flow rate, that kept the liquid level constant above the upper tie plate, was determined through a process of trial and error. After the appropriate liquid flow rate was established, the simulation was continued over a prolonged period of time to ensure that the average water level above the upper tie plate as well as in the water collection chamber remained constant. Finally the mass flow rates at the inlets, and the densities of liquid and gas and surface tension at the tie plate branch, were taken down.

A very small time step ($\Delta t \leq 1$ ms) and error tolerance ($\varepsilon = 1.0 \cdot 10^{-5}$) had to be used to get good results.

Results and discussion

The results are presented in Figure 11.2.4. The simulation results are in good agreement with the experimental data for both the simulated cases. For the 0.02 bar (0.2 m water column) -case, water accumulation above the tie plate couldn't be established for the low gas flows.

[2] Air was used as the gas in the real experiment to ease the construction of the test facility, even though in real situations it is the steam rising from the reactor core that is limiting the flow of the cold injection water. Working with air also eliminates condensation and evaporation phenomena, which have also effect on the liquid flow rate through the system.

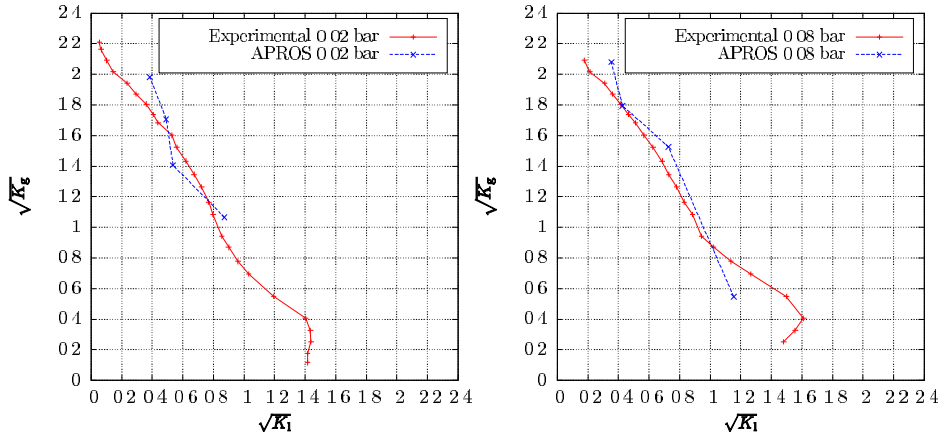

Figure 11.2.4. APROS results of the CCFL experiment simulation with the plate 12.

The simulation results show good agreement with the experimental data, but the fact that no results could be acquired for the low gas flow rates of the 0.02 bar experiment is a bit inconvenient. The failure of APROS to find a quasi-stationary state for these mass flow rates is for the large part caused by the use of non-condensable air instead of saturated steam as the flowing gas: simulation of a water/non-condensable gas system is a much stiffer problem than simulation of a system filled with water and steam, due to the lack of the interfacial mass-transfer, which tends to smooth out small perturbations, and due to the fact that steam partial pressure at 50°C is very small compared to the “normal” conditions of safety analyses. Small errors in steam mass calculation (condensation/ evaporation) have a strong influence in local gas temperature and pressure.

Conclusions

The new upper tie plate CCFL correlation of APROS was validated against experimental data obtained at a full-scale water/air experimental facility. It was observed, that when appropriate values are given to the free parameters of the correlation, the counter-current flow phenomenon is predicted with satisfactory accuracy in most cases using water and non-condensable air. However, the use of the non-condensable gas model of APROS makes the solution more sensitive to small numerical perturbations, which may make it difficult for APROS to find the quasi-stationary state. Fortunately, in real analyses, where the gas phase consists of saturated steam, these difficulties are not likely to occur.

11. Improved thermal hydraulic analyses of nuclear reactor and containment (THARE)

References

1. Hänninen, M. CCFL correlations for downcomer and upper tie plate. Research report VTT-R-08582-07 (confidential). Espoo: VTT Technical Research Centre of Finland, November 2007.

2. Hänninen, M. Implementation and validation of downcomer and upper tie plate CCFL correlations in a two-fluid code. Proceedings of the 16th International Conference on Nuclear Engineering ICONE16, May 11–15, 2008, Orlando, Florida, USA.

3. Kokkonen, I. Air/water countercurrent flow limitation experiments with full-scale fuel bundle structures. Research report IVO-A-07/89. Imatran Voima Oy, October 1989.

4. Kokkonen, I. Assessment of RELAP 5/MOD3 against CCFL tests with full-scale fuel bundle structures. Research report IVO-A-04/94. Imatran Voima Oy, September 1994.

5. Tuomisto, H. Large scale air/water flow tests for separate effects during LOCAs in PWRs. Nuclear Engineering and Design, 102, 1987, pp. 171–176.

6. Freitas, R. & Bestion, D. On the prediction of flooding phenomenon with the CATHARE code. In: Proceedings of NURETH 6, 1993. Pp. 1265–1272.

7. Glaeser, H. Downcomer and tie plate countercurrent flow in the Upper Plenum Test Facility (UPTF). Nuclear Engineering and Design, 133, 1992, pp. 259–283.

12. CFD modelling of NPP horizontal and vertical steam generators (SGEN)

12.1 SGEN summary report: CFD modeling of horizontal steam generators

Timo Pättikangas, Jarto Niemi and Ville Hovi
VTT

Tommi Rämä and Timo Toppila
Fortum Nuclear Services Oy

Abstract

A porosity model for the secondary side of the steam generator is formulated by following the ideas presented earlier by Stosic and Stevanovic [Num. Heat Transfer, Part B, **41**, 263 (2002)]. Porosity model means that the secondary side geometry is not described in detail but the tubes of the primary circuit are modeled as sources of enthalpy and as pressure loss. The Euler-Euler multiphase model of the Fluent CFD code is used, where conservation laws for mass, momentum and enthalpy of liquid and vapor are included. The source term for enthalpy is obtained by performing an APROS simulation of the primary circuit. The source terms for the conservation equations are implemented by using User-Defined Functions of Fluent. The model is tested by performing test simulations for a horizontal steam generator of a VVER-440 nuclear power plant. The main features of the test simulation are discussed.

Introduction

The detailed flow field of water and steam mixture on the secondary side of horizontal or vertical steam generators of the nuclear power plants (NPP) is fairly unknown. This is because of the lack of large experimental devices, and the difficulties related to the measurements in the real NPPs. Two-phase flow in a complicated three-dimensional geometry is also very challenging to solve numerically. Knowledge of flow fields and temperatures of water and vapor would, however, be very useful in steam generator life time management and accident analysis.

The geometry of the secondary side of a steam generator is too complicated for detailed three-dimensional CFD simulations. Therefore, some simplifications are necessary. Stosic and Stevanovic [1] have proposed using a model where the tube bundles of the primary circuit are modeled as porous media. The effect of the primary circuit on the secondary side is described with source terms of mass, momentum and enthalpy. The source terms of mass and enthalpy make possible to describe the heat transfer from the primary circuit to the secondary side. The source term of momentum describes the pressure loss caused by tubes of the primary circuit on the flow on the secondary side.

In CFD modeling, the Euler-Euler multiphase model is used, where equations for mass, momentum and enthalpy conservation are solved for two phases: liquid and vapor. The tubes of the primary circuit are described by using porosity. The numerical model contains the relevant interactions between the phases, such as the drag forces and the mass transfer between the phases due to evaporation and condensation. The source terms are implemented in the Fluent CFD code by using User-Defined Functions.

In modeling the secondary side of the steam generator, it is important to use a realistic model for the primary circuit because it determines the heat source and the distribution of the void fraction on the secondary side. Furthermore, the void fraction together with gravity determine the flow pattern on the secondary side. Therefore, the APROS code is used for modeling the primary circuit. The temperature of the outer wall of the primary circuit is calculated with APROS and interpolated to the three-dimensional CFD mesh.

The developed model is applied to horizontal VVER-440 type steam generator. As a test case, the solution of operating at full power level is presented. The main features of the coupling between the primary circuit and the flow on the secondary side are discussed. The validity of the results is examined qualitatively.

Porous media model for a steam generator

Conservation equations for phase q

$$\begin{aligned}
&\text{mass}: && \frac{\partial}{\partial t}(\alpha_q \rho_q) + \nabla \cdot (\alpha_q \rho_q \mathbf{v}_q) = S_{\text{mass},q} \\
&\text{momentum}: && \frac{\partial}{\partial t}(\alpha_q \rho_q \mathbf{v}_q) + \nabla \cdot (\alpha_q \rho_q \mathbf{v}_q \mathbf{v}_q) = \mathbf{S}_{\text{M},q} \\
&\text{energy}: && \frac{\partial}{\partial t}(\alpha_q \rho_q h_q) + \nabla \cdot (\alpha_q \rho_q \mathbf{v}_q h_q) = S_{\text{E},q}
\end{aligned} \qquad (12.1.1)$$

where α_q is the volume fraction, ρ_q is the density, h_q is the specific enthalpy and $\mathbf{v}_q$ is the velocity of the phase q, $(q=1)$ for liquid, $(q=2)$ for vapor and $(q=3)$ for solid tubes when necessary. The sum of the volume fractions is $\alpha_1 + \alpha_2 + \alpha_3 = 1$. The mass transfer between the phases, i.e., evaporation and condensation, is described with the source term $S_{\text{mass},q}$ on the right-hand side. The mass source term is discussed in detail in the next section.

The momentum source term $\mathbf{S}_{\text{M},q}$ on the right-hand side of the momentum equation contains interphase momentum transfer, lift force and virtual mass force. In addition, it includes effects of pressure gradient, gravitation and turbulence. The momentum source terms will be discussed in detail below.

The energy source term $S_{\text{E},q}$ on the right-hand side of the energy equation includes the interphase heat exchange, the effects of turbulence and changing pressure. The energy source terms are described in detail in the next section.

Momentum source terms

In the conservation law of momentum, Equation (12.1.1), the source term is

$$\mathbf{S}_{\text{M},q} = -\alpha_q \nabla p + \nabla \cdot \boldsymbol{\tau}_q + \alpha_q \rho_q \mathbf{g} + \mathbf{R}_{pq} + \mathbf{F}_{\text{CE},q} + \mathbf{F}_{\text{lift},q} + \mathbf{F}_{\text{vm},q} + \mathbf{F}_{\text{DF},q} \qquad (12.1.2)$$

where p is the pressure and $\mathbf{g}$ is the gravitational acceleration. The stress-strain tensor is denoted by $\boldsymbol{\tau}_q$ and $\mathbf{R}_{pq}$ is the interphase friction force and $\mathbf{F}_{\text{DF},q}$ is the friction caused by the tubes of the primary circuit. $\mathbf{F}_{\text{CE},q}$ is the force related to momentum transfer between phases, when mass transfer between phases occurs. The effects of the lift force $\mathbf{F}_{\text{lift},q}$ and the virtual mass force $\mathbf{F}_{\text{vm},q}$ have been neglected. The main forces driving the mixture circulation are the gravitational forces, wall friction affecting both phases and the interfacial friction.

The interphase friction force is proportional to the velocity difference between the phases: $\mathbf{R}_{21} = K_{21}(\mathbf{v}_2 - \mathbf{v}_1)$. Several models exist for the interphase momentum exchange coefficient K_{21}. The so-called symmetric model has been chosen [2].

Pressure losses in the axial and perpendicular directions caused by the tube bundles are described based on the porous material formulation. In this approximation, the drag force on the fluid phase consists of two parts: a viscous loss term proportional to flow velocity and an inertial loss term proportional to the square of the flow velocity. The linear term can often be ignored, when the flow velocity is large.

In an anisotropic porous medium, such as the tube bundles, the proportionality coefficients describing the friction forces are tensors, which vary depending on the direction:

$$\mathbf{F}_{\mathrm{DF},q} = -\mu_q \mathbf{D}_q \mathbf{v}_q - \frac{1}{2}\rho_q \left|\mathbf{v}_q\right| \mathbf{C}_q \mathbf{v}_q \tag{12.1.3}$$

The viscous loss term has been neglected: $\mathbf{D}_q = 0$.

The cross flow friction loss for the bundle, $\mathbf{C}_{\mathrm{CrossFlow}}$, may be derived by combining the friction loss coefficient for a single tube, $f_{\mathrm{CrossFlow}}$, and the summation effect resulting from several tube layers.

$$f_{\mathrm{CrossFlow}} = A\mathrm{Re}_{\mathrm{m}}^{-n} \quad \Rightarrow \quad \mathbf{C}_{\mathrm{CrossFlow}} = \frac{f_{\mathrm{CrossFlow}}}{P}, \qquad \left[\mathbf{C}_{\mathrm{CrossFlow}}\right] = \frac{1}{\mathrm{m}} \tag{12.1.4}$$

where P is the pitch in the cross flow direction and Re_{m} is calculated using mixture values. The following values for the parameter pair have been chosen: $A = 3.29$, $n = 0.18$.

The Blasius correlation can be applied in the direction parallel to the tube banks:

$$f_{\mathrm{CoFlow}} = \frac{0.3165}{\mathrm{Re}_{\mathrm{m}}^{0.25}} \quad \Rightarrow \quad \mathbf{C}_{\mathrm{CoFlow}} = \frac{f_{\mathrm{CoFlow}}}{d_{\mathrm{e}}}, \qquad \left[\mathbf{C}_{\mathrm{CoFlow}}\right] = \frac{1}{\mathrm{m}} \tag{12.1.5}$$

where d_{e} is equivalent diameter.

Mass source terms

The mass transfer between the phases is included as a source term in the continuity equation, Equation (12.1.1), for each phase. The source term for the liquid phase caused by condensation of vapor bubbles and evaporation of liquid

is $S_{\text{mass},1} = \dot{m}_{21} - \dot{m}_{12}$, where $\dot{m}_{pq}$ is the mass transfer rate from the phase *p* to the phase *q*. The source term for the vapor phase is $S_{\text{mass},2} = -S_{\text{mass},1}$.

Evaporation occurs, when the liquid enthalpy is higher than the liquid saturation enthalpy, i.e., $h_1 > h'$, whereas condensation occurs, when vapor is in contact with subcooled liquid, i.e., $h_1 < h'$. The following correlations are used for bulk evaporation and condensation

$$\begin{aligned} &\text{evaporation}: \quad \dot{m}_{12} = \frac{\alpha_1 \rho_1}{\tau_{\text{e}}} \frac{h' - h_1}{h'' - h'} \\ &\text{condensation}: \quad \dot{m}_{21} = \frac{\alpha_1 \rho_1}{\tau_{\text{c}}} \frac{h_1 - h'}{h'' - h'} \end{aligned} \tag{12.1.6}$$

where τ_{e} is the evaporation relaxation time and τ_{c} is the condensation relaxation time. Constant values of one second have been adopted for both relaxation times.

Energy source terms

In the conservation law of energy, Equation (12.1.1), the source term is

$$S_{\text{E},q} = -\alpha_q \frac{\partial p}{\partial t} + \boldsymbol{\tau}_q : \nabla \mathbf{v}_q - \nabla \cdot \mathbf{q}_q + Q_{pq} + S_{\text{EC},q} + S_{\text{PR},q} \tag{12.1.7}$$

where $\mathbf{q}_q$ is the heat flux, Q_{pq} is the intensity of heat exchange between phases *p* and *q*. The last two terms are related to condensation and evaporation and to heat transfer from the primary circuit. In the following, some of these source terms are discussed in detail.

In terms of the surface area heat transfer coefficient, the volumetric boiling heat flux is

$$q'''_{\text{wb}} = h''_{\text{wb}} \left(T_{\text{w}} - T_{\text{sat}} \right) \left(\frac{A_{\text{s}}}{V_{\text{tot}}} \right) \tag{12.1.8}$$

The surface area heat transfer coefficient, h''_{wb}, is derived from the Thom pool boiling correlation [3].

The source term of enthalpy caused by bulk evaporation and condensation in Equation (12.1.7) for the liquid phase is

$$S_{\text{EC},1} = (\dot{m}_{21} - \dot{m}_{12})(h'' - h_1) \tag{12.1.9}$$

where $\dot{m}_{pq}$ denotes the mass transfer rate due to condensation or evaporation, respectively. The corresponding source term in the enthalpy equation for vapor is

$$S_{\mathrm{EC},2} = (\dot{m}_{12} - \dot{m}_{21})(h'' - h_1) \tag{12.1.10}$$

Model of horizontal steam generator of VVER-440

APROS model of the primary circuit

The primary circuit has been divided into five horizontal layers in the APROS model. The uppermost layer is presented in Figure 12.1.1. Several tubes are modeled with the same APROS component: four consecutive tubes in the horizontal direction and fifteen in the vertical direction. The flow rate of the primary circuit is controlled by a control valve and a control circuit.

The secondary side of the steam generator is presented in Figure 12.1.2. The portion of the secondary side occupied by the tube bundles has also been divided into five horizontal layers. Five horizontally aligned downcomer nodes have been added to allow some recirculation, and the area above the tube bundles (steam dome) is modeled with two nodes. The heat transferred in each of the five layers of the primary circuit is conveyed into its own node on the secondary side. The feed water flow is adjusted with a three-point control, which monitors the water level of the uppermost downcomer node.

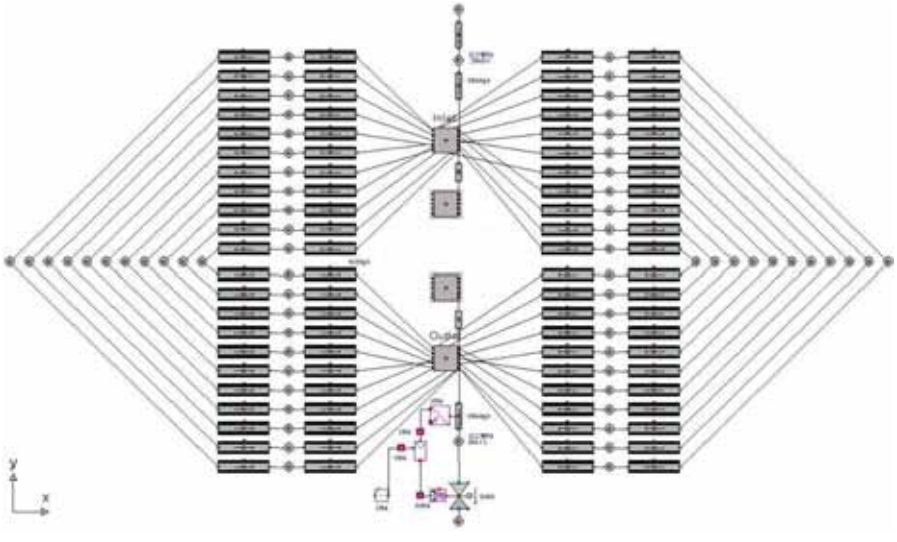

Figure 12.1.1. The uppermost level of the primary circuit in the APROS model.

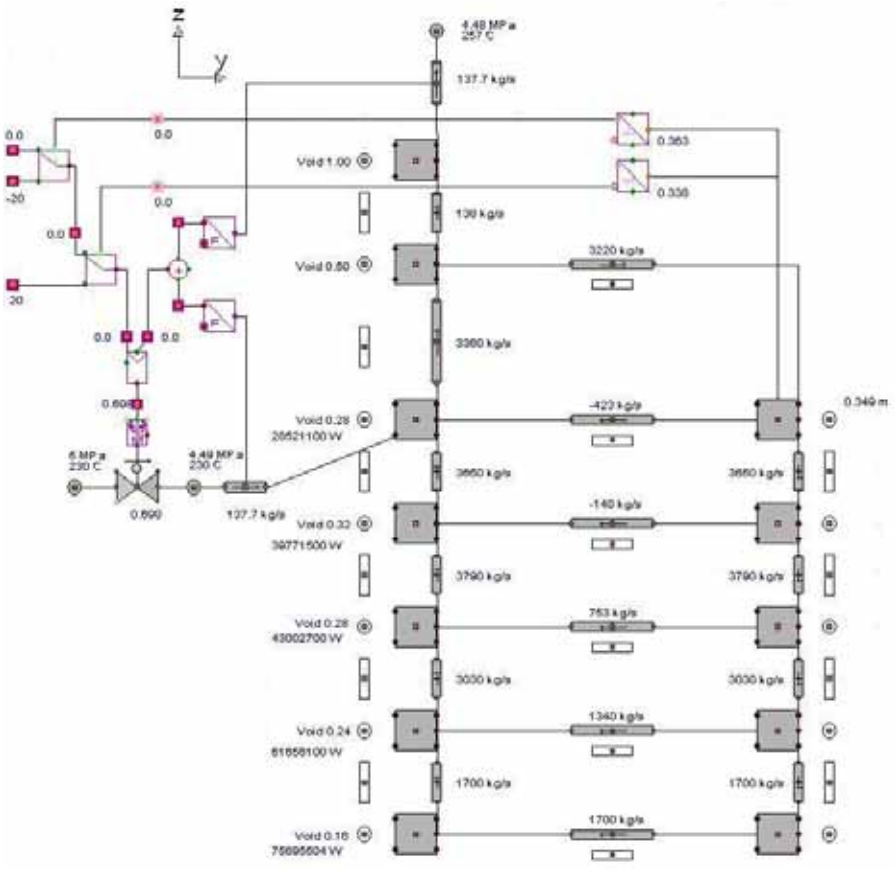

Figure 12.1.2. The secondary side of the APROS model.

Fluent model of the steam generator

The secondary side of the horizontal steam generator has been modeled using the Euler-Euler multiphase model of Fluent. The portion of the steam generator occupied by the tube bundles has been described with the porosity model of Fluent, which introduces the additional pressure loss and the enthalpy source. The source terms were included in the model by using User-Defined Functions of Fluent.

The model has been tested by using two different meshes in Fluent. The coarse mesh consists of 87 000 grid cells and the fine mesh contains 930 000 grid cells. The grid is almost purely hexahedral, only few thousand tetrahedral, pyramid and wedge cells have been used in the fine mesh. The free flow areas

are modeled with a finer mesh than the porous areas. The tube support plates are represented as thin walls. Fluent model is shown in Figure 12.1.3, where the tube banks are green and the support plates and collectors are shown in brown.

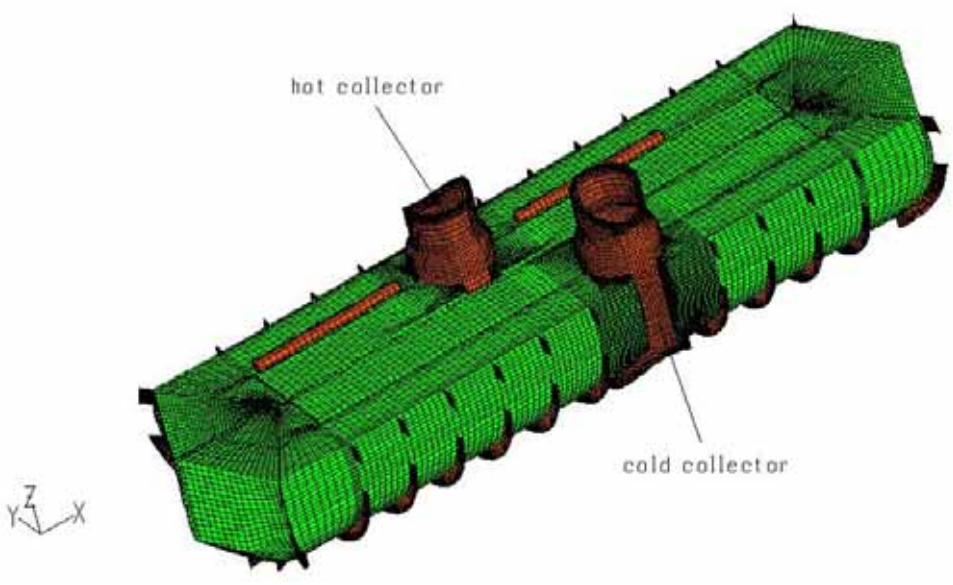

Figure 12.1.3. Fluent model of the secondary side of the steam generator.

APROS-Fluent coupling

Simulation of the primary circuit by using APROS makes possible to provide a realistic boundary condition for the CFD simulation of the secondary side. The temperatures of the outer wall of the tubes of the primary circuit are solved by using the APROS model of the steam generator. The outer wall temperatures are interpolated from the nodes of the APROS model to each grid cell in the tube bundles of the Fluent model. The interpolation is based on finding the nearest APROS node for each grid cell of the Fluent model. The outer wall temperatures are then used in the CFD simulation for calculation of the heat transfer from the primary circuit to the secondary side.

The flow on the secondary side is driven by gravitation and the density differences of the water-vapor mixture. The density differences are caused by the differences in void fraction, which are caused by differences in heat transfer on the cold and hot side of the steam generator. Therefore, it is expected that the

use of accurate estimates for the wall temperatures of the primary circuit is a crucial step in determining the correct flow field on the secondary side.

Simulation of a VVER-440 steam generator

In the following, simulation results for a horizontal VVER-440 steam generator are presented. First, the parameters for operation at full power are discussed. Then, the main features of the simulation results are described. The results that are presented have been obtained with the fine mesh shown in Figure 12.1.3.

In steam generator, the heat energy from the primary circuit is transferred to the feed water injected to the secondary side. Feed water is evaporated and the steam dried, before it flows to the steam piping and out of the steam generator. Parameters presented in Table 12.1.1 have been used for modelling the geometry and as boundary conditions in the simulation discussed below.

Table 12.1.1. Process variables for the simulation of steam generator at full power.

$P_{thermal}$	250 MW	Q_{steam}	138 kg/s
T_{prim} (in/out)	299°C / 264°C	Q_{feed_water}	138 kg/s
T_{sec}	257°C	Length	11.8 m
$T_{feedwater}$	230°C	Diameter	3.2 m
p_{prim}	123 bar	Water volume of the secondary side	44–49 m^3
p_{sec}	44.8 bar	Water volume of the primary side	10.2 m^3
Q_{prim}	1 364 kg/s	Heat transfer area	2 510 m^2

As a test case, operation at a full power of 250 $MW_{thermal}$ was simulated. Even though the calculation was carried out as time-dependent simulation, the goal was not to simulate any transient but to find a reasonable steady water level for the steam generator. Convergence towards the steady water level was evaluated by monitoring the void fractions at different horizontal planes of the steam generator.

The feed water injection is located above the tube bundles and it is the flow inlet boundary of the model (see Figure 12.1.3). The flow outlet boundary is set by the secondary side pressure at the top of the model. Heat is brought to the

model through tube bundles, which are modeled as porous media with porosity of 0.72.

In Figure 12.1.4, the outer wall temperatures in different parts of the tube bundles are shown for the full power case. The wall temperatures have been solved with APROS and interpolated to the Fluent mesh. The largest temperature values occur at the upper part of the tube bundles near the hot collector.

The results for the operation at the full power are presented in Figures 12.1.5–12.1.8. In Figures 12.1.5 and 12.1.6, one can see that the amount of water is clearly larger on the cold side. In Figure 12.1.5, the effect of the feed water is clear on the plane $x = –2.67$ m, which is located more towards the hot collector end of the steam generator. In Figure 12.1.6, one can see that on the hot collector side occurs more foaming; in total there occurs great deal of mixing and the void fraction of steam is between 0.3 and 0.8. Level of 100% pure steam is a bit upper on the hot side near the collector.

In Figure 12.1.7 and 12.1.8, the flow patterns are shown in two cross-sections of the steam generator. Water flows downwards near the walls and upwards in the tube bundle area. Small water vortexes at the bottom part of the steam generator and the feed water injection also affect the steam flow. Water flows towards the bottom along the shell from both sides of the steam generator colliding at the stagnation point at the bottom. The stagnation point is not located exactly at the center but more on the hot side, where the feed water injection is also located. Largest flow velocities are found near the outlet, otherwise the flow velocities are mostly below 2 m/s for both water and steam.

Conclusions

The coupled APROS-Fluent model of the steam generator has been found to be a promising tool for analyzing the horizontal steam generator of VVER-440 nuclear power plant. The model is numerically quite robust, which makes it possible to use it for practical applications. When a coarse mesh of about 87 000 grid cells was used, a converged stationary solution could be obtained within a few days. When a fine mesh with about 930 000 grid cells was used, the computing time was more than one week when a good initial guess for the flow field was used.

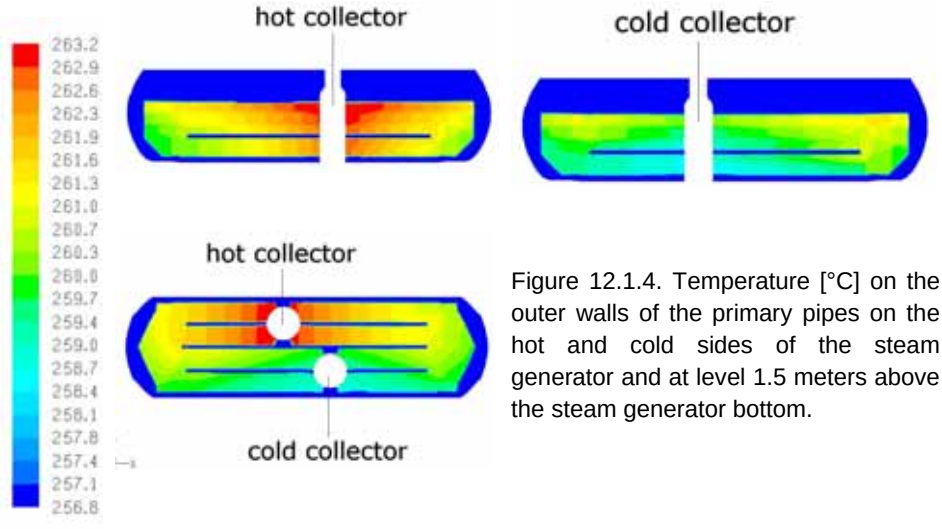

Figure 12.1.4. Temperature [°C] on the outer walls of the primary pipes on the hot and cold sides of the steam generator and at level 1.5 meters above the steam generator bottom.

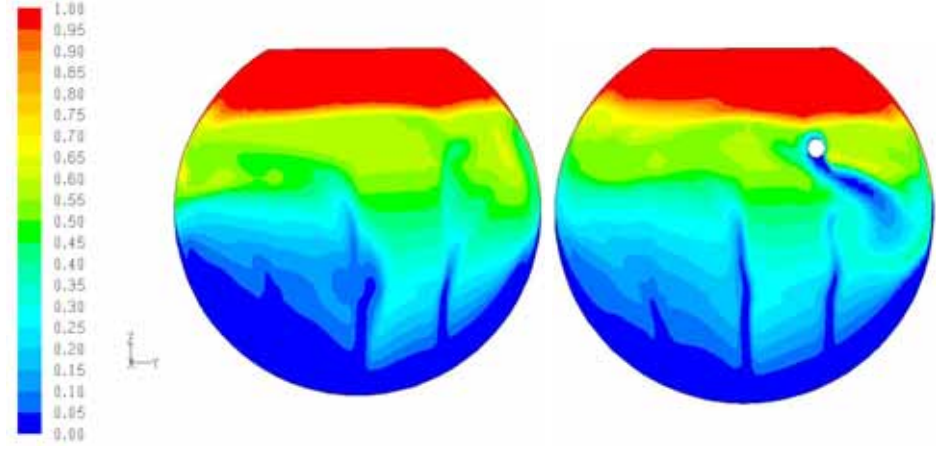

Figure 12.1.5. Void fraction in the plane x = 0 (left) and x = –2.67 m (right). Plane x = 0 is located at the center of the steam generator in the axial direction.

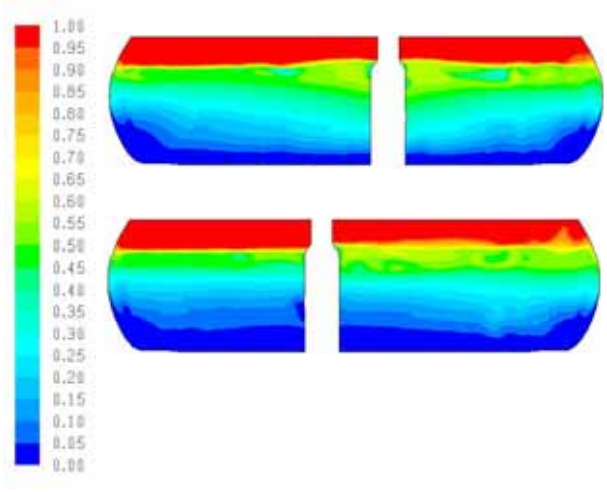

Figure 12.1.6. Void fraction on the hot side (top) and the cold side (bottom) of the steam generator.

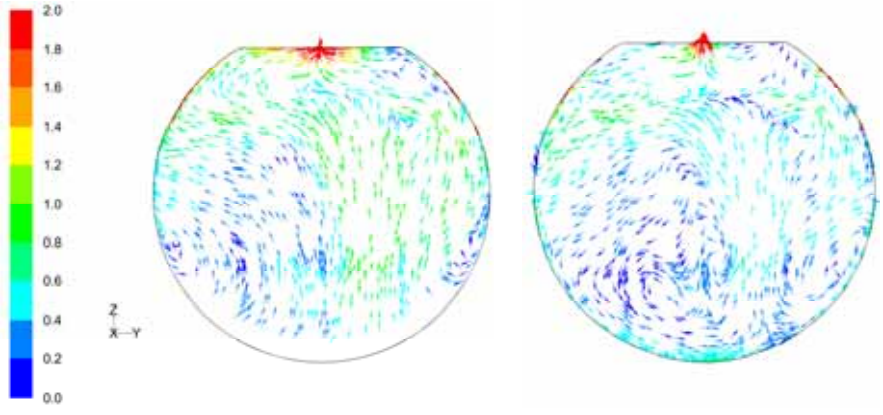

Figure 12.1.7. Velocity vectors of steam (left) and water (right) in the plane x = 0. The vectors are colored with velocity magnitude (m/s).

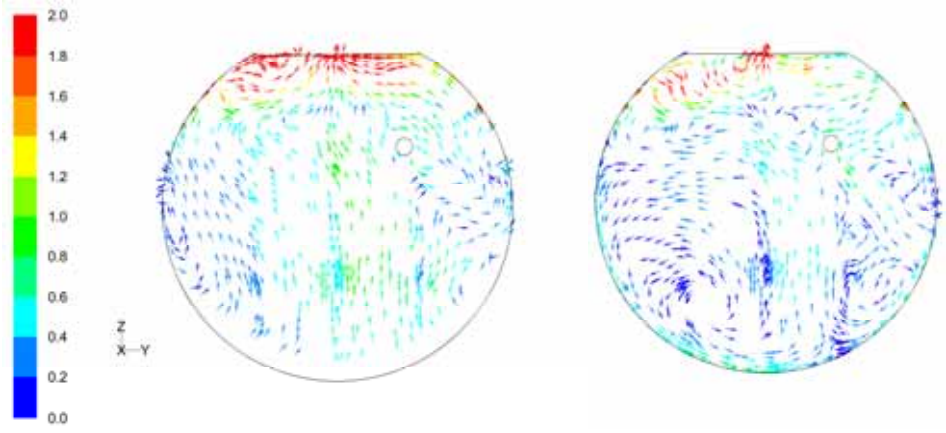

Figure 12.1.8. Velocity vectors of steam (left) and water (right) in the plane x = –2.67 m.

The results obtained for the flow fields and void fractions behave qualitatively in a reasonable manner. The distinctive features of the hot and cold side of the steam generator are found in the results, such as the high void fraction on the hot side and the shape of the water surface. The flow velocity fields of water and steam also behave in an anticipated manner. Gravitation and the density difference of the mixture between the hot and cold side of the steam generator determine the main features of the flow field. The fine hexahedral mesh used in the simulation makes also possible to describe quite accurately the regions without tubes, such as the narrow gaps between the tube bundles.

The developed novel interpolation method made possible to use the result of APROS simulation as outer wall temperatures of the primary circuit in the CFD simulation. The heat transfer from the primary side to the secondary side determines the void fraction and the flow pattern on the secondary side. Therefore, the APROS-Fluent coupling is an essential part of the present analysis.

Quantitative validation of the developed model has still to be done. This will be a challenging task because of the scarcity of the available validation data. Some information can be obtained from practical operating experience of steam generators. A well instrumented experiment would, however, be optimal for further validation studies.

References

1. Stosic, Z.V. & Stevanovic, V.D. Advanced three-dimensional two-fluid porous media method for transient two-phase flow thermal-hydraulics in complex geometries. Numerical Heat Transfer, 2002. Part B, Vol. 41, pp. 263–289.

2. Fluent, Fluent 6.3 User's Guide, Lebanon USA: Fluent Inc., September 2006.

3. Groeneveld, D. & Snoek, C. A Comprehensive Examination of Heat Transfer Correlations Suitable for Reactor Safety Analysis. In: Hewitt, G., Delhaye, J. & Zuber, N. Multiphase Science and Technology, Vol. 2. Hemisphere, 1986. Pp. 181–274. ISBN 0-89116-283-8.

13. Improvement of PACTEL facility simulation environment (PACSIM)

13.1 PACSIM summary report

Juhani Vihavainen and Antti Rantakaulio
Lappeenranta University of Technology

Abstract

The main objective of the PACSIM project is to improve the simulation environment of PACTEL facilities with TRACE thermal hydraulic code. TRACE code has been utilized for preparing different simulation models for the VVER and PWR PACTEL facilities. The Finnish Radiation and Nuclear Safety Authority, STUK, has required an independent tool to support safety and licensing analysis and chosen TRACE code for this purpose. The PACSIM project supports this requirement. The new model of VVER PACTEL was tested against pressure and heat loss experiments. Also, loss-of-feedwater experiment LOF-10 was calculated. The calculation results agreed reasonably well with the experiment although some difficulties occurred. The PWR PACTEL model with vertical steam generators was prepared and functionality was tested and found to be satisfactory.

Introduction

The Parallel Channel Test Loop (PACTEL) facility [1], constructed in the Laboratory of Nuclear Engineering at Lappeenranta University of Technology (LUT) in Finland 1990, is one of the largest facilities of its kind. It was originally designed to model the thermal hydraulic behavior of the VVER 440

type pressurized water reactors (PWR) currently used in Finland. Recent modifications in the frame of Tekes project PAOLA have introduced a new set-up of PWR PACTEL facility, which now contains two vertical steam generators and new hot and cold loops for them. Figure 13.1.1 shows VVER and PWR PACTEL facilities. The Finnish Radiation and Nuclear Safety Authority, STUK has required an independent tool to support safety and licensing analysis. According to the Code Applications and Maintenance CAMP agreement with USNRC the TRACE code and Symbolic Nuclear Analysis Package (SNAP) graphical user interface are set to use of the partners. Hence, TRACE code (currently version 5.0 Patch 1) has been recently implemented at LUT. The first modeling exercise in the way towards whole model of the PACTEL facility was to prepare a model for horizontal steam generator of the PACTEL facility using the SNAP model editor. In the frame of PACSIM project on SAFIR2010 programme full models of VVER and PWR PACTEL facilities have been prepared.

Main objectives

The main objective of the PACSIM project is to improve the simulation environment of both VVER and PWR PACTEL facilities with TRACE thermal hydraulic code. This project aims to develop the VVER PACTEL model further and prepare a complete model with three loops with necessary control modules. This gives important validation knowledge for achieving the final goal of the full-scale VVER-440 model preparation, which will be carried out outside the SAFIR2010 programme. Another objective is to prepare a new TRACE-model with vertical steam generators for the modified PWR PACTEL facility. The use of the TRACE code enhances the preparedness to give analysis support and improves education in computational thermal hydraulics. The TRACE code calculations will give valuable analysis and comparison support for the Apros calculations of the PWR PACTEL experiments.

TRACE code

TRACE code is a new thermal hydraulic system code, which is developed by USNRC. The TRACE (TRAC/RELAP Advanced Computational Engine) – formerly called TRAC-M is the latest in a series of advanced, best-estimate reactor systems codes developed by the USNRC for analyzing transient and steady-state neutronic-thermal-hydraulic behavior in light water reactors. It is the product of a long term effort to combine the capabilities of the NRC's four main systems

codes (TRAC-P, TRAC-B, RELAP5 and RAMONA) into one modernized computational tool. NRC has stated that it is committed in future to TRACE code. RELAP5 will be maintained but only for legacy purposes. TRACE is going under development process and it will have all capabilities of RELAP5. TRACE has similar or better capabilities and accuracy for most applications compared to RELAP5. The USNRC recommends CAMP members to focus their assessment on TRACE.

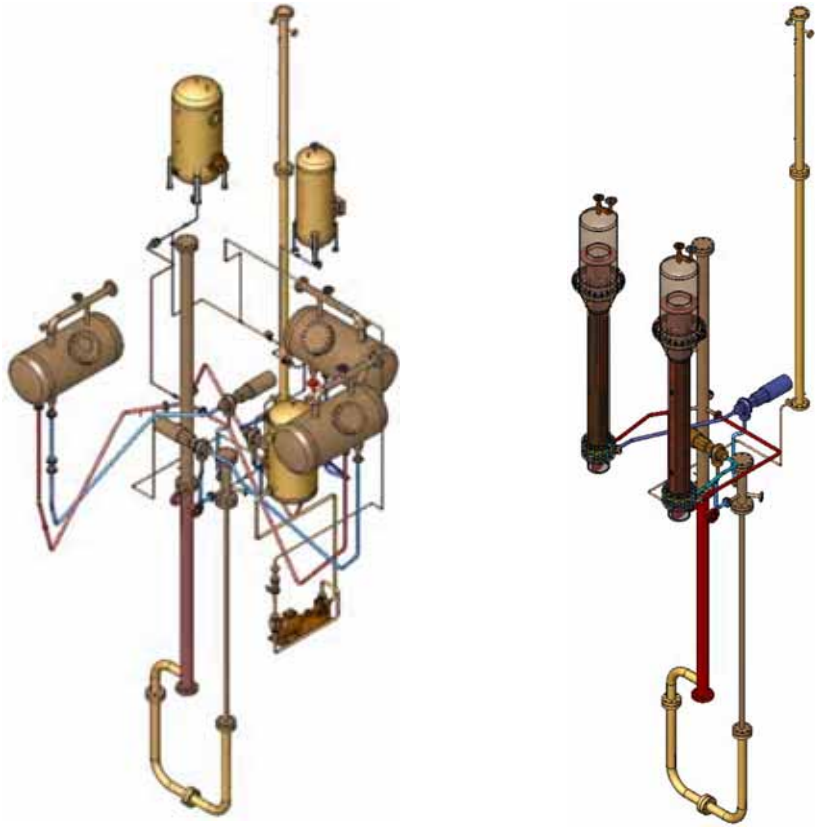

Figure 13.1.1. Views of VVER- and PWR-PACTEL facilities.

TRACE code modeling of VVER-PACTEL facility

The TRACE modelling of the VVER-PACTEL is based to the guidelines on the earlier RELAP5 model [2]. Since the RELAP5 and TRACE codes are not alike structured the transfer from RELAP5 to TRACE was not straightforward [7].

The model geometry had to be re-evaluated and re-checked for the TRACE code configuration. Figure 13.1.2 shows example of main differences between RELAP5 and TRACE code meshing. In RELAP5 pipe bend is described with two elements but in TRACE the bend is described with only one element containing the bend inside.

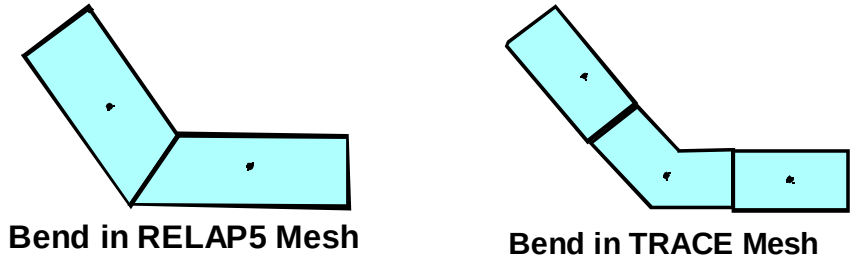

Figure 13.1.2. Differences between RELAP5 and TRACE meshing.

The primary side model of VVER-PACTEL consists of pressure vessel part modeled with U-shape piping and three primary loops modeled individually since they have geometry differences. Main circulation pumps and closing valves are also modeled. The upper plenum of the facility is modeled with two parallel pipes connected together with single junctions. This represents the diffusor structure, which consists of two nested concentric pipes in real facility. Pressurizer is modeled using standard pipe component. The core section is divided in three parallel lines and the heat production in core as well as in pressurizer heaters is implemented with POWER components, which can be controlled with time dependent functions and trips. The primary tube bank in each horizontal steam generator is divided in eight rows. Three top rows represent one tube row of real PACTEL facility. Other tube rows represent two rows of real facility. Secondary side is divided in riser and downcomer sections. The top part of the steam generator is modeled with separator component. Figure 13.1.3 presents the main view of the graphical set-up of the VVER-PACTEL created with SNAP model editor showing the loop-1 connected to the pressurizer and steam generator.

TRACE calculations of pressure loss tests

The TRACE model of PACTEL was validated against pressure loss test FLT (Runs 04, 08 and 11) [3]. Several PACTEL experiments have been performed to determine the pressure losses over the whole test loop both for normal and for reverse flow direction. Main parts of the facility, three primary circuits, a pressure vessel and a pressurizer surge line, were all measured separately. Pressure losses have been measured over a large scale of mass flow range. Usually the highest mass flow value from the top range of the experiment data was picked. Then the TRACE model pressure loss in this certain mass flow point was adjusted to match with reasonable accuracy by using additive form loss values. The model correspondence was then checked in all measured mass flow data points. The calculated results were agreeable with experiment data in most cases.

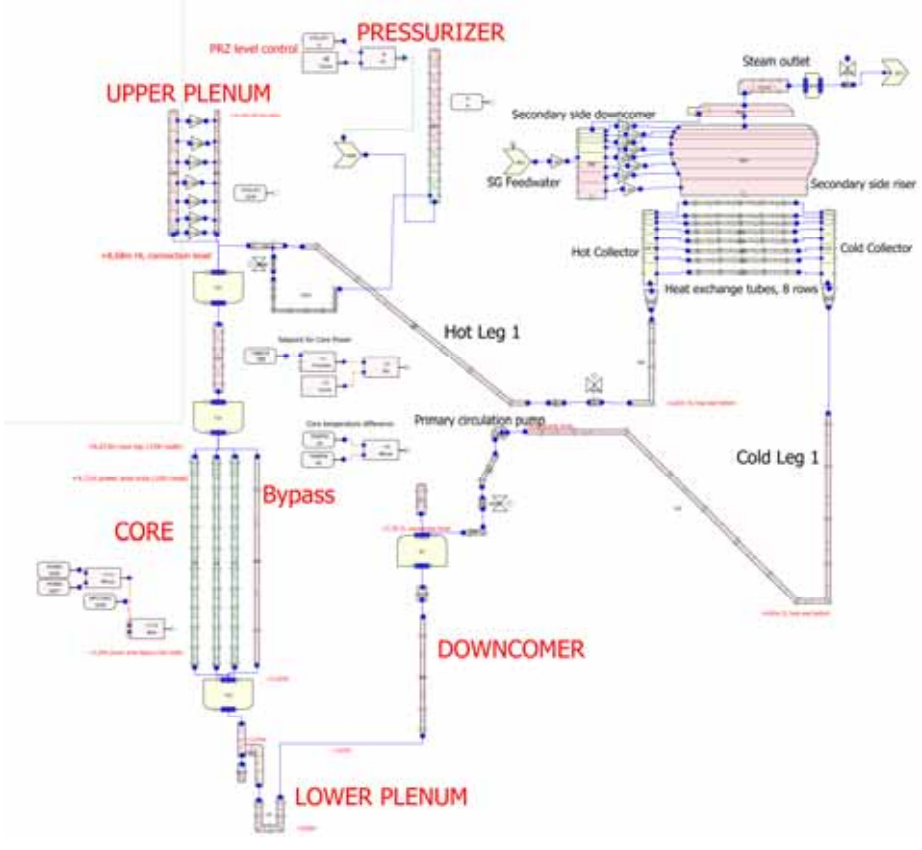

Figure 13.1.3. Main view of the VVER-PACTEL facility model by SNAP editor.

TRACE calculations of heat loss tests

Heat loss experiments were carried out during IMPAM/VVER EU-project. Primary heat losses of the PACTEL facility were defined using the heat-up and cool-down method presented by J. Sanders [4]. The model of TRACE code was modified for specific initial conditions. The secondary side of steam generators was filled with air in atmospheric pressure to minimize the heat transfer via steam generators.

It was obtained that the heat up phase of the experiment contains many uncertainties. The water was drained out from the facility several times in order to avoid pressurizer to become full. However, these drainings were not recorded in the experiment data. Also, water was injected back to the facility during the steady state phase. Therefore it was decided that the heat up phase calculation was not implemented further and only the steady state period and cooling down phases were simulated.

A steady state calculation was then introduced to achieve the thermal values in the facility just before the start of the cooling phase. Steady state option of TRACE was not used since the case was too complicated. The calculation for achieving steady state was carried out in transient mode. The model used control devices for pressurizer pressure and level and also logical setup for pressurizer heaters.

The first calculations showed that the pressurizer has significant effect to the overall behaviour of the facility. The pressurizer level started to decrease as soon as core power was switched off and cooling down began. After few thousand seconds of cooling phase the pressurizer level started to rise. This was a consequence of vapor forming in the upper plenum. Obviously, this phenomenon slowed down the pressure decrease of the facility. The heat losses were adjusted by modifying the thermal conductivity of the mineral wool and the heat transfer coefficient at outer surface.

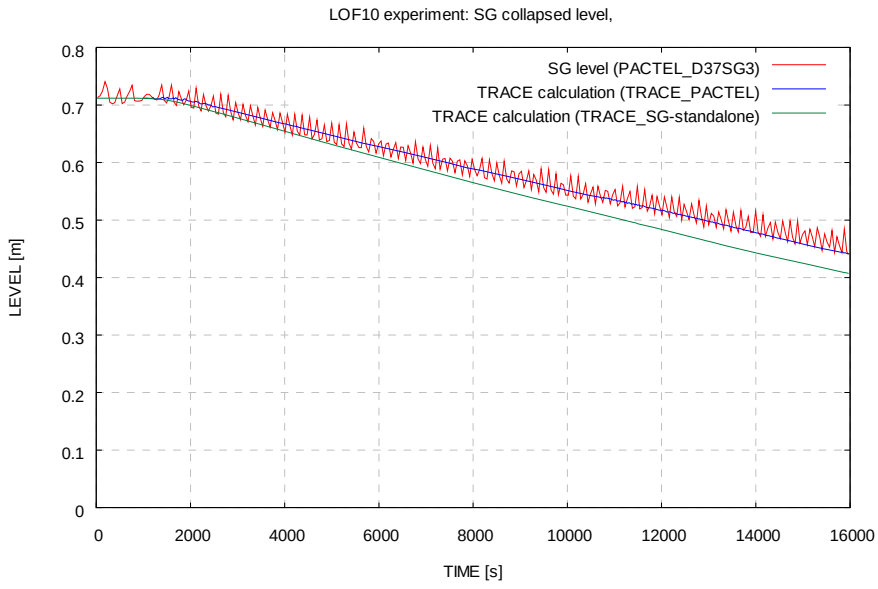

Figure 13.1.4. Measured and calculated collapsed level in steam generator. PACTEL Experiment LOF-10.

TRACE calculations of LOF-10 test

The next case was to calculate loss-of-feedwater experiment LOF-10 [5, 6]. This case had earlier been calculated and reported via CAMP programme with the separate steam generator model [8]. The objective of this calculation was to check the behaviour of the whole facility in transient case. The calculation results showed that the code is capable to model the behaviour of horizontal steam generator also in natural circulation mode. Figure 13.1.4 presents the collapsed level trend of steam generator. The calculation with the whole PACTEL facility model gives more accurate results than the stand-alone calculation. Explanation to better performance of the whole facility model derives from the fact that the mass flow rate of natural circulation and heat losses were more realistic assessed.

Modelling of PWR-PACTEL facility

The main goal of this work was to create a TRACE model of PWR PACTEL's vertical steam generator and connect it to PACTEL's TRACE model. SNAP was

used to create the model. The model consists of the primary and secondary sides. There is also a simple control system modeled, which controls the feedwater mass flow. The model is a quite accurate description of the actual steam generator. Hence, the amount of the nodes is quite high in order to take the best advantage of the high instrumentation rate in the steam generator. Although the model is quite accurate, some assumptions and simplifications were made because of restrictions of TRACE and difficulty of modelling a complex 3D apparatus into the 1D form. The basic idea in modelling was to preserve the height and the volume in the model. In TRACE geometry is defined with cell and with cell edges. Cell is defined with length, volume and average flow area. One of these three must be calculated thus the user can define two of them. In cell edges user can define flow area and hydraulic diameter. The most used component in the model is a pipe component. Although flow channels are not always circular, pipe component can be easily used. In TRACE node connections to cell/node can be done to endings or to sides. When making a connection to a side of a vertical node the elevation of connections is defined to a centerpoint of the cell.

Primary side

Primary side consists of loops, collectors and U-shaped heat exchange tubes. Hot and cold loops are modelled with pipe components and there are no simplifications with them. The hot and cold collectors are modelled with pipe components which have only one cell. Although collector is not a circular tube, average flow area and hydraulic diameter must be calculated. The length of the collector in the model is not exactly the same as in reality because of the elevation of connection loop. Loop is connected to the side conjunction of the collector cell. Thus the connection elevation is half of the length of collector. This makes it possible to keep the loop connection elevation the same as in reality.

Heat exchange tubes can be categorized into five groups by their length but if one wants to be accurate there is actually ten different groups i.e. ten different lengths. The triangular pitch causes small length differences. The tube bank consists of five heat exchange tube groups. The U-shape of heat exchange tubes causes problems because TRACE doesn’t allow round shapes. U-shape is formed with pipe cells, of which angle are approximately 45º. Modelling a U-shaped tube is a difficult task and compromises have to be made with total length, length of U-bend and tube ceiling dimensioning. Final model of a tube is

optimized between those three factors included. The center elevation of the nodes in the heat exchange tubes comply with the locations of the temperature sensors in the tubes.

Secondary side

Modelling of the secondary side is more problematic than modelling the primary system. The secondary side consists of feedwater line, downcomer, riser, steam dome and steam outlet. Inlet of feedwater is modelled with a fill component which is basically a velocity inlet. Mass flow is controlled with a level controller component. Feedwater pipe is modelled with a pipe component and it's connected to the cold side of the downcomer. Downcomer section is divided into hot and cold parts. Cold downcomer brings the feedwater flow downwards. Hot downcomer brings the condensation water from steam dome walls down through holes. The top of the hot downcomer is connected to the steam dome and the bottom is connected to the hot riser. Cold downcomer is connected to the feedwater line and to the cold riser. Riser part consists of five pipe components: hot and cold riser, the section where U-tube's ends and the section without tubes. The connection between riser and downcomer is difficult.

Calculation results

The first calculations were made with stand alone steam generator with fill and break boundaries at primary inlet and outlet. The results showed that the model is working properly. Then the steam generator model was connected to the basic PACTEL model with new primary loops. The functionality was tested and found to be satisfactory. The calculations for achieving steady state showed that model is stable. However, calculations showed that with steady state option the stationary state could not be achieved. Hence, the calculations had to be started with transient option.

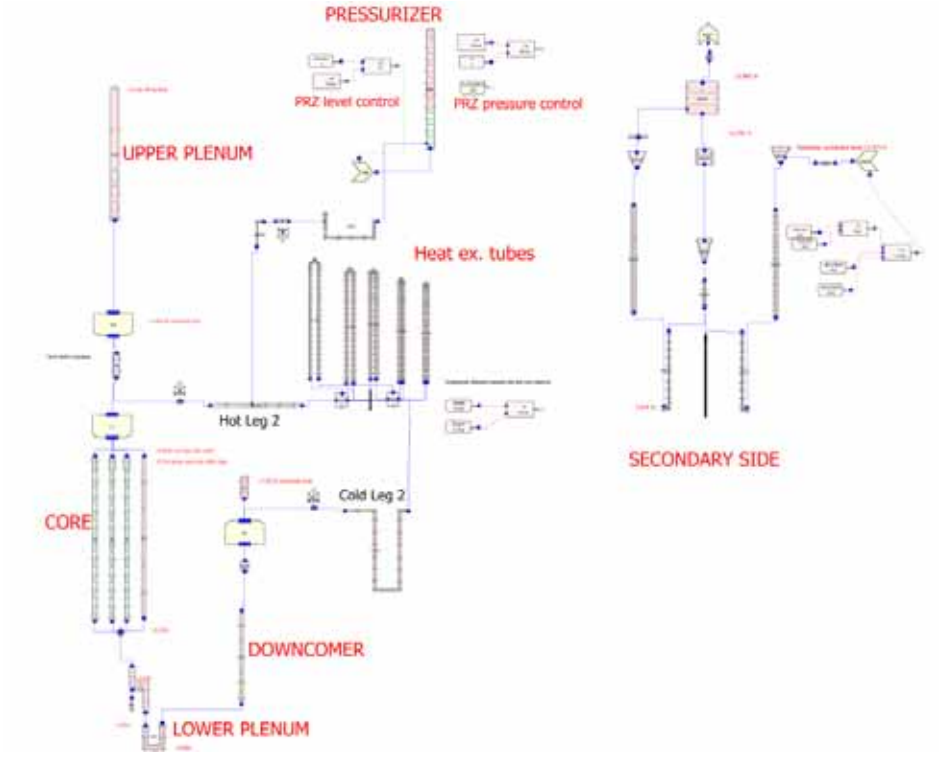

Figure 13.1.5. Main view of the PWR-PACTEL facility model by SNAP editor.

Applications

The PACSIM project has produced TRACE code calculation models for VVER and PWR PACTEL facilities. The models will be used directly to the continuous research work. The models can be used for calculating the existing VVER experiments and therefore are useful for validating the TRACE code towards full-plant VVER model. The PWR PACTEL model is usefull for calculating the very first experiments and can be compared to the results from the Tekes PAOLA project, where PWR PACTEL is modelled and calculated with the Apros code. This will pave the way for the PWR PACTEL to become an international project.

Conclusions

In the frame of the PACSIM project at LUT new models for VVER and PWR PACTEL facilities have been introduced using the TRACE thermal hydraulic system code with the SNAP graphical tool. The VVER PACTEL model was constructed to cover all main parts of the primary and secondary sides of the facility. The functionality of the model was tested with calculations of pressure and heat loss experiments. Loss-of-feedwater experiment was also calculated. The calculation results showed that the code is capable to model the behaviour of horizontal steam generator also in natural circulation mode. The PWR PACTEL model was also prepared. The model was working satisfactorily. The model is able to calculate heat transfer in natural circulation mode. The model is to be verified against characterizing tests soon after they have been carried out in 2009.

References

1. Tuunanen, J., Kouhia, J., Purhonen, H., Riikonen, V., Puustinen, M., Semken, S., Partanen, H., Saure, I. & Pylkkö, H. General description of the PACTEL test facility. Espoo: VTT, 1998. VTT Tiedotteita – Meddelanden – Research Notes 1929. 35 p. + app. 74 p. ISBN 951-38-5338-1; 951-38-5339-X. http://www.vtt.fi/inf/pdf/tiedotteet/1998/T1929.pdf.

2. Riikonen, V. RELAP5/MOD3.1 Analysis of the PACTEL Loss of secondary Side Feed Water Experiment. VTT Energy Technical Report, PROPA 8/94, 25.10.1994.

3. Kouhia, J. & Puustinen, M. Pressure loss tests at PACTEL test loop. Technical Report TOKE 7/99, VTT Energy, 1999.

4. Sanders, J. Methods of Heat Loss Measurement for a thermohydraulic Facility. Experimental Heat Transfer, 1991. Vol. 4, pp. 127–151.

5. Kouhia, J. & Puustinen, M. Experimental Data Report on LOF-10. VTT Energy, Technical Report TEKOJA 7/98, 11.12.1998.

6. Riikonen, V. RELAP5/MOD3.1 Analysis of the PACTEL Loss of Secondary Side Feed Water Experiment. VTT Energy Technical Report, PROPA 8/94, 25.10.1994.

7. TRACE V5.0 USER'S MANUAL, Volume 1: Input Specification. Input Specification. Washington DC: USNRC, Division of System Analysis and Regulatory Effectiveness, 2005. 642 p.

8. Vihavainen, J. An Assessment of the TRACE V4.160 Code against the PACTEL LOF-10 Experiment. Research report LUT/NEL 2/2007. Lappeenranta: Lappeenranta University of Technology, Laboratory of Nuclear Engineering, 2007.

14. Condensation experiments with PPOOLEX facility (CONDEX)

14.1 CONDEX summary report

Markku Puustinen, Jani Laine, Vesa Tanskanen,
Antti Räsänen and Heikki Purhonen
Lappeenranta University of Technology

Abstract

The condensation experiments with PPOOLEX facility (CONDEX) project has focused on studying phenomena occurring in different compartments of a scaled down Boiling Water Reactor (BWR) containment volume when steam/gas mixture is blown through dry well into a wet well water pool. In a BWR power generation system, the wet well pool serves as the major heat sink for condensation of steam in case of a primary system blowdown from a pipe break, or in case of a dedicated steam venting of the primary system. Experiments on the initial phase of steam line rupture, on thermal stratification and mixing processes in the water and gas volumes of the containment and on wall condensation in the dry well have been carried out with a scaled down test facility designed and constructed at Lappeenranta University of Technology (LUT). The system pressure of the steam source before discharge has ranged from 0.2 to 0.8 MPa and the pool water temperature from 20 to 50 °C. The data acquisition system has recorded measurements mainly with a frequency of 1 kHz. High-speed video equipment has been used to capture the details of the condensation process at the blowdown pipe outlet. Pressure pulses registered inside the blowdown pipe have been smaller than in the preceding project with

the open pool facility. The dry well compartment acts as a buffer and reduces the amplitude of the pulses. Experiments on thermal stratification and mixing processes have been used for the verification of the models of GOTHIC code at Kunliga Tekniska Högskolan (KTH). The coupling of computational fluid dynamics (CFD) and structural analysis codes in solving fluid-structure interactions in the SAFIR2010/NUMPOOL project has been facilitated with the aid of load measurements during rapid condensation in the CONDEX project. Furthermore, CFD calculations on wall condensation at VTT have been compared to CONDEX experiments.

Introduction

The common feature of current BWRs is the use of large condensation pools with a venting system for the mitigation of the immediate consequences of a conceivable Large Break Loss-of-Coolant Accident (LBLOCA) such as a main steam line break. Also, in certain advanced light water reactor concepts, during emergency cooling conditions, mixtures of steam and non-condensable gas are blown into a pool of water via an open pipe. In both cases, steam/gas bubbles form at the pipe exit, start to rise and then condense or break up to smaller bubbles. Pressure pulses generated by the collapse of steam bubbles due to rapid condensation, either at the pipe outlet or inside the pipe, may cause considerable loads or even damage when they impact upon a structure.

Condensation pool issues have been investigated experimentally at LUT and VTT within the national Finnish research programs on nuclear power plant safety. Experiments at LUT have been modeled with CFD and structural analyses tools at VTT and LUT as part of the INTELI, ECE, NUMPOOL and CONDEX projects. LUT and VTT have also co-operated closely in the numerical modeling of the experiments through participation in the EU/NURESIM project, where models for direct-contact condensation (DCC) have been developed.

A new PPOOLEX test facility including an adequate model of the upper dry well and withstanding prototypical pressure (0.5 MPa) was designed and constructed during the last year of the previous research program (Figure 14.1.1). Sophisticated high frequency measurement techniques and high speed video equipment are used in the experiments.

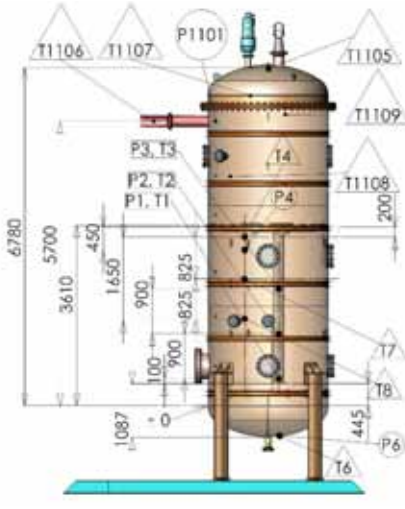

Figure 14.1.1. PPOOLEX test facility.

The new test facility has further increased the applicability of the experimental results. Condensation on the dry well walls and DCC in the wet well can be examined, and scenarios in terms of condensation modes threatening the integrity of structures can be assessed. Topics to be studied include, for example, thermal stratification and mixing processes in the pool volume, steam discharge with several blowdown pipes and the effect of counterpressure on system behavior. Possibility for open pool experiments still exists, since the vessel head of the new facility can be removed if necessary.

Experiment results of the CONDEX project can be used for the validation of different numerical methods for simulating containment behavior and steam injection through a blowdown pipe into liquid. Some of the calculation models are applicable also outside the BWR scenarios, e.g. for the quench tank operation in the pressurizer vent line of a Pressurized Water Reactor (PWR), for the bubble condenser in a VVER-440/213 reactor system, or in case of a submerged steam generator pipe break [1].

Nordic co-operation has been enhanced via the NORTHNET framework. Within Roadmap 3, the analytical and experimental work of KTH is combined to the CONDEX and NUMPOOL projects. Calculation tools and methods are examined and models of reactor containment codes such as GOTHIC can be evaluated on the basis of PPOOLEX experimental data on the behavior of a scaled down containment system.

Pre- and post-analysis of the loads on the pool structures are necessary for the experiments. Therefore, the experiments have been modeled with CFD codes at VTT. Loads calculated with CFD simulations have then been transferred to structural analysis and the stresses in the pool structures have been evaluated. [2, 3, 4.]

Main objectives

The main goal of the project is to improve understanding and increase fidelity in quantification of different phenomena in a BWR containment during steam discharge. These phenomena could be connected, for example, to bubble dynamics, DCC, pressure oscillations, thermal stratification and global circulation and mixing in the pool. These phenomena have to be measured with sophisticated, high frequency instrumentation and/or captured on video with high-speed cameras.

To achieve the project objectives, a combined experimental/analytical/ computational study programme is being carried out. Experimental part (LUT: CONDEX) of the project is responsible for the development of a database on condensation pool dynamics and heat transfer at well controlled conditions. Analytical/computational part (VTT: NUMPOOL, KTH: NORTHNET RM3, LUT: CONDEX) use the developed experimental database for the improvement and validation of models and numerical methods including CFD and system codes. Also analytical support is provided for the experimental part by pre- and post-calculations of the experiments.

The first objective in the beginning of the CONDEX project was to learn the general behaviour of the new test facility by carrying out a series of characterizing experiments with air and air/steam mixture discharge and with different initial conditions [5]. Instrumentation, data acquisition and control systems were also tested.

The main objective of the PPOOLEX experiments has been the production of measurement data to be used for different verification purposes. Load estimation, structural analysis, fluid-structure interactions, thermal stratification and mixing processes and models of wall condensation are, for example, research areas where the data produced in the CONDEX project can be utilized. Valuable co-operation between the thermal hydraulics, numerical simulation and structural analysis branches of the SAFIR2010 research programme has been created and strengthened.

The final goal of the CONDEX project is a large database containing the results of the steam/air discharge experiments. It can be used for testing and developing calculation methods used for nuclear safety analysis.

Characterizing experiments

The test program with the PPOOLEX facility accompanied by numerical modeling work started in 2007 by conducting a series of characterizing experiments with gas/steam discharge through the dry well compartment into the condensation pool and by simulating the gas experiments with CFD at VTT and LUT. Altogether eight air and four steam/air mixture experiments, each consisting of several blows (tests), were carried out. A DN200 blowdown pipe was used. Figure 14.1.2 illustrates the air and steam supply system used in the experiments.

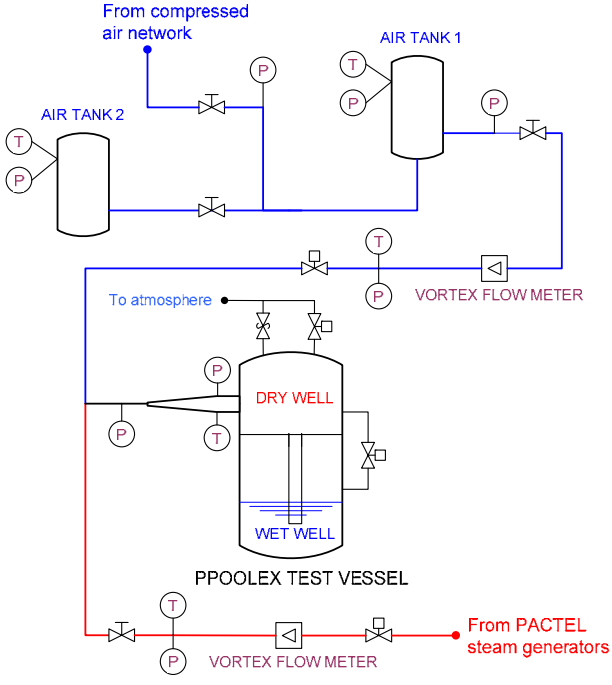

Figure 14.1.2. Arrangement of air and steam supply in the PPOOLEX facility.

The general behavior of the PPOOLEX facility differed significantly from that of the previous POOLEX facility because of the closed two-compartment

structure of the test vessel. Heat-up by several tens of degrees due to compression in both compartments was the most obvious evidence of this. Temperatures also stratified (Figure 14.1.3).

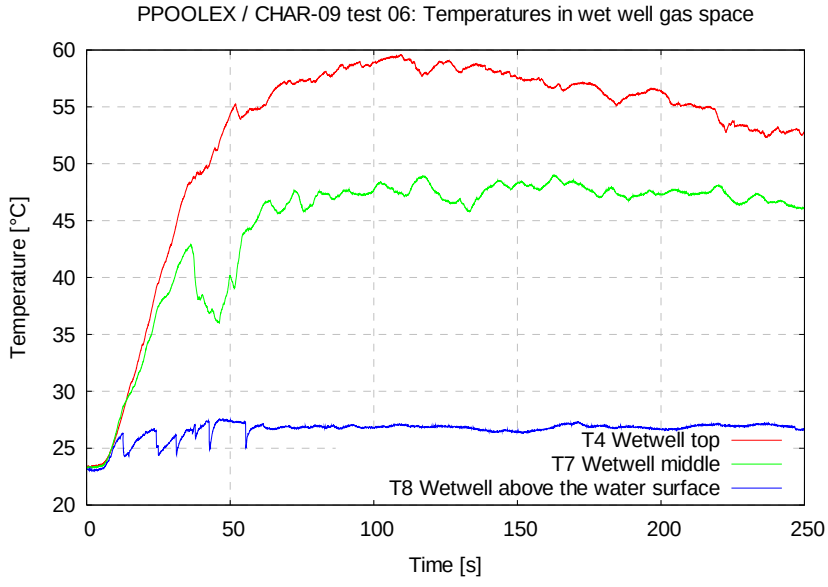

Figure 14.1.3. Stratification of temperatures in the wet well gas space in an air discharge test.

Condensation oscillations and chugging phenomenon were encountered in those tests where the fraction of non-condensables had time to decrease significantly. A radical change from smooth condensation behavior to oscillating one occurred quite abruptly when the air fraction in the blowdown pipe flow dropped close to zero (Figure 14.1.4). The experiments again demonstrated the strong diminishing effect that non-condensables have on dynamic unsteady loadings experienced by submerged pool structures. Clear BWR containment like behavior related to the beginning of a postulated steam line break was observed in the PPOOLEX tests during the steam/air mixture experiments.

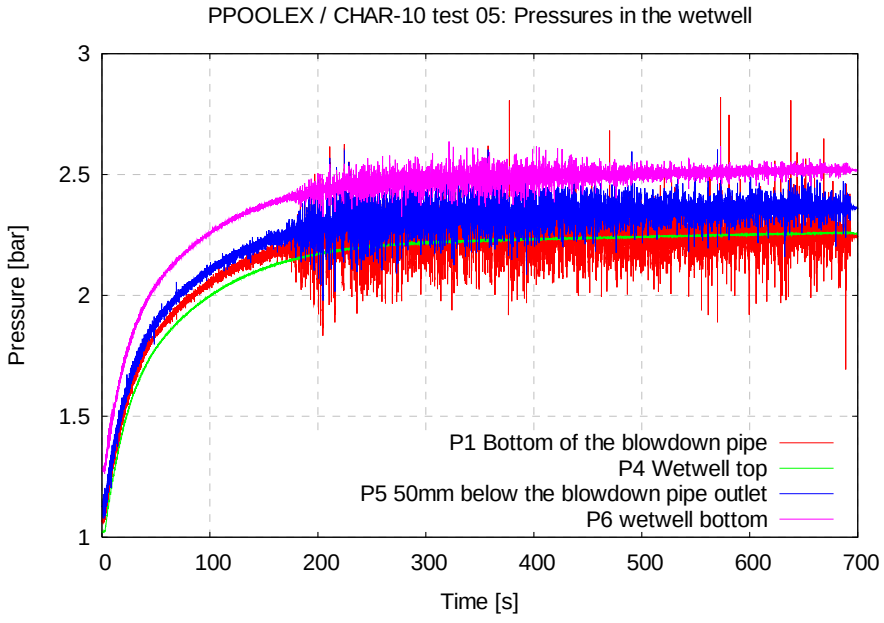

Figure 14.1.4. Radical change from smooth condensation to oscillating one as the air fraction of flow drops close to zero during discharge of steam/air mixture.

Thermal stratification and mixing experiments

Thermal stratification and mixing experiments were carried out in 2008 [6]. The objective was to study thermohydraulic loading of the wet well structures due to stratification processes as well as to produce comparison data for evaluating the capability of GOTHIC code to predict stratification and mixing phenomena. An array of properly positioned thermocouples was added to the pool volume in order to measure accurately the characteristics of thermal stratification and mixing. A cooling period of several days was also measured in some experiments. The initial pool water temperature was 20 °C. With small steam flow rates the stratification process started almost immediately after the initiation of the experiment. With higher flow rates the mixing effect of steam discharge delayed the start of the stratification process until the pool bulk temperature exceeded 50 °C (Figure 14.1.5). Table 14.1.1 lists the measured changes in wet well liquid and gas temperatures.

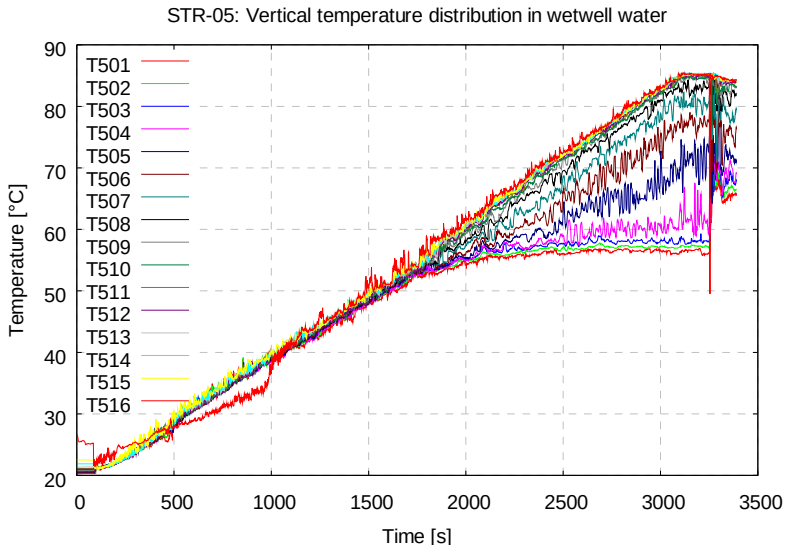

Figure 14.1.5. Due to mixing effects thermal stratification occurred only after the pool water had warmed up when higher flow rates were used.

Table 14.1.1. Maximum measured stratification in the wet well pool and gas space.

Test	Dry well final pressure [bar]	Max stratification of pool water [°C]	Max stratification of wet well gas [°C]	Final top layer temperature [°C]
STR-02	3.75	~ 70	~ 30	~ 91
STR-03	3.7	~ 70	~ 27	~ 92
STR-04	3.2	~ 53	~ 28	~ 74
STR-05	3.1	~ 30	~ 38	~ 86
STR-06	3.0	~ 36	~ 31	~ 87

Wall condensation experiments

Calculation models related to steam condensation in the dry well must be improved before proceeding to the simulation of the whole containment system. For that reason, a series of wall condensation experiments was carried out with the PPOOLEX facility [7]. The experiments aimed at estimating the amount of condensate produced with different flow rates and pre-heating levels of the dry well structures and at producing verification data for CFD calculations. A

system for collecting and measuring the amount of condensate from four different wall segments of the dry well compartment was installed before the experiments. Additional wall temperature measurements and a thermographic camera were in use as well. In Figure 14.1.6, accumulation of condensate in the collection tanks is shown when the experiment was started without pre-heating the wall structures.

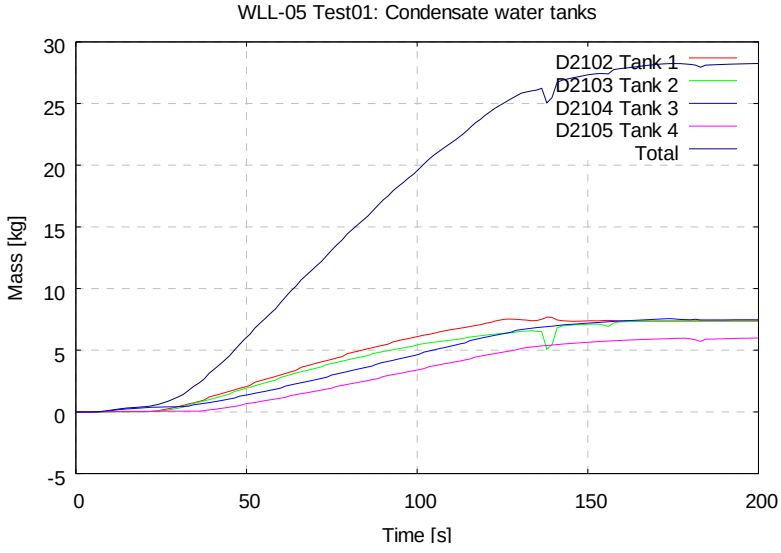

Figure 14.1.6. Accumulation of condensate in a wall condensation experiment when pre-heating of the dry well wall was not used. Steam discharge stopped at 120 seconds.

NEPTUNE_CFD simulations

Work with NEPTUNE_CFD code, developed in the EU/NURESIM project, continued with the simulation of selected POOLEX experiments. An experiment with thermally insulated blowdown pipe and a quasi-steady steam-water interface at the pipe mouth were simulated with 2D and 3D grids. The models of Hughes-Duffey and Lakehal et al. 2008 were compared [8, 9].

Simulation of another experiment related to chugging phenomenon is under way with the same calculation models. For this case, missing initial and boundary conditions are evaluated with the help of APROS and TRACE calculations. Figure 14.1.7 illustrates the development of a steam jet at the mouth of the blowdown pipe in the simulation of a chugging experiment.

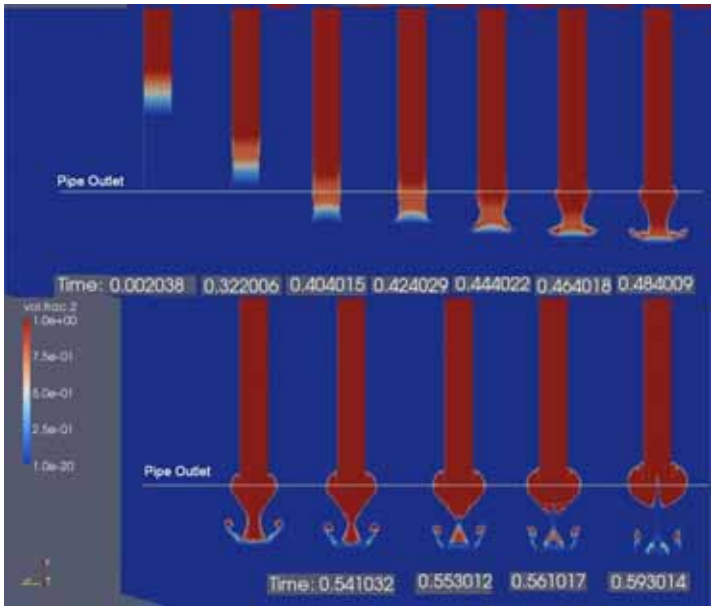

Figure 14.1.7. Emergence of a steam jet and first bubble at the blowdown pipe outlet in the NEPTUNE_CFD simulation of a POOLEX experiment.

Applications

Using the information gained in the experiments can directly solve certain open questions of suppression pool related safety systems in existing BWRs. Additional benefit from the project will be achieved through the use of the test results in developing and validating CFD and system codes for nuclear safety analysis. The connections of thermal hydraulics and structural loads will be studied in real conditions. The project outcome will allow the end users to analyze the safety risk of pool operation threatened by dynamic loading of DCC and quasi-static loading due to thermal stratification. More reliable prediction of condensation pool behavior based on combined CFD and structural analysis codes validated against experimental data can be directly utilized in the safety analysis of the Nordic power plants and thus improve the safety of their operation. The results can be used by the power companies, nuclear safety authorities and research organizations. Being part of the SAFIR2010 and NORTHNET RM3 research programs the CONDEX project gives an excellent forum for the international exchange of knowledge and experience including the Finnish and Swedish BWR operators.

Conclusions

The CONDEX project has focused on studying phenomena occurring in different compartments of a scaled down BWR containment volume when steam/gas mixture is blown through dry well into a wet well water pool. Experiments on the initial phase of steam line rupture, on thermal stratification and mixing processes in the water and gas volumes of the containment and on wall condensation in the dry well have been carried out.

The general behavior of the PPOOLEX facility differs significantly from that of the previous POOLEX facility because of the closed two-compartment structure of the test vessel. Heat-up of gas volume due to compression in both compartments is the most obvious evidence of this. A temperature increase of several tens of degrees is experienced when the system pressure is let to rise from 0.1 MPa to 0.4 MPa. Gas temperatures also stratify in both compartments.

Condensation oscillations and chugging phenomenon are encountered in the longer tests where the fraction of non-condensables has time to decrease significantly. A radical change from smooth condensation behavior to oscillating one with pressure pulses occurs quite abruptly when the air fraction of the blowdown pipe flow drops close to zero. However, dry well gas volume damps the oscillations inside the blowdown pipe by acting as a buffer. The experiments have again demonstrated the strong diminishing effect that non-condensable gases among the flow have on dynamic unsteady loadings experienced by submerged pool structures.

In the thermal stratification and mixing experiments a large difference between the pool bottom and top layer temperatures is measured when small steam flow rates are used. With higher flow rates the mixing effect of steam discharge delays the start of stratification until the pool bulk temperature exceeds 50 °C.

The most important task of the research project, to produce experimental data for code simulation purposes, can be satisfactorily fulfilled with the current version of the PPOOLEX facility. Further modifications and additions of equipment and instrumentation are, however, needed to increase the applicability of the test facility for system scale studies, too.

References

1. Fischer, K. & Häfner, W. Bubble Dynamics in the BWR Wetwell Pool. atw, Vol. 49, No. 5, May 2004, pp. 319–322.

2. Timperi, A., Pättikangas, T., Calonius, K., Tuunanen, J., Poikolainen, J. & Saarenheimo, A. Numerical Analysis of a Water Pool under Loadings Caused by a Condensation Induced Water Hammer. Espoo: VTT, 2004. Research Report BTUO72-031198.

3. Timperi, A., Pättikangas, T., Niemi, J. & Ilvonen, M. Fluid-Structure Interaction Analysis of a Water Pool under Loading Caused by Steam Injection. Espoo: VTT, 2006. Research Report TUO72-056662.

4. Pättikangas, T., Timperi, A., Niemi, J. & Kuutti, J. Modelling of Blowdown of Air in the Pressurized PPOOLEX Facility. Espoo: VTT, 2008. Research Report VTT-R-02233-08.

5. Puustinen, M. & Laine, J. Characterizing Experiments of the PPOOLEX Test Facility. Lappeenranta: LUT, 2008. Research Report CONDEX 1/2007.

6. Puustinen, M., Laine, J. & Räsänen, A. PPOOLEX Experiments on Thermal Stratification and Mixing. Lappeenranta: LUT, 2008. Research Report CONDEX 1/2008.

7. Puustinen, M., Laine, J. & Räsänen, A. PPOOLEX Experiments on Wall Condensation. Lappeenranta: LUT, 2008. Research Report CONDEX 3/2008.

8. Lakehal, D., Fulgosi, M. & Yadigaroglu, G. DNS of a Condensing Stratified Steam-water Flow. ASME J. Heat Transfer, 130(3), (2008). (Available online: DOI: 10.1115/1.2789723.)

9. Tanskanen, V., Lakehal, D. & Puustinen, M. Validation of Direct Contact Condensation CFD Models Against Condensation Pool Experiment. Poster, XCFD4NRS Workshop, Grenoble, France, September 10.–12. 2008.

14.2 PPOOLEX Wall Condensation Experiments

Markku Puustinen, Jani Laine, Antti Räsänen and Heikki Purhonen
Lappeenranta University of Technology

Abstract

An experimental study was performed in the PPOOLEX test facility designed and constructed at Lappeenranta University of Technology (LUT) to investigate wall condensation phenomenon in the dry well compartment while steam is discharged through it into the condensation pool. The effect of pre-heating of the dry well structures and steam flow rate was evaluated. Furthermore, the experiments aimed at producing relevant comparison data for computational fluid dynamics (CFD) calculations at VTT. Calculation models related to steam condensation in the dry well must be improved before proceeding to the simulation of the whole containment system.

The initial temperature (pre-heating) level of the dry well structures ranged from 23 to 99 °C. The steam flow rate varied between 85 and 690 g/s and the temperature of incoming steam between 115 and 160 °C. A system for collecting and measuring the amount of condensate was designed and constructed before the experiments. The amount of condensate that was produced during the initial phase of steam discharge was very much controlled by the level of pre-heating of the dry well structures. As the wall heated up the condensation process slowed down but never completely stopped. A small temperature difference (6 to 7 °C) between the dry well atmosphere and inner wall remained even in the case of an extended steam discharge.

Introduction

During a possible steam line break accident inside the containment a large amount of non-condensable (nitrogen) and condensable (steam) gas is blown from the upper dry well to the condensation pool through the blowdown pipes in a typical containment design of a Boiling Water Reactor (BWR). The wet well pool serves as the major heat sink for condensation of steam. However, some fraction of steam condenses also on the dry well compartment walls, particularly during the initial phase of the discharge.

Condensation pool issues have been investigated experimentally at LUT within the national Finnish research programs on nuclear power plant safety [1, 2, 3]. Experiments at LUT have been widely modeled with CFD and structural analyses tools at VTT [4, 5, 6]. The newest simulations deal with an attempt to model wall condensation in dry well with CFD. For this reason, an experiment series on steam discharge through dry well into the condensation pool was carried out with the PPOOLEX facility at LUT.

PPOOLEX test facility

A new PPOOLEX test facility including adequate models of the dry well and wet well compartments and withstanding prototypical system pressure (0.5 MPa) was designed and constructed during the last year of the previous research program. Dry well and wet well volumes of the facility are scaled down according to the corresponding compartments of the Olkiluoto plant. Steam needed during the experiments is generated with the nearby PACTEL facility [7]. Sophisticated high frequency measurement techniques and high speed video equipment are used in the experiments. The new test facility has further increased the applicability of the experimental results. Condensation on the dry well walls and direct contact condensation (DCC) in the wet well can be examined, and scenarios in terms of condensation modes threatening the integrity of structures can be assessed. Table 14.2.1 lists the main design features of the PPOOLEX facility.

Table 14.2.1. Main design features of the PPOOLEX test facility.

Volume	Total	31.1 m^3
	Dry well compartment	13.3 m^3
	Wet well compartment	17.8 m^3
Test vessel outer diameter		2.4 m
Height	Total	7.45 m
	Dry well compartment	3.18 m
	Wet well compartment	4.27 m
Max. overpressure		0.4 MPa
Max. underpressure		0.05 MPa
Max pressure difference across the intermediate floor		0.2 MPa
Max operating temperature		190 °C
Wall thickness	Vessel head	10 mm
	Bottom end	10 mm
	Lowest wall segment	10 mm
	Other wall segments	8 mm
Construction material		Stainless steel (EN1.4301)

The dry well compartment is separated from the wet well compartment (condensation pool) with a removable floor. A DN200 (∅219.1x2.5) blowdown pipe leads from dry well to wet well through the floor. Horizontal piping for injection of gas and steam penetrates through the side wall of the dry well compartment (Figure 14.2.1). The length of the inlet plenum (DN200) is 2.0 m. A remote-controlled valve in the steam line is used for initiating steam discharge. Six windows allow visual observation of the internals. The test facility is not thermally insulated.

Figure 14.2.1. Dry well compartment of the PPOOLEX test facility.

A system for collecting and measuring the amount of condensate from four different wall segments of the dry well compartment was installed before the wall condensation experiments. The system includes slightly tilted drain gutters on the dry well inner wall on two elevations, piping from the lowest points of the gutters through the compartment wall to the floor level of the lab and condensate collection tanks with water level measurements (Figure 14.2.2). Two of the four wall segments are located on the opposite half of the dry well in relation to the inlet plenum and the other two on the same side. The area of the each two upper wall segment is 2.08 m^2 and of the two lower segment 5.32 m^2. Thus, condensate is collected from a total wall area of ~14.8 m^2. Condensate is not collected from a 0.45 m high segment between the lower gutter and the separating floor and from the vessel head.

Figure 14.2.2. Drain gutters and condensate tanks for collecting condensate from dry well walls.

Thermocouples were installed on the inner and outer surface of the dry well wall on two locations. Additional measurements include thermocouples and a pressure transducer at the top of the blowdown pipe in order to better determine relevant initial and boundary conditions for the simulations. The outside view of the dry well compartment was filmed with a thermo graphic camera in a couple of experiments at the location where the steam jet hits the wall.

Experiment program

The wall condensation experiments program consisted of five experiments (labeled from WLL-01 to WLL-05). Each experiment included 2 to 6 separate steam discharge tests. Before each experiment the condensation pool was filled with about 20 °C water to the level of 2.14 m i.e. the blowdown pipe was submerged by 1.05 m. The used steam flow rates ranged from 85 to 690 g/s. Steam mass flow rate was calculated on the basis of volumetric flow rate and density of steam, which was determined on the basis of steam pressure by assuming saturated steam flow. Initially, the dry well compartment was filled with air at atmospheric pressure. Pre-heating of the wall segments was executed with steam. After pre-heating (and between individual tests) the test vessel was shortly ventilated with compressed air before the initiation of the actual test discharge to dry the wall surfaces and to clear the windows. The shortest duration of an individual blow was 60 seconds and the longest 800 seconds. The values of the main test parameters of the performed wall condensation experiments are listed in Table 14.2.2.

Table 14.2.2. Main test parameters of the wall condensation experiments

Exp/Test no.	Initial steam line pressure [bar]	Steam flow rate [g/s]	Initial temperature of the dry well wall (T2111) [°C]	Temperature of incoming steam [°C]
WLL-01-1	~ 1.8	85–140	~ 77	~ 115
WLL-01-2	~ 2.5	180–205	~ 90	~ 128
WLL-01-3	~ 3.5	270–290	~ 95	~ 137
WLL-01-4	~ 4.4	325–350	~ 99	~ 145
WLL-02-1	~ 2.1	205–245	~ 80	~ 120
WLL-02-2	~ 2.0	150–240	~ 84	~ 119
WLL-02-3	~ 3.2	320–350	~ 95	~ 134
WLL-02-4	~ 3.3	325–355	~ 89	~ 135
WLL-02-5	~ 6.2	580–660	~ 99	~ 159
WLL-02-6	~ 6.5	450–690	~ 97	~ 160
WLL-03-1	~ 2.1	190–225	~ 49	~ 120
WLL-03-2	~ 2.1	120–220	~ 45	~ 120
WLL-03-3	~ 3.3	340–355	~ 50	~ 135
WLL-03-4	~ 3.3	320–355	~ 43	~ 136
WLL-04-1	~ 4.5	450–480	~ 24	~ 145
WLL-04-2	~ 4.5	425–480	~ 42	~ 145
WLL-04-3	~ 4.5	425–480	~ 70	~ 145
WLL-05-1	~ 5.3	500–560	~ 26	~ 152
WLL-05-2	~ 5.2	480–550	~ 64	~ 150

Experiment results

In the experiments, the amount of generated condensate depended on the pre-heating level of the dry well wall. In Figure 14.2.3, the total accumulation of condensate from all four wall segments is presented with no pre-heating and with about 42 and 70 °C pre-heating of the dry well wall. The moderate pre-heating of 42 °C had only a minor decreasing effect on the generation of condensate while the higher pre-heating level of 70 °C clearly reduced wall condensation. The steam flow rate and temperature was practically the same in all three cases during the first 60 seconds that are compared. As a basic rule it can be said that with a pre-heating of 60–70 °C it takes roughly twice the time to generate the same amount of condensate as with no pre-heating, when the same steam flow rate is used. Very definitive conclusions of the effect of pre-heating level on the condensation process at different wall surfaces can not be drawn, since the initial test temperatures (after the pre-heating process) were not exactly uniform on all wall segments.

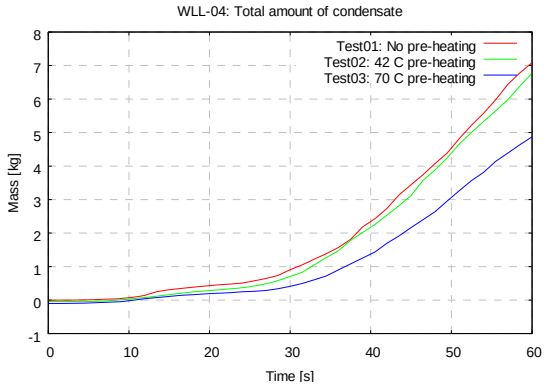

Figure 14.2.3. Total accumulated condensate with and without pre-heating of the dry well wall.

A small temperature difference (6 to 7 °C) between the dry well atmosphere and inner wall remained even in the case of an extended steam discharge (Figure 14.2.4). Therefore, wall condensation never stopped completely, although it diminished considerably in the long duration tests.

The collected amount of condensate from the four wall segments differed from each other. For example, the level of pre-heating and the used steam flow rate had an effect on the generation of condensate on different wall segments. In general, the two upper segments generated more condensate than the two lower segments. This was most evident in those tests where the used steam flow rate was small. It is also consistent with the fact that the inlet plenum is on the level of the upper segments and the steam flow first hits on those. However, it seemed that with no or only moderate pre-heating, condensation took place most effectively on the wall segments opposite to the inlet plenum (Figure 14.2.5).

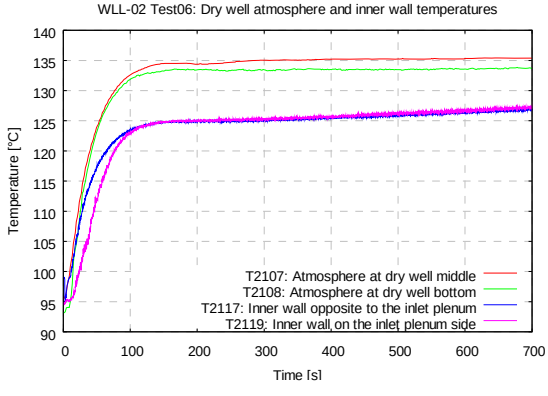

Figure 14.2.4. Temperature difference between the dry well wall and atmosphere remained even in the long duration experiments.

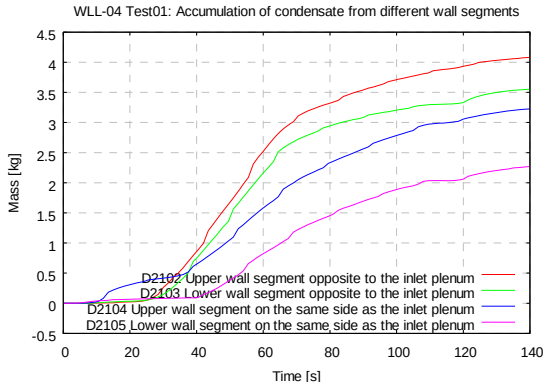

Figure 14.2.5. Accumulation of condensate from different wall segments without pre-heating.

Inside and outside surface temperatures of the dry well wall are measured at the same location in two places, opposite and on the same side as the inlet plenum. These measurements indicate that a clear temperature difference develops between the inner and outer surface on both sides of the dry well compartment (Figure 14.2.6). The difference gets smaller along the tests but remains a couple of degrees wide even in the long duration tests.

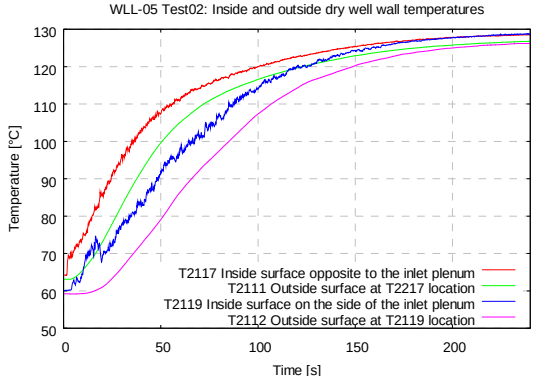

Figure 14.2.6. Temperature difference between the inside and outside surface of the dry well wall.

Figure 14.2.7 shows a view captured from the recording of a thermo graphic camera that was used in a couple of experiments to film the outside surface of the dry well wall. The view is from experiment WLL-05-1 about 60 seconds into

the steam discharge period. It shows the upper segment of the wall that is opposite to the inlet plenum. Steam hits to the inside surface of the area that is on the right edge of the view.

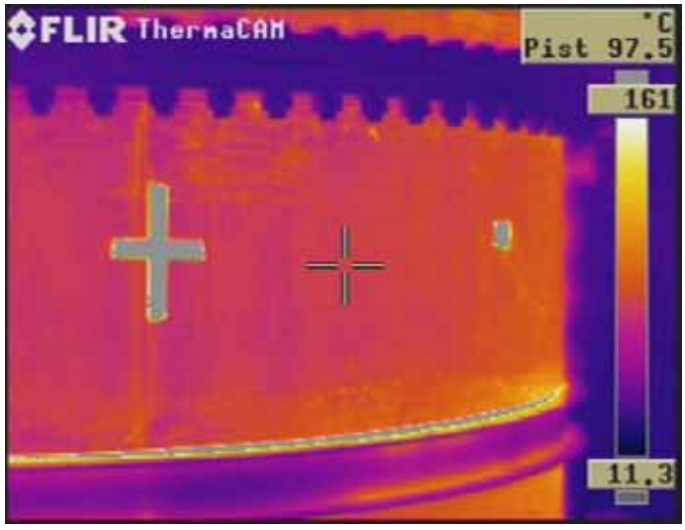

Figure 14.2.7. Capture of thermo graphic camera recording from the wall opposing the inlet plenum.

Conclusions

An experimental study was performed in the PPOOLEX test facility designed and constructed at LUT to investigate wall condensation phenomenon in the dry well compartment. The effect of pre-heating of the dry well structures and steam flow rate was evaluated. The main goal of the experiments was to produce relevant comparison data for CFD calculations at VTT.

The amount of generated condensate depended on the pre-heating level of the dry well wall. With high pre-heating (60–70 °C) it takes roughly twice the time to generate the same amount of condensate as with no pre-heating when the same steam flow rate is used. Moderate pre-heating (35–45 °C) had only a minor decreasing effect on the generation of condensate.

Wall condensation diminished considerably when steam discharge continued for several hundreds of seconds. However, it didn’t stop completely, because a small temperature difference between the dry well atmosphere and inner wall remained throughout the tests.

The collected amount of condensate from the four wall segments differed from each other. Usually, more condensate was collected from the two upper segments than from the two lower segments. In the case of no or only moderate pre-heating, the highest amount of condensate was, however, generated by the wall segments opposite to the inlet plenum.

References

1. Laine, J. & Puustinen, M. Steam Blowdown Experiments on Chugging. Lappeenranta: Lappeenranta University of Technology, 2005. Research Report POOLEX 2/2005.

2. Puustinen, M. Combined Effects Experiments with the Condensation Pool Test Facility. Lappeenranta: Lappeenranta University of Technology, 2006. Research Report POOLEX 1/2006.

3. Puustinen, M. & Laine, J. Characterizing Experiments of the PPOOLEX Test Facility. Lappeenranta: LUT, 2008. Research Report CONDEX 1/2007.

4. Timperi, A., Pättikangas, T., Calonius, K., Tuunanen, J., Poikolainen, J. & Saarenheimo, A. Numerical Analysis of a Water Pool under Loadings Caused by a Condensation Induced Water Hammer. Espoo: VTT, 2004. Research Report BTUO72-031198.

5. Timperi, A., Pättikangas, T., Niemi, J. & Ilvonen, M. Fluid-Structure Interaction Analysis of a Water Pool under Loading Caused by Steam Injection. Espoo: VTT, 2006. Research Report TUO72-056662.

6. Pättikangas, T., Timperi, A., Niemi, J. & Kuutti, J. Modelling of Blowdown of Air in the Pressurized PPOOLEX Facility. Espoo: VTT, 2008. Research Report VTT-R-02233-08.

7. Tuunanen, J., Kouhia, J., Purhonen, H., Riikonen, V., Puustinen, M., Semken, R.S., Partanen, H., Saure, I. & Pylkkö, H. General Description of the PACTEL Test Facility. Espoo: VTT, 1998. VTT Research Notes 1929. ISBN 951-38-5338-1. http://www.vtt.fi/inf/pdf/tiedotteet/1998/T1929.pdf.

15. Large break loss of coolant accident test facility study (LABRE) and Large break loss of coolant accident test rig (LABRIG)

15.1 LABRE/LABRIG summary report

Arto Ylönen and Heikki Purhonen
Lappeenranta University of Technology

Abstract

The initiative for the new LBLOCA test facility came from the code developers. Full background study was done as master's thesis during year 2007 [1]. LABRE project gave an overall view of the needs and challenges concerning the construction of new test facility for large break blowdown testing. The new needs of the data for the validation of the current codes were also identified. The task of the LABRIG project is to continue the work done in LABRE project and to design small scale test facility which could be used to gather measurement data for code developers. Moreover, the original goal was to get to know from a small scale facility, if it is possible to achieve missing data with a larger test facility to be constructed later.

The main objective of this new test facility and following test program is to gain new validation data for the code validation purposes. The main interest is in the fluid-structural analysis issues. Existing code capabilities can be improved by using measurement data gained from the facility. It is also relevant to have active research on the subject to educate new structural analysis experts. Simultaneous analytical and experimental work is needed to fully understand the phenomena during the blowdown.

Introduction

The facilities like HDR and Battelle-Frankfurt facility were nearly full scale and built to study fluid-structure interactions during the blowdown phase of LBLOCA. Building of such a large scale facility is expensive. The size of the existing laboratories may also set some limitations. Therefore one solution is to build a small scale facility with a lot of instrumentation. The initiative to design a new test facility came from the code developers. They are searching for suitable test data to validate fluid-structure interaction calculations done with coupled CFD and structural analysis codes. Some calculations have been done with the HDR geometry, but there are some flaws in the facility that restrict the use of experimental data for code validation purposes. For obvious reasons (tests were done in the 70's and 80's) the facility was not designed to validate CFD codes. For that purpose there must be a dense grid of pressure and temperature measurements. In this case the pressure measurements would be enough. When the task is to validate coupled CFD and structural analysis codes extensive structural measurements are also needed. Certain important aspects have to be taken into account when designing a new separate effects test facility; scaling, structural questions, instrumentation and planned test program.

Main objectives

The main objective of this new test facility and following test program is to gain new validation data for the code validation purposes.

Originally the facility was planned to be relatively small in scale, so the direct results for code validation would have been somewhat limited. Based on the problems related to a small scale facility the scale was increased to be in somewhere in the middle of the scales of "original" pilot facility and the next, larger one. This also means that only one facility will be needed.

Test facility description

As the scale of the test facility is still relatively small, it is necessary to use external heating and cooling circuits. Even if there would be enough space for the internal heaters, it would be better to use external heaters instead. The reason for this is that temperature distribution inside the pressure vessel has relevant effect on depressurization (effect was observed in Battelle experiments). There is also the risk of damaging the electric heaters during the blowdown if they are

located inside the pressure vessel. External circuits also are needed to adjust the system pressure. The principle of the circuits is adopted from the HDR test facility and modified to fit to a smaller scale test facility [2].

Pressure vessel is the main component in the blowdown test facility. The principles of the pressure vessel have been adopted from Semiscale test facility (Bettis Flask) [3].

Dimensions of the designed facility will be larger than in Semiscale test facility. One reason for this is the break opening time versus the time of the pressure wave to reach the pressure vessel internals. Inner diameter of the pressure vessel will be 700 mm. The pressure vessel itself forms a rigid outer boundary for the annular flow channel. The most challenging part of the pressure vessel design is the internal part, simulating the core barrel. Combined CFD and structural analysis code calculations are needed to define the final design of internals. Material thicknesses and arrangement of the weight simulating the core mass are to be studied before construction of the facility to achieve a reasonable response to the early phase of a LBLOCA. It was not possible to perform these analyses parallel to the other design of the facility due to budget limitations of the project in 2008.

Pressurizer is attached to the heater circuit. It is needed to obtain the initial pressure and control the volume of the test facility. Height of the pressurizer will be about 2.5 m and inner diameter 470 mm. Heating power will be about 100 kW.

External heater is needed to achieve the desired temperature inside the pressure vessel. Internal heaters are not used due to the risk to damage the heaters during the blowdown transient. Cooler is not needed in the preparation of the planned tests.

Blowdown pipe would be separate from the circuits. The pipe would basically have two parts, break assembly and straight pipe part. The opening time of the break will be varied by changing the break assembly and its settings. Length of the straight pipe part will be varied to modify the break location.

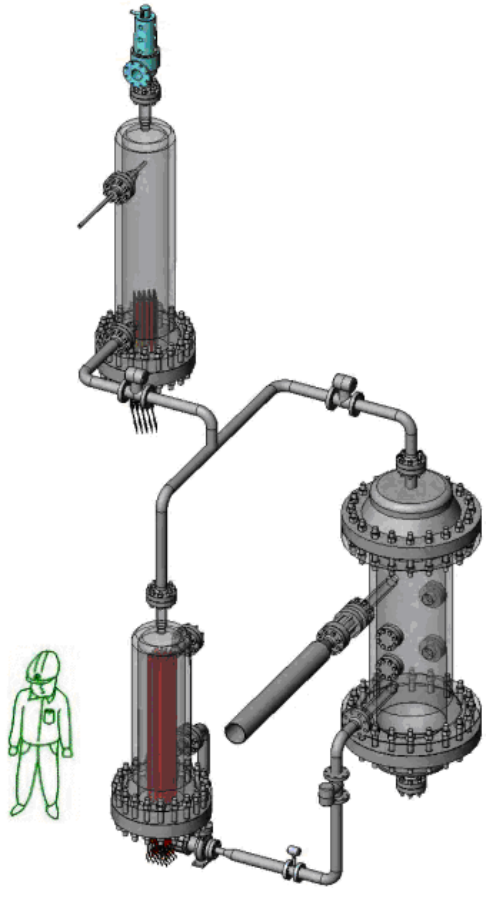

Figure 15.1.1. The main components of the “LABRIG” facility.

Applications

The new test facility is designed to provide data from the blowdown phase of a LBLOCA for the validation of CFD and structural analysis codes, combined and separately used. Originally one goal was to evaluate the quality of the experimental data of a larger LBLOCA facility by constructing and using a small scale pilot test facility. According to scaling laws and due to speed of sound (effecting on the scaling of the break opening time and speed of data acquisition system) the scale of this facility was decided to be in between those two abovementioned sizes. This means that all the main phenomena should be present and recordable already in this facility.

Conclusions

The new test facility would provide new validation data for code developers, more accurate and more detailed information about system behaviour during blowdown phase. This would benefit both code developers and utilities. Ultimate goal of this new facility is to increase the safety of the nuclear power plants.

One important aspect to consider is the education of future experts. One master's thesis has already been done on this subject and if the project continues there will be more to come. The new test facility with vast instrumentation is also ideal for academic research and education purposes. Structural integrity of the reactor vessel and the core is a key issue in accident situations.

The results gained from the new test facility can be used also as benchmarking exercises instead of old experiments like Edward's pipe. Research program would also improve the international status of the research unit and the nuclear safety research in Finland.

References

1. Ylönen, A. Large Break Blowdown Test Facility Study. Master's thesis. Lappeenranta: Lappeenranta University of Technology, 2008.

2. Krieg, R., Schlechtendahl, E.G. & Scholl, K.-H. Design of the HDR experimental program on blowdown loading and dynamic response of PWR-vessel internals. Nuclear Engineering and Design, 1977. 43(2): pp. 419–435.

3. Oehlberg, R.N. A Review of the EPRI Hydroloads Program. Transactions of 7th International Conference on Structural Mechanics in Reactor Technology, 1983.

16. Participation in development of European calculation environment (ECE)

16.1 ECE summary report

Vesa Tanskanen, Heikki Purhonen and Markku Puustinen
Lappeenranta University of Technology

Abstract

Lappeenranta University of Technology (LUT) as well as Technical Research Centre of Finland (VTT) participated in the Nuclear Reactor Simulations (NURESIM) Integrated Project in the Sixth Framework Programme of EU. The aim of the NURESIM project was to take the initial steps towards a common European standard software platform for the next generation nuclear reactors simulations. The specified participation of LUT and VTT focused on the thermal hydraulic (TH) part of the project. The main products of the project were the information transfer to Finland of the European development of simulation software, and the new platform of two-phase CFD code calculations for advanced safety analysis. The existing POOLEX test data was reviewed, but the existing test cases were considered to be too complex to be used in the validation of NEPTUNE CFD module in SALOME platform. It was decided to carry out a tailored experiment for NURESIM, with an insulated blowdown pipe. The NEPTUNE CFD module was installed in a Linux system at LUT. Simulations with the Hughes-Duffey based DCC model of the NEPTUNE CFD code indicated two orders of magnitude higher condensation rates than the experiment. This overestimation was reduced by one order of magnitude by decreasing the numerical truncation parameter and by disabling the residual

droplet handling. By implementing the direct numerical simulation (DNS) based model of Lakehal et al. (2008) the heat transfer coefficient reached the same order of magnitude as indicated by experiments. More stable transfer rate values were also attained. However, uncertainties prevail in the experimental and simulation results as the presence of non-condensables, has not been taken into account.

Introduction

Lappeenranta University of Technology (LUT) as well as Technical Research Centre of Finland (VTT) participated in the Nuclear Reactor Simulations (NURESIM) Integrated Project in the Sixth Framework Programme of EU. The goal of the ECE project was to take part in the development and validation process of the new Common European Standard Software Platform for modeling of the problematic two-phase flow simulations of present and next generation nuclear reactors. A key activity of the project was also to maintain good relations and increase contact intensity to the European nuclear research community. The participation ensured the access to use the new platform and new simulation tools. The project gave new possibilities to increase educational competence and to acquire readiness to use new two phase flow simulation tools. Also, an important aspect in the project was to maintain the domestic preparedness to the new challenges in the forefront of nuclear simulation. The aim of the NURESIM project was to take the initial steps towards a common European standard software platform for the next generation nuclear reactors simulations. The specified participation of LUT and VTT focused on the thermal hydraulic (TH) part of the project, which was one of the subprojects of NURESIM. The VTT part was included in the SAFIR/THEA project. The funding share from EU was limited, but it was strategically important to stay involved in NURESIM. The SAFIR funding in the ECE project enhanced the possibilities of LUT to be also involved in the calculation work and to concentrate on the preparation of the experimental data.

Main objectives

The main products of the project were the information transfer to Finland of the European development of simulation software, and the new platform of two-phase CFD code calculations for advanced safety analysis. The new calculation environment would increase the prediction capability of the simulation tools and enhance safety of current and future nuclear installations.

The development process of a new code is very extensive task especially in the area of challenging two-phase CFD simulation. During the NURESIM-project (three years), the simulation tools were validated on selected experiments to gain acceptance within utility and regulatory organizations. However, validation and development work is still needed, and will be continued in continuation projects like NURISP, which was initiated in year 2009. Power companies, research organizations, safety authorities and technical universities in Finland should be able to utilize the research results obtained from these projects.

The goal of the ECE project was to take part in the development and validation process of the new Common European Standard Software Platform for the simulations of next generation nuclear reactors, NURESIM. The participation ensured the access to use the new platform and new simulation tools. The project gave possibilities to increase educational competence and to acquire readiness to use new two phase flow simulation tools. The objectives of ECE project were as follows:

- To select, evaluate and convert suitable steam blowdown experiment data from the condensation pool test series carried out in SAFIR/POOLEX project.
- To use these selected experiment results for the development and validation of new simulation tools.

Experimental data for validation

The existing POOLEX test data was reviewed and one test of rapidly condensing steam bubbles was selected and proposed to be used in the validation of NEPTUNE CFD module in SALOME platform [1]. However, this suggested test was considered to be too complex as a validation case for the version of the software of that time. After reviewing again the experiment database, an experiment with a stable steam-water interface was proposed to be used as a validation case. As the pipe simulated a normal blowdown pipe as it exists in a condensation pool, it was not insulated. The heat flux through the pipe wall was neither measured nor possible to estimate accurately. Missing this information made it difficult to use this experiment as a test case for validation.

After these problems, it was decided to carry out a tailored experiment for NURESIM in the POOLEX project [2]. An insulated blowdown pipe was introduced and a test series was carried out. One test of this series was used for validation, see Figure 16.1.1.

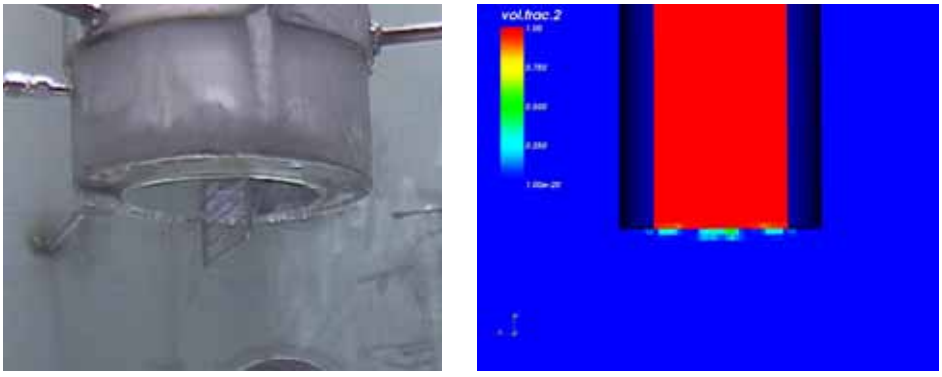

Figure 16.1.1. Stable steam-water interface at blowdown pipe exit in POOLEX test and simulation for NURESIM.

CFD Validation

The NEPTUNE CFD module was installed in a Linux system at LUT. Use of SALOME platform was not crucial and NEPTUNE CFD was functional also with other free/commercial pre- and postprocessing tools. Two 2D-axisymmetric and 3D calculational grids were developed and tested. Grids were imported to NEPTUNE CFD from FLUENT/GAMBIT and free tools (ParaView and Visit) were used in postprocessing. SALOME was briefly tested in postprocessing. Grid dependency in the results was not tested comprehensively, but there were no significant differences in the results between the two 2D grids and between the 2D and 3D grids.

The simulations [3, 4] indicated clearly higher condensation rates than in the experiment, when the original implementation of Hughes-Duffey stratified flow condensation model of NEPTUNE CFD was used. This overestimation was decreased remarkably by decreasing a numerical truncation parameter and by disabling the residual droplet condensation auxiliary model. After these modifications, at least one order of magnitude over-estimation of the mass transfer rate still prevailed. For comparison, the condensation model of Lakehal et al. (2008) was implemented into the code. This model is an adapted variant of the Banerjee et al. (2004) model for passive scalar transport across sheared turbulent streams. Using Lakehal's model, the condensation rates were significantly decreased to the same order of magnitude as in the experiment. The model appeared also to be more stable than the previous one, see Figure 16.1.2. One

reason for this is probably the fact, that in the Lakehal et al. (2008) model the turbulence kinetic energy was damped by the turbulence dissipation rate whereas in the Hughes-Duffey model this seemed to dominate the heat transfer coefficient.

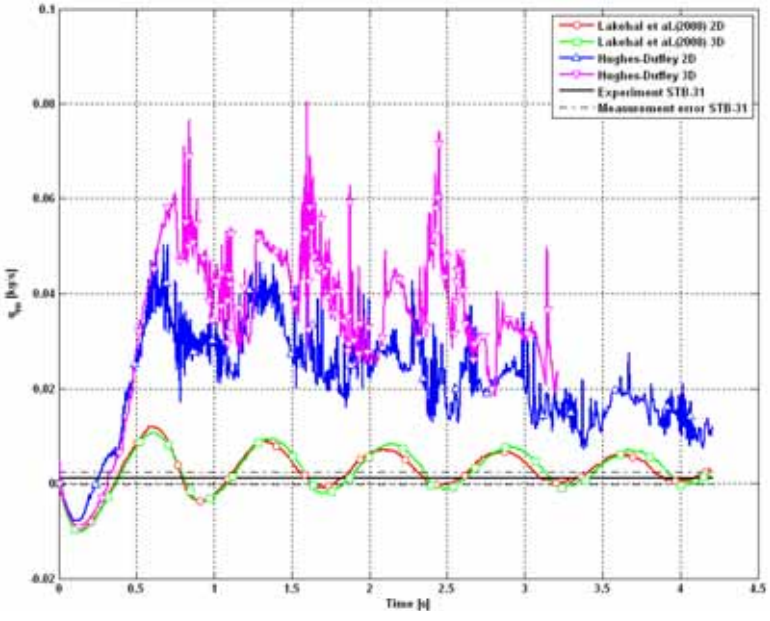

Figure 16.1.2. Vapour mass flow rates recorded next to the blowdown pipe inlet in simulations where the pressure inlet boundary (1.186 bar) is used.

High uncertainties exist concerning the comparability of these models with this POOLEX experiment, because the contribution of non-condensable air layer was not included. It is likely, that these condensation models could yield much lower condensation rates if this logarithmically concentrated, approximately 1–6 mm thick layer of non-condensables were modelled [4]. In NEPTUNE CFD, air could be simulated by setting an air fraction into the steam phase, but this model was not fully tested by developers and its effect to steam-water interface was unpredictable in the POOLEX case.

Concerning the implemented version of the Lakehal et al. (2008) model, it would have been more preferable to use the inner scaling version of the model, because the steam-water interface in the experiment was not significantly turbulent. Now, the outer scaling (surface divergence theory) version was used, because its implementation into NEPTUNE CFD was simple and possible to be done according to the schedule of the project.

During the project, a researcher visit to CEA Grenoble was done. The duration of this visit was approximately 3 months, and this visit gave a good opportunity to get acquainted with two-phase model development of NEPTUNE CFD code. During this visit, the access to coding was also granted.

Conclusions

Lappeenranta University of Technology as well as Technical Research Centre of Finland participated in the Nuclear Reactor Simulations (NURESIM) Integrated Project in the Sixth Framework Programme of EU. The aim of the NURESIM project was to take the initial steps towards a common European standard software platform for the next generation nuclear reactors simulations. The specified participation of LUT and VTT focused on the thermal hydraulic part of the project. The main products of the project were the information transfer to Finland of the European development of simulation software, and the new platform of two-phase CFD code calculations for advanced safety analysis.

A tailored experiment with an insulated blowdown pipe was performed for NURESIM in the POOLEX project. Achieving a stable steamwater interface at the mouth of blowdown pipe was the main goal of this experiment.

The NEPTUNE CFD module was installed in a Linux system at LUT. Simulations with the Hughes-Duffey based DCC model of the NEPTUNE CFD code indicated two orders of magnitude higher condensation rates than the experiment. This overestimation was reduced by one order of magnitude by decreasing the numerical truncation parameter and by disabling the residual droplet handling. By implementing the DNS-based model of Lakehal et al. (2008) the heat transfer coefficient reached the same order of magnitude as indicated by experiments. More stable transfer rate values were also attained. However, uncertainties prevail in the experimental and simulation results as the presence of non-condensables were not taken into account.

References

1. Vihavainen, J. & Puustinen, M. Review of the existing data basis for the validation of models for PTS. European Commission 6th Euratom framework programme 2005–2008, Integrated project (IP): NURESIM, Nuclear Reactor Simulations, Subproject 2: Thermal Hydraulics, Deliverable D2.1.2.

2. Laine, J. & Puustinen, M. Condensation Pool Experiments With Steam Using Insulated DN200 Blowdown Pipe. POOLEX 3/2005, Technical Report, Nuclear Safety Research Unit, Lappeenranta University of Technology, 2006.

3. Tanskanen, V., Puustinen, M. & Laine, J. Validation of NURESIM-CFD against POOLEX condensation pool experiment: Final Report. 6th Euratom Framework Program NURESIM, Deliverable D2.1.15.2b, (2008), European Commission, 6th Euratom Framework Programme 2005–2008, Integrated Project (IP): NURESIM Nuclear Reactor Simulations Sub-Project 2: Thermal Hydraulics, European Commission, 2008.

4. Tanskanen, V., Lakehal, D. & Puustinen, M. Validation of Direct Contact Condensation CFD Models Against Condensation Pool Experiment. 2008, XCFD4NRS, Experiments and CFD Code Applications to Nuclear Reactor Safety, OECD/NEA & IAEA Workshop, September 10–12, 2008, CEA, Grenoble, France.

17. The integration of thermal-hydraulics (CFD) and finite element (FEM) computer codes in liquid and solid mechanics (MULTIPHYSICS)

17.1 MULTIPHYSICS summary report

Tellervo Brandt, Ville Lestinen, Timo Toppila and Jukka Kähkönen
Fortum Nuclear Services Oy

Antti Timperi, Timo Pättikangas and Ismo Karppinen
VTT

Abstract

In this article, we study a large-break loss of coolant accident (LBLOCA) where a guillotine break of one of the main coolant pipes occurs near the reactor pressure vessel (RPV). This initiates a pressure wave which propagates inside the RPV. The simulation of bidirectional fluid-structure interaction phenomena has been found important for accurate prediction of the resulting deformation and loads. In this article, fully coupled simulation results are validated against the German HDR (Heißdampfreaktor) experiments. The computational fluid dynamic (CFD) software Fluent and Star-CD are applied to modeling of three-dimensional, viscous, turbulent fluid flow. The MpCCI code is used for bidirectional coupling of the CFD simulation to the structural solver Abaqus. Pressure boundary condition at the pipe break is obtained in a two-phase simulation with the system code APROS. Comparisons are made for break mass flow, wall pressure, displacement and strain. The simulation results follow the

experimental data fairly well. The sensitivity of the results to pressure boundary condition and water temperature is studied. In addition, the necessity of using bidirectional coupling instead of one-way pressure mapping is demonstrated.

Introduction

Large-break loss of coolant accident (LBLOCA) is one of the design basis accidents of Finnish nuclear power plants (NPP). In a hypothetical accident scenario, a “guillotine” break of one of the main coolant pipes of the primary circuit causes a rapid pressure drop at the break location. The pressure transient propagates inside the reactor pressure vessel (RPV), and within the first hundreds of milliseconds after the break, the pressure loads induce deformations on the structures and threat their integrity. In this article, the pressure transient is simulated by coupling commercial computational fluid dynamic (CFD) and structural solvers using the MpCCI interface [1]. The pressure boundary condition required in the CFD model, is calculated using the system code APROS [2]. The results are validated against the HDR (Heißdampfreaktor) experiments [3, 4], where LBLOCA was studied in a full-scale geometry using realistic initial conditions. The main focus here is to validate a simulation environment which can be utilized in safety analysis of the Loviisa NPP which includes two VVER-440 type pressurized water reactors (PWR) owned by Fortum.

In earlier studies of pressure transient resulting from the pipe break during LBLOCA, accounting for bidirectional fluid-structure interaction (FSI) phenomena has been found important (see e.g. [4–7]). The HDR experiments and simulations with system codes like APROS show that the FSI problem can be simulated as a one-phase flow approximately for the first 100 ms after the break [4, 8]. However, two-phase phenomena have to be accounted for in evaluating the boundary condition at the break.

In the present work, the CFD solvers Star-CD [9] and Fluent [10] is applied together with the structural solver Abaqus [11], and the pressure at the break nozzle is taken from simulations with the system code APROS.

HDR blowdown experiments

The HDR blowdown experiments were carried out in the early 1980’s in Germany. FSI phenomena caused by the flexibility of the core barrel during the initial depressurization phase of LBLOCA were studied in particular, and one of

the main emphases was to provide reference data for validation of three-dimensional FSI codes.

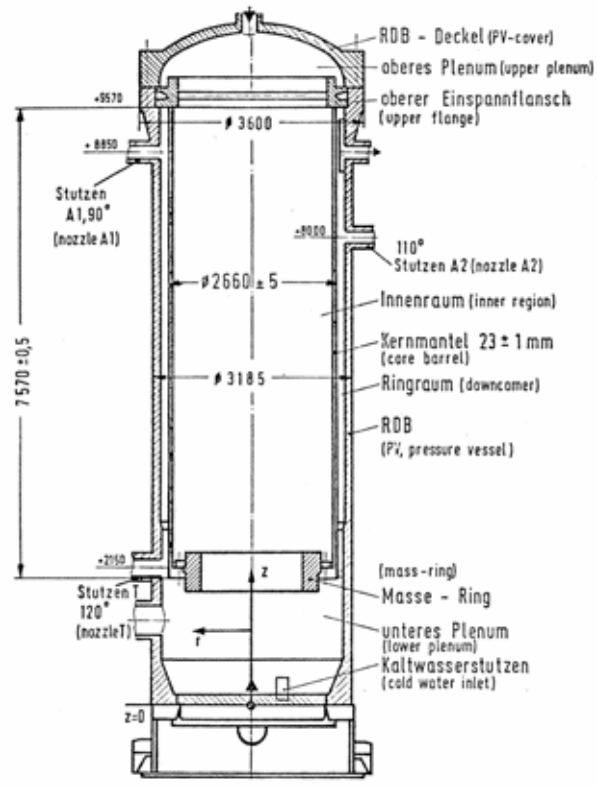

Figure 17.1.1. HDR reactor [4].

The lay-out and the main dimensions of the test facility are shown in Figure 17.1.1. The break occurs in the nozzle A1. Most of the other nozzles of the reactor were closed in order to provide clear boundary conditions for CFD calculations, and the effect of those left open was estimated to be small [3]. The construction of the test facility is quite realistic when compared to Loviisa NPP [8].

Blowdown experiment V32, which was the base case in the experiment series, was chosen for this work. In this experiment, the downcomer and break nozzle temperature was 240 °C and the core temperature varied axially from *308* °C at the upper core to *283* °C at the lower core barrel end. Subcooling in the downcomer and break nozzle area was quite large in the experiment V32, i.e. *78* °C which increased the loads on the core barrel.

Numerical models

Two-phase system code simulations

The system code APROS was utilized to evaluation of the pressure boundary condition for the CFD simulation. The external pressure boundary for APROS calculation was adjusted with the measured pressure from the HDR experiment to get correct pressure reduction rate in the outlet of the nozzle, i.e. break opening time of 1 ms. Actual shredding out of the break disk was not simulated. Instead, a constant opening rate was assumed.

The break nozzle was modeled with 5, 15 and 45 nodes. To be able to provide a detailed time dependent pressure evolution during the first milliseconds after the break opening, the result from the case with 45 nodes was chosen as the CFD boundary condition. In this case, the node length in the break nozzle was 3 cm.

The pressure boundary condition for the CFD calculation was taken from a point inside the nozzle where there were not yet a significant void to allow single-phase CFD simulation. Pressure in this point using 5, 15 and 45 nodes in the nozzle is plotted on the left-hand side of Figure 17.1.2. In addition, pressure in the end of the nozzle is included from the case with 45 nodes and from the measurements. Pressure is depicted only for the first *0.01* s to show the details of the pressure drop. After $t = 0.01$ s, pressure at the break location remains almost constant. The main difference between the APROS result and the measurement is the sharp drop of pressure when the break starts to open.

On the right-hand side of Figure 17.1.2, the calculated break mass flows obtained with 5, 15 and 45 nodes in the break nozzle are compared to experimental result. In addition, the mass flow from a fully coupled FSI-simulation is included. The FSI-result is somewhat below the experiments. The difference is mainly caused by the smaller density used in the FSI-simulation.

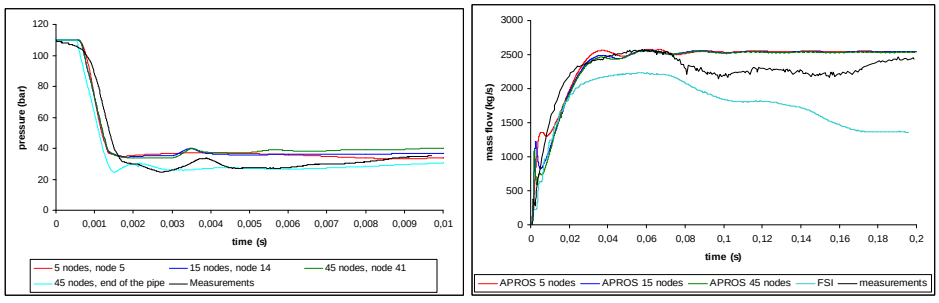

Figure 17.1.2. Comparison to experiments. Pressure boundary condition for the CFD model (left). Measured and calculated blowdown flow (right).

CFD model

The simulations were performed with a CFD grid of approx 78000 cells. The grid is depicted in Figure 17.1.3 together with the model used in the structural solver. The grid dependence and resolution were discussed in more detail in [12, 13].

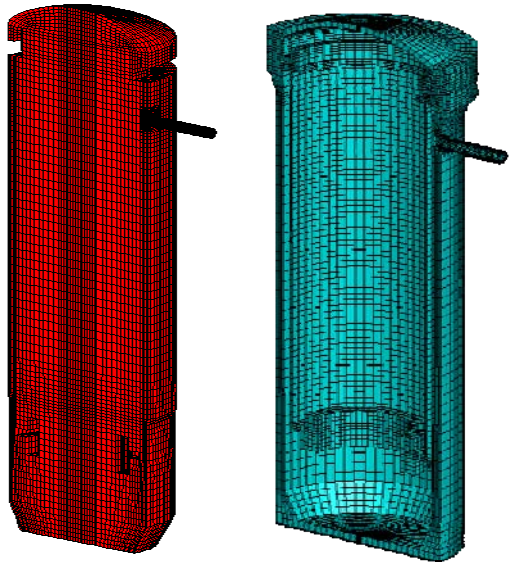

Figure 17.1.3. Computational meshes used in the CFD (left) and structural (right) models.

It can be seen from the experimental data that temperature remains almost constant during the first *0.20* s after the pipe break. Thus in the present simulations, a constant temperature corresponding to the average of maximum and minimum temperatures obtained in the measurements (*274* °C) was assumed. The corresponding dynamic viscosity is $\mu = 0.0001$ Pa·s.

Fluent and Star-CD are both finite-volume based CFD solvers. In both codes, the pressure-based solver was utilized with the PISO pressure-correction. The so-called standard k-ε turbulence model of Launder and Sharma with the standard wall functions was applied [10]. The solid walls were treated as viscous walls using wall functions, and pressure was given at the pipe break. The applied numerical methods were discussed in more detail in [8, 12, 13].

Structural model

In the finite-element based structural solver Abaqus, a linear finite-element model of the reactor with about 15000 8-node hexahedral elements was applied. Continuum shell elements, which have only displacement degrees of freedom but model shell behavior accurately, were mainly used. Conventional solid elements were used in a few necessary regions. One layer of continuum shell elements was used in the core barrel wall and four layers in the RPV wall. The mesh of the structural model is shown in Figure 17.1.3. The structural model had a preliminary static load step in which the static pressure condition was achieved. After the static load step, applied pressure was provided by CFD code.

Material properties $E = 175$ GPa, $\nu = 0.3$ and $\rho = 7900$ kg/m^3 were used for elastic modulus, Poisson's ratio and density of the core barrel, respectively. For the RPV, values $E = 190$ GPa, $\nu = 0.3$ and $\rho = 7850$ kg/m^3 were applied. A small amount of stiffness proportional Rayleigh damping was included in the RPV wall. Value $\beta = 6\times10^{-6}$ was used which results in *2%* of critical damping at frequency *1000* Hz. The maximum frequency of interest was estimated as *400* Hz.

Coupling of CFD and structural model

The external coupling software MpCCI was applied to bidirectional coupling of the CFD and structural solvers. In this approach, the CFD and structural analysis codes run simultaneously and coupling information is exchanged during the simulation. Interpolation is used for transferring coupling quantities between the fluid and structure meshes. In this work, the coupling quantities were fluid pressure and nodal coordinates of the structure, and the codes exchanged

information in the beginning of each time step. The simulations were run on a PC with Intell Core 2 CPU 1.86 Ghz processor in the Windows environment. A simulation for the time period *t = 0* to *0.20* s took approximately *96* hours of wall clock time.

Simulation results

Propagation of the pressure wave and the resulting stress and displacement are demonstrated in Figure 17.1.4. In the figures depicting the stress, the deformation is scaled by the factor of 200.

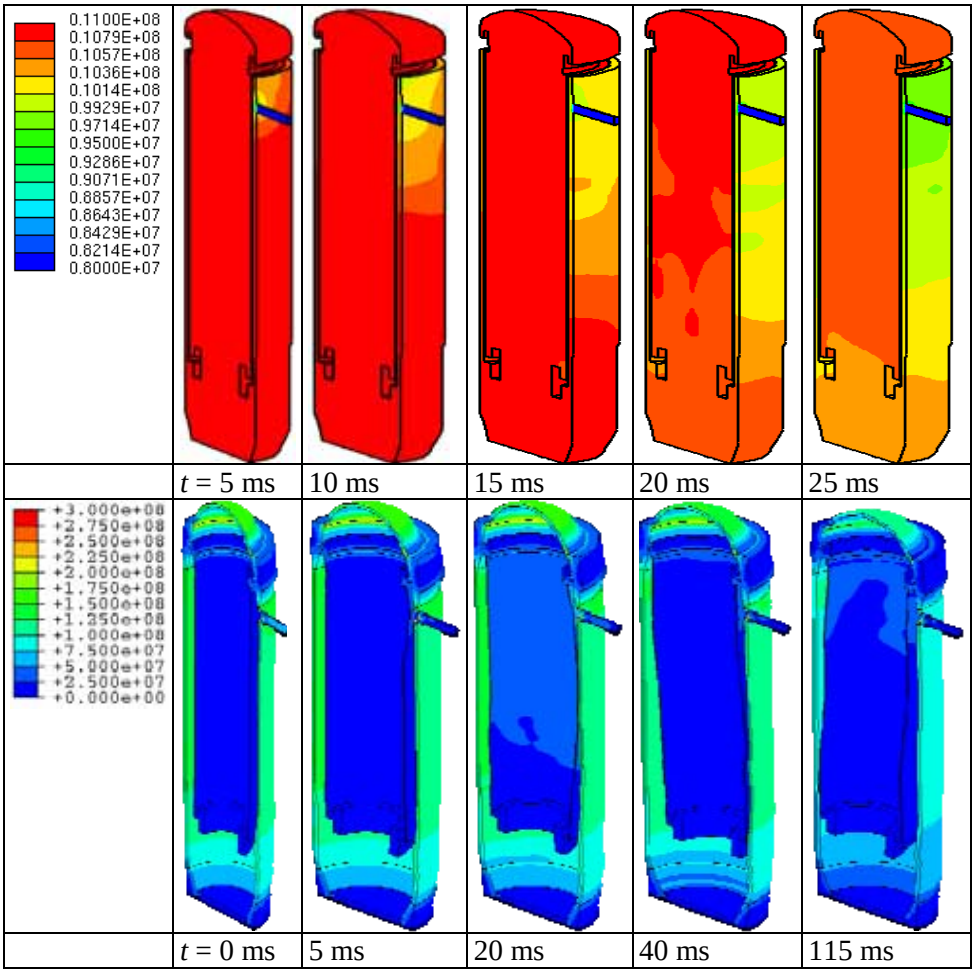

Figure 17.1.4. Pressure in the CFD model (upper). Von Mises stress in the structures, displacements are scaled with the factor of 200 (lower).

Pressure on the inner wall of the downcomer at the nozzle location (in cylindrical coordinates of Figure 17.1.1 at φ = 90○, z = 8.85 m) and somewhat below the nozzle (φ = 90○, z = 2.3 m) are depicted in Figure 17.1.5. Pressure on the opposite side of the downcomer (φ = *270*○, z = *7.78* m) and on the core axis are given in Figure 17.1.6. The pressure field is slightly underpredicted in both simulations, but it follows the experiments fairly well until approximately t = *0.1* s. After this, flashing occurs [4] and the one-phase model fails to describe the pressure rise. During the first *20* ms, both simulations predict an oscillation of approximately *380* Hz in the pressure field. This frequency corresponds to a pressure wave travelling back and forth in the nozzle. The oscillation is not shown in the experiment which may be caused by boiling inside the nozzle (and outside it) which makes the water "soft" in this region.

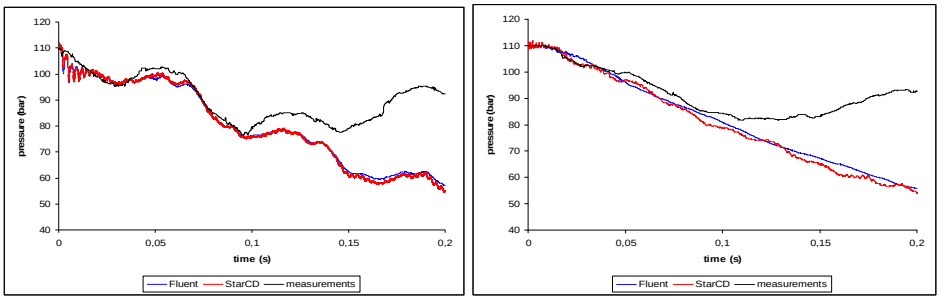

Figure 17.1.5. Pressure on the inner downcomer wall at φ = *90*°, z = *8.85* m at φ = *90*°, z = *2.3* m.

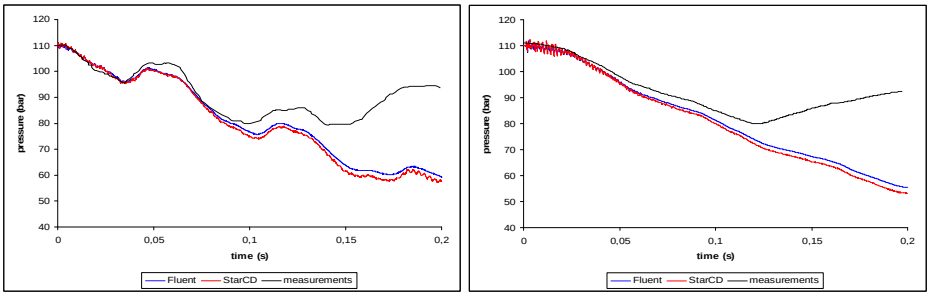

Figure 17.1.6. Pressure on the inner downcomer wall at φ = *270*°, z = *7.78* m at φ = *270*°, z = *5.05* m.

The pressure on both sides of the wall of the core barrel is underpredicted in a similar manner. Because of this, the pressure difference across the wall follows

the experiment even better than the wall pressure. This is visible in the resulting relative displacements between the walls of the core barrel and RPV which are depicted on several locations of the downcomer wall in Figures 17.1.7 and 17.1.8. Here, we notice that the displacements are predicted fairly well for the entire duration of the simulations.

The hoop and axial strain on the wall of the core barrel are shown in Figures 17.1.9 and 17.1.10. The strain oscillates with the frequency corresponding to the pressure wave travelling in the nozzle. This frequency was also visible in the pressure field. The result obtained with Star-CD oscillates clearly more than the one obtained with Fluent which is caused by different time-integration methods.

The two CFD solvers produce almost identical results. However, the Fluent result is somewhat smoother. Since the same computational grid and pressure boundary condition were applied in the simulations with Fluent and Star-CD, the main difference between the two models is in the numerical methods. The sensitivity to numerical methods was discussed in more detail in [12]. Based on these studies, we can conclude that the results are not strongly sensitive to numerical methods.

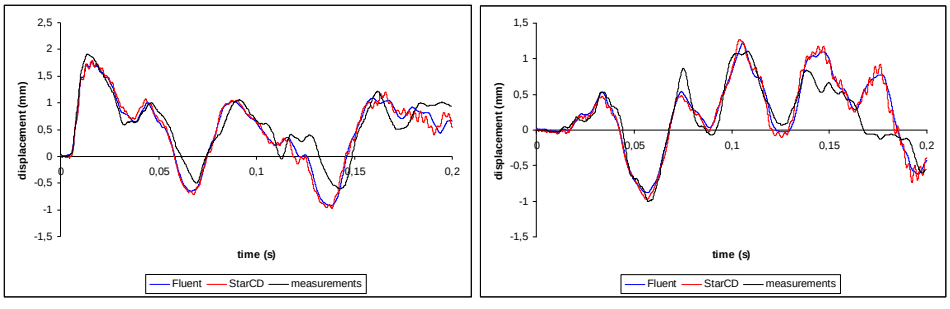

Figure 17.1.7. Relative radial displacement between the core barrel and RPV at $z = 7.15$ m, $\varphi = 90^\circ$ (left) and at $z = 7.15$ m, $\varphi = 270^\circ$ (right).

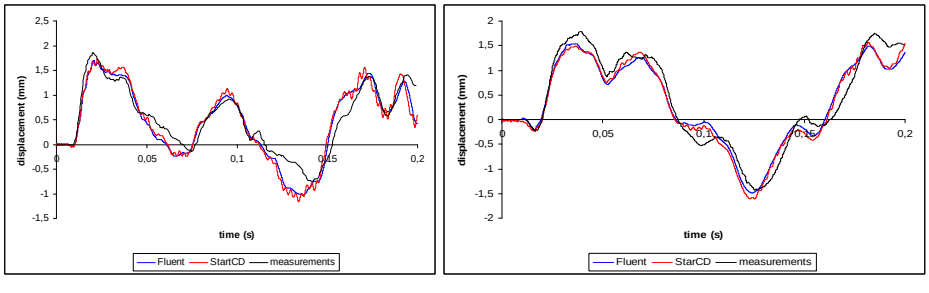

Figure 17.1.8. Relative radial displacement between the core barrel and RPV at $z = 5.55$ m, $\varphi = 90^\circ$ (left) and at $z = 2.3$ m, $\varphi = 90^\circ$ (right).

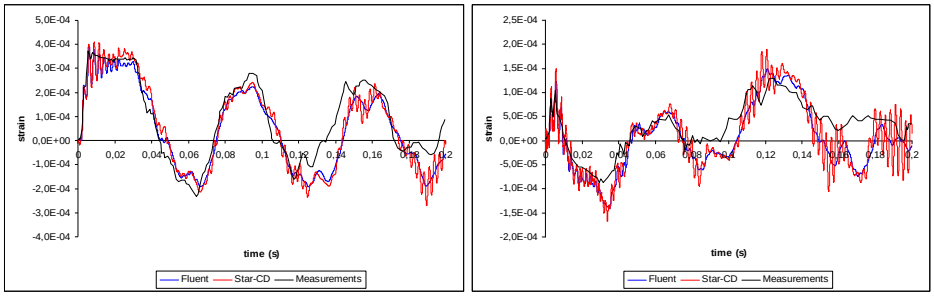

Figure 17.1.9. Hoop strain (left) and axial strain (right) on the outer surface of the core barrel at $z = 8.85$ m, $\varphi = 90^{\circ}$.

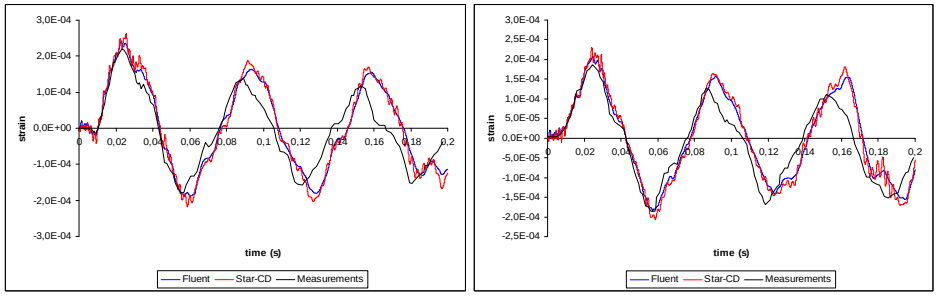

Figure 17.1.10. Hoop strain on the inner surface of the core barrel wall at $z = 8.85$ m, $\varphi = 135^{\circ}$ (left) and at $z = 8.85$ m, $\varphi = 225^{\circ}$ (right).

Conclusions

In this article, we have presented results from simulations of the pressure transient occurring in the early phase of LBLOCA. The results were obtained by bidirectional coupling of CFD and structural solvers. The pressure boundary condition was obtained in a two-phase system code simulation with APROS. The main aim of this work was to validate the simulation environment against the HDR experiments and to describe the sensitivity of the results to pressure boundary condition, numerical methods and grid resolution.

The assumption of one-phase flow used in the CFD model was valid until approximately $t = 100$ ms and after this, the pressure field clearly deviated from the experimental result. During the first *100* ms, the obtained pressure field was fairly close to the experiments. The pressure on both sides of the core barrel was

underpredicted in a similar manner, and thus the pressure difference, which determines the wall movement, followed the experimental result even better. In addition, the pressure difference was not as sensitive to flashing as the wall pressure and the wall displacement was predicted quite accurately for the entire simulation, i.e. until $t = 200$ ms.

Based on the present results, we can conclude that the simulation environment is capable of simulating the FSI phenomena related to the early phase of LBLOCA where the flow can be considered as a one-phase flow.

References

1. MpCCI 3.0.6-12 Documentation User manual. Fraunhofer Institute for Algorithms and Scientific Computing SCAI. Germany, 2007.

2. APROS. The Advanced Process Simulation Environment, http://apros.vtt.fi/. VTT Technical Research Centre of Finland.

3. Wolf, L. Design report for the HDR-RPV-I blowdown experiments V31.2, V32, V33 and V34 with specifications for the pretest computation. HDR Safety Program, Report No. 3.243/81. Kernforschungszentrum Karlsruhe, 1981.

4. Wolf, L., Schall, M. & Bader, H. Untersuchungen von RDB-Einbauten bei Bruch einer Reaktorkühlmittelleitung. HDR Sicherheitsprogramm, Technischer Fachbericht 29–82. Kernforschungszentrum Karlsruhe, 1983.

5. Andersson, L., Andersson, P., Lundwall, J., Sundqvist, J., Nilsson, K. & Veber, P. On the validation and application of fluid-structure interaction analysis of reactor vessel internals at loss of coolant accident. Computers & Structures, 2003. Vol. 81, pp. 469–476.

6. Lestinen, V., Toppila, T., Timperi, A., Pättikangas, T. & Hänninen, M. Determination of thermal-hydraulic loads on reactor internals in a DBA-situation. In: ASME Pressure Vessels and Piping Conference. Vancouver, Canada, July 23–27 2006, PVP2006-ICPVT11-93456, 2006.

7. Casadei, F. & Potapov, S. Permanent fluid-structure interaction with non-conforming interfaces in fast transient dynamics. Computer methods in applied mechanics and engineering, 2004. Vol. 193, pp. 4157–4194.

8. Timperi, A., Pättikangas, T., Karppinen, I., Lestinen, V., Kähkönen, J. & Toppila, T. Validation of fluid-structure interaction calculations in a large-break loss of coolant accident. In: Proc. of the 16th International Conference on Nuclear Engineering ICONE16, Orlando, Florida, USA, May 11–15 2008, 2008.

9. CD adapco Group, Star-CD Version 3.20. Methodology, 2004.

10. Fluent 6.3 Documentation. User's guide. Fluent inc, 2007.

11. Abaqus/CAE 6.7 User's manual. Dassault systems simulia corp., 2007.

12. Brandt, T. Lestinen, V., Kähkönen, J., Toppila, T., Timperi, A., Pättikangas, T. & Karppinen, I. Fluid-Structure interaction analysis of large-break loss of coolant accident. In: Proc of Experiments and CFD code application to Nuclear Reactor Safety, XCFD4NRS, Grenoble, France, September 10–12, 2008.

13. Brandt, T., Lestinen, V., Kähkönen, J., Toppila, T., Timperi, A., Pättikangas, T. & Karppinen, I. Validation of fluid-structure interaction simulation environment in analysis of large-break loss of coolant accident. In: Proc of of Asia Simulation Conference 2008/ 7th International Conference on System Simulation and Scientific Computing (ICSC7), Beijing, China, October 9–10, 2008.

18. Release of radioactive materials from a degrading core (RADECO)

18.1 RADECO summary report

Riitta Zilliacus, Tommi Kekki, Ilona Lindholm and Atso Suopajärvi
VTT

Abstract

The formation of organic iodine on painted surface in water and in N_2 was studied with and without radiation. The water pH in the experiment was 9.3 or 7. In neutral solution small amount of volatile organic iodide was detected. In high pH all volatile iodine was very small amount of inorganic iodine. Experiments performed in gas phase show some formation of volatile compounds, but most of these were rapidly adsorbed on other surfaces and only a negligible amount of organic iodine was detected.

The severe accidents during shutdown conditions were examined with MELCOR code. Olkiluoto 1 was selected for the reference plant. Two accident scenarios starting during shutdown conditions with pressure vessel upper head opened were studied: a station blackout with initially intact pressure vessel (RPV) and a LOCA starting with a break in the bottom head of the RPV. The results of the calculation suggest that even a small hole in the RPV Bottom Head may allow some air ingress to the core region. If the Lower Head is intact no air ingress to the RPV would take place. Station blackout scenario resulted in high zirconium oxidation fraction, about 60%. The oxidation fraction in the Bottom Head LOCA case was 14%. In the calculated cases Ru release from the core equaled to 8–23% of the initial core inventory. The highest Ru release was obtained in the station blackout scenario.

Introduction

Iodine is one of the most important fission products released in a severe nuclear reactor accident. The main reason for this is that a significant fraction of iodine may exist in a volatile form. The understanding of iodine behavior in containment has advanced considerably over the last decades, but there are still some areas where further investigation is needed. Organic iodide formation in post accident containment could result from gas or aqueous phase homogeneous processes, or from processes initiated at the painted surfaces in the containment. There is some data available on the production of organic iodides from painted surfaces, but reactions of iodine with different types of paints may be different [1]. VTT participate in OECD/BIP project (2007–2010). The information from that project will be useful to compare with our own experimental results.

The second subtask in the RADECO project is the investigation of severe accident phenomena related to accidents commencing during plant shutdown state. Specific to shutdown conditions is that the containment may be air-filled even in plants with nitrogen inerting during power operation and the pressure vessel may be open for refueling operations. The containment personnel and equipment hatches may be open. Hydrogen generation and possibility of combustion during shutdown conditions and the release and formation of volatile ruthenium compounds as a consequence of air ingression into the reactor pressure vessel have gained special interest.

Main objectives

The main objective of iodine behavior studies was to assess if the paints applied in Finnish nuclear power plants will contribute in formation of organic iodides under the chemical containment conditions prevailing in Finnish nuclear power plants during a severe accident. Organic iodides are highly volatile compounds which are difficult to remove from atmosphere with the existing filter technology.

The target of investigations of severe accidents during shutdown conditions was to examine overall performance of MELCOR code for accident scenarios occurring during maintenance outage. Olkiluoto 1 and 2 were selected for the reference plant. Special goals of the work were to assess air ingression into opened pressure vessel, the effects on cladding oxidation and potential hydrogen combustion and ruthenium release. Concerning the ruthenium issue, the strategy was to adjust the existing ruthenium release models in MELCOR to account for

the recent measured data on ruthenium behavior under oxidizing conditions. The modifications were limited to the available sensitivity coefficients and material data specified in the MELCOR input. The calculations were purposed to be scoping studies for envisioning the possible effects of ruthenium behavior to plant scale. Increasing the accuracy of the results would need modifications to the MELCOR source code.

The selected two accident scenarios starting during shutdown conditions with pressure vessel upper head opened were a station blackout with initially intact pressure vessel (RPV) Lower Head and a LOCA starting with a break in the bottom of the RPV.

Formation of organic iodine on painted surface in water

The formation of organic iodine on painted surfaces in the radiation field was studiedirradiating painted concrete blocks in bottles filled with water. The solution had the same chemical composition as the sump water in Loviisa reactors containing boric acid, sodium metaborate, NH_3, KOH and HCl. The iodine (5.6 mg/kg-water) was added to the solution. The pH of the solution in the first set of tests was 9.3. The second set was performed using the same base solution after neutralization with hydrochloric acid. The gas flow was lead through the apparatus during the irradiation to collect the volatile reaction products by trapping the inorganic I_2 in a solution of NaOH (2 g/l) and organic iodides in ethanol. Air or N_2 were used gas cover gas in the experiments. The water and gas temperature in the experiments was 25 °C.

The size of the cubic painted samples was 3 cm x 3 cm x 2 cm and the amount of solution 500 cm^3. The gas flow during the irradiation was 0.1 l/min. Figure 18.1.1 illustrates schematically the experimental set up.

The total iodine inventory of Loviisa reactor core is 7.3 kg giving the I-concentration 3.6 mg/kg if all iodine is released. The water volume of the test reaction vessel was 500 cm^3. The total painted area of the concrete block was 26 cm^2. Most of the experiments were made by using 7 years old blocks. The new blocks were used in two experiments.

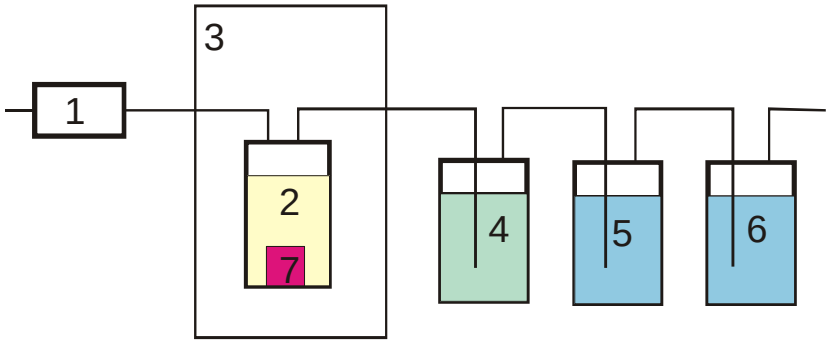

Figure 18.1.1. Schematic diagram of the experimental set up. 1. Flow meter, 2. Reaction vessel, 3. Irradiation facility, 4. NaOH-solution (2g/l, 5 and 6. Ethanol traps and 7. painted block.

A radioactive tracer ^{131}I with the total activity of 50 kBq was used in each experiment. The tracer was added into the reaction solution in vessel 2 in Figure 18.1.1. The activities of trap solutions were measured by using a gamma-spectrometry. The fraction of tracer in each location was determined and the production of elemental iodine and organic iodides was calculated based on the tracer material information. The detection limit of iodine in each trap was 0.001% of the total iodine in the experiment.

Gamma cell ^{60}Co source was used to irradiate the samples during the experiments. The relatively low radiation dose rate (220 Gy/h) of the gamma cell yielded long measurement times, with the longest being 11 days for dose of 48 kGy. The production of organic iodides was measured by leading a slow flow of air or N_2 through the reaction vessel and trapping the inorganic iodine into a NaOH-solution and organic iodides into ethanol. The different experiments performed are presented in the following Table 18.1.1.

Table 18.1.1. Results of the formation of organic iodine on painted surface in water.

Test	gas flow	dose kGy	paint	I abs. on paint (%)	released I_2, %	released org.I, %	pH
1	air	0	-	-	<0.001	<0.001	9.3
2	air	0	-	-	<0.001	<0.001	9.3
3	N_2	0	old	0.2	<0.001	<0.001	9.3
4	N_2	4.6	-	-	<0.001	<0.001	9.3
5	N_2	4.6	old	1.7	<0.001	<0.001	9.3
6	N_2	10.2	old	1.2	<0.001	<0.001	9.3
7	N_2	19.6	old	0.6	<0.001	<0.001	9.3
8	N_2	20.0	old	0.7	0.001	<0.001	9.3
9	N_2	20.0	old	3.9	0.03	0.12	7
10	N_2	10.0	old	4.2	0.09	0.42	7
11	N_2	0	old	0.8	<0.001	<0.001	7
12	air	43	old	1.0	<0.001	<0.001	9.2
13	N_2	43	old	0.9	<0.001	<0.001	9.3
14	air	44	old	0.8	<0.001	<0.001	7
15	air	48	new	10.2	<0.001	<0.001	7
16	air	41	4 month	1.8	<0.001	<0.001	9.3

The results show that the adsorption of iodine on the paint surface is possible even without radiation [2]. The adsorption increased in lower pH and especially on the newly painted surface with air flow (experiment 15). The newly painted surface was less than one month old in the beginning of the experiment. The adsorption on a four months old paint surface (experiment 16) had already decreased to the same level as with several years old paint (experiment 12). According to these results some of the iodine adsorbed on the paint in the beginning of the irradiation may be released later in the course of a longer irradiation.

In the experiments with pH 9.3 only in one experiment some release of inorganic iodine was noticed. In higher pH no release of organic iodides was noticed. When pH was decreased to 7, small amounts of organic iodide were present in the ethanol traps. The tests with long irradiations (higher dose rate) show no release of iodine in any form. It may be possible, that during the long experiment part of the organic iodine will run through the traps. This should not be possible with I2. The production of volatile iodine in these conditions is so small, that the precision of the measurements may be insufficient (0.001%). One explanation is the absorption on the surfaces of trap vessels or pipelines. It is not possible to determine in which chemical form iodine is adsorbed on the surface.

Formation of organic iodides on painted surfaces in gas phase

The formation of organic iodides in gas phase was performed by impregnating the paint surfaces with elemental iodine and then exposing the test blocks to gas atmosphere with or without radiation field to see if any iodine is revolatilized from the painted surfaces.

Iodide solution (I_2 in KJ solution) containing ^{131}I as radioactive tracer was poured at the bottom test vessel and painted blocks were kept above the liquid surface (Figure 18.1.2). Sulfuric acid was added into the solution to vaporize iodine and the bottle was closed. The iodine volatilizes rapidly and the paint adsorbs part of the iodine. The iodine concentration near the surface was adjusted by using different amounts of iodine in the solution and changing the exposure time. The gamma activity originating from ^{131}I was measured and the amount of iodine adsorbed on the surface was calculated. The amount of the adsorbed iodine on the paint surface varied 0.015–0.13 mg/cm^2. The blocks were then inserted into the bottles and nitrogen flow was lead through the bottle. Otherwise the experimental setup was as shown in Figures 18.1.1 and 18.1.3. Each experiment was made as two parallel runs, one in the radiation field and one without radiation. The amount of volatile iodine was determined by measuring the amount of ^{131}I in the traps, in the blocks, in the reaction vessels and in the gas lines. The experiments performed in gas phase are presented in the Table 18.1.2.

Figure 18.1.2. The painted blocks adsorbed gaseous iodine on the surface from the air.

Figure 18.1.3. Traps to collect different forms of iodine.

Table 18.1.2. Results of the experiments performed in gas phase.

Number of exp.	**Total I in the experiment [mg/cm^3]**	**Radiation dose [kGy]**	**I released from the surface % of total I**	**Trapped I_2 % of total I**	**Trapped organic I % of total I**
1	0.06	47 -	5.3 1.5	< 1 < 1	< 0.2 < 0.2
2	0.13	12 -	0.93 0.99	< 0.2 < 0.2	<0.2 < 0.2
3	0.015	43 -	4.6 1.5	< 0.2 < 0.2	< 0.2 < 0.2

In all performed experiments, part of the iodine was released from the surface, but it is immediately adsorbed on the other surfaces, reaction vessel, and gas lines [3]. The reaction on the surface was so rapid that it was impossible to determine the chemical form of iodine. The amount of organic or elemental iodine trapped in the filters was negligible.

Severe accidents during shutdown conditions

Severe accident phenomena related to plant shutdown conditions were studied using Olkiluoto 1 and 2 as a reference plant. Two accident scenario types were selected for assessment: station blackout and a LOCA in one control rod guide tube in the reactor pressure (RPV) vessel bottom. Analyses of these accidents were carried out with MELCOR code version 1.8.6YT. The existing MELCOR input of Olkiluoto 1 was modified by adding a new volume for reactor pool above RPV and by adjusting the decay heat of the core to a value representable to the time when RPV lid is opened. Further, ruthenium was separated into a new fission product group. The release of fission products was modeled with Corsor-Booth correlation which allowed binding of the release rate with cladding oxidation fraction with coarsely approximate temperature criterion. The material properties of the new fission product were determined to be those of RuO_4. This seemed to be sufficient for scoping studies. Any refinement of accuracy would need modifications to the MELCOR source code. This is currently not possible due to code development limitations posed by MELCOR code Maintenance Quality Assurance policy.

The station blackout accident scenario is assumed to begin with the total loss of off-site and on-site power at 18 hours after the plant shutdown. The pressure vessel is assumed to be open for maintenance. The lower drywell material hatch is closed. No pedestal flooding is assumed to take place. No breaks in the reactor coolant system or shutdown cooling system are assumed to occur. As a consequence of complete loss of power, decay heat is removed into the RPV water pool but heat is not removed by shutdown cooling system (321). The unmitigated accident progresses to long-term boil-off of coolant from the RPV and steam release to the auxiliary building. Table 18.1.3 collects the timing of key events and key figures-of-merit from the calculated station blackout scenario.

A loss-of-coolant accident is assumed to occur during a plant shutdown. The location of the leak is at the bottom of the RPV, and the diameter of the leak (71 mm) is equal to the diameter of a control rod guide tube. The pressure vessel is assumed to be open for maintenance. The lower drywell personnel door is assumed to be open. The water in the pedestal flows thus out of the containment. No breaks in the reactor coolant system or shutdown cooling system are assumed to occur. The water escapes from the RPV and the core is exposed. Table 18.1.4 collects the timing of key events and key figures-of-merit from the calculated LOCA scenario.

Table 18.1.3. Key figures-of-merit from the scenario of station blackout commencing during shutdown.

	Station blackout, reactor pool initially empty	**Station blackout, reactor pool initially full**
Reactor pool empty (hr)	0	46
Time of core uncovery (TAF) (hr)	8	54
Time of total core uncovery (hr)	14	61
Pressure vessel failure (hr)	22.5	74
Cavity failure by concrete erosion (hr)	53	>83
Hydrogen production in the core(kg)	1095	1123
Hydrogen production in the cavity (kg)	586	186
Fraction of Zr oxidized	0.59	0.63
End of calculation (hr)	53	83

Table 18.1.4. Key figures-of-merit from a scenario with RPV bottom head LOCA the scenario commencing during shutdown.

	LOCA, reactor pool initially empty	**LOCA, reactor pool initially full**
Reactor pool empty (hr)	0	5.3
Time of core uncovery (TAF) (hr)	1.2	6.3
Time of total core uncovery (hr)	2.5	7.5
Pressure vessel failure (hr)	4.3	9.6
Cavity failure by concrete erosion (hr)	23.1	29
Hydrogen production in the core(kg)	157	147
Hydrogen production in the cavity (kg)	651	673
Fraction of Zr oxidized	0.080	0.138
End of calculation (hr)	23.1	29

In the station blackout case the zirconium is practically completely oxidized by steam as there is not yet air available in the core region. The total amount of hydrogen generated is approximately 1100 kg independent of initial reactor pool water inventory. In case the reactor pool is initially dry the oxidation begins at about 14 hours after loss of power. If the reactor pool is initially full of water the oxidation starts 61 hours (= 2.5 days) after the station blackout.

In case of Bottom head LOCA scenario the water in the reactor pool drains out through the bottom head hole in about 5 hours. If the reactor pool is dry in the beginning, the oxidation begins in 2.8 hours after the initiation of the accident. In case the reactor pool is initially full, the oxidation commences 7 hours after the beginning of the accident (Figure 18.1.4). Zirconium and steel are oxidized mainly by steam but there is some oxygen in the core atmosphere at the end of the oxidation process. The shutdown cooling system 321 injects water into the pressure vessel. The average oxidation fraction is significantly lower than in station blackout case. This may be due to lower coolant temperature in the RPV during feed and bleed.

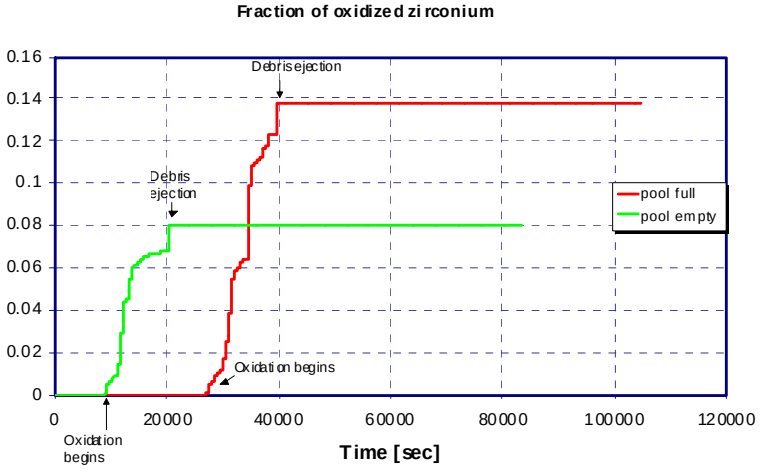

Figure 18.1.4. Zirconium oxidation fraction. Bottom head LOCA accident with reactor pool initially filled with water (pool full) and with reactor pool initially empty.

The release of fission products from the core is presented in Tables 18.1.5 and 18.1.6 and the history of release in case of station blackout is illustrated in Figure 18.1.5. The higher oxidation fraction in the station blackout scenario results in higher ruthenium release than in the LOCA scenario. Ruthenium tetroxide can also be formed also in the presence of steam, the only necessary condition has been observed to be that practically all zirconium in the cladding needs to be oxidized before RuO_4 can form. The ruthenium tetroxide is assumed to remain as gas and thus remains in the atmosphere of the reactor hall and the reactor pool (Figure 18.1.6). The reduction of ruthenium inventory starting at about 24 hours (85 000 s) is due to hydrogen deflagrations mostly in the Pedestal

(Figure 18.1.8). The pressure difference between the Pedestal and the environment pushes gases through the failed RPV bottom head to the reactor hall and out to the environment.

Table 18.1.5. Initial fission product inventories in the core and release from the core in case of station blackout scenario.

Fission product	**Initial core inventory (kg)**	**Release fraction from the core**	
		Reactor pool initially full	**Reactor pool initially empty**
Noble gases	403.0	1	1
Cs	219.5	0.745	0.702
I (as CsI)	41.05	0.881	0.970
Te	39.96	0.731	1
Ru	181.0	0.231	0.230

Table 18.1.6. Initial fission product n the core and release from the core in case of Bottom Head LOCA scenario.

Fission product	**Initial core inventory (kg)**	**Release fraction from the core**	
		Reactor pool initially full	**Reactor pool initially empty**
Noble gases	403.0	0.985	0.997
Cs	219.5	0.185	0.257
I (as CsI)	41.05	0.965	0.981
Te	39.96	0.861	0.465
Ru	181.0	0.084	0.116

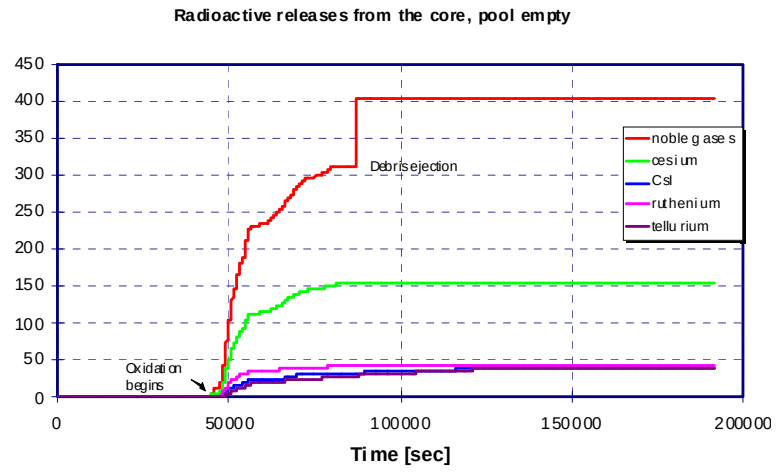

Figure 18.1.5. The history of radioactive material release from the core. Station blackout accident, reactor pool initially empty.

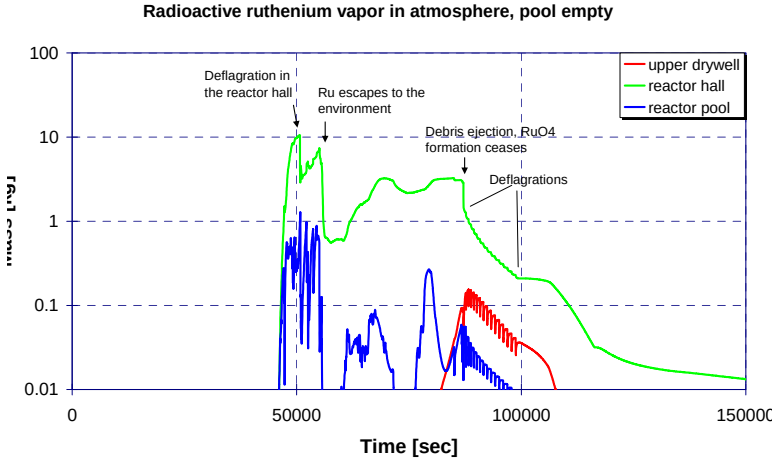

Figure 18.1.6. Ruthenium vapor mass in the containment and reactor building atmospheres. Station blackout during shutdown.

The ruthenium release from the core was 50% lower in the Bottom Head LOCA case than in the station blackout scenario. The airborne ruthenium inventory reaches a peak value of about 6.3 kg in about 1 hour after the release from the core begins (Figure 18.1.7). After the pressure vessel failure a large release path to the environment opens through the failed RPV bottom and further through the

open Lower Drywell Personnel hatch. The release to the environment is enhanced by hydrogen deflagrations following RPV failure. Ruthenium is transported out of the reactor hall through blow-off panels that are opened by deflagrations early during the accident. Air flows in through lower drywell personnel door and exits via impaired RPV and reactor hall through blow-off panels (Figure 18.1.9).

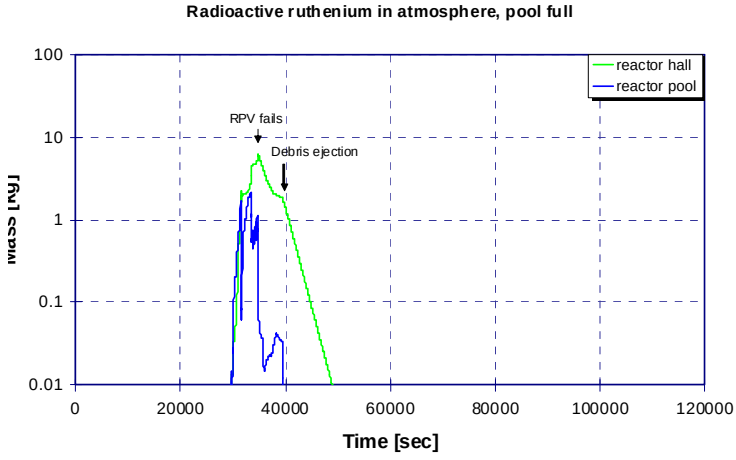

Figure 18.1.7. Ruthenium in atmosphere. Bottom Head LOCA accident. Reactor pool initially full.

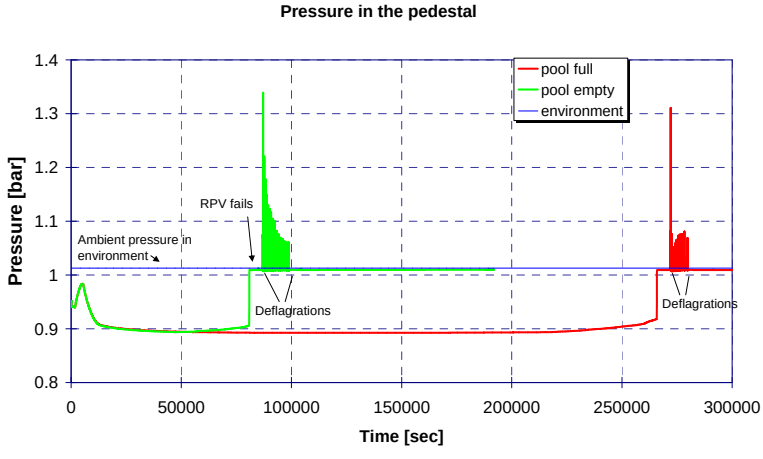

Figure 18.1.8. Pressure in the pedestal. Station blackout during shutdown.

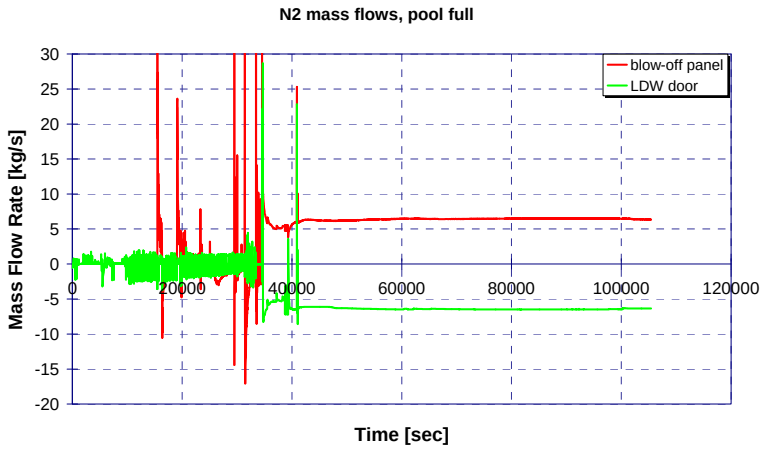

Figure 18.1.9. Nitrogen mass flow rate out of the containment (red) and pedestal (green) to the environment. Negative values indicate opposite direction. Bottom Head LOCA. Reactor pool initially full.

Conclusions

In all performed experiments, part of the iodine was released from the surface, but it is immediately adsorbed on the other surfaces, reaction vessel, and gas lines. The reaction on the surface was so rapid that it was impossible to determine the chemical form of iodine. The amount of organic or elemental iodine trapped in the filters was negligible.

According to these experiments the formation of the organic iodine is very limited. The painted containment surfaces exposed to atmosphere can be effective traps for iodine in severe accident conditions. However, some migration of iodine on the surfaces may be possible by sequential revolatilization and re-trapping. Furthermore, the effects of flooding the painted surfaces which carry iodine with moderate to high pH water still needs to be studied.

The results of the calculation with MELCOR code suggest that even a small hole in the RPV Bottom Head may allow some air ingress to the core region. If the Lower Head is intact, no air ingress to the RPV would take place. Station blackout scenario resulted in high zirconium oxidation fraction, about 60%, and hydrogen generation. The oxidation fraction in the Bottom Head LOCA case remained lower, less than 14%. The reason for lower oxidation is the drainage of coolant through the RPV leak and injection of cold coolant to the RPV by

shutdown cooling system, which suppressed steam production. Air ingression was not sufficient to support strong oxidation.

In the calculated cases Ru release from the core equaled to 8–23% of the initial core inventory. The highest Ru release was obtained in the station blackout scenario. If a large portion of the released ruthenium is volatile RuO_4, the vapor is easily transported to the reactor pool and reactor hall residing outside the containment barrier. In the performed calculation a total of 41 kg of Ru was released from the containment and reactor building. The activity release with Ru is of the order of 2700 TBq. Due to several conservatisms and modeling simplifications this exercise can be considered only as crude approximation and encouragement to study further the behavior of Ru during severe accidents during plant shutdown conditions and its effects on source term.

References

1. Zilliacus, R., Koukkari, P., Karjunen, T. & Sjövall, H. Formation and behaviour of organic iodine. NKS-42. ISBN 87-7893-095-2. January 2002.

2. Zilliacus, R. & Kekki, T. Formation of organic iodine in water. VTT-R-01090-08. March 2008.

3. Zilliacus, R. & Kekki, T. Formation of organic iodine on painted surface in gas phase. VTT-R-00503-09. January 2009.

19. Primary circuit chemistry of fission products (CHEMPC)

19.1 CHEMPC summary report

Teemu Kärkelä, Ari Auvinen, Riitta Zilliacus, Jussi Lyyränen,
Jouni Pyykönen, Unto Tapper, Tapani Raunio, Tommi Kekki,
Tuula Kajolinna, Leif Kåll and Jorma Jokiniemi
VTT

Abstract

This report summarizes the activities performed in CHEMPC project. The aim of the project was to study transport and chemistry of fission products in primary circuit as well as in containment during a hypothetical severe accident. Experimental studies on fission product chemistry in primary circuit were conducted at VTT and at IRSN. Fission product transport in SGTR sequences was experimentally studied in international ARTIST program at PSI. Experiments on radiolytic oxidation of iodine in containment conditions were carried out together with Chalmers University of Technology at VTT. Based on previous experiments, modelling studies on the behaviour of ruthenium oxides in air-ingress accident were conducted. As a part of international collaboration, CHEMPC project also included follow-up of Phebus FP and ISTP programs as well as ISTC program project EVAN.

CHEMPC project is funded by Finnish Research Programme on Nuclear Power Plant Safety 2007–2010 (SAFIR2010), VTT, Nordic Nuclear Safety Research (NKS), Institut de Radioprotection et de Sûreté Nucléaire (IRSN) and Fortum Nuclear Services Ltd.

Introduction

CHEMPC project is focused on studying transport and chemistry of fission products during a hypothetical severe accident. Especially of interest have been ruthenium oxides and iodine, which are considered very harmful because of their volatility and high radiotoxicity [1, 2]. The aim is to find out the possible gaseous and aerosol species transporting through the primary circuit as well as their behaviour in containment.

Due to the extremely high costs involved with experiments on real spent fuel, project includes active international collaboration. In addition to separate effect experiments conducted at VTT, instrumentation, experimental expertise and interpretation help has been provided to several large international research programs. As an example of the interpretation work, behaviour of volatile ruthenium oxides in decreasing temperature gradient (1700–300 K) during previously conducted experiments could be explained by detailed CFD modelling of the facility. The results of the study have been shared with international experts in the frame of SARNET network.

Another important topic in CHEMPC project has been the transport of FPs in possible steam generator tube rupture scenarios. Despite their fairly low probability such containment by-pass scenarios are considered risk dominant because of their estimated large source term to the environment. Currently, retention to the circuit is not taken into account in risk analysis due to lack of crucial aerosol models and experimental data. VTT participated in international ARTIST program carried out at PSI, in which retention of particles to various structures of a vertical steam generator was experimentally studied. In addition, separate effect experiments were carried out at VTT to quantify resuspension of particles from broken steam generator tube. As a result, a unique database on particle retention in steam generator to be utilized in safety assessments was gathered.

Fission product chemistry in primary circuit

As a result of Phebus FP program, it is known that the codes applied in severe accident analysis are not able to model the high temperature chemistry of most important fission products. In order to resolve this issue, ISTP program project CHIP was launched at IRSN to study gas phase chemistry of FPs in primary circuit. Sampling system for high and low temperature sections of the CHIP facility were designed and constructed at VTT. In addition, EXSI facility aimed at studying iodine chemistry at primary circuit surfaces at VTT was manufactured as well.

One of the main objectives of the constructed sampling system was to minimize losses of the hot leg sample during cooling of the flow. In order to accomplish that, a special two stage diluter was designed for the system. The system was tested by sampling saturated NaCl vapour from 750°C and cooling it down to 150 °C. In these tests, the combined losses due vapour condensation, thermophoresis and chemical reactions were 8% to the preheated inlet of the diluter and 0.08% to the diluter itself. Simultaneous measurements conducted using online mass balance without the special diluter indicated greater than 50% losses to the sampling lines. As expected, losses to the cold leg sampling system were insignificant.

As CHIP facility needs to be remotely operated, the sampling system had to be fully automated. The graphic interface of the control program provides an overview to the state of the system at a glance as well as easy step-by-step navigation through the sampling sequence. All measurement data from sampling line is logged to a single file in order to facilitate further processing.

In the qualification tests the sampling system was shown to perform very well in the expected experimental conditions. The system maintained constant dilution ratio, even if the test parameters went far beyond those required in actual experiments. Moreover, the accuracy and relatively fast response time of the flow controls enable adaptation of the system to accommodate various online measuring instruments. The accuracy of the computer controlled dilution was tested using CO_2 tracer and Fourier Transformation Infrared Spectrometer (FTIR) for online analysis of the gas composition. A result from a test with a dilution ratio 1/10 is presented in Figure 19.1.1. It can be seen that estimated and measured CO_2 concentrations match closely despite stepwise changes in the system pressure.

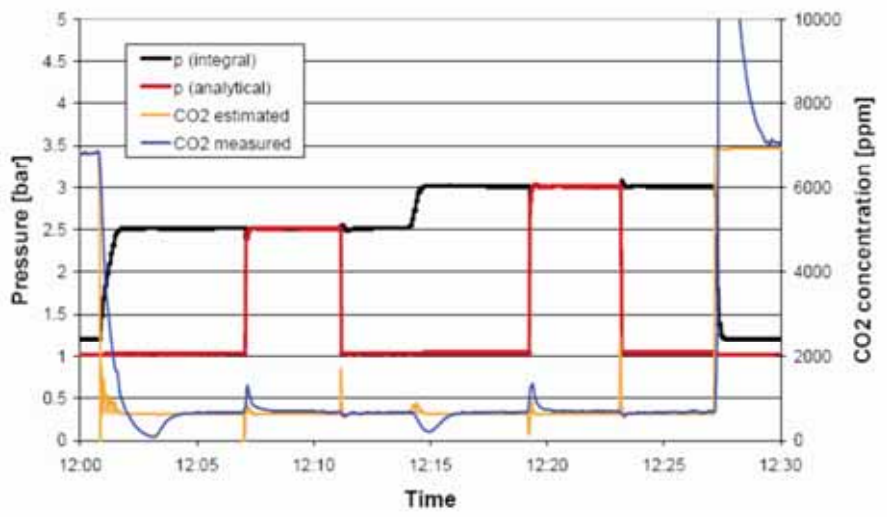

Figure 19.1.1. This figure shows the measured and estimated CO_2 concentrations in hot leg sampling line with argon and H_2 sample flow mixture and dilution ratio of 1/10. Pressure measured in lines to integral and analytical filters during different stages of sampling is presented as well.

Follow-up of international programs

CHEMPC project has included follow-up of international Phebus FP and ISTP programs as well as ISTC program project EVAN.

During the first two years of SAFIR2010 program a major undertaking was the review of the Phebus FP FPT-2 final report regarding fission product transport in the primary circuit of the facility. The experiment was highly interesting as revaporisation of all volatile fission products in the circuit was directly measured for the first time in realistic conditions. The results from the experiment indicated also significant change in the FP transport close to the end of the fuel degradation phase. Furthermore, the changes in iodine concentration in the containment seemed to be almost exactly the opposite to the predictions of severe accident codes [3].

ISTP program includes the aforementioned CHIP experiments, in which VTT has participated. In addition, iodine and ruthenium chemistry in containment has been studied in EPICUR project, B_4C degradation in BECARRE project and cladding degradation in MOZART project. The construction of the VERDON

facility for HBU and MOX fuel degradation experiments has also been followed-up in ISTP program.

ISTC program project EVAN included several subprojects of which fission product release from molten pool and resuspension experiments were reviewed by VTT. Progress on these issues will be presented at ICAPP 09 conference in Tokyo.

Modelling of ruthenium transport in oxidising conditions

In previous experiments the chemistry of ruthenium oxides proved to be complex with a number of reaction pathways in gas phase and on the surfaces. Particle formation, impurities and gas composition all played an important role in the experiments [4]. In order to interpret the results a detailed CFD-modelling of the facility was deemed necessary.

According to the modelling study, diffusion-limited reactive condensation of RuO_3 and direct condensation of RuO_2 seemed to explain majority of the wall deposition observed in the experiments. Simulated ruthenium deposition profiles and comparison with the measured data are presented in Figure 19.1.2. Particle formation and subsequent thermophoretic deposition especially at the part of the tube close to the outlet of the furnace are likely to explain majority of the remaining differences between the calculated and measured results.

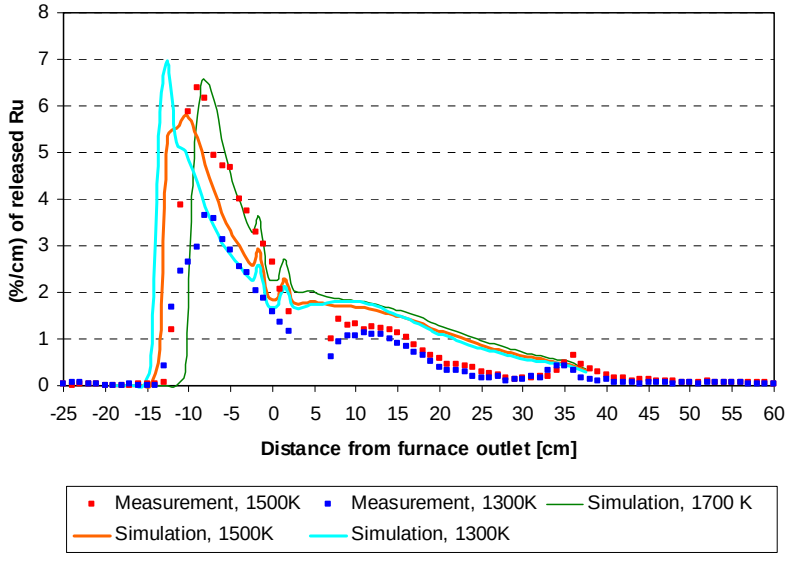

Figure 19.1.2. Simulated ruthenium deposition profiles and comparison with the measured data.

The conclusions that this study allows to make is that wall condensation and particle formation are the dominant processes, when the cooling rate is relatively fast. As the cooling rate was fast in every experiment, it is harder to extend the understanding beyond the conditions encountered in the test facility.

According to thermal equilibrium, there should be significant gaseous RuO_4 concentration especially at the temperature of 1300 K. This would explain the overestimated wall deposition at that temperature. At higher temperatures increasing RuO_2 particle mass concentration is likely to catalyse decomposition reaction of RuO_4 to RuO_2. Impurities in the gas flow seemed to decrease the catalytic activity and increase the transport of gaseous RuO_4 through the facility.

Radiolytic oxidation of iodine

One hypothesis in modelling iodine behaviour in the containment has been that radiolytic processes destroy gas phase molecular iodine to form iodine oxide or iodine nitrogen oxide particles. The objective of this study was to verify the possible formation of iodine containing aerosol when gaseous iodine is exposed to radiation. In addition, the produced particles were to be characterised.

The radiolytic oxidation of iodine in containment conditions was studied in 27 experiments. The source of ionising radiation was ultraviolet light (UVC). The effect of oxygen, ozone and iodine concentrations as well as that of radiation intensity on IO_x aerosol formation was studied. Temperature of the facility was always constant at 120 °C and the gas contained always some humidity.

It was find out that the nucleation of aerosol particles was almost instant when ozone and iodine were present in the facility. Even few ppm concentration of ozone was enough to convert molecular iodine to particles in few seconds. The size of the nucleated particles was less than 10 nm and their number concentration was very high. The primary particles grew by agglomeration and by surface reaction. The mobility diameter of agglomerates ranged from 60 to 120 nm. UV-radiation by itself was not efficient in promoting IO_x particle formation. However, ozone produced by UV-radiation caused nucleation to take place. Presence of ozone also promoted iodine retention to the facility probably by surface reaction. The decrease in iodine transport, when the concentration of ozone increases, is presented in Figure 19.1.3.

As significant concentration of ozone is expected to form in the containment during a severe accident, it is very likely that iodine would be primarily in the form of aerosol particles. If the particles are formed after most material has

settled, they may remain in the containment atmosphere for a long time due to their small size. It was also found out that iodine retained on the tube surfaces evaporates later. Such process may lead to a steady-state gas phase concentration of iodine in the containment.

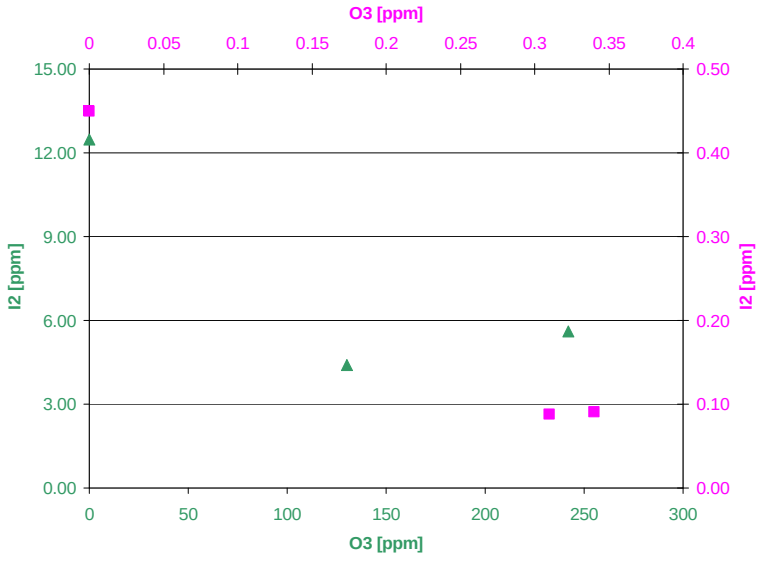

Figure 19.1.3. The effect of ozone concentration on the concentration of iodine transported through the facility.

Images of the formed particles could only be taken with low-voltage SEM. In TEM particles seemed to easily evaporate under the electron beam. According to SEM-EDX analysis particles contained both iodine and oxygen. Due to literature study, there are three probable iodine oxide species what to expect – I_2O_4, I_2O_5 and I_4O_9. When the iodine oxides are in contact with water they form hydrated species and the final product is likely iodic acid [5, 6]. Concerning the conditions during severe accident it is probable that iodic acid (HIO_3) would form, but that was not verified in this study.

Study of SGTR sequences

Particle resuspension experiments

Particularly in containment by-pass sequences retention of FPs in the circuit would significantly decrease the source term. While deposition processes of

aerosol particles are fairly well known, great uncertainty remains in estimating the removal of deposited material by high velocity flow. Current integral codes do not even have validated models for particle resuspension.

In this work experiments, in which particle deposition and resuspension were measured with online instrumentation, were carried out [7]. The experiments were unique as the amount of deposited material was monitored simultaneously at several locations within a tube. The deposition mechanism, deposition velocity and flow velocity could also be adjusted independently. Particle size, shape and density were well characterised in the experiments.

According to the results, the most important parameter affecting resuspension seemed to be particle size. Flow rate during the deposition phase seemed to also influence on adhesion force distribution. Deposition mechanism did not directly influence resuspension. However, it affected on the size of deposited particles. Particles that had resuspended from the walls seemed to fell to the floor of the tube. This would indicate that the resuspension must have taken place as fairly large agglomerates. Also simultaneous deposition and resuspension seemed to be significant in laminar as well as in turbulent flow.

Experimental phase of the resuspension study has now been finished. However, further analysis of the results and modelling studies have been carried out within SARNET network at the University of Newcastle, IRSN, ENEA as well as at VTT.

ARTIST Program

Aim of the ARTIST program has been to provide an international forum to create and share information on SGTR scenarios. High quality experimental data for development of both fundamental and application oriented models have been produced during the program. Data have also facilitated evaluation of effectiveness of severe accident management guidelines. During the project methodology for SGTR risk assessment using ARTIST experimental data have been further developed. The objective is to produce international consensus on re-assessment of SGTR induced environmental risk during DBA and SA. Preliminary results from the re-assessment have been published.

ARTIST program consist of seven phases, in which various mechanisms related to FP retention during SGTR sequence have been experimentally studied. These include aerosol retention in broken SG tubes, retention in bundle at break stage and at far-field, aerosol and droplet retention in separator and dryer,

retention in flooded bundle as well as integral experiments with complete vertical steam generator.

As a result, aerosol retention in SG was determined for spherical monodisperse SiO_2 and latex particles as well as polydisperse TiO_2 agglomerates. Tests were conducted for different particle concentrations in dry conditions, in condensing conditions and in flooded bundle. In broken SG tubes the retention was dynamic depending on particle size and concentration. Steam condensation increased decontamination factor significantly [8]. Largest retention in dry conditions was found to take place however in the break stage depending primarily on particle size and concentration [9]. Retention in the far-field of the bundle was rather limited [10]. The most effective retention took place in flooded bundle with submersion of the break between at least 3.2 and 3.8 meters. In such case the decontamination factor was found to vary between 300 and 2000 [11]. VTT participated in ARTIST integral experiments, which yielded results consistent with the separate effect experiments. In the integral tests the highest retention was observed at the break stage of the SG [12].

Conclusions

The CHEMPC project started in 2007 focused on the transport and chemistry of fission products in primary circuit and in containment. The aim is to gather data about the behaviour of fission products, which can be utilized in safety assessment and plant analysis codes. The project continues to the end of year 2010.

During the project a fully automated system, capable of extracting gaseous samples from high temperature (700–1000 °C) and cooling them down to 150 °C with only negligible losses, was constructed. The sampling system is applied at IRSN to study the gas phase high temperature chemistry of FP compounds at CHIP facility. At VTT similar sampling system is used in EXSI facility dedicated to measure reactions of FP compounds at the surfaces of the primary circuit.

EXSI facility was also applied in the study of radiolytic oxidation of iodine in containment conditions conducted together with Chalmers University of Technology. It was found out that UV-radiation alone was not able to oxidise elemental iodine in gas phase. However, UV-radiation produced significant amount of ozone even with fairly low oxygen concentration (2 %-vol). Ozone reacted with gaseous elemental iodine causing almost instant nucleation of iodine oxide aerosol particles. The particle growth took place by agglomeration and by surface reaction to final mobility diameter of 60–120 nm depending on

the initial iodine concentration. It seemed that ozone increased the retention of iodine, probably by surface reaction, in the facility. The observed formation of iodine oxide particles would largely explain the particularly peculiar behaviour of gaseous iodine in Phebus FP experiments.

The modelling study of ruthenium transport was successful. According to the study diffusion-limited reactive condensation of RuO_3 and direct condensation of RuO_2 seemed to explain majority of the wall deposition observed in the experiments. The modelling results agreed closely with the observed ruthenium transport during previous separate effect experiments. The conclusions that this study allows to make is that wall condensation and particle formation are the dominant processes, when the cooling rate is relatively fast.

ARTIST program has provided high quality experimental data for development of both fundamental and application oriented models for retention of FPs during SGTR sequences. During the project methodology for SGTR risk assessment have been further refined. Data have also facilitated evaluation of effectiveness of severe accident management guidelines.

References

1. Mun, C., Contrel, L. & Madic, C. Review of literature on ruthenium behaviour in nuclear power plant severe accidents. Nuclear Technology 156, 332, 2006.

2. Girault, N., Dickinson, S., Funke, F., Auvinen, A., Herranz, L. & Krausmann, E. Iodine behaviour under LWR accident conditions: Lessons learnt from analyses of the first two Phebus FP tests, Nuclear Engineering and Design, 236, 2006, pp. 1293–1308.

3. Gregoire, A., March, P., Payot, F., Ritter, G., Zabiego, M., de Bremaecker, A., Biard, B., Gregoire, G., Schlutig, S. & Phebus, P.F. FPT2 Final Report. IRSN DPAM/DIR-2008-272, Document Phébus PF IP/08/579, 2008.

4. Kärkelä, T., Backman, U., Auvinen, A., Zilliacus, R., Lipponen, M., Kekki, T., Tapper, U. & Jokiniemi, J. Experiments on the behaviour of ruthenium in air ingress accidents – Final Report. VTT-R-01252-07, 2007.

5. Daehlie, G. & Kjekshus, A. Iodine oxides, I. I2O3.SO3, I2O3.4SO3.H2O, I2O3.SeO3, and I2O4. Acta Chemica Scandinavica, 18(1), 1964b, pp. 144–56.

6. Chase, M.W. NIST-JANAF thermochemical tables for the iodine oxides. Journal of Physical and Chemical Reference Data, 25(5), 1996, pp. 1297–1340.

7. Raunio, T. Experimental Study on Fine Particle Resuspension in Nuclear Reactor Safety. Masters Thesis, Helsinki University of Technology, Faculty of Information and Natural Sciences, 2008.

8. Lind, T., Suckow, A. & Dehbi, A. Summary report on ARTIST Phase I tests for in-tube retention. Paul Scherrer Institut, TM-42-08-03, ARTIST-71-08, 2008.

9. Lind, T., Suckow, A. & Dehbi, A. Summary report on ARTIST Phase II tests for retention in the break stage. Paul Scherrer Institut, TM-42-08-04, ARTIST-72-08, 2008.

10. Lind, T., Suckow, A. & Dehbi, A. Summary report on ARTIST Phase III tests for retention in the far field. Paul Scherrer Institut, TM-42-08-05, ARTIST-73-08, 2008.

11. Dehbi, A., Suckow, A. & Lind, T. Summary report on ARTIST Phase V tests for retention in the flooded bundle. Paul Scherrer Institut, TM-42-08-18, ARTIST-75-08, 2008.

12. Lind, T., Suckow, A. & Dehbi, A. Summary report on ARTIST Phase VII tests for retention in the integral mock-up facility. Paul Scherrer Institut, TM-42-08-08, ARTIST-77-08, 2008.

20. Core melt stabilization (COMESTA)

20.1 COMESTA summary report

Tuomo Sevón and Ilona Lindholm
VTT

Abstract

COMESTA project has investigated core melt behavior in a severe accident. Experiments have been conducted both at VTT and in international projects on the subjects of molten core – concrete interactions, melt pool coolability and steam explosions. Competence for computational modeling of severe accidents has been developed.

Introduction

In the very unlikely event of a severe accident, the core of a reactor melts. The target of severe accident management is to keep the containment intact and to prevent the release of radioactive materials to the environment. To reach this target, the molten corium must be cooled down. COMESTA (Core Melt Stabilization) project was set up to investigate the behavior of molten corium in the containment. In particular, the phenomena of molten core – concrete interactions (MCCI) and coolability of core melt were investigated and competence for computational modeling of severe accidents was developed.

Main objectives

The project consisted of several separate tasks. The largest task was performing HECLA experiments on melt–concrete interactions. The objective was to test the behavior of the special sacrificial concrete in the EPR reactor pit under pouring of metallic melt. The HECLA experiments are described in more detail in a separate article in this publication.

The project involved participation in several international research programs. International cooperation allows expensive experiments to be conducted in an affordable way for the participating countries. In the OECD MCCI-2 project, the objective is to experimentally investigate interactions between molten corium and concrete and coolability of core melt. In the OECD SERENA2 project, experiments on steam explosions are conducted. Both of these international projects employ real nuclear reactor materials, which makes the experiments very challenging. In addition, Finland's membership in the U.S. NRC's CSARP (Cooperative Severe Accident Research Program) is part of the COMESTA project. Through CSARP, licenses for using the integral severe accident simulation program MELCOR are obtained for all Finnish nuclear energy organizations.

In the frame of the MCCI-2 project, CORQUENCH computer code was got into use. It contains state-of-the-art models for melt pool coolability, developed on the basis of the CCI and SSWICS experiments. One task of the COMESTA project was to learn the use of the CORQUENCH code and perform some test calculations.

One detail in simulating a severe accident progression is the behavior and failure of the core support plate under the thermo-mechanical loads of a severe accident. A task of the COMESTA project was to develop methods for mechanical analysis of the core support plate and to compare the results with the simple supporting structure model in MELCOR.

OECD MCCI-2 (Melt Coolability and Concrete Interactions)

MCCI-2 is an international project for investigating core melt coolability and its interactions with concrete. There are 13 participating countries in the project, and it is managed by OECD NEA. The project extends from 2006 to 2009, and it is a continuation of the MCCI project (2002–2005). The experiments are conducted at Argonne National Laboratory in the United States. By the end of 2008, four SSWICS (Small Scale Water Ingression and Crust Strength) tests and two CCI (Core Concrete Interaction) tests have been performed in the frame of MCCI-2.

The SSWICS tests involve forming a pool of molten corium and flooding the surface with water. The objectives of the tests are twofold. The first objective is to measure the heat transfer rate from the melt pool to the boiling water. This data is used in developing heat transfer models for melt pool coolability. The latest, SSWICS-11 test showed that gas flow from the decomposing concrete significantly enhances the cooling rate by water ingression. After the melt pool has solidified and cooled down, strength of the solid corium is tested. This data can be used in assessing whether a crust on the top of the melt pool can carry its own weight and the overlying water pool. A strong crust means that, if the crust gets attached to the cavity sidewalls, a gap may form between the melt pool and the crust. This would inhibit coolability of the melt. The results of the SSWICS experiments indicate that the crust would probably be too weak to stay intact in the plant scale.

In the CCI experiments, a pool of molten corium interacts with concrete basemat and sidewalls. At a later phase, the melt surface is flooded with water in order to measure the cooling rate. CCI-4 test was conducted with limestone – common sand (LCS) concrete, and some metals were included in the melt. The test confirmed the earlier result that the basemat and sidewall ablation rates are similar to each other with LCS concrete. Oxidation of the metals created thermal energy and thus accelerated concrete ablation in the beginning of the test, but the presence of metals did not have other significant effects. CCI-5 test employed siliceous concrete. The long term ablation rates were similar as in CCI-3 with the same concrete type, i.e. sidewall ablation was much faster than basemat ablation. However, the initial transient during the first 150 minutes was very different.

At VTT, a detailed heat transfer analysis of the CCI experiments 1, 2 and 3 was conducted. Traditionally, heat conduction in the concrete has been ignored when analyzing such experiments. In the newly developed method, the heat conduction is taken into account. The new method gives better results during slow concrete ablation, and its time resolution is significantly better. Three new correlations for the bubbling-enhanced heat transfer were developed (see example in Figure 20.1.1). The results were published in the Nuclear Engineering and Design journal [1]. A simple Excel macro was written for testing the new correlations. The results were satisfactory, but the initial transient in the case of siliceous concrete is very difficult to simulate.

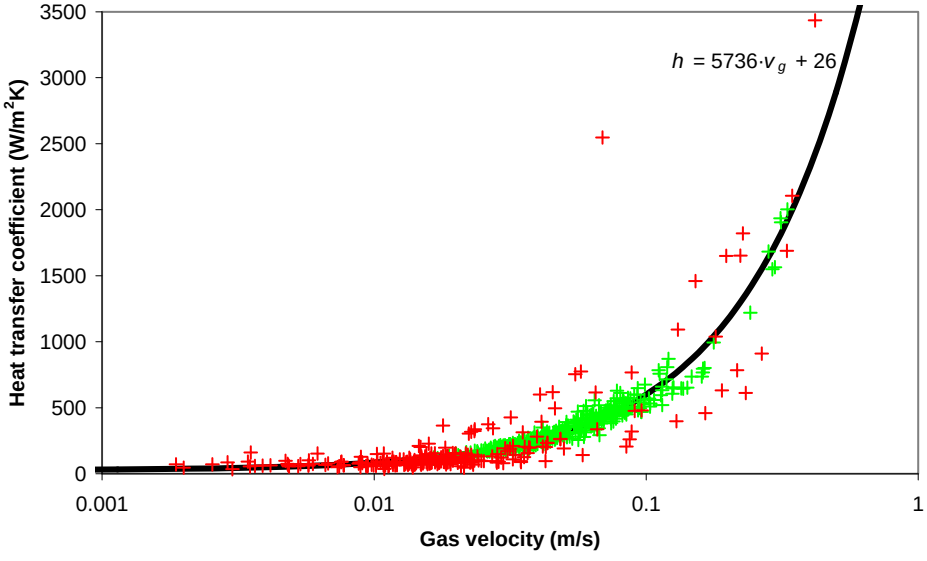

Figure 20.1.1. Sidewall heat transfer coefficients as a function of the superficial gas velocity for siliceous concrete. The red marks are from the CCI-1 experiment and the green marks from CCI-3. A linear function has been fitted to the data. The gas velocity scale is logarithmic.

OECD SERENA2 (Steam Explosion Resolution for Nuclear Applications)

OECD has launched an experimental research program – SERENA2 – to investigate steam explosions with two existing facilities: the KROTOS facility in France and TROI facility in South Korea. The purpose of the SERENA2 project is to bring the uncertainties related to steam explosion phenomena under containment conditions to an acceptable level for applications of risk analysis. Finland joined the SERENA2 project in 2008 particularly to enhance insight to cavity flooding prior to pressure vessel failure as a severe accident management strategy.

The preceding OECD project SERENA1 comprised code benchmarks of selected fuel fragmentation and steam explosion tests and calculation benchmark of in-vessel and ex-vessel steam explosions for a hypothetical plant situation. The code comparison showed a markedly wide span of results for maximum pressure and reaction efficiency. Some of the calculations underestimated the measured pressures and impulses. Another uncertainty had come up with the Korean TROI experiments related to the occurrence of steam explosions with

real corium material. The previous KROTOS test program at JRC Ispra had never yielded a spontaneous – or even triggered – steam explosion with core melt mixture of 80% UO_2 – 20% ZrO_2. The first set of TROI experiments with a mixture 70% UO_2 – 30% ZrO_2, however, was reported to yield an explosion in three tests out of five even without a trigger. The mixture composition was considered the key reason for the different results.

The experimental work in SERENA2 comprises six "twin" tests with KROTOS and TROI facilities to address material effects, coolant temperature and premixture void effects on explosion behavior and reproducibility of steam explosion tests. Voluntary analytical work by participating partners supports the experimental program. To date, one experiment per facility has been performed. The first twin test was targeted to yield the highest maximum pressure by applying highly subcooled water (~30^{o}C) at 4 bar system pressure. No spontaneous explosions took place with either facility. The next three twin tests are planned for the year 2009 and the last two tests for the year 2010.

VTT is participating in the analytical work by performing post test calculations with TEXAS V code, developed by the University of Wisconsin. Figure 20.1.2 illustrates the end state of a steam explosion and the progression of a pressure spike during the 10 ms of interaction.

CORQUENCH Code

CORQUENCH is a computer code for simulating molten corium behavior in the reactor pit. It has state-of-the-art models for melt pool coolability by bulk cooling, melt eruption and water ingression mechanisms [2]. The code also simulates the interaction between the melt and concrete. CORQUENCH is being developed at Argonne National Laboratory. The code was obtained via the OECD MCCI-2 program.

In the frame of the COMESTA project, CORQUENCH was taken into use. The code was tested by simulating the CCI-1 experiment. The results were reasonably good. Basemat ablation and heat transfer to the water were predicted within ten percent of the measured values. The code is very fast, which makes it possible to conduct uncertainty analyses. CORQUENCH was also used by VTT in a benchmark calculation exercise that was organized within the SARNET network of excellence [3].

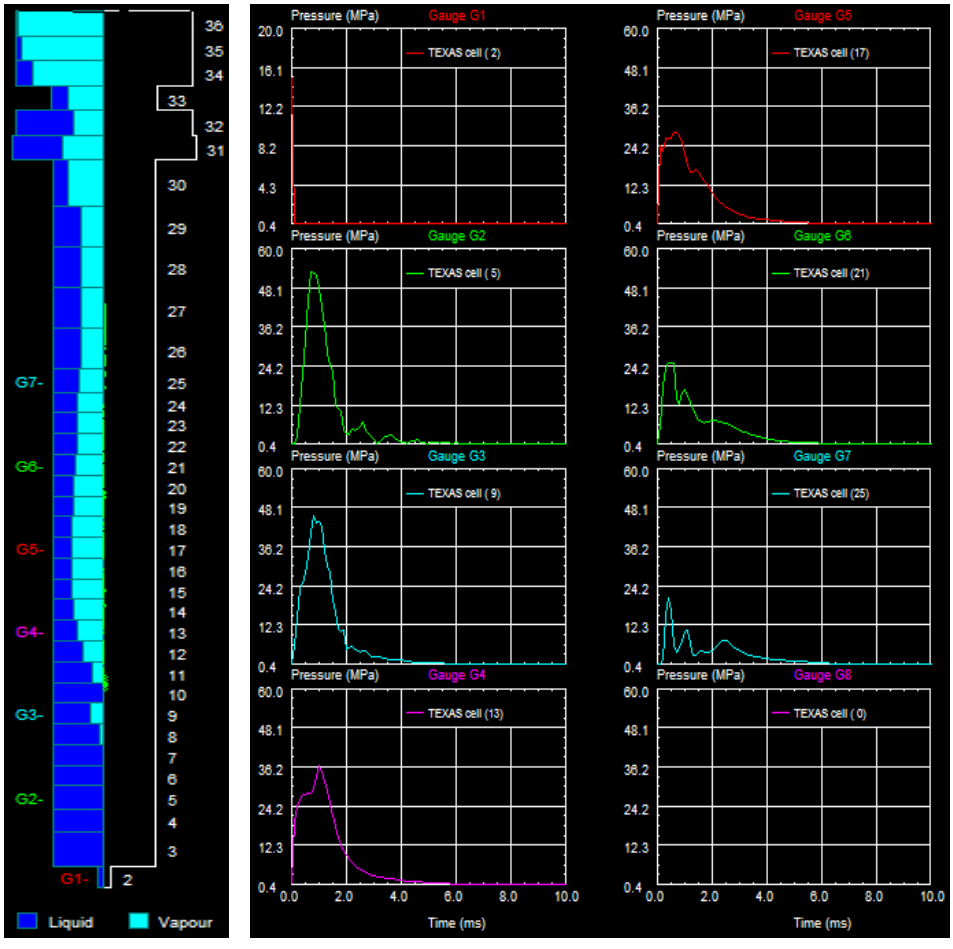

Figure 20.1.2. A typical estimate of steam explosion pressures in a KROTOS experiment calculated with the TEXAS V code. The 1-dimensional calculation nodalization at the end state with pressure gauge locations is illustrated on the left hand side and the evolution of pressure following a triggering from node 2 is shown in the plots on the right hand side. The core melt fragments are distributed between nodes 10 and 27. The melt is poured from node 30.

Core Support Plate Mechanical Analysis

In simulating a severe accident, it is often assumed that the debris from the failed fuel rods forms a particle bed on the top of the core support plate. The debris then heats up the plate. Eventually the structure becomes so hot that it loses its strength, and the debris falls to the bottom of the reactor pressure vessel. In the

COMESTA project, the behavior of the core support plate under the thermo-mechanical loads from the hot fuel debris is analyzed. The Loviisa VVER-440 reactor is used as an example case. Results of detailed finite element modeling are compared with the simple supporting structure models in MELCOR.

Applications

The results from the OECD MCCI project have been employed in Olkiluoto 3 safety analyses for STUK. The CORQUENCH code has been used in Olkiluoto 1&2 severe accident analyses. The MELCOR code, the license of which is acquired through the COMESTA project, is constantly being used for safety analyses of nuclear power plants by VTT, Fortum and TVO.

Conclusions

The HECLA experiments have given new information on the behavior of concrete, especially the special sacrificial concrete used in the EPR reactor pit, under pouring of metallic melt. The OECD MCCI-2 program has increased the state of knowledge of two-dimensional melt–concrete interactions and coolability of melt pool, with real nuclear reactor materials. Similarly, the OECD SERENA program generates new information on steam explosions with prototypic materials. The international research programs are also good opportunities for networking and sharing of knowledge. Through Finland's membership in the CSARP program, the COMESTA project provides VTT, STUK, Fortum and TVO with a license to use the MELCOR severe accident analysis computer code.

The CORQUENCH code for simulating melt pool coolability was taken into use and tested. Advanced methods for analyzing the thermo-mechanical behavior of a core support plate under the loads of a severe accident are being developed and compared with the simple structural models in MELCOR.

References

1. Sevón, T. A Heat Transfer Analysis of the CCI Experiments 1–3. Nuclear Engineering and Design, 2008. Vol. 238, p. 2377–2386.

2. Farmer, M.T., Lomperski, S., Kilsdonk, D., Aeschlimann, R.W. & Basu, S. A Summary of Findings from the Melt Coolability and Concrete Interaction (MCCI) Program. Proceedings of International Congress on Advances in Nuclear Power Plants (ICAPP), Nice, France, May 13–18, 2007. Paper 7544.

3. Spindler, B., Dufour, E., Dimov, D., Foit, J., Sevon, T., Cranga, M., Atkhen, K., Garcia Martin, M., Schmidt, W. & Spengler, C. Simulation of corium concrete interaction in a 2D geometry: Recent benchmarking activities concerning experiment and reactor cases. 3rd European Review Meeting on Severe Accident Research (ERMSAR), Nessebar, Bulgaria, September 23–25, 2008. Paper S2-10. http://www.sar-net.org/upload/2-10_ermsar08-s2-10-final.pdf.

20.2 HECLA Experiments on Melt–Concrete Interactions

Tuomo Sevón, Stefan Holmström, Jouko Virta and Tuomo Kinnunen
VTT

Abstract

The HECLA experiments investigate interactions between metallic melt and concrete. They involve pouring of 50 kg of stainless steel into a cylindrical concrete crucible. Three full-scale experiments have already been performed, one with ordinary siliceous concrete and two with hematite-containing concrete, similar to the sacrificial concrete in the EPR reactor pit. The ablation depths have been between 0 and 30 mm. Clear differences between the two concrete types have not been observed. Dramatic effects, e.g. explosive spalling, have not taken place.

Introduction

In a severe accident, molten corium may penetrate the reactor pressure vessel and flow to the concrete cavity under the reactor. This causes a molten core – concrete interaction (MCCI). The concrete in the floor and sidewalls of the cavity starts to melt. The process is driven by the high initial temperature of the molten corium and the decay heat that is generated inside the melt by the radioactive decay of the fission products. If the interaction cannot be stopped, it may cause a failure of the containment and release of radioactive materials to the environment.

The HECLA experiments are motivated by the severe accident management strategy of the EPR, in which an intentional core–concrete interaction takes place in the reactor pit. There the melt is temporarily retained before it melts itself through the sacrificial concrete layer and flows into the spreading area. [1]

The main objective of the HECLA experiments is to investigate the initial, pouring phase of the MCCI. The experiments are transient, i.e. no decay heat simulation is used. In most previous MCCI experiments, the melt has been generated inside the concrete crucible. In the HECLA experiments, the melt is poured into a cylindrical concrete crucible, which is more prototypic of a reactor accident.

Experimental Facilities

A schematic presentation of the HECLA test facility is shown in Figure 20.2.1. Photographs of the facility are shown in Figure 20.2.2. The facility consists of an induction furnace and a closed steel chamber. The furnace has a capacity of 50 kg steel and power of 175 kW. The furnace lining is a ZIRCOA crucible of composition 72% zirconia and 27% silica. The melt in the furnace if protected by a graphite cover and nitrogen gas. The melt is poured into a pre-heated tundish above the steel chamber. From the tundish, the melt flows through the bottom hole and melt nozzle into the chamber and falls into the concrete crucible. The pouring height is about 80 cm. The chamber volume is approximately 2.2 m^3. A video camera records the events through the window. To prevent hydrogen burns, nitrogen gas is fed into the chamber for oxygen evacuation and dilution of the MCCI reaction gases. The chamber gases are exhausted by a fan and conducted out.

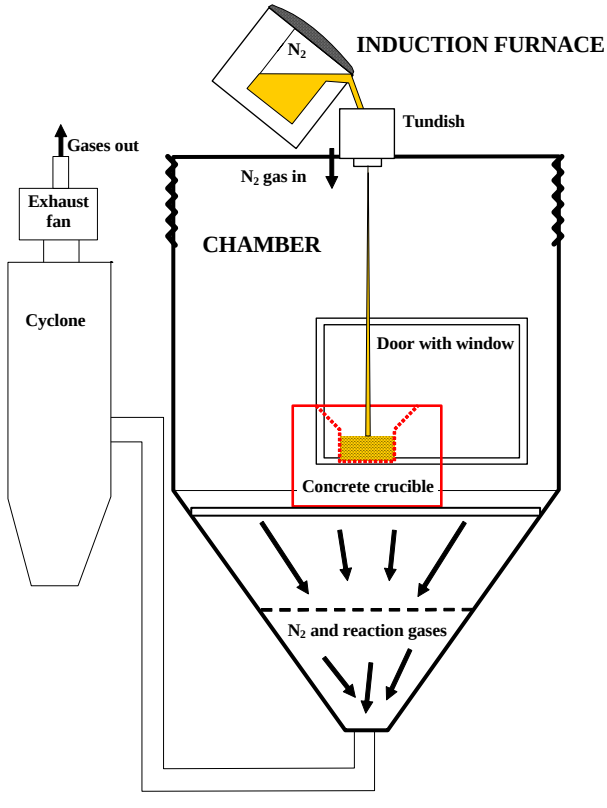

Figure 20.2.1. Schematic presentation of the HECLA facility.

Figure 20.2.2. Photographs of the HECLA facility and its induction furnace.

Dimensions of the cylindrical concrete crucible are shown in Figure 20.2.3. The melt pool depth is about 150 mm. In order to make the crucible stronger, steel reinforcement is installed at the outer periphery of the crucible. The reinforcement is so far from the inner surfaces that it has no effect on the heat transfer and ablation behavior. A ready crucible is shown in Figure 20.2.4. The reddish color comes from the hematite aggregate in the concrete.

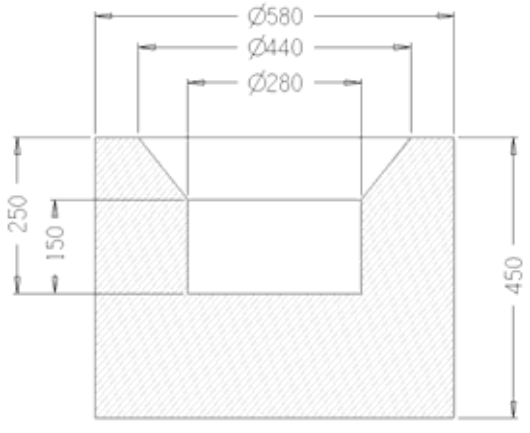

Figure 20.2.3. Dimensions of the cylindrical concrete crucible (mm).

Figure 20.2.4. HECLA-3 concrete crucible before the experiment.

Temperature within the crucible was measured with 46 K-type thermocouples. For the measurement of the melt temperature, two C-type (with Ta sheath and HfO_2 insulation) and two S-type thermocouples were used. The C-type thermocouples were mounted in alumina and steel protection tubes and installed through the bottom of the crucible. The S-type thermocouples were installed in quartz glass tubes and attached to the crucible lifting ring. The melt thermocouples can be seen in Figure 20.2.4.

Main parameters of the four HECLA experiments conducted thus far are shown in Table 20.2.1. The first test was a small-scale test with limited instrumentation to make sure that the facility works well and safely. The FeSi concrete is similar to the sacrificial concrete used in the Olkiluoto 3 reactor pit. It includes about 35% of hematite (Fe_2O_3) and about 40% of SiO_2. The hematite aggregates for HECLA-3 were obtained from Rautaruukki corporation. For HECLA-4 concrete, the ingredients were obtained from Areva. However, it is not exactly the same concrete as in the Olkiluoto 3 plant because a problem with plasticizer caused a far too large amount of air to be entrained in the concrete. This decreased the concrete density to 2250 kg/m^3, while normal value for the FeSi concrete is around 2600 kg/m^3. Stainless steel was used as the molten material in all the four experiments.

Table 20.2.1. Test matrix of the first four HECLA experiments.

	HECLA-1	HECLA-2	HECLA-3	HECLA-4
Date	19.12.2006	19.6.2007	14.3.2008	9.12.2008
Concrete type	Siliceous	Siliceous	FeSi	FeSi
Melt mass (kg)	20.4	50	50	50
Melt temperature (°C)	1560	1700	1650	1770

Results

All the experiments have been operationally successful. The largest deviation was in HECLA-3 when, due to the manual nature of the process, the melt pouring lasted 50 s. In the other tests the pouring time was around 20 s. A picture from the melt pouring in HECLA-4 is shown in Figure 20.2.5.

Figure 20.2.5. Melt pouring in the HECLA-4 experiment.

Measuring the very high temperatures of the metallic melt is challenging. HECLA-3 test (Figure 20.2.6) is thus far the only one where reliable melt temperature data has been obtained throughout the melt solidification period. In this case the temperature data from the four thermocouples is very consistent and can be considered reliable.

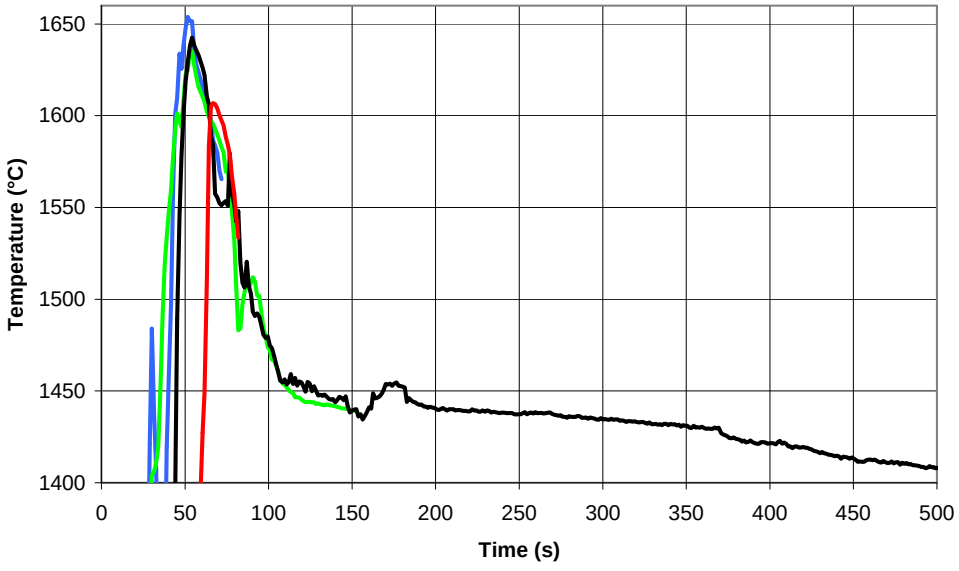

Figure 20.2.6. Melt temperature in the HECLA-3 experiment, measured with four thermocouples.

The progression of the concrete ablation can be tracked from the temperature measurements inside the concrete. As an example, Figure 20.2.7 shows temperature data from selected thermocouples at five different depths inside the sidewall of HECLA-4. The first four thermocouples are destroyed by the melt, but the thermocouple at 20 mm depth remains below the concrete melting temperature. Thus, the final ablation depth is between 15 and 20 mm in this case.

After the experiments, the concrete crucible was cut into half and the metal ingot was removed. A photograph of the split crucible after HECLA-2 test is shown in Figure 20.2.8. About 25–30 mm of concrete has eroded from the basemat and about 15 mm from the sidewall. The initially sharp corners have become round. The final ablation depths of each experiment are shown in Table 20.2.2. Detailed information on the experiments is available in the test reports, references [2–4]. A report of HECLA-4 is still unfinished.

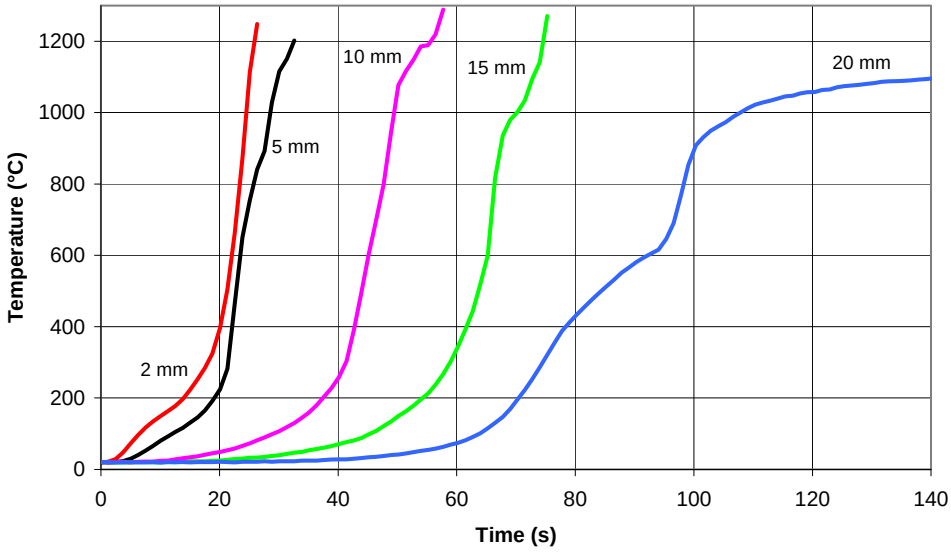

Figure 20.2.7. Temperatures from selected K-type thermocouples at different depths inside the concrete sidewall in HECLA-4 experiment.

Figure 20.2.8. The HECLA-2 concrete crucible after splitting and removing the metal ingot.

Table 20.2.2. Final ablation depths in the first four HECLA experiments.

	Ablation depths (mm)	
	Basemat	**Sidewall**
HECLA-1	0	0
HECLA-2	25–30	15
HECLA-3	25	0
HECLA-4	15	20

Conclusions

In the HECLA experiments, 50 kg of molten stainless steel is poured into a cylindrical concrete crucible. The concrete ablation is measured with thermocouples embedded in the concrete. After the first, preliminary small-scale test, three full-scale experiments have been conducted. One of them employed ordinary siliceous concrete, and the next two used a special hematite-containing FeSi concrete type, similar to the sacrificial concrete in the EPR reactor pit.

The measured ablation depths have been between 0 and 30 mm. Clear differences between siliceous and FeSi concretes have not been observed. In HECLA-3 test with FeSi concrete, the ablation was very anisotropic, with practically no ablation in the sidewall. This result was not reproduced in HECLA-4 with a similar concrete type. Thus, it is probable that the reason for the anisotropy was the slower melt pouring in HECLA-3 (50 s as compared with 20 s in HECLA-4). When planning the experiments, a concern was explosive spalling, causing pieces of concrete to crack off from the surface due to the very rapid temperature change. This has been observed in some fire tests of concrete [5], but not in the first four HECLA experiments.

The experiments have been simulated with MELCOR 1.8.6 and CORQUENCH 3.0 computer codes. Neither of the codes can satisfactorily simulate the pouring phase of the interaction between metallic melt and concrete. This is not surprising, since the codes have been developed mostly on the basis of oxidic melts and sustained heating. In particular, both codes tend to underestimate the ablation rate and, on the other hand, significantly overestimate the duration of the interaction.

There is one more HECLA experiment left in the planned test program. It will be similar to HECLA-4, but the concrete should be identical to the sacrificial concrete used in the Olkiluoto 3 reactor pit. The problem with excessively high

air content in the HECLA-4 concrete seems to have been solved now. During the second half of 2009, it is planned to perform an experiment with FeSi concrete and oxidic melt (UO_2 and ZrO_2) with sustained heating at the VULCANO facility in Cadarache, France. The name of the experiment will be FESICO.

References

1. Fischer, M. The Severe Accident Mitigation Concept and the Design Measures for Core Melt Retention of the European Pressurized Reactor (EPR). Nuclear Engineering and Design, 2004. Vol. 230, pp. 169–180.

2. Sevón, T., Pankakoski, P.H., Virta, J., Ylä-Mattila, R., Koskinen, P., Kauppinen, P., Holmström, S., Kinnunen, T., Pesonen, P. & Lindholm, I. HECLA-1 Experiment on Melt–Concrete Interactions. Espoo: VTT Technical Research Centre of Finland, 2007. Research Report VTT-R-01176-07. 33 p.

3. Sevón, T., Pankakoski, P.H., Holmström, S., Virta, J., Kinnunen, T., Ikonen, K., Pesonen, P., Koskinen, P. & Kekki, T. HECLA-2 Experiment on Melt–Concrete Interactions. Espoo: VTT Technical Research Centre of Finland, 2007. Research Report VTT-R-11203-07. 38 p.

4. Sevón, T., Holmström, S., Virta, J., Kinnunen, T., Koskinen, P. & Kekki, T. HECLA-3 Experiment on Melt–Concrete Interactions. Espoo: VTT Technical Research Centre of Finland, 2008. Research Report VTT-R-04906-08. 32 p.

5. Kalifa, P., Menneteau, F.-D. & Quenard, D. Spalling and Pore Pressure in HPC at High Temperatures. Cement and Concrete Research, 2000. Vol. 30, pp. 1915–1927.

21. Hydrogen risk in containments and particle bed issues (HYRICI)

21.1 HYRICI summary report

Eveliina Takasuo, Stefan Holmström, Juha Kyttälä and Ilona Lindholm
VTT

Abstract

The HYRICI project conducted during 2007 and 2008 was divided in two different research topics in the field of severe accident investigations: hydrogen distribution and the pressure and thermal loads caused by hydrogen combustion in the containment, and the coolability of ex-vessel particle beds formed after the discharge of molten corium into a deep water pool. Computational fluid dynamics codes were utilized in the hydrogen risk analysis. The evaluation of particle bed coolability consisted of both experimental and numerical studies. Experimentally, the effect of lateral bottom inflow into the particle bed was investigated in the STYX 10–13 test series. The project was connected to two international research programmes.

Introduction

Several phenomena related to the hydrogen behaviour and the behaviour of porous beds with volumetric decay heat generation are of complex nature. For instance, modeling of deflagrations and mixing of hydrogen requires advanced turbulence models. The interest in numerical modeling of hydrogen behaviour derives from the need to update and validate computational tools applied to severe accident management at Finnish nuclear power plants. The codes have to

be capable of describing the physical phenomena with adequate accuracy. This is the case also with particle bed coolability. Debris coolability in the containment is the remaining severe accident key issue for Olkiluoto 1 and 2 BWRs. The assessment of the possibilities to reach quenched conditions in a gravel bed formed of core material requires evaluation of the effects of bed geometry and rheology. This often incorporates multi-dimensional, multi-phase modeling.

The French TONUS computational fluid dynamics (CFD) code owned by CEA and IRSN is especially developed for modeling of hydrogen problems in closed volumes and it was taken into use at VTT in 2006 within the preceding CAPHORN project [1]. The work was started by modeling the large-scale deflagration tests performed in the FLAME test series of the Sandia National Laboratories [2].

The WABE code developed at Stuttgart University was taken into use in 2006 for the purpose of modeling the particle bed coolability tests performed in the STYX test series [1]. Previously the tests had been analyzed by using simple correlation models and in-house porous media codes [3]. The analysis of the STYX tests was initiated in the CAPHORN project and it has been continued in the present project.

The particle bed of the STYX test facility at VTT consists of irregularly shaped alumina particles arranged in a cylindrical configuration which has a typical height of 60 cm and a diameter of 30 cm [4]. The bed is heated by resistance heaters arranged in layers within the test bed to simulate the decay heat generation of the core material. The original tests conducted between 2002 and 2005 within the framework of the MOSES and SANCY projects examined a configuration where only top flooding was present [1]. However, in realistic accident scenarios, it is likely that the particle bed, which is formed from melt pour into a flooded lower drywell, is not evenly distributed. Instead, lateral coolant flows may be allowed from the sides of the heap which is expected to increase the coolability. The experiments including lateral flooding provide valuable data for code validation and they can also be seen as a first step from the original STYX test rig towards more realistic reactor scenarios.

Main objectives

The objective of the first subproject dealing with hydrogen issues was to model hydrogen distribution, combustion and the hydrogen mitigation by recombiners

in order to assess the capability of the available computational tools to predict hydrogen behaviour in the case of Olkiluoto 3 and Loviisa nuclear power plants. The follow-up of the OECD-NEA research project THAI was included in this subproject and a part of the analytical work was to be conducted by participating to a benchmark calculation conducted within the framework of the international programme. Co-operation with CEA which was initiated in 2006 was to be continued in the development of the French TONUS CFD code.

The objective of the second subproject addressing particle bed issues was to continue the modeling of the original STYX test series and to conduct a new test series in order to investigate the effect of lateral coolant inflow near the bottom of the test best. This was expected to increase the dry-out heat fluxes and thus increase the coolability of the debris. The modeling work aimed at validating the WABE 2D code for applications at Finnish nuclear power plants, particularly the BWRs at Olkiluoto. Another aim of the subproject was to perform the analytical and experimental work in co-operation with the EU project SARNET participants and the IKE institute at Stuttgart University.

Modeling of hydrogen combustion using the TONUS code

In severe accident management it is important to be able to predict the thermal and pressure loads resulting from hydrogen combustion since they may threaten the containment integrity. In containment scenarios the combustion is likely to start as a laminar flame near the ignition source and possibly develop to a turbulent deflagration due to flame acceleration and finally to a fully developed detonation by deflagration-to-detonation-transition (DDT) if certain criteria are met. Turbulent deflagration and detonation, in which the flame front travels coupled with a shock wave, are the most severe forms of combustion. The work utilizing TONUS was initiated by calculating the deflagration tests which are described in [2]. In the present project, the FLAME F-19 hydrogen combustion test performed at the Sandia National Laboratories was modeled using the gas detonation model implemented in the TONUS CFD code [5]. The detonation model solves the reactive Euler equations and the reaction rate is obtained by the Arrhenius global rate equation. Compared to the previous effort of simulating hydrogen deflagrations, the modeling of detonations is relatively straightforward since there is no need to take viscous and buoyancy effects into account due to the high velocity of the combustion front.

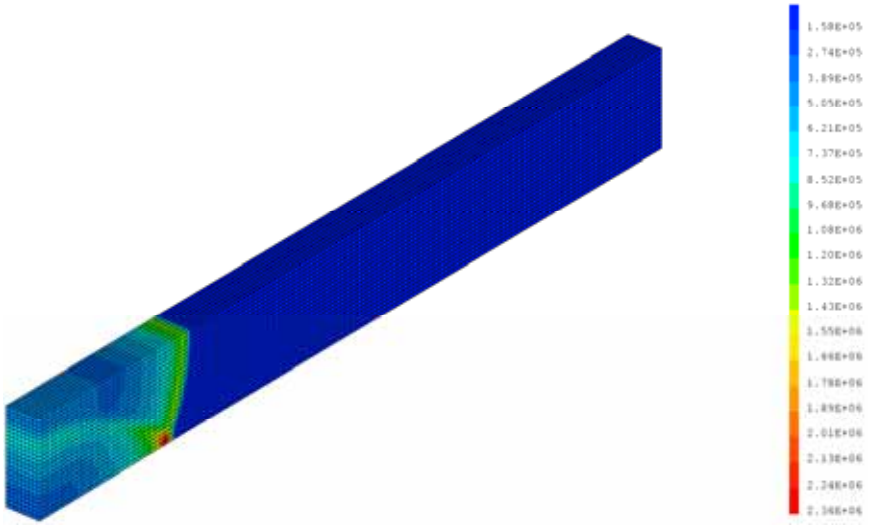

Figure 21.1.1. The position of the combustion front can be seen as a discontinuity in the pressure field during the simulation. The basic Cartesian 3-D grid is shown in the figure.

The study was conducted in phases as follows. First, a parametric study of the chemistry model was performed in order to find out if the basic computational results would approach the experimental results by model adjustments. Secondly, the Chapman-Jouguet (C-J) post-shock equilibrium conditions and the detonation structure for the gas mixture were examined by chemical kinetics calculations using the Cantera software. The results given by the CFD model and the chemical kinetics calculations were compared to each other. The C-J velocity obtained by the CFD model was slightly higher than the one obtained by Cantera which may be due to differences in the calculation of chemical reactions. It was noticed that it is not possible to affect the results by adjusting the model parameters because this will lead to decoupling of the pressure wave and the flame front. See reference [5] for more details.

Modeling of the THAI hydrogen distribution tests

The objective of the first two tests, HM-1 and HM-2, in the OECD THAI project (Thermal-Hydraulics, Hydrogen, Aerosols, Iodine) was to study hydrogen mixing and distribution under steam condensing conditions and compare the results to those obtained by helium which is often used as simulator material in experimental facilities where combustion has to be ruled out. The test HM-2 was

calculated using the commercial FLUENT CFD package prior to the release of the full test data. The work was related to an analytical exercise of the THAI project participants [6].

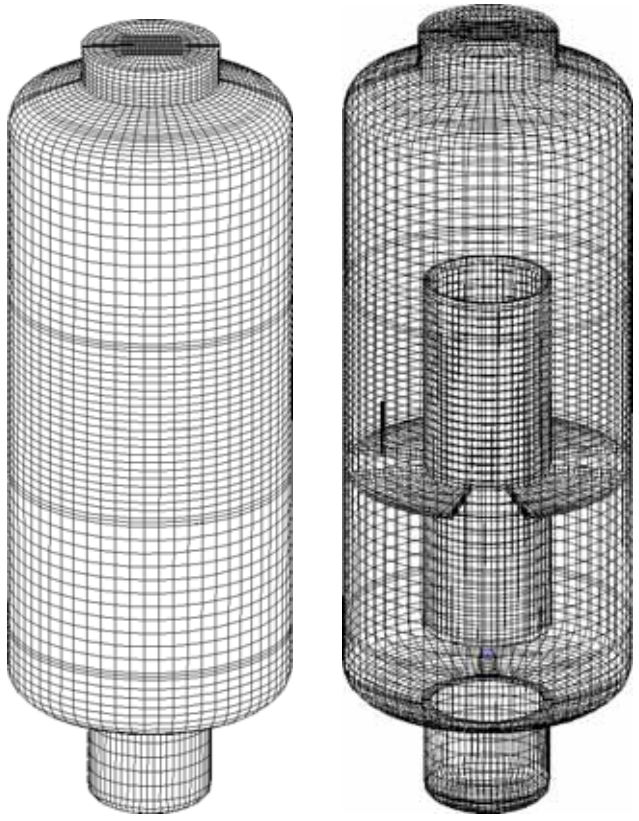

Figure 21.1.2. 3D surface grid (left) and the modeled internal structures of the THAI test vessel. The model contains 144 429 computational cells.

The first phase of the test is hydrogen injection into the middle section of the closed test vessel during which a hydrogen-rich cloud is formed in the upper part of the vessel and atmospheric stratification is achieved. Then, in the second phase, steam is injected through a cylinder installed on the axis of the facility. The steam flow gradually erodes the hydrogen cloud and homogenizes the mixture by convective flow from the top of the inner cylinder to the bottom of the vessel through the outer annulus. Wall condensation plays an important role in the simulation case due to the high steam concentration accumulated in the second phase.

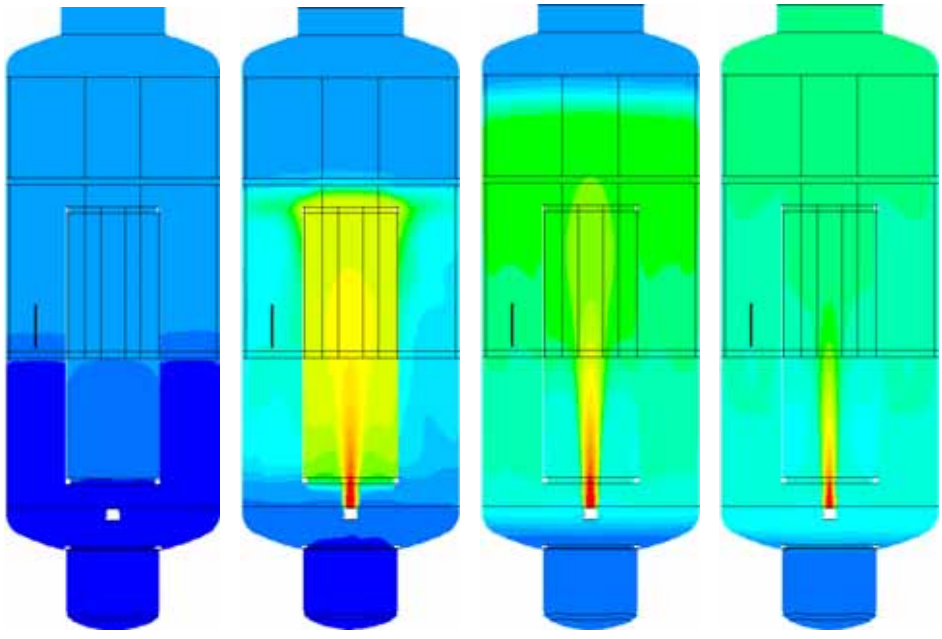

Figure 21.1.3. The contours of steam concentration at 4300 s, 4850 s, 5600 s and 6820 s. Steam is injected at the axis near the bottom and hydrogen inlet is seen on the left of the inner cylinder.

The standard k-ε model with wall functions and full buoyancy effects was utilized in the modeling of turbulence. Submodels previously implemented into the code at VTT were used to calculate wall and bulk condensation and one-dimensional heat transfer through solid structures. The results show that the atmospheric conditions are well approximated by the model in the hydrogen injection phase. In the second phase, the decrease of the hydrogen concentration and increase of temperature are also well approximated but the velocity of the hydrogen could dissolution is somewhat underestimated. Possibly, this could be improved by increasing the grid density in the dome part of the vessel. The evolutions of steam and hydrogen distributions from the onset of steam injection to the complete atmospheric homogenization are presented in Figure 21.1.3 and Figure 21.1.4. Comparison of calculations between the benchmark participants revealed that code and user dependent variation exists in the results. In the model of VTT, a numerical problem was found in the 1-D model that describes heat conduction through solid structures which results in too small increases in wall temperature. The model is currently being revised and an improved model will be used in future calculations.

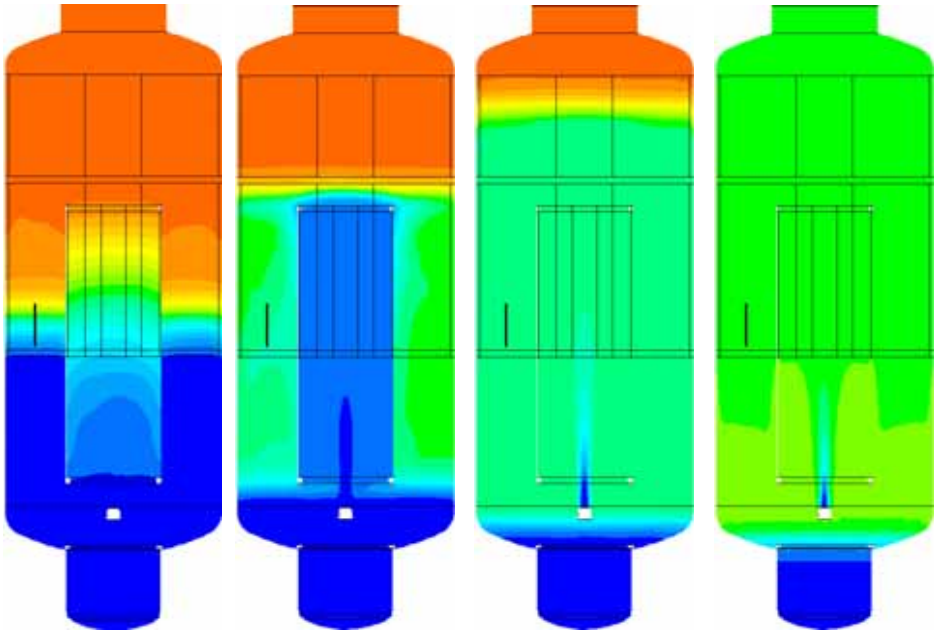

Figure 21.1.4. The contours of hydrogen concentration at 4300 s, 4850 s, 5600 s and 6820 s. The break-up of the hydrogen-rich cloud is clearly seen.

STYX 10–13 particle bed coolability experiments

In the STYX test series 10–13 the effect of downcomers which provide water inflow into the test bed from three directions near the bottom of the bed was investigated [4]. The previous test series 1–9 investigated top flooding at different pressures and the effect of a stratification layer [1]. The test facility consists of 600 mm deep cylindrical bed of alumina oxide particles installed into a cylindrical vessel. The average porosity of the bed is 0.37 and the mass-averaged particle size is 3.46 mm. Hydrodynamic measurements showed that the particle mixture obeys the behaviour of a bed with much smaller average particle size: 0.804 mm [3]. The inner cylinder is contained in a pressure vessel allowing testing up to 7 bar. The bed depth and pressure range in the facility account for the anticipated conditions in Olkiluoto 1 and 2 containment during a severe accident. A total of 13 tests have been conducted. Two different sizes of downcomers were used, 5 mm and 8 mm. The inner cylinder with the downcomer tubes and the measured dry-out power for homogenous beds with and without downcomers are presented in Figure 21.1.5.

The measured power needed for local dry-out was 20–25% higher for the homogenous bed with the 8 mm downcomers than for the corresponding bed without downcomers. This indicates a relatively small increase in the coolability margin for reactor senarios. In the earlier tests without downcomers it had been observed that the 600 mm homogenous beds in general were coolable when compared to realistic values of decay heat power at pressure levels higher than 2 bar. However, the margins between coolable and non-coolable conditions were smaller than expected based on other experimental studies [3]. It was also noticed that bottom flooding with downcomers tends to shift the vertical position of the local dry-out higher in the bed.

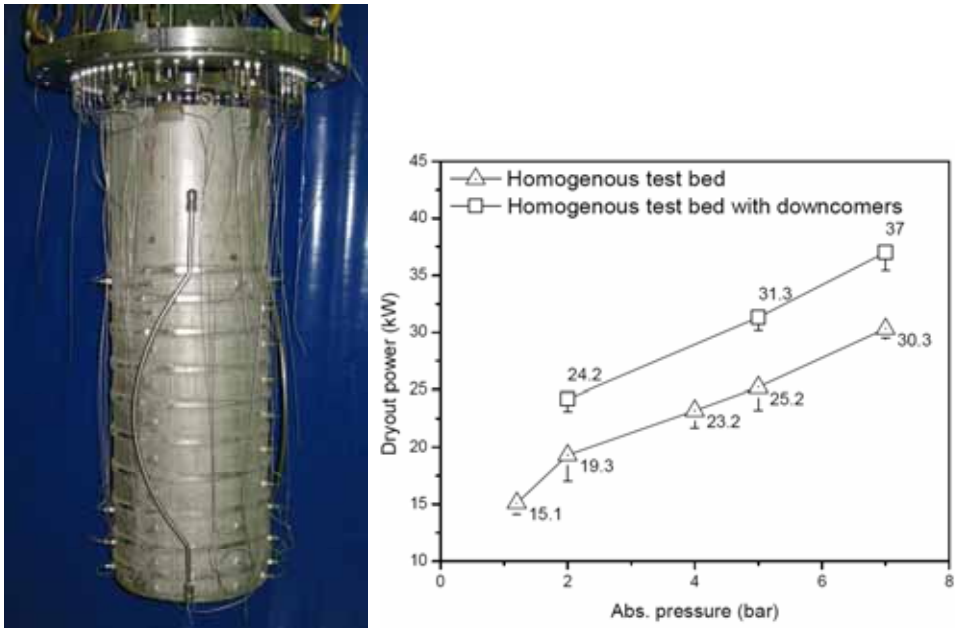

Figure 21.1.5. The inner cylinder of the test rig with downcomers (left) and the measured dry-out heat fluxes as a function of pressure for test beds with and without downcomers.

For the stratified beds, no significant improvement in the coolability was measured with the present configuration. It can be speculated that this may be due to a counter-current flow limitation in the downcomer pipes which could result from the layer of fine particles preventing steam from escaping the top surface. In this case, steam flow would favor the downcomers for escaping the bed instead of the top layer which provides high flow resistance. The results

indicate that the benefit gained from higher pressure is partially lost in the presence of the stratification layer which is consistent with earlier results [7]. The repeatability of the results was verified by running the tests with blocked downcomers in the series STYX-11. The repeatability tests showed that the bed characteristics had remained unchanged even though the facility had been moth-balled for two years before the current application. A separate special report of the tests and their modeling is given in this publication.

Computational methods in assessing the coolability of particle beds

The WABE code contains a porous media model which can be used for simulating the coolability of heat-generating particle configurations. Thus far the focus has been on quasi-1-D calculations but explicit consideration of gas-liquid friction provides the possibility to model two-dimensional flows in a detailed fashion [8]. The STYX test series 1–3 have been calculated with extensive parameter variations with respect to modeling of heating arrangement, nodalization, porosity, particle size and the friction model coefficients [9]. Prior to this, the dry-out heat fluxes were evaluated using simple correlations and models such as Lipinski 1-D [3]. The dryout heat fluxes were reasonably well predicted by the correlations and the 1-D models developed during the test programme in 2002–2005. The location of the incipient dryout, however, was never predicted correctly with the developed models. The POBEDA model developed by J. Hyvärinen parametrically incorporated the interfacial friction of steam and water flow, but the formulation of the interaction terms was not completed.

It has been concluded that accurate results can be obtained by the Reed or Theofanous models for turbulent friction in the WABE simulations and the correlation model calculations if representative bed properties such as effective particle size are appropriately selected. The modeling of the heating method in which the resistance heaters provide at least somewhat local heating, rather than heating the particles uniformly, did not cause remarkable discrepancies in the results. However, the real three-dimensional arrangement includes local effects which can not be predicted by WABE (or the 1-D and 0-D correlations) and the transient development towards dry-out has not been accurately simulated in the present study. The code validation for multi-dimensional flows will continue within the framework of the HYBCIS project in 2009.

Conclusions

The performed analytical exercises using the TONUS code on hydrogen combustion and the FLUENT code on hydrogen mixing have supported the assessment of reliability of the computational results in plant applications. The calculation of the FLAME F-19 hydrogen combustion test by the TONUS code and the comparison of the TONUS results to chemical kinetics calculations showed that the code is capable of modeling combustion in the detonation regime with good accuracy which was an expected result. User observations of the TONUS code were communicated to the code developers at CEA who provided user assistance with the code.

The THAI computational exercise in which the break-up of a hydrogen cloud from the upper domain of the THAI facility by injection of steam was investigated was successfully simulated using FLUENT and the user-defined functions incorporated into the model. On their part, the results and comparison to other codes used in the benchmark indicate that the present turbulence and condensation models are at a good level considering realistic containment applications. The follow-up of the OECD-NEA THAI research project was included in the HYRICI project.

The STYX test series 10–13 showed that the dry-out heat flux is increased approximately 20–25% for the homogenous beds in which three downcomer tubes to feed water into the bottom of the test bed in lateral direction were used. For the stratified beds with a fine particle layer on top of the bed, no significant increase in the dry-out heat flux and the coolability of the bed was observed. The first series of calculations of the original STYX tests with no downcomers was finalized using WABE and reasonably accurate results were obtained. The STYX experiments contribute to the experimental data base applied for code validation. WABE code is a state-of-the-art model that is needed for plant scale evaluations of debris bed stability.

In addition, the WABE work as well as the FLUENT and TONUS simulation efforts served as training for young generation research scientists.

References

1. Lindholm, I., Holmström, S., Miettinen, J., Kekki, T., Pankakoski, P., Sevón, T., Takasuo, E., Virta, J. & Zillicaus, R. SANCY/CAPHORN summary report. SAFIR The Finnish Research Programme on Nuclear Power Plant Safety 2003–2006 Final Report. VTT Research Notes 2363. Espoo: VTT Technical Research Centre of Finland, 2006. Pp. 225–236. ISBN 951-38-6886-9. http://www.vtt.fi/inf/pdf/tiedotteet/2006/T2363.pdf.

2. Takasuo, E. & Kudriakov, S. Modeling of the FLAME hydrogen combustion tests F-8 and F-22 using the TONUS CFD code. CEA Rapport DM2S/SFME/LTMF/RT/06-046/A. CEA Centre de Saclay, 2006.

3. Lindholm, I., Holmström, S., Miettinen, J., Lestinen, V., Hyvärinen, J., Pankakoski, P. & Sjövall, H. Dryout Heat Flux Experiments with Deep Heterogeneous Particle Bed. Nuclear Engineering and Design 236, 2006, pp. 2060–2074.

4. Holmström, S., Kinnunen, T., Pankakoski, P.H. & Hosio, E. STYX dry-out heat flux testing with lateral coolant inflow. Research Report VTT-R-06910-08. Espoo: VTT Technical Research Centre of Finland, 2008. 23 p.

5. Takasuo, E. Modeling of Hydrogen-Air Detonations in the TONUS CFD Code and its Application to the FLAME F-19 Test. Proceedings of the 16th International Conference on Nuclear Engineering (ICONE-16). May 11–15, 2008, Orlando, Florida, USA.

6. Schwarz, S. Comparison and Evaluation of Experimental Data and Blind Calculations of OECD-NEA THAI Test HM-2. Technische Notiz TN1-08. GRS, Germany, December 2008.

7. Holmström, S. & Pankakoski, P.H. STYX dry-out heat flux testing with different test bed thicknesses. Part II: homogenous and stratified tests with 600 mm and 400 mm test beds. Research Report BTUO74-051381. Espoo: VTT Technical Research Centre of Finland, December 2005.

8. Buck, M., Pohlner, G. & Rahman, S. Documentation of the MEWA code. Stuttgart: Universität Stuttgart, June 2007.

9. Miettinen, J., Lindholm, I., Bürger, M., Buck, M. & Pohlner, G. 2008. WABE calculations for STYX experiments. VTT Research Report VTT-R-01360-07. Espoo: VTT Technical Research Centre of Finland, 2008.

21.2 STYX dry-out heat flux testing with lateral coolant inflow

Eveliina Takasuo, Stefan Holmström, Tuomo Kinnunen, Pekka H. Pankakoski, Ensio Hosio, Ilona Lindholm and Jaakko Miettinen
VTT

Abstract

The STYX test facility which is designed to investigate the coolability of heat-generating core debris beds has been applied to study the effect of lateral flooding on the dry-out heat fluxes of porous particle beds. The test rig was modified by installation of three downcomer tubes that feed cooling water to inlets near the bottom of the particle bed by natural circulation. It was observed that the dry-out heat flux in a homogenous test bed was increased approximately 20–25%. For a stratified bed with a layer of fine particles on top of the bed no significant increase was observed. The WABE/MEWA porous media code has been utilized in modeling of the coolability tests.

Introduction

At the Finnish BWRs in Olkiluoto the flooding of the lower drywell of the containment is a key part of the severe accident management strategy. If the reactor pressure vessel fails in the course of an accident molten core material is discharged from the pressure vessel into a deep water pool in the lower drywell. The corium is fragmented and it is expected that it forms a porous particle bed from which decay heat must be removed in order to prevent re-melting of the material. The objective of the STYX tests was to measure the heat fluxes which will result in local dry-out in the interior of the porous bed and thus verify the coolability of the debris for severe accident scenarios in a conservative arrangement.

The formation of particle beds has been recently studied e.g. by Karbojian et al. [1] who indicate that highly irregular configurations with porosities as high as 60% may be formed depending on the water subcooling. The STYX test series performed at VTT during the preceding MOSES and SANCY projects investigated cylindrical particle beds consisting of irregular alumina particles with the porosity of approximately 37% [2]. The effects of particle size stratification, particle bed height and pressure on the heat flux required for a local dry-out were studied. The particle size distribution was chosen based on various

experiments investigating the debris bed formation. The depth and the pressure ranges characterize the conditions expected at the Olkiluoto containments during a core melt accident. Decay heat is simulated using resistance heater bands.

However, in realistic accident scenarios the debris bed resulting from fragmentation, is not expected to be evenly distributed to the pedestal floor of the containment. Instead, a heap-like geometry which allows coolant inflow from the sides of the bed is a more likely configuration. In addition, vigorous boiling is occurring inside the porous medium which may prevent the settling of smaller particles on top of the bed. For example, increases of about 45% in the overall coolability have been predicted by calculations of multi-dimensional flows in homogenous configurations [3]. In a top flooding configuration, such as the one that was examined in the original STYX series 1–9, the counter-current flow limitation (CCFL) restricts the water flow into the bed interior at a point when high enough vapor flux is reached. The allowed vapor flux is significantly higher for bottom or side flooding cases where co-current flows of steam and water are possible [4]. In the present test series STYX 10–13 the effect of lateral coolant inflow on the dry-out power was studied by means of three downcomer tubes which provide cooling water to the bottom of the test rig by natural circulation [5].

Currently, the main tool for analyzing the coolability of particle beds is the MEWA 2D code (also known as WABE prior to the code version of August 2008) which is developed at the IKE institute of Stuttgart University. The code contains models for calculating heat transfer and friction between the solid, liquid and gas phases and capillary forces. Models which explicitely consider interfacial friction of gas and liquid are included [6]. Thus far, the code has been applied for modeling of the STYX test series 1–3 with parameter variations with respect to modeling of the heating method, nodalization scheme, porosity and particle size [7]. These calculation cases are effectively one-dimensional because the bed is homogenous in the lateral direction. The results for dry-out heat flux obtained by MEWA/WABE have been consistent with those given by more simple models such as Lipinski-0D. Modeling of the two-dimensional cases in the STYX 10–13 series is an on-going activity.

The experimental set-up

The main components of the test rig are feed water tank, feed water pump, feed water pre-heater, pressure vessel, test bed with heating element, steam line,

condenser, process controls and measurement equipment as presented in Figure 21.2.1. The test bed is otherwise similar as the homogenous and stratified beds used in the previous tests [8] but downcomers have been connected to provide natural circulation from the overlaying water reserve to the bed bottom. The principal measured test parameters are temperature, pressure, and the input power of the heating element. To record the bed temperatures thermocouples are distributed within the 600 mm test bed in 9 levels. Additional thermocouples are placed on the inner and outer pressure vessel wall surfaces and in the water pool on top of the bed. The rig makes use of two pressure gauges, one for pressure control and one for pressure monitoring. A water level gauge controls the water level on top of the test bed.

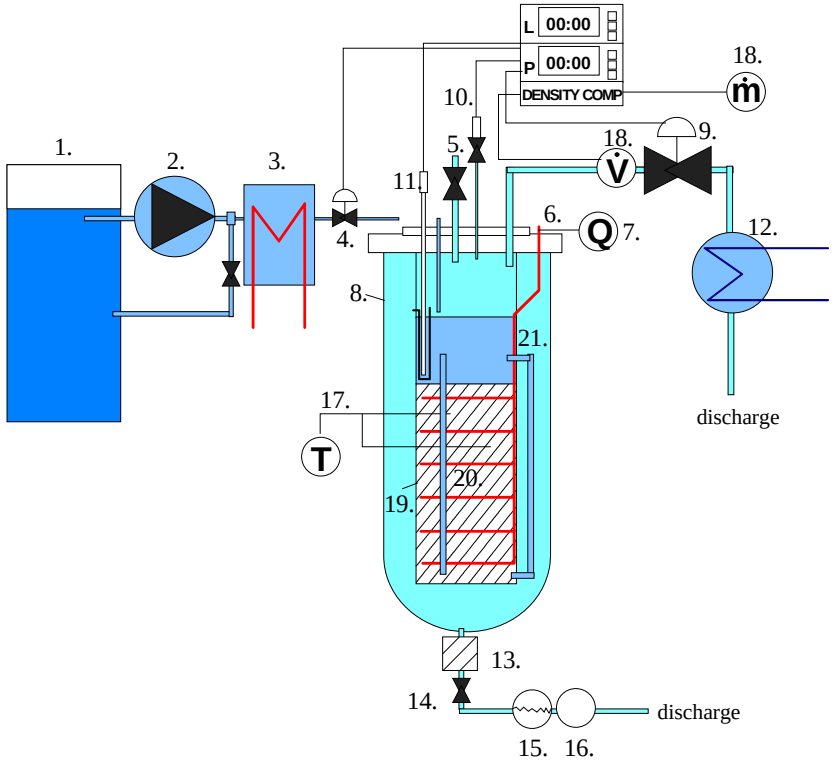

Figure 21.2.1. The modified dryout heat flux test rig. 1) feedwater tank, 2) feedwater pump, 3) pre-heater 4) feed water valve, 5) pressure gauge (measurement), 6) heating element, 7) power input and measurement, 8) pressure vessel 9) pressure valve (control), 10) pressure gauge (control), 11) water level indicator (control), 12) condenser, 13) impurities sifter, 14) valve (condensate line), 15) condensate level indicator, 16) condensate separator, 17) thermocouples (measurement), 18) flow meter (mass or energy flow), 19) inner vessel, 20) test bed, 21) downcomers.

The total power of the heating elements is recorded online from a calibrated 3-phase power meter. The inputs to this device are the line voltages and currents. The currents are measured with measurement transformers that were incorporated in the calibration setup and the voltages are directly measured from each phase. The dry-out power values are read from the 3-phase power meter at the time of power increment. Mean power values for each power step are calculated from the online data. The nominal holding time between power increments in all the tests was 25 minutes. In this study, dry-out is considered to be reached in a location where the temperature sensor reading is 5 °C higher than the saturation temperature at actual pressure at specified time. This temperature margin was chosen to eliminate false dry-out indications due to momentary fluctuations in the pressure and sensor offsets.

In the first tests, STYX-10, three downcomer tubes of 5 mm inner diameter installed at 120° divisions were used. The STYX-11 tests were performed with plugged downcomers and in the test series STYX-12 and STYX-13 the inner diameter of the downcomers was increased to 8 mm. The STYX-12 test series was conducted with a stratified bed and the STYX-13 with a homogenous test bed. The stratified bed represents a condition where a layer of fine particles has been settled on top of the bed as a result of a steam explosion during the fragmentation. The tests with plugged downcomers verified that the results are reproducible and that there had been no changes in the bed properties during storage and transportation.

The tests STYX-10b and STYX-12b consisted of separate measurements of mass flows through the downcomers. The two tests were conducted to verify that each downcomer was open and thus could maintain the natural circulation. However, there were no means to measure the downcomer flow during the tests. The size range of the particles in the homogenous bed is 0.25 mm – 10 mm with the mass-averaged diameter of 3.46 mm. In the fine stratification layer the particle diameter is 0.25 mm – 0.4 mm. The porosity of the bed is approximately 0.37. Figure 21.2.2 shows the downcomer connections near the top and bottom of the bed. The test matrix is given in Table 21.2.1.

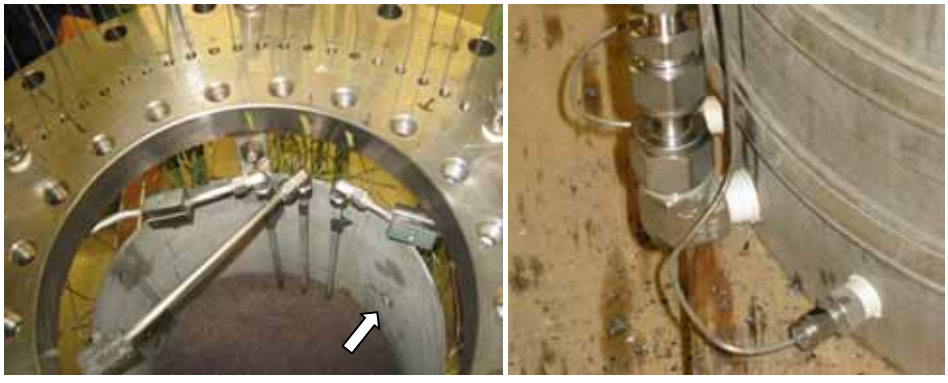

Figure 21.2.2. The surface of the stratified test bed with the upper downcomer connection (left) and the downcomer connection near the bottom.

Table 21.2.1. The test matrix.

Test code	Test type	Pressure [bar]	Downcomer diameter [mm]
STYX-10	Stratified 600 mm test bed (60 mm stratification layer Ø 0.25–0.4 mm)	2, 4, 5, 7	5
STYX-10 b	Downcomer flow-through measurement	-	-
STYX-11	Stratified 600 mm test bed (60 mm stratification layer Ø 0.25–0.4 mm)	2, 5, 7	-
STYX-12	Stratified 600 mm test bed (60 mm stratification layer Ø 0.25–0.4 mm)	2, 5, 7	8
STYX-12 b	Downcomer flow-through measurement	-	-
STYX-13	Homogenous 600 mm test bed with Ø 8 mm 3 downcomers	2, 5, 7	8

Results of the stratified bed tests

The measured dry-out powers for the stratified bed with 5 mm and 8 mm downcomers are presented in Figure 21.2.3 and Figure 21.2.4, respectively. In the STYX-10 tests the dry-out was observed in the lower middle section of the test bed, between the temperature sensor levels of 200 mm and 400 mm. In the

STYX-12 tests, with the larger capacity downcomers, the dry-out was first found near the lowermost levels and below the 267 mm level.

The difference between the previous results [8] and results with the 5 mm downcomers is approximately 13% in the 2 bar case and 6% at in the 4 bar case. In the 7 bar case the dry-out power was unexpectedly small and the temperature excursion was observed already at 25 kW. For the 8 mm downcomers, the dry-out power increased some 10% compared to the 5 mm downcomers. Otherwise, the results indicate that the downcomers have only little influence on the dry-out heat fluxes in the stratified beds. It can be speculated that the reason for this behaviour is a counter-current flow limitation in the downcomer tubes which might result if the friction in the fine particle layer is high enough to make the top layer impermeable to the steam escaping the bed. In this case the steam would favour flowing up through the downcomer tubes instead of escaping through the top surface. In addition, the effective hydrodynamic particle size in the bed is only 0.8 mm according to flow resistance measurements [2] while it has been shown that the role of gas-liquid friction which increases the coolability in bottom and side flooding conditions diminishes for smaller particles with this order of diameter [4].

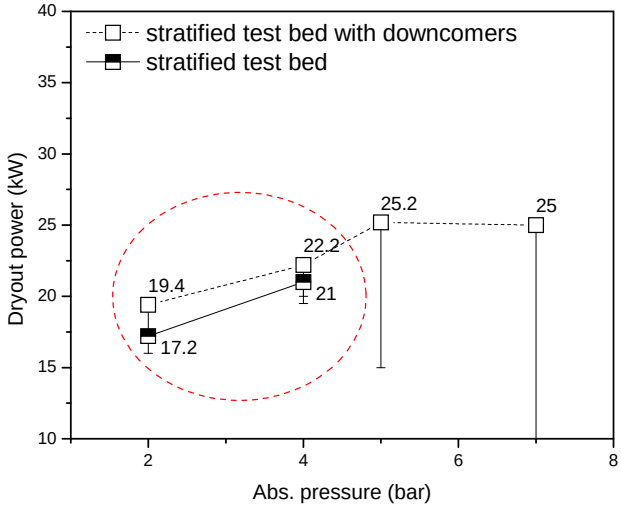

Figure 21.2.3. The dry-out power for the stratified test bed with 5 mm downcomers compared to the previous results with no downcomers.

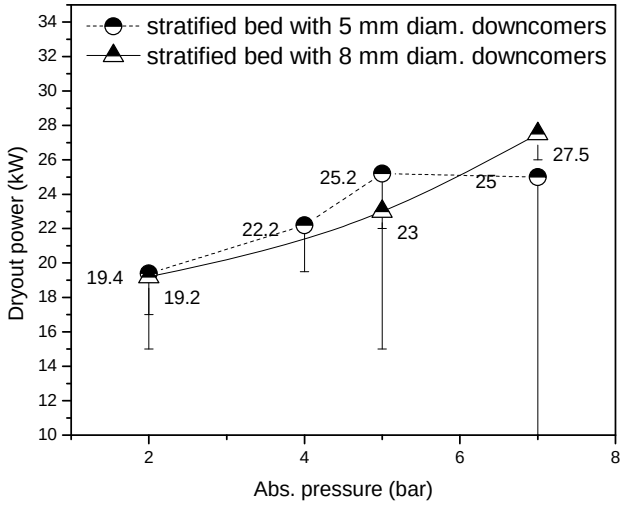

Figure 21.2.4. The dry-out power for the 8 mm downcomers compared to the dry-out power for the 5 mm downcomers. The test bed is stratified.

It was found out that the results with the plugged downcomers in the test sequence STYX-11 agree with the earlier results signifying that the results are reproducible. The results also indicate that the coolability benefit obtained from a higher pressure level could be partially lost in the presence of the stratification layer. Earlier experiments show a similar trend with the 400 mm test bed [8].

Results of the homogenous bed tests

A comparison between the results of the STYX-13 test sequence and the earlier results [8] of homogenous beds are shown in Figure 21.2.5. In this sequence the effect of the downcomers is clearly seen. The difference to the previous results is 22–25% which indicates a rather modest increase in the coolability. The dry-out was first observed near the top of the bed at 533 mm level. Apparently, in this case the availability of water in the bottom of the bed results in dry-out in the upper levels where a larger amount of steam has been accumulated.

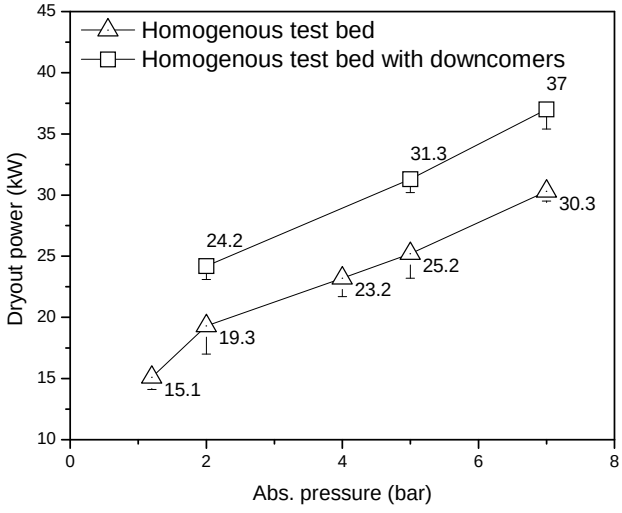

Figure 21.2.5. The dry-out power for the homogenous test bed with 8 mm downcomers compared to the earlier results with no downcomers.

Porous media model of the MEWA/WABE code

The MEWA/WABE code includes a 2D porous media model which solves the momentum and mass conservation equations for the fluid phases and the energy equation for the liquid, gas and solid phases. Several studies have shown that an explicit model of gas-liquid drag is necessary to predict the pressure gradient inside the bed correctly and to capture the effect of multi-dimensional flow on coolability [4, 9]. In the present study the modified Tung and Dhir model is used. The approach is based on separating the flow regime ranges of bubbly, slug and annular flow and deriving expressions for relative passability and permeability for each regime [10]. Boiling heat transfer is modeled by using the boiling curve model which accounts for the following boiling modes: pool boiling which is calculated by the Rohsenow correlation, film boiling which is calculated by the Lienhard correlation and the transition regime obtained by linear interpolation from these two modes.

The results of a MEWA simulation of the STYX-13 test at 2 bar pressure are illustrated in Figure 21.2.6. The field images represent the particle temperature with liquid velocity vectors and saturation (i.e. liquid volume fraction) at about 4000 s after dry-out has occurred. An area with zero saturation has been developed above 44 cm elevation and a clear increase in solid temperature is

seen in the corresponding location. The location of the incipient dry-out seen in the experiment (53 cm) is slightly higher in the bed. Nonetheless, both the experiments and the simulation indicate dry-out in the upper section of the configuration. In the symmetrical geometry seen in the figures the narrow passages in the lowermost cells represent the downcomer flow paths connected to a water reserve on the other side of an impermeable wall. The rather coarse grid which contains 19x64 cells is strongly refined towards the downcomer gap.

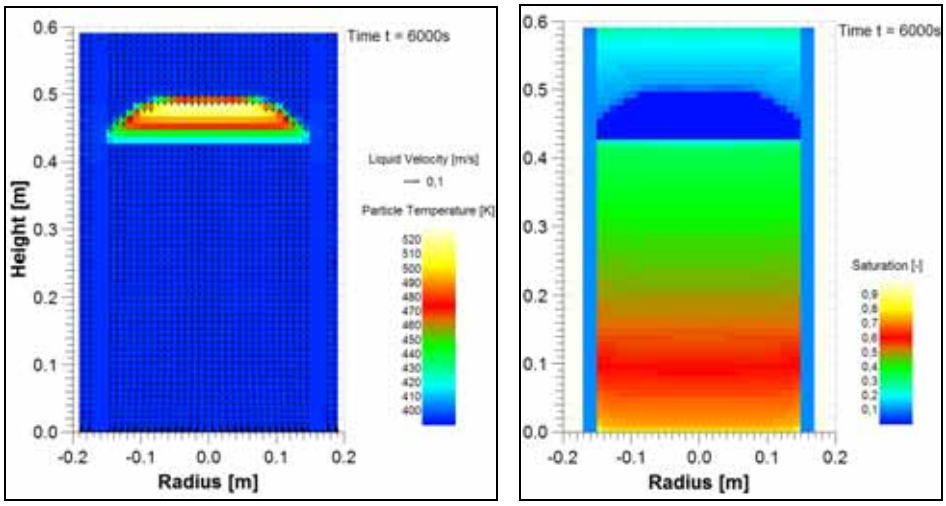

Figure 21.2.6. Particle temperature (left) and saturation fields after dry-out has occurred. The bed porosity is 0.37 and the particle diameter is 0.8 mm.

The maximum coolable steady state power in this calculation is roughly 24.6 kW and the minimum power leading to dry-out is about 25.4 kW. This result is within 5% of the dry-out power measured in the experiment. In these first simulation runs, the deviation from the test results in the pressure range of 2 to 7 bar is between 5–19%. The effectiveness of water spreading near the downcomer region may partly explain the differencies in the results and remains an issue of further studies.

Conclusions

The effect of lateral bottom flooding on the dry-out heat fluxes in the STYX particle bed has been investigated. In the case of a stratified bed the downcomers providing lateral flooding have no significant influence on the dry-out power.

For a homogenous bed, the downcomers have a clear but relatively small beneficial impact on the needed dry-out power. In this case, the dry-out occurs in the uppermost thermocouple levels near the top of the bed because a water-rich region remains in the lower bed. A dependency was observed between the dry-out location and the rate and magnitude of power increase during the test sequence. The tests provide a valuable contribution to the experimental data base that can be used for code validation.

The MEWA/WABE 2D code has been used to model the STYX test series in the cases of top and lateral flooding. The effective parameters (particle diameter and bed porosity) applied in the simulations were selected based on the measurements of the test bed hydraulic resistance. The first calculations of lateral flow configurations indicate that the code is capable of producing realistic results with this choice of parameters.

References

1. Karbojian, A., Ma, W.M., Kudinov, P., Davydov, M. & Dinh, T.N. A Scoping Study of Debris Formation in DEFOR Experimental Facility. 15th International Conference on Nuclear Engineering (ICONE-15). Nagoya, Japan, April 22–26, 2007.

2. Lindholm, I., Holmström, S., Miettinen, J., Lestinen, V., Hyvärinen, J., Pankakoski, P. & Sjövall, H. Dryout Heat Flux Experiments with Deep Heterogeneous Particle Bed. Nuclear Engineering and Design 236, 2006, pp. 2060–2074.

3. Ma, W.M., Dinh, T.N., Buck, M. & Bürger, M. Analysis of the Effect of Bed Inhomogeneity on Debris Coolability. 15th International Conference on Nuclear Engineering (ICONE-15). Nagoya, Japan, April 22–26, 2007.

4. Schäfer, P. & Lohnert, G. Boiling experiments for the validation of dryout models used in rector safety. Nuclear Engineering and Design 236, 2006, pp. 1511–1519.

5. Holmström, S., Kinnunen, T., Pankakoski, P.H. & Hosio, E. STYX dry-out heat flux testing with lateral coolant inflow. Research Report VTT-R-06910-08. Espoo: VTT Technical Research Centre of Finland, 2008. 23 p.

6. Buck, M., Pohlner, G. & Rahman, S. Documentation of the MEWA code. Stuttgart: Universität Stuttgart, June 2007.

7. Miettinen, J., Lindholm, I., Bürger, M., Buck, M. & Pohlner, G. 2008. WABE calculations for STYX experiments. Research Report VTT-R-01360-07. Espoo: VTT Technical Research Centre of Finland, 2008.

8. Holmström, S. & Pankakoski, P.H. STYX dry-out heat flux testing with different test bed thicknesses. Part II: homogenous and stratified tests with 600 mm and 400 mm test beds. Research Report BTUO74-051381. Espoo: VTT Technical Research Centre of Finland, December 2005.

9. Bürger, M., Buck, M., Schmidt, W. & Widmann, W. Validation and application of the WABE code: Investigations of constitutive laws and 2D effects on debris coolability. Nuclear Engineering and Design 236, 2006, pp. 2164–2188.

10. Schmidt, W. Influence of Multidimensionality and Interfacial Friction on the Coolability of Fragmented Corium. Doctoral Thesis. Stuttgart: Universität Stuttgart, Institut für Kernenergetik und Energiesysteme, May 2004. ISSN 0173-6892.

22. Risk-informed inspections of piping (PURISTA)

22.1 PURISTA summary report

Kaisa Simola, Otso Cronvall, Ilkka Männistö, Matti Sarkimo and Ari Vepsä
VTT

Abstract

The overall objective of the PURISTA project is to support the implementation of risk-informed in-service inspection (RI-ISI) at Finnish nuclear power plants by studying relevant issues related to RI-ISI. Main objectives are the development of structural reliability methods for quantification of piping leak and break probabilities, the development of methods for evaluating inspection capability and the link between inspection qualification, detection probability and RI-ISI, and studying issues related to risk-ranking, selection of inspection sites and acceptance criteria of a RI-ISI programme. The project includes several international activities, the most important being the participation in the European Network for inspection and Qualification (ENIQ), especially in the work of its Task Group on Risk (TGR).

Introduction

Risk-informed in-service inspections (RI-ISI) aim at rational in-service inspection management by taking into account the results of plant-specific risk analyses in defining the inspection programme and focusing the inspections efforts to the most risk-significant locations. Ideally this could lead to improved safety and availability, reduced doses of radiation and reduced inspection costs.

Even if RI-ISI has been widely applied in the US, European utilities and safety authorities think that several issues need further research. Furthermore, the US RI-ISI approaches cannot always be adopted as such since they have been originally developed to the US regulatory environment, and do not comply as such with national regulations and different standards in many European countries.

The overall objective of the PURISTA project is to support the implementation of RI-ISI at Finnish nuclear power plants by studying relevant issues related to it. In Finland, the use of risk-informed methodology in planning new ISI programmes is a regulatory requirement, and both domestic utilities are developing RI-ISI programmes for the existing plants. Also the ISI programme for the new EPR unit will consider risk insights.

Main objectives of the PURISTA project are the following:

- To develop structural reliability methods for quantification of piping leak and break probabilities
- To develop methods for evaluating inspection capability and the link between inspection qualification, detection probability and RI-ISI
- To study issues related to risk-ranking, selection of inspection sites and acceptance criteria of a RI-ISI programme.

In this paper, the phases of a RI-ISI process are summarised and research activities of the PURISTA project are described.

Phases of a RI-ISI process

From a technical perspective, a typical RI-ISI process consists of the following main steps:

- Definition of RI-ISI scope, collection and analysis of the required input data
- Identification and evaluation of piping failure consequences
- Identification and evaluation of piping failure potential
- Risk ranking
- Definition of the new inspection programme.

Typically, before implementing the RI-ISI programme, the results of the RI-ISI analysis are required to be submitted to the national regulatory body for approval.

Figure 22.1.1 illustrates these phases of the RI-ISI process, and is followed by a brief discussion on each of them.

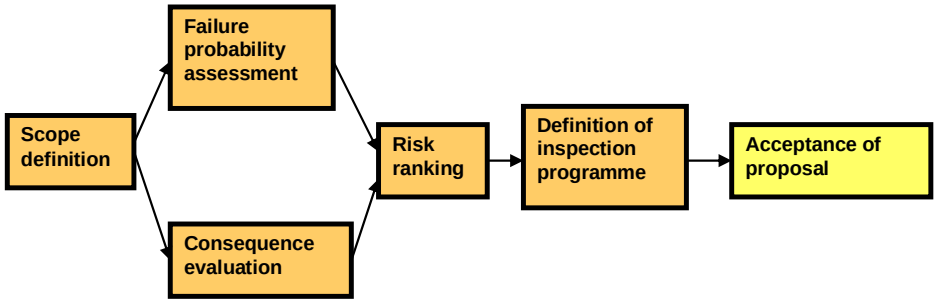

Figure 22.1.1. Phases of a RI-ISI development process

The first step is to decide the scope of the RI-ISI programme, i.e. which piping systems are included in the RI-ISI application. In principle, the scope can vary from a very limited one, such as the reactor coolant system, or ASME Class 1 piping only, up to a large scope covering both safety and non-safety systems. In Finland, the regulatory requirements state that “while drawing up the risk informed inspection programme the systems of classes 1, 2, 3, 4 and EYT (not safety related) must be regarded as a whole” [1]. In practice, the screening of systems is made on the basis of the results from probabilistic safety analysis (PSA).

In the consequence evaluation, both direct and indirect consequences of pipe failures are analysed. Once the consequences of the piping failures have been identified, their importances are determined by using the plant-specific PSA. In PURISTA project, there are no specific studies related to the consequence assessment, but valuable information is obtained through participation in the RISMET project benchmarking RI-ISI methodologies (see Section International co-operation).

There are alternative ways to assess the probability of failure, ranging from purely qualitative assessment to quantification with either statistical analysis of service data or structural reliability models. The disadvantage of a qualitative approach is that the relative importance/severity of the degradation potential is not addressed, and quantitative comparison of e.g. alternative inspection strategies cannot be done. In PURISTA project, methods and tools for quantification of piping failure probabilities are developed.

Based on the failure probability and consequence assessments, the piping segments or elements are ranked according to their risk importance. The risk ranking is the most important, but not the only criterion for selection of inspection sites. It is recommended that an expert panel reviews the initial ranking and selection of risk important piping elements.

The definition of the inspection programme includes the selection of inspection elements, inspection intervals and techniques. In this connection, an evaluation of risk impact of changes to inspection programme is to be made to verify that any acceptance criteria are met. Typically the main acceptance criterion is that the risk should not increase when moving from the old ISI programme to the risk-informed ISI. When evaluating the risk reduction due to inspections, the probability of detection (POD) of defects is an essential parameter. PURISTA project addresses the inspection reliability issues in relation to RI-ISI and inspection qualification.

After the acceptance of the RI-ISI proposal, the new programme is implemented. The RI-ISI should be kept “living”, i.e. the inspection programme should be reviewed, and – if needed – updated on regular basis. A document on RI-ISI updating is under preparation in the ENIQ Task Group on Risk, and this work is coordinated by VTT.

Evaluation of piping failure potential

In a quantitative evaluation of piping degradation potential, failure probabilities are developed based on their susceptibility to degradation mechanisms. For the evaluation of the most common degradation mechanisms, structural reliability models (SRM) have been developed, but typically there is only a limited acceptance that these estimates can be seen as representing some form of true or absolute value. Quantitative values may however serve to quantify relative differences in the probability of failure through taking into account piping component geometry, material properties, loads and inspection strategies. One promising way to improve the accuracy of the SRMs is to use statistical estimates based on both plant specific and global databases in order to provide anchoring/calibrating points for single SRM estimates, in relation to which they could be improved in other locations as well. Quantitative approaches can also be used to conduct sensitivity studies, for instance to assess the impact of inspection capability and interval on the failure probability.

Probabilistic fracture mechanics modelling

Research work on structural reliability analysis methods at VTT has resulted in further development of a probabilistic fracture mechanics (PFM) tool. This tool is a modified version of fracture mechanistic analysis code VTTBESIT, developed by the Fraunhofer-Institut für Werkstoffmechanik (IWM), Germany and by VTT. With the VTTBESIT code it is possible to quickly compute the stress intensity factor values along the crack front and, based on this, simulate the crack growth. VTTBESIT was modified by adding probabilistic capabilities to the code, which was originally intended for deterministic fracture mechanics based crack growth analyses. Assessment of probabilistic distributions for depth and length of the existing fabrication cracks has been added to the analyses, assessment of initiation probability of low-cycle fatigue induced cracks has been developed, and probabilistic treatment of cyclic loads in PFM analyses concerning low-cycle fatigue induced cracking has been developed. The new features were tested in a pilot analysis of the auxiliary feedwater system of a Finnish BWR unit [2].

A joint Nordic research activity has started to benchmark the VTT PFM analysis tool against PRoSACC and NURBIT tools used in Sweden by applying them to selected structural reliability cases and comparing the results. Depending on the benchmarking results, the study either identifies differences and their reasons, or (if results are coherent) provides added confidence on the use of the benchmarked approaches.

Vibration induced high cycle fatigue

Vibration in operational conditions is a potential source of high cycle fatigue in piping systems. This damage mechanism is such that application of non-destructive testing (NDT) is not expected to decrease the risk. When a crack has nucleated in heavy vibration conditions, it grows rapidly through the pipe wall. Therefore it is unlikely to be detected in the inspections before a leak occurs. This fact in turn necessitates other control methods to be applied. Traditionally, control of piping vibration has been carried out by measuring velocity of vibration and comparing the measured values against recommendations and guidelines that can be found in codes, standards and other type of literature.

Potentiality of fatigue is partly determined by magnitude and frequency of occurrence of stress variation in piping material. These factors can be assessed by strain gauge measurements. However, this method has also its own disadvantages. A study within PURISTA concentrates on investigating a method with which vibration induced stress variation can be estimated without performing strain gage measurements [3]. In the investigated method, operational displacements shapes, as actually measured at the system, are used as an input in the forced vibration analysis. This analysis is in turn performed with a finite element model of the system. As a result of the analysis, estimate for the vibration induced stress variation can be obtained at every location of the system that is included into the model.

Test subject of the study is a pipeline of the secondary feed water system at Loviisa 1 WWER plant. In order to verify the investigated method, strain gage measurements were carried out at the system. The results of these measurements were then processed with a computer code which was developed to support the evaluation. The work will be continued in 2009 with further development of the evaluation code. Additionally, computed estimates for the vibration induced stress variation will be processed with the developed code. The obtained results will be compared against their measured counterparts. This way, validity of the investigated method will be verified.

Reliability of in-service inspections

The impact of ISI on plant safety depends on the capability of the inspection system to detect flaws. The reliability of inspections is an important input for RI-ISI analysis. If a quantitative RI-ISI analysis is to be performed, then a quantitative measure of inspection effectiveness is needed in order to calculate the reduction in risk associated with the inspections.

The project addresses the ISI reliability from two directions. On one hand, the reliability of inspections is investigated through NDT simulations. On the other hand, the importance of inspection capability assumptions in risk-informed ISI is studied. In this connection the relationship between inspection qualification and flaw detection probability are studied.

NDT simulations

When considering detection capability of NDT inspections there are always many parameters that are contributing to the final outcome. Examples of the

factors that have influence on the inspection result are component properties (geometry, material), inspection technique (probe, setting values, scanning path), and flaw parameters (geometry, size, location, orientation). These parameters must be taken into account during the development phase of the inspection and also in the assessment of the inspection performance. Usually some experimental trials using test blocks are carried out to verify the capability of the technique. The coverage of all the different parameters and their variations is often challenging using real experimental tests because of the number of test blocks and inspection runs needed. Therefore computer simulations can be considered as a convenient option and extension for the practical trials. Using simulations many parameters can be varied rapidly and flexibly.

The noise originating from the material (especially from weld material) and the attenuation of signals are two factors that are always present in the ultrasonic inspections. Signal detection is possible only, if the signal originating from the flaw can be distinguished reliably from the surrounding noise. When the noise level increases or the attenuation suppresses the useful signal, the flaw signal is buried into noise and detection is more difficult or impossible. To simulate the real inspection conditions it is important that simulations can also produce noise and take into account the signal attenuation. When also these two factors are included into simulations it is possible to produce simulated inspection cases that could be used for POD assessments.

The CIVA simulation software is able to take into account both material noise and attenuation. Simulation trials using different noise parameters have been used to adjust the noise characteristics to resemble those of real experimental measurements. Also several simulations using different ultrasonic transducers were performed in varying noise environments to test probe performance [4].

The Figure 22.1.2 shows a simulation example where a phased array ultrasonic probe is applied to scan over some test reflectors (flat bottom holes) in a square test block to measure detectablity of defects in a weld layer. In the side view it can be seen that the noise level the middle layer imitating weld zone is higher than in the base material (top and bottom layers of the block). The reflectors reaching the upper surface and the middle of “the weld zone” are producing clear indications and can be easily detected. The reflector below “the weld zone” is quite completely hidden in the noise in the top view presentation. On the other hand some indication of this reflector is visible at the lower surface of “the weld zone” in the side view which is in fact presenting just a narrow slice of the data taken along the plane of the reflector locations.

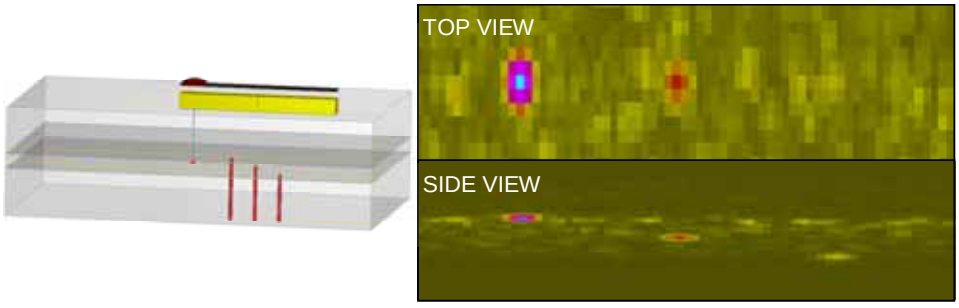

Figure 22.1.2. Simulation configuration (left) includes flat bottom holes penetrating to different depths into a noisy zone located in the middle of the block. Simulation result (right) is shown as colour coded maps where indications from reflectors as well as the higher noise level in the middle of the block is visible.

Relationship between inspection qualification and probability of detection

A POD curve could provide ideal data for evaluating ISI reliability, but there can be significant problems associated with generating realistic POD curves by practical trials. The ENIQ inspection qualification methodology [5], based on a combination of a qualitative technical justification and practical trials, is used to provide high confidence that an inspection system will achieve its objectives. However, it is not designed to provide a quantitative measure of the type that can be used in RI-ISI analysis. A European project was set up to investigate and demonstrate via pilot studies approaches to quantify the confidence which comes from inspection qualification according to the ENIQ procedure [6].

Two pilot qualification studies were performed to demonstrate the application of the quantification methods in practice, and to identify needs of further work and issues to be addressed in the guidelines. The most structured quantification approach is based on weighting and scoring the elements of the technical justification, and combining the information from a quantified technical justification with the results of practical trials. The pilot studies highlighted a number of issues that require further work or that should at least be drawn to the attention of those who intend to apply the methodology. Guidelines were developed for the application of the structured quantification approach. Consideration should also be given to how to construct a technical justification to facilitate the quantification of the NDT capability.

Sensitivity of risk reduction to the assumptions on inspection capability

Studies were also carried out to investigate the sensitivity of risk reduction due to inspections to the level of detail of the POD. The simpler the shape of the POD curve is, the easier it would be for the qualification body to make judgements on POD. The simplest case will be a step function where a fixed POD is assumed for defects above the qualification size, and no detection capability assumed for defects below that size. It will also be easier the lower the POD required. However the risk reduction associated with an inspection will tend to increase if credit is taken for detecting defects below this “cut-off” qualification size, and will also tend to increase the higher the POD for a given defect size. It is therefore useful to understand the sensitivity of risk reduction to the level of detail in the POD curve.

Preparation, acceptance, follow-up and updating of RI-ISI programme

Studies are performed on issues related to risk-ranking, selection of inspection sites and acceptance criteria of a RI-ISI programme. The project has participated in the international RI-ISI benchmarking project RISMET (see section on International co-operation). This increases knowledge on what are the main uncertainties related to risk ranking, and how important the differences in RI-ISI results obtained by various methodologies are. For instance, in the consequence assessment the PSA quality, conservatism, success criteria, and crediting of operator actions play important roles.

After the risk ranking of piping segments or elements, the next step is to decide which welds will be included in the inspection programme. The risk measure, determined on the basis of PSA analyses and failure potential analyses, is not the only decision criterion. Also insights from several other disciplines should be integrated in the decision making process, preferably through a well structurised expert panel process. VTT has led the development of an ENIQ recommended practice on guidance on expert panels in RI-ISI [7]. The document gives guidance on responsibilities and composition of a RI-ISI expert panel, and how to plan, conduct and document the panel sessions.

The main criterion for the acceptance of a RI-ISI programme is that the risk will not increase when moving from the old ISI programme to the risk-informed. This calls for the evaluation of the change in risk. The previously described research work on quantification of the failure probabilites and NDT capability

support the delta-risk assessment. In this evaluation it is recommended to begin with a simplified approach and move to more detailed analyses only if needed. If the total number of inspections is not reduced, it is very easy to justify the safety improvement when inspections are targeted to more risk-significant sites. If the number of inspections is reduced, more quantitative delta-risk analyses are needed.

VTT has started the development of an ENIQ document on RI-ISI updating. The document is meant to assist on how to maintain and update a RI-ISI programme. The document provides also an overview of current ISI updating practices in the majority of EU member states having operating nuclear power plants. The document is expected to be finalised in 2009.

International co-operation

International co-operation is an essential part of the PURISTA project. A large part of the research work is done in co-operation with European organisations and in international networks. The main networking activities are summarised in the following.

VTT has participated in the international project for benchmarking RI-ISI methodologies, RISMET [8]. RISMET was initiated by ENIQ TGR and coordinated by the JRC and OECD/NEA, and it was conducted in 2006–2008. In the project, various RI-ISI methodologies and the deterministic ASME XI approach were applied to the same case, consisting of four selected piping systems of Ringhals 4 PWR unit. The applied methodologies and the aspects considered in the evaluation are presented in Figure 22.1.3. More than twenty organizations from Europe, U.S., Canada and Japan participated in the project. The final report of the benchmark exercise will be published in 2009.

VTT has actively participated in the work of the Task Group Risk of the European Network for Inspection and Qualification, ENIQ TGR, and the chairperson of this working group is from VTT. The TGR works towards developing European best practices for RI-ISI methodologies. Besides leading the work on writing recommendations for expert panels and RI-ISI updating, VTT has also contributed to the development of a recommended practice on verification and validation of structural reliability models used in RI-ISI [9].

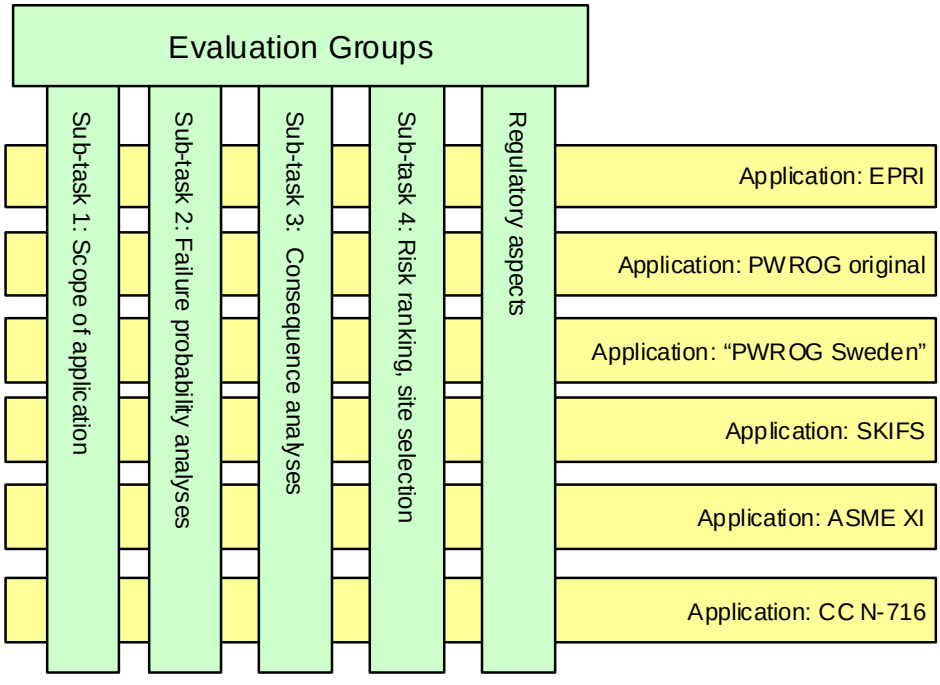

Figure 22.1.3. RISMET RI-ISI benchmark application and evaluation tasks.

Additionally, VTT has participated in IAEA consultancy meetings to draft a technical document on RI-ISI. The publication describes the general process of developing and implementing risk-informed in-service inspection (RI-ISI) methodologies, the technological issues which lie behind the methodologies, application status, and the current development activities. The report will be published in 2009.

Conclusions

The basic idea of RI-ISI is to make the ISI more effective by considering safety, economy and worker radiation exposure. Piping failure potential is evaluated in detail, and this information is combined with the assessment of consequences of the failure in order to understand the piping risk-importance. The risk-importance, together with other aspects, such as inspection methods, accessibility, radiation doses and inspection costs, are used to support decision on locations to be inspected.

The applications of risk-informed approaches to redefine in-service inspection programmes are increasing all over the world, and RI-ISI projects are presently going on at Finnish nuclear utilities. The PURISTA project aims at supporting the RI-ISI implementation in Finland.

The results of the PURISTA project can be applied in performing and reviewing the risk-informed ISI applications. The main focus is on assessment of piping degradation potential, and inspection capability, and in issues related to the acceptance and updating of RI-ISI programmes. Through the PURISTA project VTT is participating in international projects and in the development of European and international recommendations on RI-ISI related issues.

Many results of the PURISTA project are not restricted to RI-ISI application, but can be used more widely in the safety management of structural components. Probabilistic structural integrity assessment tools may be applied in structural safety analyses, and in updating PSA initiating event frequencies. Sufficiently reliable estimates of stresses and their fluctuations allow better evaluation of low-cycle fatigue risks. Inspection reliability studies support the development of the link between inspection qualification and quantification of inspection capability. The results of inspection simulation studies can be used in connection to the inspection qualification. Studies of RI-ISI implementation can also be utilised in other risk-informed applications, such as testing and maintenance planning.

References

1. STUK. YVL 2.8. Probabilistic safety analysis in safety management of nuclear power plants. 28 May 2003. http://www.stuk.fi/saannosto/YVL2-8e.html.

2. Cronvall, O., Simola, K., Vepsä, A. & Alhainen, J. RI-ISI pilot study of the auxiliary feed water system of the Olkiluoto OL1 NPP unit. Espoo: VTT, 2008. VTT Research Report VTT-R-01414-08. 47 p. + 12 p. app.

3. Vepsä, A. Operational Displacement Shape Based Estimation of Vibration Borne Stress Variation in a Pipeline. Proceedings of the IMAC XXVI A Conference and Exposition on Structural Dynamics. 4–7 February 2008, Orlando, USA. 14 p.

4. Sarkimo, M. Application of noise in the ultrasonic inspection simulation. Espoo: VTT, 2008. VTT Research Report VTT-R-00628-08. 13 p.

5. ENIQ. European methodology for qualification of non-destructive testing: third issue. European Commission, 2007. EUR 22906 EN. 40 p.

6. Shepherd, B., Gandossi, L. & Simola, K. Link Between Risk-Informed In-Service Inspection and Inspection Qualification. Doosan Babcock report TR-08-071, 2008. http://safelife.jrc.ec.europa.eu/eniq/publications/RI-ISI.php.

7. ENIQ. ENIQ Recommended practice 11: Guidance on expert panels in RI-ISI. European Commission, 2008. EUR 22234 EN. 22 p.

8. Simola, K., Eriksson, A. & Huerta, A. OEDC/NEA and JRC RISMET Project: Benchmarking of RI-ISI Methodologies. Proceedings of PSAM 9 Conference on Probabilistic Safety Assessment & Management. 18–23 May 2008, Hong Kong, China.

9. Cueto-Felgueroso, C., Simola, K. & Gandossi, L. ENIQ Recommended Practice 9: Verification and validation of structural reliability models and associated software to be used in risk-informed in-service inspection programmes. European Commission, 2007. EUR 22228 EN. 12 p.

23. Fatigue endurance of critical equipment (FATE)

23.1 FATE summary report

Jussi Solin, Jouni Alhainen and Wade Karlsen
VTT

Abstract

Progress in research for clarifying the fatigue mechanism in stainless steels, transferability of data into primary circuit ageing assessment and development of related new research capabilities is summarised by introducing the motivation, challenges and main results.

Fatigue properties and microstructural changes in cyclic deformation of Alloy 316 are reported. Secondary hardening and formation of α' martensite was found at very low strain amplitudes. The RT air fatigue endurance data is in conflict with the new stainless steel design curve, which was recently endorsed by the US NRC.

Introduction

In line with the general orientation of the national research programme, the current project aims in understanding the material and component ageing mechanisms caused by cyclic stressors during plant operation and their relation to practical fatigue assessment of primary loop pressure boundaries. Development of reliable capabilities to perform critical experiments and modelling work plays an important role in this work. It should be noted that generation of material data bases for design purposes goes beyond the scope of this project (and programme), but critical tests need to be performed

- to create a basis for long term development of quantitative mechanism based and risk informed fatigue models, and
- to check validity of (sometimes hidden) assumptions in component assessment.

Quantitative models are sought for not only to improve accuracy of remaining safe life prediction, but also to realistically evaluate effects of different factors. In some cases, the current state of the art is very good for qualitative assessment, but problems arise when the plant operators and regulators need numeric values, e.g., for fatigue usage. This need cannot be ignored and in parallel with the long term research, practical applications are also discussed. Continuous contact to reality is not necessary bad for modelling either.

This presentation will briefly describe the research challenges, project activities in 2007–2008 and finally focus to the issue of selecting fatigue design curve for stainless steel.

State of the art as starting point of this study

Planning of the preceding and current project has been guided by international debates on applicability of ASME, KTA and RCC-M fatigue design curves for stainless steels in primary loop pressure boundaries. The environmental effects of coolant water were originally selected as the main focus. Potential effects of service loading as variable amplitude and rate transients are also considered. More recently the claims on relevance of the basic reference curve grew in interest – and will be particularly addressed also in this presentation.

Laboratory data for environmental effects

Extensive studies to quantify hot water effects on fatigue life have been realised, mainly in USA and in Japan. The research in Argonne National Laboratory (ANL) resulted to statistical models for estimating the fatigue lives in air and in variable LWR environments [1]. An alternative approach for presenting the environmental effects in terms of an environmental fatigue correction factor F_{en} was proposed by Higuchi and Iida [2]. Mehta used the ANL statistical models for calculating F_{en} in an approach known as the EPRI/GE methodology [3]. To account for the latest data Chopra and Higuchi have several times updated the expressions to calculate F_{en} [4–7].

French type 304 L stainless steel has been tested in PWR environments at GE in a large EDF programme. The results presented by Solomon, Amzallag et al. indicate that for this alloy specific cyclic deformation mechanisms may have notable effects in fatigue endurance and in particular in the endurance limit in environment [8]. For most industrial alloys, the stability of austenite phase is not perfect in room temperature. The effect of austenite stability types has been studied and fatigue behaviour of different alloy types have been compared in PSI Switzerland by Kalkhof et al. [9–10].

It should be noted that the above cited regression models for F_{en} have been developed without consideration of the underlying mechanisms. The mechanisms responsible for environmental effects for stainless steels in PWR's are still unknown. On the other hand, though the experimentally mapped effects are generally accepted, consensus on significance of the laboratory data on small specimens to component behaviour in real plants is still missing. It is often claimed that operational experience confirms applicability and conservatism of the classical fatigue design procedures, which account for moderate environmental effects only.

Codes and guidelines

Fatigue design curves given in the ASME Code Section III – and in other related international codes – are based on strain controlled low cycle fatigue tests in room temperature. Protection against environmental effects was left as a responsibility of the designer [11].

Environmental effects have been discussed in terms of proposed fatigue curve revisions [12], but it is obvious that such curves would not be generally applicable and common agreement has not been reached. In all relevant applications, environmental effects are described through F_{en} models.

In Japan the utilities were notified in 2000 to adopt MITI guidelines for evaluating fatigue initiation life reduction in LWR environments, a revised approaches were published in 2002 as TENPES Guidelines and in 2006 in the JSME code [13].

The EPRI/GE methodology [3] was applied for license renewals in USA and it has been reviewed by the Pressure Vessel Research Council (PVRC/CLEE). In 2004 this methodology was introduced in the ASME Code with the following wording: "proposed in the form of a nonmandatory Appendix … and may possibly be considered for Code implementation" [14].

The US Nuclear Regulatory Commission published in 2007 guidelines for fatigue analyses incorporating life reductions due to LWR environment [15]. This guide refers to the NUREG/CR-6909 report [5] and is applicable to new reactors to be built in USA only, but it is a globally important reference. In addition to environmental effects, the NRC endorsed even a new air curve for stainless steels.

In Finland consideration of fatigue damage rate in high temperature water environment has been mandatory for new designs since 2002 [16]. Related measures have been adopted also in plant life management of the running plants. This new YVL 3.5 guide was naturally an important starting point for the current research.

Test facility for LCF in primary coolant

To be able to accurately measure specific environmental effects and perform parametric studies, a novel experimental facility was developed by VTT [17]. Although a couple other facilities have been launched, the VTT facility is still the only hot water facility in Europe claimed to meet the basic requirements (ASTM E-606, ASTM E-1012) for determination of qualified ASME design curve data. A specimen diameter (4 mm) slightly less than the minimum recommended by ASTM has been used so far, but this was not considered crucial, at least as long as the aim has not been to develop accredited design data.

Three grades of austenitic stainless steel have been tested in PWR waters, Figure 23.1.1. Our results are well in line with predictions by the F_{en} models. Additional details of these experiments can be found in previous papers [18–20].

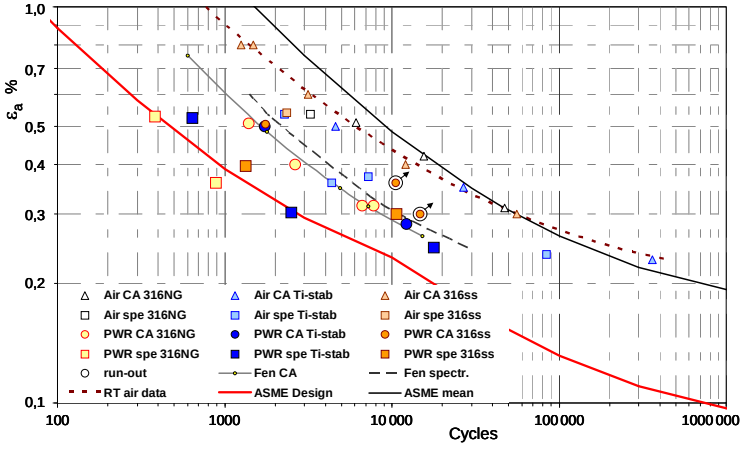

Figure 23.1.1. Summary of previous hot water fatigue data for three stainless steel grades.

Main achievements in 2007–2008

Transmission electron microscopy

The long term goal of developing quantitative mechanism based and risk informed fatigue models requires full understanding of the mechanisms for cyclic deformation, strain localisation, crack initiation and growth.

Transmission electron microscopy (TEM) studies combined with careful evaluation of the cyclic behaviour were started in 2007. This approach has already been proven valuable. The work [21, 22] has been successful in revealing specific dislocation microstructures in different phases of fatigue process and in improving our understanding of fatigue mechanisms without environmental effects. The challenge of identifying relevant changes due to temperature and environment is ahead.

Modelling of cyclic stress strain response for stainless steels is complex due to hardening and softening processes which can act consecutively and/or simultaneously. The latest results proved formation of α' martensite during the secondary hardening phase in a specimen fatigued at low strain amplitude (0,25%), Figure 23.1.2. This is particularly interesting because most of the martensite formation studies [9, 10] deal with higher strains and because the austenite in our test material (alloy 316) should be relative stabile.

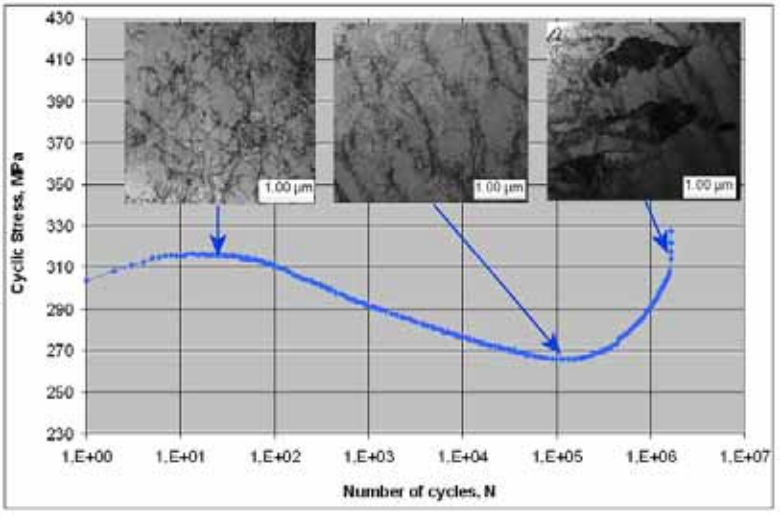

Figure 23.1.2. Development of representative microstructures in Alloy 316 during a fatigue test in RT air at 0,25% strain amplitude. Small volumes of martensite are found after a million cycles of secondary hardening (right) [22] .

Sequence effects and transient simulation

The importance of real loading sequence has been pointed out both in RT air and in PWR water environment. Our tests using an arbitrary variable amplitude sequence showed an additional life reduction, Figure 23.1.1. But also an opposite, less damaging effect with a typical plant transient in PWR environment has been recently reported [23].

Looking at the available data as a whole, it seems that the sequence effects are highly depending on the plant transient type and material cyclic response at the particular strain ranges. If accuracy of fatigue assessment is to be improved by considering sequence effects, alloy sub-class specific effects may need to be evaluated. In other words, austenitic stainless steels cannot be considered as a uniform material group. Further research to clarify transferability of existing laboratory data to relevant materials and real plant conditions is needed. Such activity is planned for the second half of the project.

Verification of transient simulation and indirect strain control

The control and measuring system applied in our previous autoclave tests had been designed for constant amplitude loading. In 2007 we built a new system suitable for effective and flexible simulation of complex plant transients. The new capability was verified and it will be used for controlling next autoclave tests, which are planned for 2009 after completion of the ongoing update of bellows fatigue loading units.

Figure 23.1.3 shows a typical fatigue relevant transient expected in operation of the EPR reactor. This transient (with and without suppression of slow decreasing strain part) was simulated as part of our verification tests, Figures 23.1.4–23.1.5.

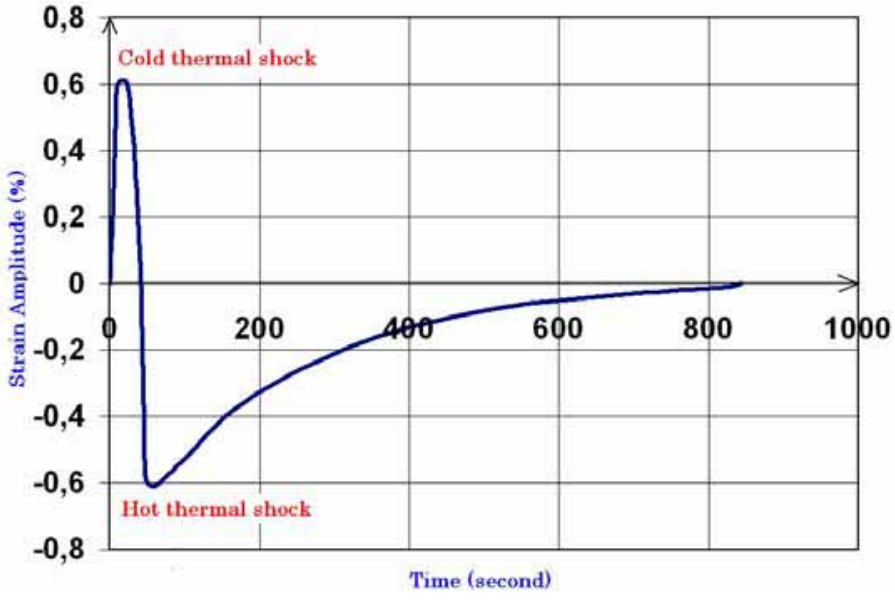

Figure 23.1.3. Typical strain history of cold and hot thermal shocks corresponding to a safety injection transient in a PWR. [23]. Note: the original transient is actually assumed symmetric with slow return of strain to 0 after the peak. This part has been omitted to save time in autoclave tests.

Strain measurement within the gage section is not easy to arrange and some laboratories (not VTT) utilise indirect strain control based on a "companion specimen" strategy [1] for calibration of the measurements in the autoclave. Applicability of indirect strain measurement was investigated by attaching another extensometer reaching over the rounded fillet area, see on right in Figure 23.1.4. The blue curves in Figure 23.1.4 show the remote strain response which is not linearly correlated to the true strain (red curves) during the transient. Figure 23.1.6 show the non-controlled strain responses during constant amplitude tests run with direct and indirect strain controls. Calibration between the two strains drifted about 10% during both tests. This demonstrates severe difficulties in accurate control of strain by the companion specimen strategy and confirms the benefit of direct strain control. Switching to indirect strain control would simplify the experimental work in hot water autoclaves, but it cannot be recommended.

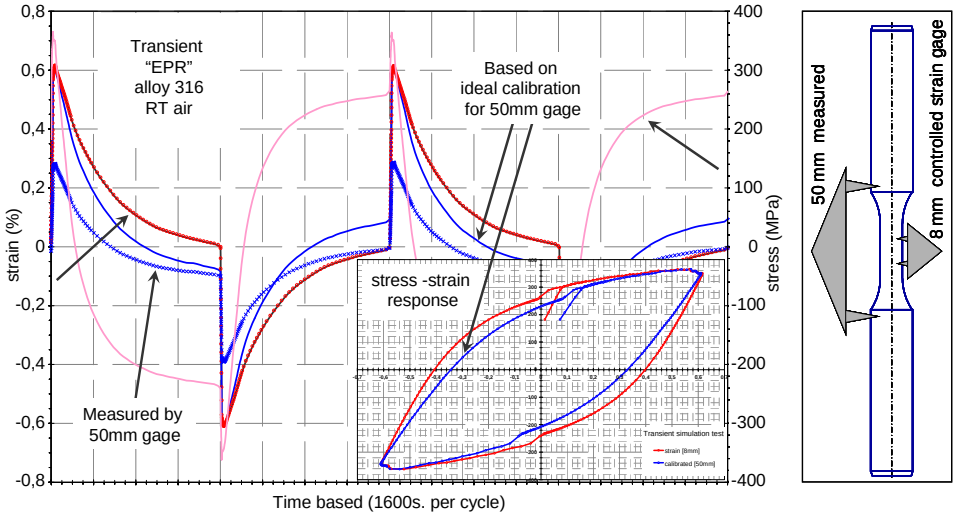

Figure 23.1.4. Simulation of the transient shown in Figure 23.1.3. Strain in middle of specimen gage section (8 mm) is controlled to follow the desired time history. Stress and strain over the 50 mm section depend on the material response shown both as time based and in hysteresis loop form.

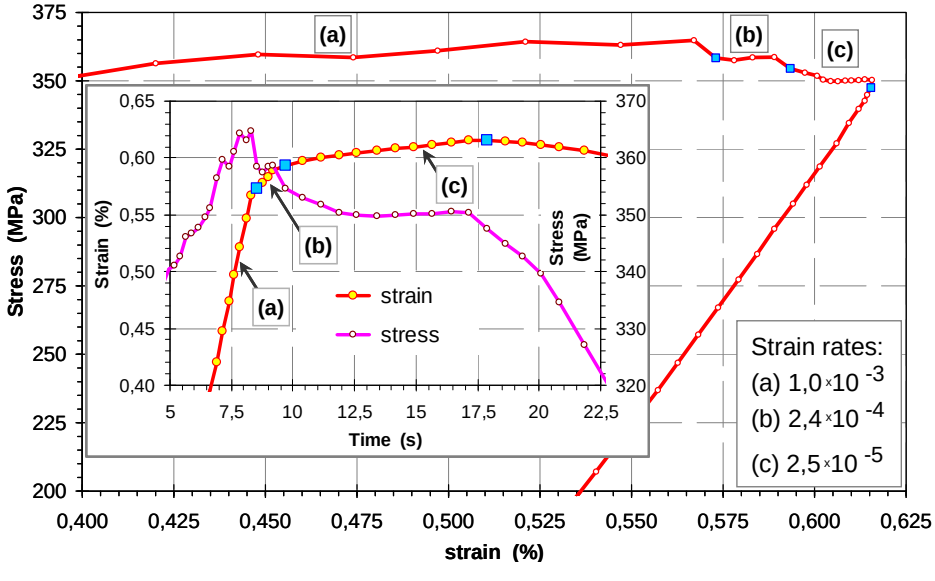

Figure 23.1.5. Strain rate effect at the peak strain (top of hysteresis loop in Figure 23.1.4).

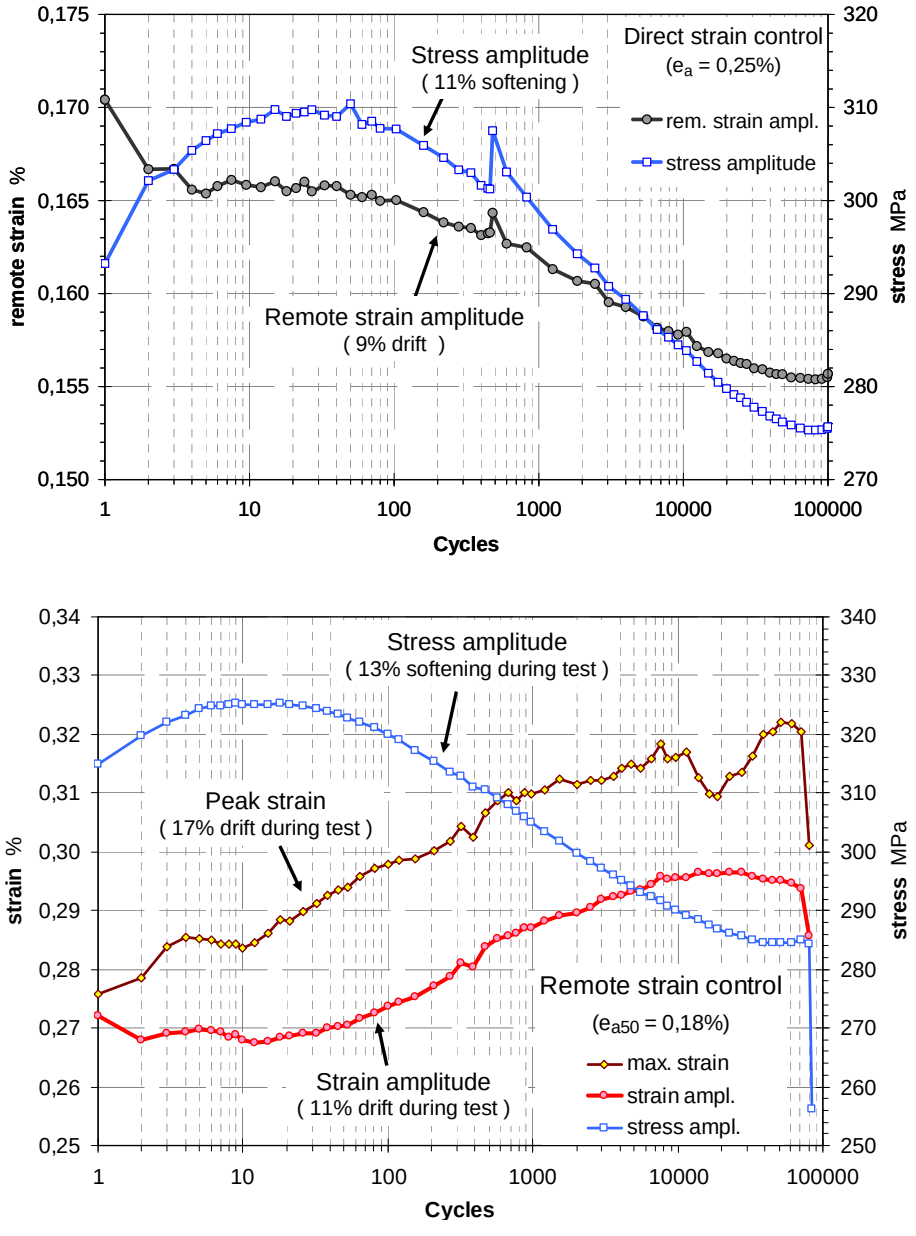

Figure 23.1.6. Drift in the other strain measurements during direct and remote strain controlled tests.

Design curve for stainless steels

Applicability of fatigue design curves for stainless steels is an issue of current debate. Laboratory data have shown environmental effects in coolant waters, but applicability of the proposed new design criteria to current plant components has been questioned in many instances. It is often claimed that operational experience confirms applicability and conservatism of the existing design procedures as a whole. However, environmental effects larger than "the moderate effects" already included in the ASME curve have been addressed e.g. for licence renewals in USA.

Another issue for debate is the air curve. In part this is due to the fact that the development of the ASME code was primarily aiming to prevent catastrophic fractures of pressure vessels and the fatigue assessment was focussing on severe but rare thermal transients that can cause notable low cycle fatigue damage. Later on, higher numbers of small stress cycles have been addressed in the piping (for small bore pipes in particular) and fatigue tests have been conducted to longer lives. Encouraged by new experimental data and a proposal by ANL experts [5], the NRC endorsed a new air curve for stainless steels as part of a Regulatory Guide for new designs un USA [15].

Much data and regression curves in line with the ANL/NRC air curve (often referred as "Chopra curve") have been published, e.g. in Japan and France [4, 6, 24]. In the LCF end the new data and proposed curves do not much differ from the Lager curve, which is the basis of the ASME design curve. The difference grows notable (an order of magnitude in life) in the HCF regime. At least part of the new data refers to very soft steel grades.

Discussion based on the VTT data

Only a few tests in air were performed along with the previous autoclave tests for three grades of stainless steel, Figure 23.1.1, but is was quite obvious that our data did not follow the same trend as Chopra's. More research was needed to remove or confirm this discrepancy with international literature. The same batch of alloy 316 used in this programme had been tested in as machined condition in another project and with kind permission of Fortum Nuclear Services, the data could be used also in Safir programme. The regression curve for this 316 base material is shown as "not polished" in Figure 23.1.7. In spite of higher surface roughness, this curve is very close to Langer curve in the HCF regime. Additional testing with polished samples within the current project showed some improvement

in fatigue life, but even more strikingly, faced us with a behaviour indicating an endurance limit, Figure 23.1.7. Two specimens were broken at about 1,5 million cycles in the gripping area of the specimen, indicating that the standard recommended geometry for LCF testing is not good for this purpose. With reinforced gripping design we obtained almost 5 million cycles at 0,2% strain amplitude without any indication of crack or other fatigue damage.

Together with some other data available, this observation clearly demonstrates that different grades of stainless steels exhibit different fatigue performance, and that the new air curve endorsed by the NRC is applicable only to part of the stainless steels. Based on general experience, it seems probable, that many soft grades developed particularly to exclude sensitivity to stress corrosion cracking will comply with the Chopra curve, but many grades used in the existing plants will not. So, as the NRC also states, the Regulatory Guide 1.207 as such may be applicable to new (US) designs only.

The endurance limit type behaviour of this 316 alloy is clearly associated with notable secondary hardening, Figure 23.1.2. Further details and discussion on the secondary hardening phenomena go beyond this presentation, but it is worth of noting that it may occur also in operation temperatures. The GE/EDF programme actually resulted to extreme secondary hardening just in 300 ºC [8].

In principle, one might even find or develop material specifications ensuring “traditional ASME level” fatigue strength for HCF critical components also in new designs. Together with aims for complete understanding of the ageing processes in running plants, that will be a guiding vision for the second half of this project.

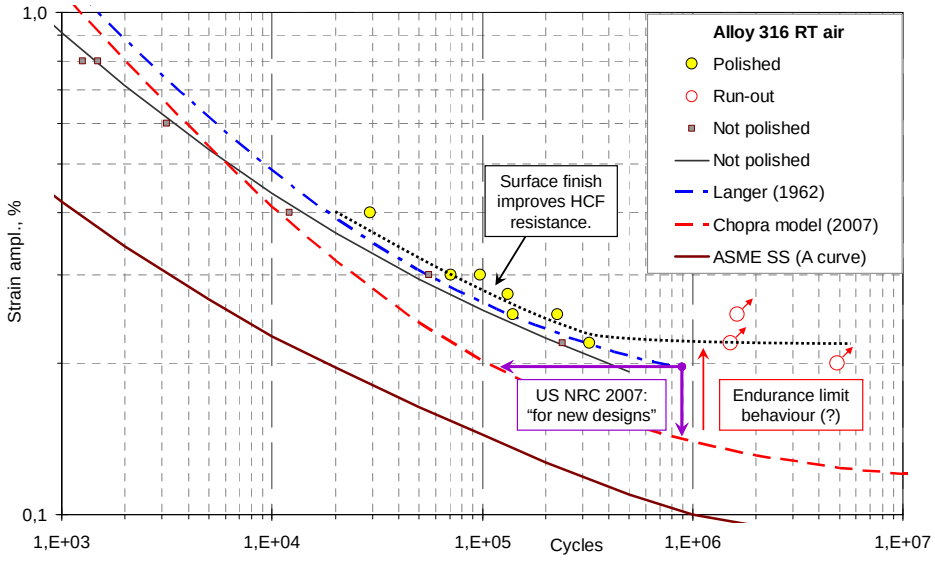

Figure 23.1.7. Comparison of our data for alloy 316 with the old and proposed reference curves.

Conclusions

The research capability developments in this project progress slowly but steadily and the facility for transient simulations should be in use 2009. Comparison of direct and indirect strain control strategies confirmed that, in spite of many practical difficulties, our approach for direct strain control also in hot water is more than well justified.

A stainless steel grade of type 316 has been studied in this project. The microstructural changes revealed by TEM are well in line with the cyclic stress strain responses observed in fatigue tests. The extent of secondary hardening and α' martensite formation at low strain amplitude is important finding for a material with relatively stabile austenite.

Secondary hardening may play important role for increasing fatigue endurance in high cycle fatigue to much higher level than the data in the newest international data sets. The in NUREG/CR-6909 proposed and by NRC Reg. Guide 1.207 endorsed air curve gives a particularly poor description of the RT air fatigue behaviour of this alloy.

References

1. Majumdar, S., Chopra, O.K. & Shack, W.J. 1993. Interim fatigue design curves for carbon, low-alloy, and austenitic stainless steels in LWR environments, NUREG/CR-5999 (ANL-93/3) for U.S. Nuclear Regulatory Commission, Washington DC. 48 p.

2. Higuchi, M. & Iida, K. 1991. Fatigue strength correction factors for carbon and low-alloy steels in Oxygen-containing high-temperature water. Nucl. Eng. Des. 129, pp. 293–306.

3. Mehta, H. 1999. Update on the EPRI/GE environmental fatigue evaluation methodology and its applications. Probabilistic and Environmental Aspects of Fracture and Fatigue – 1999, PVP-Vol 386, ASME, 1999, pp. 183–193.

4. Chopra, O.K. 1999. Effects of LWR coolant environments on fatigue design curves of austenitic stainless steels. NUREG/CR–5704, ANL–98/31 for U.S. Nuclear Regulatory Commission, Washington DC. 42 p.

5. Chopra, O. & Shack, W. 2007. Effect of LWR Coolant Environments on the Fatigue Life of Reactor Materials, Final Report. NUREG/CR-6909, ANL-06/08, Argonne Nat. Lab. 118 p.

6. Higuchi, M. 2004. Japanese program overview. 3rd International Conf. on Fatigue of Reactor Components. 3–6.10.2004, Seville, Spain, EPRI/OECD. 15 p.

7. Higuchi, M. 2008. Comparison of environmental fatigue evaluation methods in LWR water. Proceedings of PVP 2008-ICPVT11 2008 ASME Pressure Vessel and Piping Division Conference. July 27–31, 2008, Chigago, USA. Paper PVP2008-61087. 11 p.

8. Solomon, H., DeLair, R.E., Vallee, A.J. & Amzallag, C. 2004. 3rd Int. Conf. on Fatigue of Reactor Components, 3–6.10.2004, Seville, EPRI/OECD, 22 p.

9. Kalkhof, D., Grosse, M., Niffenegger, M., Stegemann, D. & Weber, W. 2000. Microstructural investigations and monitoring of degradation of LCF damage in austenitic steel X6CrNiTi 18-10. Int. Conf. on Fatigue of Reactor Components, 31.7–2.8.2000. Napa, California, EPRI. 12 p.

10. Leber, H., Niffenegger, M. & Tirbonod, T. 2007. Microstructural aspects of low cycle fatigued austenitic stainless tube and pipe steels. Materials Characterization 58, pp. 1006–1015.

11. Criteria of the ASME Boiler and Pressure Vessel Code for design by analysis in sections III and VIII division 2. Pressure Vessels and Piping: Design and Analysis. A Decade of Progress, Vol. One, ASME 1972, pp. 61–83.

12. O'Donnell, W.J. & O'Donnell, W.J. 2008. Temperature dependence of reactor water environmental fatigue effects on carbon, low alloy and austenitic stainless steels. Proceedings of PVP 2008-ICPVT11 2008 ASME Pressure Vessel and Piping Division Conference. July 27–31, 2008, Chigago, USA. Paper PVP2008-61917. 11 p.

13. JSME. 2006. Codes for Nuclear Power Generation Facilities. Environmental Fatigue Evaluation Method for Nuclear Power Plants, JSME S NF1-2006. The Japan Society of Mechanical Engineers, Tokyo, Japan, 2006.

14. ASME. 2004. Corrosion fatigue and crack growth. ASME Code, issue 2004 Section III, Division 1, Appendices, article W-2700, pp. 416–418.

15. U.S. Nuclear Regulatory Commission Regulatory Guide 1.207. 2007. Guidelines for evaluating fatigue analyses incorporating the life reduction of metal components due to the effects of the light-water reactor environment for new reactors. 7 p.

16. STUK. 2002. YVL-guide 3.5. Ensuring the strength of nuclear power plant pressure devices, issue 5.4.2002. (Original in Finnish, translations exist.)

17. Solin, J., Karjalainen-Roikonen, P., Moilanen, P. & Marquis, G. 2002. Fatigue testing in reactor environments for quantitative plant life management. 2nd Int. Conf. on Fatigue of Reactor Components. 29–31 July, 2002, Snowbird, Utah, EPRI. 16 p.

18. Solin, J., Karjalainen-Roikonen, P., Arilahti, E. & Moilanen, P. 2004. Low cycle fatigue behaviour of 316 NG alloy in PWR environment. 3rd Int. Conf. on Fatigue of Reactor Components. 3–6.10.2004, Seville, EPRI/OECD. 19 p.

19. Solin, J. 2006. Fatigue of stabilized SS and 316 NG alloy in PWR environment. Proceedings of PVP 2006-ICPVT11 2006 ASME Pressure Vessel and Piping Division Conference. July 23–27, 2006, Vancouver, BC, Canada. Paper PVP2006-ICPVT11-93833.

20. Solin, J. 2006. Fatigue behaviour of 316 NG alloy and plant aged titanium stabilised stainless steel in PWR environments. Proceedings of Fontevraud 6, SFEN International symposium. 18–22.9.2006, Fontevraud, France. Vol. 2. Pp. 1121–1132.

21. Karlsen, W. & Solin, J. 2007. TEM examination of low-cycle fatigue deformation microstructures in 316 stainless steel. VTT Research Report VTT-R-07810-07. Espoo: VTT. 15 p.

22. Karlsen, W. 2008. Deformation microstructures of 316L stainless steel after interrupted low-cycle fatigue tests. VTT Research Report VTT-R-07909-08. Espoo: VTT. 16 p.

23. Le Duff, J.-A., Lefrançois, A. & Vernot, J.P. 2008. Effects of surface finish and loading conditions on the low cycle fatigue behavior of austenitic stainless steel in PWR environment – Comparison of LCF test results with NUREG/CR-6909 life estimations. Proceedings of PVP 2008-ICPVT11 2008 ASME Pressure Vessel and Piping Division Conference. July 27–31, 2008, Chicago, USA. Paper PVP2008-61894. 10 p.

24. Faidy, C. 2008. Status of French fatigue analysis procedure. Proceedings of PVP 2008-ICPVT11 2008 ASME Pressure Vessel and Piping Division Conference. July 27–31, 2008, Chicago, USA. Paper PVP2008-61911. 9 p.

24. Water chemistry and oxidation in the primary circuit (WATCHEM)

24.1 WATCHEM summary report: Development and verification of in situ techniques to study oxidation and water chemistry effects in the primary circuit

Timo Saario and Petri Kinnunen
VTT

Abstract

The focus in the WATCHEM project has been in development of in situ methods (a) to study oxidation of fuel cladding alloys and (b) to study optimisation of passivation (i.e. Hot Conditioning) of PWR reactor circuit surfaces prior to first fuel loading.

The Controlled Distance Electrochemistry (CDE) -method has been shown to be reliable and to give consistent and repeatable results both in BWR and in PWR conditions. Comparisons of the effects of elevated Li^+ (PWR) and K^+ (WWER) concentrations on fuel cladding oxidation were performed as part of this project. In studying the sensitivity limits of the CDE method the effects of F^- concentration in the beginning of cycle conditions of WWER on Zr-1Nb alloy oxidation were found to be negligible at levels below 100 ppb.

Based on a literature study the optimal water chemistry conditions in PWRs for Inconel 600 and 690 materials are 0.5–1 ppm Li^+ and 25–30 ccH_2/kgH_2O. There is a considerable uncertainty in determining the effect of boric acid and the minimum required hot conditioning time. Two new methods were developed in co-operation with Bhabha Atomic Research Centre (BARC), India, to study

the optimisation of the hot conditioning procedure and verified for carbon steel under PHWR water chemistry conditions. Preliminary studies with Inconel 690 under PWR conditions are underway.

Introduction

Water chemistry forms an integral part of the safety of a nuclear power plant. At the moment, there is a trend for extended fuel cycles and higher burn-ups of fuel in nuclear power plants which results in a demand for an elevated level of the alkali in the water, LiOH in case of PWR's and PHWR's, KOH in case of WWER's. Oxidation rate of fuel cladding alloys is known to increase with increasing concentration of the alkali, at least above some threshold level and for some cladding alloys. There are also other concerns on the effect of water chemistry (e.g. impurity levels) on the cladding oxidation rate. These issues together with the continuous need for developing new and better cladding alloys indicate a need for an efficient in situ technique for studying the growth and properties of the oxide layer forming on the cladding alloys under relevant water chemistry conditions. This paper describes the results from development of the Controlled Distance Electrochemistry (CDE) in situ -technique and discusses the main experimental findings and modelling results with regard to cladding alloy oxidation.

Corrosion products released from component surfaces of a nuclear power plant primary loop can be carried with the coolant flow to the core, then deposit on the fuel elements and become activated. These activated corrosion products may again be released and carried by the coolant flow and subsequently deposited onto other component surfaces in the primary loop. This process which causes an increase in the local radiation levels is called activity build-up. The source term of this process, i.e. initial corrosion product release rate, is governed by the surface film properties of the component in question.

Steam generator surface area forms about 70% of the total surface area exposed to the coolant. Thus the corrosion product release from steam generator surfaces is dominating the extent of activity build-up in Pressurised Water Reactors (PWRs). In case of a new PWR plant the first passivation treatment during the hot conditioning period (also called Hot Functional Test (HFT)) is crucial in creating a surface film with as low as possible corrosion product release rate. This paper describes results from a literature study on the optimisation of the hot conditioning water chemistry as well as development of new tools for monitoring the progress of passivation during the hot conditioning period.

Fuel cladding alloy oxidation

The CDE method developed for studying fuel cladding oxidation in situ has been described in detail earlier [1]. The main measurement technique used within the CDE method has been the Electrochemical Impedance Spectroscopy (EIS) and its variation called Contact Electric Impedance (CEI) Spectroscopy. Interpretation of the EIS and CEI results has been performed through the development of the Mixed Conduction Model [2]. The combination of an in situ method and the modelling tool, both developed as part of this project (in co-operation with the University of Chemical Technology and Metallurgy in Sofia, Bulgaria) has several advantages. Firstly, a ranking order for cladding alloys from different manufacturers and with different material chemistry can be established in a very short time, less than 100 hrs, when comparing with the exposure times of several hundred days when using the conventional weight gain technique. This has been verified for both BWR and PWR water chemistries [5, 4]. Figure 24.1.1 shows, as an example, the comparison of Zircaloy-2 (nominally same composition) from five different suppliers (exposure time 72 hrs, BWR water at 288 ^{o}C). The higher the impedance (resistance to alternating current) at low frequencies the lower is the oxidation rate of the cladding alloy. Secondly, the modelling approach gives a totally new view of the rate limiting steps in the oxidation process and thus helps in determining the dominating mechanisms of the process [5].

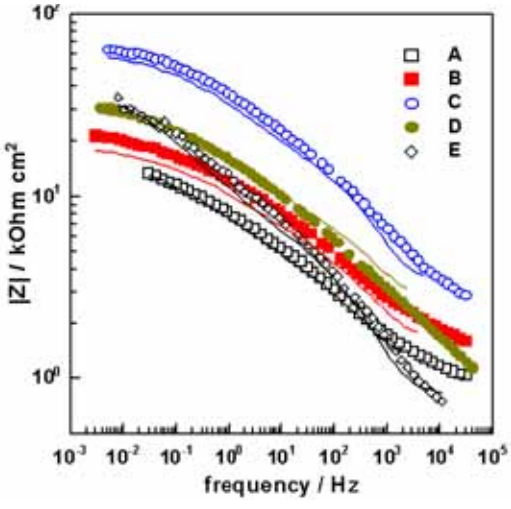

Figure 24.1.1. EIS results for Zircaloy-2, five different suppliers, 72 hrs test in BWR water at 288 °C. Alloy C showing the largest impedance and thus highest resistance for oxidation has also shown the best in-reactor performance [5].

For a PWR plant, water chemistry guidelines typically set a maximum allowed concentration of alkali at 2.2 ppm of Li^+ (corresponding to 12.5 ppm of K^+ in case of a WWER plant). There is a trend to extend the fuel cycle from the typical 12 months to 18 or even 24 months. This calls for a higher concentration of boron (as boric acid) in the coolant in beginning of cycle. The higher concentration of boric acid then needs to be compensated with a higher concentration of alkali, i.e. LiOH, to achieve the high temperature pH of about 7.2 which is optimal from corrosion point of view. One of the threats in increasing the alkali concentration is increasing oxidation rate of the fuel cladding alloy.

The CDE method was modified for PWR usage and verified by investigating the effect increased alkali concentration on fuel cladding oxidation as revealed by changes in the impedance response. Figure 24.1.2 shows a comparison of impedance of the Zr-1Nb alloy (E110) as a function of alkali (K^+) concentration. While an increase from 12 ppm to 28 ppm showed no effect on impedance, further increase to 56 ppm of K^+ resulted in a decrease of impedance by a factor of about two. This indicates that the Zr-1Nb fuel cladding alloy is not very sensitive to a moderate increase of alkali concentration above the current specified upper limit.

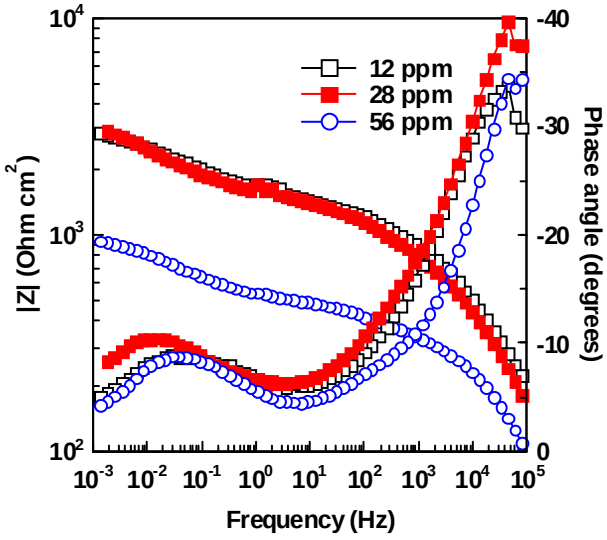

Figure 24.1.2. Effect of increasing alkali (K^+) concentration on the impedance of Zr-1Nb (E110) fuel cladding alloy under WWER water chemistry conditions at 310 ^oC.

Optimisation of hot conditioning

The tubing material selected for steam generators in modern PWR's is mainly Alloy 690. This has been the trend after Alloy 600 tubing was found to suffer from IGSCC in several plants. PWRs in Germany have used also Alloy 800 with good history, while in the Russian type PWR reactors (WWER) Ti-stabilised stainless steel has been used in steam generator tubing, also with a rather good history. The conditions (water chemistry, temperature) under which the first layer of the surface films forms largely determine the properties of the film in the long term. The water chemistry used during the first hot conditioning phase of a new plant is thus crucial with regard to the future behaviour of the plant (e.g. activity build-up rate and other corrosion product related degradation phenomena).

Until late 1970's the water chemistry used during the initial exposure period (hot conditioning) for PWRs was deaerated ion purified water. For Westinghouse PWRs (as reported by Garbett [13] in 1996) the normal method for reactor cooling system (RCS) passivation during the hot functional test (HFT) is to operate under alkaline conditions at 1–2 ppm lithium (added as LiOH) at T>260 °C, with Cl^- and F^- < 150 ppb, O_2 < 100 ppb (when T > 82 °C), SiO_2 < 200 ppb before boration and suspended solids < 100 ppb at the end of passivation. Originally passivation lasted six weeks but was later reduced to four weeks. EdF and Siemens (nowadays AREVA) performed the passivation under similar conditions, EdF at about 300 °C for 240 hrs continuous operation at 2 ppm Li and Siemens at 1–2 ppm Li (as ^7Li) for > 50 hrs continuous operation until suspended solids were < 100 ppb. Although deoxygenated conditions were specified in each case, operation with normal concentrations of dissolved hydrogen was not required.

Yamada et al. [6] performed autoclave studies on the effect of Hot Conditioning water chemistry on corrosion product release rate from Alloy 600 and Alloy 690. After a 600 hr test run under simulated hot conditioning environment part of the specimens were exposed to simulated power operation conditions for an additional maximum 3000 hrs. The result shown in Figure 24.1.3 indicates that a combination of added dissolved hydrogen (H_2) and added lithium hydrogen (LiOH) results in the lowest release of Ni in the corrosion product.

Based on these results Yamada et al. proposed an "improved HFT water chemistry", which contained 0.5 ppm Li (as LiOH) and 30 $cm^3/kg\text{-}H_2O$ of dissolved H_2. This water chemistry was used for the HFT period of Tomari 1

plant in 1989. The Fe and Ni concentrations during the HFT period of the Tomari 1 plant shown in Figure 24.1.4 indicate a dramatic improvement over that in earlier plants using deaerated water during the HFT period. The dose rates measured at the 1st annual inspection were on average 40% lower than those at preceding plants (where dearated water was used during HFT). About half of the improvement was evaluated to be the result of the improved HFT water chemistry. Since then, similar hot conditioning water chemistry has been used in Japanese PWR plants with good results (e.g. Ikata 3 in 1994 [7] and Genkai 4 in 1997 [8]).

In all PWRs the boric acid make-up systems are tested during hot conditioning, but the boric acid concentrations used are variable and do not approach start-of-the-cycle boron levels. Based on loop results [9] and data from Emsland PWR plant it is known that an addition of boric acid causes a considerable increase in corrosion product levels. The use of boric acid during hot conditioning as well as the minimum time required for proper passivation are still open issues for further research.

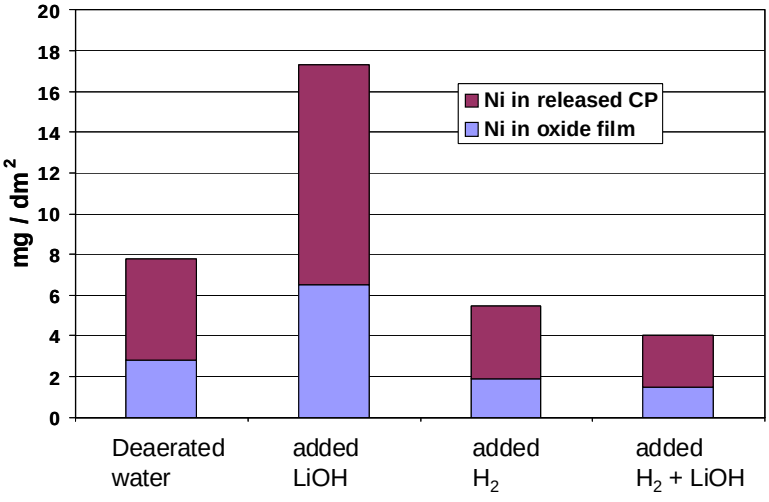

Figure 24.1.3. Relations between the water chemistry and amount of Ni in CP (Alloy 600), CP = Corrosion Product (redrawn from [6]).

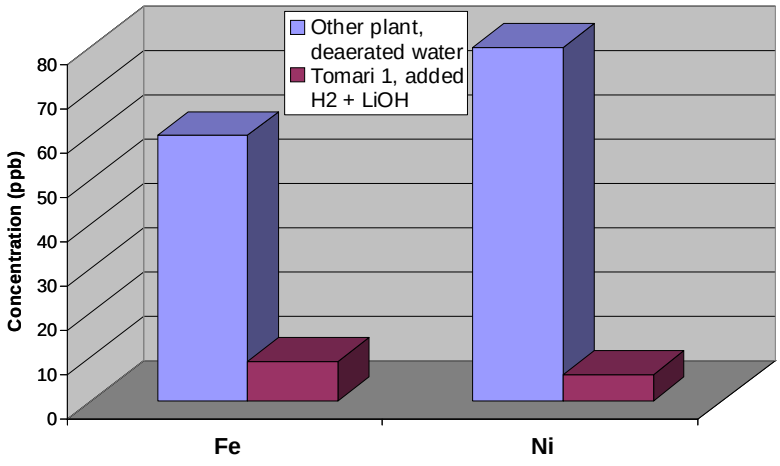

Figure 24.1.4. Concentrations of Fe and Ni in two Japanese reactor coolant systems during Hot Conditioning period (redrawn from [6]).

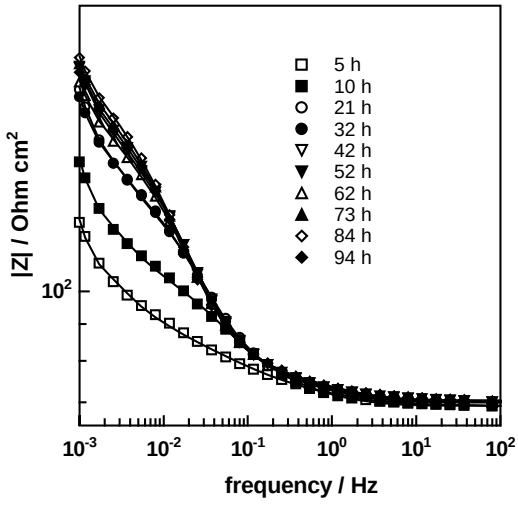

Figure 24.1.5. Impedance of carbon steel (250 °C, 30 ccH_2/kgH_2O, 1 ppm Li^+) as a function of exposure time [3].

The quality of passivation during Hot Conditioning has been traditionally measured using coupon type specimens which are extracted after certain exposure times and investigated using weight gain measurement as well as microscopy. In this work new methods based on electrochemistry have been

developed to allow on-line monitoring of the passivation. In co-operation with the Bhabha Atomic Research Centre (BARC), India, the CDE method was modified and verified for carbon steel in the Pressurised Heavy Water Reactor (PHWR) environment. The results [3] show that the magnetite oxide layer growing on carbon steel at 250 °C and in a typical water chemistry of PHWR hot conditioning saturates within about 30 hrs exposure time, Figure 24.1.5. As an alternative method, estimation of the defect density in the formed oxide layer by Mott-Schottky plots generated from room temperature EIS measurements was studied [10].

Conclusions

Based on the results gained the following conclusions can be made:

- The CDE-method developed for in situ investigations of surface oxides forming on nuclear power plant structural materials has been shown to be a reliable and versatile tool. Together with the modelling method (Mixed Conduction Method) a ranking order for fuel cladding alloys can be formed based on a very short exposure time (less than four days). This represents a considerable improvement on the traditional weight gain method requiring exposures up to several hundred days.
- Additional insight on the mechanism of oxidation as well as on the effect of water chemistry variables can be effectively gained by the new CDE method.
- The in situ method based on impedance spectroscopy has been verified to be applicable also in case of carbon steel in PHWR hot conditioning studies.
- The optimal water chemistry for hot conditioning of PWRs consists of 0.5–1 ppm Li^+ and 25–30 ccH_2/kgH_2O. The minimum time required as well as the role of boric acid are issues for further research.

References

1. Bojinov, M., Laitinen, T., Moilanen, P., Mäkelä, K., Mäkelä, M., Saario, T. & Sirkiä, P. Development of a controlled-distance electrochemistry arrangement to be used in typical power plant environments. VTT Research Notes 2039. Espoo: VTT Technical Research Centre of Finland, 2000. Pp. 1–48.

2. Beverskog, B., Bojinov, M., Kinnunen, P., Laitinen, T., Mäkelä, K. & Saario, T. A mixed-conduction model for oxide films on Fe, Cr and Fe–Cr alloys in high-temperature aqueous electrolytes—II. Adaptation and justification of the model. Corros. Sci., 2002. Vol. 44, No. 9, pp. 1923–1940.

3. Bojinov, M., Gaonkar, K., Ghosh, S., Kain, V., Kumar, K. & Saario, T. Characterisation of the oxide layer on carbon steel during hot conditioning of primary heat transport systems in heavy-water reactors. Proposed for publication in Corrosion Science Journal.

4. Bojinov, M., Cai, W., Kinnunen, P. & Saario, T. Kinetic parameters of the oxidation of zirconium alloys in simulated WWER water – effect of KOH content. J. Nuclear Materials. Accepted for publication.

5. Bojinov, M., Hansson-Lyyra, L., Kinnunen, P., Mäkelä, K., Saario, T. & Sirkiä, P. In-Situ Studies of the Oxide Film Properties on BWR Fuel Cladding Materials. Journal of ASTM International, 2005. Vol. 2, No. 4, pp. 183–198.

6. Yamada, E., Suzuki, S., Hirao, T., Hashimoto, Y., Hisamune, K. & Yokoyama, J. Corrosion rate reduction by chemical control during Hot Functional Testing. Proc. of 1991 JAIF International Conference on Water Chemistry in Nuclear Power Plants. Fukui, Japan. Pp. 151–156.

7. Kadoya, M. Countermeasures for radiation dose reduction at Ikata Unit No.3. Ikata Unit No.3 countermeasures for radiation dose reduction. Proc. 10. International congress of the International Radiation Protection Association. Hiroshima (Japan), 14–19 May 2000. Paper number P-6a-296. 6 p.

8. Ito, A., Murata, K. & Yokoyama, J. Water chemistry during stratup testing at the latest PWR: Genkai Unit No. 4. Proc. 1998 JAIF international conference on water chemistry in nuclear power plants. Kashiwazaki, Japan, 13–16 Oct 1998. Pp. 806–811.

9. Eley, C., Thomas, D., Libaert, D., Cattell, R., Garbett, K. & Woolsey, I. Monitoring of soluble species in the NP SCEPTRE loop. Water chemistry of nuclear reactor systems 6, BNES, London, 1992. Pp. 224–226.

10. Bojinov, M., Gaonkar, K., Ghosh, S., Kain, V., Kumar, K. & Saario, T. Estimation of the minimum time needed for saturation of the oxide layer on carbon steel during hot conditioning of primary heat transport systems in heavy-water reactors. To be proposed for publication in Journal of Nuclear Materials.

25. Monitoring of the structural integrity of reactor circuit (RAKEMON)

25.1 RAKEMON summary report

Ari Koskinen
VTT

Abstract

Developing techniques and monitoring systems that can be used to monitor the structural integrity of the primary circuit components is quite essential. Pilot monitoring system was developed and constructed during 2007 and 2008. Monitoring test will be performed in the later stage with austenitic stainless steel (316LN) pipe. The final aim will be to develop measurement systems both for detection and analysis of macroscopic flaws and microscopic changes in the material that are often preceding the macroscopic failure

It is also necessary to develop inspection techniques that can be applied to reactor circuit components where the access is restricted and decreasing the reliability of inspection. The geometry and the material properties of the component to be inspected must always be considered when an ultrasonic test is planned. Ultrasonic inspection simulations for difficult geometries (nozzles) and anisotropic weld metals were done with simulation program CIVA 8.

Fibre optical monitoring methods have been developing rapidly in recent years and nowadays there are already fibres that can resist radiation. Also methods for correcting measurement errors arising from radiation induced attenuation have been developed. The potential of using fibre optical monitoring technology in nuclear environments was evaluated in 2008. It was noticed that metal embedded fibres are in strong compression and polymer coating is eliminated. Therefore it

could be possible that drift in Bragg wavelength due to volumetric changes and radiation induced hydrogen evolution from the polymer coating on the fibre could be eliminated with metal embedded fibres.

Closed cracks are very dangerous because they can stay undetected for many inspection cycles due to inspection restrictions related to closed cracks. A new ultrasonic method has been developed for these closed cracks. The subharmonic ultrasonic inspection is developed at Tohoku University Japan and it seems to be very promising for these dangerous closed cracks.

Introduction

Non-destructive testing techniques are used to monitor the condition of the structures of reactor circuit during the operation of nuclear power plants. The in-service inspections (ISI) are normally performed during the shutdown period but there is also increasing need to monitor the condition of components during service by on-line methods. The tendency worldwide and also in Finnish nuclear power plants is to improve the efficiency of in-service inspections by applying risk-informed methods to the selection of inspection items, methods and timing of in-service inspections. This kind of ISI-programme is supported by on-line monitoring techniques that are used to focus the inspections to areas where failures are most probable and/or consequences are most severe.

There is a specific need to improve the reliability of NDE-techniques used for the ISI of bimetallic welds and inspection items where access is limited. Ultrasonic simulation can be used to optimize the inspection techniques for these problematic inspection areas.

The aim of RAKEMON project is to develop techniques and monitoring systems that can be used to monitor the structural integrity of the primary circuit components. The aim is to develop measurement systems both for detection and analysis of macroscopic flaws and microscopic changes in the material that are often preceding the macroscopic failure.

It is also necessary to develop inspection techniques that can be applied to reactor circuit components where the access is restricted and decreasing the reliability of inspection. This kind of inspection items are e.g. welds with coarse grain size and nozzle welds where the difficult geometry is restricting the performance of inspection.

International atomic energy agency (IAEA) has launched a coordinated research programme (CRP) on advanced, surveillance, diagnostics and prognostics techniques used for health monitoring of systems, structures and components in

nuclear power plants. RAKEMON project is taking part of this international project which started in 2008 and lasts for three years.

Monitoring of the structural integrity of reactor circuit

On-line monitoring is defined as an automated method of monitoring instrument output signals and assessing instrument calibration while the plant is operating, without disturbing the monitored channels. In the simplest implementation, redundant channels are monitored by comparing each individual channel's indicated measurement to a calculated best estimate of the actual process value. This best estimate of the actual process value is referred to as the process variable estimate or estimate. By monitoring each channel's deviation from the process variable estimate, an assessment of each channel's calibration status can be made. An on-line monitoring system can also be referred to as a signal validation system or data validation system [1].

Data transfer and archive

The data amount produced in the typical ultrasonic inspection is large and transfer of this data from the primary circuit to monitoring room is challenging. Also because of the large amount of data, properly working archiving system is essential. The possibilities for data transfer from transducers placed on primary components to monitoring room or data storage locating outside the containment are being reviewed. Information concerning the existing instrumentation cabling used for temperature and vibration monitoring currently on site was gathered from the literature. Also different types of archiving systems in different industrial applications have been gathered from the literature. Possibilities for wireless data transfer will be studied in cooperation with data transfer experts at VTT.

Pilot monitoring system and monitoring tests

Pilot monitoring system is designed for monitoring the structural integrity of a component in nuclear power plant's primary circuit. In 2007 the basics for the design of monitoring system was studied and the components were outlined. In 2008 construction of pilot monitoring system for ultrasonic online monitoring has been done and preliminary tests have been started. After successful tests on conventional methods, more advanced probes and inspection methods for the monitoring system will be studied. Advanced version of the monitoring system will be constructed in the later stage of the project.

The system itself includes the inspection item, ultrasonic and heating equipment and adjustable frame. The inspection item is austenitic stainless steel pipe (316LN). Dimensions of the pipe are:

- Length is 300 mm
- Outer diameter is 168.7 mm
- Wall thickness is 14.1 mm.

The basic idea of this system is to monitor flaws in this pipe for longer periods. Typically flaws appear in the welding zone but in this case they are produced in the base material. The actual cracks are produced by thermal fatigue and their dimensions and locations are precisely documented (Figure 25.1.1). There are also EDM-notches for comparing the indications from cracks and notches.

ANNEX 2. DETAILED FLAW INFORMATION

Red dye penetrant image		
	Trueflaw 308AIB875 1 mm	
Crack characteristics	Cracking mechanism:	thermal fatigue
	Crack location:	base material
	Material grade:	AISI 316LN
	Material group:	austenitic stainless steel
	Material thickness:	14.1
	Length:	16.6 mm
	Depth:	4.5 mm
	Skew:	7°
	Average opening:	36.2 µm
	Median opening:	35.1 µm
	Macroscopic branching:	0
	Turns:	1
	Discontinuities:	0
Measurement anomalies	No anomalies.	
Measurement information	Image resolution:	976.3 px/mm
	Signal to noise threshold:	6.0
	Measurement length for Ra etc.:	1500 µm
	Measurements length for turns:	500 µm
	Date and time of measurement:	2008-12-21 14:25:15

Figure 25.1.1. Example of detailed flaw information.

The cracks are produced in-situ to the inspection item with controlled thermal fatigue loading. The cracks grow with natural thermal fatigue damage mechanism. The crack location in the inspection item is affected by the local material properties. Especially if the sample contains stress risers or marked homogeneities the cracks grow in to the natural weakest location. There are no artificial initiators used in the process and the microstructure of the inspection item has not been changed. The true crack depth is known through Trueflaw destructive validation [2].

Inspection of items with limited access, difficult geometry or unfavourable grain structure

The geometry and the material properties of the component to be inspected must always be considered when an ultrasonic test is planned. In many cases these factors can be challenging and careful examination of the case is needed to ensure reliability of the inspection. Simulation of the ultrasonic inspection using computer program (CIVA 8) can be one part of necessary work providing tools to study how the ultrasonic beam is propagating in structure and what kind of signals can be expected to be received from the reflectors in the inspection area. The difficult inspection geometries (nozzles) and anisotropic weld metals (Figure 25.1.2) have been modelled in 2007 and 2008 with simulation program CIVA version 8.

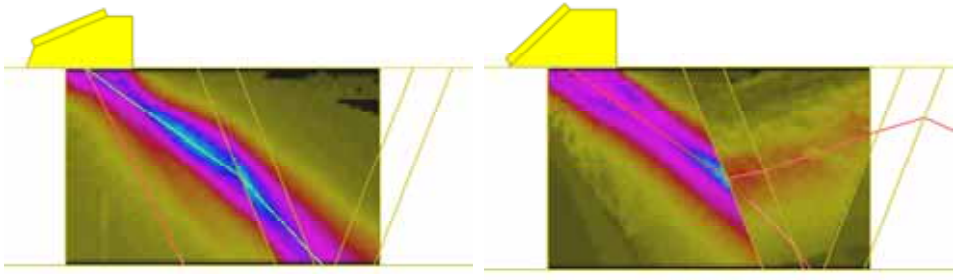

Figure 25.1.2. The ultrasonic beam in anisotropic weld material (55° / 2 MHz probe). Left using longitudinal wave mode, right using shear wave mode [3].

Recently promising results have been achieved by applying Phased Array-technique to in-service inspection of piping and components of nuclear power plant. One challenging task is to detect and determine defects locating below or inside the austenitic cladding of reactor pressure vessel. By applying phased

array technique in data acquisition and SAFT-algorithm for data analysis the reliability of the inspection can most probably be remarkably improved. In 2008 the application of phased array technique to anisotropic weld metal was experimentally tested by using test blocks containing defects. Inspections were done with Omniscan phased array system and with two 32 channel probes (transmit-receiver). The data collected with Omniscan phased array system was transferred to Ultravision for data analyse.

Choice of fibre optical monitoring methods

It has generally been assumed that fibre optical sensors cannot be used in high radiation environment due to radiation induced light attenuation in the fibre. This is not completely true anymore because radiation resistant fibres have been developed as well as methods for correcting measurement errors arising from radiation induced attenuation. Raman distributed temperature sensing has been demonstrated for example with fibres wound along the primary loop of the experimental fast reactor JOYO in Japan. In this experiment the fibre got a total gamma dose of more than 7.7 × 103 C/kg (0.26 MGy in air). For a fibre placed on the primary loop of a commercial light water reactor this dose would correspond to more than 35 years of use [4].

Fibre Bragg gratings (FBGs) can be used to measure for example temperature and/or strain. For FBGs the strain and/or temperature information in wavelength coded, so a variation in intensity is not critical as long as the Bragg peaks can be detected well above the noise level. SCK-CEN has tested a special type of Bragg gratings (so called Chemical Composition Gratings, CCGs) in the core of their BR2 reactor to a total gamma dose in excess of 1.5 GGy and to a neutron fluence of 7.5 × 1019 n cm-2 [4]. The CCGs remained fully functional but a drift in Bragg wavelength was observed. This shows that all problems are not solved, but that the FBGs have potential even for incore monitoring.

It has been assumed that radiation induced hydrogen evolution from the polymer coating on the fibre degrade the FBGs. Further, radiation induced volumetric changes of the fibre may be responsible for the drift in Bragg wavelength. Metal embedded fibres are in strong compression and the volumetric changes may therefore be minimal; the polymer coating is also eliminated. It would be essential to repeat the irradiation tests with metal embedded high temperature stable FBGs.

The potential of using fibre optical monitoring technology in nuclear environments was evaluated in 2008. Also international research networks have been utilized in the evaluation process. The focus has been on monitoring needs where traditional electrical sensors do not work well and on monitoring issues where an electrical sensing solution exists.

Subharmonic ultrasonic inspection

The new ultrasonic method for imaging closed cracks based on subharmonic ultrasound has been developed at Tohoku University in Japan. Reliability and applicability to inspection of real NPP components with this method will be studied in 2009. Reliable inspection would be an important progress in the detection of dangerous closed cracks. The focus of this study in 2008 has been on a literature study and international networks by contacting the involved scientists in Japan and also elsewhere.

Steam Generator lifetime monitoring

In 2009 there will be new area of research concerning steam generator lifetime monitoring attached to RAKEMON project. Steam generators are one part in the PWR type nuclear power plant that can be restricting the lifetime of the plant. In those steam generators there is magnetite deposition on tubing and between tubes. The inspection data of steam generators contain also additional information than flaw indications. Recently eddy current data has been applied to show locations of magnetite deposition on tubing. Improvement of eddy current analysis, e.g., concerning magnetite deposition on tubing or between tubes and flaw sizing will be started in 2009 by performing literature review. Also an experimental study on detecting magnetite deposition between tubes will be made in 2009.

Understanding the variations in the local environmental condition facilitating iron deposition in steam generators should be improved. Pertinence of water chemistry based predictions, NDE monitoring results concerning iron deposition and plant observations and experience should be discussed and documented.

Conclusions

Developing techniques and monitoring systems that can be used to monitor the structural integrity of the primary circuit components is quite essential. The aim

is to develop measurement systems both for detection and analysis of macroscopic flaws and microscopic changes in the material that are often preceding the macroscopic failure.

It is also necessary to develop inspection techniques that can be applied to reactor circuit components where the access is restricted and decreasing the reliability of inspection. This kind of inspection items are e.g. welds with coarse grain size and nozzle welds where the difficult geometry is restricting the performance of inspection.

Fibre optical monitoring methods have been developing rapidly in recent years and nowadays there are already fibres that can resist radiation. Also methods for correcting measurement errors arising from radiation induced attenuation have been developed.

Closed cracks are very dangerous because they can stay undetected for many inspection cycles due to inspection restrictions. There has been new ultrasonic method developed for these closed cracks. The subharmonic ultrasonic inspection is developed at Tohoku University, Japan and it seems to be very promising for these dangerous closed cracks.

References

1. On-line Monitoring for Improving Performance of Nuclear Power Plants, Part 1: Instrument Channel Monitoring. IAEA-NE-D-NP-T-1, IAEA, VIENNA, 2007. 137 p.

2. Kemppainen, M. Realistic Artificial Flaws for NDE Qualification – A Novel Manufacturing Method Based on Thermal Fatigue. Doctoral dissertation. TKK Dissertations 35. Espoo: TKK, 2006. 93 p.

3. Sarkimo, M. Study about the Applicability of Civa Version 8 in Difficult Inspection Geometries. VTT-R-01108-08, VTT Research Report. Espoo: VTT, 2008. 15 p.

4. Sandlin, S. Applicability of Distributed Fibre Optical Temperature Sensing and Fibre Bragg Gratings in Nuclear Radiation Environments. VTT-R-13509-07, VTT Research Report. Espoo: VTT, 2007. 16 p.

25.2 Ultrasonic inspection simulations with Civa version 8

Ari Koskinen and Matti Sarkimo
VTT

Abstract

The geometry and the material properties of the component to be inspected must always be considered when an ultrasonic test is planned. In many cases these factors can be challenging and careful examination of the case is needed to ensure reliability of the inspection. Simulation of the ultrasonic inspection using computer program can be one part of necessary work providing tools to study how the ultrasonic beam is propagating in structure and what kind of signals can be expected to be received from the reflectors in the inspection area. The well done preparation including simulation of the inspection usually decreases inspection time drastically and therefore can also decrease total inspection costs. There are also other aspects that can be improved with simulations. For example health aspect in nuclear power plants where it is essential to keep the inspection time as low as possible due to radiation exposure.

The features and possibilities of Civa version 8 ultrasonic simulation program to take into account material properties and geometry of the inspection object are discussed in this article. Using examples some possibilities are shown how the inspection of a challenging nozzle geometry could be performed and which echoes are seen in the simulation results.

Introduction

The geometry and material properties of a component set in many cases limitations and conditions that have to be considered when an ultrasonic inspection is planned and performed. Issues that have to be taken into account are for example:

- how the ultrasonic beam is formed in the component geometry and material and how well it is hitting the volume to be examined
- what kind of geometric echoes produces the structure itself
- how the changing material properties or different material layers influence on the sound propagation.

Simulation of the ultrasonic inspection can provide tools to study the questions presented above. It helps to plan the inspection for example in the design of the scan plans and optimisation of the probes. During the signal interpretation phase simulations can be helpful in reasoning of signal origins.

Some of the features of Civa version 8 ultrasonic simulation program which make it possible to take into account different geometric and material properties of the component are described in this article. This is mainly done through simulation examples of a difficult nozzle geometry.

Possibilities to apply different inspection geometries in Civa

NDT inspection geometries can vary from plane or cylindrical piece to almost any kind of complex geometry. In Civa program there are “standard” component models available in the program itself and more complex geometries can be added with CAD tools [1].

Available “standard” components

The user can define the component to be inspected just by giving parameters of available “standard” component models. The available geometry types are: plane, cylindrical piece, conical piece, spherical piece, elbow and nozzle. In Figure 25.2.1 is shown as an example the way how two different simple inspection components can be defined in Civa program just by giving the values for component main dimensions. The geometry of the other “standard” components is defined in similar way.

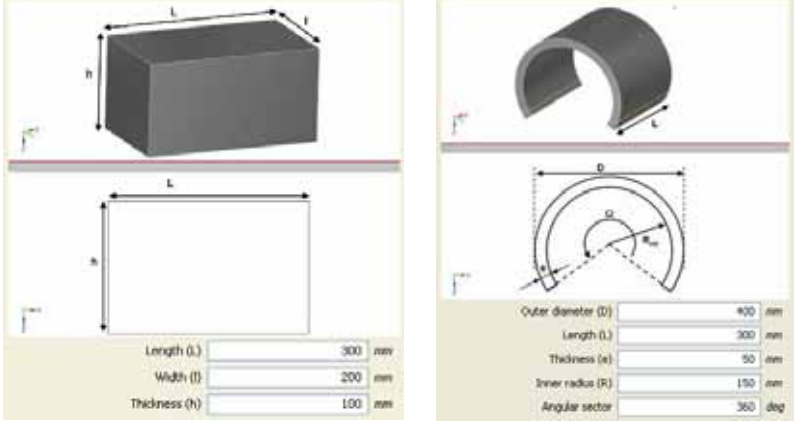

Figure 25.2.1. Two examples of definition of “standard” components in Civa. Planar component (left) and cylindrical component (right).

Component design using CAD tools

More complicated geometric details can be included in planar and cylindrical components using two dimensional CAD option. The component profile is designed using some external CAD program or using simple drawing tools included in Civa. The three dimensional component is finally defined in Civa by extrusion or rotation of the profile as shown in Figure 25.2.2. Both beam computation and defect response computation modules of Civa are able to use this type component models.

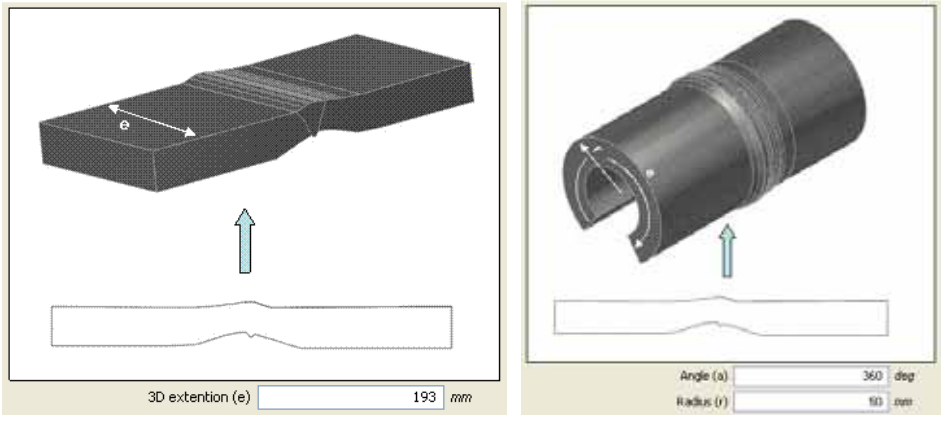

Figure 25.2.2. Definition of component using extrusion and rotation of a profile designed in a CAD program.

A component can also be designed as 3D model using an external CAD program and then be imported into Civa in STEP or IGES file format. But in the current Civa version (version 8) this kind of component models can be applied only in the beam computation module. Thus shapes of the ultrasonic beam and sound propagation can be examined in these component models but it is not possible to compute ultrasonic responses from reflectors.

Nozzle geometry example

A nozzle geometry with conical sections on the outer surface and complex weld design as shown in Figure 25.2.3 is a challenging inspection object for ultrasonic method. In such a case simulations can clearly help to plan the inspection. Some simulation examples with this geometry are given in the sections below. The applied probe model is a 70° transmit-receiver longitudinal wave probe operating

with 2 MHz frequency (70°TRL 2) which is scanning on the conical surface of the nozzle. Examples of both modelled beam form and defect response results are given.

The 3D model of the example nozzle can be produced using the rotation of a 2D profile as shown at the top of Figure 25.2.3. Because some computation options are possible only in planar component models the tubular nozzle model had to be simplified for those cases to a planar component which is shown at the bottom of Figure 25.2.3. This planar component presentation also reveals the details of the weld construction.

Figure 25.2.3. The original tubular nozzle geometry and the simplification to planar geometry model. In the planar geometry the weld design details can be seen.

Ultrasonic beam computation in nozzle geometry

An example of the sound field computation and visualization in the original tubular geometry is shown in Figure 25.2.4.

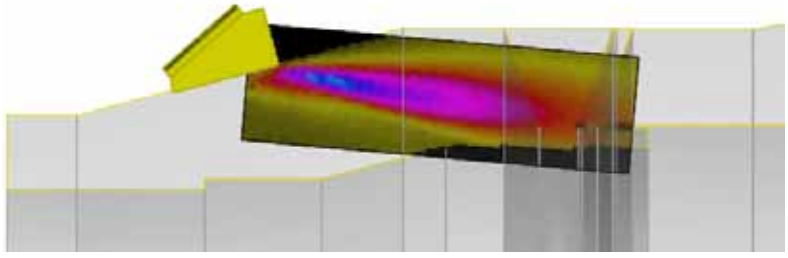

Figure 25.2.4. Ultrasonic field of 70° TRL 2 probe in cylindrical geometry.

Further examples of the sound field computation were produced using the planar geometry, see Figure 25.2.5. In these simulations the sound beam is presented in different phases when the probe is moving along the conical surface. It can be seen that the sound beam form is quite similar with the result in the tubular geometry but the component details are more clearly visualized.

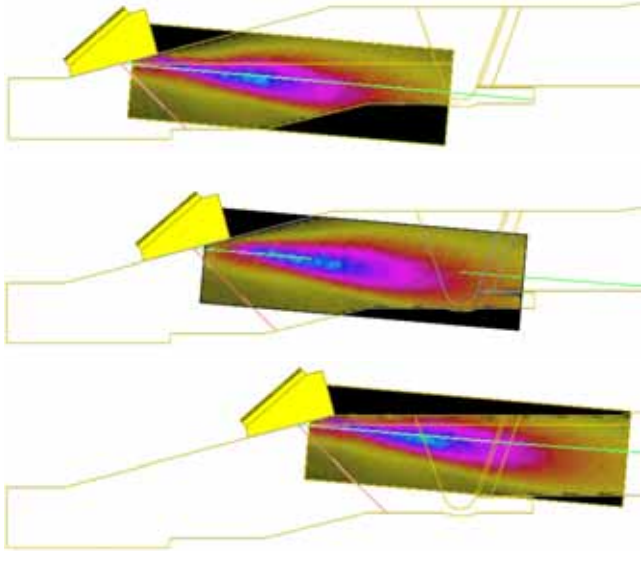

Figure 25.2.5. Ultrasonic field of 70° TRL 2 probe in three phases of the scan.

The simulation results show that the focus area of the sound field (the probe is focussed at 60 mm along the sound path) is not reaching the weld root, only the zones of the beam with lower sound pressure values are hitting the root area. On the other hand the sound beam direction is optimal for detection of vertical defects at the weld root.

Reflector response computation in nozzle geometry

When reflector responses are computed using Civa version 8 there are limitations concerning applicable component geometry. In the nozzle example case only the planar geometry can be used to compute the back wall echoes when the scan direction is towards the weld. A further limitation for back wall echo computation is that the component has to consist of homogenous material. Only signals produced by flaws are computed if the component includes several material layers as shown in Figure 25.2.6. This realistic model of the example nozzle geometry consist of different materials zones (carbon steel, stainless steel and buttering between those).

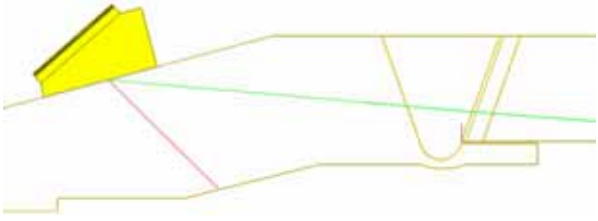

Figure 25.2.6. Inspection geometry with weld and buttering layer connecting carbon steel and stainless steel parts. A vertical, rectangular flaw shown with red colour in the weld root area.

In Figure 25.2.7 below are shown two examples of defect response computation using component geometry with several material layers. Rectangular defect (5 x 10 mm) is located above the weld backing as shown in Figure 25.2.6 in vertical and tilted orientation. During the simulation the probe has been scanning the whole length of the conical section of the component. Thus the sound path is long and sound beam opening is large producing indication pattern that continues far above the flaw. It can be noticed that the influence of the flaw tilt is very small on the indication pattern received.

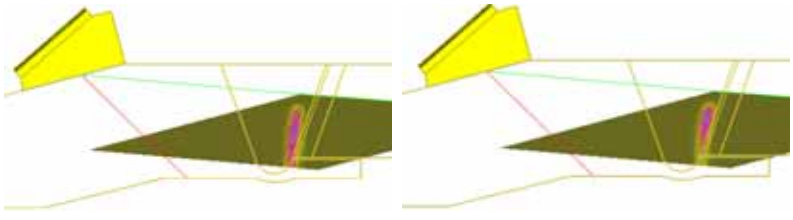

Figure 25.2.7. Flaw indication in the component geometry with different material layers. Vertical flaw (left), flaw tilted along the weld groove (right).

To be able to include also the geometric indications from the back wall in the simulation result the component geometry was changed in such way that it consisted only of homogenous material without any material boundaries as shown in Figure 25.2.8. In this geometry different flaw sizes and positions were applied in the simulations performed. The weld backing is leaving a narrow gap near the weld root. In the simulation the height of this gap was 0.5 mm. The flaws applied in the simulations were located to start upwards and downwards from the end of the gap as shown in Figure 25.2.8.

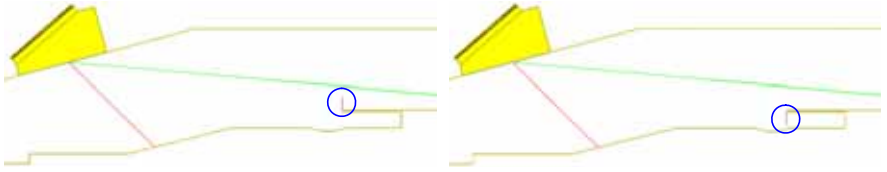

Figure 25.2.8. Nozzle geometry consisting of homogeneous material. The two flaw positions in relation to the gap formed by the weld backing are shown: defect upwards from the gap (left) and defect downwards from the gap (right).

The Figure 25.2.9 shows the principle how the indications are formed in simulations using the homogenous material. Two indications can be seen in the B scan presentation. One of these indications is produced by the end of the narrow gap and the flaw at this same location (summary indication) and the other indication is formed by the end of the weld backing.

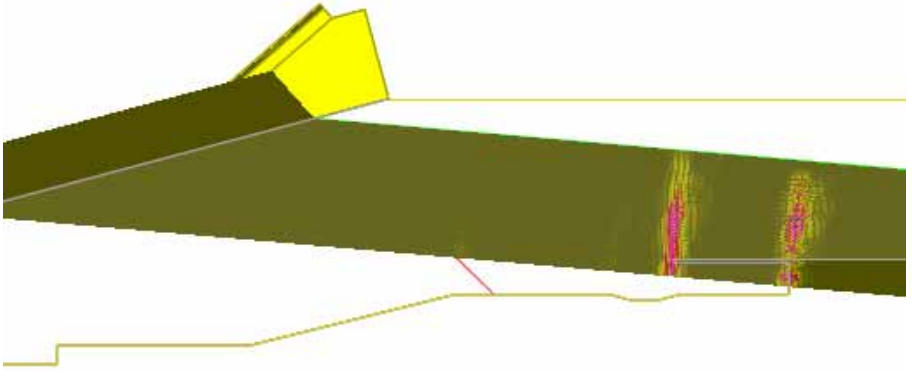

Figure 25.2.9. Simulation result showing the signals from component geometry and defect located at the gap formed by the weld backing.

To examine how the defect position and size are influencing on the indication signals different simulation results in B scan format are recorded in Figure 25.2.10. In these simulations the whole conical length of the component was scanned. In these results it can be seen that the component geometry itself produces two indications: one at the end of the weld backing and the other (smaller) at the end of the narrow gap. It can also be seen that the flaw signal at end of the gap is always summarized with the geometric echo but it clearly increases the signal amplitude even if the flaw depth is small. The location of the flaw upwards or downwards from the gap end has very small influence on the signal amplitude, pattern and position. Anyhow a third indication can be seen when a large (4 mm) flaw is applied downwards. This third indication seems to be multiple echo from the end wall of the weld backing.

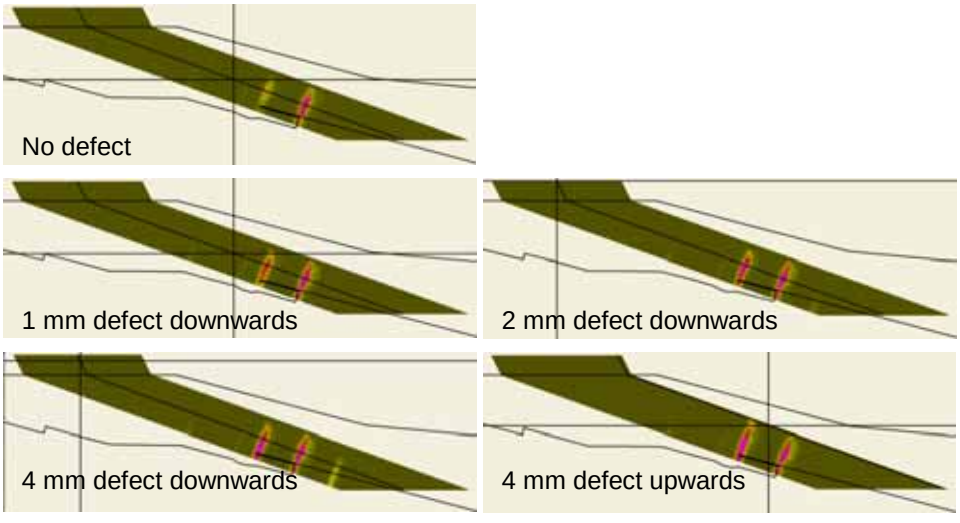

Figure 25.2.10. Indications computed with different defect sizes and positions in relation to the gap formed by the weld backing. B scans shown.

If the inspection scan is performed in the simulation in axial and circumferential directions the result is dominated by the strong and wide geometrical echoes. The D scan view (end view) is shown in Figure 25.2.11 where the high amplitude geometric echo from weld backing geometry is continuous in the circumferential direction. The flaw can be seen in this pattern as a rather small extension relating to the length of the flaw (total scan length in Figure 25.2.11 40 mm, flaw length 10 mm).

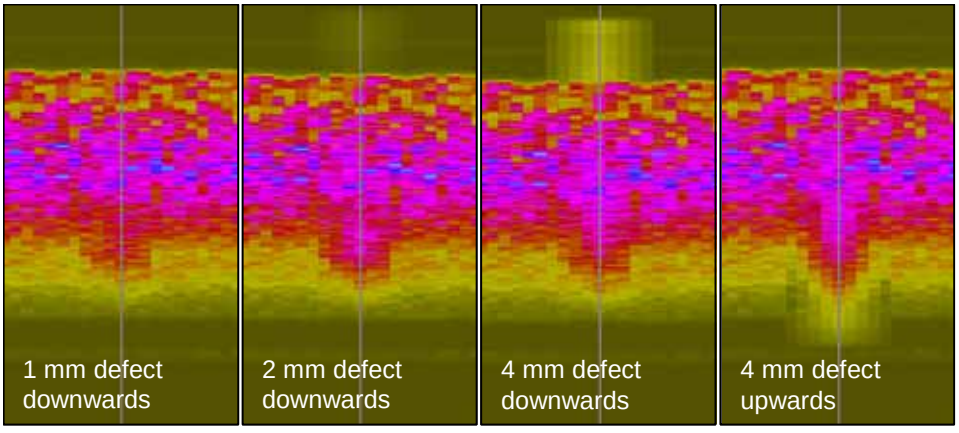

Figure 25.2.11. D scan results when scan is performed on the nozzle model conical sections both in axial and circumferential directions. The circumferential scan movement is in this presentation horizontal. The influence of the defect to signal pattern can be seen as an extension downwards at the cursor position.

The simulation was performed also using only circumferential scan. In this scan result the signals coming from weld backing end and from the end of the gap above the weld backing can be seen as separate lines because of the different arrival times, see Figure 25.2.12. The flaw located at the end of the gap produces stronger amplitude levels and can be thus distinguished from the geometric echo. Also the multiple weld backing end echo caused by large downwards directed flaws is visible in these simulation results.

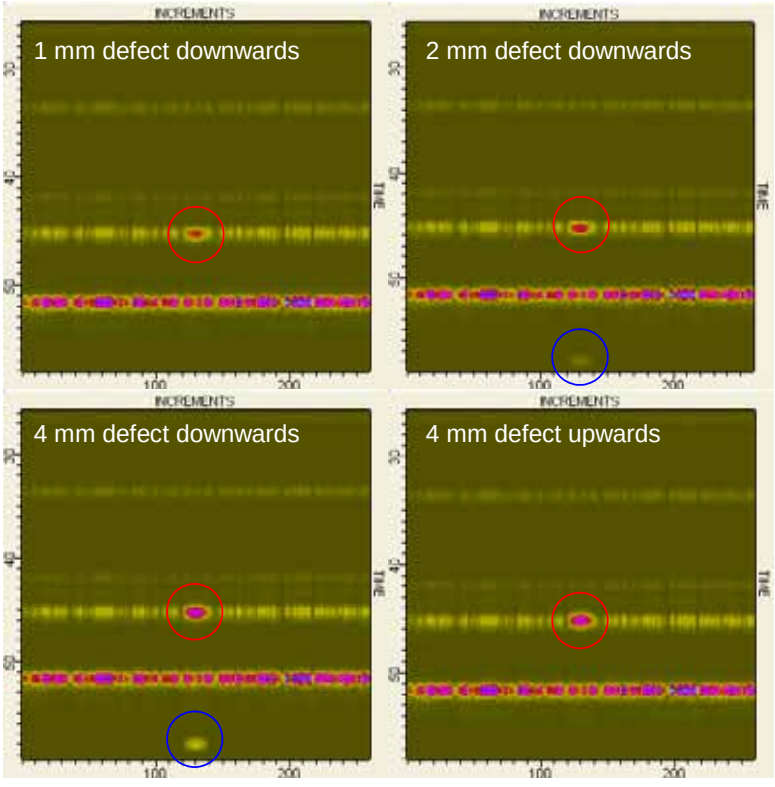

Figure 25.2.12. D scan results when scan is performed on the conical sections only in circumferential direction, total scan length 260 mm (horizontal increments of figures). The indication from defect marked with red circle, the multiple weld backing end echo marked with blue circle.

Conclusions

Simulation of an ultrasonic inspection is a fast developing area and in the future it will be used more and more for designing the scan plans and optimisation of the used probes. The current version of Civa (version 8) ultrasonic simulation program is able to produce simulations of rather demanding geometries. It has also options which can be used to take into account for example the anisotropic material properties. On the other hand the application of these features includes some limitations which lead in many cases to a need for simplification of the simulation case. For example the computation of the back wall echoes is limited to certain geometry models. Therefore the computation of the back wall echoes may require the change of a tubular component to a planar case. Also the application

of different material layers in the component construction sets certain limits to simulations that are possible to be computed.

The new version (version 9) of the Civa program is already available and it includes quite many new features. Some limitations presented in this article are therefore already solved in this new version.

References

1. CEA. Civa 8 user manual. Paris: Commissariat à l'énergie atomique, 2007.

26. Fracture assessment of reactor circuit (FRAS)

26.1 FRAS summary report

Päivi Karjalainen-Roikonen, Pekka Nevasmaa, Kim Calonius,
Antti Timperi, Otso Cronvall, Heikki Keinänen, Anssi Laukkanen,
Lauri Elers, Matti Valo and Tapio Planman
VTT

Abstract

The FRAS project (Fracture assessment of reactor circuit) project aims at (i) calculation of design and unforeseeable loads and their effects on a structure by applying numerical modelling; (ii) development of advanced fracture mechanics assessment tools and analysis methods based on material characterisation, damage mechanisms models and structural performance, in order to control structural failure both in cases of postulated initial flaw and environmentally assisted (internal) material damage; (iii) determination of degradation in material properties during service. This report summarises the results of the FRAS project after two years (2007–2008) of the four year project.

Introduction

During recent years several structural analysis assessment methods have been established. Nonetheless, need for more accurate methods in load definition, true 3D flaw assessment, as well as irradiation embrittlement evolution assessment, still remains. Generally, numerical simulation of loads has treated different components as separate, even though they belong to the same aggregate, thereby

disregarding the interaction of support loads on the entire system. Concerning loads, also local manufacturing process induced and often relatively high residual stresses, especially in load carrying welds, need to be researched further, including both the physical phenomenology as well as more realistic 3D numerical simulations. Applicability and limits of sub-modelling techniques in numerical simulation of crack growth need to be investigated further. Feasible 'engineering assessment tools' cannot be reliably applied, unless they have been tailored and verified for the particular plant and component in question. Traditionally, material's fracture toughness has been determined applying deep-notched 'high-constraint' specimens enabling conservative estimates to be derived. Sophisticated constraint corrections are required for shallow surface cracks with lower constraint, particularly in the case of asymmetric crack fronts during crack growth and to acquire representative assessment fracture properties. Present limitations for specimen's measuring capacity in fracture resistance testing and under ductile crack growth are presumably unrealistic and hence need revision. Unified model for irradiation embrittlement is still lacking, despite of intensive previous research. Recently, advanced multi-scale modelling techniques of material damage micromechanism have allowed micro-scale investigation of relevant damage mechanisms, without a necessity to postulate a pre-existing flaw and extent the usability of traditional fracture mechanics. This provides means for realistic material damage assessment for environmentally assisted failure, such as stress corrosion cracking, irradiation embrittlement, ageing embrittlement and hydrogen embrittlement that do not require the existence of pre-existing flaw. In conjunction with modern FEM structural analysis methods, the application of advanced modelling techniques enables realistic structural integrity assessment of a component, or structure, over an entire 'chain' from micro- to macro-scale.

Main objectives

The objectives for fracture risk assessment comprise (i) calculation of design and unforeseeable loads and their effects on a structure by applying numerical modelling; (ii) development of advanced fracture mechanics assessment tools and analysis methods based on material characterisation, damage mechanisms models and structural performance, in order to control structural failure both in cases of postulated initial flaw and environmentally assisted (internal) material damage; (iii) determination of degradation in material properties during service.

Definition of loads

The greatest uncertainties in the assessment of structural integrity of a component are often associated with accurate determination of loads. The subproject aims at calculating of design and unforeseeable loads & welding stresses and their structural effects by applying numerical modelling and analyses methods. These calculations contribute to crack growth analyses for reactor circuit components and, finally, the assessment of component's defect sensitivity. The study was concentrated in three specific areas.

Loads transferred by supports

The objective is to define the external loads transferred to the reactor circuit components by supports. During 2007–2008, finite element modelling methods provided by commercial Abaqus code for pipes and different types of supports and restraints were delineated. Stiffness propertises of pipes and supports were calculated with separate and combined models. A guillotine pipe break was chosen as a dynamic test case that was simulated with different kind ofs of three dimensional models. Larger models consisted of shell and solid elements. In smaller models they were substituted with special purpose elements. Simple and typical pipeline geometry and materials were chosen. Material properties were linear and everything was considered to be in room temperature. The results were compared with each other and their reliabilities were evaluated.

It was seen that in respect to the eigenmodes the pipe element model was adequate and almost as accurate as a shell element model with a fine mesh, especially when the pipe bend was modelled with elbow elements. Nonlinear spring elements were found to act realistically and seemed very suitable for moodelling restraints in this kind of dynamic problems. The dynamic analysis results of the pipe element model corresponded well to the ones of the much larger shell element model. [1]

Fluid-structure interaction

Thermal loads caused by static operational conditions and by various yearly anticipated and nonanticipated transients are usually the most significant loading input for crack growth calculations of reactor circuit components. For many components the detailed spatial variation of fluid temperature and heat transfer coefficient has to be known in order to determine stresses and hence the crack

growth rate. Therefore, simplified methods may not often provide sufficient data for these kinds of analyses and Computational Fluid Dynamics (CFD) calculations have to be pursued.

Buoyancy-driven flows have significance in many nuclear power plant applications where large temperature differences may exist in water. CFD calculations of buoyancy-driven flows have been validated for two simple geometries by using different turbulence models and settings. Buoyancy-driven flow around a thermal sleeve of an inlet nozzle in a HDR (Heißdampfreaktor) experiment was used as a more realistic validation case. Large-Eddy Simulations (LES) of thermal striping in a similar HDR experiment has been also performed. In the experiment, temperature fluctuations caused by instability between layers of cold and hot water flowing in a horizontal pipe were studied. The vortex method was implemented and validated for fully developed pipe flow in order to have realistic turbulent inlet conditions for LES. [2]

Weld residual stresses

Assessment of the structural integrity of critical components and structures in NPPs is of vital importance for safe operation. When assessing the structural integrity of a component, both the loading and the load carrying capacity are determined. The residual stresses are included in the analysis on either the loading or capacity side, depending on the design strategy.

Since residual stresses with various magnitudes and distributions are present in virtually all structurally engineered components, there is a demand for accurate assessment of the residual stress distributions, especially in critical components, e.g. NPP primary circuit component welds. The residual stress distributions present in a structure are the result of the manufacturing history and the elasticplastic properties of the structure. The former referring to the mechanical and thermal processes executed during the whole production sequence and the latter to the elasticplastic behaviour of the structure.

Because the elasticplastic properties influence the severity and distribution of the residual stresses, it follows that a structure comprised of several materials, i.e. a composite, will experience the development of the residual stresses in a completely different way than one made of a single material. Depending on the importance of the residual stresses, different approaches have been introduced for the assessment of the structural integrity. In the structures where the integrity of the structure is of vital importance for the reliability, a thorough and accurate

assessment of the residual stress state is of primary concern. Relevant examples of such structures are e.g. the NPP primary circuit components where typically the residual stress levels in welds in as-welded state are of the scale of tensional yield stress in and near the inner surfaces.

This study concerns welding process induced residual stress distributions in Nuclear Power Plant (NPP) reactor circuit component welds. The covered residual stress definition procedures this far are the ASME recommendations [3, 4], the British Standard BS 7910: 1999 [5], the R6 Method, Revision 4 [6], the SAQ handbook [7], the SINTAP Procedure [8], the API 579 procedure [9] and the FITNET Procedure [10]. In the first phase of the study the weld residual stress distributions are calculated with the above mentioned seven procedures for welds in representative small, medium and large NPP reactor circuit pipes in Finnish BWR NPP units. The dimensions of these pipes are:

- Small pipe; outer diameter = 60 mm, wall thickness = 4.0 mm
- Medium pipe; outer diameter = 170 mm, wall thickness = 11.0 mm
- Large pipe; outer diameter = 510 mm, wall thickness = 26.0 mm.

For these three pipe sizes weld residual stress distributions through wall are calculated for both ferritic steels and austenitic stainless steels (SSs) in both perpendicular and parallel to weld directions. The covered weld conditions in the calculations are aswelded state, after Post Weld Heat Treatment (PWHT) and after weld repair. The temperature is set to 286°C in all calculations, corresponding to operational temperature in Finnish Boiling Water Reactor (BWR) NPP units. The more recent weld residual stress procedures are backed by more measured residual stress data and Finite Element Method (FEM) analysis result data than the older ones, so for the assessment of the weld residual stress distributions through wall and perpendicular to weld in as welded state these procedures are recommended, i.e. the API 579, R6 Method Rev. 4 and FITNET, even though their match is not so good in some cases. These more recent procedures are also recommended for the assessment of weld residual stresses in all other directions and for all other weld types and treatments. Of these three procedures the API 579 appears to give the most conservative weld residual stress distributions, the R6 Method Rev. 4 and the newer FITNET, on their behalf, give exactly same residual stress values for all cases covered in this study.

A set of fracture mechanics based crack growth analyses were performed to the above mentioned three pipe welds. Semielliptic axial and circumferential crack postulates located in the inner pipe weld surface were considered, the

initial size of all of which as 0.1 mm in depth and 0.6 mm in length. The aspect ratio, i.e. depth divided by length, of this crack postulate is that of the reference crack as defined in Section III of ASME code [11], corresponding to the crack shape having the highest growing potential. According to results from the fracture mechanics based crack growth analyses the compared crack growth rates show both discrepancies and similarities.

The largest discrepancies and highest crack growth rates resulted for welds in aswelded state. According to analysis results the quickest crack growth through wall for circumferential crack postulate in weld in aswelded state was approximately 27 years, in case of the Small pipe and the ASME recommendations, and for corresponding axial crack postulate approximately 12 years, again in case of the Small pipe and the ASME recommendations, respectively. For other cases, i.e. the crack growth rates through wall in weld after PWHT and in repair weld, the analysis results matched with each other for the covered procedures either quite or very well. In the light of the analysis results PWHT appears to remarkably decrease the growth rates of the piping weld cracks as compared to those for welds in as-welded state. The crack growth rates in repair welds fall according to analysis results between the aswelded and after PWHT conditions.

The study continues by implementing relevant weld residual stress procedures/standards/codes to numerical simulations concerning NPP reactor circuit components. The selected components are a feedwater nozzle and connecting safe-end and pipe in a BWR Reactor Pressure Vessel (RPV), and the examined locations are the two circumferential welds joining these components. The models are created and analyses performed with FEM code ABAQUS. Firstly, 2D models were created, and some elastic-plastic analyses performed. Also 3D FEM analyses have been started concerning reactor circuit component welds; these include weld residual stress distributions and consequent cracking analyses with fracture mechanics based analysis tool VTTBESIT, which has been partly developed at VTT.

Advanced fracture mechanical assessment methods

The sub-project aims at developing advanced finite element method assessment tools and fracture mechanics analysis methods based on material characterisation, damage mechanisms models and structural performance, in order to control structural failure both in cases of postulated initial flaw (surface-flaw) and environment assisted (internal) material damage, such as in case of irradiation

embrittlement, ageing embrittlement and stress-corrosion cracking. Coupled with Subproject 1, this finally enables the assessment of component's defect sensitivity.

Engineering assessment tools

As regards to the integrity of the reactor circuit and its components, T-junctions among other components belong to the most important structural parts. Due to the complexity of the case, no simple engineering methods are available. Thus the solution is sought by using finite element method (ABAQUS, ANSYS) together with the Zencrack code and integrating its application to existing geometric and loading data, e.g., plant database. In the beginning, the needed initial data has been specified. The basic testing and application of the procedure is presented under the sub-task "Development of sub-modelling technique".

In the case of T-joint the Zencrack code was applied to introduce an elliptical crack into a pre-existing Ansys finite element model of a T-joint generated using TVO macros. Stress intensity factor under combined thermal and pressure loading was studied [12]. Further work will consider the T-joint geometry and application of real existing geometry and loading data.

Assessment of 3D flaws

Transferability of fracture mechanics material data associated with different levels of specimen constraint has been investigated by performing numerical work to assess the fracture toughness transition between standard CT and SENB -type specimens and 3D cracks of various geometries and crack shapes for cleavage initiation and propagation using the WST model (EUROCURVE, VOCALIST and PERFECT data from Areva). Experimental companion work is in progress. The work assesses how fracture toughness is affected by different crack types as well as "realistic" crack features (such as asymmetric crack fronts). The results have been coupled to the constraint formalism build within the Master curve methodology and fracture mechanical constraint assessment methods of Fitnet [10], Sintap [8] and R6 [6]. The results provide complete means for assessing the effects of constraint on fracture mechanical material properties, both with respect to reduction of analysis conservatism and enabling optimized material usage, as well as presenting methods for handling situations where otherwise unconservative assessment results would result using traditional methods. These methods are as such suited for assessment of "real" structural material properties.

Micromechanical modelling

Micromechanical modelling of fracture mechanics related micro-mechanisms of failure deals with usage of phenomena-based models to quantify the failure of a structural component and the associated material properties. Failure micro-mechanism specific models are used to derive material properties and multi-scale material models to perform structural integrity evaluation against the modelled fracture micro-mechanisms and model changes in material properties, arising for example from mechanisms of embrittlement. In 2008, micromechanical modelling of cleavage fracture was performed in liaison with the PERFECT project to develop the WST fracture model to be applied further in assessing fracture toughness constraint response of specimens and structures with 3D flaws. Studies aiming at understanding how sub-grain plastic flow affects and ties in to the cleavage fracture process were initiated as well as development of related probabilistic models. Computational work regarding how different parameters affect cleavage fracture toughness in the DBT and its modelling has been completed.

Development of sub-modelling technique

Assessment of size limits of cracks of which growth rate could be determined solely on the basis of 3D FEM stress analysis, i.e., without the use of sub-models, is continued. In this case, as an alternative to sub-modelling, the crack growth rate is determined by using an analysis code based on weight functions, or by using some other computationally economic method. In 2007, the limitations and possibilities of sub-modelling had been studied. Crack growth results obtained with, and without, sub-modelling were compared with each other in a RPV nozzle using separate models with different crack sizes. In 2008, the ZENCRACK code working with FE codes like a “cracked sub-model” has been tested through computational examples [12].

The target of the first computation was a benchmark exercise of the project NULIFE, and the second round robin exercise on Civaux 1. This was basically a simple case concerning a straight pipe having a sinusoidal temperature fluctuation on the inner surface without other loads. The growth of an infinitely long axial crack was computed using the Paris equation. Abaqus FE code together with Zencrack code was utilised in the computation. The computational results were delivered to the Nulife project for comparison.

The second target was a thick-walled cylinder with an internal axial crack. The cylinder was subjected to a cyclic internal pressure loading. The growth of an elliptic internal axial crack was computed using the Paris equation, and the computed stress intensity factor was compared to a handbook solution.

The third target was a case studied in a former EU project concerning fast fracture of a reactor pressure vessel. The computation was performed for a given pressure and thermal loads simulating a selected transient. An elliptic axial though-clad crack was modelled on the inside surface. The computed stress intensity factor versus temperature was compared to previously computed one.

The present experience shows that the Zencrack code is suitable for engineering crack growth applications utilising the Paris law. It is useful for developing cracked finite element models of complex 3D shapes. The concept of crack blocks, which allow the user to control mesh density and distribution, makes this program applicable to any cracked structure in principle. The crack front of the crack block having a curved crack is oriented perpendicular to the surface of the crack block, which sets some limits to the modelling of crack front geometry.

Advanced surveillance techniques

The sub-project aims to develop an improved quantitative model, which accounts for micro-structural features developed in irradiation. Currently the measured transition temperature shifts (trend curves) are described directly by material composition, i.e., Cu, P and Ni contents, and the descriptions have large scatter when compared to surveillance data. The improved model defines the microstructures that harden the material and aims to describe the effect of coexistent phosphorus and copper based formations important especially in VVER steels.

Ductile crack growth measuring capacity

The experimental part consisting of fracture resistance measurements of different materials using various specimen types (e.g., CT, SENB) was initiated in 2007. In 2008, experimental work was extended to additional materials and specimen geometries including also non-standard ‘shallow’ specimens allowing crack growth lengths beyond those in standard specimens. During 2009, numerical cohesive zone modelling calculations and experimental results on additional materials will be continued. The main aim is to produce ductile fracture resistance (J-R) data to be applied in later numerical calculations in

order to define realistic criteria for specimen's true measuring capacity and development of related material characterisation standardisation. [13]

Irradiation embrittlement

Within IAEA CRP-8 "Master Curve Approach to Monitor Fracture Toughness of Reactor Pressure Vessels in NPPs", fracture toughness data on various reactor pressure vessel (RPV) steels were analysed for quantifying the toughness issues associated with RPV surveillance testing and integrity analyses, using the Master Curve approach. The work covered three topic areas: constraint/ geometry effects, fracture toughness vs. temperature and dynamic loading conditions. [14, 15, 16]

Ten laboratories contributed to a round robin in the framework of the consolidation of analytical tools needed to support loss of constraint issues in the application of the Master Curve. It was found that the ANSYS code produces systematically higher forces. Remaining differences for the other finite element codes were very small. It was also found that shallow crack specimens are more sensitive to loss of constraint than deep crack for a given specimen size. The difference in term of reference temperature was evaluated to be of about 40°C.

Based on Master Curve analyses performed for a variety of RPV steels the constant C-parameter assumption given in ASTM E 1921 provides a good approximation for most irradiated materials exhibiting moderate fracture toughness. Irradiation may slightly lower the fracture toughness in the upper transition region in relation to that predicted by the standard curve shape, but the effect after moderate T_0 shift values seems to be negligible.

Based on investigations performed on the loading rate, the ratio between stress intensity factor and time at cleavage (or test termination) can be used to effectively estimate the average loading rate dK/dt in a fracture toughness tests. From the round-robin exercise the Master Curve approach proved to be fully applicable to impact fracture toughness measurements obtained in the ductile-to-brittle transition region.

During 2007–2008, the applicability of a non-linear neural network technique to the IAEA VVER-440 surveillance data base was studied and a draft reported was prepared [17]. The new method enables to separate the timely (neutron fluence) occurrence of copper and phosphorus effects on embrittlement. As compared to the Russian norm description of irradiation embrittlement, where the effect of phosphorus and copper are descruibed by linear separate terms, the

best new description indicated stronger and accelerating response when phosphorus content increases.

The evolution of microstructure in irradiation, anneling and reirradiation treatments of VVER-440 steels was studied by SANS in co-operation with Forschungszentrum Rossendorf (FZR). The data [18] indicates that during the first irradiation large population of particles of around 2nm size will occur. This particle popularion disappears in anneling fully. During the reirradiation a very minor population of these particles is observed and this population does not grow in further irradiation. The data is a strong indication that copper reach particles play a big role in first irradation. The absence of these particles in reirradiation can be explained only by the fact that copper particles grow in annealing and number density of the particles is largely reduced. Hence copper will not play a role in reirradiation. SANS assumably do not detect phosphorus formation as they are believed to be one or two dimensional. SANS is sensitive to volume type particles.

Within frame of co-operation between VTT/ Tohoku University large number of ATOM probe and Positron annihilation samples were prepared at the end of 2008. The sampled materials represent VVER-440 steels in different I-, IA- and IAI-conditions as well as model alloys with varying chemical composition. The samples have been packed for radioactive transport and they are waiting for formal acceptance from Japan.

Applications and conclusions

The results will be applied to assess structural safety of nuclear reactor components, as well as to evaluate their remaining lifetime during service, by coupling between advanced numerical modelling tools and material's characterisation data, in order to cover the entire chain of structural safety related aspects coupling the interaction of effects of loads, existing flaws, material's relevant damage mechanisms and degradation of properties during service.

References

1. Calonius, K. Preliminary numerical studies on dynamic behaviour of pipelines. VTT Research Report VTT-R-01637-08. Espoo: VTT, 2008. 69 p.

2. Timperi, A. Numerical simulations of turbulent buoyancy-driven flows. VTT Research Report VTT-R-11339-07. Espoo: VTT, 2008. 49 p.

3. Section XI Task Group for Piping Flaw Evaluation, ASME Code. Evaluation of Flaws in Austenitic Steel Piping. Journal of Pressure Vessel Technology, 1986. Vol. 108, pp. 352–366.

4. Shack, W.J. et al. Environmentally Assisted Cracking in Light Water Reactors: Annual Report, October 1981 – September 1982. NUREG/CR-3292. Washington D.C.: U.S. Nuclear Regulatory Commission, June 1983.

5. British Standard BS 7910: 1999. Guide on methods for assessing the acceptability of flaws in fusion welded structures. 4th draft after public comment. England, 8 April, 1999.

6. R6 Method. Assessment of the Integrity of Structures containing Defects. Revision 4. 2004 update of 2001 edition. British Energy (BE).

7. Andersson, P. et al. A Procedure for Safety Assessment of Components with Cracks – Handbook. 3rd revised edition. SAQ/FoU-Report 96/08. Stockholm, Sweden: SAQ Kontroll AB, 1998. 104 p.

8. SINTAP. Structural Integrity Assessment Procedures for European Industry. Final Procedure: November 1999. Project funded by the European Union (EU) under the Brite-Euram Programme: Project No. BE95-1426. Contract No. BRPR-CT95-0024.

9. American Petroleum Institute (API). Recommended practice for fitness-for-service. API 579. Washington D.C.: American Petroleum Institute, 2000.

10. FITNET Fitness-for-Service PROCEDURE – FINAL DRAFT MK7. Koçak, M. et al. (Eds.). European Fitness-for-Service Thematic Network – FITNET. Germany. 1.5.2006.

11. ASME Boiler and Pressure Vessel Code Section III, Division 1, Article G-2000. 2005 Update of 2004 Edition.

12. Keinänen, H., Kaunisto, K. & Kuutti, J. Application of Zencrack code for crack initiation and growth cases. VTT Research Report VTT-R-00513-09. Espoo: VTT, 2009. 36 p.

13. Elers, L. The validity of fracture resistance curve characterization methods for extended ductile crack growth. VTT Research Report VTT-R-10197-08. Espoo: VTT, 2008. 58 p.

14. Lidbury, D., Diard, O., Marini, B., Bugat, S., Keim, E., Wallin, K. & Planman, T. Prediction of irradiation damage effects in reactor components: update of progress in RPV mechanics subproject. Proc.Conf. ASME PVP 2007/ CREEP 8:2007. ASME Pressure Vessels and Piping Conference. San Antonio, Texas, July 22–26, 2007. ASME. Pp. PVP2007–26076.

15. Planman, T., Onizawa, K., Server, W. & Rosinski, S. IAEA coordinated research project on Master Curve approach to monitor fracture toughness of RPV steels: applicability for highly embrittled materials. Proc. Conf. ASME PVP 2007/CREEP 8:2007. ASME Pressure Vessels and Piping Conference. San Antonio, Texas, July 22–26, 2007. ASME. Pp. PVP2007–26097.

16. Planman, T., Server, W., Wallin, K. & Rosinski, S. Application of the Master Curve approach for abnormal material conditions. Proc. Conf. ASME PVP 2007/CREEP 8:2007. ASME Pressure Vessels and Piping Conference. San Antonio, Texas, July 22–26, 2007. ASME. Pp. PVP2007–26257.

17. Valo, M. & Bulsari, A. Non-linear analyses of VVER-440 surveillance data. VTT Research Reporti VTT-R-03047-08. Espoo: VTT, 2008. 55 p.

18. Ulbricht, A., Bergner, F., Böhmert, J., Valo, M., Mathon, M.-H. & Heinemann, A. SANS response of VVER440-type weld material after neutron irradiation, post-irradiation annealing and reirradiation. Philosophical Magazine, 21 April 2007. Vol. 87, No. 12, pp. 1855–1870.

26.2 Simulation of thermal striping in a HDR experiment

Antti Timperi
VTT

Abstract

Computational Fluid Dynamics (CFD) calculations of thermal striping in a HDR (Heißdampfreaktor) experiment were performed with the commercial Star-CD code. In the experiment, temperature fluctuations caused by instability between layers of cold and hot water flowing in a horizontal pipe were studied. Large-Eddy Simulation (LES) with the Smagorinsky sub-grid scale model was mainly used for turbulence modelling. The vortex method was implemented and validated for simple pipe flow in order to have realistic turbulent inlet conditions for LES. Different geometries and meshes for simulating the experiment were tested. Results obtained with realistic geometry seemed qualitatively correct but the magnitude of temperature fluctuations was too low. This could be connected to too coarse mesh in the model.

Introduction

Thermal striping, characterized by relatively high-frequency fluid temperature fluctuations near a solid wall, has caused material fatigue in certain components of nuclear power plants [1]. Typical locations susceptible to thermal striping are piping T-junctions, where mixing of cold and hot water occurs. Another example are horizontal pipe sections, where a layer of cold water flows in the lower part while a layer of hot water flows with different velocity in the upper part. Large-scale fluctuations of the cold-hot interface, caused by fluid dynamic instability and/or turbulence, may cause significant temperature fluctuations in the pipe wall.

It has been found that the Reynolds Averaged Navier-Stokes (RANS) turbulence models are usually unsuitable for modeling these situations because fine time-dependent flow details need to be captured. The Large-Eddy Simulation (LES) and recently also the Detached-Eddy Simulation (DES) models have been used for studying thermal striping in T-junctions [2, 3, 4, 5]. Comparison to experiments has shown that at least LES is a suitable tool for these calculations.

No CFD calculations of thermal striping between layers of cold and hot water in a horizontal pipe are known to the author.

In this work, thermal striping in a horizontal feedwater pipe in a HDR (Heißdampfreaktor) experiment is analyzed with LES. The Smagorinsky sub-grid scale model is used. Calculated temperature fluctuations are compared with experimental data. The Vortex Method (VM) is used for generating turbulent inlet conditions for LES. The calculations are performed with the Star-CD 4.02 code.

Generation of synthetic turbulent inflow conditions

VM was implemented into Star-CD as a user subroutine for generating transient inflow conditions for LES. Traditional methods for generating the inflow conditions include superimposing simple random perturbations on the mean velocity profile and using data from separate or simultaneous LES. The former of these usually requires a long region to develop into realistic turbulence whereas the latter is quite laborious to perform. VM can be conveniently used for generating close to realistic turbulent inflow conditions which require only a short development region [6, 7].

In VM, a two-dimensional random vorticity field is generated on the inflow plane normal to the streamwise direction. Properties of the vorticity field are estimated from distributions of turbulence quantities at the inlet. In addition, methods for adding also streamwise perturbations have been developed. In this work, also the streamwise component is added because this gave more realistic turbulence spectra downstream of the inlet plane.

The method was first tested in a pipe flow at Reynolds number 10000. A corresponding calculation with cyclic boundary conditions was also carried out to have a good reference for the VM calculations. With cyclic boundary conditions, length of the pipe was four times the pipe radius. In the following, the VM results have been taken eleven pipe radii from inlet. Instantaneous velocity fields obtained with VM and with cyclic boundary conditions are compared in Figure 26.2.1, it is seen that the velocity fields are similar. The instantaneous fields obtained from VM resemble the fully developed state already at the inlet plane. Profiles of time averaged velocity and velocity fluctuation are shown in Figure 26.2.2. The profiles are quite well represented in all calculations. Turbulence spectra near the pipe wall are shown in Figure 26.2.3. Results of the different calculations are close to one another and the -5/3 slope is realized in the mid-range.

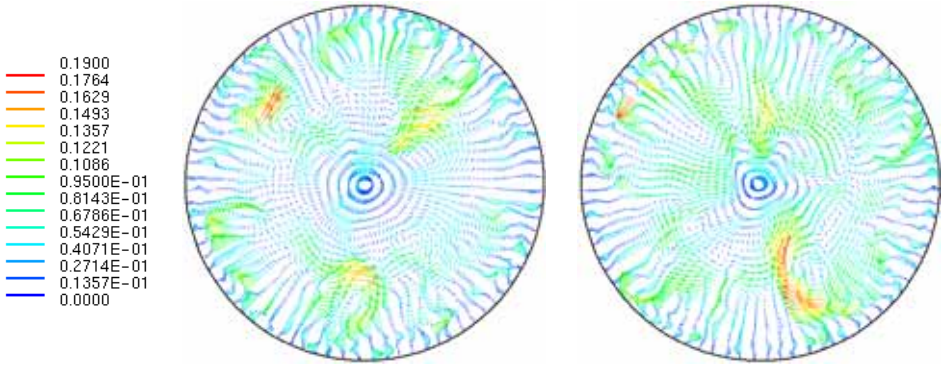

Figure 26.2.1. Instantaneous perpendicular velocity field [m/s] obtained with cyclic boundary conditions (left) and with VM (right).

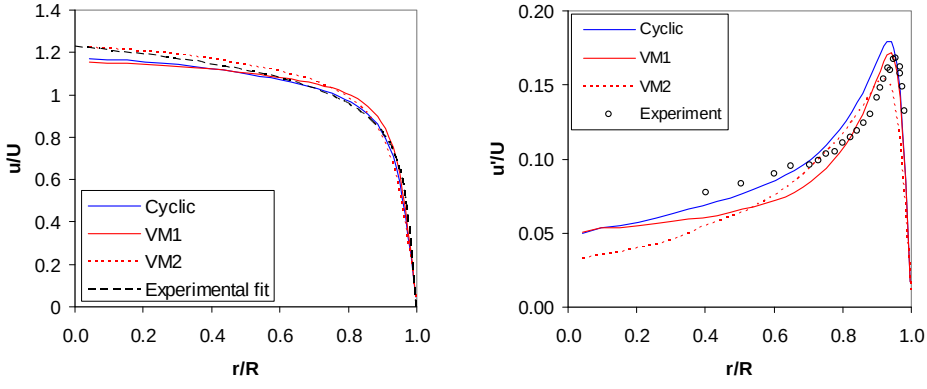

Figure 26.2.2. Profiles of time averaged axial velocity and velocity fluctuation. The experimental data is from Refs. [8, 9].

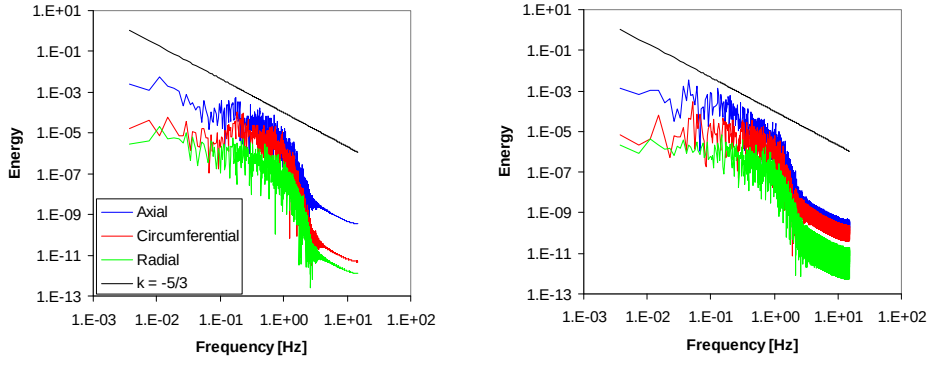

Figure 26.2.3. Turbulence spectra at location of maximum axial fluctuation obtained with cyclic boundary conditions (left) and with VM (right).

HDR experiment TEMR-T33.19

In the HDR experiment, thermal striping in a horizontal pipe section was studied in a full-scale reactor geometry [10, 11, 12]. Schematics and dimensions for the experiment are shown in Figure 26.2.4. The reactor pressure vessel and the horizontal part of the feedwater pipe are initially at temperature 210 °C. Cold water at temperature 60 °C is injected with a constant flow rate of 46 t/h into the pipe. Due to buoyancy and relatively low flow rate, a stream of cold water is formed on the bottom of the horizontal part of the pipe. Difference between velocities of the cold and hot layers causes the interface to become unstable and thermal striping occurs. Measured temperature in the transition layer 10 mm from pipe wall is presented in Figure 26.2.5. The range of the temperature fluctuations is around 100°C and the most dominant frequency is a little less than 1 Hz.

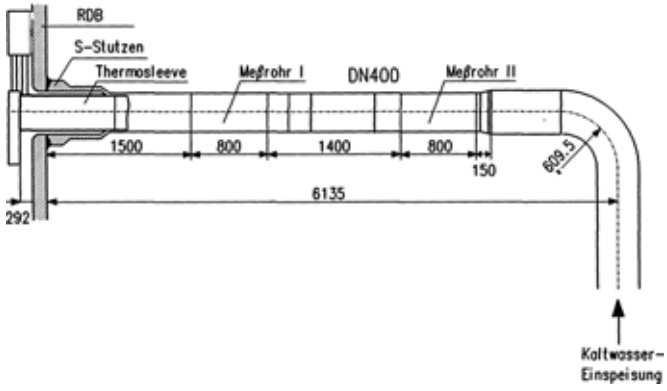

Figure 26.2.4. Cold water inlet pipe in the HDR experiment [10].

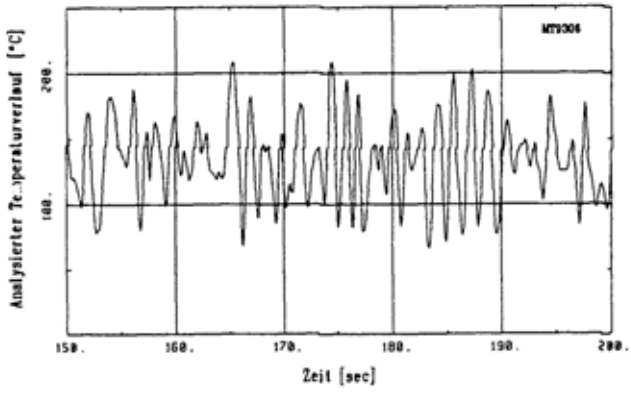

Figure 26.2.5. Temperature fluctuations in the transition layer in the HDR experiment [10].

LES of the HDR experiment

Unsteady RANS calculations of the experiment were first performed by using different k-ε turbulence models. With two-dimensional models some temperature fluctuations could be seen but with three-dimensional models the fluctuations were completely suppressed resulting only to a time-averaged field.

LES were first performed in straight pipe sections having highly refined mesh in the mixing layer. Length of the pipe was 3 m at maximum, i.e. about half of that in the experiment. The maximum number of cells was 1.2 million. Temperature fluctuations obtained with the straight pipes were clearly smaller than the measured values. Reducing the eddy-viscosity through the Smagorinsky constant was also tested but this had little effect.

A calculation was finally performed in a more realistic geometry which had the whole horizontal part of the feedwater pipe including the small contraction and the 90º bend shown in Figure 26.2.4. The same mesh density was used throughout the horizontal pipe which took about 5 million cells. The mesh of the model is presented in Figure 26.2.6. Cell size in the lower part of the pipe is approximately 5.5 mm and at wall $y^+ \approx 1$. It should be noted that the lower part is still too coarse for accurate LES. Time step size in the calculation was 0.01 s. Calculating up to 40 seconds took about three weeks with four CPU cores.

Figure 26.2.7 presents instantaneous temperature fields in the middle cross-section. The Kelvin-Helmholtz instability waves can be seen after about halfway of the pipe. Large-scale unsteady motion of the transition layer can be seen also between the bend and contraction. Figure 26.2.8 shows calculated temperatures at the location of “Meßrohr 1” in Figure 26.2.4. The calculated fluctuations have lower amplitude near the wall compared to the experiment.

Height of the cold layer is approximately 105 and 183 mm in the calculation and experiment, respectively. This could be caused by too low flow resistance due to the coarse mesh. In addition, the calculation should be continued up to about 100 s from which the measurements were made. A RANS calculation, which is expected to describe the overall flow field more accurately than the LES with coarse mesh, gave height of the cold layer of 140 and 160 mm at t = 40 s and t = 100 s, respectively.

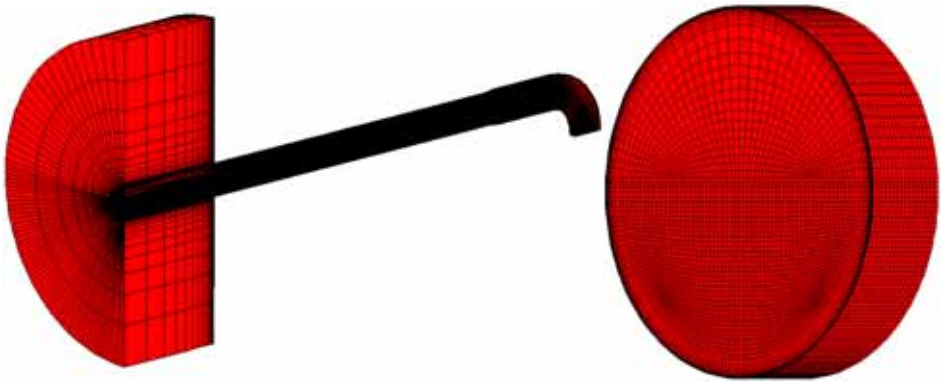

Figure 26.2.6. Mesh used for LES of the HDR experiment.

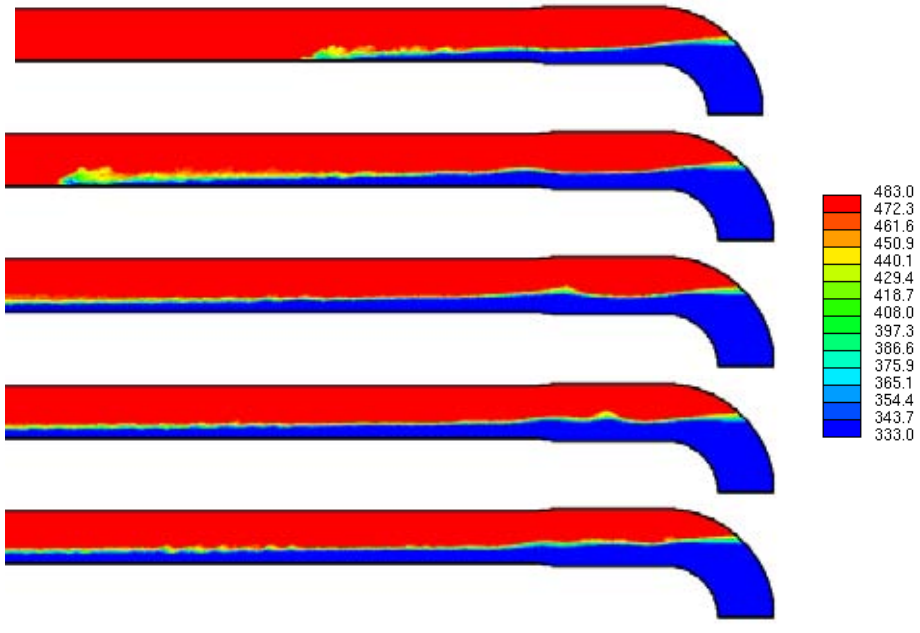

Figure 26.2.7. Instantaneous temperature fields [K] from t = 12 … 33 s in LES of the HDR experiment.

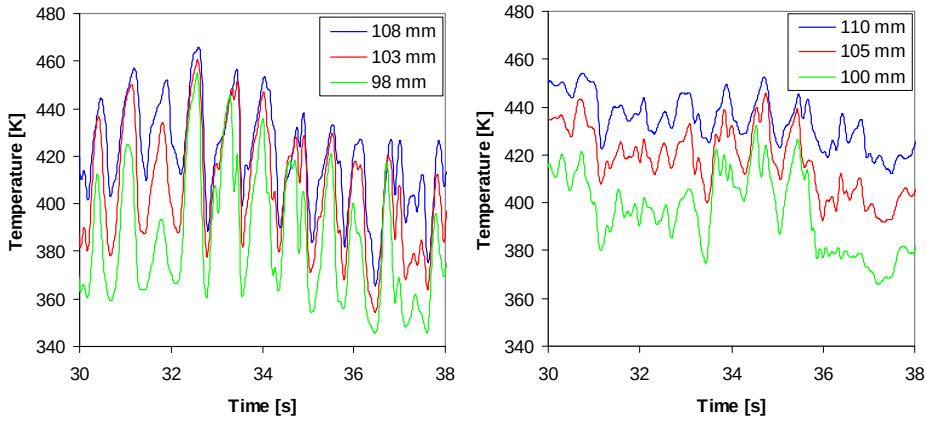

Figure 26.2.8. Temperature fluctuations at different heights at the centre (left) and 10 mm from pipe wall (right) in LES of the HDR experiment.

Conclusions

LES of thermal striping in a horizontal feedwater pipe, caused by a mixing layer between cold and hot water streams, were performed. The analysed case was the HDR TEMR-T33.19 experiment. In order to have realistic turbulent inlet conditions, the vortex method was implemented into Star-CD and validated for fully developed pipe flow. Calculations of the HDR experiment with short pipe sections predicted clearly too small temperature fluctuations. With realistic geometry, better agreement with the experiment was found but too low fluctuations were still obtained near the wall. Height of the cold layer was clearly lower in the calculation which could be caused mainly by too coarse mesh. The low cold layer could partly cause the too low amplitude of the calculated temperature fluctuations. The case proved to be challenging in terms of demands for computing power and non-conservative temperature loads were easily obtained. A more refined and optimized mesh as well as the computationally less expensive DES model could be tested in future work.

References

1. Shah, V.N. & MacDonald, P.E. (Eds.). Aging and life extension of major LWR components. Elsevier, 1993.

2. Hu, L.-W. & Kazimi, M.S. LES benchmark study of high cycle temperature fluctuations caused by thermal striping in a mixing Tee. International Journal of Heat and Fluid Flow, 2006. Vol. 27, pp. 54–64.

3. Tanaka, M., Ohshima, H. & Monji, H. Numerical simulation of thermal striping phenomena in T-junction piping system using large eddy simulation. ICONE16-48667, 16th International Conference on Nuclear Engineering. Orlando, USA, May 11–15, 2008.

4. Westin, J., Veber, P., Andersson, L., Mannetje, C., Andersson, U., Eriksson, J., Henriksson, M., Alavyoon, F. & Andersson, C. High-cycle thermal fatigue in mixing Tees. Large-eddy simulations compared to a new validation experiment. ICONE16-48731, 16th International Conference on Nuclear Engineering. Orlando, USA, May 11–15, 2008.

5. Frank, T., Adlakha, M., Lifante, C., Prasser, H.-M. & Menter, F. Simulation of turbulent and thermal mixing in T-junctions using URANS and scale-resolving turbulence models in Ansys CFX. OECD/NEA & IAEA Workshop “Experiments and CFD Code Applications to Nuclear Reactor Safety” (XCFD4NRS). Grenoble, France, September 10–12, 2008.

6. Mathey, F., Cokljat, D., Bertoglio, J.P. & Sergent, E. Assessment of the vortex method for large eddy simulation inlet conditions. Progress in Computational Fluid Dynamics, 2006. Vol. 6.

7. Benhamadouche, S., Jarrin, N., Addad, Y. & Laurence, D. Synthetic turbulent inflow conditions based on a vortex method for large-eddy simulation. Progress in Computational Fluid Dynamics, 2006. Vol. 6.

8. White, F.M. Viscous Fluid Flow. McGraw-Hill, 1991.

9. den Toonder, J.M.J. & Nieuwstadt, F.T.M. Reynolds number effects in a turbulent pipe flow for low to moderate Re. Physics of Fluids, 1997. Vol. 9, pp. 3398–3409.

10. Häfner, W. Thermische Schicht-Versuche im horizontalen Rohr. Technischer Fachbericht PHDR 92-89. HDR Sicherheitsprogramm. Kernforschungszentrum Karlsruhe, 1990.

11. Wolf, L., Häfner, W., Geiss, M., Hansjosten, E. & Katzenmeier, G. Results of HDR experiments for pipe loads under thermally stratified flow conditions. Nuclear Engineering and Design, 1992. Vol. 137, pp. 387–404.

12. Schygulla, U. & Wolf, L. Thermal stratification experiments in horizontal piping section. Design report. HDR Sicherheitsprogramm. Kernforschungszentrum Karlsruhe, 1986.

27. Influence of material, environment and strain rate on environmentally assisted cracking of austenitic nuclear materials (DEFSPEED)

27.1 DEFSPEED summary report

Ulla Ehrnstén, Matias Ahonen and Wade Karlsen
VTT

Hannu Hänninen
Helsinki University of Technology, TKK, Engineering Materials

Abstract

The DEFSPEED project (Influence of material, environment and strain rate on environmentally assisted cracking on austenitic nuclear materials) aims to increase the understanding of environmentally assisted cracking (EAC) and irradiation assisted stress corrosion cracking (IASCC) mechanisms in austenitic nuclear materials. Several sub-tasks are performed to achieve the set objectives during the four year project. Initiation studies using Super Slow Strain Rate Testing technique (SSSRT) are performed in LWR environments on austenitic nuclear materials and in-depth investigations on deformation mechanisms are performed using versatile methods. The role of dynamic strain ageing in austenitic nuclear materials is evaluated using internal friction measurements and tensile tests at different strain rates. The effect of environment and strain rate on fracture toughness properties in nickel-based welds is determined both on materials from dissimilar metal welds as well as on pure weld metal specimens.

Irradiated austenitic stainless steels from plant internals are characterized using transmission electron microscopy to increase the knowledge of radiation induced segregation and defect structures, which both play a role in IASCC. The latest international knowledge, applied for research as well as failure analyses, is brought to Finland by participating in international co-operation within the fields of EAC and IASCC. Education of new experts in the field of nuclear materials is an important objective for the DEFSPEED project, which may become even more important when taking into account the clear indications of a nuclear renaissance in Finland in conjunction with the skewed age distribution of the experts. This report summarises the results obtained during the first two years of the four year DEFSPEED project.

Introduction

Intergranular environmentally assisted cracking (EAC) of austenitic stainless steels has been the major failure mode in BWR's. The risk has been minimised by changing high-carbon stainless steels to low carbon, nitrogen-alloyed stainless steels, improving welding techniques and improving the water chemistry [1]. However, EAC has also been reported in non-sensitised stainless steels and in austenitic stainless steels in PWR's, connected to non-specified water chemistry conditions [2–5]. Further, EAC in nickel-based alloys has today a major influence of the usability of both PWR's and BWR's. As the world's fleet of light-water reactor nuclear power plants age, cracks have emerged in components which have been exposed to neutron irradiation. An ability to predict the instances and extent of such cracking could enable better assessment of the performance and integrity of reactor core components for safe extension of the operating lifetime of power plants.

Localisation of plastic deformation and the interaction between strain localisation and oxide film formation are most probably playing a key role in EAC and IASCC [6]. Several mechanisms, such as dynamic strain ageing, recovery, environmentally enhanced creep, relaxation, segregation and dislocation channel formation (especially in internals) can affect localisation of deformation [7]. Understanding of these phenomena is important, e.g., in order to be able to predict and quantify the risk for environmentally assisted cracking in austenitic nuclear materials. These predictions can be used e.g. for selection of reliable criteria for NDE programs. Better mechanistic understanding of EAC and

IASCC mechanisms is particularly important in the context of the ageing fleet of existing NPPs and of long lifetimes planned for new NPPs.

Main objectives

The main objective of the DEFSPEED project is to increase the mechanistic understanding of environmentally and irradiation assisted stress corrosion cracking (EAC and IASCC) in austenitic nuclear materials. Several sub-tasks are performed to achieve the set objectives during the four year project. Initiation studies using Super Slow Strain Rate Testing technique (SSSRT) are performed in LWR environments on austenitic nuclear materials and in-depth investigations on deformation mechanisms are performed. Sophisticated and versatile methods are used, such as transmission electron microscopy (TEM) and electron back-scatter diffraction (EBSD). The role of dynamic strain ageing in austenitic nuclear materials is evaluated using internal friction and tensile tests at different strain rates. The effect of environment and strain rate on fracture toughness properties in nickel-based welds is determined both on materials from dissimilar metal welds as well as on pure weld metal specimens. All these investigations focus on a better understanding of precursors for crack initiation and phenomena affecting EAC. Irradiated austenitic stainless steels from plant internals are characterized with transmission electron microscopy to increase the knowledge of radiation induced segregation and defect structures, which both play a role in IASCC. The latest international knowledge is brought to Finland by participating in international co-operation within the field of EAC and IASCC. Education of new experts in the field of nuclear materials is an important objective for the DEFSPEED project and its role may become even more emphasized when taking into account the clear indications of a nuclear renaissance and the skewed age distribution of the experts.

Strain localisation in austenitic stainless steels

Slow strain rate tests are used worldwide as a method to investigate the susceptibility of materials to stress corrosion cracking. However, the method, using conventional strain rates on the order of $>10^{-6}$ s^{-1}, is not regarded as sensitive enough for evaluation of the behaviour of modern, less EAC-susceptible nuclear materials in clean LWR environments. VTT has developed a bellows loading system which enables a very slow strain rate with truly constant extension rate and measurement of the strain from the specimen itself. Super

slow strain rate tests, SSSRT's, were started by evaluating the technique using two strain rates ($1 \cdot 10^{-7}$ s^{-1} and $1 \cdot 10^{-8}$ s^{-1}) and two material conditions, i.e., sensitised Type 304 stainless steel with or without 10% cold work. These tests were performed in simulated BWR environment (400 ppb O_2, 300 °C). Further SSSRT's will be performed on austenitic nuclear materials in both BWR and PWR environments and tests are ongoing using non-sensitised Type 316L stainless steel deformed to different levels in simulated BWR environment.

The results from the evaluation tests using sensitised stainless steel showed an increased sensitivity of the test with decreasing strain rate, manifested by a higher amount of intergranular cracking and smaller strain to fracture with decreasing strain rate, Figure 27.1.1 [8]. Thus, the technique seems applicable for investigations of also less susceptible materials, e.g., non-sensitised stainless steels. The results from the evaluation test also showed a detrimental influence of deformation, manifested by a higher amount of intergranular cracking in specimens that had been cold-deformed 10% before the SSSR-testing.

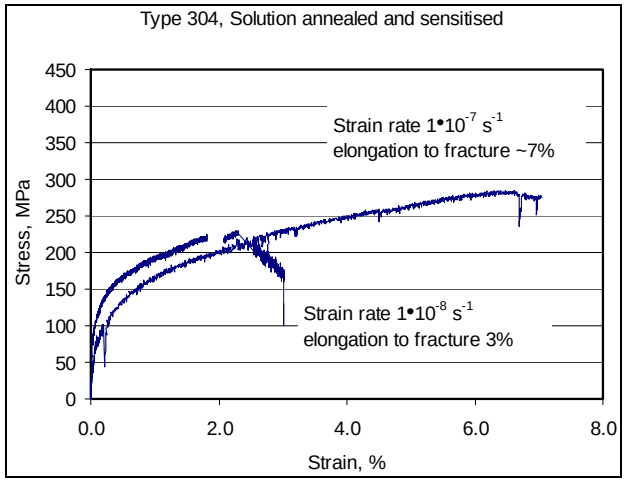

Figure 27.1.1. Stress vs. strain for solution annealed and sensitised Type 304 austenitic stainless steel specimens tested using different strain rates, i.e., $1 \cdot 10^{-7}$ s^{-1} and $1 \cdot 10^{-8}$ s^{-1}, in simulated BWR environment.

Electron back-scattered diffraction, EBSD, is a very versatile method for characterising crystalline materials. EBSD maps can be formed in numerous ways to reveal desired properties. Intra-grain mis-orientation mapping is one method, and can be calibrated for quantitative measurement of local plastic strain. This calibration was preformed within this project [9], before specimens

from the SSSR-tests were characterised using EBSD. The results [10] show a non-uniform distribution of plastic strain, with higher plastic strains in the vicinity of grain boundaries than inside the grains, Figure 27.1.2.

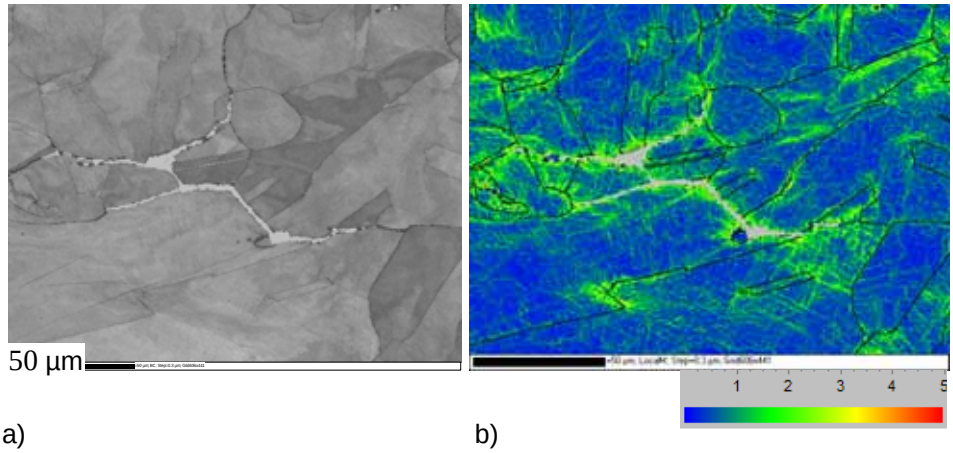

Figure 27.1.2. Pattern quality map (a) showing the microstructure of a crack tip area in a solution annealed and sensitised Type 304 stainless steel after SSSR-testing in simulated BWR environment and the local mis-orientation map in the same area (b). Blue, through green to red colour correspond to smallest to highest degree of mis-orientation, respectively, i.e., from lowest to highest amount of plastic strain.

Further observations include local non-uniform distributions of plastic strain at the surfaces and an influence of local changes in the grain size on the localisation of plastic deformation. The non-homogeneous microstructure of materials thus results in non-homogenous distribution of local plastic strain, which in turn affects the crack initiation and growth.

In addition to characterisation of SSSRT specimens, the local strain distribution in a **welded pipe** made of nuclear grade Type 304 austenitic stainless steel was characterised using EBSD [11], and the results were compared to the results of residual stress measurements made on the same pipe. The highest degrees of plastic strain (10–20%) were measured in the heat affected zone (HAZ) close to the root area of the weld, Figure 27.1.3, with the deformed zone extending 5–7 mm from the fusion line to the base material.

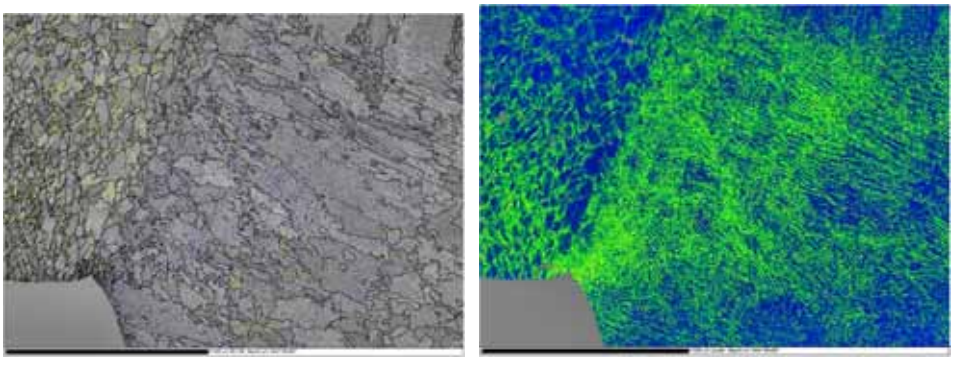

Figure 27.1.3. Pattern quality map (a) showing the microstructure of the fusion line area at the weld root, and local mis-orientation map from the same area of the investigated weld.

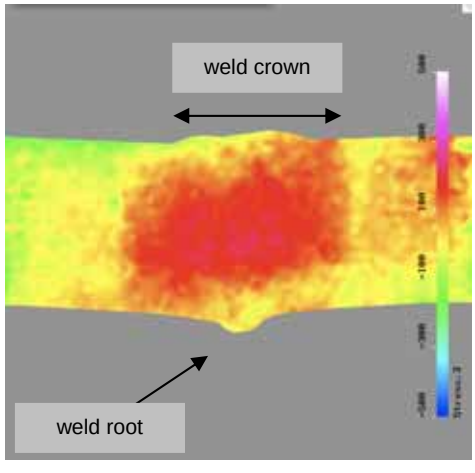

Figure 27.1.4. Residual stresses obtained by Contour method in the nuclear pipe weld made of Type 304 austenitic stainless steel. The inner surface of the pipe is on the lower side of the picture.

The amount of residual plastic strain in the base material decreased towards the outer surface of the pipe. Plastic strains were also observed in the weld metal, where they were measured to be highest in the areas of the weld bead boundaries. The residual stress measurements showed high tensile stresses at the inner surface of the pipe, Figure 27.1.4. Both the residual stresses and the plastic strains were higher on one side of the weld fusion line compared to the other.

Dynamic strain ageing of austenitic nuclear materials

Dynamic strain aging (DSA) is a material phenomenon most commonly associated with the appearance of serrations in tensile stress-strain curves at particular test temperatures. DSA is important for structural stainless steels because it has also been associated with the anomalous evolution of strength and ductility with temperature, both for tensile and fatigue tests. Further, the DSA phenomenon may be important to the overall deformation behaviour of stainless steels as a contributor to strain localisation. Dynamic strain ageing properties of austenitic nuclear materials has been investigated using tensile testing at different strain rates and internal friction measurements during several years both at VTT and Helsinki University of Technology, TKK [e.g. 12, 13]. A doctoral thesis work is ongoing on the subject at TKK and the DEFSPEED-project funds a part of this work. Additionally, transmission electron microscopy has been applied in investigations of deformation structures in Type 316 stainless steels showing and not showing serrated yielding.

Based on the tensile tests using different strain rates, DSA-maps have been constructed for austenitic stainless steels of Type 304 and 316 and for nickel-based materials Alloy 600 and 690 [14–16]. Serrated yielding starts at a lower temperature in Alloys 600 and 690 (observed between 150 and 600 °C) compared to Type 316NG austenitic stainless steel (observed above ~200 °C.) However, DSA-behaviour as manifested by serrated yielding is observed at LWR-relevant temperatures in all of the above mentioned materials at strain rates below 10^{-4} s^{-1}. An example of a DSA-map is shown in Figure 27.1.5. The activation energies for the onset of DSA have been determined for both Alloy 600 and 690, and it has been observed to be about the same both, at ~1.65 eV. The results indicate that plastic deformation causes redistribution of interstitials (e.g. nitrogen and carbon), which can affect localisation of plastic deformation.

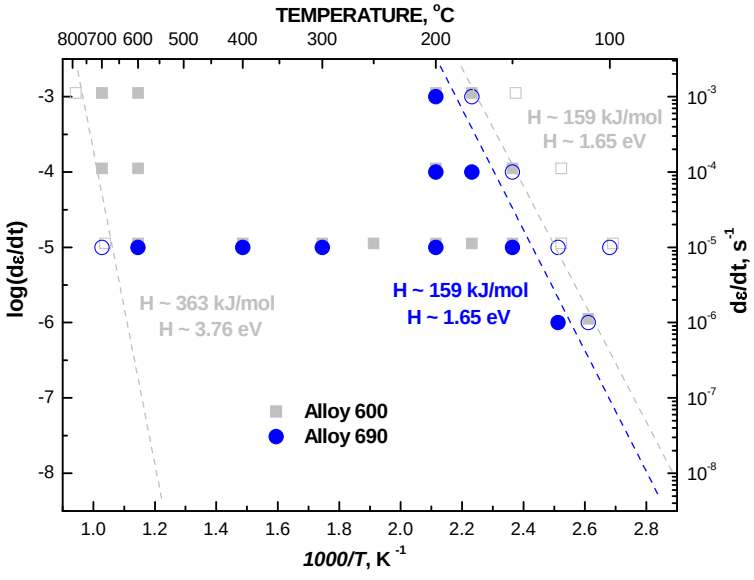

Figure 27.1.5. DSA-map for Alloys 600 and 690, where serrated yielding is observed at temperature between 150 and 600 °C at strain rates $<10^{-4}$ s^{-1}.

The deformation microstructures of Type 316 stainless steel specimens tested inside and outside the DSA regime were examined by transmission electron microscopy, [17]. Though post-mortem TEM cannot directly observe solute interactions with dislocations, the observed long-range planarity in the dislocation structures at 400 °C, and short-range planarity at 288 °C, in conjunction with the serrations observed in the tensile curves, gives indirect evidence that the mechanism of DSA is operating in the material. DSA affects the deformation behaviour of the material by restricting cross-slip and therefore promoting strain localisation to the principle slip planes. The work has demonstrated that DSA is present in commercial Type 316 SS, and occurs at temperatures relevant to nuclear power plant operation.

Characterisation of irradiated stainless steels

As the world's fleet of light-water reactor nuclear power plants age, cracks have emerged in core structures which have been exposed to neutron irradiation. An ability to predict the instances and extent of such cracking can enable better assessment of the performance and integrity of reactor core components for safe extension of the operating lifetime of power plants. Conducting transmission

electron microscope (TEM) examinations of materials that have been removed from service in real reactors makes an important contribution towards understanding the phenomenon better.

Continuing from its initiation in Safir, this project has so far conducted analytical TEM examinations for the Halden project of specimens prepared from a Type 304 austenitic stainless steel centre filler assembly plate exposed to neutron irradiation in the French Chooz A PWR, from a Type 304L control rod blade from the Barsebäck 1 BWR, and from three cold deformed and irradiated Type 316 stainless steels. The dose levels extend from ~1.5 dpa to 30 dpa.

The presence of a high density of dislocation loops was confirmed in all of the materials, a consequence of the fact that the density rapidly saturates at about 1 dpa. However, the median loop diameter ranged from about 3–4 nm at 1.5 dpa, up to 6.7 nm at 30 dpa. Small voids or bubbles were also found within the matrix of the high dose material, having about 3–4 nm in diameter in the control rod blade material, but 1–2 nm in diameter in the centre filler assembly plate material. The low dose materials had no evidence of such void features. Compositional analyses indicated the expected depletion of chromium at the grain boundaries in the high dose materials, while at 1.5 dpa the difference between Cr composition in the matrix and at the grain boundary was less apparent, Figure 27.1.6. There was also a strong tendency for co-segregation of nickel and silicon at the grain boundaries, and in the higher dose materials as precipitates in the matrix [18–20]. Figure 27.1.7 shows the silicon segregation.

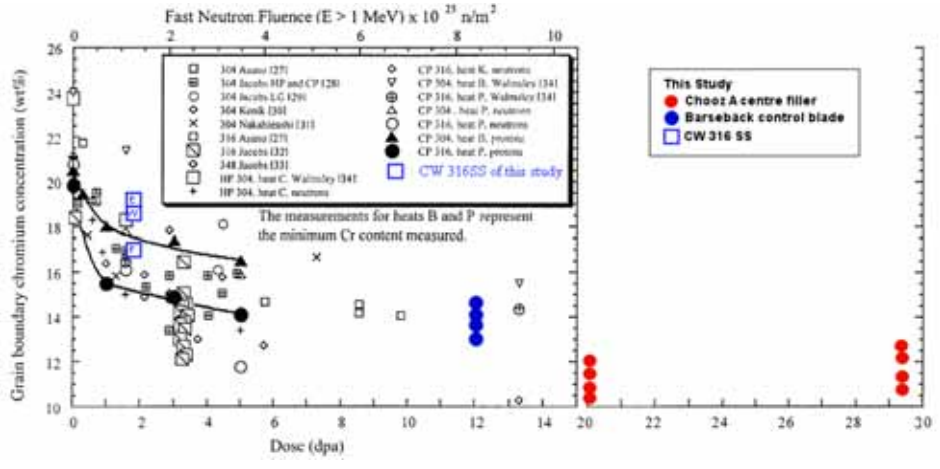

Figure 27.1.6. Radiation induced depletion of Cr at the grain boundaries of the irradiated materials of this project, compared to literature data.

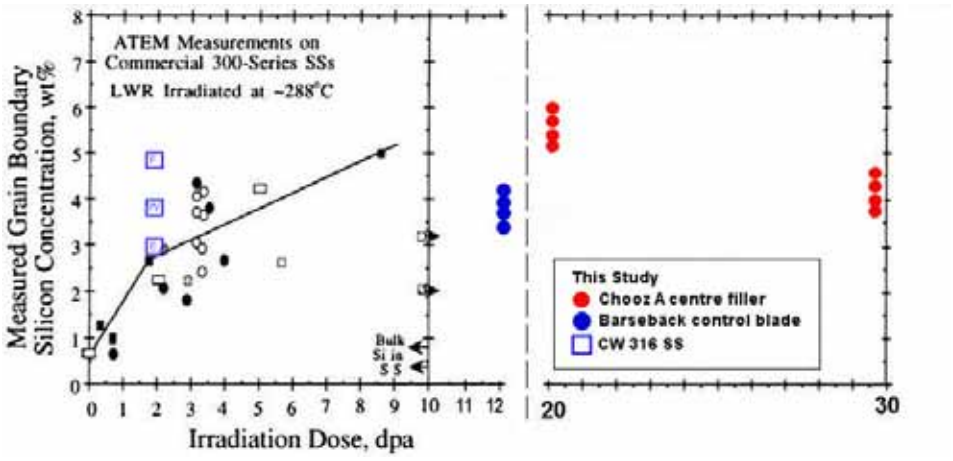

Figure 27.1.7. Radiation induced segregation of Si at the grain boundaries of the irradiated materials of this project, compared to literature data.

Influence of the strain rate and environment on fracture toughness properties of austenitic materials

Recent international research has indicated a clear influence of stain rate and environment on fracture resistance and tearing modulus in the case of nickel-based weld materials. Literature data on this **L**ow **T**emperature **C**rack **P**ropagation (LTCP) show a remarkable influence of hydrogen containing environment on fracture toughness properties of e.g. Alloy 182. The most susceptible temperature, according to the literature, is 55 °C. No open literature data is available on fracture toughness of welded joints, but only on pure weld metals. The work within the DEFSPEED-project was started as a Master of Science work [21] and is continued with a broader test matrix. The influence of environment and strain rate is measured using sub-size specimens prepared from dissimilar metal welds (DMW), where the weld material is Inconel 52 and 182 and from pure weld metals made of Inconel 52, 152, 82 and 182. A pneumatic servo-controlled loading device and potential drop technique to measure the crack growth continuously during the test is used. Tests are mainly performed at 55°C in hydrogenated water with 100 cc H_2/kg H_2O and loading rates of either 0.1 or 6.7 mm/h. The selected hydrogen content for the fracture toughness tests is higher (100 cc H_2/kg H_2O) than the typical hydrogen content of PWR primary water (~30 cc/kg H_2O), i.e., the selected environment for the fracture toughness

tests is accelerated and will obviously result in overly conservative results compared to real PWR environments. However, the main objective is to compare and evaluate the behaviour of different weld metals and to compare pure weld metals to dissimilar metal welds.

The results reveal a decrease in the fracture toughness of Ni-based weld materials in hydrogenated (100 cc H_2/kg H_2O) water at 55 °C at low strain rate. The decrease is more remarkable in pure weld metals than in the specimens from dissimilar metal welds. Concerning the welded joint specimens, the decrease in fracture toughness value J_{IC} was remarkable for Alloy 182, from >260 kJ/m^2 in air to as low as 40 kJ/m^2 in hydrogenated water. The fracture toughness of specimens cut from the DMW made using Alloy 52 filler material showed no influence of hydrogenated water, and the toughness was so high (>300 kJ/m^2), that valid J_{IC} values were not obtained. However, low J_{IC} values, down to 46 kJ/m^2, were measured on pure Alloy 52 weld metal specimens, Figure 27.1.8. Also the J_{IC} values of pure Alloy 182 specimens were lower than those from DMW specimens, but the difference was smaller (the lowest J_{IC}-value was 40 kJ/m^2 in DMW specimen and 31 kJ/m^2 in a pure weld metal specimen). A summary of selected results obtained so far are presented in Figure 27.1.9. The reasons for the difference between welded joints and pure weld metals will be further investigated. One reason may be the dilution of nickel in the weld metal during welding.

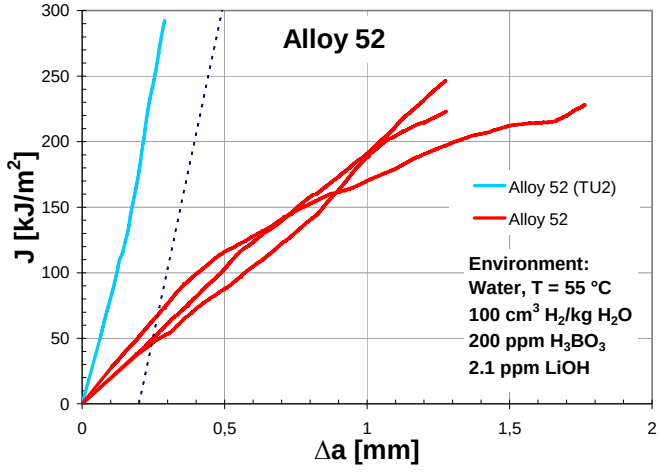

Figure 27.1.8. Fracture toughness, i.e., J-R curves for pure weld metal specimens made of Alloy 52 and from Alloy 52 dissimilar metal welds (TU2) in hydrogenated water at 55 °C sing a loading rate of 0.1 mm/h.

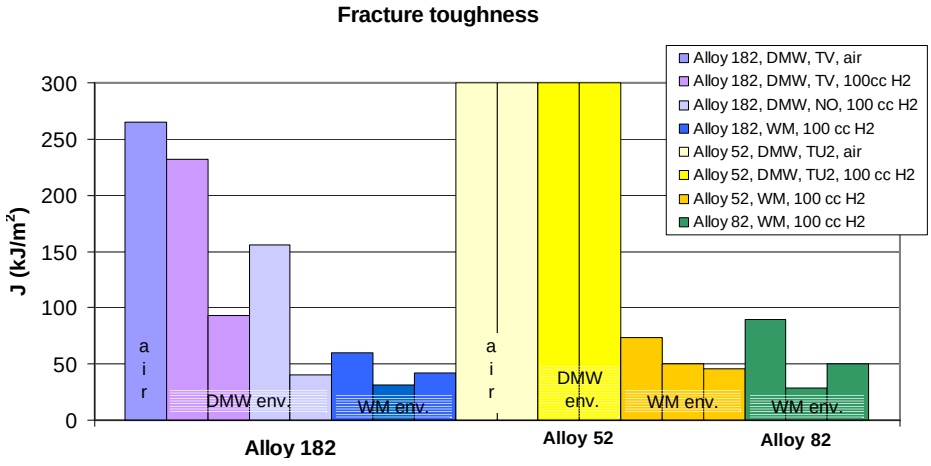

Figure 27.1.9. Fracture toughness, J_{IC} or J_Q, values obtained in air and hydrogenated water at 55 °C ("env.") using a loading rate of 0.1 mm/h. WM denotes pure weld metal specimens and DMW specimens from welded dissimilar metal welds.

International co-operation and education

Education of new experts in the field of nuclear materials is an important objective for the DEFSPEED project, which may become even more important when taking into account the clear indications of a nuclear renaissance in Finland in conjunction with the skewed age distribution of the experts. Young persons; students, researchers and technicians; are encouraged to work within the DEFPSEED-project. Through active participation in international expert working groups and conferences, the latest international knowledge is brought to Finland, where it is then utilised in research projects as well as in conducting failure analyses. The international meetings also have an important educational aspect.

Applications and conclusions

Non-homogeneous microstructures always occur in welded structures and materials fabricated by different methods and subjected to complex strain paths. Investigations on strain localisation are important e.g. for old plants with respect to life extension and increased power outputs, but also for new components for modernisations and utilized in new builds. Materials having non-homogeneous microstructures do not deform uniformly, even though engineering design often assumes uniform deformation. Mechanistic understanding and data on different

phenomena are important for enabling things like the prediction and quantification of the risk for environmentally assisted cracking in austenitic materials in BWRs and PWRs. Such predictions can be used for guiding the selection of reliable criteria for NDE programs. It is also needed when trying to understand and predict the very long incubation times for crack initiation, as observed e.g. for Ni-based materials in operating power plants. The increased knowledge on EAC is particularly useful when conducting failure analyses on plants components.

Conducting transmission electron microscope (TEM) examinations of materials that have been removed from service in real reactors makes an important contribution towards better understanding the role of irradiation in promoting EAC and IASCC. This information could possibly also be used for evaluation of a need for adjustments of chemical composition requirements for materials for new internals.

Knowledge and data on the behaviour of nickel-based materials in hydrogenated environments is important for the structural integrity assessment of nuclear components. Facture toughness data as a function of strain rate, environment and material is a prerequisite to enable evaluation of the risk for low temperature crack propagation, LTCP, in nuclear components in different operational conditions. The results obtained within the DEFSPEED project so far indicates, that dissimilar metal welds have higher fracture toughness values compared to those of pure weld metals. The reasons for this will be further investigated in this project.

References

1. Danko, J. (Ed.). Proceedings on Seminar on Countermeasures for Pipe Cracking in BWRs. EPRI Report NP-3684-S4, 1984.

2. Ehrnstén, U., Aaltonen, P., Nenonen, P., Hänninen, H., Jansson, C. & Angeliu, T. Intergranular Cracking of AISI 316NG Stainless Steel in BWR Environment. 10th Symposium on Environmental Degradation of Materials in Nuclear Power Systems – Water Reactors. Nevada, USA, 5–9 August, 2001, ANS, NACE, TMS. 10 p.

3. Tähtinen, S., Hänninen, H. & Trolle, M. Stress Corrosion Cracking of Cold Worked Austenitic Stainless Steel Pipes in BWR Reactor Water. 6th Symposium on Environmental Degradation of Materials in Nuclear Power Systems – Water Reactors. San Diego, CA, USA, August 1–5, 1993, TMS. Pp. 265–275.

4. Horn, R., Gordon, G., Ford, P. & Cowan, R. Experience and Assessment of Stress Corrosion Cracking in L-Grade Stainless Steel BWR Internals. Nuclear Engineering and Design, 1997. Vol. 174, pp. 313–325.

5. Angeliu, T. Microstructural Characterization of L-Grade Stainless Steels Relative to the IGSCC Behavior in BWR Environments. Proc. of Corrosion 2001. NACE, Houston, Texas, March 11–16, 2001. Paper No. 01121. 14 p.

6. Aaltonen, P., Saario, T., Karjalainen-Roikonen, P., Piippo, J., Tähtinen, S., Itäaho, M. & Hänninen, H. Vacancy-creep Model for EAC of Metallic Materials in High Temperature Water. Corrosion ’96. Denver, CO, 24–29 March 1996. NACE International, Houston. Paper No. 81. 12 p.

7. Ehrnstén, U. & Hänninen, H. Environmentally Assisted Cracking of Non-sensitised Stainless Steels – Possible Affecting Phenomena. Fontevraud 6, Contribution of Materials Investigations to Improve the Safety and Performance of LWRs. Fontevraud Royal Abbey, France, 18–22 Sept. 2006. French Nuclear Energy Society, SFEN (2006). Pp. 1–10.

8. Ehrnstén, U. Interim report on Super Slow Strain Rate Tests of Austenitic Materials in Nuclear Environments – Report on Work Performed in 2007. Research Report VTT-R-00795-08.

9. Saukkonen, T. & Hänninen, H. Determination of Calibration Curves for Measuring Plastic Strain by EBSD in AISI 316 and AISI 304 Stainless Steel Power Plant Materials. Work Report for the DEFSPEED project.

10. Saukkonen, T., Ehrnstén, U. & Hänninen, H. Microstructure and Plastic Strain Distribution of an AISI 304 Stainless Steel Power Plant Pipe Weld Studied by EBSD. Submitted for Journal of Microscopy for publication.

11. Saukkonen, T., Ehrnstén, U. & Hänninen, H. Microstructure and Plastic Strain Distribution in an AISI 304 Stainless Steel Power Plant Pipe Weld Studied by EBSD. Royal Microscopical Society, 15th Electron Backscatter Diffraction Meeting, 31 March-1 April 2008. England: University of Sheffield, 2008.

12. Ehrnstén, U., Ivanchenko, M., Nevadacha, V., Yagodzinskyy, Y., Toivonen, A. & Hänninen, H. Dynamic Strain Ageing of Nitrogen-alloyed AISI 316L Stainless Steel. Proc. of Eurocorr 2004. Nice, France, 13–16.9 2004. Event No. 226. 10 p.

13. Ehrnstén, U., Ivanchenko, M., Nevdacha, V., Yagodzinskyy, Y., Toivonen, A. & Hänninen, H. Dynamic Strain Ageing and EAC of Deformed Nitrogen-Alloyed AISI 316 Stainless Steels. 12th Symposium on Environmental Degradation of Materials in Nuclear Power Systems – Water Reactors, TMS, 2005. Pp. 1475–1482.

14. Hänninen, H., Ivanchenko, M., Yagodzinskyy, Y., Nevdacha, V., Ehrnstén, U. & Aaltonen, P. Dynamic Strain Ageing of Ni-base Alloys Inconel 600 and 690. 12th Symposium on Environmental Degradation of Materials in Nuclear Power Systems – Water Reactors, TMS, 2005. Pp. 1423–1430.

15. Ivanchenko, M., Yagodzinskyy, Y. & Hänninen, H. Effect of Plastic Deformation on Anelastic Mechanical Losses in Multicomponent Substitutional Austenitic Alloys. Materials Science and Engineering A, 2006. Vol. 442, pp. 458–461.

16. Ivanchenko, M., Yagodzinskyy, Y. & Hänninen, H. Effect of DSA on Interstitial Redistribution in AISI 316NG steel and Inconel 600 Alloy. Proceedings of Third Nordic Symposium for Young Scientists in Metallurgy. TKK, Espoo, Finland, May 14–15, 2008. HUT, Faculty of Chemistry and Material Science, Department of Material Science and Engineering. Espoo: Multiprint Oy, 2008. Pp. 68–71.

17. Karlsen, W. Examination of Dynamic Strain Ageing Microstructures in 316 Stainless Steel by TEM. Research Report VTT-R-10235-07. Espoo: VTT, 2007.

18. Karlsen, W. & Aaltonen, P. FEGSTEM Study of 12 dpa Barsebäck 304L and 20 dpa and 130 dpa Chooz A 304 SS. VTT Research Report VTT-R-01215-07. Espoo: VTT, 2007.

19. Karlsen, W. Characterisation of LWR Irradiated Stainless Steel Internal Components by FEG-STEM. VTT Research Report No VTT R-07773-07. Espoo: VTT, 2007.

20. Karlsen, W. Grain Boundary Analyses of 30 dpa Chooz A 304 SS Centre Filler Assembly. VTT Research Report VTT-R-01344-08. Espoo: VTT, 2008.

21. Ahonen, M. Ympäristön ja muodonmuutosnopeuden vaikutus austeniittisten materiaalien murtumisvastuskäyttäytymiseen. Tutkimusraportti VTT-R-06172-08. Espoo: VTT, 2008.

27.2 Strain localisation in sensitised Type 304 stainless steel in simulated BWR-environment

Ulla Ehrnstén
VTT

Tapio Saukkonen and Hannu Hänninen
Helsinki University of Technology, Engineering Materials

Abstract

Intergranular, environmentally assisted cracking (EAC) has been observed, not only in sensitised austenitic stainless steels in oxidising BWR conditions, but also in non-sensitised, cold deformed stainless steels. Further, EAC has recently been reported also in PWR plants, in connection to local non-specified water chemistry conditions. Environmentally assisted cracking in nickel-based weld metals is considered to be one of the most challenging issues for operating power plants today. Mechanistic understanding of the effects of main factors affecting environmentally assisted cracking of austenitic materials is important, especially as the trend in the NDE inspection strategy is moving towards risk-informed inspection.

In the SAFIR 2010 DEFSPEED project (Influence of material, environment and strain rate on environmentally assisted cracking of austenitic nuclear materials), investigations are performed using super slow strain rate tests (SSSRT) in LWR environments and the deformation is characterised using versatile methods such as FE-SEM EBSD and TEM. The investigations aim to increase the mechanistic understanding of precursors to crack initiation as well as factors affecting crack growth in austenitic nuclear materials. The results achieved from the SSSRT's on deformed and sensitised austenitic stainless steel of Type 304 and from EBSD characterisation of a Type 304 nuclear pipe weld show non-uniform distribution of micro-strains in the material, being higher in the vicinity of grain boundaries than inside the grains. The results indicate that several phenomena can occur during extremely slow deformation, such as heterogeneous creep, dynamic recovery and relaxation leading to grain boundary sliding, dynamic strain ageing and short range ordering. The results also show

that non-homogeneous microstructures, e.g. local changes in the grain size, affect strain localisation.

Introduction

Intergranular stress corrosion cracking (IGSCC) of sensitised stainless steels in oxidising boiling water reactor (BWR) environments caused major capacity factor losses in the 1970 and 1980's. Large research programmes to solve the problem were launched, major factors contributing to the problem were identified and quantified and remedial actions were taken [e.g., 1]. Consequently, the amount of IGSCC in sensitised stainless steels decreased remarkably, and the capacity factor of the BWRs has increased. The remedial actions included development and employment of low-carbon stainless steels, new welding techniques decreasing the residual stresses and sensitisation as well as improvement of the water chemistry with different measures.

Non-sensitised stainless steels can, however, also suffer from intergranular, environmentally assisted cracking (EAC). This type of cracking has so far been connected to cold-worked stainless steels and it has been reported to occur in oxidising environments [2–7], but it seems to be also a potential degradation mode in the non-oxidising environments [8], i.e., both in BWR and PWR conditions.

Table 27.2.1. Examples of IGSCC cases in non-sensitised stainless steels in BWR and PWR environments.

Location	**Assumed main affecting parameters**	**Ref.**
BWR: HAZ in AISI 316NG piping	High shrinkage strains from welding at difficult location	2
BWR: Cold bent pipe elbow of AISI 304	Initiation in highly deformed surface layer from bending with mandrel	3
BWR: Core shrouds of AISI 304L or AISI 347	Surface grinding resulting in high hardness, high ECP, thermal ageing	7
BWR: Core spray annulus pipe of AISI 316L	not mentioned	4
BWR-like: RBMK downcomer pipes of Ti-stab. SS	Weld defects, surface cold work, high residual stresses	9
PWR: Pressurizer heater	Cold deformation, off-normal local conditions (T and environment)	8

Several projects worldwide focus today on intergranular cracking investigations of cold-deformed stainless steels in BWR and PWR environments [e.g. 7, 10]. Cold work of components in operating plants can, e.g., be caused by shrinkage during welding, surface grinding or machining. Weld shrinkage can cause high residual strains, and up to 20% residual strains have been measured in the HAZ of a weld with IGSCC [2], welded at a difficult location. Recognition of possible sites for cracking and predictability of ageing becomes increasingly important, e.g., due to increased application of risk-informed inspection strategies and increasing demands on operation efficiency factors. In the case of sensitised stainless steels in BWR NWC (normal water chemistry) environment, welds joining stainless steel pipes with high carbon content (>0.03%) are usually classified to have a risk for sensitisation (thermal during welding or low temperature sensitisation during long term operation) and are therefore included in the NDE programs as sites of special interest. Classification of high risk welds in non-sensitised stainless steels is not easy due to the fact that the degree of cold-work is generally not known and that all affecting parameters causing increased risk are not understood or quantified. Welding with narrow-gap welding technique decreases remarkably the risk for crack initiation due to the smaller residual stresses and strains in this type of welds. However, if a crack initiates within the first few grains from the fusion line (which is typical for deformed, non-sensitised stainless steels), the crack path follows the fusion line and is thus perpendicular to the pipe axis. This is also the direction of the most likely principal stresses. This crack growth can occur without any inclination of the crack path, which could be connected to slower crack growth rate or even suppression.

Localisation of plastic deformation and the interactions between oxidation and strain localisation are most probably playing a key role in cracking of cold-worked stainless steels. Mechanistic understanding of the effects of main factors affecting intergranular stress corrosion cracking of cold-worked, non-sensitised austenitic stainless steels is important, especially as the trend in the NDE inspection strategy is moving towards risk-informed inspection. Further, mechanistic understanding is also important to increase the understanding of the possible risk for IGSCC in PWR-plants, where this failure mode mostly is regarded as negligible, and for increased understanding of the reasons for the very long incubation times for crack initiation, as observed, e.g. for Ni-based materials in operating nuclear plants.

Super slow strain tests of sensitised Type 304 stainless steel

Slow strain rate tests are used as a method to investigate susceptibility of materials to stress corrosion cracking. The strain rates typically used are in the order of 10^{-6} s^{-1}, which are several decades faster than the slow dynamic loading which may locally occur in real plants. The technique has mainly been used as an accelerated test for screening purposes to evaluate e.g. the suitability of different materials to different environments. However, the method using 'conventional' strain rates is not regarded to be sensitive enough for evaluation of the behaviour of modern, less EAC-susceptible nuclear materials in clean (i.e., free of impurities) LWR environments. VTT has developed a bellows loading system which enables very slow strain rate with truly constant extension rate and measurement of the strain from the specimen itself [11]. Super slow strain rate tests, SSSRT's, were started by evaluating the technique using two strain rates ($1 \cdot 10^{-7}$ s^{-1} and $1 \cdot 10^{-8}$ s^{-1}) and two material conditions, i.e., sensitised AISI 304 stainless steel with or without 10% cold work were performed in simulated BWR environment (400 ppb O_2, 300 °C). Further SSSRT's will be performed on austenitic nuclear materials in BWR and PWR environments and tests are ongoing using non-sensitised stainless steel of Type 316L in BWR-environment.

The results from the evaluation tests showed an increased sensitivity of the test with decreasing strain rate, manifested by a higher amount of intergranular cracking and smaller strain to fracture with decreasing strain rate, Figure 27.2.1 [12]. The results also showed a detrimental influence of deformation manifested by a higher amount of intergranular cracking in specimens, which had been cold-deformed 10% before SSSR-testing. Scanning electron microscopy revealed intergranular initiation and typically small steps at the crack mouths indicating a shear strain component, Figure 27.2.2.

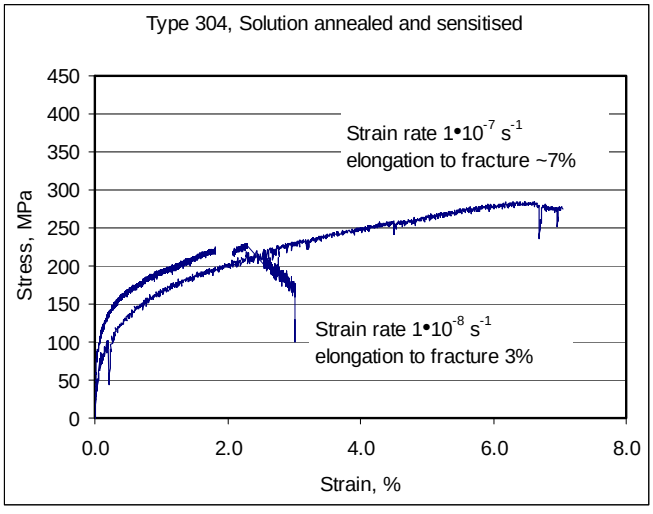

Figure 27.2.1. Stress vs. strain for solution annealed and sensitised Type 304 austenitic stainless steel specimens tested using different strain rates, i.e., $1 \cdot 10^{-7}$ s^{-1} and $1 \cdot 10^{-8}$ s^{-1}, in simulated BWR environment.

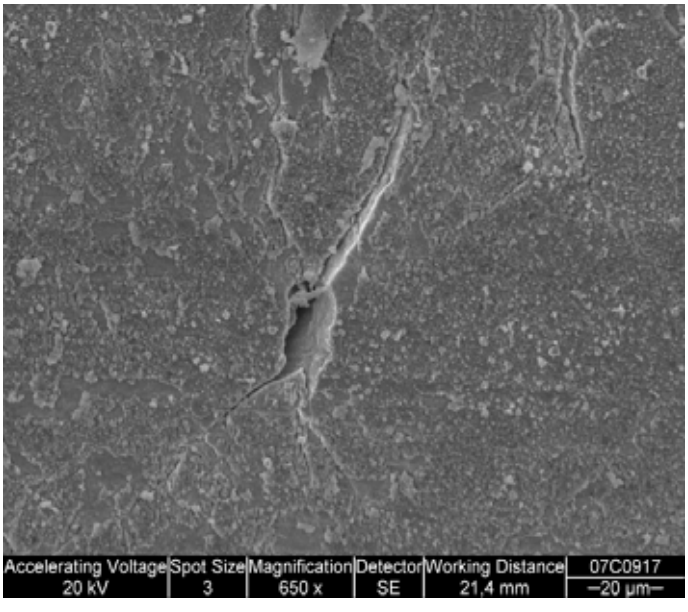

Figure 27.2.2. SEM-picture of a solution annealed and sensitised specimen surface after SSSRT using a strain rate of $1 \cdot 10^{-8}$ s^{-1}, showing a small step at the crack mouth of a small secondary crack.

Electron back-scattered diffraction, EBSD, is a very versatile method for characterising crystalline materials. EBSD maps can be formed in numerous ways to reveal desired properties, e.g., grain boundaries, texture, orientation gradients, etc. Intra-grain mis-orientations can be calibrated for quantitative measurement of local plastic strain [13]. This method was employed to characterise specimens from the SSSR-testing. The results show non-uniform distribution of plastic strains in the specimens, with higher plastic strains in the vicinity of grain boundaries than inside the grains, Figure 27.2.3. Non-uniform distribution of the plastic strains was also observed at the surface of the specimens, indicating local strain gradients. It seems that local strain distributions at the surface may affect the location of crack initiation, which would occur at the location with local smallest degree of strain, Figure 27.2.4. Also the local differences in grain sizes affected the strain distribution, being higher in the region with smaller grain size compared to a neighbouring area with larger grain size, Figure 27.2.5.

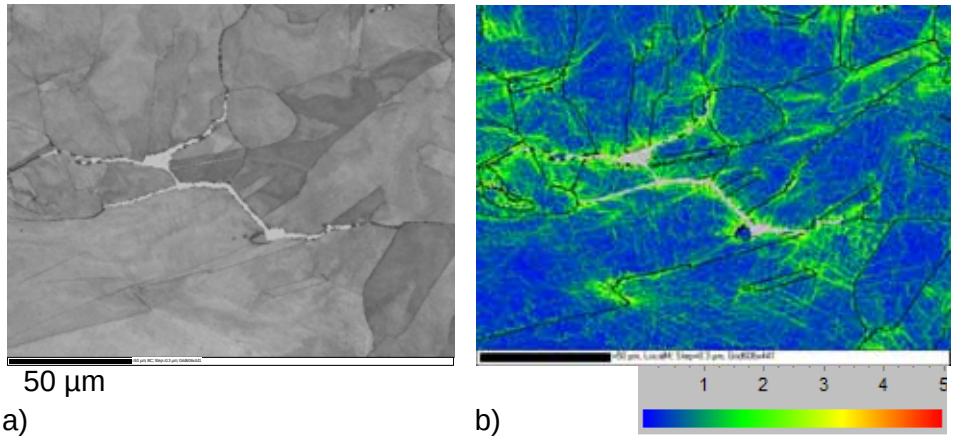

Figure 27.2.3. Pattern quality map (a) showing the microstructure of a crack tip area in a solution annealed and sensitised Type 304 stainless steel after SSSR-testing in simulated BWR environment and the local mis-orientation map in the same area (b). Blue, through green to red colour correspond to the range from smallest to highest degree of mis-orientation, i.e., from lowest to highest amount of plastic strain.

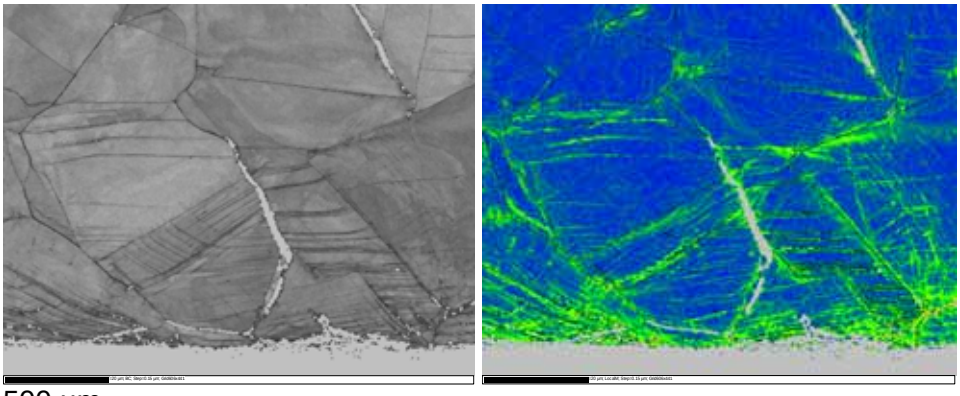

500 µm

a) b)

Figure 27.2.4. Pattern quality map (a) and mis-orientation map (b) close to the surface of an SSSRT specimen showing less strain at the location of the crack initiation site compared to the immediate surrounding.

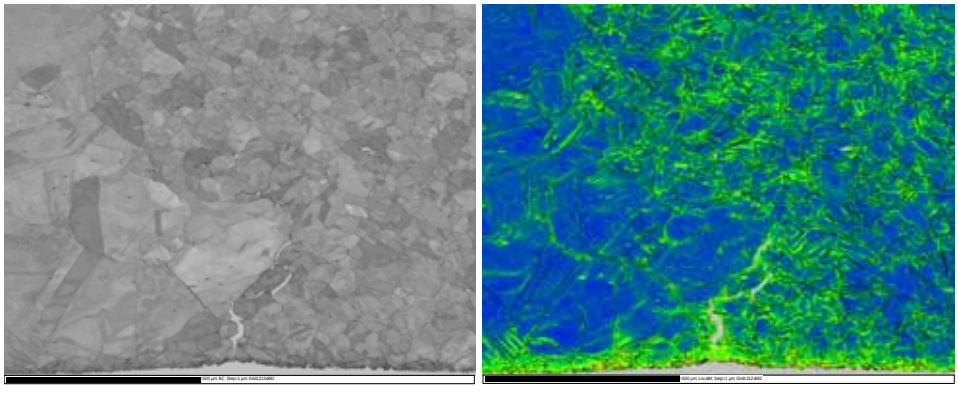

500 µm

a) b)

Figure 27.2.5. Pattern quality map (a) and mis-orientation map (b) close to the surface of an SSSRT specimen showing more strain in the area with smaller grain size compared to that with larger. The strain is localised at the grain boundaries.

Measurement of local strain distribution in a Type 304 weld

A Type 304 austenitic stainless steel pipe with nominal dimensions of 275x22 mm, which had been welded for a nuclear power plant using tungsten inert gas welding, TIG, was characterised using different methods. The strain distribution in the typical nuclear pipe weld was determined using EBSD [14]. Additionally, micro-hardness measurements were performed and the results were converted to local amount of strain using the calibration curves for hardness and mis-orientation versus plastic strain. Further, measurements of residual stresses were made using the Contour method as a part of another project.

The highest degrees of plastic strain (10–20%) were measured in the heat affected zone (HAZ) close to the root area of the weld, Figure 27.2.6, and the highly deformed zone extends 5–7 mm from the fusion line to the base material. The amount of plastic strain in the base material decreases towards the outer surface of the pipe. Plastic strain was also measured in the weld metal, where it varies in the different directions of solidification, being highest in the areas of weld bead boundaries. The strain values obtained by hardness measurements are in fairly good agreement with the EBSD results. The measured plastic strain distributions based on EBSD and hardness are summarised in Figure 27.2.7. The results from the residual stress measurements showed highest tensile stresses in the middle of the weld, which extend to the base material on both sides of the weld, Figure 27.2.8. The residual stresses are higher on one side of the weld compared to the other. Also the EBSD measurements showed different amounts of plastic strain on each side of the weld.

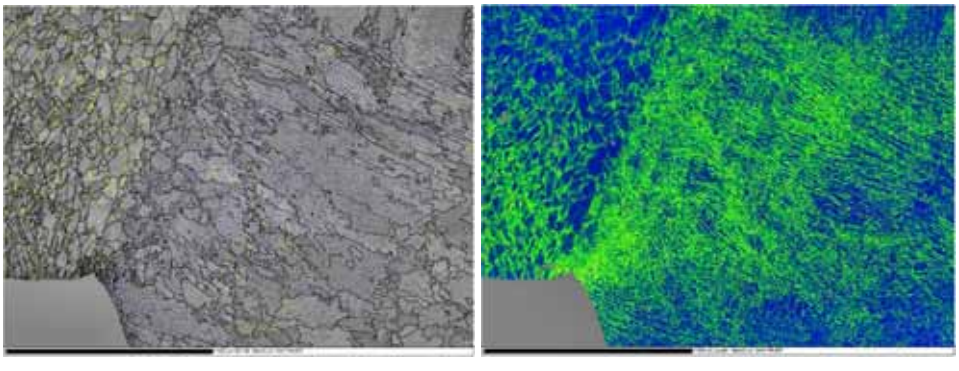

a) b)

Figure 27.2.6. Pattern quality map (a) showing the microstructure of the fusion line area at the weld root, and local mis-orientation map from the same area of the investigated weld.

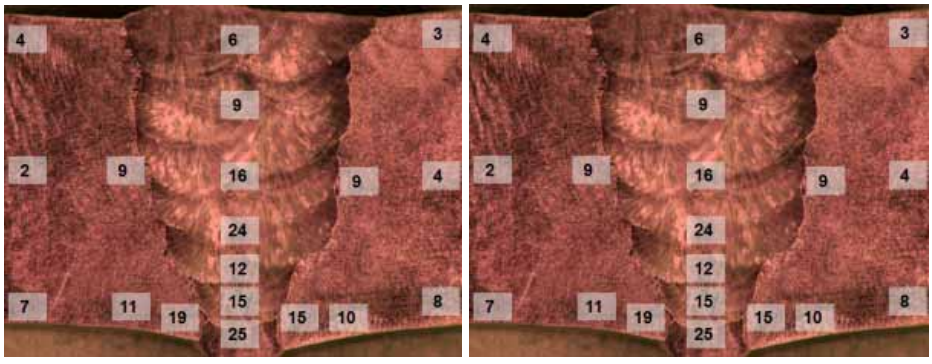

a) b)

Figure 27.2.7. Measured values of plastic strain (%) in different areas of the cross-section of the weld using a) EBSD and b) hardness measurements.

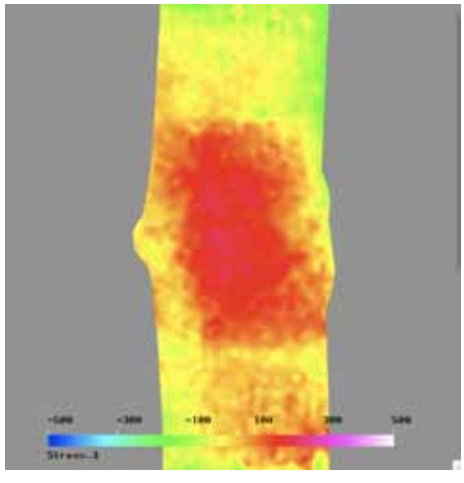

Figure 27.2.8. Residual stresses in the nuclear pipe weld made of the Type 304 austenitic stainless steel.

Conclusions

The results from the super slow strain rate tests on deformed and non-deformed, sensitised Type 304 austenitic stainless steel showed an increased sensitivity of the test with decreasing strain rate, manifested by a higher amount of intergranular cracking and smaller strain to fracture with decreasing strain rate. It also revealed

a detrimental influence of deformation. EBSD-measurements on these sensitised stainless steel specimens revealed non-uniform deformation, with higher plastic strains in the vicinity of grain boundaries than inside the grains. These techniques are further employed in the investigations on deformed, non-sensitised austenitic stainless steels in BWR- and PWR-environments as well as on nickel-based materials.

The EBSD method is a powerful tool to measure local residual plastic strains and localisation of deformation. The method can, and should, be utilised to characterise typical nuclear components or mock-ups, such as specimens from welding procedure tests, from parts removed from operation and from failed sections.

Non-homogeneous microstructures always occur in welded structures and materials fabricated by different methods and subjected to complex strain path. Investigations on strain localisation are important e.g. for old plants related to life extension and increased power, but also for new components for modernisation and utilized in new builds. Materials having non-homogeneous microstructures do not deform uniformly, even though engineering design often assumes uniform deformation. Mechanistic understanding and data on different phenomena are important for enable things like the prediction and quantification of the risk for environmentally assisted cracking austenitic materials. Such predictions can be used for guiding the selection of reliable criteria for NDE programs. It is also needed when trying to understand and predict the very long incubation times for crack initiation, as observed e.g. for Ni-based materials in operating power plants. The increased knowledge on EAC is particularly useful when conducting failure analyses on plant components.

References

1. Danko, J. (Ed.). Proceedings on Seminar on Countermeasures for Pipe Cracking in BWRs. EPRI Report NP-3684-S4, 1984.

2. Ehrnstén, U., Aaltonen, P., Nenonen, P., Hänninen, H., Jansson, C. & Angeliu, T. Intergranular Cracking of AISI 316NG Stainless Steel in BWR Environment. 10th Symposium on Environmental Degradation of Materials in Nuclear Power Systems – Water Reactors. Nevada, USA, 5–9 August, 2001, ANS, NACE, TMS. 10 p.

3. Tähtinen, S., Hänninen, H. & Trolle, M. Stress Corrosion Cracking of Cold Worked Austenitic Stainless Steel Pipes in BWR Reactor Water. 6th Symposium on Environmental Degradation of Materials in Nuclear Power Systems – Water Reactors. San Diego, CA, USA, August 1–5, 1993, TMS. Pp. 265–275.

4. Horn, R., Gordon, G., Ford, P. & Cowan, R. Experience and Assessment of Stress Corrosion Cracking in L-Grade Stainless Steel BWR Internals. Nuclear Engineering and Design, 1997. Vol. 174, pp. 313–325.

5. Angeliu, T. Microstructural Characterization of L-Grade Stainless Steels Relative to the IGSCC Behavior in BWR Environments. Proc. of Corrosion 2001. NACE, Houston, Texas, March 11–16, 2001. Paper No. 01121. 14 p.

6. Andresen, P., Emigh, P., Morra, M. & Horn, R. Effects of Yield Strength, Corrosion Potential, Stress Intensity Factor, Silicon and Grain Boundary Character on the SCC of Stainless Steels. 11th Symposium on Environmental Degradation of Materials in Nuclear Power Systems – Water Reactors. Stevenson, WA, Aug. 10–14, 2003. Pp. 816–833.

7. Ooki, S., Tanaka, Y., Takamori, K. & Suzuki, S. Study on SCC Growth Behavior of BWR Core Shroud. 12th International Conference on Environmental Degradation of Materials in Nuclear Power Systems – Water Reactors, TMS, 2005. Pp. 365–376.

8. Couvant, T., Moulart, P., Legras, L., Bordes, P., Capelle, J, Rouillon, Y. & Balon, T. PWSCC of austenitic stainless steels of heaters of pressurizers. Proceedings of the 6th International Symposium on Contribution of Materials Investigations to Improve the Safety and Performance of LWRs. French Nuclear Society, Fontevraud. 18–22 September, 2006. Paper A100-TO3. 12 p.

9. Timofeev, B., Federova, V. & Buchatskii, A. Intercrystalline Corrosion Cracking of Power Equipment Made of Austenitic Stainless Steels. Materials Science, 2004. Vol. 40, No. 1, pp. 48–59.

10. Couvant, T., Valliant, F., Boursier, J.-M. & Delafosse, D. Effect of Strain-Path on Stress Corrosion Cracking of AISI 304L Stainless Steel in PWR Primary Environment at 360 °C. Proc. of Eurocorr 2004. Nice, France, 13–16.9.2004. Event No. 226. 11 p.

11. Moilanen, P. Pneumatic Servo-Controlled Material Testing Device Capable of Operating at High Temperature Water and Irradiation Conditions. VTT Publications 532. Espoo: VTT, 2004. 154 p. http://www.vtt.fi/inf/pdf/publications/2004/P532.pdf.

12. Ehrnstén, U. Interim report on Super Slow Strain Rate Tests of Austenitic Materials in Nuclear Environments – Report on work performed in 2007. Research Report VTT-R-00795-08. Espoo: VTT, 2008.

13. Saukkonen, T. & Hänninen, H. Determination of Calibration Curves for Measuring Plastic Strain by EBSD in AISI 316 and AISI 304 Stainless Steel Power Plant Materials. Work Report for the DEFSPEED project.

14. Saukkonen, T., Ehrnstén, U. & Hänninen, H. Microstructure and Plastic Strain Distribution in an AISI 304 Stainless Steel Power Plant Pipe Weld Studied by EBSD. Royal Microscopical Society, 15th Electron Backscatter Diffraction Meeting. 31 March – 1 April 2008. Sheffield, England: University of Sheffield. 16 p.

28. Service life management system of concrete structures in nuclear power plants (SERVICEMAN)

28.1 SERVICEMAN summary report

Erkki Vesikari and Liisa Salparanta
VTT

Esa Turunen
ÅF Consult Oy

Abstract

The objective of the project is to develop a service life management system (SLMS) for concrete structures in nuclear power plants. By the SLMS the safety, performance and serviceability are secured during the operational life of the plant. The SLMS helps in conducting systematic maintenance policy and in finding optised maintenance strategy with regard to life cycle costs and environmental impacts. The core of the system is formed by the service life management tool ServiceMan but the system includes also special risk analyses and structural analyses focused on the containment building.

Introduction

A service life management system of concrete structures in nuclear power plants is being developed in VTT in cooperation with the Finnish nuclear companies TVO and FORTUM. The work started in 2006 as a preliminary study and is continued under the auspices of SAFIR 2010 (The Finnish Research Programme

on Power Plant Safety) as the actual research project in 2007–2010. The service life management system is developed for the maintenance engineers of nuclear power plants for conducting systematic maintenance policy and for planning, organising and optimising maintenance strategy of concrete structures in nuclear power plants.

Objectives

The main objective of the project is to develop a predictive service life management system for concrete structures in nuclear power plants. The management system is capable of predicting the condition of structures, guarding of safety and serviceability limits, timing of intervention actions including inspection, maintenance and repair actions, and evaluating life cycle costs, environmental impacts and structural risks. The core of the SLMS is formed by the service life management tool "ServiceMan" but the system includes also special risk analyses and structural analyses for safety related structures. By the SLMS the safety, accepted structural performance and uninterrupted service of concrete structures are ensured during the planned service life of a nuclear power plant.

The SLMS is connected with the in-service inspection system of NPP by special inspections. Thus the observed condition of structures is brought to the process of service life prediction and decision making on maintenance and repair actions. The methodological ground of the service life management system was developed during the EU project LIFECON (2001–2003) [1].

Service life management tool ServiceMan

ServiceMan is a program for life cycle planning and management of concrete structures in nuclear power plants. The basic ideas of program ServiceMan could be expressed by the following characteristics of the system: predictive, integrated, life-cycle based and probabilistic. The attribute "predictive" refers to the ability of the tool to predict the condition of structures over a long period of time, and to specify future MR&R actions in order to keep the condition of structures within an accepted level. "Integrated" means that not only the condition of structures but also other indicators of lifetime quality, such as life cycle costs, environmental impacts, and risks can be considered in the decision making on maintenance strategy. The condition, costs and environmental impacts are evaluated over the remaining licenced operating time of the plant or longer if necessary. The condition analysis is probabilistic in order to make the

theory of reliability applicable for the timing of special inspections and MR&R actions.

The plant units are divided into structures. The structures are still divided into smaller parts which are called “modules”. The modules can be treated roughly as homogenous with respect to materials, structural features and environmental conditions. The modules serve as basic structural units in the analysis and planning processes of the system. The structural and modular databases which serve as initial data sources in the calculation processes are consistent with the modular breakdown of structures.

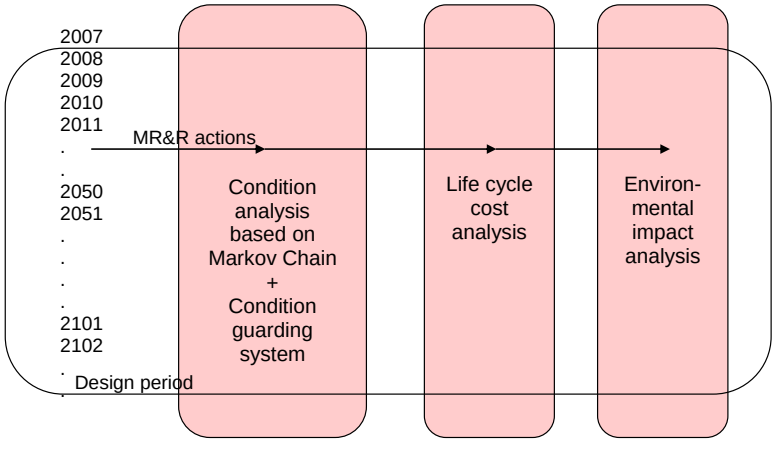

Figure 28.1.1. Combined Life Cycle Analysis.

The core of the planning process consists of a combined condition, cost and environmental impact analysis (Figure 28.1.1). The condition analysis is produced automatically based on degradation models and predefined limit states of condition. The condition analysis is stochastic (based on the Markov Chain method) and is capable of predicting the probability of the structure to be at any of the condition states during the treated design period. The analysis consists also of an automatic condition guarding system which is able to trigger MR&R actions whenever the predefined limit state of condition is exceeded. [2, 3, 4]

Risk analyses

The purpose of the risk analysis is to address the aging problems of containment buildings with higher level of accuracy than other structures. The risk analyses focus degradation phenomena occurring in both steel and concrete parts of the containment and try to summarize the total risk. The probability of corrosion in pre-stressing tendons and the steel liner are evaluated using reliability based methods with time dependent degradation models. Thus the evaluated probability of a tendon damage or corrosion of steel liner is a time-dependent quantity with an increasing trend. Also traditional methods of PSA such as logical trees are used to describe and summarize the effects of different risk factors. In 2008 a report on risk analysis methods and procedures for concrete structures in nuclear power plants was produced. [7]

Structural analyses

Structural degradation analyses

The structural degradation analyses support the risk analyses by bringing the risk evaluation to the structural level. Structural degradation analyses assume changes in material properties, damages and long-term deformations in structures and try to answer what is the total effect of ageing to the structural safety? One objective of the analyses is to find out acceptance limits for various types of degradation.

Structural degradation analyses are conducted using different methods with different levels of accuracy. High accuracy level analyses are performed using the Finite Element Method (FEM). The relaxation of the pre-stressed tendons and the time-dependent nonlinear behaviour of concrete as well as the interaction between steel and concrete (slip of tendons) are considered. At lower level of accuracy pre-stressed concrete structures are analysed using Excel based programs in which the structure is simplified and divided into smaller parts.

Serviceability limit state design

The development of serviceability limit state design for reinforced concrete structures was started in 2007 and continued until the end of year 2008. The system is utilising the results of a FEM analysis and dimensioning is done through the in-house computer program according to the selected standard (National building code of Finland: B4, DIN 1045, SNiP-84). The system is

applicable within structural analysis and limit state design especially in reinforced concrete structures of nuclear power plants.

During the year 2007 the design algorithm of serviceability limit state design accordance with Eurocode 2 was developed. In 2008 the developed design algorithm was programmed into the in-house computer program developed for structural design and analysis of reinforced concrete structures. Also the design algorithm of ultimate limit state was developed and programmed and necessary verification tests were conducted. Reliability of the program was ensured by simple hand calculations for limited number of shell and beam elements and loading conditions. [5, 6]

Research Cooperation on Concrete Material Technology

Partners in the BTS-research cooperation are: Finnish Road Administration, Finnish Rail Administration, Radiation and Nuclear Safety Authority, City of Helsinki, City of Tampere, City of Espoo, City of Turku. The research in BTS has been focused around durability and aging management of concrete structures.

In 2007 a field study DURAFIELD on durability of concrete materials and structures was started. In 2008 this project was extended international and the project name was changed to DURAINT. The results of this research can be utilised in the degradation models of NPP structures.

In Table 28.1.1 some BTS research topics from years 2007–2008 are presented.

The reports of the BTS-research cooperation are written in Finnish as a rule. They are available for the participants of SAFIR 2010 by request (Liisa Salparanta).

Table 28.1.1. Research topics BTS.

Topic	Objective/ State
1. SILKO-test of concrete repair materials, a two-year study (2007–2008)	1. Criteria and test programme for concrete repair materials. List of suitable repair materials for different applications and grading of their properties. Completed.
2. Design and practice of cathodic protection	2. Guidelines for the use of cathodic protection for concrete structures. Completed.
3. Quality requirements and verification of conformity of concrete substrate for reparation	3. Quality requirements and verification methods of conformity of concrete substrate for reparation. Completed.
4. Correlation between shrinkage measurement methods (In preparation)	4. Correlation between shrinkage measurement methods. Criteria for shrinkage measured in construction site. Completed.
5. The effect of formliner on the Cl-permeability of concrete, continues from 2007	5. The effect of hydrophobic impregnation and using of formliner on the Cl-permeability of concrete. Completed.
6. RH measurement method of the substrate for waterproofing and RH criteria	6. Knowledge of the applicability of new RH measurement methods for site measurements. RH criteria for the substrate for waterproofing. Ongoing.
7. Electrochemical chloride extraction form reinforced concrete	7. Applicability and efficiency of electrochemical chloride extraction form reinforced structures. Completed.
8. Rapid, cheap and simple chloride content measurement method for site	8. Applicability and accuracy of rapid, cheap and simple chloride content measurements method for site. State of the art of development of such methods. Methods that could be developed to be used for site measurements. Completed.

Reserch Cooperation on Aging Problems of Concrete Structures in Nuclear Power Plants

VTT has participated in the work of OECD/NEA/CSNI/IAGE (Integrity and Aging) work group by SAFIR financing (in 2003–2008). The IAGE work group is divided into three subgroups: IAGE Seismic, IAGE Metal and IAGE Concrete. The IAGE Concrete group deals with aging phenomenon and aging management of concrete structures in nuclear power plants.

VTT is also participating in the activities of COST C25 “Sustainability of Constructions: Integrated Approach to Life-time Structural Engineering” in years 2007–2010. COST C25 is a European network which aims at promoting scientific understanding of life-time engineering and sustainable construction in

Europe. The meetings and seminars are financed by EC for travels and accommodation. Cooperation in COST C25 is useful for the implementation of the service life management system of NPP structures.

Conclusions

The Service Life Management System (SLMS) addresses the needs stated in the Finnish Regulatory guide YVL 1.1: “A plan shall be presented for how the design and qualification of the components and structures, their operation and operating experience, in-service inspections and tests, and maintenance are integrated so as to form a comprehensive ageing management programme.” The system provides the utilities with the following information:

- present condition state of structures
- predicted condition and service life of structures over the licensed operating time
- specified and timed maintenance and repair actions and special inspections during the whole operating time
- costs of maintenance and repair actions
- identification of potential risks related to performance of concrete structures.

The SLMS can convince authorities and the utilities that the concrete structures in the NPPs fulfil the serviceability and safety requirements during the whole licensed operating time. For maintenance staff and designers the SLMS helps conducting systematic maintenance policy which guarantees long service lives for NPP concrete structures.

References

1. Söderqvist, M.-K. & Vesikari, E. 2003. Generic technical handbook for a predictive life-cycle management system of concrete structures (LMS). Lifecon GIRD-CT-2000-00378 Lifecon Deliverable D1.1, final report. 170 p. http://lifecon.vtt.fi/.

2. Vesikari, E. 2007. Service life management system of concrete structures in nuclear power plants. Espoo: VTT Technical Research Centre of Finland. VTT Publications 648. 82 p. http://www.vtt.fi/inf/pdf/publications/2007/P648.pdf.

3. Vesikari, E. 2008. Degradation and service life of concrete structures in nuclear power plants. The Finnish Research Programme on Nuclear Power Plant Safety 2007–2010. Espoo: VTT Technical Research Centre of Finland. Research Report VTT-R-02323-08. 40 p.

4. Vesikari, E. 2009. Service Life Management System SERVICEMAN. Part I User manual & Part II Calculation principles. The Finnish Programme on Nuclear Power Plant Safety 2007–2010. Espoo: VTT Technical Research Centre of Finland. Research Report VTT-R-11305-08. 45 p.

5. Turunen, E. 2007. Halkeilevan teräsbetonirakenteen jäykkyyden redusointi ja mitoitusalgoritmi toteuttaen Eurokoodin määräykset (Stiffness reduction and a design algorithm of cracking concrete structures in compliance with Eurocode regulations). Espoo: Helsinki University of Technology. Master's Thesis. 17 December 2007. 119 p.

6. Turunen, E. & Iivonen, P. 2009. Serviceability limit state and crack width analysis of concrete structures according to Eurocode 2. The Finnish Programme on Nuclear Power Plant Safety 2007–2010. Espoo: VTT Technical Research Centre of Finland. Research Report. 31 p.

7. Vesikari, E. & Rissanen, T. 2009. Risk Assessment Methods with Special Reference to Aging Effects in Containment Buildings of Nuclear Power Plants. The Finnish Programme on Nuclear Power Plant Safety 2007–2010. Espoo: VTT Technical Research Centre of Finland. Research Report VTT-R-10610-08. 51 p.

28.2 Service Life Management System of Concrete Structures in Nuclear Power Plants

Erkki Vesikari
VTT

Abstract

A service life management system of concrete structures in nuclear power plants is being developed in VTT in cooperation with the Finnish nuclear companies TVO and FORTUM. The work started in 2006 as a preliminary study and is continued under the auspices of SAFIR 2010 (The Finnish Research Programme on Power Plant Safety) as the actual research project in 2007–2010. The service life management system is developed for the maintenance engineers of nuclear power plants for conducting systematic maintenance policy and for planning, organising and optimising maintenance strategy of concrete structures in nuclear power plants.

Introduction

The objective of the project is to produce a predictive service life management system (SLMS) for concrete structures in nuclear power plants. The service life management tool ServiceMan is able to predict the degradation of structures, to guard the safety and serviceability limits, to time special inspections and to specify and time maintenance, repair and rehabilitation (MR&R) actions in an optimal way. The system also evaluates life cycle costs, environmental impacts and structural risks over a long period of time. By the SLMS the safety, accepted structural performance and uninterrupted service of concrete structures are ensured during the licenced lifetime of a nuclear power plant. The methodological ground of the management system was developed during the EU project LIFECON in 2001–2003 [1].

The plant units are divided into structures. The structures are divided into still smaller parts which are called “modules”. The modules can be treated roughly as homogenous with respect to materials, structural features and environmental conditions. The modules are the basic structural units in the analysis and planning processes of the system. The structural and modular databases which

serve as initial data sources in the calculation processes are consistent with the modular breakdown of structures.

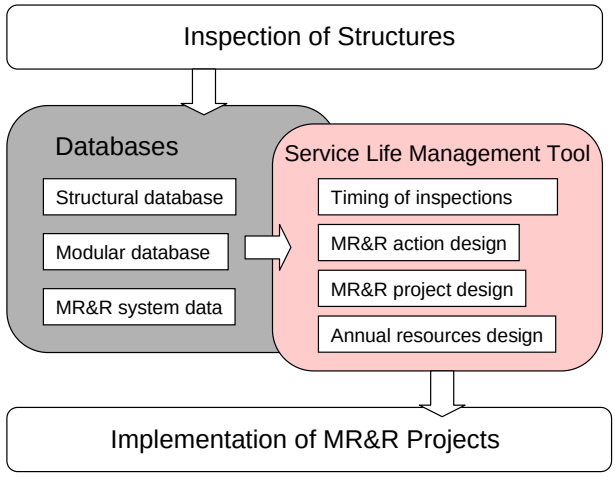

Figure 28.2.1. Service Life Management System. Database and Service Life Management Tool.

The process of the service life management system is presented in Figure 28.2.1. The process starts from the inspection of structures and ends in the implementation of MR&R actions. The SL management tool gives timings for special inspections and makes preliminary plans for the MR&R actions. The management tool helps also in grouping the MR&R actions into projects and in preparing annual project lists to be in balance with the annual budget [2].

Procedure of the SLMS

Figure 28.2.2 shows a scheme on the calculation procedure and the data flow of the service life management system. On the top the databases of structures, modules and MR&R systems with their contents are presented. The structural and modular databases contain identification data, measuring data, data on exposure, observed degradation (inspection data), data on MR&R actions that have already performed and actions that will be performed in the future, and data on damages (observed degradation that cannot be predicted by models) etc. The database of MR&R Systems consists of data on protection systems, repair systems and renovation systems. It contains for each system group material data, cost data, environmental impact data, service life data, and effect-on-condition data. The last mentioned data type is different for protection systems and for

structural repair systems. The effect-on-condition data for protection systems define how the rate of degradation of the structure is reduced by the protection system (considering each degradation type). The effect-on-condition data for repair and renovation systems define the condition of the structure immediately after the repair or renovation.

The life cycle action planning is performed for each module in row. Accordingly, each module in turn is selected and the data pertaining to that module is gathered and checked before inserting into the life cycle analysis procedure. When gathering the data, part of the necessary information is obtained from the modular database and the rest part from the MR&R system database. E.g. in case of service life of a module the specifications of MR&R system as well as the exposure data are defined in the modular database while data on service lives pertaining to MR&R systems are defined in the database of MR&R systems. So, these data must be combined to determine the actual service life of a module.

The LC analysis process is systemised so that the calculations are performed as a routine using the same analysis procedure irrespectively on the module at hand. So, the procedure itself is the same, only the initial data is changed according to the active module.

Following each life cycle analysis the data on the MR&R actions are gathered into the datatable of specified and timed actions. This is done by a macro program which controls the analysis processes. After this the design may continue with MR&R project design (combining MR&R actions into groups) and Annual Resources Design (balancing the annual MR&R costs with the budget). These design phases entail sorting, filtering and supplementing of the table of specified actions.

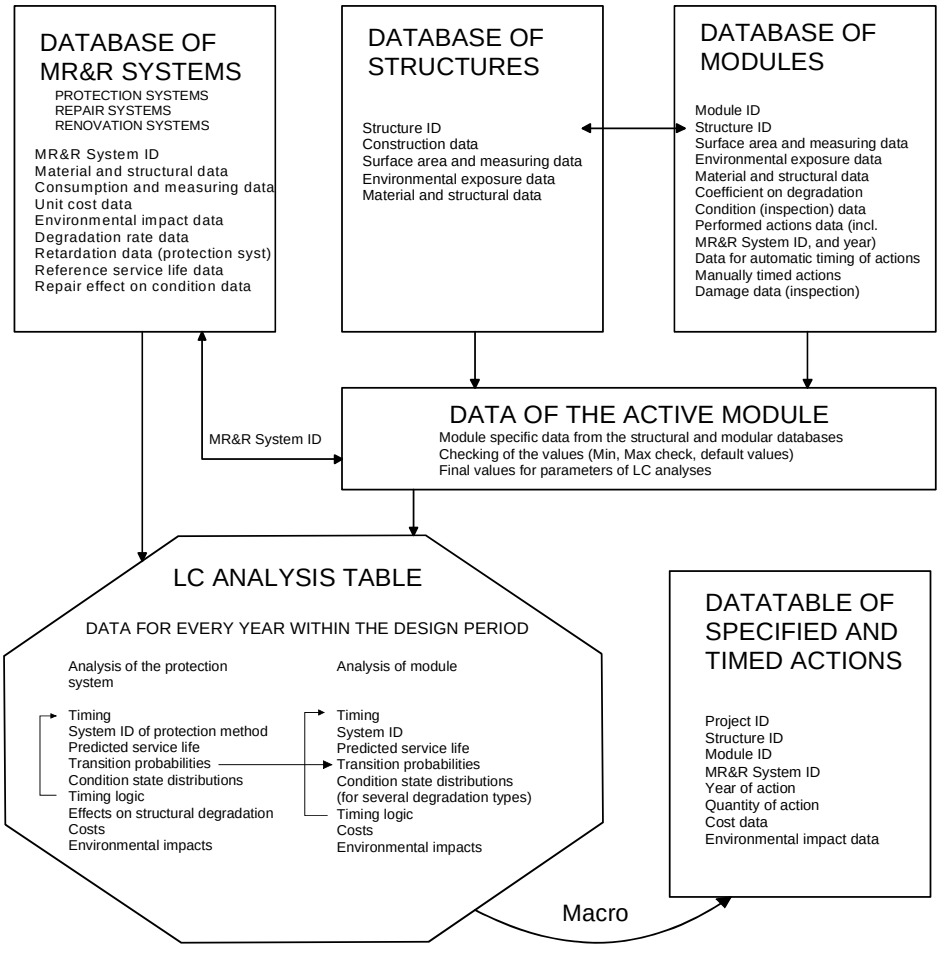

Figure 28.2.2. The procedure of Management in ServiceMan.

Combined Life Cycle Analysis

The core of the management system consists of a combined condition, cost and environmental impact analysis. A scheme on the system is presented in Figure 28.2.3. The annual condition state distributions are determined by the Markov Chain method in the analysis table on the left hand side of the figure. The condition state distributions show the probability that the module is at any of the condition states (in this case the states range from 0 to 4). The annual changes in the condition state distributions are predicted by the transition probability matrices (degradation and action effect matrices in the upper left corner of the

figure). The transition probabilities of the degradation matrix are automatically determined based on the model formula of degradation. The transition probabilities of the action effect matrices are specific to each MR&R action.

In this example the limit condition state is defined to be 3 and the maximum allowable probability for exceeding the limit state is 50%. In the column Prob >3 the probability that the module exceeds the limit state (3) is determined. Following this column over the years whenever Prob >3 is greater than the maximum probability (50%) a repair action is automatically triggered. In the next year the repair is implemented and the action effect matrix is applied (instead of the degradation matrix) to define the condition state distribution after the repair. At the same time the repair costs are added in cost calculator on the right. The cost calculator totals the costs and environmental impacts from the whole design period. Thus the data presented in the upper right corner of Figure 28.2.3 can be determined.

Figure 28.2.3 presents the analysis procedure in a simplified way. In reality several degradation types are taken into account in the analyses [3]. The following degradation types are determined and any of them can trigger MR&R actions:

- carbonation and corrosion
- chloride penetration and corrosion
- carbonation and corrosion at cracks
- chloride penetration and corrosion at cracks
- degradation of concrete
- degradation of possible protection system.

The degradation rate of a module can be retarded by protection measures. Some of them are applied on the whole surface of the module (e.g. coatings) and others are applied only to cracks. The retarding effect of a protection system depends on the condition of the protection system so that the retarding effect is greatest at the beginning and smallest at the end of the service life (of the protection system). This is modelled by the Markov Chain so that the transition probabilities of the structure change with time depending on the condition of the protection system.

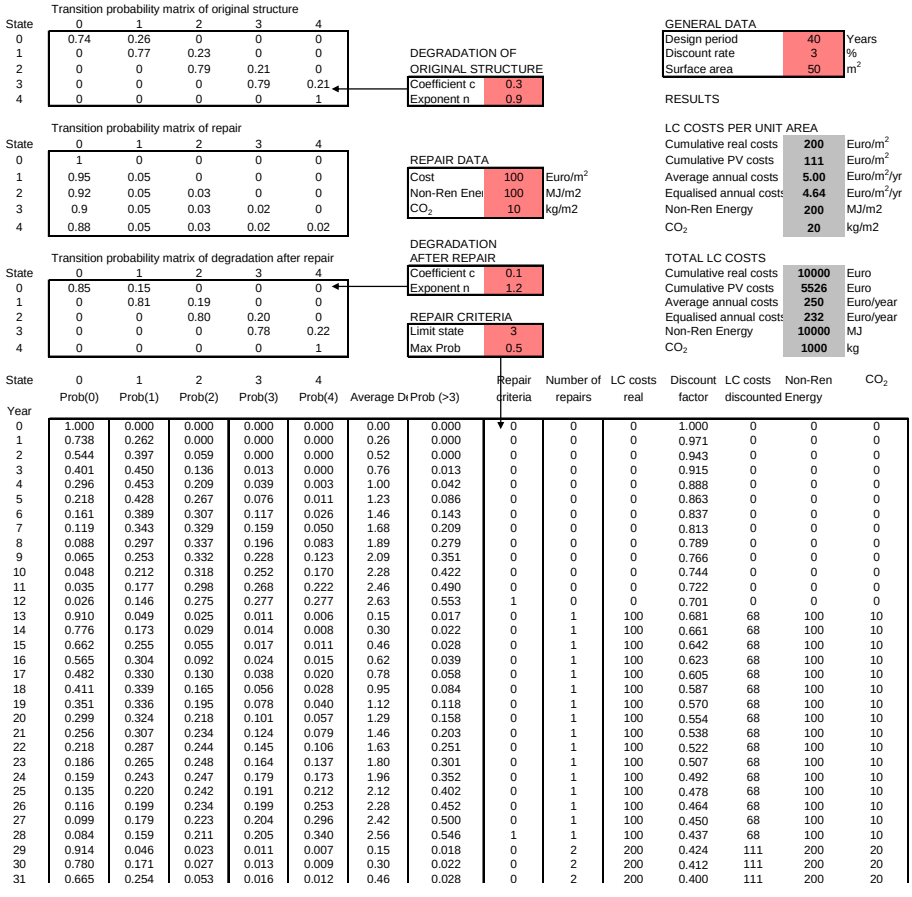

Transition probability matrix of original structure

State	0	1	2	3	4
0	0.74	0.26	0	0	0
1	0	0.77	0.23	0	0
2	0	0	0.79	0.21	0
3	0	0	0	0.79	0.21
4	0	0	0	0	1

DEGRADATION OF ORIGINAL STRUCTURE

Coefficient c	0.3
Exponent n	0.9

GENERAL DATA

Design period	40	Years
Discount rate	3	%
Surface area	50	m^2

RESULTS

Transition probability matrix of repair

State	0	1	2	3	4
0	1	0	0	0	0
1	0.95	0.05	0	0	0
2	0.92	0.05	0.03	0	0
3	0.9	0.05	0.03	0.02	0
4	0.88	0.05	0.03	0.02	0.02

REPAIR DATA

Cost	100	Euro/m^2
Non-Ren Ener	100	MJ/m2
CO_2	10	kg/m2

LC COSTS PER UNIT AREA

Cumulative real costs	200	Euro/m^2
Cumulative PV costs	111	Euro/m^2
Average annual costs	5.00	Euro/m^2/yr
Equalised annual costs	4.64	Euro/m^2/yr
Non-Ren Energy	200	MJ/m2
CO_2	20	kg/m2

Transition probability matrix of degradation after repair

State	0	1	2	3	4
0	0.85	0.15	0	0	0
1	0	0.81	0.19	0	0
2	0	0	0.80	0.20	0
3	0	0	0	0.78	0.22
4	0	0	0	0	1

DEGRADATION AFTER REPAIR

Coefficient c	0.1
Exponent n	1.2

REPAIR CRITERIA

Limit state	3
Max Prob	0.5

TOTAL LC COSTS

Cumulative real costs	10000	Euro
Cumulative PV costs	5526	Euro
Average annual costs	250	Euro/year
Equalised annual costs	232	Euro/year
Non-Ren Energy	10000	MJ
CO_2	1000	kg

State / Year	0 Prob(0)	1 Prob(1)	2 Prob(2)	3 Prob(3)	4 Prob(4)	Average Dr	Prob (>3)	Repair criteria	Number of repairs	LC costs real	Discount factor	LC costs discounted	Non-Ren Energy	CO_2
0	1.000	0.000	0.000	0.000	0.000	0.00	0.000	0	0	0	1.000	0	0	0
1	0.738	0.262	0.000	0.000	0.000	0.26	0.000	0	0	0	0.971	0	0	0
2	0.544	0.397	0.059	0.000	0.000	0.52	0.000	0	0	0	0.943	0	0	0
3	0.401	0.450	0.136	0.013	0.000	0.76	0.013	0	0	0	0.915	0	0	0
4	0.296	0.453	0.209	0.039	0.003	1.00	0.042	0	0	0	0.888	0	0	0
5	0.218	0.428	0.267	0.076	0.011	1.23	0.086	0	0	0	0.863	0	0	0
6	0.161	0.389	0.307	0.117	0.026	1.46	0.143	0	0	0	0.837	0	0	0
7	0.119	0.343	0.329	0.159	0.050	1.68	0.209	0	0	0	0.813	0	0	0
8	0.088	0.297	0.337	0.196	0.083	1.89	0.279	0	0	0	0.789	0	0	0
9	0.065	0.253	0.332	0.228	0.123	2.09	0.351	0	0	0	0.766	0	0	0
10	0.048	0.212	0.318	0.252	0.170	2.28	0.422	0	0	0	0.744	0	0	0
11	0.035	0.177	0.298	0.268	0.222	2.46	0.490	0	0	0	0.722	0	0	0
12	0.026	0.146	0.275	0.277	0.277	2.63	0.553	1	0	0	0.701	0	0	0
13	0.910	0.049	0.025	0.011	0.006	0.15	0.017	0	1	100	0.681	68	100	10
14	0.776	0.173	0.029	0.014	0.008	0.30	0.022	0	1	100	0.661	68	100	10
15	0.662	0.255	0.055	0.017	0.011	0.46	0.028	0	1	100	0.642	68	100	10
16	0.565	0.304	0.092	0.024	0.015	0.62	0.039	0	1	100	0.623	68	100	10
17	0.482	0.330	0.130	0.038	0.020	0.78	0.058	0	1	100	0.605	68	100	10
18	0.411	0.339	0.165	0.056	0.028	0.95	0.084	0	1	100	0.587	68	100	10
19	0.351	0.336	0.195	0.078	0.040	1.12	0.118	0	1	100	0.570	68	100	10
20	0.299	0.324	0.218	0.101	0.057	1.29	0.158	0	1	100	0.554	68	100	10
21	0.256	0.307	0.234	0.124	0.079	1.46	0.203	0	1	100	0.538	68	100	10
22	0.218	0.287	0.244	0.145	0.106	1.63	0.251	0	1	100	0.522	68	100	10
23	0.186	0.265	0.248	0.164	0.137	1.80	0.301	0	1	100	0.507	68	100	10
24	0.159	0.243	0.247	0.179	0.173	1.96	0.352	0	1	100	0.492	68	100	10
25	0.135	0.220	0.242	0.191	0.212	2.12	0.402	0	1	100	0.478	68	100	10
26	0.116	0.199	0.234	0.199	0.253	2.28	0.452	0	1	100	0.464	68	100	10
27	0.099	0.179	0.223	0.204	0.296	2.42	0.500	0	1	100	0.450	68	100	10
28	0.084	0.159	0.211	0.205	0.340	2.56	0.546	1	1	100	0.437	68	100	10
29	0.914	0.046	0.023	0.011	0.007	0.15	0.018	0	2	200	0.424	111	200	20
30	0.780	0.171	0.027	0.013	0.009	0.30	0.022	0	2	200	0.412	111	200	20
31	0.665	0.254	0.053	0.016	0.012	0.46	0.028	0	2	200	0.400	111	200	20

Figure 28.2.3. Combined Life Cycle Analysis with automatic trifggering of actions.

Special inspections

Special Inspections are an essential part of the SLMS. During Special inspections samples are taken from structures and the a condition assessment is performed based on the samples. A data form is reserved for inputting the condition assessment data in to the modular database. The input data includes

- special inspection year
- measured carbonation depth
- measured depth of critical chloride content
- measured thickness on concrete cover
- measured crack width
- measured amount of cracks.

Based on the results of special inspections the degradation models are re-evaluated. Subsequently, the calibrated models are used in the anlyses instead of the original ones. Now, the timings of MR&R actions are based on observed data and they can be considered more reliable. However small changes in the timings of actions can be done by the designer in the other phases of design, project design and annual resources design.

Other Features of the Service Life Management System

The service life management system as described above is supplemented by risk analyses and structural analyses for containment buildings. The purpose of this is to study the aging problems of containment buildings with a higher level of accuracy than other structures.

The risk analyses focus degradation phenomena occurring in both steel and concrete parts of the containment trying to evaluate the total risk from aging phenomena. The probability of corrosion in pre-stressing tendons and the steel liner are evaluated using reliability based methods with time dependent degradation models. Traditional PSA methods such as logical trees are used to describe and summarize the total effect as a result of aging phenomena.

The structural degradation analyses support the risk analyses by bringing the evaluation of risk to the structural level. Structural degradation analyses consider damages and long-term deformations of structures and evaluate their effect on structural safety. One objective of the analyses is to find out acceptance limits for various types of degradation. The probability of cracking is studied by a special application for serviceability limit state design.

Conclusions

The project SERVICEMAN (Service life management system of concrete structures in nuclear power plants) under the auspices of SAFIR 2010 (A Finnish research programme on power plant safety), that started in 2007, aims at producing a predictive service life management system for concrete structures in nuclear power plants in Finland. The service life management system is capable of predicting degradation in structures with respect to different degradation types and of timing special inspections and MR&R actions for the remaining operating life of the plant and longer if necessary [4].

The service life management tool can be used for systematic and proactive maintenance of concrete structures in nuclear power plans. The core process of

the system is a combined condition, cost and environmental impact analysis. The condition analysis is based on special degradation models and the Markov Chain method.

References

1. Söderqvist, M.-K. & Vesikari, E. 2003. Generic technical handbook for a predictive life-cycle management system of concrete structures (LMS). EC FP5 project LIFECON. Deliverable D1.1. 170 p. http://lifecon.vtt.fi/.

2. Vesikari, E. 2007. Service life management system of concrete structures in nuclear power plants. Espoo: VTT Technical research Centre of Finland. VTT Publications 648. 82 p. http://www.vtt.fi/inf/pdf/publications/2007/P648.pdf.

3. Vesikari, E. 2008. Degradation and service life of concrete structures in nuclear power plants. The Finnish Research Programme on Nuclear Power Plant Safety 2007–2010. Espoo: VTT Technical research Centre of Finland. Research Report VTT-R-02323-08. 40 p.

4. Vesikari, E. 2009. Service Life Management System SERVICEMAN. Part I User manual & Part II Calculation principles. The Finnish Programme on Nuclear Power Plant Safety 2007–2010. Espoo: VTT Technical research Centre of Finland. Research Report VTT-R-11305. 45 p.

29. IMPACT2010 (IMPACT) and Structures under soft impact (SUSI)

29.1 IMPACT and SUSI summary report

Kim Calonius, Ilkka Hakola, Simo Hostikka, Juha Kuutti, Auli Lastunen, Hannu Martikainen, Arja Saarenheimo and Ari Silde
VTT

Markku Tuomala
Tampere University of Technology

Ari Kankkunen
Helsinki University of Technology

Abstract

The IMPACT testing facility has been built to investigate the impact of deformable missiles on concrete structures [1]. The test facility is designed for medium scale tests the maximum missile weight of 50 to 100 kg depending on the missile velocity in the range 100 to 200 m/s. The Impact project is mainly concentrated to the research of soft missile impacts on concrete walls, but also several tests have been carried out using hard steel missiles. The main purpose of the project is to produce data for verifying and developing numerical models and methods. This work has been carried out within the SUSI project [2, 3].

The spread of liquid fuel as a result of an intentional or accidental aircraft crash may cause a sudden fire with hazardous effects on the safety of the NPP. The spread phenomena have been studied at VTT in the IMPACT tests where the missile is filled by water (called wet missile tests) [4]. The goals of the study are to increase a general knowledge of the liquid dispersion phenomena under

impact conditions, measure the most important test parameters to be used in validation of simulation techniques, and take in use and validate suitable simulation methods than can be used for the determination of fuel spread and fire risk following an airplane crash. The Fire Dynamics Simulator (FDS) program is found to be a useful tool for the problem, and the program will be applied in future also.

Introduction

In order to obtain reliable numerical results the methods and models should be verified against experimental data. The accuracy and capability of numerical methods in analysing reinforced concrete structures under soft missile impacts are studied. Test results used in this study are recorded within the IMPACT project. All the calculation work presented is performed within the SUSI project.

Numerical studies were carried out with ABAQUS code using shell elements and with simplified two degrees of freedom models. Some numerical simulations were carried out also by LS-DYNA code. Due to uncertainties in measuring the force-time functions for impacting missiles load functions needed in analyses were calculated by using the Riera method and adjusted according to the experimental findings. Parameters for material models used in the analyses are based on the available material test data.

The spread of liquid fuel as a result of an intentional or accidental aircraft crash may cause a sudden fire with hazardous effects on the safety of the NPP. The liquid spread phenomena have been studied at VTT in the IMPACT tests where the missile is filled by water [4, 5]. In the tests, a deformable cylindrical or a more prototypical 3-D missile impacted a solid concrete wall or a steel force plate [1, 6]. The cylindrical missiles were filled completely, whereas in the 3-D missiles only the wings were filled by liquid. Water mass inside the cylinder ranged from 15 to 68 kg. Total water mass in the wings of a 3-D missile was about 8 kg. The impact velocity in the wet missile tests varied from 70 to 177 m/s.

Because very little experimental information can be found from the literature concerning the fuel dispersal from impacted projectile, more experimental data are needed for the validation of the applied simulation/analysing techniques, and for the determination of fuel spread and fire risk following an airplane crash. Some parameters, like a discharge speed of liquid, direction and propagation speed of liquid release, and drop size of liquid spray are essential input parameters to be used as boundary conditions for the suitable simulation methods.

Only limited number of IMPACT tests is conducted with fluid filled missile, and hence, effects of all important parameters associated with the dispersion phenomena are not studied systematically so far. However, the measurements have given vital new information about liquid spread phenomena. The experience and experimental results so far form a good basis for further investigation and validation of the simulation techniques.

Impact tests and measurements

A flexible experimental platform has been created at VTT for intermediate scale impact tests. The test apparatus consists of two main parts. First, a 13.5 m long pressure accumulator is used to provide the required initial energy for the test. Second, a 12 m long acceleration tube is used to accelerate test missiles to a final velocity of 100 m/s to 200 m/s. The mass of the missile can be up to 100 kg. In the tests, missile impacts on a concrete wall or on a steel force measurement plate. The test facility has been further developed and improved since the first version was taken in use in 2003.

Two versions of the force plate system are shown in Figure 29.1.1. The force plates have been supported directly to the back wall using only the back pipes. The 3D missile tests were performed by using heavy steel frame, horizontal beams and three force plates installed in front of the frame, depicted in Figure 29.1.1 on the right.

Figure 29.1.1. The second model (left) and third model of force plate construction.

Figure 29.1.2. Dry (empty) aluminium (Al) pipe missile and wet (water filled) missile.

Tests have been done with a steel piston inside the acceleration tube and the missile installed on the rails at the top of the acceleration tube. An aluminium pipe missile with a diameter of 0.25 m and wall thickness of 5 mm was used in impact tests of slabs with a thickness of 0.15 m (see Figure 29.1.2). The aircraft model tests on force plate have been done using a smaller aluminium pipe, with a diameter of 200 mm and wall thickness of 4 mm. At the end of the test series wings and engines were included in the model (see Figure 29.1.3) and also in some tests wings were filled with water in order to study the spreading of fuel [7].

Pre-stressed concrete slabs with a thickness of 250 mm were tested using rigid hard steel missiles with a diameter of 150 mm, wall thickness of 10 mm and filled with concrete, shown in Figure 29.1.3 on the left.

Figure 29.1.3. The rigid steel pipe missile with a diameter of 150 mm (left) and an aeroplane model with wings (right).

The dimensions of the concrete slab in the soft missile tests were: width 2 m, length 2.3 m, support length 2.2 m and thickness 0.15 m. Bending and in some cases also shear reinforcement was applied. The slabs were supported on the vertical edges by the test frame shown in Figure 29.1.4 on the left.

The pre-stressed concrete slabs were of the same size except the thickness was 0.25 m. The slab contained bending and in some cases also shear reinforcement. In the new test frame the slabs are simply supported on all the four edges. The new test frame is shown in Figure 29.1.4 on the right.

Figure 29.1.4. One way support system and test slab in soft missle test (left). Pre-stressed test slab with a thickness of 0.25 m and support system 2 in hard missile test (right).

The missile tests onto force plate in the Impact project phase 1 are composed of 7 test series given in Table 29.1.1 and of concrete slab tests shown in Table 29.1.2.

Table 29.1.1. Missile impact tests on force plate.

Missile type	Launch type	Number of tests
Pretests with steel piston	Inside	5
Pretests with steel pipe	Inside	5
Thin walled steel pipe, dry, water or light concrete inside	Inside	14
Al. pipe, dry	Inside	3
3D missile	Outside	12

Table 29.1.2. Concrete plate tests in the phase 1.

Test type	Number of tests
Soft missile on 0.15 m thick plate	12
Hard missile on 0.25 m thick pre-stressed wall	13

Measurements

The data from sensors have been gathered using a sampling frequency of 100 kHz. In measuring anti-aliasing filtering and simultaneous sampling was applied. The maximum number of channels used in the tests has been 32. The following sensors have been used in Impact tests:

- Force transducers behind the force plate (used also in measuring the post-tension force of Dyvidag bars)
- Strain gauges on back pipes to measure reaction forces
- Strain gauges on supporting frame to control the bending stresses of beams
- High speed cameras to video collision
- Strain gauges in rebars inside concrete to measure strains of rebars
- Strain gauges on surface of concrete slab to measure strains of concrete
- Deflection transducers to measure horizontal deflections of the slab
- Laser sensors to measure the speed of missile
- Accelerometer at the back of the missile (wired measurements)
- Accelerometers at the back of the concrete wall
- Pressure sensors to measure the air pressure inside the acceleration tube or near the concrete slab.

The measuring device and deflection transducers are shown in Figure 29.1.5. The transducer is a mechanical sensor, which is fixed on the surface of the slab and is also working during the test.

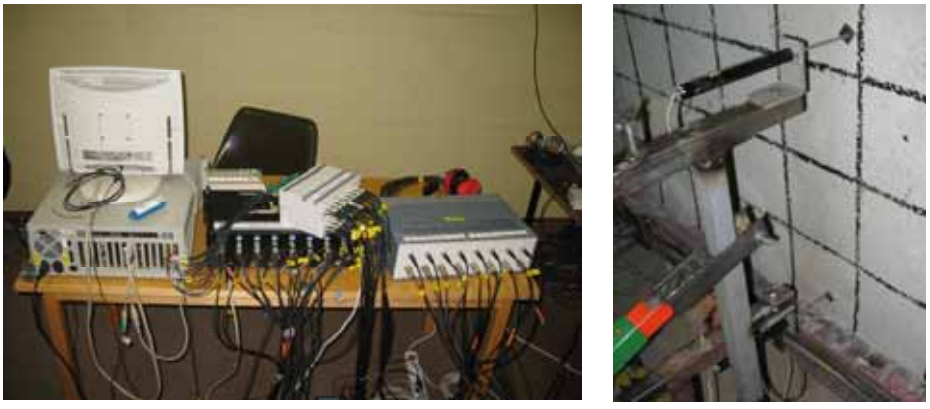

Figure 29.1.5. Measuring data collection device (left) and deflection transducers in front of the slab (right).

The high frequency laser sensors are used to measure the velocity of the missile before hitting the target and reaction forces are measured by strain gauges glued on the back pipes (Figure 29.1.6).

Figure 29.1.6. The laser sensors (left) and a strain gauge on the back pipe (right).

The post-tension force of Dyvidag bars and the force-time function due to missile impact is measured by force transducers shown in Figure 29.1.7.

Figure 29.1.7. The force transducers of Dyvidag bars (left) and the force transducers behind the force plate (right).

The strains of rebars and concrete are measured by high capacity strain gauges, which are attached on rebars and on the surface of concrete, see Figure 29.1.8.

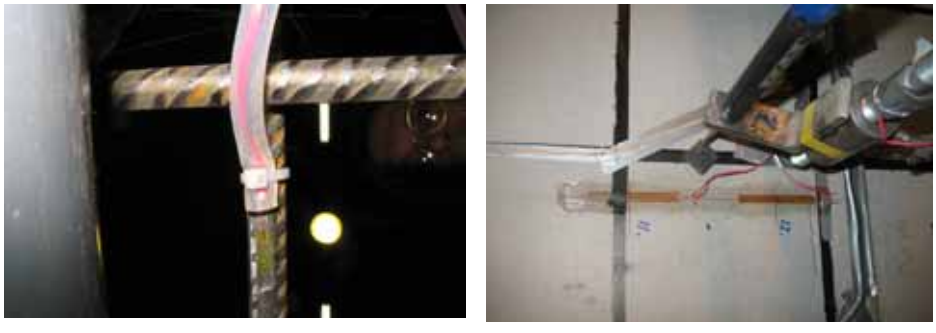

Figure 29.1.8. A strain gauge glued on rebar (left) and a strain gauge on the front surface of the slab (right).

Structural analyses

Nonlinear structural analyses of Tests 642 and 644 were carried out with Abaqus/Explicit code [8] and with a two degree of freedom (TDOF) model [9]. In addition, Test 642 was simulated by LS-Dyna FE code [10]. All these models will be described below.

This chapter concentrates on structural analyses of Tests 642 and 644, but shows also some main results of several other tests with 150 mm thick reinforced concrete walls. Two types of missiles were used in those test series. The first type was an empty aluminium missile (dry) and it was used for instance in Test 642. The missile of the second type used in Test 644 was shorter and filled with water (wet). The photographs of the missiles are shown in Figure 29.1.2 and their dimensions and other specifics in Figure 29.1.9. The main characteristics of Tests 642 and 644 are shown in Table 29.1.3 and the load time functions calculated by the Riera method and applied in all these calculations are shown in Figure 29.1.16.

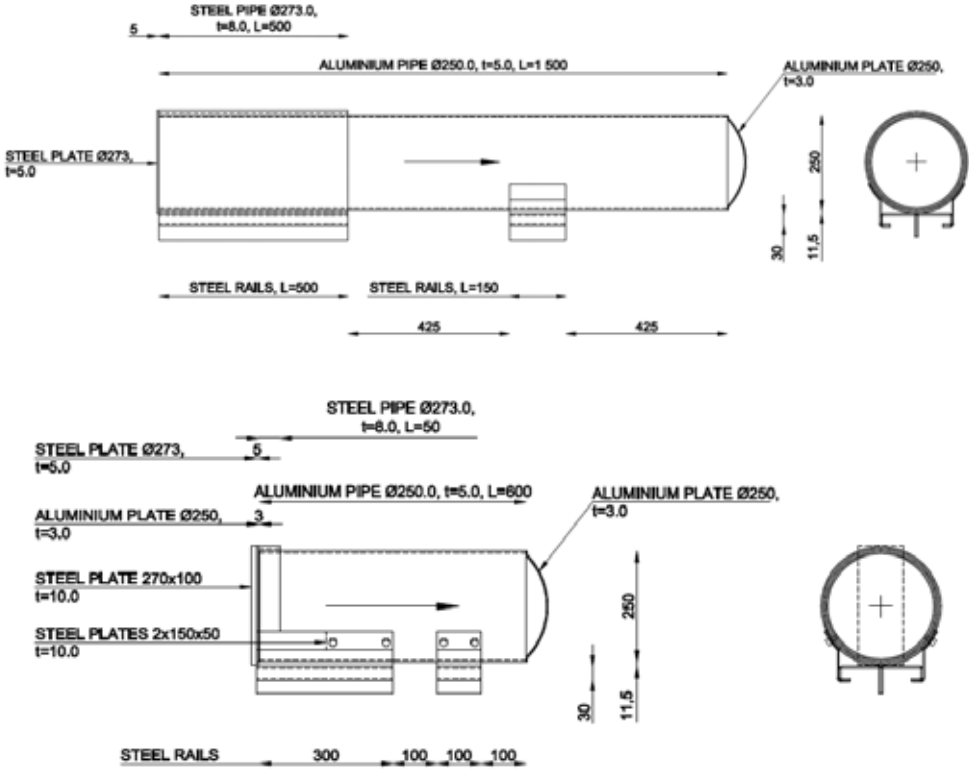

Figure 29.1.9. Aluminium pipe missiles of both types, the empty one above and the one filled with water below.

Table 29.1.3. Main characteristics of Tests 642 and 644.

Test	v_o [m/s]	m [kg]	L_o [1)] [mm]	L_{cr} [2)] [mm]	ΔL [3)] [mm]
642	109	51.5	1500	800	700
644	105	50.9	600	0	600

1) L_o is the initial length of the missile
2) L_{cr} is the length of the missile after the test
3) $\Delta L = L_o - L_{cr}$

The reinforced concrete wall type used in the impact tests is depicted in Figure 29.1.10. The dimensions of the slabs in the test series are: width 2 m, length 2.3 m, support length 2.2 m and thickness 0.15 m. The slab was simply supported on two opposite vertical sides (dot-and-dash lines) and free on the two other sides. The locations of the displacement sensors used in Tests 642 and 644 are shown in Figure 29.1.10.

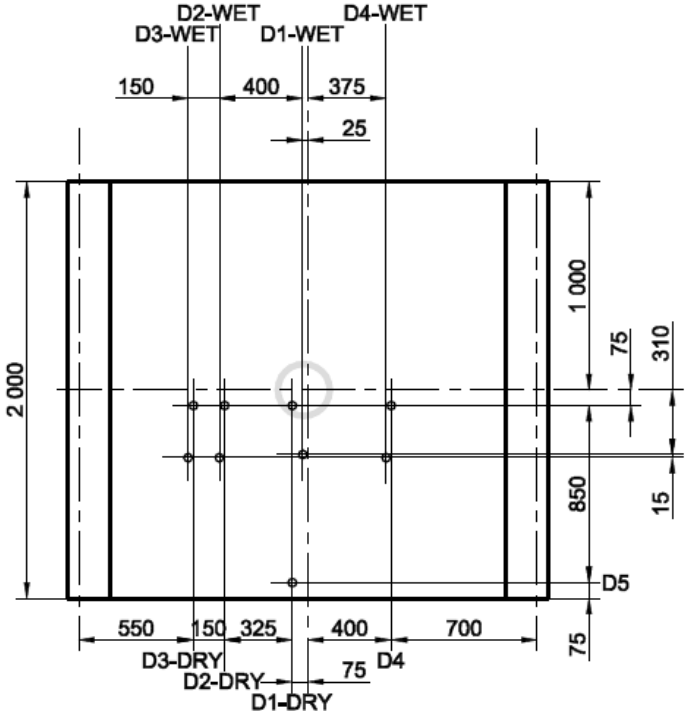

Figure 29.1.10. Instrumentation of the wall in Tests 642 (DRY) and 644 (WET): Displacement sensors are at locations D1–D5.

The slabs were reinforced using bars with a diameter of 8 mm and a spacing of 50 mm, in each way and on each face. The amount of reinforcement (on both the bottom and top faces) is $A_s = A_{st} = A_{sb} = 0.00100531$ m^2/m. The reinforcement ratio is in this case $A_s / h = 0.0067$ or $\rho_s = 0.67\%$.

Shell element model without frame (Abaqus)

The finite shell element models for one quarter of the target structure are shown in Figure 29.1.11. The reinforcement in the concrete wall is modelled as layers in the four-noded shell elements. There are two symmetry lines in the model. When the supporting structure, which includes the heavy frame around the wall and the back pipes anchored to the rock wall, is not modelled, the upper edge of the model is free and the right hand side edge is simply supported. The loaded area is determined by assuming a load spreading angle of 45^o in the slab thickness direction. The load area is indicated by red colour on the left hand side model.

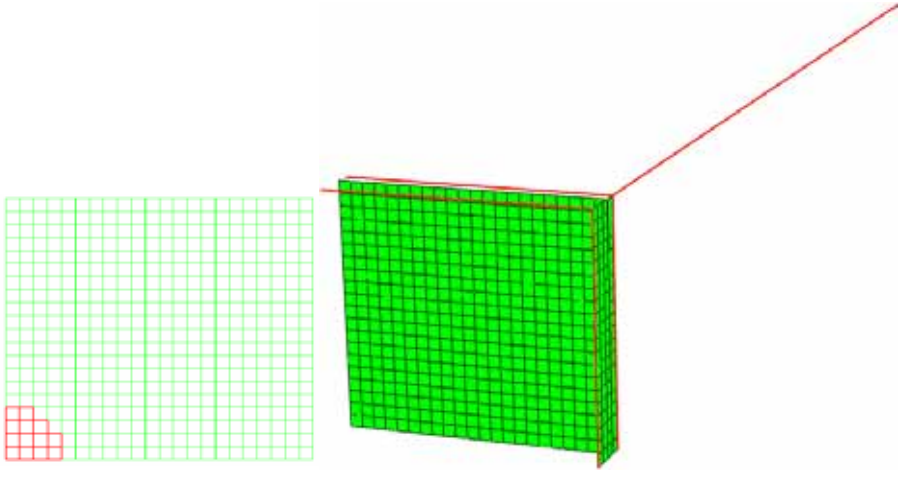

Figure 29.1.11. One quarter finite element models of impact test walls with (on the right) and without (on the left) the frame structure and back pipes.

Shell element model with frame (Abaqus)

A finite element model of the frame supporting the reinforced concrete wall was built in order to study the effects of the supporting frame to the behaviour of the wall and the measurements. When designing the real frame itself, the aim was to construct as rigid support for the wall as reasonably possible. This way the boundary conditions applied to the wall would be ideal.

The wall is supported by a steel frame that has been built from various beam profiles and plates. The frame is connected to a rock wall with long back pipes. In this simple study the frame was modelled simplified using linear beam and shell elements. The finite element mesh of the frame and the wall is shown on the right in Figure 29.1.11. The beam elements are shown in red colour.

Solid element model (LS-Dyna)

A simulation of Test 642 was also carried out using LS-DYNA (version ls971d R3.1, revision 43919) [10]. Only a quarter of the model was modelled mainly with solid brick elements (Figure 29.1.12). The rebars were modelled using beam elements. There were altogether 130122 elements in the model. The wall was supported using two rigid bars. The Winfrith material model was used. The load area is indicated by light grey colour.

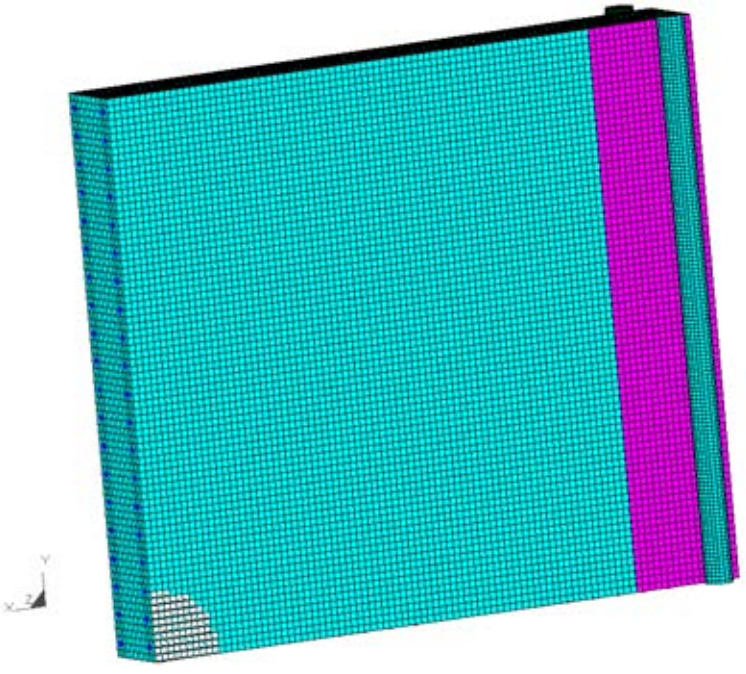

Figure 29.1.12. LS-DYNA solid element model.

Two degree of freedom model for shear deformable plate

A two degree of freedom model (TDOF model), e.g. the CEB model [8], can be used in analysing the overall impact behaviour of concrete slabs. In this model spring 1 and mass 1 are connected to the global bending deformation and movement of the plate while spring 2 and mass 2 are used in modelling the local shear behaviour in the missile impact area. The behaviour of element 1 (bending spring $\boldsymbol{r}_1$) and the local behaviour connected with the possible formation of a shear cone (shear spring $\boldsymbol{r}_2$) are shown in Figure 29.1.13.

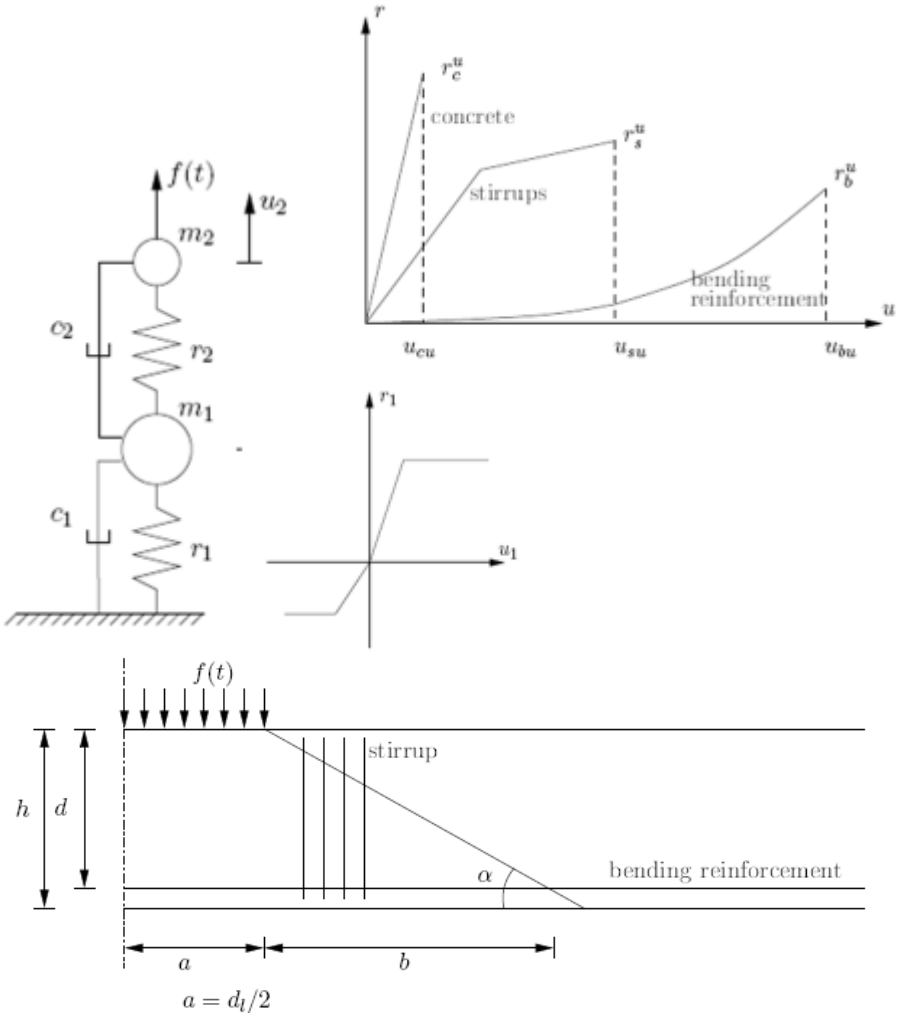

Figure 29.1.13. Two degrees of freedom model.

Material properties

One dimensional nonlinear stress strain curve of concrete is presented on the left hand side in Figure 29.1.14. According to the material tests, the compression strength of concrete is 58 MPa and the tensile strength 2.8 MPa. Stress-strain behaviour of concrete after tensile cracking is predicted according to the method given in Reference [11]. This dependency was assumed in FE analyses carried out with shell elements.

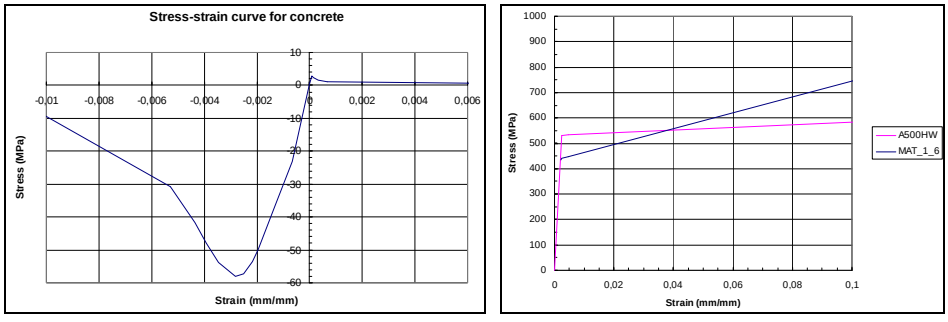

Figure 29.1.14. Nonlinear tensile stress-strain curves of concrete (left) and steel (right).

The use of the average (smeared) steel stresses in combination with the corresponding concrete stresses allows the tension stiffening effect (of steel bars by concrete) to be considered and deformations of the steel concrete composites to be correctly evaluated [11]. The stress-strain curves for reinforcement used in the nonlinear analyses carried out with Abaqus are presented together with the measured stress-strain curve obtained by tensile test in the right hand side of Figure 29.1.14. The yield strength of reinforcement steel is highly strain rate dependent and increases with the strain rate. This dynamic yield strength of steel was taken into consideration by the Cowper-Symonds formula for uniaxial tension or compression.

Calculated and measured results of Tests 642 and 644

The measured and the corresponding calculated wall deflections in Tests 642 and 644 are shown in Figure 29.1.15. The main results of some of the wall tests are collected in Table 29.1.4. The maximum deflection value can be calculated accurately. The vibration of the damaged wall was not predicted that well. The frequency of the oscillation is nearly the same for both Abaqus models,

approximately 36 Hz for the model without the frame (Abaqus shell, dark blue lines) and approximately 34 Hz for the model with the frame (Abaqus shell+beam, red lines). The corresponding measured frequency (thick cyan line) is approximately 20 Hz. The two-degrees-of-freedom model (TDOF, dotted brown line) behaves very similarly to the Abaqus model without the supporting structure. The results are either from the center of the wall (Dmax) or from the displacement sensor location D1 (see Figure 29.1.12). LS-Dyna gives somewhat different kinds of results.

Even though the impulse is slightly higher in the dry missile test, the maximum deflection is clearly smaller than the one in the wet missile test in accordance both to the measurements and calculations (see Table 29.1.4). According to the calculations with the shell element model the maximum strain, by a clear margin, occurred in the horizontal reinforcement in the dry missile test. This is due to the fact that the wall loaded by the deformable empty missile behaves like a wide bending beam. In tests where the water missile was used the calculated strain values in the vertical back surface reinforcement were nearly as high as in the horizontal back surface reinforcement. This is due to the fact that the missiled filled with water has a much higher maximum peak value in the load time function at least according to the Riera method (see Figure 29.1.16). Besides the contained water, also the rather stiff steel rail below the water missile affects the impact load.

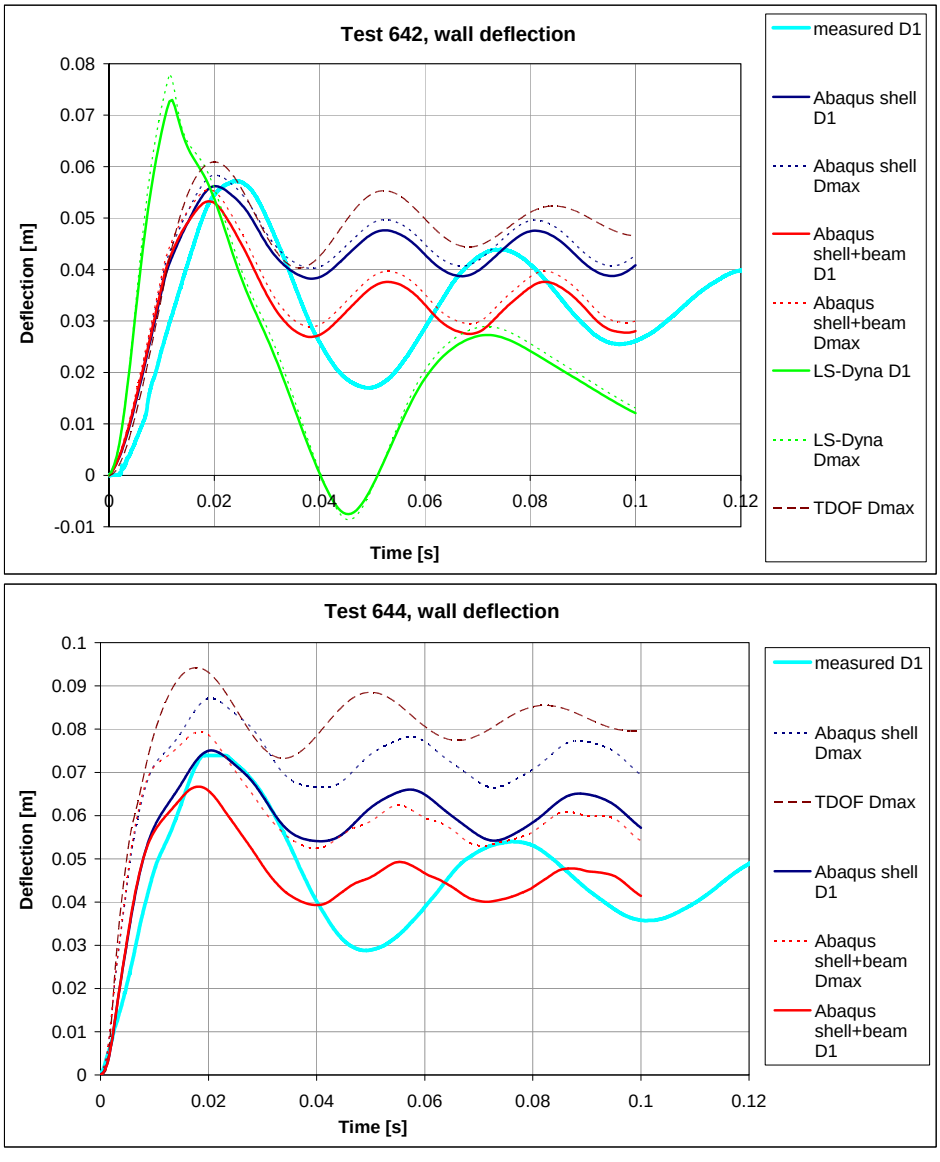

Figure 29.1.15. Measured and calculated wall deflections in Test 642 (above) and 644 (below).

Figure 29.1.16 shows the load time function (load) according to the Riera method and used in simulations, the reaction force measured from the back pipes (back pipes) and the calculated reaction at the end of the back pipes (Abaqus shell+beam) for both tests. As can be seen, the missile filled with water (blue

curves) has a much higher force peak than the empty one (red curves). Respectively, the measured reaction force has also slightly higher peak values, but the forces are clearly evened out within the distance the stress wave travels through the wall and its supporting structure. The calculated reaction force corresponds relatively well to the measured one in case of Test 642, but in case of Test 644 simulation the impact seems to hit a resonance point and the reaction force starts to strongly vibrate. However, there has not been any clear sign of water hammer effect with the water filled missiles.

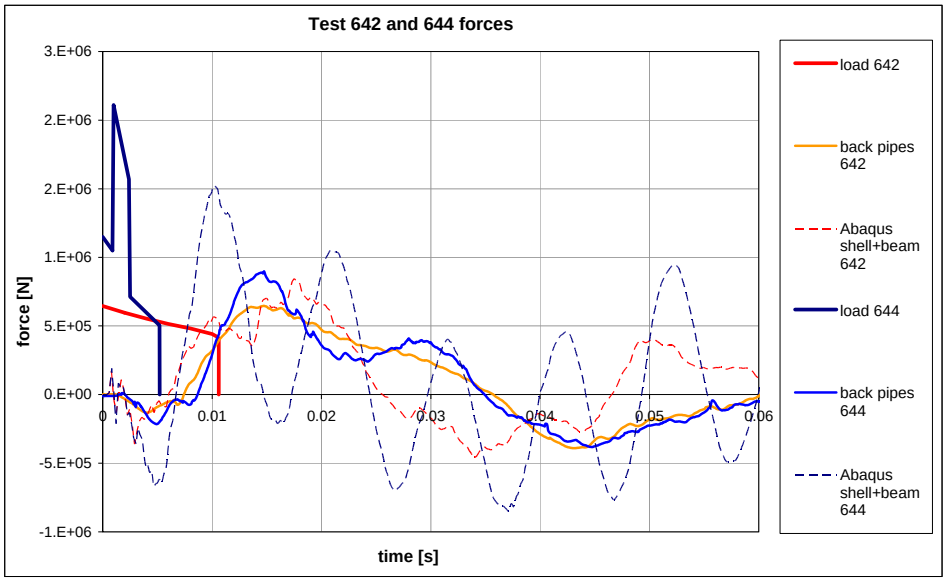

Figure 29.1.16. The load time function (load), the measured reaction force in the back pipes forces (back pipes) and the calculated reaction at the end of the back pipes (Abaqus shell+beam).

Table 29.1.4. Summary of experimental and numerical results.

Test number	**642 (DRY)**	**663(DRY)**	**673(DRY)**	**644(WET)**	**650(WET)**
Velocity (m/s)	109	129	127	105	105
Impulse (Ns)	5630	6230	6400	5344.5	5292
Collapse mode	bend	bend	bend	bend	bend
D1 (m)	0.057	0.07	0.07	0.075	0.08
Calculated results					
FE **D1 (m)** **Dmax (m)** **Strain (%)**	 0.058 3.2	 0.058 3.0	 0.062 0.064 3.0	 0.075 0.087 4.6	 0.073 0.084 4.3
FE f_{ctk_zero} **D1 (m)** **Dmax (m)**	 0.059	 0.063 0.067	 0.068 0.07	 0.075 0.087	 0.076 0.086
Simplified Dmax (m)	0.061	0.069	0.072	0.09… 0.12	

Liquid spreading

The preliminary measuring system and procedure to detect the important parameters/phenomena associated with liquid release and spread process have been developed and documented [5]. The use and further development of the system have been continued in the SUSI project, and the system will be used in the future “wet” IMPACT tests as well. So far, the measured parameters relating to liquid dispersal have been the discharge speed and direction of liquid release, propagation speed of liquid front, extent of liquid spray, liquid pooling area on the floor, and size of deposited and airborne droplets of liquid spray. Partly because the main objective of the IMPACT tests has been directed towards the structural aspects, it has not been possibly to study systematically all important parameters associated with fluid dispersal phenomena. However, based on the experience and information gained from the measurements of the previous tests, a procedure for measurements has been developed that can be used more systematically in the future wet missile tests. The main aim will be to get

quantitative data detailed enough to be utilised in the validation of the simulation methods (FDS code) that are to be used for determination of fuel spread and fire risk following an airplane crash.

The speed and direction of liquid spray coming out from a ruptured missile is measured using a high-speed video camera (1000 fps). Figure 29.1.17 shows a typical splash pattern around two different missiles: a cylindrical (left) and a prototypical 3D missile (right). The deceleration of the missile is very rapid in impact, and consequently, liquid spurts out from the missile when the liquid container fails resulting in dispersal around the target. In case of cylindrical missile, the liquid release starts along the surface quite perpendicularly to the missile direction, and forms a fairly “flat” and uniform circular splash pattern. The pattern becomes thicker as the breakup of the liquid core begins. According to the measurements, the initial discharge speed of the liquid is in some cases even as high as 2.5 times the impact velocity of the missile, but the propagation speed of the spray front decreases rapidly when the distance from the impact target increases. The furthest splashes found on the floor were located about 15 meters sidewards from the impact target. In case of a 3D missile, totally different splash pattern is observed. The front edges of the wings are ruptured first, and liquid spurts out relatively non-uniformly, mostly to vertical directions. The extent of liquid spray to the vertical direction is much higher than directly sidewards. The fragments of the missile interfere with the free surface of the liquid front, and the splash pattern becomes very asymmetric. That is why it is more challenging to measure the speed of the liquid front in case of a 3D missile than in the tests with cylindrical missiles.

Figure 29.1.17. Typical liquid plash pattern from a cylindrical (left) and a prototypical 3D missile (right).

A typical propagation speed of a liquid (spray) front coming out from the cylindrical missile with associated deceleration can be seen in Figure 29.1.18. Also two simulation results of the FDS program with different droplet initial mean diameter are shown. The impact velocity in the test was 125 m/s and the initial discharge velocity of liquid was about 250 m/s. The x-axis of the Figure 29.1.18 indicates the distance from the missile meanwhile the y-axis shows the ratio of liquid velocity to its initial velocity. Within 1.5 meters distance from the impact target the speed of liquid front decreases to a value which is about half of the initial speed. The FDS simulation with a 300 μm droplets diameter yields reasonable results comparing to the experimental data.

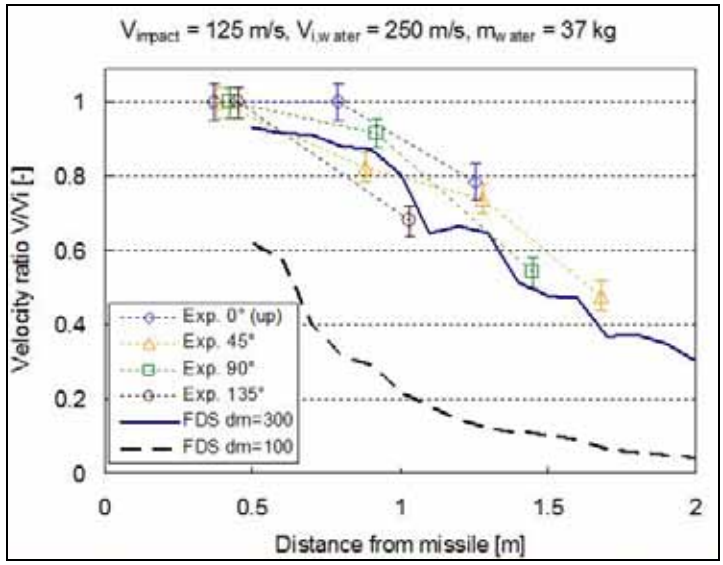

Figure 29.1.18. Measured and simulated speed of liquid front in an IMPACT test.

Initial droplet size of liquid spray is an important parameter that must be given as a boundary condition for the applicable simulation techniques, like FDS. The size of the deposited droplets is measured in the IMPACT tests using collection trays coated with 1–2 mm thick high-viscosity oil layer. The droplet size in the oil layer is measured with a specific image analysis software. Figure 29.1.19 shows the measured data of three different tests with a different impact velocity: 105, 125 sand 165 m/s. The legend indicates also the distance of the measuring point from the impact target. The Figure 29.1.19 demonstrates that the mean diameter of deposited droplets is around 200–300 μm, in some measurements

even lower. The smallest droplet diameter that can be detected within this method is around 15 μm. It is worth mentioning that the size of droplets detected on the oil-coated trays does not represent necessarily the size of airborne droplets of the “primary” liquid spray.

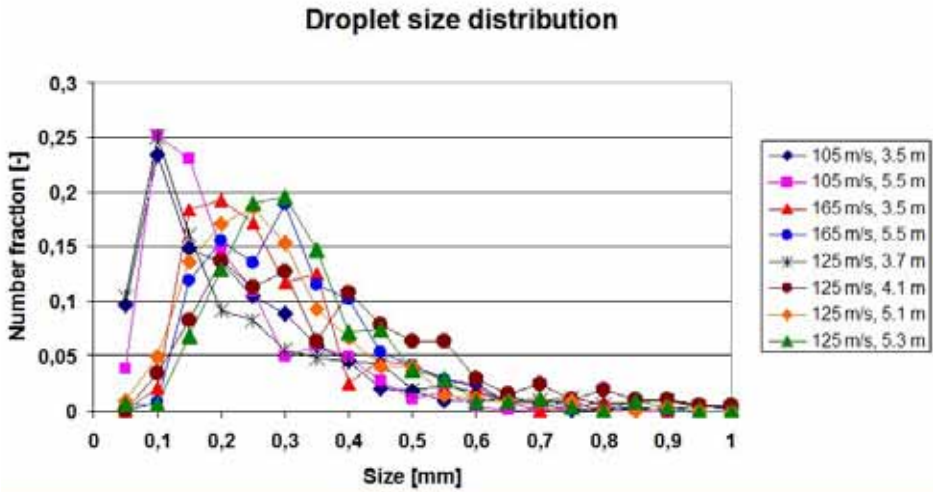

Figure 29.1.19. Example of droplet size measurement on oil-coated collection trays.

A measuring arrangement to detect the size of airborne droplets was also developed. The system consists of two different, parallel cameras with a proper backlighting illumination: a high-speed camera and a high-shutter-speed camera [5]. A high-speed camera (500 fps) is used for drop-size measurement. The camera is synchronised with a high-speed stroboscope to enable an exposure time of 1 μs that “stopped” the motion of single drops. This measuring system has been tested under the small scale laboratory conditions. In order to move and take the system in use under IMPACT test conditions, the most challenging tasks will be building proper shielding for the system and attenuation of the electrical disturbances caused by the high-voltage stroboscope that interrupts the triggering system.

Fire Dynamics Simulation

Model description

The simulation domain was the same as used earlier for the water spray simulations. The domain was 12 m long, 10 m wide and 5.0 m high, as shown in Figure 29.1.20. Three of the four side boundaries were defined open for flow, and all the other surfaces were concrete.

The impact speed was 125 m/s and the release speed of liquid droplets was 250 m/s. In the simulation, the impact itself was accounted for by a pulse of air entering the domain at speed of 125 m/s. 37 litres (25 kg) of heptane (C7H16) was released during a 10 μs period to a release angle $0^o \ldots 15^o$ from the direction parallel to the target surface. The mean diameter of liquid droplets was set to 300 μm.

Simulation was performed using version 5 of Fire Dynamics Simulator [12]. The most important physical models and some of their limitations in the current application are listed below:

- Fluid motion is computed using weakly compressible Large Eddy Simulation (LES)-based solver. This model can not predict the increase of pressure by detonation.
- Two phase flow is computed using Eulerian-Lagrangian concept where the liquid droplets have zero volume in Eulerian space. This means that the liquid-air and liquid-liquid interactions, that may have importance in dense sprays and early phase of the impact, can not be taken into account.
- Combustion is modelled using a mixture-fraction based model that assumes fast, mixed-is-burned chemistry, except for the CO-formation under oxygen limited conditions. The model can not consider the progress of flame surface in the gas-liquid mixture and possible situations where some of the fuel is left unburned.
- Thermal radiation is computed using Finite Volume Method with specialized model for spray-radiation interaction [13]. In the model, the detailed radiative properties are only available for water, and the other liquids are assumed to be some type of oil with simple absorption properties.
- The surface heat conduction is computed using a one-dimensional solver that is considered to be accurate enough for the current application.

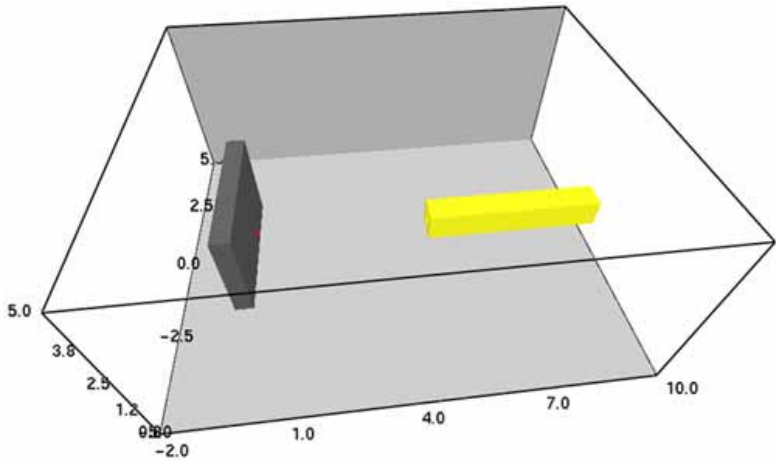

Figure 29.1.20. Simulation domain for impact fire.

Results

The simulation was performed on a single 3.0 GHz Intel Xeon processor. The simulation of 15 s (15033 time steps) took about 11 hours.

The development of the flame after the release of droplets is shown as a series of pictures for the first 1.83 s in Figure 29.1.21. During the first 0.5 s the flame has travelled from the impact location to the domain boundaries. Since some of the domain boundaries are open, we must assume that some fraction of the fuel leaves the computational domain unburned. In future work, domain boundaries should be far enough to allow for an accurate accounting of energy.

Figure 29.1.22 shows the total heat release rate curve of the fire (on the left). The fire ball phase continues about three seconds, during which the heat release rate is order of 100 MW. After the fire ball has burned away, the fire continues to burn as a liquid pool on the floor. However, in the numerical model the pool at that point consists of droplets fallen on the floor, and the evaporation rate is computed by the droplet equations – not by the liquid pool surface model. Therefore, the predicted burning behaviour after the initial flame ball has very high uncertainty. In the future, a feature may be added that transfers the mass of the droplets fallen on the floor to a mass in the pool model.

A cumulative integral of the released energy is shown on the right in Figure 29.1.22. According to the present simulation, about 25% of the total available energy is released in the initial flame ball, but as mentioned above, some uncertainty is related to the results due to the outflow of unburned fuel.

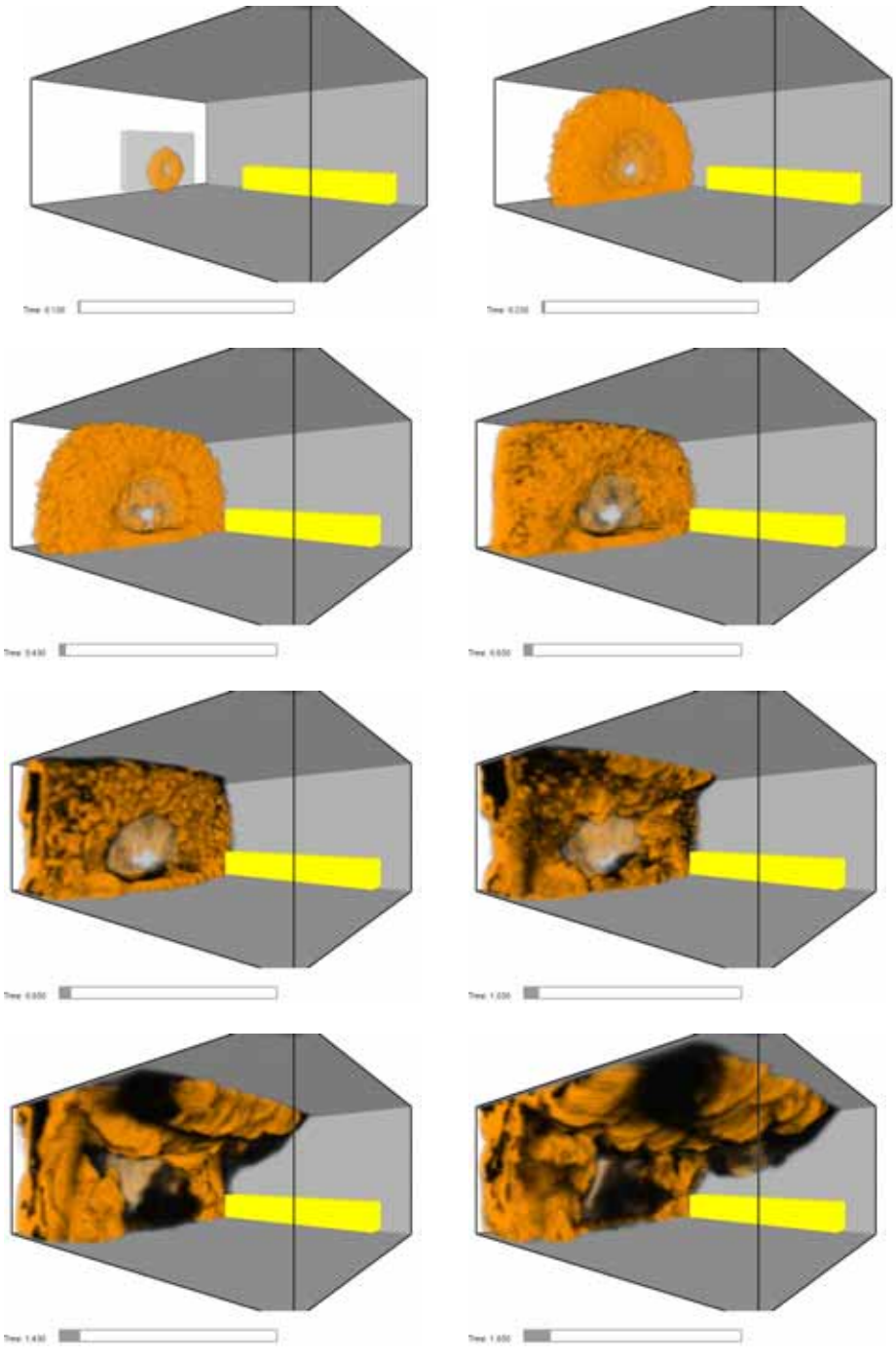

Figure 29.1.21. Development of the flame during the first 1.83 seconds.

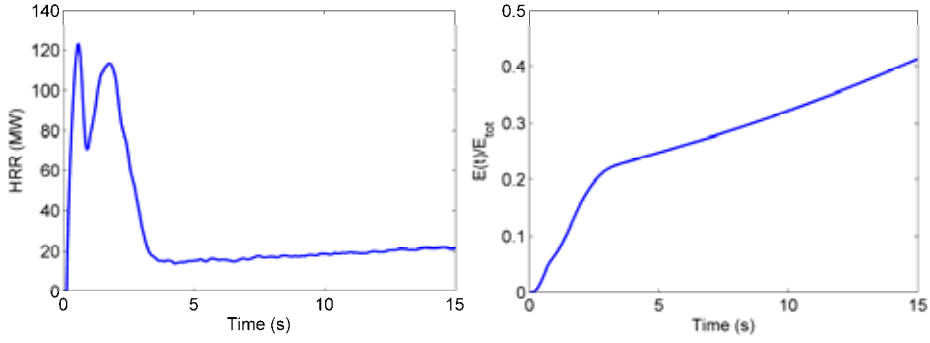

Figure 29.1.22. Total heat release rate (HRR) and cumulative integral of released energy in the impact fire.

The incident heat flux to the target wall is shown on the left in Figure 29.1.23. During the flame ball phase, the heat flux is close to 100 kW/m^2, corresponding to a black body radiation from 880 °C temperature. The surface temperature of the concrete wall is shown on the right in Figure 29.1.23. During the first 15 s, the surface temperature reaches about 200 °C, which would have no effect on the strength of the concrete. It is clear, that the safety relevant heating of the massive structures requires a longer period of heating from a resulting pool fire.

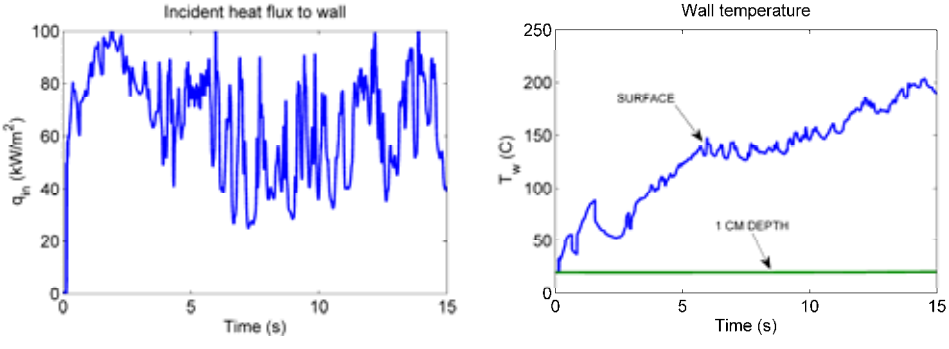

Figure 29.1.23. Incident heat flux to the target wall and target wall surface temperature.

Conclusions

The IMPACT facility has been developed starting from 2003 and has reached now a mature status where well repeatable tests can be conducted and broad range of dynamic data acquired reliably. Most important measurements are the

force-time function of impact (including effects of liquid, possibly contained in the missile) and for walls dynamic displacement (at selected locations) and strains in wall reinforcement. The first phase of the international test campaign has now been completed.

Simplified models that are valuable when judging the reliability of both the test results and the more extensive numerical simulations are studied. Bending or shear failure of a reinforced concrete slab subjected to a projectile impact can be very simply modelled with a two mass system (TDOF). The two mass system is, however, sensitive to the assumed angle of shear failure cone and 3D finite element solutions are needed for comparison. Experimental findings can be used in defining the shear angle for different kind of slabs. Also the determination of proper damping requires carefully conducted experiments.

Based on these studies it can be concluded that these simple four-node shell element models where the transverse nonlinear shear deformation is not considered are capable for calculating the deflection behaviour of a reinforced concrete wall loaded by a deformable missile.

The simplified method and shell element model without the frame somewhat overestimated the permanent deflection. The frequency of the calculated bending vibration after impact was higher than the one recorded during the test. The model with the frame predicted similarly the vibration behaviour for the damaged wall although estimated the permanent deflection reasonably well.

Even though the impulse is slightly higher in the dry missile test, the maximum deflection is clearly smaller than the one in the wet missile test in accordance both to the measurements and calculations. According to the calculations with the shell element model the maximum strain, by a clear margin, occurred in the horizontal reinforcement in the dry missile test. This is due to the fact that the wall loaded by the deformable empty missile behaves like a wide bending beam. In tests where the water missile was used the calculated strain values in the vertical back surface reinforcement were nearly as high as in the horizontal back surface reinforcement. This is due to the fact that the missiled filled with water has a much higher maximum peak value in the load time function at least according to the Riera method.

Some preliminary calculations were carried out also by LS-Dyna code. The maximum deflection was somewhat overestimated and the permanent deflection was underestimated. However, the model was able to simulate the frequency of the global bending mode of the damaged wall reasonably well.

The liquid spread phenomena have been studied at VTT in the IMPACT tests where the missile is filled with water. New vital information on the dispersal phenomena under the impact conditions is gained. Relevant measuring system and procedure have been developed and used in selected IMPACT tests so far.

The measurements indicate that the discharge speed of liquid coming out from the ruptured missile is in some tests even 2.5 times the impact velocity, but the propagation speed of the spray front decreases rapidly due to liquid atomization when the distance from the impact target increases. The splash patterns of cylindrical and 3D missiles behave qualitatively very differently. The mean diameter of deposited droplets on the floor is measured to be around 200–300 μm, in some samples even smaller.

The simulation of liquid fuel dispersal and burning was performed using FDS software in the geometry of laboratory impact tests. The purpose of the work was to study the feasibility of the FDS code for the simultaneous simulation of extremely fast fluid release, flame formation and progress of heat and combustion products. The simulation results were both qualitatively and quantitatively plausible, although the actual uncertainties are difficult to estimate.

References

1. Lastunen, A., Hakola, I., Calonius, K., Järvinen, E. & Hyvärinen, J. Impact Test Facility. SMiRT-19 Conference. August 2007, Toronto, Canada.

2. Calonius, K., Tuomala, M., Hakola, I., Saarenheimo, A., Hostikka, S., Silde, A. & Lastunen, A. IMPACT Tests: Test Facilities and Application Methods, Part 1. VTT Research Report. VTT-R-00731-08. 2008.

3. Saarenheimo, A., Tuomala, M., Calonius, K., Lastunen, A., Hyvärinen, J. & Myllymäki, J. Numerical Studies on Impact Loaded Reinforced Concrete Walls. SMiRT-19 Conference. August 2007, Toronto, Canada.

4. Silde, A., Hostikka, S., Kankkunen, A., Hakola, I. & Hyvärinen, J. Experimental and Numerical Studies on Liquid Dispersal from Projectile Impacting on Wall. SMiRT-19 Conference. August 2007, Toronto, Canada.

5. Silde, A., Hostikka, S. & Kankkunen, A. Study of liquid dispersal in IMPACT tests: Summary report. VTT Research Report No. VTT-R-12084-06. 2.3.2007.

6. Saarenheimo, A., Hakola, I., Kärnä, T., Hyvärinen, J. & Tuomala, M. Numerical and experimental studies on impact loaded concrete structures in Icone-14 2006 Miami (Florida, USA).

7. Kuutti, J. Design of Projectile for Impact testing. Master Thesis. Helsinki University of Technology, 2007.

8. Abaqus Theory Manual, Version 6.7. SIMULIA. Dassault Systemes, 2007.

9. Structural Analysis and Design of Nuclear Power Plant Facilities. ASCE 0-87262-238-X. ASCE, 1980. 571 p.

10. Hallquist, J.O. LS-DYNA Theory Manual. Livermore Software Technology Corporation, March 2006.

11. Wang, T. & Hsu, T. 2001. Nonlinear Finite Element analysis of concrete structures using new constitutive models. Computers & Structures, 2001. Vol. 79, pp. 2781–2791.

12. McGrattan, K., Hostikka, S., Floyd, J., Baum, H. & Rehm, R. 2007. Fire Dynamics Simulator (Version 5) Technical Reference Guide. National Institute of Standards and Technology, MD. USA. NIST Special Publication 1018-5. 86 p.

13. Hostikka, S. & McGrattan, K. Numerical modeling of radiative heat transfer in water sprays. Fire Safety Journal, 2006. Vol. 41, pp. 76–86.

30. Challenges in risk-informed safety management (CHARISMA)

30.1 CHARISMA summary report

Ilkka Karanta, Jan-Erik Holmberg and Ilkka Männistö
VTT

Abstract

The CHARISMA (CHAllenges in Risk-Informed MAnagement) project consists of research tasks related to the use of probabilistic safety assessment (PSA) in decision making, developing assessment methods for nuclear plant operation and maintenance, and developing solutions to problem areas within PSA. In addition to the research tasks, advancement of skills, transfer of skills to the new generation and international cooperation are achieved within CHARISMA. In 2007–2008 research tasks were conducted under the headings risk-informed decision making, human reliability, reliability of automation and level 2 & 3 PSA.

Introduction

Challenges in risk-informed management are two-fold: the use of risk-information as a support for decision making, and the problem areas within the PSA itself. The use of risk information in decision making is challenging, because PSA is a complex model integrating different kinds of statistical and subjective information into a probabilistic model. The concurrent use of both deterministic and probabilistic safety analyses as the basis for decision making is the subject of ongoing discussion. Proper documentation of the assumptions behind both the analysis and the probability model enhances the transparency of the PSA model

and interpretation of the results. Communications process between the PSA experts and other experts is crucial for drawing the conclusion on the risk significance of different components in the risk analysis.

Due to a nuclear power plants nature as a complex socio-technical system the challenges in the risk assessment are numerous:

- Identification of hazards and screening of hazard to be modelled. Recent issues here include the identification of external hazards (e.g. severe weather phenomena) and common cause initiators (e.g. plants disturbances caused by power system or control system failures).
- Identification of dependencies and interactions between systems and processes. This includes e.g. dependencies between human interactions, I&C systems and power supply systems.
- Reliability modelling of dynamically behaviouring systems. Recent issues include computer based systems and accident phenomena in level 2 PSA.
- Estimation of probabilities for events and issues where statistical data is rare or totally missing. This includes e.g. estimation of human error probabilities, software error probabilities and frequencies for rare external events.

Main objectives

The main objectives are to develop risk-informed decision making methods integrating results from risk and reliability analyses with other expertise in the problem domain, to develop assessment methods for plants' operation and maintenance to enhance planning of activities and acting in situations, to develop methodologies in the problem areas of PSA, to advance skills in risk analysis, to assure the competence transfer to the new generation and to participate in international co-operation.

Risk-informed decision making

PSA-related safety goals

The outcome of a probabilistic safety assessment (PSA) for a nuclear power plant is a combination of qualitative and quantitative results. Quantitative results are typically presented as the Core Damage Frequency (CDF) and as the

frequency of an unacceptable radioactive release. In order to judge the acceptability of PSA results, criteria for the interpretation of results and the assessment of their acceptability need to be defined. Ultimately, the goals are intended to define an acceptable level of risk from the operation of a nuclear facility. However, safety goals usually have a dual function, i.e., they define an acceptable safety level, but they also have a wider and more general use as decision criteria. The exact levels of the safety goals differ between organisations and between different countries. There are also differences in the definition of the safety goal, and in the formal status of the goals, i.e., whether they are mandatory or not.

The Nordic project has explored the issue of probabilistic safety goals for nuclear power plants, of important concepts related to the definition and application of safety goals, and of experiences in Finland and Sweden [1]. In parallel, additional context information has been surveyed by contributing to and benefiting from an international activity related to PSA criteria within the OECD/NEA Working Group Risk. Figure 30.1.1 shows results related to criteria for large release, i.e., the outcome of level 2 PSA. [2]

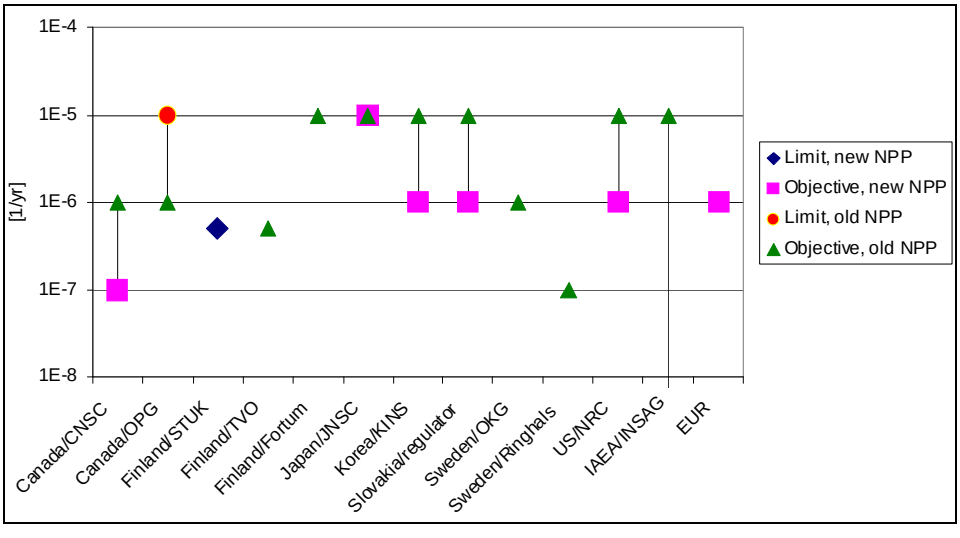

Figure 30.1.1. Criteria for level 2 PSA defined by different organisations. The definition for “large (early) release” varies.

The final goal will be to provide guidance on the formulation, application and interpretation of probabilistic criteria. The results from the project can be used as

a platform for discussions at the utilities on how to define and use quantitative safety goals. The results can also be used by safety authorities as a reference for risk-informed regulation. The outcome can have an impact on the requirements on PSA, e.g., regarding quality, scope, level of detail, and documentation.

Risk-informed defence-in-depth

The concept of defence-in-depth (DID) is fundamental to safety of nuclear power plants. It calls for multiple successive methods or barriers to radioactive release to the environment. A methodology to assess the DID levels using a plant-specific PSA has developed in this subtask. The first stage of the work included: 1) mapping of conditions that should be considered for the DID levels, and 2) definition of quantitative measures that should be considered for the defence in depth levels [3].

Figure 30.1.2 shows the correspondence between levels of PSA and DID framework. The work has been limited to loss-of-coolant accidents (LOCA) and DID levels 1 and 2, i.e., prevention of abnormal operation and failures and control of abnormal operation and detection of failures. Examples were chosen both from power operation LOCAs and LOCAs during cold shutdown. Many DID activities against LOCA are not explicitly modelled in typical PSA-studies. The risk importance of in-service-inspection is analysed and quantified in RI-ISI applications but so far results from RI-ISI have not been incorporated into PSA. Very few leakage detection systems are modelled in PSA-studies. Normally leakage detection systems that is part of the automatic actuation system are modelled while leakage detection systems in the DID levels 1 and 2 typically are omitted. DID activities and systems identified in this study can play a role in several DID levels, and the evaluation of the DID level must therefore be judged by the initiating event.

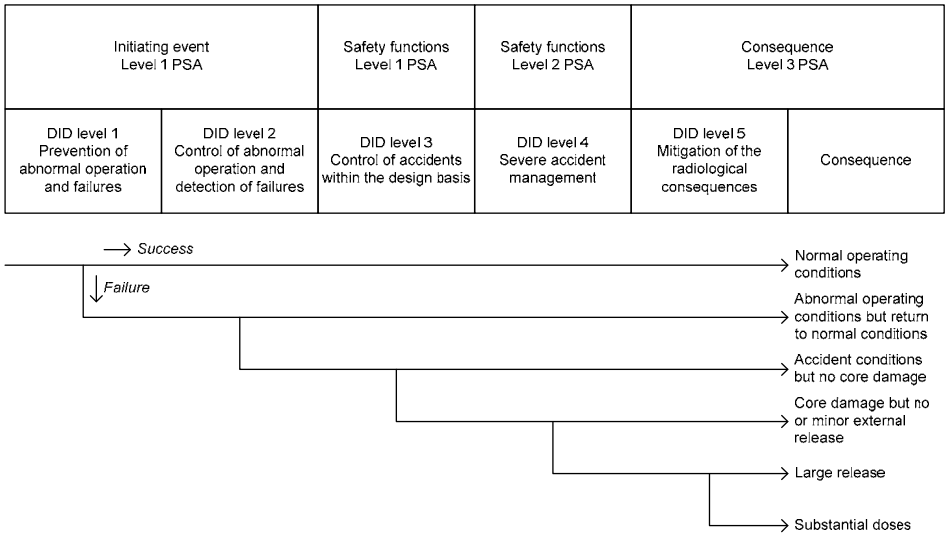

Figure 30.1.2. PSA event tree and the levels of defence-in-depth.

Risk evaluation of technical specification conditions

The use of risk informed methods in daily operation at nuclear power plants as well as for long term evaluation and definition of rules and regulations is increasing. Risk informed methods have been applied on a case by case basis during the past few years, but it is expected that these methods will be applied in a quite different manner in the coming years.

A literature study and interviews with representatives of the Swedish and Finnish utilities and authorities were carried out on the use of risk-informed approaches to evaluate Technical Specifications (TS). According to the interviews, there is a reasonable agreement on the existing TS evaluation methods on a general level. However, there is no common agreement on the basis for the TS analyses, e.g. types of initiating events and risk measures to be studied. Further, especially concerning the risk-informed approaches for evaluating allowed outage times, the Finnish and Swedish views are diverging.

The report [4] summarises the interviews and provides a short background to the current TS and to the role of PSA in the TS evaluation process. Methods, discussions and comments with regard to surveillance test interval and allowed outage time analyses respectively are presented. In a second phase of the study, to be started in 2009, the aim is to develop guidance to facilitate the use of PSA in interpretation and evaluation of TS criteria.

Human reliability

Risk-informed management of fire situations

Collaboration between CHARISMA and FIRAS project has been started in order to integrate the different methodological approaches to fire safety and the management of fire risks. The long term goal is to develop a comprehensive, more holistic approach to operational fire safety. The integration will be made with the help of common fire scenarios, related to fire-risk relevant rooms at the plants. The results can be taken into account in fire risk analyses and in the development of procedures and training at the plants.

The approach developed in the CHARISMA project and applied in this subtask is based on a systemic analysis of the management of fire situations [5]. In the analysis, the management is regarded as a functional and cooperative whole. The emphasis is on the actual situation-specific conditions of decision-making and cooperation and on how they influence on the fire brigades' and the control room crews' possibilities to cope with the situation in cable room fires. The results produced in the FIRAS project, concerning the characteristics and way of spreading of the fire, are used in the analysis. Respectively, the principles of conceptualizing fire situations from the human activity point of view can be used in the quantitative assessments of the FIRAS project.

In this subtask, the work carried out thus far has been concentrated on collaborative development of means for integrating the approaches. In addition, a conceptual framework for the identification of the ways fire may limit and impede decision-making and cooperation and, vice versa, of the ways human actions may affect the behaviour of the fire has been developed. In the next phase the aim is to develop the analysis further and to apply it to relevant fire scenarios, in cooperation with the representatives of the plants.

Emerging human reliability analysis

The subtask aims at reviewing different new approaches to HRA. The work will be carried out by participating into an international empirical study of HRA methods organised by the OECD/NEA Halden Reactor Project [6]. In the Halden study, simulator runs were run for two scenarios relevant in PSA context. Several HRA teams from different countries analysed the scenarios with their own HRA methods, and the approaches will be compared. Two studies (Steam generator tube rupture, STGR scenario and Loss-of-feedwater, LOFW

scenario) were run utilizing a set of simulator runs performed in Halden HAMMLAB for studying performance shaping factors and effects of masking information.

VTT is one of the HRA teams using a method called the enhanced Bayesian THERP (Technique for Human Reliability Analysis). The method is based on the use of the time-reliability curve introduced in the Swain's human reliability analysis (HRA) handbook and on adjustment of the time-dependent human error probabilities with five performance shaping factors (PSFs): (1) support from procedures, (2) support from training, (3) feedback from process, (4) need for co-ordination and communication, (5) mental load, decision burden. In the enhanced Bayesian THERP, the PSFs are elicited by expert judgments, which are then aggregated in a Bayesian manner. This approach has been successfully used in real PSA-studies, where the plant operators have been the experts assessing the levels of the PSFs. The method has proven to be a systematic way to qualitatively and quantitatively analyze operator actions [7].

Reliability of automation

Reliability of distributed control systems

In current PSAs, distributed control systems are analysed and modelled very simply. The subtask aims at bringing the analysis of digital systems reliability to the systems architecture level. The application case has been the feedwater system of a boiling water reactor, and the method used the dynamic flowgraph methodology (DFM) [8]. International research work in this field is followed by participating in the task group on digital I&C (DIC) reliability of OECD/NEA/WGRISK. For a more in-depth description of the work, see the article "Reliability analysis of digital control systems in nuclear power plants" in this SAFIR interim report.

Level 2 and 3 PSA

Modelling of phenomenological uncertainties

The Master's Thesis [9] surveyed how phenomenological uncertainties are modeled in level 2 PSA. The methods were applied to a study case of Loviisa nuclear power plant. The accident scenario is a small loss-of-coolant accident where in addition the emergency core cooling is lost. The most important

phenomena in severe accidents in Loviisa are hydrogen burns, in-vessel retention, and depressurization of primary circuit. A dynamic PSA modeling tool, STUK PSA [10], was used to modify Loviisa containment event tree. The dynamic modeling approach was compared to the conventional event tree-fault tree modeling.

The results show that delay in taking the safety actions has impact in several phenomena. Probabilistic models are constructed that take the delay into account. To support probability quantification, accident simulations are performed using a MELCOR [11] model of Loviisa. The delay is sampled, and the results are presented as distributions in order to quantify the uncertainty of the results. The dynamic approach enables more detailed modeling. Uncertainty analysis is simpler to perform than with the conventional point estimate approach.

Level 3 PSA

Long duration release

In the ARANO dispersion and dose calculation model [12], it is assumed that weather is constant during the whole release duration. This prerequisite can be estimated to hold the shorter the release is. But during long releases dispersion conditions can be expected to change. To evaluate significance of weather changes on off-site doses, the existing calculation model was modifred to calculate consequences on a hourly base.

Essentially compared with the old model the intermediate results now include a new parameter that is the dispersion sector. Placing dispersion in 12 sectors enables usage of the preliminary approach of calculating effect, e.g. dose in the sector and in the adjacent sector. When doses or ground concentrations from one hour pieces of the release are calculated, the results have to be summarized in polar coordinates before effects or interdiction times can be calculated. The intermediate results are outputted into a file from where they are again read when finally cumulative probabilities of the results are calculated. The aim was to make minor modifications into ARANO. This means that dose calculation procedures were not touched [13].

Further processing and presentation of results

Due to changes in calculation procedures of long release duration and general features of probabilistic approach, a large amount of results will be produced,

requiring development in result treatment. The amount of results depends also on the input data, as environmental data, that may not always be available. Results consist of i.a. radiation doses, acute and late health effects and economic losses. Results are presented as complementary cumulative distribution functions (CCDF).

Calculations were done in purpose to compare results of the same dose calculation model employing two different approaches in weather sequence definition. Comparisons indicate that there can be differences in the results but they are not remarkable, if the release duration is only few hours. A reason for this may be that in the traditional ARANO, release duration expands plume dispersion in the horizontal direction decreasing at the same time concentration at the x-axis. In the renewed model this horizontal meandering is bounded into one hour plume and then the x-axis concentration may remain higher than in the traditional ARANO [14].

ASAMPSA2

ASAMPSA2 (Advanced Safety Assessment Methodologies: Level 2 PSA) is a 3-year EU-project (2008–2010) aiming to develop best practice guidelines for the performance of Level-2 PSA methodologies with a view to harmonization at EU level and allowing a meaningful and practical uncertainty evaluation in a Level-2 PSA. For more information, see the homepage of the project http://www.asampsa2.eu/.

Conclusions

Challenges in risk-informed management are two-fold: the use of risk-information as a support for decision making, and the problem areas within the PSA itself. The PSA safety goals usually have a dual function, i.e., they define an acceptable safety level, but they also have a wider and more general use as decision criteria. The use of risk informed methods in daily operation at nuclear power plants as well as for long term evaluation and definition of rules and regulations is increasing. Risk informed methods have been applied on a case by case basis during the past few years, but it is expected that these methods will be applied in a quite different manner in the coming years. An example is the assessment of the defence-in-depth as demonstrated in CHARISMA.

Methods for human reliability analysis can be tested by benchmarking them against simulator studies. For dynamically behaviouring systems, other reliability modelling methods than static event tree-fault tree approach may be

needed. In CHARISMA, alternative methods have been tested for modelling of digital I&C systems and accident phenomena in level 2 PSA. Integration of the qualitative, human activity based approach with the quantitative approach to fire safety and the management of fire risks has been started with the FIRAS project.

The PPRISMA project has been also active in international co-operation through e.g. OECD/NEA Working Groups Risk (WGRISK), Nordic Nuclear Safety Research (NKS), Nordic PSA Group (NPSAG), Halden reactor project and ASAMPSA2 project in the EU FP7 programme. Results have been presented internationally at the most important conferences in this field.

References

1. Holmberg, J.-E. & Knochenhauer, M. Probabilistic Safety Goals. Phase 1 – Status and Experiences in Sweden and Finland. SKI Report 2007:06. Stockholm: Statens kärnkraftinspektion (SKI), 2007.

2. Holmberg, J.-E., Björkman, K., Rossi, J., Knochenhauer, M., He, X., Persson, A. & Gustavsson, H. Probabilistic Safety Goals. Phase 2 Status Report. NKS-172. Roskilde: Nordic nuclear safety research (NKS), 2008.

3. Holmberg, J.-E., Nirmark, J. & Männistö, I. Risk-informed assessment of defence in depth, LOCA example. Phase 1: Mapping of conditions and definition of quantitative measures for the defence in depth levels. SKI Report 2008:33. Stockholm: Swedish Nuclear Power Inspectorate (SKI), 2008.

4. Bäckström, O., Häggström, A. & Simola, K. NPSAG/NKS: Interpretation and Evaluation of the Technical Specification Criteria. NKS-171. Roskilde: NKS. 33 p.

5. Hukki, K. & Holmberg, J.-E. 2007. Systemic Approach to Development of Risk-Informed Management of NPP Fire Situations. In: Proceedings of the Joint 8th Conference on Human Factors and Power Plants and 13th Annual Workshop on Human Performance / Root Cause / Trending / Operating Experience / Self Assessment. August 26–31, 2007, Monterey, California.

6. Lois, E., Dang, V.N., Forester, J., Broberg, H., Massaiu, S., Hildebrandt, M., Braarud, P.Ø., Parry, G., Julius, J., Boring, R., Männistö, I. & Bye, A. International HRA empirical study – pilot phase report. Description of overall approach and first pilot results from comparing hra methods to simulator data. Report HWR-844, OECD Halden Reactor Project. Halden, Norway, April 2008.

7. Holmberg, J.-E., Bladh, K., Oxstrand, J. & Pekka, P. The Application of the Enhanced Bayesian THERP in the HRA Methods Empirical Study Using Simulator Data. In: Proceedings of PSAM 9 – International Conference on Probabilistic Safety Assessment & Management. 18–23 May 2008, Hong Kong, China. Paper 0180, IAPSAM – International Association of Probabilistic Safety Assessment and Management, Hong Kong, 2008.

8. Karanta, I. & Maskuniitty, M. Reliability of digital control systems in nuclear power plants – Modelling the feedwater system. VTT-R-01749-08. Espoo: VTT, January 2009.

9. Suopajärvi, A. Modeling of Phenomenological Uncertainties in Level 2 Probabilistic Safety Assessment of a Nuclear Power Plant. VTT-R-03384-08. Espoo: VTT, May 2008. (Also Master's Thesis at Helsinki University of Technology.)

10. Niemelä, I. SPSA level 2 user's guide. Addendum to SPSA user's guide. Helsinki: Finnish centre for radiation and nuclear safety, 1996. 51 p.

11. U.S. Nuclear regulatory commission. NUREG/CR-6119, MELCOR computer code manuals. Vol. 1 & 2. SAND2005-5713. Washington, DC: Division of systems analysis and regulatory effectiveness, Office of nuclear regulatory research, 2005.

12. Ilvonen, M. Software development of models that simulate the dispersion of atmospheric radioactive releases and predict the resulting radiation doses. Master's Thesis. Espoo: Helsinki University of Technology, Department of Information Technology, 1994. 119 p. (In Finnish.)

13. Rossi, J. Use of hourly weather data in ARANO. Research report VTT-R-08408-08. Espoo: VTT, November 2008.

14. Rossi, J. Presentation of the results calculated from the hourly weather data. Research report VTT-R-08409-08. Espoo: VTT, November 2008.

30.2 Reliability analysis of digital I&C systems in nuclear power plants

Ilkka Karanta, Jan-Erik Holmberg and Matti Maskuniiitty
VTT

Abstract

Assessing the reliability of digital I&C systems is an important but challenging task. Traditional tools of reliability and risk analysis, such as event and fault trees, have limitations. Some dynamic reliability analysis methods, such as dynamic flowgraph methodology (DFM) and Markov models may provide a solution to analyse digital I&C systems of nuclear power plants, such as feedwater control system. Here we will consider DFM. For safety systems (such as reactor protection system) dynamic reliability analysis methods may not be needed.

Introduction

Digital protection and control systems are appearing as upgrades in older nuclear power plants (NPPs) and are commonplace in new NPPs. Due to their important functional role for the safety of NPP, quantitative reliability models are needed along with data for digital systems that are compatible with existing probabilistic safety assessments (PSAs). Due to the many unique attributes of these systems (e.g., software), several challenges exist in modeling and data collection.

In CHARISMA project, VTT's focus has been to develop approaches to model digital control systems. The software reliability issue has been studied in previous research projects of the SAFIR programme using the Bayesian belief network (BBN) approach to combine evidence from expert judgements, testing, different analyses and operating experience [1, 2]. From various methods proposed for the reliability analysis of digital systems, the dynamic flowgraph methodology (DFM) was chosen for further consideration because the physical system can be incorporated in it in a natural way. DFM is based on state and time discretization, and a DFM model is a directed graph where variables are connected to each other by edges. A simple model of the feedwater system was implemented in DFM.

International research work in this field has been followed by participating in the task group on digital I&C reliability of OECD/NEA Working Group RISK (http://www.nea.fr/download/dicrel/). The focus of this activity is on current experiences with reliability modeling and quantification of these systems in the context of PSAs of NPPs. The objectives are to make recommendations regarding current methods and information sources used for quantitative evaluation of the reliability of digital I&C systems for PSAs of NPPs, and identify, where appropriate, the near- and long-term developments that would be needed in order to improve modeling and evaluating the reliability of these systems.

Reliability analysis methods for digital I&C systems

Reliability analysis methods for digital I&C systems can be categorised according to purposes of the methods. The following methods are worth discussing in this context:

- System level quantitative reliability methods used e.g. in PSA context. The traditionally used fault tree analysis (FTA) and failure modes and effects analysis (FMEA) are mostly used to model digital control systems in PSAs for NPPs. Dynamic reliability analysis methods are still at the research and development stage.
- Software reliability analysis methods focussing on the software part of the system. These include methods like reliability growth models, test based models, subjective (Bayesian) methods, software metric based methods and “rule based” methods. For more discussion, see e.g. [3].
- Formal methods aiming at proofing that a hardware design and software is defect-free. Formal methods are not probabilistic, but in methods like model checking [4] a presentation of the functional dependencies of a system is constructed as in a system reliability analysis. In practice, a reliability model and a model checker model can be developed with approximately same effort or jointly, e.g., based on common system FMEA. This line of research will be further studied jointly in SAFIR projects CHARISMA and MODSAFE.

The task group on digital I&C reliability of OECD/NEA/WGRISK concluded that the contribution of software failures to the reliability of a digital I&C system should be accounted for in the models. However, there is little agreement on

how to assess this contribution, and this is probably the most vexing issue associated with probabilistic modeling of digital I&C systems. It is generally agreed that software fails differently than hardware and that obtaining or using software failure data is probably not practical. Some organizations have attempted to quantify software failure probability in limited applications. Some others have included software failures in reliability models as simple common-cause-failure events and quantified them using expert judgment.

The dynamic flowgraph methodology

The dynamic flowgraph methodology (DFM) is an approach to modeling and analyzing the behaviour of dynamic systems for reliability/safety assessment and verification [5]. DFM models express the logic of the system in terms of causal relationships between physical variables and states of the control systems; the time aspects of the system (execution of control commands, dynamics of the process) are represented as a series of discrete state transitions. DFM can be used for identifying how certain postulated events may occur in a system; the result is a set of timed fault trees, whose prime implicants (multi-state analogue of minimal cut sets) can be used to identify system faults resulting from unanticipated combinations of software logic errors, hardware failures and adverse environmental conditions.

DFM models are directed graphs that may contain cycles (feedback). In simple terms, a DFM graph consists of time-valued discrete variable nodes and causality edges.

The variable nodes can represent physical variables (these nodes are called process variable nodes) or states of the system (called condition nodes) components. If the process variable is originally continuous, it must be discretized into a finite number of states. Each variable has an integer time index T referring to a specific time point.

The edge nodes indicate graphically the dependencies between variables nodes. The dependencies are explicitly expressed in decision tables. A decision table is a generalized truth table, where for each combination of the states of input variables, the state of the output is given. The decision table tells what the state of the output variable, at time point T = t, is for a given combination of states of the inputs, at previous time points.

Figure 30.2.1 shows an example of a DFM model. For instance, the variable Level[t] is dependent on two variables: 1) Level[t–1] and 2) Flow[t–1]. It should

be noted that, the DFM formalism allows to model also longer time delays than one time step. Thus the whole DFM model can be expressed as a difference equation

$$X[t] = f(X[t–1], ..., X[t–n]),$$

where X[t] is the vector of variables represented by the nodes, n is the longest time delay used in the decision tables and f(·) is a "super decision table."

The DFM model can be analyzed in two different modes, deductive and inductive. In inductive analysis, event sequences are traced from causes to effects; this corresponds to simulation of the model. In deductive analysis, event sequences are traced backward from effects to causes.

A deductive analysis starts with the identification of a particular system condition of interest (a top event); usually this condition corresponds to a failure. To find the possible root causes of the top event, the model is worked backward in the cause-and-effect flow to find what states of variables (and at what time instances) are needed to produce the top event. The result of a deductive analysis is a set of prime implicants.

A prime implicant consists of a set of triplets (V, S, T); each triplet tells that variable V is in a state S at time T. The circumstances described by the set of triplets causes the top event. Prime implicants are similar to minimal cutsets of fault tree analysis, except that prime implicants are timed and they deal with multivalued variables. A useful analogy is that deductive analysis corresponds to minimal cut set (MCS) search of a fault tree. Once prime implicants have been found, the top event probability is quantified as in the MCS analysis of a fault tree.

In inductive analysis, all the possible consequences of a given system initial condition or boundary condition are generated. These initial or boundary conditions can be defined to represent desired and undesired states. Starting from a combination of desired states, an inductive analysis can be used to verify system requirements. Starting from a combination of undesired states, inductive analysis can be used to verify the system's safety behaviour.

Applications and potential

DFM has been used to assess the reliability of nuclear power plant control systems [6], but also of space rockets [7] and chemical batch processes [8]. The application scope of DFM is large. The most important current areas of application include

- Determination of prime implicants or minimal cutsets and computation of probabilities of top events for PSA purposes. These can be used to construct timed fault trees.
- Inspection of a given design for requirements compliance. Compared to model checking, which stops when a counterexample is found, DFM searches for all counterexamples. On the other hand, model checking models may include temporal logic operators not possible in DFM.
- Setting up a testing plan by examining what events (i.e., the prime implicants found by DFM) might lead to failure.

The main benefits of the approach are as follows:

- the simplicity of its formalism: the main entities – discrete state space, state transition tables and delays – are immediately graspable
- possibility to model time-dependencies and loop dependencies
- possibility to model multi-state logic and incoherent reliability structures
- possibility to analyse different top events using a single system model.

The main drawback and limitation of DFM is that a more realistic modelling easily causes a combinatorial explosion as the number of states in the decision tables grows. This can be controlled somewhat by giving more constraints in the top event.

The main use of DFM in PSA context could be to support the construction of fault trees for dynamic systems and systems with loop dependencies, e.g., feedback control systems and back-upped electric systems.

An application example

The model is a simplified representation of the feedwater system of a boiling water reactor. The model was constructed to analyze restart after a short term loss of offsite power transient, which causes a reactor scram and stopping of the feedwater system.

Several simplifications have been made. The full power flow control valve has been left out because it does not participate in the restart of the feedwater system. Only low power flow control valves and one of the four feedwater pumps have been incorporated in the model because even one working pump

will supply sufficient water flow, and therefore the rest only affect the reliability and availability of the pump subsystem. Further, a significant simplification is that only a small part of control signals is included in the model.

The number of states of the process parameter variables has been limited to max 3 states. This is typical in reliability analysis, since the primary purpose is to analyse particular system states, and not to accurately model process dynamics. In principle any number of states can be attached to a variable in a DFM model; determining the sufficient amount of states for each variable is a case specific issue. Figure 30.2.1 shows the simplified DFM model and the meaning of some variables is explained in Table 30.2.1.

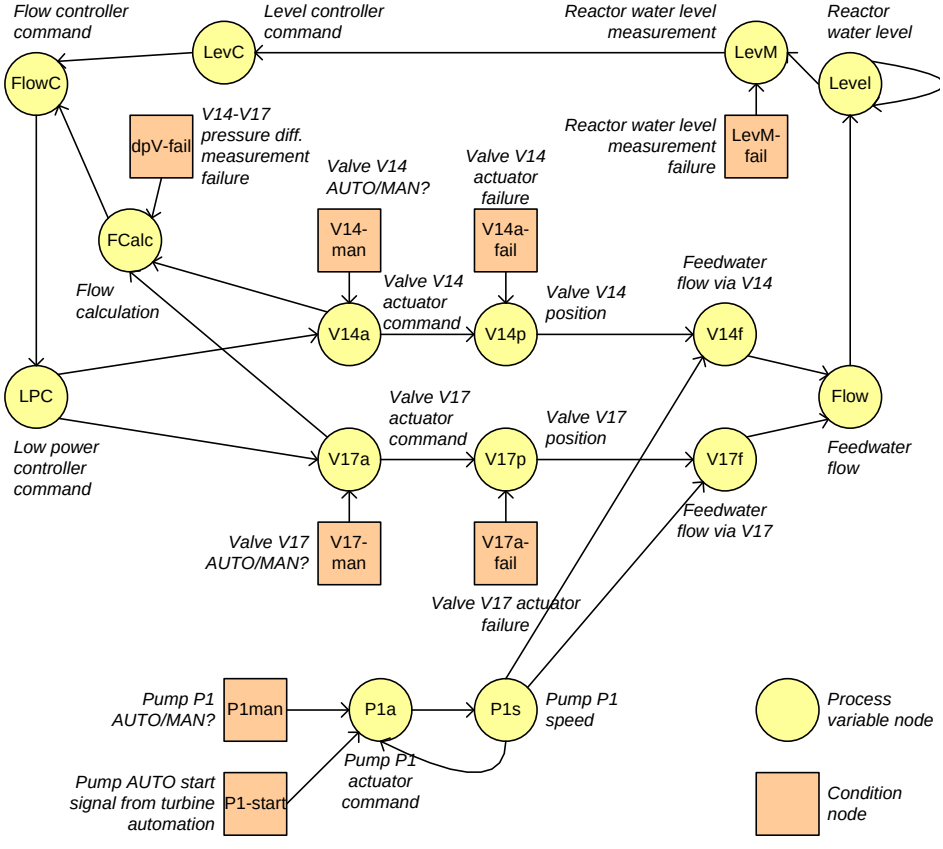

Figure 30.2.1. The DFM architecture of an NPP feedwater system.

Table 30.2.1. Some variables of the simple DFM model.

Variable	Description	Possible states
V14a	The direction to which the actuator tries to direct the position of the feedwater flow control valve (V14)	increase, stationary, decrease
V14f	The feedwater flow through the valve V14	high, normal, low
V17a	The direction to which the actuator tries to direct the position of the feedwater flow control valve (V17)	increase, stationary, decrease
V17f	The feedwater flow through the valve V17.	high, normal, low
Level	Water level in the reactor pressure vessel	too_low, normal, too_high

The decision table for our example variable Level is shown in Table 30.2.3. For instance, if the total flow is “high” and the water level in reactor is “too_low” at time point T = t–1, then at the next time point T = t, the water level in reactor is “normal.”

Table 30.2.2. Decision table for the variable WaterLevel.

Input variables		Output variable
Flow[t–1]	**Level[t–1]**	**Level[t]**
high	too_low	normal
high	normal	too_high
high	too_high	too_high
normal	too_low	too_low
normal	normal	normal
normal	too_high	too_high
low	too_low	too_low
low	normal	too_low
low	too_high	normal

The model contains three kinds of variables:

- Physical state variables describe a physical variable such as amount of flow, a measurement variable, or an electrical signal. In this model, these are V14f, V17f, P1s, P1a, LevM, LevC, V14p, V17p, Flow and Level
- Logical variables. These are variables that describe the behaviour of a software or networking component. In this model, these are FCalc, FlowC, LevC, LPC, P1-man, V14-man, and V17-man
- Fault condition variables. These are indicator variables that tell whether the system component they are attached to is working properly or not. In this model, these are dPVfail, LevM-fail, V14a-fail, V17a-fail and P1-start. Fault condition variables correspond to basic events in a fault tree model.

As an example top event for the system, consider the case that the water level of the reactor is too low for three consecutive time instances. This is expressed as

(Level[0] = too_low) & (Level[–1] = too_low) & (Level[–2] = too_low).

When setting the total number of time steps to 3, DYMONDA gives 2082 prime implicants for this top event. A sample prime implicant is

(Level[–3] = normal) & (P1s[–3] = low) & (P1s[–3] = incorrect measurement)

The prime implicant can be interpreted as follows. “Level[–3] = normal“ means that the reactor level is initially normal. This variable was not fixed in the analysis. “P1s[–3] = low“ means that the pump is not initially running. The actual failure event here is “P1s[–3] = incorrect measurement” meaning that the pump P1 does not start. In the next time step T = –2, the reactor level is low and will stay low, since the pump does not function.

The model was implemented in DYMONDA, available from Asca, Inc. (http://www.ascainc.com/). The software is currently in beta version, and it was received by VTT for testing and evaluation. VTT’s experience was that only simple models and top events could be analysed with this code version. DYMONDA also contains the capability of computing the top event probability from cause probabilities, but in this beta version this functionality was not functioning correctly.

Conclusions

Assessing the reliability of digital control systems is an important but challenging task. Traditional tools of reliability and risk analysis, such as event and fault trees, have limitations. Some dynamic reliability analysis methods, such as dynamic flowgraph methodology (DFM) and Markov models may provide a solution to analyse digital control systems of nuclear power plants, such as feedwater control system. For safety systems (such as reactor protection system) dynamic reliability analysis methods may not be needed.

In CHARISMA project, VTT's focus has been to develop approaches to model digital control systems. The dynamic flowgraph methodology (DFM) seems a promising way to assess the reliability of digital systems. Its central elements would seem sufficient for modelling a control system to desired accuracy. Its representation is geared towards modelling of hardware-software systems such as the control systems at an NPP. The main drawback and limitation of DFM is that a more realistic modelling easily causes a combinatorial explosion as the number of states in the decision tables grows.

References

1. Helminen, A. & Pulkkinen, U. Reliability assessment using bayesian networks. Case study on quantative reliability estimation of a software-based motor protection relay. Helsinki: Radiation and nuclear safety authority, 2003. 28 p. + app. 3 p. STUK-YTO-TR 198. http://www.stuk.fi/julkaisut/tr/stuk-yto-tr198.pdf.

2. Haapanen, P., Helminen, A. & Pulkkinen, U. Quantitative reliability assessment in the safety case of computer-based automation systems. Helsinki: Radiation and nuclear safety authority, 2004. 36 p. STUK-YTO-TR 202. http://www.stuk.fi/julkaisut/tr/stuk-yto-tr202.pdf.

3. Pulkkinen, U. Software-based System Reliability. Technical Note. Paris: OECD Nuclear Energy Agency, 2007. 16 p. NEA/SEN/SIN/WGRISK(2007)1. http://www.nea.fr/download/dicrel/Background%20info/sen-sin-wgrisk2007-1.pdf.

4. Valkonen, J., Pettersson, V., Björkman, J., Holmberg, J.-E., Koskimies, M., Heljanko, K. & Niemelä, I. Model-Based Analysis of an Arc Protection and an Emergency Cooling System – MODSAFE 2007. Espoo: VTT, 2008. VTT Working Papers 93. http://www.vtt.fi/inf/pdf/workingpapers/2008/W93.pdf.

5. Garrett, C.J., Guarro, S.B. & Apostolakis, G.E. The dynamic flowgraph methodology for assessing the dependability of embedded software systems. IEEE Transactions on Systems, Man and Cybernetics, May 1995. Vol. 25, No. 5, pp. 824–840.

6. Aldemir, T., Stovsky, M.P., Kirschenbaum, J., Mandelli, D., Bucci, P., Mangan, L.A., Miller, D.W., Sun, X., Ekici, E., Guarro, S., Yau, M., Johnson, B., Elks, C. & Arndt, S.A. Dynamic reliability modeling of digital instrumentation and control systems for nuclear reactor probabilistic risk assessments. NUREG report NUREG/CR-6942, October 2007. http://www.nrc.gov/reading-rm/doc-collections/nuregs/contract/cr6942/cr6942.pdf.

7. Yau, M., Guarro, S. & Apostolakis, G. Demonstration of the dynamic flowgraph methodology using the Titan II space launch vehicle digital flight control system. Reliability Engineering and System Safety, 1995. Vol. 49, pp. 335–353.

8. Houtermans, M., Apostolakis, G., Brombacher, A. & Karydas, D. Programmable electronic system design & verification utilizing DFM. In: Koornneef, F. & van der Meulen, M. (Eds.). SAFECOMP 2000. Lecture Notes in Computer Science 1943 (2000). Implementation of quantitative fire risk assessment in PSA (FIRAS). Pp. 275–285.

31. Implementation of quantitative fire risk assessment in PSA (FIRAS)

31.1 FIRAS summary report

Simo Hostikka, Anna Matala, Johan Mangs and Jukka Hietaniemi
VTT

Abstract

Implementation of Quantitative Fire Risk Assessment in PSA (FIRAS) -project aims at development and application of modelling techniques for fire spread on cables and other fire loads found at NPPs, integration of the quantitative fire risk assessment methods into the NPP fire PRA, and carrying out fire simulations related to but outside OECD PRISME-project aiming to (i) guidance for the design of experiments and (ii) validation of the developed fire models. New experimental techniques have been developed to study the vertical flame spread, and analysis methods have been developed to estimate pyrolysis model parameters from the small scale experiments.

Introduction

The recent developments in numerical fire simulation and computer capacity allow the use of fire simulation as a predictive sub model for the fire-PRA of NPPs. In the previous NPP fire safety projects, promising results were obtained for both the deterministic methods for fire spread simulation and the probabilistic methods allowing risk estimation. The usability of the methods has been shown by applying them on some relatively simple geometries. In the current project, the fire spread simulation is further developed by utilizing the

new experimental information and co-operation with the plant personnel and fire brigades to estimate the effectiveness of the active fire safety measures.

The long term objective is the comprehensive assessment and management of fire risks. In 2008, a co-operation with the CHARISMA-project was started to integrate the quantitative fire simulation method (FIRAS) with the systemic approach of risk-oriented decision making in CHARISMA.

VTT transforms new information from the international fire research community into Finland, utilizing the good contacts with NIST/USA, NRC/USA, IRNS/France and GRS/Germany. VTT also generates new information in the areas where sufficient knowledge is not readily available.

Main objectives

(1) Application of modelling of fire development and spread to fires involving cables and other fire loads found at NPPs, including the potential fire loads during shut down and refuelling outages and reconstruction periods.

(2) Integration of the quantitative fire risk assessment methods into the NPP fire PRA, which will be initiated through a study of fire-risk relevant rooms with potential to comprehensive testing of the models. The work will be carried out in close co-operation with the personnel involved in safety and PRA work of the NPPs.

(3) Carrying out fire simulations related to but outside OECD PRISME-project aiming to (i) guidance for the design of experiments and (ii) validation of the developed fire models.

Results

Fire spread modelling and experiments

The numerical fire simulations are used in the quantitative PRA, to predict the effects of accidental fires on the NPP components, and during the design phase of new plants to assess the reliability of safety measures and performance of the fire loads. In most of these applications, the fire spreading and heat release rate must be *predicted* rather than *prescribed*. There are several challenges associated with the fire spread simulations: (1) the difference in scales of close field heat transfer and the largest resolved scales of the geometry, (2) physical and

numerical modelling of the mass and heat transfer phenomena within the condensed phase, and (3) the definition of the necessary model parameters.

In years 2007 and 2008, the focus of the modelling activities was in the development of methods for the estimation of condensed phase model parameters. Good results were obtained by applying of Genetic Algorithms for the estimation of kinetic reaction coefficients from thermogravimetric data [1]. Later, the method was extended to estimate thermal parameters from cone calorimeter tests, and applied on the pyrolysis of electrical cables. These results are reported in this publication as a special report titled “Estimation of pyrolysis model parameters for condensed phase materials”.

To increase the understanding of flame spread physics and to provide validation data for the simulation models, flame spread experiments have been performed on well-characterized reference materials (birch wood) and electrical cables. A new experimental apparatus has been developed for the implementation of flame spread tests at different ambient temperatures. The purpose is to obtain a continuous preheated air supply throughout the experiment to be able to measure flame spread velocity at different initial temperatures, starting from ordinary room temperatures up to temperatures near auto-ignition level. Basic requirements are: sample length 2 m, diameter at maximum less than 100 mm, and initial temperature at maximum 400 °C. Description of the device and the initial results are reported in [2].

A schematic picture of the developed apparatus is shown in Figure 31.1.1. The device consists of a heating channel and a test channel (width 300 mm, depth 330 mm), separated from each other by a thin stainless steel sheet and connected to each other at the upper and lower parts of the channels. The device is insulated with 100 mm thick Kaowool insulation between 0.5 mm stainless steel plates. There is a door on the front side to the channels, an air inlet in the upper part of the heating channel and a smoke outlet at top of the test channel. The device is pivoted to a massive steel support at its lower end, and can be used in either vertical or horizontal position.

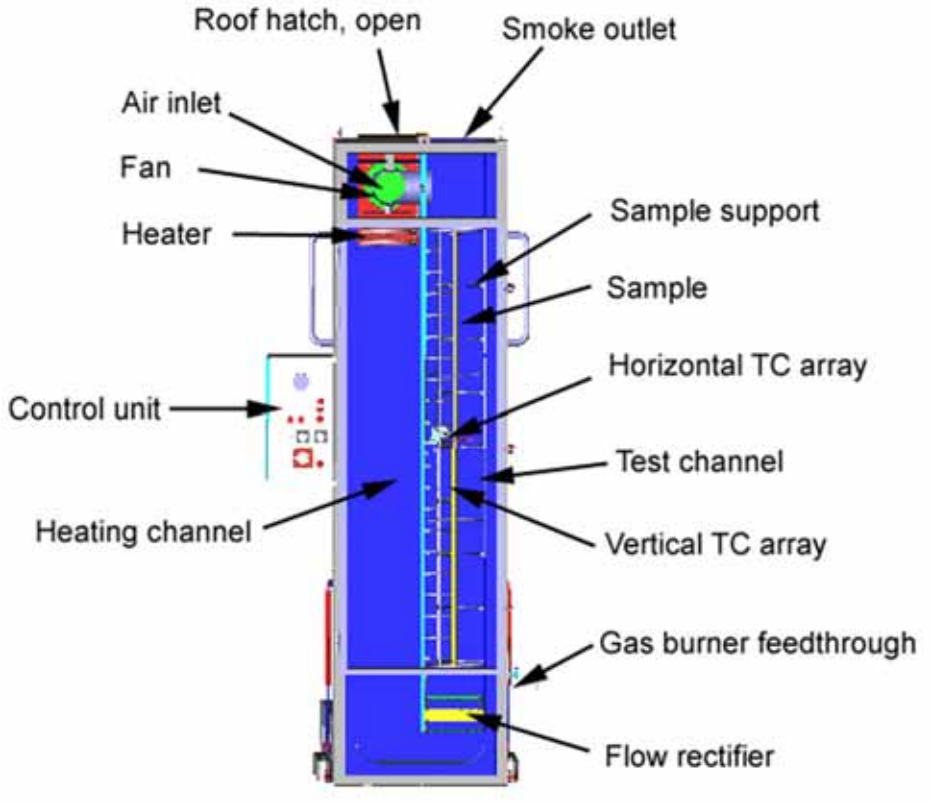

Figure 31.1.1. 2 m test rig *for flame spread experiments* in vertical position. Cross-section with essential features.

During the years 2007 and 2008, start-up tests of the test rig were performed to ensure consistent flow and temperature conditions, and to characterize the temporal and spatial variations of temperature. Actual flame spread tests were performed for birch wood and PVC-cable. Figure 31.1.2 shows the measured rate of flame spread for 8-mm birch samples as a function of the ambient temperature. Results are shown for both oven-dry and normal moisture samples. The temperature dependence is roughly exponential. The flame spread rate of PVC-cable (MMJ 4 × 1.5 mm^2) with outer diameter of 9.5 mm are shown in Figure 31.1.3.

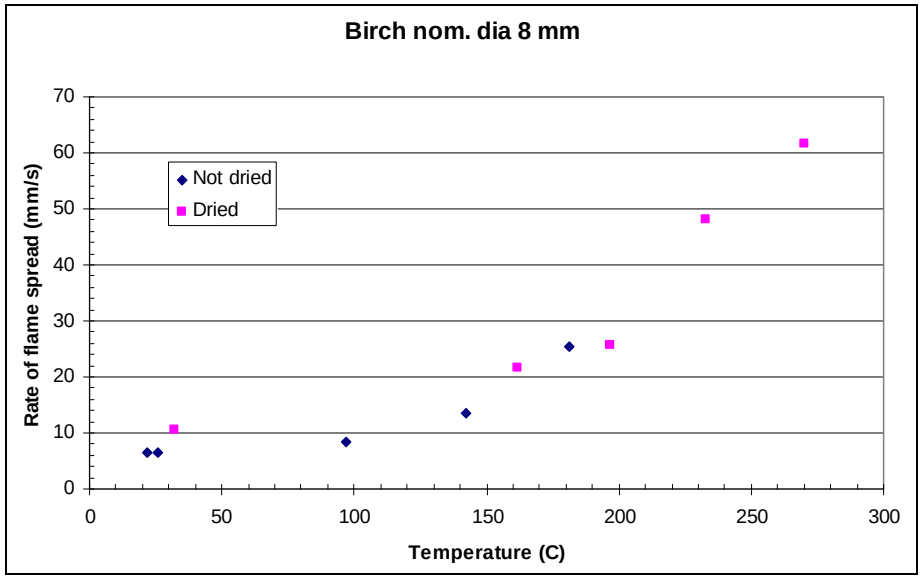

Figure 31.1.2. Rate of flame spread as a function of ambient temperature for cylindrical birch samples 8 mm in nominal diameter.

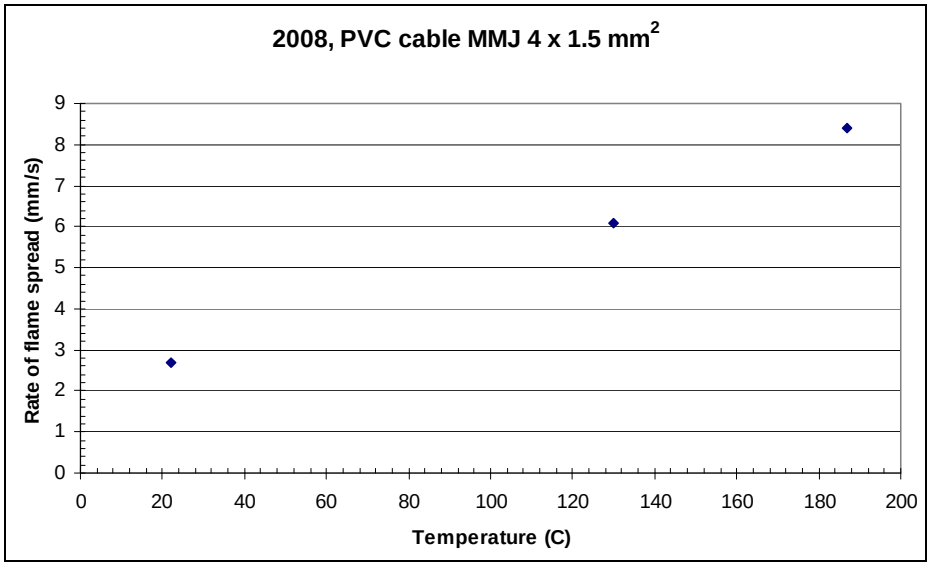

Figure 31.1.3. Rate of flame spread as a function of ambient temperature for MMJ cable samples.

For the validation of flame spread simulations, the birch wood material model, developed in [1], was implemented in version 5 of Fire Dynamics Simulator (FDS) CFD-code [3], and simulations of 2-mm thick birch sample was started. A very thin sample was first used to get first estimates of the code behaviour in short time (at thin samples, the steady-state flame spread rate is obtained faster). The initial simulations showed that the flame spread rates were considerably higher than those obtained using the previous version of the code. Reasons for the differences were searched by performing a series of parametric tests for various gas and condensed phase properties.

Integration of quantitative fire risk assessment into NPP PSA systems

During 2008, the two SAFIR2010 projects, FIRAS and CHARISMA, have started co-operation that ultimately aims at creating a novel, comprehensive approach to improve fire protection and prevention, preparedness to fires, assessment and mitigation of fire risks as well as management of fire situations at nuclear power plants (NPPs). Though both projects address fire safety at NPPs, their approaches differ notably. FIRAS employs natural-sciences based methodologies with emphasis on physical phenomena and technology. CHARISMA deals with human actions and interactions to achieve a systemic approach to development of risk-informed management of fires and fire hazards NPPs. Acknowledging the fundamental differences of the approaches – one is thoroughly quantitative and the other more qualitative – it is quite evident that attempts to create a fully integrated unified methodology of these approaches are likely to be very tedious and in fact unnecessary. A more fruitful way forward is to make these two methods to support each other as far as is reasonable and advantageous for the main goal, fire safety of NPPs. That is, the methodologies should be made commensurable enough that one can make use of the information of the other. In the FIRAS project the focal point in the work carried out in 2008 has been in laying the basis for the information exchange through drafting a computational platform that utilises input from both FIRAS and CHARISMA. This platform is implemented as a rather rudimentary EXCEL worksheet tool, which in no account shall be considered as a solution of FIRAS-CHARISMA co-operation, but as a tool that gives concrete guidelines for the further development steps.

A model to quantify the timing of NPP fire-brigade (FB) intervention has been developed. The model considers the time-line of FB using both literature study and experimental information collected from TVO plant FB and on municipal FBs. A literature study was performed to model the ability of the FB to fight successfully a fire of a given size. One result is illustrated in Figure 31.1.4, showing the fire extinguishing success probability of an average fire department as a function of the fire area.

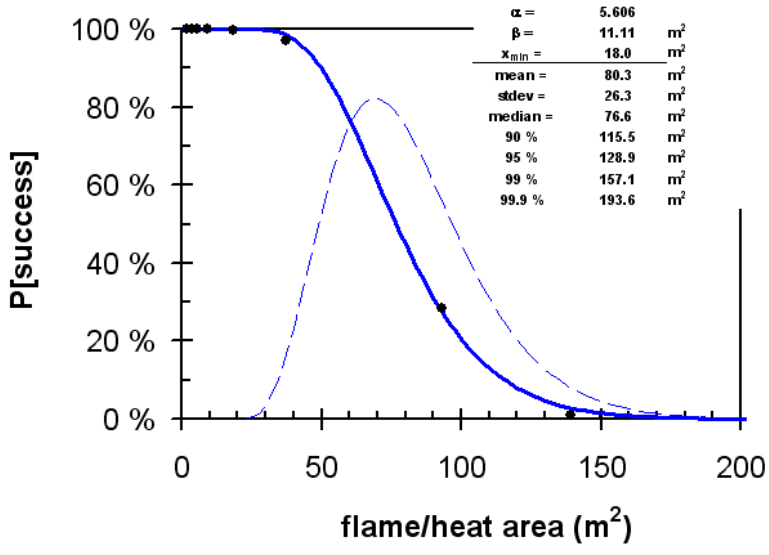

Figure 31.1.4. Fire extinguishing success probability of an average fire department.

A NPP FB intervention model (NPP-FBIM) is developed. The model addresses specifically the FB operations in an NPP. In particular this means that principal emphasis is on the FB actions and the potentially needed interactions with other actors, such as the control-room personnel or electricians after the FB has arrived at the fire scene. The response time, i.e., the time from alarm to arrival at the fire scene is given less weight as it typically is not the dominant factor in NPP FB operations. The time-line is formulated according to the format used in NPP FB exercises with each factor treated as a stochastic quantity. The use of the model is exemplified by applying it to a specific cable room considered in the FIRAS project fire simulation studies as well as in the systemic approaches to development of risk-informed management of fires in the SAFIR2010 CHARISMA project.

International activities

Within FIRAS, VTT has participated in the planning, steering and utilization of OECD PRISME programme. This programme aims at analysing the mechanisms governing smoke and heat propagation from the room containing the fire to adjacent rooms. Propagation modes were selected: through a door; along a ventilation duct that crosses the room containing the fire and that ventilates an adjacent room; along a ventilation duct when flow is reversed within; through leakages between several rooms. It is to provide critical information such as time elapsed before malfunction of target equipments, and to qualify computer codes modelling of heat and smoke propagation phenomena. The PRISME tests are performed by IRSN/France.

Formally outside PRISME, there is a parallel benchmarking exercise (BE) to validate fire models by performing blind and open simulations. VTT has participated BE #1 by simulations using FDS code version 5. The results have been in accordance with the general FDS validity database.

Applications

The developed simulation techniques are used to study the cable fires and their consequences at two different target rooms of real plants. The objective is two find out the failure probabilities of second sub-system in rooms where two of the four sub-systems are paired, i.e. placed in the same space, and to estimate the effectiveness of the water sprinkler systems in the protection of the adjacent trays. The first application was a long cable tunnel, of which a 95-m long section was simulated. The second application was a complicated cable room.

A cross section of the tunnel is shown in left part of Figure 31.1.5. The fire load consists of power cables on the few uppermost cable trays. For modelling, a material model of NOKIA AHXCMK 10 kV 3 x 95/70 mm^2 cable (Figure 31.1.5 right) was created.

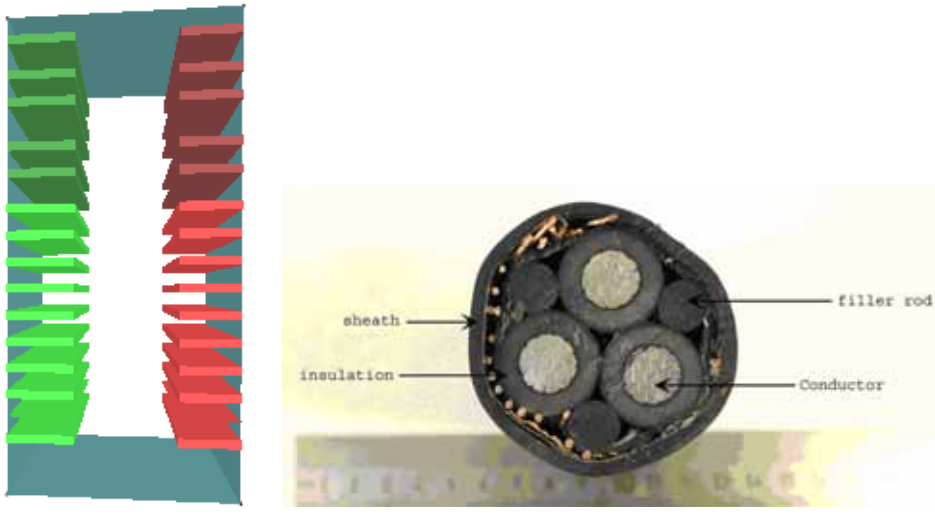

Figure 31.1.5. Cross-section of the cable tunnel (left) and power cable used as fire load (right).

Models of the water sprinkler nozzles were created by first measuring the water flux distributions at 5.0 bar pressure and adjusting the water droplet boundary conditions to match the experiments. The simulated spray (horizontal direction) and comparison of the measured and simulated water flux distributions are shown in Figure 31.1.6. The results indicate, that if the sprinklers are not used, the failure probability of second-sub IC cables is between 0.6 and 0.7. The probability is practically zero during the first 1000 s from the ignition, and reaches the final level at about 2000 s from the ignition. The simulations of the cases with sprinklers were not finished at the time of this publication.

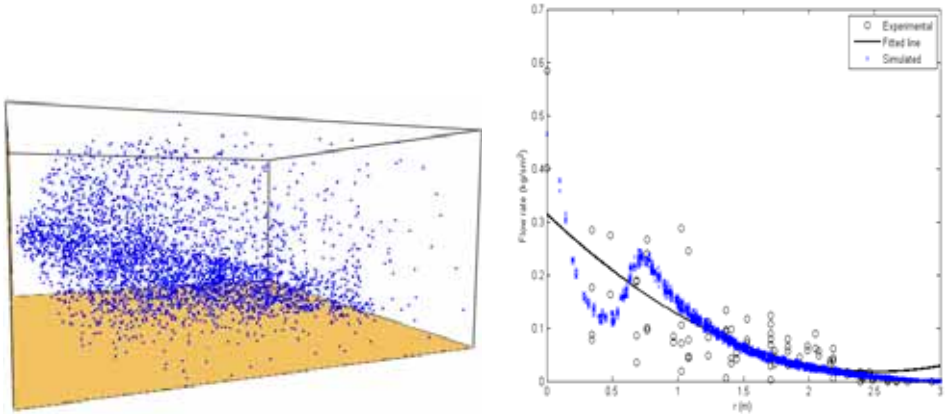

Figure 31.1.6. Simulated water spray (left) and comparison of the simulated and measured water flux distributions (right).

Conclusions

Several aspects of the fire safety analysis methods have been studied on the way towards better integration and utilization of fire simulation methods in the quantitative Fire-PRA. The methods used for predicting the fire spread and heat release rate have been studied both experimentally and by developing the analysis methods. A new 2-m test apparatus has been developed for studying the effect of ambient temperature on the flame spread rate on thin objects, such as electrical cables. Techniques for estimating the pyrolysis model parameters from thermogravimetric and cone calorimeter, i.e. small scale experiments have been developed. The techniques are based on genetic algorithms and have been demonstrated and successfully applied in real cable tunnel simulations.

New methodology for integration of quantitative fire simulations and more qualitative human reliability assessment has been proposed. It can be used to identify the dominating factors on for example efficiency of fire brigade.

Fire in a NPP cable tunnel was simulated using Monte Carlo technique. Without sprinklers the probability of IC cable failure is 0.6. This number is most sensitive to the starting height of the fire. Next step will be modelling the similar Monte Carlo with sprinklers, comparing the old sprinkler system to the new one.

The future work includes the validation of flame spread models using the vertical flame spread experiments and development of more efficient parameter estimation techniques. Future applications will look at the efficiency of water sprinklers in the protection of secondary targets.

References

1. Matala, A., Hostikka, S. & Mangs, J. Estimation of pyrolysis model parameters for solid materials using thermogravimetric data. Fire Safety Science – Proceedings of the Ninth International Symposium, International Association for Fire Safety Science. 2008. (Preprint.)

2. Mangs, J. A new apparatus for flame spread experiments. VTT Working Papers 112. Espoo, Finland: VTT Technical Research Centre of Finland, 2008.

3. McGrattan, K.B., Hostikka, S., Floyd, J.E., Baum, H. & Rehm, R. Fire Dynamics Simulator (Version 5): Technical Reference Guide. NIST SP 1018-5. NIST Special Publication 1018-5. October 2007. Building and Fire Research Laboratory. National Institute of Standards and Technology.

31.2 Estimation of pyrolysis model parameters for condenced phase materials

Anna Matala, Simo Hostikka and Johan Mangs
VTT

Abstract

Determination of the material parameters is one of the key challenges of numerical fire simulation attempting to predict, rather than prescribe the heat release rate. In this work, we use common fire simulation software and genetic algorithms to estimate the kinetic and thermal reaction parameters for PVC, black PMMA and a power cable. Parameters are estimated by modelling thermogravimetric and cone calorimeter experiments and minimizing the error between the experimental and numerical results.

Introduction

The numerical simulation of fires is used in the quantitative PRA to predict the effects of accidental fires on the NPP components, such as electrical cables. Simulations are also used in the design phase of new plants to assess the reliability of safety measures and performance of the fire loads. In most of these applications, the fire spreading and heat release rate must be *predicted* rather than *prescribed*. There are several challenges associated with the fire spread simulations, including the difference in scales of close field heat transfer and the largest resolved scales of the geometry, physical and numerical modelling of the mass and heat transfer phenomena within the condensed phase and the definition of the necessary model parameters. During the recent update of the Fire Dynamics Simulator (FDS) to version 5 [1], the treatment of the condensed phase pyrolysis reactions was significantly changed, allowing the definition of a wide range of reactions of varying complexity. Increased complexity has an evident drawback of increased number of model parameters. Quite often, these parameters can not be found directly from literature because the parameters are not material constants by nature. Instead, they are always associated with a specific model of the material, and they should be determined using the exactly same or very similar model.

The reaction parameters for fire models are often estimated by varying the parameters until the model reproduces the measured behaviour in some laboratory experiment. Small scale experiments are typically preferred for the estimation while larger experiments serve as validation tests. It depends on the type of the test, whether it can yield estimates for the thermal parameters or kinetic reaction parameters or both. Mathematically, the parameter estimation process can be presented as an optimization problem. In the recent papers of Lautenberger et al. [2] and Rein et al. [3], Genetic Algorithms (GA) were used for the optimization to estimate the thermal material properties from bench scale experiments [2] and kinetic parameters from thermogravimetric experiments [3]. In this work, we use the ideas of the above mentioned authors to determine the kinetic reaction parameters for the modelling of pyrolysis behaviour of selected solid materials, including polyvinylchloride (PVC), polymethyl methacrylate (PMMA) and a power cable and its components. The reactions are modelled using FDS and the practical aspects associated with the use of genetic algorithms are studied. The developed method has already been successfully applied for the determination of kinetic coefficients for cellulosic materials [4].

Methods

Experiments

In this work, the kinetic parameters of selected solid materials were determined using Thermogravimetric Analysis (TGA) [5]. In addition, Differential Scanning Calorimetry (DSC) was used to determine if the reaction is endo- or exothermic. In both experiments, just 10–50 mg of sample material is needed. A small furnace is heated at constant heating rate (heating rate typically 2–20 K/min) so that the temperature of the sample is in equilibrium with the environment all the time. The purge gas can be air or nitrogen (N_2). These thermoanalytical experiments were carried out at the Laboratory of Inorganic and Analytical Chemistry, Helsinki University of Technology, using Netzsch STA 449C equipment. The sample materials are listed in Table 31.2.1.

TGA measures the sample mass as a function of temperature. In this paper, the results are presented as a fraction of the current mass to the initial mass

$$M = \frac{m}{m_0} \tag{31.2.1}$$

The main difference between TGA experiments conducted in air and in N_2 is that in air, direct oxidation reactions may take place parallel or after the pyrolysis reaction. Oxidation decreases the mass of material, so the residual mass is usually smaller in air than in N_2. This is true for all the sample materials discussed in this work. In DSC, temperature of a sample is kept identical with reference sample and the energy needed for that is measured. In DSC data it is possible to see if the reaction is endothermic or exothermic. Sometimes it is even possible to measure the heat of reaction by integrating over the peak in the DSC curve. Nitrogen should be used as a purge gas if the heat of reaction is going to be measured. However, sometimes many parallel reactions take place simultaneously or the measurement is not accurate enough, and the DSC graph does not give the expected results.

The thermal parameters are estimated from the cone calorimeter (ISO 5660-1) results.

Table 31.2.1. Sample properties. The moisture-% is wet based.

Material	**Description**	**ρ (kg/m^3)**
PVC	Almost pure PVC pipe material.	1440
Black PMMA	ICI, Perspex	1180
Power cable	NOKIA AHXCMK 10 kV 3 x 95/70	
Sheath	PVC	1501
Insulation	PEX	1039
Filler rods	-	950
Conductor + other metals	Aluminium + copper	3042

Kinetic modelling of pyrolysis reactions

The condensed phase materials are modelled as mixtures of material components. In the modelling of condensed phase reactions, the rate of an individual condensed phase reaction β converting material α to something else is expressed as an Arrhenius equation

$$r_{\alpha\beta}(T) = A_{\alpha\beta}\left(\frac{\rho_\alpha}{\rho_{s0}}\right)^{n_{\alpha\beta}} e^{-\frac{E_{\alpha\beta}}{RT}} \qquad (31.2.2)$$

where ρ_α is the mass concentration of component α and ρ_{s0} the original density of the material. The rate of change for the mass concentration of component α is

$$\frac{\partial}{\partial t}\left(\frac{\rho_\alpha}{\rho_{s0}}\right) = -\sum_\beta r_{\alpha\beta} + S_\alpha \tag{31.2.3}$$

where S_α is the production rate of material α. In words, the mass is consumed by all the reactions converting material α to something else and created by the reactions converting something else to α. If none of the reactions leaves solid residue, the sample volume is reduced correspondingly, thus retaining constant density.

Kinetic parameters *A*, *E* and *n* depend both on the material and the assumed reaction scheme. They must be determined using some sort of experimental data. To estimate the kinetic parameters for Eq. (31.2.1), a numerical model of the TGA experiment was created using Fire Dynamic Simulator (FDS) version 5.0.2 [1]. The model is very simple, consisting of only few gas phase control volumes and a single surface element to describe the sample material. A thin layer of sample material is heated by radiation from the surroundings with linearly increased temperature. The layer is thin enough to remain in equilibrium with the surroundings with a tolerance of few Kelvins. Gas phase convection and reactions are neglected and the sample backing is adiabatic.

Correct interpretation of the model output is important when comparing the experimental results and model predictions. TGA results are presented as mass fractions *M*. The model, in turn, provides us with a sample density ρ which is sum of the individual mass concentrations. Direct comparison between *M* and ρ/ρ_0 is possible if the sample volume does not change. For non-charring materials, such as PMMA, the sample volume is reduced and the mass fractions leading to ρ/ρ_0 must be based on the initial sample volume.

Parameter estimation

The parameter estimation was performed by minimizing the error between a measured and simulated TGA and Cone calorimeter result using Genetic Algorithm (GA) as a minimization technique. GA was chosen because it is effective for problems with several unknown variables, and can usually find a global minimum instead of converging to some local minimum. Recently, GA has been used for the parameter estimation of condensed phase reactions by Lautenberger et al. [2] and Rein et al. [3].

Genetic algorithms are based on the idea of evolution and the procedure and the terminology is adapted from references [2], [3] and [6]. The process is iterative, and each iteration round corresponds to one *generation*. The first generation is initialized by generating random numbers for candidate solutions (*individuals*). An individual is a vector with real numbers corresponding to the unknown variables of the model. The individuals of a generation form a *population*. Population can be divided from the beginning into smaller *subpopulations* to keep up the variety of candidate solutions. Each generation goes through several processes. First, the goodness of an individual is tested using a *fitness function* returning a *fitness value*. According to the fitness value, the individuals are ranked, and the best of them are selected to produce *offspring*. The offspring are formed by *crossover*, where the chosen individuals are set to pairs and each pair are changing *alleles* (values of variables) according to the conditions of crossover. After that occur *mutations*, stochastically according to a predetermined mutation rate. In mutation, one value in an individual is replaced by a new random number. Then fitness values are calculated for the offspring and the best parents and offspring are chosen to the next generation. If population is divided into isolated subpopulations, some individuals *migrate* then between subpopulations bringing new genes and so maintaining variety. After each generation, the best individual is plotted, which enables the user to observe the action of algorithm. The process is repeated until the maximum number of iterations is finished or the user is satisfied with the result and stops the algorithm from outside.

The fitness function compares experimental data to model and returns a metrics of how good is the fit. This is often made by using least mean squares. Based on the numerical experiments, another feature was added to the fitness function: The results of the parameter estimation process are not unambiguous and several well-fitting parameters can be found for the same material. On the other hand, high values of pre-exponential factors A were found to make the FDS simulations more prone for numerical fluctuations. An additional term was thus added to the fitness function to prefer the smaller values of A. The formula for the fitness value is

$$fV = \omega_1 \left(1 - \frac{\sum_i \left(M_{\exp} - \overline{M}_{\exp} \right)^2 - \sum_i \left(M_{\exp} - M_{\mathrm{mod}} \right)^2}{\sum_i \left(M_{\exp} - \overline{M}_{\exp} \right)^2} \right) + \omega_2 A_p \qquad (31.2.4)$$

where M is mass fraction in TGA or mass loss rate in cone calorimeter experiment and i goes over all the data. ω_1 and ω_2 are the weights of fitness function so that $\omega_1+\omega_2=1$. A_p is the penalty of high parameter A, and has a form

$$A_p = \frac{A - A_{\min}}{A_{\max}} \tag{31.2.5}$$

where A is the current value of the pre-exponential factor, $A_{\min}$ is its lower bound and $A_{\max}$ the upper bound. Weight $\omega 2$ should be in the same order of magnitude as the differences in the fitness values of the best solutions. In the tests, these differences were around 15/1000. Too high weight would lead to small pre-exponential factors giving inaccurate predictions.

The population size and the division of one big population into smaller subpopulations are important when fast convergence to a possible local minimum must be avoided. Inside one population, the solution converges quite fast towards the best candidate solution. If there are many independent populations, the probability that one of the solutions is near the global minimum, is much higher. In test simulations, division to subpopulations was found to be even more important than the population size. The populations without separation converged very fast, no matter how big the number of individuals was in the population. On the other hand, when there were at least four subpopulations, each of them could have as few as 20 individuals and the diversity was still maintained well enough. Mutation rate is used to control the maintenance of diversity. It expresses the probability of an individual to mutate during one generation. If the mutation rate is too low, the solution may converge to a local minimum, and if it is too high, good solutions may be lost. A good rule of thumb is to choose a mutation rate close to ratio $1/N$, where N is number of variables.

When TGA experiments are available at many different heating rates, the fitness value should be calculated considering all the rates, thus ensuring that the model is good in general, not only with one heating rate. It can happen that some parameters provide very good results at some heating rates but poor predictions of the residue mass at others.

The Genetic Algorithm application was implemented using Genetic Algorithm Toolbox for Matlab, developed by the Department of Automatic Control and Systems Engineering of The University of Sheffield, UK [7]. The toolbox is available for free at http://www.shef.ac.uk/acse/research/ecrg/getgat.html. The parameters used in the estimation are listed in Table 31.2.2. Many different combinations were studied and the listed parameters were found to give the best

results in estimation of kinetic parameters. The variable and function names are consistent with the Genetic Algorithm toolbox.

Despite the simplicity of the FDS models used for TGA and Cone calorimeter simulations, the computational cost of the parameter estimation was quite high because the model had to be solved for every individual of every generation, and with each heating rate separately. Estimations for this work took from about 10 h to one day to run on a single CPU of a modern workstation.

Table 31.2.2. Parameters of Genetic Algorithm application.

Parameter	**Symbol in GA Toolbox**	**Value**
Number of individuals.	NIND	20
Generation gap: The fractional difference between the new and old population sizes.	GGAP	0.8
Crossover rate.	XOVR	0.7
Mutation rate.	MUTR	1/Number of variables
Maximum number of generations.	MAXGEN	1200
Insertion rate: Fraction of offspring reinserted into the population.	INSR	0.9
Number of subpopulations.	SUBPOP	4
Migration rate.	MIGR	0.2
Number of genes per migration.	MIGGEN	20

Results

The kinetic and thermal parameters of several materials were estimated using genetic algorithm. TGA experiments were made in nitrogen (N_2) because the focus was on the modelling of the pyrolysis (degradation) reactions. For each of the kinetic parameters, a range of possible values was defined, as shown in Table 31.2.3. The ranges can be chosen according to the literature values, if available, or initial estimates. In the tests, the ranges were set unnecessarily wide on purpose to be able to study the variety of solutions. Unfortunately, the choice of the range may affect the results, as was demonstrated by running two versions of the black PMMA with different bounds for the reaction order *n*. Experimental

results at four different heating rates (2, 5, 10 and 20 K/min) were used for the estimation. The thermal parameters were estimated using the cone calorimeter data. Heat of reaction and combustion were fixed manually after the estimation process. The iterations normally converged during the first 50 generations, but often the iteration process was continued at least up to 100, sometimes even 1000 generations. The numerical results are presented in Table 31.2.4 and as model behaviour in figures below.

Table 31.2.3. Estimation ranges for sample materials.

Material	**A (s^{-1})**	**E (kJ/mol)**	**n**	**residue**	**k (W/m·K)**	**c_p (kJ/kg·K)**
PVC (all reactions)	[10^8,10^{20}]	[100,300]	[0,4]	[0,1]	[0.05,0.7]	[1,3]
Black PMMA -estimation 1	[10^2,10^{10}]	[100,300]	[0,2]	-	[0.05,0.7]	[1,3]
Black PMMA -estimation 2	[10^2,10^{10}]	[100,300]	[0,7]	-	[0.05,0.7]	[1,3]
Power cable (all)	[10^5,10^{15}]	[100,300]	[0,3]	[0,1]	[0.05,0.7]	[1,3]

PVC

The first sample was almost pure polyvinyl chloride (PVC) pipe material. PVC undergoes two reactions: Release of hydrochloric acid between 200 and 300 °C and the pyrolysis reaction of the remaining solid at about 400 °C. The pyrolysis products are HCl, benzene and toluene [8]. Reactions were modelled by two pseudo-components, of which the first does not yield any tar and the second does.

The mass fraction of volatiles was assumed to be 0.54 (taken directly from the graphs). A comparison of the measured and predicted TGA curves at the end of the parameter estimation is shown in Figure 31.2.1. The solid lines denote the experimental data and the dash lines the model. Good predictions of the PVC pyrolysis are achieved at all heating rates. The numeric values of the kinetic and thermal parameters are given in Table 31.2.4.

PMMA

PMMA (Polymethyl methacrylate) is a non-charring thermoplastic that melts and then burns. The pyrolysis product is 100% monomer [8] with no significant

residue yield. Different from charring materials where the density decreases, in PMMA model the sample thickness decreases instead. This may cause problems when modelling TGA test where the sample is very thin from the beginning. As a result, care must be taken to define a sufficiently high sampling frequency for the numerical results.

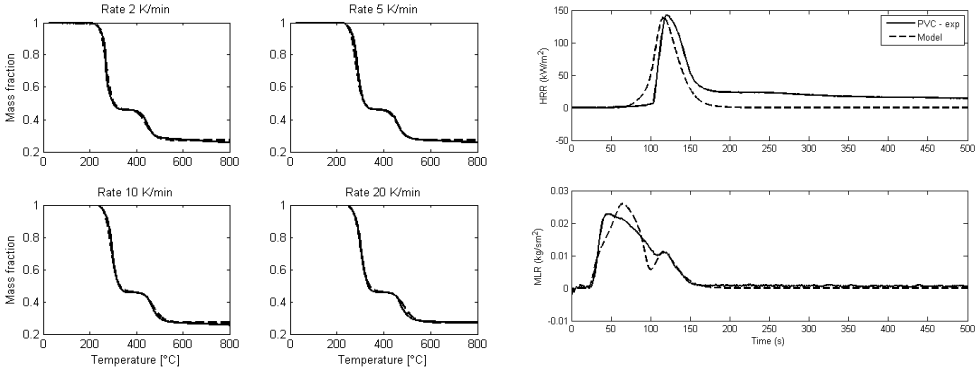

Figure 31.2.1. Left: TGA model of PVC in N_2. Right: Heat release rate and mass loss rate in cone calorimeter at 50 kW/m^2.

The estimation was made twice using different range for the reaction order parameter *n*. In the first run, the range was [0, 2] and in the second, it was [0, 7]. The result of estimation run 1 is shown in Figure 31.2.2. Again, the solid line denotes the experimental data and the dash line the model. An accurate prediction of the mass loss is achieved at heating rates 5 and 10 K/min, and reasonably well at heating rates 2 and 20 K/min. The results of the estimation run 2 look very much the same and the model is considered as accurate as in estimation run 1. That suggests that the parameter sets can be chosen among various alternatives and the genetic algorithm can find solutions from desired range. The numeric values of the kinetic and thermal parameters are given in Table 31.2.4.

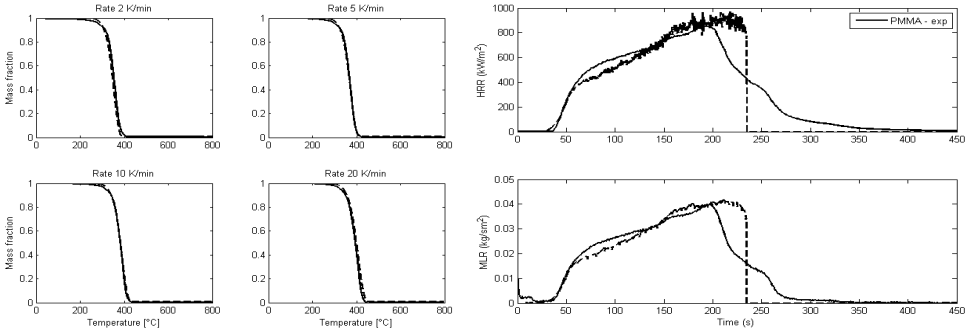

Figure 31.2.2. Left: TGA of black PMMA in N_2. Right: Heat release rate and mass loss rate in cone calorimeter at 50 kW/m^2.

Power cable

More complicated material to model would be a power cable with many layers and components. Here, the sample was NOKIA AHXCMK 10 kV 3 x 95/70 power cable with main parts sheath, filler rods, insulation and conductors. Sheath was PVC, and insulation PEX. The parameters (kinetic and thermal) were estimated for each component separately. After that, results were collected together to simulate the cone calorimeter experiment of the whole cable. These results are seen in Figure 31.2.3 and listed in Table 31.2.4.

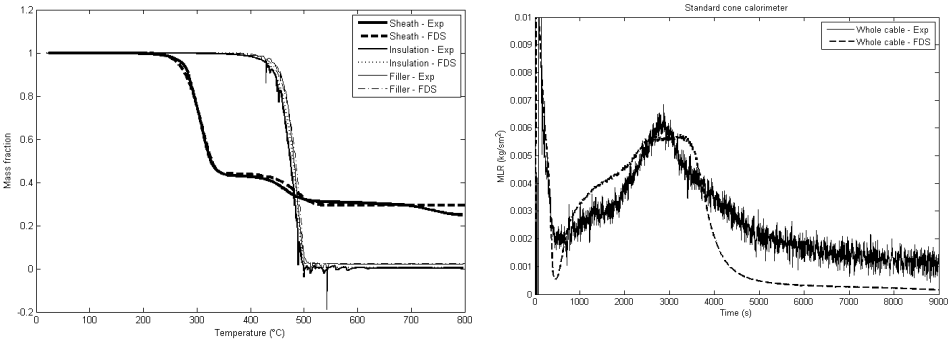

Figure 31.2.3. The results of power cable. Left TGA results for components and right cone calorimeter results for the whole cable, at 50 kW/m^2.

Conclusions

Kinetic and thermal pyrolysis model parameters were estimated for various solid materials using FDS fire model and genetic algorithm for the estimation. The estimation parameters, such as variable bounds and time step size, were carefully chosen to minimize the effect of the estimation procedure. The results were promising and indicated that genetic algorithm can successfully be used for the parameter estimation in fire engineering. All the TGA predictions were very accurate. Cone calorimeter results were slightly less precise, but the ignition time and the shapes of the curves are predicted correctly. As the material models were created using the actual fire simulation tool, the results can be directly used in applications. The estimation process is computationally expensive, taking several hours to a day on a single computer, but needs to be performed only once for each material. Validation of the current parameters and estimation of the lacking ones is still needed to build a full parameter set for fire spread computation.

Some of the resulting kinetic parameter values were quite different from those previously presented in literature. This demonstrates that the kinetic parameters are model dependent and should not be considered as fundamental material properties. The parameters should therefore be used only in models with similar structure. In addition, the estimation results are not unambiguous and there may be many suitable sets of parameters that predict the mass loss accurately.

Table 31.2.4. Kinetic and thermal parameters of materials, estimated using genetic algorithm.

Material	**A (s^{-1})**	**E (kJ/mol)**	**n**	**residue**	**k (W/m·K)**	**c_p (kJ/kg·K)**	**ΔH (kJ/kg)**	**ΔH_c (MJ/kg)**
PVC (chlorides) k_1	$6.12 \cdot 10^{16}$	198	2.18	0	0.15	2.2	700	-
PVC (solid) k_2	$3.63 \cdot 10^{13}$	219	2.08	0.589	0.15	3	500	12.5
Black PMMA – 1	$2.43 \cdot 10^{9}$	146	1.758	0	0.19	1.8	1000	22.4
Black PMMA – 2	$1.35 \cdot 10^{9}$	143	4.01	0	0.19	1.8	1000	22.4
Sheath 56%	$1.78 \cdot 10^{9}$	127	1	0	0.1	2.5	200	-
11%	$8.64 \cdot 10^{12}$	290	1	0.474	0.05	1	300	20
33%	$6.61 \cdot 10^{8}$	159	1	0.618443	0.05	1	1700	50
Insulation	$6.53 \cdot 10^{12}$	218	0.308	0	0.16	2	2200	35
Filler rods	$6.27 \cdot 10^{12}$	220	0.135	0	0.25	3	7000	35

References

1. McGrattan, K., Hostikka, S., Floyd, J., Baum, H. & Rehm, R. Fire Dynamics Simulator (Version 5) Technical Reference Guide. National Instititute of Standards and Technology, MD, USA, 2007. NIST Special Publication 1018-5. 86 p. (Draft: August 26, 2007.)

2. Lautenberger, C., Rein, G. & Fernandez-Pello, C. The application of a genetic algorithm to estimate material properties for fire modeling from bench-scale fire test data. Fire Safety Journal, 2006. Vol. 41, pp. 204–214. doi:10.1016/j.firesaf.2005.12.004.

3. Rein, G., Lautenberger, C., Fernandez-Pello, C., Torero, J. & Urban, D. Application of genetic algorithms and thermogravimetry to determine the kinetics of polyurethane foam in smoldering combustion. Combustion and Flame, 2006. Vol. 146, pp. 95–108. doi:10.1016/j.combustflame.2006.04.013.

4. Matala, A., Hostikka, S. & Mangs, J. Estimation of pyrolysis model parameters for solid materials using thermogravimetric data. Fire Safety Science – Proceedings of the Ninth International Symposium, International Association for Fire Safety Science, 2008. (Preprint.)

5. Kellner, R., Mermet, J.-M., Otto, M., Valcárcel, M. & Widmer, H.M. Analytical Chemistry: A Modern Approach to Analytical Science, Second editition. Wiley-VCH Verlag GmbH & Co. KGaA, Weinheim, 2004.

6. Reeves, C.R. & Rowe, J.E. Genetic algorithms – principles and perspective. Kluwer Academic Publishers, 2002.

7. Chipperfield, A., Fleming, P., Pohlheim, H. & Fonseca, C. Genetic Algorithm Toolbox for Use with Matlab. Version 1.2. User's Guide. University of Sheffield, Department of Automatic Control and Systems Engineering.

8. Harper, C. (Ed.). Handbook of building materials for fire protection. McGraw-Hill Handbooks. The McGraw-Hill Companies Inc., 2004.

32. Extreme weather and nuclear power plants (EXWE)

32.1 EXWE summary report

Ari Venäläinen, Jenni Rauhala, Natalia Pimenoff and Seppo Saku
Finnish Meteorological Institute

Milla Johansson, Kimmo Kahma, Antti Kangas, Hilkka Pellikka and Hanna Boman
Finnish Institute of Marine Research

Abstract

The main objective of the research conducted in the EXWE project is to produce a comprehensive study about the frequency, intensity, spatial and temporal variation and the impacts of the extreme weather events that are relevant from the point of safety of nuclear power plants. In this study both instrumental meteorological records, as well as, climate model simulations have been utilized. The study aims also to clarify the influence of climate change on extreme weather. Beside meteorological parameters, the sea level in the Baltic Sea has been included into the study. The return periods of extreme air temperature, precipitation, and length of dry, hot and cold spells have been analysed. As well, occurrences of freezing rain and heavy snowfall events in combination with high wind speed have been examined. The risk of hit of a tornado or a downburst on power plant is also a relevant subject that has been studied. Human induced global warming might trigger abrupt climate changes, which could lead to fatal consequences in continental or even global scale. The risk of abrupt climate changes grows the higher the more the global mean temperature rises above

present. Due the large impact these abrupt changes have also their probability have been examined as a part of EXWE.

Introduction

On the global scale during 1980–2003 the economical losses caused by natural catastrophes have been estimated to be about 1260 milliard US dollars and 77.5% of the losses are estimated to be caused by weather (e.g. http://www.wmo.int/pages/prog/drr/). Due to the influence of an intensified greenhouse effect the climate is expected to continue changing during the coming decades and this change may have an influence also on the occurrence of extreme weather events (e.g. [1, 2, 3]). During the past few years, major natural catastrophes have also drawn increased attention to the possible effects of extreme external events on nuclear power plants.

In the planning of nuclear power plants the risks caused by the harsh weather conditions are taken into account. However, some exceptional weather phenomena may prevent normal power operation and simultaneously endanger safe shutdown of the plant. Extreme weather events could affect, for example, the external power grid connection, emergency diesel generators (blockage of air intakes), ventilation and cooling of electric and electronics equipment rooms and the seawater intake. The nuclear power plant units now in use or under construction are planned to be operational several decades, up to the 2070's, and according to present knowledge climate will change considerably within the coming decades and it may have influence on the occurrence of relevant extreme weather events as well as on the most effective ways to operate the plants.

Main objectives

The main objective of the research conducted in the EXWE is to produce a comprehensive study about the frequency, intensity, spatial and temporal variation and the impacts of the extreme weather events that are relevant from the point of safety of nuclear power plants. In the framework of SAFIR2010 EXWE project the return periods of extreme air temperature, precipitation, and length of dry, hot and cold spells have been examined. As well, occurrences of freezing rain and heavy snowfall events in combination with high wind speed have been examined. The study in 2008 focused on the risk of the hit of a tromb or a down burst in the nuclear power plant area. As well, the sea water level in the Baltic Sea has been examined. This subject became topical issue in January 2005 when

sea water level in the Baltic Sea reached new records. One of the impacts of climate change is the rise of the sea water level globally and eventually it will also increase the probability of extremes. The aim of this study has been to update earlier done studies on the occurrence of exceptionally high sea water levels in the Baltic Sea. Human induced global warming might also trigger abrupt climate changes, which could lead to fatal consequences in continental or even global scale. The probability of the abrupt climate changes have examined as a part of EXWE.

Main results

Extreme temperatures

As a part of EXWE project the return levels of extreme temperatures were calculated. The return levels of the extreme daily maximum and minimum temperature were calculated for 12 stations located in different parts of the country. The calculation of heat waves was based on the number of consecutive days when the daily maximum temperature was above 25 °C. The calculation of cold spells was done using two thresholds -20 °C and -30 °C. According to the results the 1000-year return level of daily minimum temperature is in southern Finland about -35 °C and in Lapland colder than -50 °C. The 1000 year return level of daily maximum temperatures is around 33…35 °C. In Helsinki once in 10 years for one week temperature does not dropt below 17 °C even during the nights. When the cold spells were analysed it was found that in Helsinki once in 10 years temperature stays below -12…-13 °C for at least one week. The details of results are given in [4] and [5].

The return levels of extremely hot and humid conditions have also been examined. As well, the return levels of extreme values of enthalpy have been analysed. The results of this study will be published early 2009. An example of the analyses is given in Figure 32.1.1.

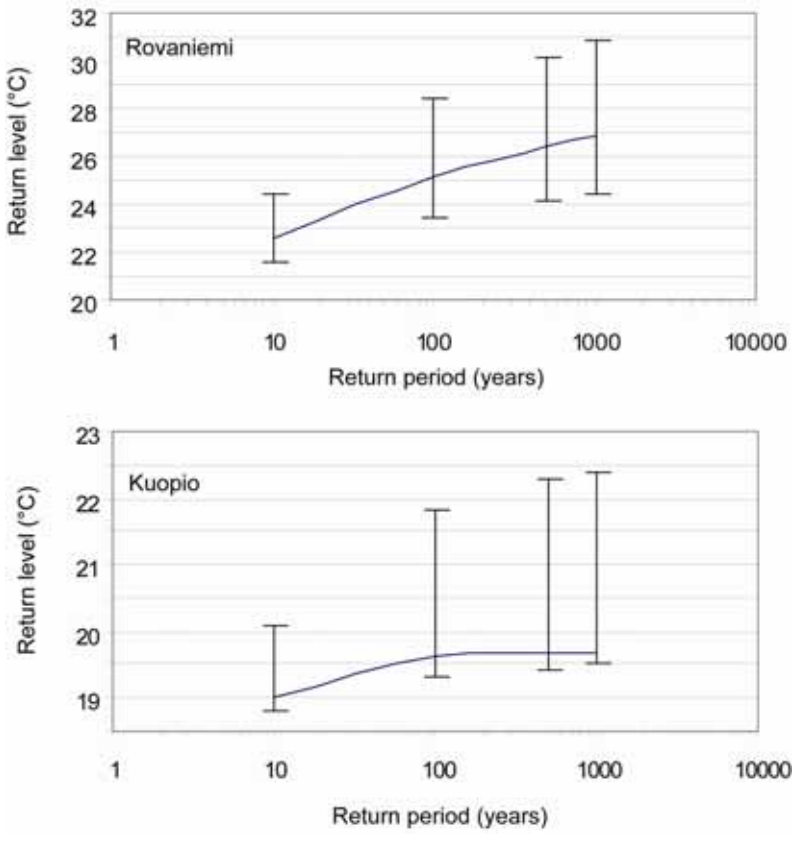

Figure 32.1.1. The return levels of daily maximum temperature at Rovaniemi and Kuopio in case relative humidity is more than 80%. The continuous line indicates the best estimate and vertical bars the 95% confidence limits.

Tornadoes and downbursts

In case of tornado and downbursts there can occur very high wind speed. In Finland there are known tornado observations since 1796. However, as the oldest observations are not directly comparable with the recent years the hit probability analyses are based on observations made 1930–2007. Only tornadoes that can be regarded strong enough to have remarkable influence on constructions (significant tornado, F2 or stronger) were used. According to the analyses made into an 80km*80km grid, the yearly probability that there occurs at least one significant tornado in the grid shell is around 5% in some parts of the country. When the seasonal variation of all tornadoes was analyzed, it was found

that the highest risk over land is in July and over water covered surfaces (including both lakes and sea), in August.

In connection with intensive thunderstorms there occur frequently downbursts that can have in some cases wind speed comparable with tornadoes. The analysis of the probability of these strongest downbursts is very difficult because there is very little information available about the frequency and impact area of these phenomena. In EXWE an area of 100 km*100 km in south-eastern Finland was used as test area. Based on the information available from the regional rescue services in 2002–2007 the cases when there were trees fallen due to strong winds were analyzed. Those cases when there had been lighting were regarded as obvious downburst cases. According to the analysis there were 210 downburst inside the test area during the six year period. The highest risk is in July. As we do not know the impact area of a down burst we can only make assumptions about the probability of a hit of downburst. According to the estimate this probability is 0.00003–0.002. However, as most of the down bursts are not strong enough to cause major damage on constructions the estimation of these strong down bursts.

Abrupt non-linear climate changes

Some of the possible abrupt climate changes could affect the safety of the nuclear power plants. The major concern is the possible abrupt sea level rise which could be triggered by changes in the Atlantic thermohaline Circulation or by melting of continental ice sheets. Also the melting of the Arctic sea-ice would quite likely accelerate the melting of the Greenland ice sheet. In the following there is a short summary of the possible abrupt climate changes and their impacts. [6.]

The complete melting of the Greenland ice sheet is considered possible if the global mean temperature rises 1–2 degrees Celsius above present. According to model simulations, the melting would take millennia. However, since the models have not been able to simulate the resent fast melting, an even faster total melting has to be taken into consideration and the lower limit is presented to be 300 years. The total melting of the Greenland ice sheet could raise the sea level by several meters. The complete melting of the West-Antarctic ice sheet is considered possible if the global mean temperature rises 3–5 degrees Celsius above present. Also the total melting of this ice sheet would according to today's knowledge take at least several hundred years. The total melting of the West-Antarctic ice sheet could raise the sea level by up to five meters.

The weakening of the Atlantic thermohaline circulation during the current century is according to model simulations very likely. None of the models, however, show a total shutoff of the circulation in the next 100 years, although according to some simulations it might happen later in time. Experts estimate that the shutdown of the Atlantic thermohaline circulation might be possible if the global mean temperature rose by 3–5 degrees Celsius above present. After passing the threshold the shutdown would occur gradually in approximately 100 years. In the north Atlantic area the weakening of the Atlantic thermohaline circulation seems to slow down the warming of the climate but will not stop it.

Baltic sea level

As a part of EXWE project the Finnish Institute of Marine Research examined the Baltic Sea levels at the coast of Loviisa and Olkiluoto. Scenarios of mean sea level rise until the year 2100 were made using an extensive literature review. According to the results the mean sea level will rise at Loviisa region 20 cm until year 2100, the uncertainty limits are from 20 cm descent to 150 cm rise. At Olkiluoto sea level will descent according to most obvious scenario 10 cm. The uncertainty limits are from 50 cm descent to 120 cm rise.

The extreme sea levels at the Baltic Sea are a result of several factors that occur simultaneously. According to the study the probability of that sea level would reach higher values than +200 cm (in the N60 height system) at Loviisa is approximately 0.001 occurrences/year.

Applications

One most important question related to climate change is the influence of climate change on climate extremes and the results of the proposed study would benefit several sectors in society like the energy sector, safety and rescue services, traffic and health care. From the point of nuclear safety the results of the study extend the knowledge about external risk caused by the weather and help the licensees and authorities to make the current PSA analyses more reliable and to identify needs for modifications of the plant and/or operating procedures. Regarding new nuclear power plant units the results can be used for determining the design basis for extreme weather events. In addition to the direct impact on nuclear power plants, the simultaneous effects of extreme weather conditions on the infrastructure should be considered in emergency response planning.

Conclusions

We are currently undergoing the most dramatic climate change in thousands of years. This change may change the limits of climate extremes and also trigger new potentially dangerous weather phenomena. Though climate models are an excellent tool to examine future climate there are still many research themes that need a large amount of future work. Storm tracks and small scale convective weather systems that potentially can cause large damage are some of the main challenges for further research. Like earlier mentioned climate change may also trigger unlinear and abrupt changes. Though the probability of these changes is very small their impacts are so large that they can no be neglected totally.

References

1. Christensen, J.H., Hewitson, B., Busuioc, A., Chen, A., Gao, X., Held, I., Jones, R., Kolli, R.K., Kwon, W.-T., Laprise, R., Magaña Rueda, V., Mearns, L., Menéndez, C.G, Räisänen, J., Rinke, A., Sarr, A. & Whetton, P. Regional Climate Projections. In: Climate Change 2007: The Physical Science Basis. Contribution of Working Group I to the Fourth Assessment Report of the Intergovernmental Panel on Climate Change. Solomon, S., Qin, D., Manning, M., Chen, Z., Marquis, M., Averyt, K.B., Tignor, M. & Miller, H.L. (Eds.). Cambridge University Press, Cambridge, United Kingdom and New York, NY, USA, 2007.

2. Trenberth, K.E. Conceptual Framework for Changes of Extremes of the Hydrological Cycle with Climate Change. Climatic Change, 1999. Vol. 42, No. 1, pp. 327–339(13).

3. Beniston, M. & Stephenson, D.B. Extreme climatic events and their evolution under changing climatic conditions. Global and Planetary Change, 2004. Vol. 44, pp. 1–9.

4. Venäläinen, A., Saku, S., Kilpeläinen, T., Jylhä, K., Tuomenvirta, H., Vajda, A. Ruosteenoja, K. & Räisänen, J. Sään ääri-ilmiöistä Suomessa (Aspects about climate extremes in Finland, in Finnish, English Abstract). Finnish Meteorological Institute, Reports 2007:4.

5. Gregow, H., Venäläinen, A., Laine, M., Niinimäki, N., Seitola, T., Tuomenvirta, H., Jylhä, K., Tuomi, T. & Mäkelä, A. Vaaraa aiheuttavista sääilmiöistä Suomen muuttuvassa ilmastossa (Danger-causing weather phenomena in changing Finnish climate, in Finnish, English Abstract). Finnish Meteorological Institute, Reports 2008:3.

6. Pimenoff, N., Venäläinen, A., Pilli-Sihvola, K. Tuomenvirta, H., Järvinen, H., Ruosteenoja, K., Haapala, J. & Räisänen, J. Epälineaariset ja äärimmäiset ilmaston muutokset. Selvitys Vanhasen II hallituksen tulevaisuusselontekoa varten. Valtioneuvoston kanslian julkaisusarja 14/2008.

32.2 Abrupt climate change and nuclear power plant safety

Natalia Pimenoff, Seppo Saku and Ari Venäläinen
Finnish Meteorological Institute

Abstract

Human induced global warming might trigger abrupt climate changes, which could lead to fatal consequences in continental or even global scale. The risk of abrupt climate changes grows the higher the more the global mean temperature rises above present.

One of the possible abrupt climate changes followed from the global warming is the total loss of summer Arctic sea-ice. According to present knowledge, the Arctic sea could become ice free during summer already within the next decades. Experts also estimate that a global warming of 1–2 degrees (3–5 degrees) Celsius above present might trigger the total melting of the Greenland (West-Antarctic) ice sheet. When started, the total melting would take at least 300 years and it could raise the sea level by several meters. The Atlantic thermohaline circulation is predicted to weaken during the current century, however a shutoff is considered unlikely. In the north Atlantic area the weakening will slow down the warming of the climate but won't stop it.

Introduction

Human induced global warming is followed by feedback effects in the climate system. These feedbacks might restrain (so called negative feedback) or force (so called positive feedback) the initial warming. Strong climate feedbacks might lead to abrupt climate changes [1].

An abrupt climate change occurs when the climate system is forced to cross some threshold, tipping point, triggering a transition to a new state at a rate determined by the climate system itself and faster than the cause [2], see Figure 32.2.1. Examples of possible non-linear abrupt climate changes are the melting of the summer Arctic sea-ice and the shutdown of the Atlantic thermohaline circulation.

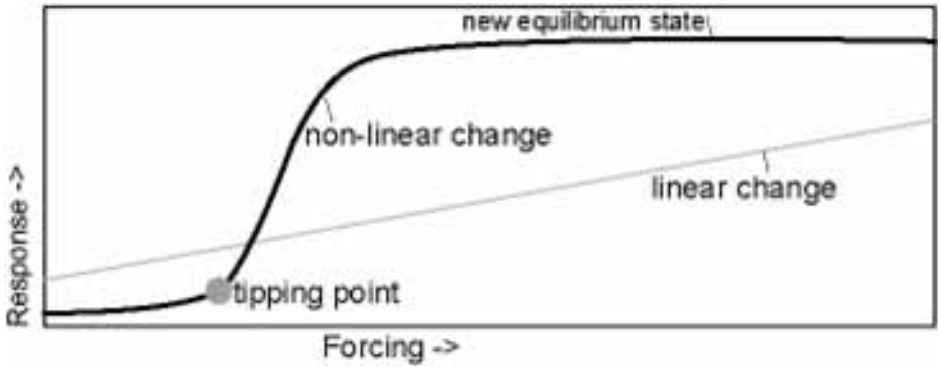

Figure 32.2.1. Schematic figure of a linear and a non-linear climate change.

The human induced climate change is projected with climate models. In these models the effects of external forcing – e.g. enhanced greenhouse gas concentrations – to the climate system are simulated. There are large uncertainties in the climate change projections, uncertainties like natural variation of climate, the uncertainties in the future emissions and model's simplicities. When projecting the feedback effects of the ecosystems, the uncertainty is caused also by the uncertainty of human action and nature's ability to adapt to the changing environment. The estimation of the non-linear and abrupt climate changes is extremely difficult and uncertain. However, the possible abrupt climate changes introduced in this report are connected with significant social and ecological impacts on the world.

A workshop entitled "Tipping points of the Earth System" [3] attempted to expand the definition of non-linear climate change by including social and political aspects. They defined "policy-relevant tipping elements" to be phenomena:

- which are in horizontal scale at least 1 000 km,
- which have a critical threshold from which any significant change leads to a qualitative change in mankind's welfare or destroys unique ecosystems,
- which are affected by human activities in that manner that decisions taken within current century determine whether the critical value is reached,
- in which changes could be observed in so near future (not later than within a couple of centuries) that they influence today's decisions.

According to these definitions tipping elements are illustrated in the Figure 32.2.2. The critical tipping points and transition times defined by leading experts [3] are also illustrated in the Figure 32.2.2. In the following chapters we introduce only those possible abrupt climate changes which might influence the safety of the nuclear power plants. These are the loss of summer Arctic sea-ice, the melting of continental ice sheets and the projected changes in the North Atlantic thermohaline circulation.

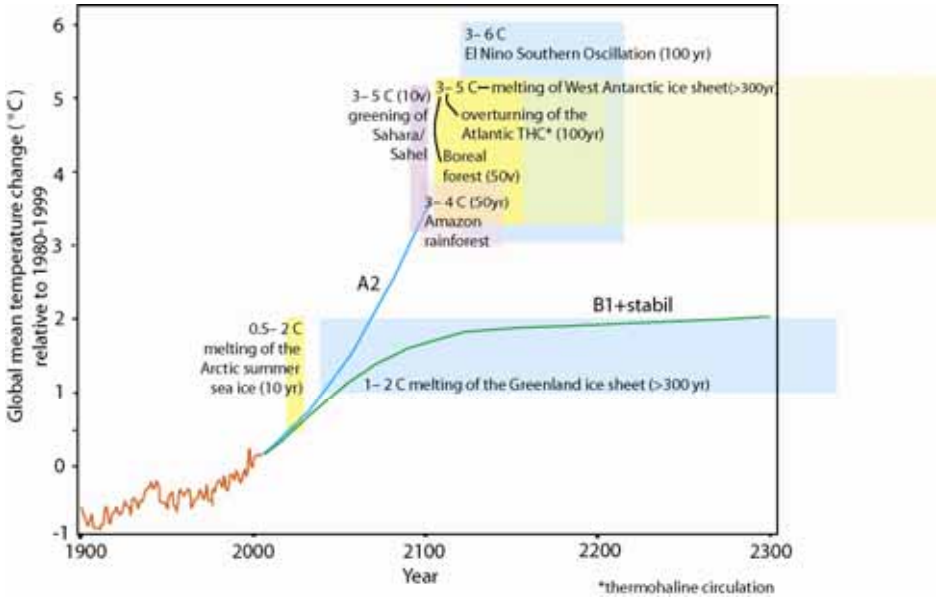

Figure 32.2.2. Tipping elements and their threshold values defined by the experts of [3] compared to the warming projections of the A2- and B1- scenarios [4]. The size and the location of the boxes describe the timings and the transition times of these phenomena. The height of a box describes the range of the threshold value; the left lower edge is approximately on that spot of the warming projection where the lowest value of the threshold range is reached. The width of the box describes the transition time of each phenomenon. The box of the melting of the summer Arctic sea ice is narrow (in horizontal) because the transition is estimated to occur in about one decade. The box of the melting of the Greenland ice-sheet extends outside the picture because the melting is estimated to take at least 300 years and that crosses the x-axis of the figure.

Arctic Sea-Ice

Arctic sea-ice is responding sensitively to the global warming. Measurements show that the area of the Arctic sea-ice has decreased by an accelerating rate during the last 30 years especially in summer time. A number of positive feedbacks in the climate system accelerate the melt back of sea-ice. The ice-albedo feedback allows open water to receive more heat from the sun during summer, and the increase in ocean heat transport to the Arctic through the advection of warmer waters and stronger circulation further reduces the ice cover.

Minimum Arctic sea-ice cover is observed in September. In September 2007 the amount of sea-ice was record low since 1978. In September 2008 the amount was second smallest since 1978. These record low sea-ice cover amounts are due to natural variation in the general circulation of the atmosphere, human induced climate change, and the ice-albedo feedback. The recent fast melting of the Arctic sea-ice suggests that this system might already have passed a tipping point [5], although others disagree [6].

About one half of the ocean-atmosphere general circulation models used in the IPCC [7] projections, become ice-free in September during this century, at a polar temperature of -9 °C that is 9 °C above present. In many of the models the transition to ice-free conditions happens non-linear, but a common critical threshold value has yet to be identified. In an extreme forcing situation – when the polar temperature rises above -5 °C (13 °C above present) – two of the IPCC models exhibit a complete loss of the Arctic sea-ice (the Arctic sea would be ice-free also during winter) [8]. One of these models shows a nonlinear transition to a new state in less than 10 years, whereas the other model shows a more linear transition. It is assumed by [3] that the tipping point of the summer Arctic sea-ice loss could occur well within this century, if not already passed. The further threshold for year-round ice free conditions is less accessible this century.

Changes in Continental Ice Sheets

Changes in continental ice sheets affect directly the sea level. During the last interglacial, about 120,000 years ago, the Greenland ice sheet was at least partly melted and the sea level was 4 to 6 m higher than at present. From this higher sea level, the proportion of Greenland ice sheet is estimated to be about 2 meters [9].

The observed global sea level change for 1993 to 2003 was 3.1 ± 0.7 mm/year [7], if continued with a constant rate: 31 cm/century. The sea level rise results from the thermal expansion of the warming oceans, melting of glaciers and

continental ice sheets and the rise/descent of the sea bed. It is estimated that for 1993 to 2003 the effect of thermal expansion was 1.6 ± 0.5 mm/year, the proportion of melting of the glaciers an ice caps was 0.77 ± 0.22 mm/year and the proportion of melting of the continental ice sheets was 0.42 ± 0.42 mm/year.

Descent of the sea bed occurs when melting waters from the continental ice sheets return in the ocean. The additional weight of the returning water isostatically depresses the oceanic crust. This leads to a corresponding rise in the continental crust so that the isostatic balance remains between oceans and continents. The calculations of [10] show that if an amount melting water corresponding to one meter thick layer on the oceans, was transferred to the ocean, the oceans would deepen on average by 0.25 meters and at the same time the continents would rise on average by 0.6 meters. Thus, the average sea level would rise by only 0.15 meters. However, these isostatic adjustments take millennia and therefore only an equally slow change in sea level will be damped by isostatic adjustment. If the melting of continental ice sheets is going to be rapid, the earth's crust won't be able follow the change with the same speed, and the sea level could rise on the cost areas a lot more than calculated above.

Greenland Ice Sheet

It is estimated that the total melt of the Greenland ice sheet could cause sea level to rise by seven meters. Satellite and *in situ* measurements show that the melting of Greenland ice sheet and the glacial streams have accelerated during the last 25 years. During summers 2004 to 2007 the Greenland ice sheet has lost on average 380 to 490 milliard tonnes of ice each year, which is on average 150–200 milliard tonnes more than snow is accumulated during winter time [11]. This causes a rise of sea level 0.5 mm/year.

The few simulations of long-term ice sheet simulations suggest that the size of the ice sheet is significantly reducing in next centuries in the warming world. However, the ice sheet models have not been able to predict the recent observed rapid melting. The experts are quite unanimous about the fact that if the global warming continues the Greenland ice sheet is unavoidable going to melt. However, the question is still: how fast? The melting of the Arctic sea-ice is quite likely going to accelerate also the melting of the Greenland ice sheet. The IPCC [7] gave an estimate that a global temperature rise of 1.4 to 4.2 °C above present would trigger an unstoppable melting of Greenland ice sheet, whereupon the melting would take several centuries. Some of the model simulations also

suggest that even if temperatures were to decrease later the melting of the Greenland ice sheet might be irreversible because the climate of an ice-free Greenland could be too warm for snow accumulation. The positive feedbacks involved here are that once the ice sheet gets thinner, temperatures in the accumulation region are higher, increasing the melting and causing more precipitation to fall as rain rather than snow; that the lower albedo of the exposed ice-free land causes a local climatic warming; and that surface melt water might accelerate ice flow.

It is estimated by [3] that the total melting of the Greenland ice sheet is possible if the global mean temperature rises 1 to 2 °C above present. They give a lower threshold value than the value of the IPCC [7] because they estimate that the amplification of warming over Greenland may be greater than assumed because of more rapid sea-ice decline than modelled. It is estimated by [3] that the lower limit for the melting of the Greenland ice sheet is 300 years due to the fact that both Greenland ice sheet and the Arctic sea-ice are observed to melt faster than in the model simulations [11].

West Antarctic Ice Sheet

The ice streams from the West Antarctic ice sheet to the Amundsen Sea are observed to have accelerated. The possible collapse of the West Antarctic ice sheet due to global warming has been researched for many years. The West Antarctic ice sheet has retreated at least once in during the last two million years [12], but the exact extent and timing of the retreat is not known. A complete collapse could cause a sea level rise of about 5 m [13].

Most of the present West Antarctic ice sheet is grounded below sea level. This part has a potential to collapse if grounding-line retreat triggers a strong positive feedback whereby ocean water undercuts the ice sheet and triggers further separation from the bedrock. The retreat of the West Antarctic ice sheet might also be preceded by the acceleration of ice streams and the ice shelf collapse. The disintegration of ice shelves could be triggered by the intrusion of warming ocean water beneath them or by surface melting. The major ice shelves, Ross and Fisher-Ronne, will exceed the melting point in summer, if the local surface atmospheric temperatures will rise by at least 5 °C. The threshold for ocean warming is estimated to be lower [14]. The West Antarctic ice sheet itself would reach the melting point in summer if the local surface atmosphere at 75–80°S will warm by at least 8 °C.

The IPCC [7] declines to give a threshold for the melting of the West Antarctic ice sheet because the present ice sheet models have not been able to simulate the recent observed rapid and large scale changes in the continental ice sheets. In spite of this, it is estimated by [3] that a threshold of global warming of 3 to 5 °C could trigger the irreversible melting of West Antarctic ice sheet. They argue this by the recent observations of the mass loss of the West Antarctic ice sheet [15]. The experts of [3] consider the timescale of the melting highly uncertain, but suggest that qualitative changes could occur already during the current millennium and a total collapse within 300 years being a worst-case scenario. They also estimate that rapid sea level rise (bigger than 1 meter per century) is more likely to com from the melting of the West Antarctic ice sheet than the Greenland ice sheet.

Atlantic Thermohaline Circulation

The large-scale Atlantic Ocean circulation, the Atlantic thermohaline circulation (THC), is driven by global density gradients created by surface heat and freshwater fluxes. Wind-driven surface currents (such as the Gulf Stream) head polewards from the equatorial Atlantic Ocean, bringing warm and salty water to high latitudes where the water cools and eventually sinks forming North Atlantic Deep Water. In the deep layers of the ocean, this dense water flows southwards, where the water eventually upwells. Theoretically it has been proven that temperature and salinity changes affect non-linear to the thermohaline circulation. This means that even a small change in the energy or water balance could cause a large change in the Atlantic Ocean circulation.

Observations of the strength of the THC and its changes are sparse. However, the ocean currents can be estimated indirectly with temperature and salinity observations. Unfortunately there are not enough of these measurements to make an extensive analysis. According to studies by [16] the deep water southward flow of the deep water on the 25°N has slowed between years 1957 and 2004. However in later studies [17] it has been shown that this reduction was due to natural variation during that time period.

At the end of the last ice age (at the time when the climate already had begun to warm but continental ice sheets were still covering Fennoscandia and North America) abrupt cooling of climate has been observed in paleoclimatological reconstructions. The cooling might have been caused by a sudden influx of fresh

water or icebergs from deglaciation in North America, which caused a significant reduction or shutdown of the North Atlantic thermohaline circulation.

During the last ten years it has been especially examined how the fresh water influx affects the Atlantic thermohaline circulation. In numerical simulations large amounts of fresh water are added to the surface layer of the ocean. These fresh water influxes have led to a weakening of the THC. Under sufficient freshwater forcing, some models exhibit a collapse of the THC leading to a cooling of North Europe by several degrees Celsius.

In the light of the latest simulations it is very likely that the THC will weaken during the current century. In simulations based on the A1B scenario [4] the THC would weaken on average by 25% (between 0 and 50% in different simulations) [7]. In spite of this reduction of THC the temperatures are projected to rise even in the North Atlantic area, because the direct greenhouse case induced global warming is so strong. The IPCC argues that it is very unlikely (probability less than 10%) that an abrupt transition of the THC would occur before 2100. The experts of [3] give an estimate that a global warming of 3–5 degrees Celsius could trigger the shutoff of the THC.

In model simulations where the THC has been brought to halt [18] the northern hemisphere cools and the southern warms. This change shifts the thermal equator to the south, and thus the intertropical convergence zone and the associated tropical rainfall belts.

The halt of the THC in model simulations also lead to sea level changes. The ocean surface currents and sea surface slopes are in geostrofic balance. Therefore changes in surface currents lead to rapid dynamic adjustment of the sea surface topography. Due to deep water formation in the northern Atlantic, the sea level is almost a meter lower in the northern Atlantic than in comparable parts of the North Pacific. In case of a shutdown of the North Atlantic deep water formation – and a change in surface currents due to this – the sea level would quickly rise up to a meter around the northern Atlantic. On the southern hemisphere and especially on the Southern Ocean the sea level would in proportion fall, and the global average sea level change would be zero [19].

Other possible consequences of the shutdown of the THC are according to [20] e.g. increased icing of northern ports and seas. However, the total halt of the THC in the near future is very unlikely. The experts of [3] give an estimate that a global warming of 3–5 degrees Celsius could trigger the shutoff of THC.

Conclusions

Some of the possible abrupt climate changes could affect the safety of the nuclear power plants. The major concern is the possible abrupt sea level rise which could be triggered by changes in the Atlantic thermohaline Circulation or by melting of continental ice sheets. Also the melting of the Arctic sea-ice would quite likely accelerate the melting of the Greenland ice sheet. In the following there is a short summary of the possible abrupt climate changes and their impacts.

Arctic sea-ice is responding sensitively to the global warming. All simulations based on the SRES-scenarios [4] project a decrease in the area of sea-ice in both hemispheres [7]. At the end of the current century the summer Arctic sea-ice melts in the all model simulations almost entirely. The recent, unpredicted fast loss of Arctic sea-ice has lead to estimates that the Arctic sea could be ice free during summer already in a couple of decades.

The complete melting of the Greenland ice sheet is considered possible if the global mean temperature rises 1–2 degrees Celsius above present. According to model simulations, the melting would take millennia. However, since the models have not been able to simulate the resent fast melting, an even faster total melting has to be taken into consideration and the lower limit is presented to be 300 years. The total melting of the Greenland ice sheet could raise the sea level by several meters.

The complete melting of the West-Antarctic ice sheet is considered possible if the global mean temperature rises 3–5 degrees Celsius above present. Also the total melting of this ice sheet would according to today's knowledge take at least several hundred years. The total melting of the West-Antarctic ice sheet could raise the sea level by several meters.

The weakening of the Atlantic thermohaline circulation during the current century is according to model simulations very likely. None of the models, however, show a total shutoff of the circulation in the next 100 years, although according to some simulations it might happen later in time. Experts estimate that the shutdown of the Atlantic thermohaline circulation might be possible if the global mean temperature rose by 3–5 degrees Celsius above present. After passing the threshold the shutdown would occur gradually in approximately 100 years. In the north Atlantic area the weakening of the Atlantic thermohaline circulation seems to slow down the warming of the climate but will not stop it.

References

1. Pimenoff, N., Venäläinen, A., Pilli-Sihvola, K., Tuomenvirta, H., Järvinen, H., Ruosteenoja, K., Haapala, J. & Räisänen, J. Epälineaariset ja äärimmäiset ilmaston muutokset. Selvitys Vanhasen II hallituksen tulevaisuusselontekoa varten. Valtioneuvoston kanslian julkaisusarja 14/2008.

2. Alley, R.B. et al. Abrupt Climate Change: Inevitable Surprises. US National Research Council Report, National Academy Press, Washington, DC, 2002. 230 p.

3. Lenton, T.M., Held, H., Kriegler, E., Hall, J.W., Lucht, W., Rahmstorf, S. & Schellnhuber, H.J. Tipping Elements in the Earth System. Proceedings of the National Academy of Sciences USA, 2008, 105, 6. Pp. 1786–1793.

4. Nakicenovic, N. et al. Special Report on Emissions Scenarios. A Special Report of Working Group III of the Intergovernmental Panel on Climate Change. Cambridge University Press, Cambridge, UK, 2000.

5. Lindsay, R.W. & Zhang, J. The thinning of arctic sea ice, 1988–2003: have we passed a tipping point? J. Climate, 2005, 18, pp. 4879–4894.

6. Holland, M.M. Future abrupt reductions in the summer Arctic sea ice. Geophys. Res. Lett., 2006, 33, L23503.

7. IPCC. Climate Change 2007: The Physical Science basis. Contribution of Working group I to the Fourth Assessment Report of the Intergovernmental panel on Climate Change. Solomon, S., Gin, D., Manning, M., Chen, Z., Marquis, M., Averyt, K.B., Tignor, M. & Miller, H.L. (Eds.). Cambridge University Press, Cambridge, UK, 2007.

8. Winton, M. Does the Arctic sea ice have a tipping point? Geophys. Res. Lett., 2006, 33, L23504.

9. Cuffey, K., Marshall, M. & Shawn, J. Substantial contribution to sea-level rise during the last interglacial from the Greenland ice sheet. Nature, 2000, 404, pp. 591–594. doi:10.1038/35007053.

10. Kivioja, L.A. Effects of mass transfers between land-supported ice caps and oceans on the shape of the earth and on the observed mean sea level. Bull. Geod., 1967, 85, pp. 281–288.

11. Witze, A. Climate change: Loosing Greenland. Nature, 2008. doi:10.1038/452798a, http://www.nature.com/news/2008/080416/full/452798a.html.

12. Scherer, R.P., Aldahan, A., Tulaczyk, S., Possnert, G., Engelhardt, H. & Kamb, B. Pleistocene Collapse of the West Antarctic Ice Sheet. Science, 1998, 281, pp. 82–85.

13. Vaughan, D.G. West Antarctic Ice Sheet collapse – the fall and rise of a paradigm. Climatic Change, 2007. http://nora.nerc.ac.uk/769/. (In Press.)

14. Oppenheimer, M. & Alley, R.B. The West Antarctic Ice Sheet and long term climate policy. Climatic Change, 2004, 64, pp. 1–10.

15. Velicogna, I. & Wahr, J. Measurements of Time-Variable Gravity Show Mass Loss in Antarctica. Science, 2006, 311, pp. 1754–1756.

16. Bryden, H.L., Longworth, H.R. & Cunningham, S.A. Slowing of the atlantic meridional overturning circulation at 25°N. Nature, 2005, 438, 1, pp. 655–657.

17. Cunningham, S.A. et al. Temporal variability of the Atlantic Meridional Overturning Circulation at 26.5°N. Science, 2007, 317, pp. 935–937.

18. Rahmstorf, S. Thermohaline Ocean Circulation. Encyclopedia of Quarternary Sciences. Elsevier, Amsterdam, 2006.

19. Levermann, A. et al. Dynamic sea level changes following changes in the thermohaline circulation. Clim. Dyn., 2005, 24, pp. 347–354.

20. Alcamo, J. et al. Europe. Climate Change 2007: Impacts, Adaptation and Vulnerability. In: Contribution of Working Group II to the Fourth Assessment Report of the Intergovernmental Panel on Climate Change. Parry, M.L., Canziani, O.F., Palutikof, J.P., van der Linden, P.J. & Hanson, C.E. (Eds.). Cambridge University Press, Cambridge, UK, 2007. Pp. 541–580.

Series title, number and
report code of publication

VTT Research Notes 2466
VTT-TIED-2466

Author(s)
Eija Karita Puska (Ed.)

Title

SAFIR2010
The Finnish Research Programme on Nuclear Power Plant Safety 2007–2010. Interim Report

Abstract

Major part of Finnish public research on nuclear power plant safety during the years 2007–2008 has been carried out in the SAFIR2010 programme. The steering group of SAFIR2010 consists of representatives from Radiation and Nuclear Safety Authority (STUK), Ministry of Employment and the Economy (MEE), VTT Technical Research Centre of Finland (VTT), Teollisuuden Voima Oyj (TVO), Fortum Power and Heat Oyj, Fortum Nuclear Services Oy (Fortum), Tekes – the Finnish Funding Agency for Technology and Innovation (Tekes), Helsinki University of Technology (TKK) and Lappeenranta University of Technology (LUT). In addition to representatives of these organisations, the Steering Group has permanent experts from the Swedish Radiation Safety Authority (SSM) and Fennovoima Oy (Fennovoima).

SAFIR2010 research programme is divided in eight research areas that are Organisation and human, Automation and control room, Fuel and reactor physics, Thermal hydraulics, Severe accidents, Structural safety of reactor circuit, Construction safety, and Probabilistic Safety Analysis (PSA).

Research projects of the programme are chosen on the basis of annual call for proposals. The annual volume of the SAFIR2010 programme in 2007–2008 has been 6,3–6,7 M€ and approximately 50 person years. Main funding organisations in 2007–2008 were State Waste Management Fund VYR with 2,7–3,0 M€ and VTT with 2,4–2,5 M€ annually. In 2008 research was carried out in 30 projects.

The research in the programme has been carried out primarily by VTT Technical Research Centre of Finland. Other research units responsible for the projects solely or in co-operation with other institutions include Lappeenranta University of Technology, Helsinki University of Technology, Tampere University of Technology, Fortum Nuclear Services Oy, Finnish Institute of Occupational Health and Finnish Meteorological Institute. In addition, there have been a few minor subcontractors in some projects.

The programme management structure consists of the steering group, a reference group in each of the eight research areas and a number of ad hoc groups in the various research areas.

This report gives a summary of the technical results of the SAFIR2010 programme from the years 2007–2008.

ISBN
978-951-38-7266-3 (soft back ed.)
978-951-38-7267-0 (URL: http://www.vtt.fi/publications/index.jsp)

Series title and ISSN
VTT Tiedotteita – Research Notes
1235-0605 (soft back ed.)
1455-0865 (URL: http://www.vtt.fi/publications/index.jsp)

Project number
VTT-V-23935-08

Date
February 2009

Language
English

Pages
535 p.

Name of project
SAHA2008/SAFIR2010

Commissioned by
TEM

Keywords
nuclear safety, safety management, nuclear power plants, human factors, automation systems, operating practices, control room technology, nuclear fuels, reactor physics, thermal hydraulics, core transient analysis, steam generators, modelling, accidents, structural safety

Publisher
VTT Technical Research Centre of Finland
P.O. Box 1000, FI-02044 VTT, Finland
Phone internat. +358 20 722 4520
Fax +358 20 722 4374

SAFIR2010

Major part of the Finnish public research on nuclear power plant safety during the years 2007–2008 has been carried out in the SAFIR2010 programme. The steering group of SAFIR2010 consists of representatives from Radiation and Nuclear Safety Authority (STUK), Ministry of Employment and the Economy (MEE), Technical Research Centre of Finland (VTT), Teollisuuden Voima Oyj (TVO), Fortum Power and Heat Oyj, Fortum Nuclear Services Oy (Fortum), Finnish Funding Agency for Technology and Innovation (Tekes), Helsinki University of Technology (TKK) and Lappeenranta University of Technology (LUT). In addition to representatives of these organisations, the Steering Group has permanent experts from the Swedish Radiation Safety Authority (SSM) and Fennovoima Oy (Fennovoima).

SAFIR2010 research programme is divided in eight research areas that are Organisation and human, Automation and control room, Fuel and reactor physics, Thermal hydraulics, Severe accidents, Structural safety of reactor circuit, Construction safety, and Probabilistic Safety Analysis (PSA).

Research projects of the programme are chosen on the basis of annual call for proposals. The annual volume of the SAFIR2010 programme in 2007–2008 has been 6,3–6,7 M€ and approximately 50 person years. Main funding organisations in 2007–2008 were State Waste Management Fund VYR with 2,7–3,0 M€ and VTT with 2,4–2,5 M€ annually. In 2008 research was carried out in 30 projects.

VTT Technical Research Centre of Finland has been the major research unit in 2007–2008. Other research units responsible for the projects solely or in co-operation with other institutions have been Lappeenranta University of Technology, Helsinki University of Technology, Tampere University of Technology, Fortum Nuclear Services Oy, Finnish Institute of Occupational Health and Finnish Meteorological Institute.

This report gives a summary of the technical results of the SAFIR2010 programme from the years 2007–2008.

ISBN 978-951-38-7266-3 (soft back ed.)
ISSN 0357-9387 (soft back ed.)

ISBN 978-951-38-7267-0 (URL: http://www.vtt.fi/publications/index.jsp)
ISSN 1455-0873 (URL: http://www.vtt.fi/publications/index.jsp)